Jan Drzymała

Mineral Processing

Foundations of theory and practice of minerallurgy

Mineral Processing

Foundations of theory and practice

of minerallurgy

1st English edition

JAN DRZYMALA, C. Eng., Ph.D., D.Sc.

Member of the Polish Mineral Processing Society

Wroclaw University of Technology

2007

Contents

4

6

Introduction

Mineral processing is a branch of science and technology dealing with processing of natural and synthetic mineral materials as well as accompanying liquids, solutions and gases to provide them with desired properties. It is a part of technical sciences, although it contains elements originating from other fields of knowledge, especially natural sciences. Mineral processing is based on separation processes and is involved in performing and description of separations, as well as their analysis, evaluation, and comparison.

Various terms are used in different countries for *mineral processing*. In English speaking countries (USA, UK, Canada, Australia, etc.) it is also termed, *dressing*, *preparation*, *beneficiation*, and recently *mineralurgy* or *minerallurgy*. The Poles mostly use *przeróbka kopalin*, the Russians *obogashchenie poleznykh iskopaemykh*, the Germans *Die Aufberaitung,* and the Spanish *Procesamiento de minerals.*

The term *mineralurgia* becomes more and more popular in Poland, Italy, Portugal, Spain, Slovakia, Hungry, Czech Republic, Russia, *minéralurgie* in France, and *mineralurgy* or *minerallurgy* in Canada and Australia. In spite of the fact that the term *mineralurgy* precisely characterizes our branch of knowledge and practice, it finds difficulties among both scientists and technologists to be commonly applied.

The word *minerallurgy* is a combination of the word *mineral* meaning a substance resulting from geological processes and a Greek word *lurgia* (streactly speaking *lourgeion*) denoting the place of processing.
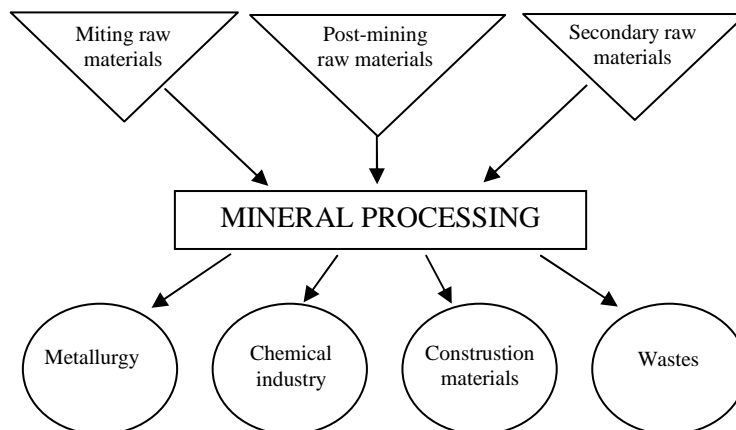
Fig. 1. Place of mineral processing in science and practice

The history of mineral processing is as old as that of a man. Cleaving stones, sharpening flint stones and sorting were one of the first mineral processing activities practiced by humans. A considerable development of mineral processing and its physicochemical basis took place within the last hundred years. Processing of useful minerals has become a branch of science and technology closely cooperating with mining and chemical industry as well as other branches of industry. Minerallurgy also deals with utilization of industrial an municipal wastes. The products manufactured by minerallurgists are utilized by metallurgical, chemical, civil engineering, and environmental protection industries (Fig.1.).

EXTRACTIVE METALLURGY

MINERALLURGY
(MINERAL PROCESSING)
(separations without chemcial changes)

METALLURGY
(separations with chemcial changes)

feed → **grinding screening flotation & other** — **concentrate** → **smelting leaching electrolysis** → **metal**

other industries

tailing

tailing
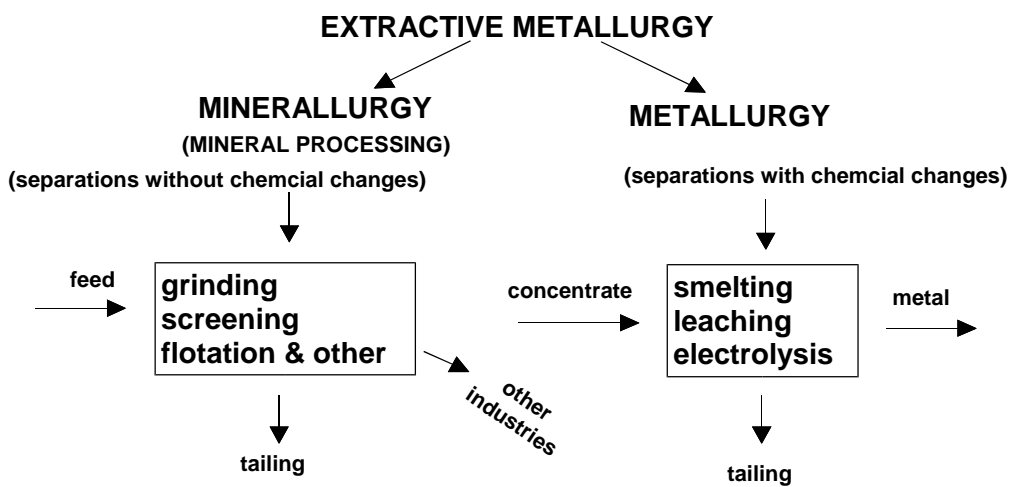
Fig. 2. Mineral processing is a part of extractive metallurgy

Mineral Processing, together with metallurgy, constitute extractive metallurgy (Fig. 2). Extractive metallurgy is a wide branch of knowledge as it covers many raw materials and numerous methods of separation.

Mineral processing is sometimes divided into mechanical and physicochemical parts. Another classification of mineral processing leads to coal preparation and processing of mineral raw materials. These divisions are frequently the source of misunderstanding because there is a tendency to use different terms for the same phenomena, parameters and properties. For example, the fraction of a particular component which is transferred from the feed to a product of separation can be called recovery, separation number, release degree, efficiency, transfer probability, and so on. In this book an attempt was undertaken to treat all mineral processing operations as separation and four basic terms, yield, recovery, content, and separation feature will be used for delineation, analysis, assessment, and comparison of separations and their results

hoping that in the future this will unify all branches of mineral processing as to its philosophy and terminology.

The advances in mineral processing can be noticed in the papers and books published in different countries. The best ones, written in English, still full of useful information are the works by Taggart (Handbook of mineral dressing, Wiley 1945), Gaudin (Flotation, McGraw-Hill, 1957), Wills (Mineral processing technology, Pergamon 1979 and further editions), Kelly and Spottiswood (Introduction to mineral processing, Wiley 1982), Leja (Surface chemistry of froth flotation, Plenum Press 1982), Wiess (chief ed., SME Mineral processing handbook, AIMME/SME, 1985), Fuerstenau, Miller, and Kuhn (Chemistry of flotation, AIME/SME, 1985), Tarjan (Mineral processing, Akademai Kiado 1986), Laskowski (Coal flotation and fine coal utilization, Elsevier, 2001).

The goal of this book is to present the bases of mineral processing with emphasis on treating all operations as separation processes having similar structure, which can be subjected to the same procedure of delineation, analysis, and evaluation. The present, most common treatment of mineral processing operations is shown in Fig. 3.
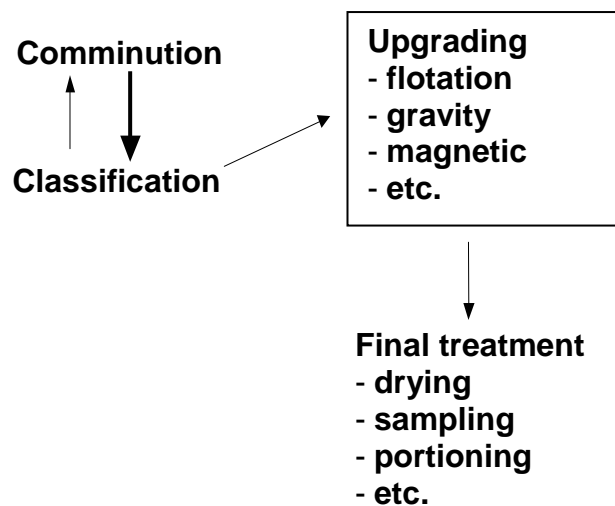
Fig. 3. Typical treatment of mineral processing operations

while the treatment used in this book in Fig. 4:

Introduction

MINERAL PROCESSING SEPARATIONS

Mechanical separation
(Comminution)

Size separation
(Classification)

MAIN SEPARATION
- **Flotation**
- **gravity**
- **magnetic**
- **etc.**

ADDITIONAL SEPARATION
- **drying**
- **sampling**
- **portioning**
- **etc.**
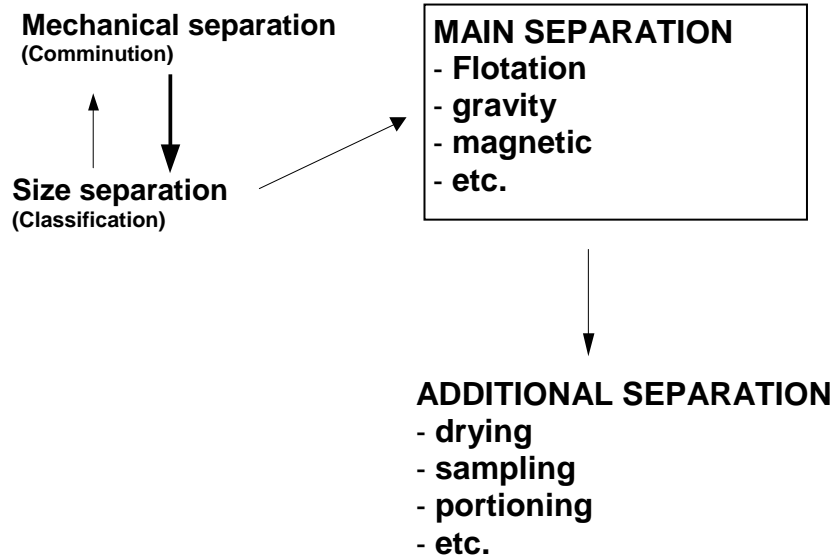
Fig. 4. Treatment of mineral processing operations proposed in this monograph

Acknowledgements

Part I

Introduction to mineral processing

1. From the Big Bang to mineral processing

1.1. The formation of matter

According to the Big Bang theory mostly based on the Einstein equations for homogenous and isotropic space-time continuum, the present universe had its origin about 15 billion ($15 \cdot 10^9$) years ago (Gribbin, 1998). At that time everything was condensed in a form of an embryo of 10^{-33} cm in size. The quantum embryo, which developed into the universe, came into existence as fluctuation. The time of this fluctuation was 10^{-43} s because this is the smallest interval of time, i.e. the quantum of time. The embryo co-existed with gravitation as an independent parameter. One of the fluctuations was too big and initiated a reaction analogical to a phase transition leading to energy release. This energy, operating against gravity, caused explosion called inflation. The universe inflation lasted about 10^{-34} s. As a result, the universe increased the size and reached a diameter of about 10 cm. Further expansion of the universe was linear with inertia as a driving force. Since then, such parameters as time and temperature have gained their physical meaning. The Big Bang put in motion processes which lead to diversification, evolution and appearance of new forms of matter and its equivalents. Evolution of the universe, based on the hypothetical Big Bang, is schematically shown in Fig. 1.1.
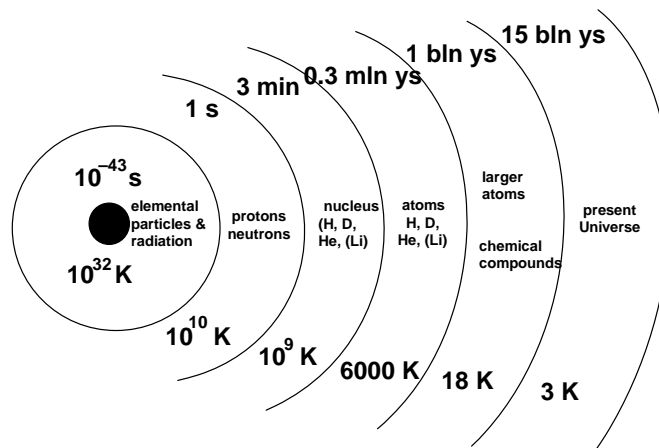
Fig. 1.1. The evolution of the universe based on the Big Bang theory (after Wiedza i Zycie, 10/1998)

At the moment of its origin the age of the universe was 10^{-43} s and its average temperature was 10^{32} kelvins (K). When the universe was 10^{-34} s "old" its temperature fell to 10^{27} K and it consisted of the mixture of elementary matter and antimatter particles. With time and temperature decrease, the particles of matter and antimatter reacted producing radiation. The reactions had been taking place until antimatter and many exotic particles disappeared leaving such particles as quarks, electrons, neutrinos, and photons. It lasted several seconds and the temperature dropped to approximately 10^{10} K. Then, the quarks started to form protons and neutrons.

Further spreading of the universe made protons and neutrons to interact, forming nuclei of hydrogen and deuterium. Soon after that, a period of nuclear reactions took place, which led to formation of helium nuclei and, to a smaller extent, heavier nuclei of lithium. Within the first million years, the atoms of hydrogen, deuterium, helium and small amounts of lithium were formed from nuclei and electrons. Further expansion of the universe caused that it became huge and cold as its temperature decreased to a few tens of kelvins (presently it is about 3 kelvins). Some hydrogen, deuterium and helium atoms, although highly disseminated, started to accumulate locally. This phenomenon also takes place today. The density of cumulating deuterium increases, while the temperature of the surroundings continuously drops. At the same time local temperature is growing until initiation of nuclear reactions leading to the formation of a star. A star is a huge "crucible" in which synthesis of heavy chemical elements takes place. At the end of their lives the stars explode, releasing chemical elements produced during their life. The chemical elements form stable compounds and create planets and solar systems. Stars with planets and their moons form galaxies like our Milky Way.

Stable chemical compounds, due to their electronic structure, are for instance H_2O, SiO_2, and CO_2. It is believed that current chemical composition of the universe is: 77% hydrogen, 23% helium, and trace amounts of heavy elements and their compounds (Polański, 1988).

The Sun, Earth and other our solar system planets were formed about 5 billion years ago. Probably about one billion years later, according to the theory of evolution, life on the Earth came into being as a result of chemical reactions. The mankind (*homo sapiens*) appeared on the Earth about two hundred thousand years ago.

The Earth consists of solid, liquid and gaseous substances which can be found mostly in the form of chemical compounds. Currently, there are 116 known and two further speculated elements. About 90 elements are present on our planet, while the remaining ones can be artificially produced by nuclear reactions. Most elements are solid at room temperature and pressure. Mercury and bromine are liquids, some elements are gases (oxygen, nitrogen, noble gases, and some others).

Atoms consist of smaller units: atomic nuclei and electrons. The number of negatively charged electrons in an atom is the same as positively charged protons. Apart from protons, there are neutrons which are electrically neutral. The number of neutrons in a nucleus is usually equal or higher than the number of protons. The elements,

which contain in their nuclei identical numbers of protons but differ in the number of neutrons, are called isotopes. Particular isotopes are referred to as nuclides. Atoms can be found in a single form (for instance argon, Ar), as molecule (oxygen, O_2), or form complex structure (macromolecules such as polymers, solid, etc.). The properties of the elements can be generally characterized with the periodic table of elements. Details regarding the periodic table, are taught during physics and chemistry courses, and therefore will not be presented in this work.

1.2. Elementary particles

Atoms consist of smaller units called elementary particles. They are divided into matter carriers called fermions and particles that are associated with force carriers, which are called bosons (Table 1.1). There are two types of fermions - leptons and quarks and four types of fields (forces) – electromagnetic, weak, strong and gravity. The elementary particle associated with force interactions are photons, bosons, gluons, and gravitons, respectively. The existence of graviton has not been confirmed.

Table 1.1. Presently known elementary particles of the universe

Elementary particles					
Fermions (matter carriers)		Bosons (force carriers)			
Leptons	Quarks	Weak (bosons)	Strong (gluons)	Electro-magnetic (photon)	Gravity (graviton)
electron neutrino	up	W_- boson	color 1	$E_1 = h\nu_1$	*
electron	down	W_+ boson	color 2	$E_2 = h\nu_2$	
muon neutrino	charm	Z_o boson	color 3	$E_2 = h\nu_2$	
muon	strange			$E_3 = h\nu_3$	
tau neutrino	top			$E_n = h\nu_n$	
tau	bottom				

* not yet discovered

There are three pairs of quarks and separately three pairs of leptons. The quarks are called up and down, charm and strange, top and bottom while leptons are electron and neutrino, muon and muon neutrino, tau particle and tau neutrino. Ordinary matter contains the simplest fermions that is the up and down quarks, as well as electrons and electronic neutrinos. Higher quarks and leptons existed only during the Big Bang. They and their antiparticles can be produced in special physical laboratories.
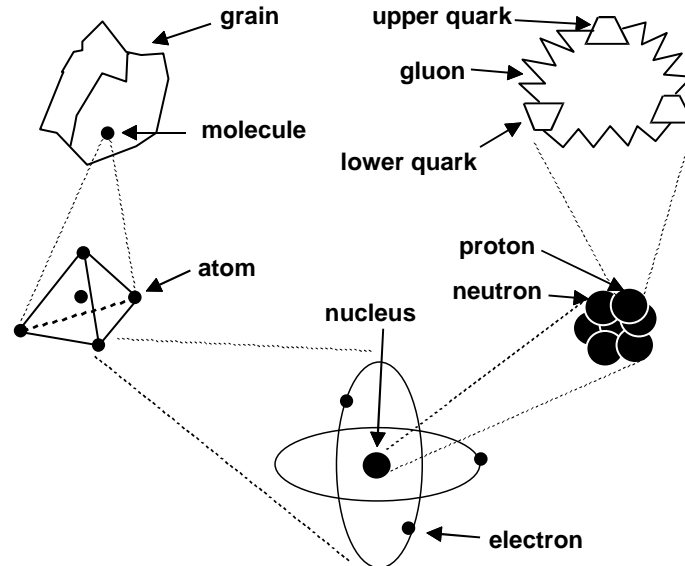
Fig. 1.2. Elemental components of matter (base on Kane, 1986)

Quarks form protons and neutrons in which quarks are bound by gluons (Fig. 1.2). Proton consists of two up quarks and one down quark. Since the electric charge of the up quark is 2/3 and the down quark -1/3, the electric charge of proton (2·2/3–1/3) is equal to one and is positive (+1) and numerically equal to the electron elementary charge. Neutron consists of one up quark and two down quarks. It is easy to calculate that electric charge of neutron is zero (2/3 – 1/3 – 1/3 = 0).

Elementary particles, as well as the objects they form, can mutually interact. As it has been mentioned, currently we know four interactions: gravitational, electromagnetic, strong and weak.

Gravitation energy of the universe is, in approximation, equal to the energy equivalent of its mass ($E=mc^2$) and, therefore, is negative. According to the Einstein theory, gravity effects are realized by means of gravitons, electromagnetic effects (electrical field, magnetic field, electromagnetic field) by photons, strong forces effects by gluons (which are responsible for nuclei cohesion) and weak forces by bosons, which are of certain importance for radioactivity. The quarks are subjected to strong, electromagnetic, and weak interactions, leptons (without neutrino) to weak and electromagnetic, while neutrinos are under the influence of weak interactions.

Elementary particles (proton, neutron, quarks, leptons, and so on) have their counterparts called antiparticles. Their name is formed by adding prefix „anti". Hence, there are antielectron (i.e. positron), antineutron, antiproton, antiquark, antineutrino, and so on. For instance photons do not have their equivalent „anti", since they are their own antiparticles. If a particle has a charge, an antiparticle features an opposite charge.

If a particle does not have a charge, its antiparticle has a spin opposite to it. A collision of a particle and antiparticle causes their vanishing (annihilation) and forming new particles or a field. As a result of electron and position annihilation two photons are usually formed. Opposite reaction of forming electron and position is also possible (Pajdowski, 1993).

Each particle possesses its time of life. Many of them feature a very short life-span and therefore we cannot find them in everyday life. Extremely stable are quarks, protons, neutrons, electrons (the matter carries) and photons.

1.3. Molecules

The molecules are formed as a result of the reaction between chemical elements or other molecules. Molecules appear in the space due to explosion of stars creating nuclei providing different chemical elements, and finally molecules. Molecules formed in the space are mostly stable, except for the radioactive ones. Under favorable conditions molecules undergo alterations. Such conditions exist in various spots of the universe, including planets, moons and comets. Also the Earth is the place of reactions leading to formation of chemical compounds. It takes place during magmatic, post-magmatic, weathering, transportation, sedimentation, diagenesis, metamorphosis, anatexis, and palingenesis, geological processes (Gruszczyk, 1992). Since there are presently 90 available chemical elements theoretical number of possible diatomic molecules originating from different atoms is 90! (symbol „!" means a mathematical function called factorial).

As it has already been mentioned, the properties and structure of chemical elements is well characterized by the periodic table of elements. In the case of molecules, their description requires other than periodic table approaches. The diatomic molecules can delineate, for instance, with the Goerlich triangle (1965, 1997), which is shown in Fig. 1.3. According to the Goerlich triangle the character of a diatomic compound depends on the so-called Pauling electronegativity of atoms forming molecule. The diatomic molecule is characterized by three parameters: ionicity (I), non-metallic (A), and metallic character (M). According to Goerlich (1965) diatomic compounds can be divided into four categories:

I.   alkaline metals and their intermetallic compounds
II.   amphoteric metals and their compounds with alkaline metals
III.   metalloids (semimetals) and their semiconducting compounds
IV.   non-metals and their compounds. The fourth group can be subdivided in the following way:
IVA.   salts structurally similar to metals
IVB.   compounds structurally similar to metalloids
IVC.   compounds structurally similar to nonmetals.

Ionic I and non-metallic character A of a particular compound for silicon carbide (SiC, broken lines) is shown in Fig. 1.3. The scale is based on three chemicals: FrF (fully ionic), Fr (fully metallic), and F (fully ionic).
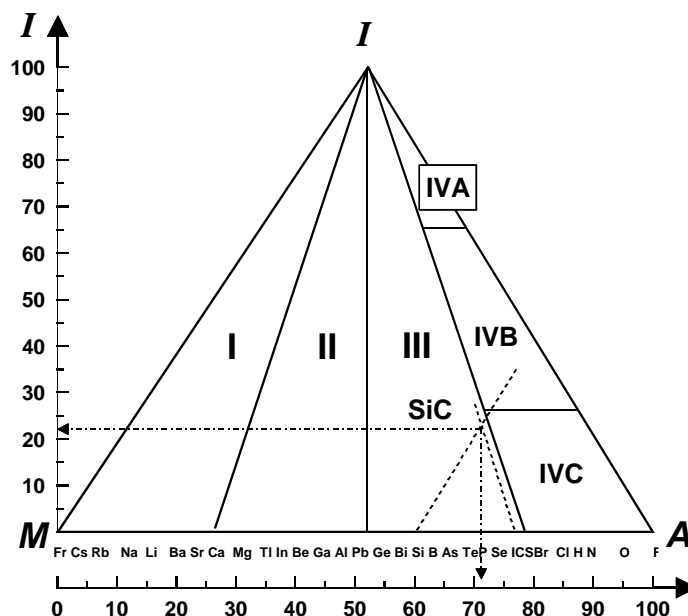
Fig. 1.3. The Goerlich triangle characterizing bonds in diatomic molecules (after Goerlich, 1965)

The Goerlich triangle covers and classifies only diatomic 1:1 compounds. It covers a small number of compounds since many molecules have more than two atoms in their structure. Sulfuric acid, H_2SO_4, can serve as an example of multiatom molecule. The multiatom molecules can be reduced, after appropriate procedures, to 1:1 structures. Other classifications of molecules have been also proposed (Górecki, 1994).

1.4. Solids

Most molecules do not occur in a single isolated form, but as their collection forming either solid, liquid, or gas phase. In the solid phase, due to mutual interactions, molecules form crystalline structures. Depending on electronic structure of the atoms forming the solid, especially the properties of outer electrons, four types of crystalline structures: ionic, covalent, metallic, and molecular, are distinguished (Bielański, 1999). The atoms are held together with ionic, covalent, metallic, and molecular bonds, respectively. The covalent bonds are the strongest when compared with other bonds. Therefore, the covalent crystals are hard, melt at high temperatures and feature

low solubility. Among substances which form covalent structures are diamond and silicon carbide which are used as abrasives.

In ionic crystals the atoms are bound with ionic bonds. Many ionic crystals are soluble in polar solvents. The lattice of molecular crystals is built of molecules held together due to dispersion forces also called the van der Waals interactions. Such a structure is formed for instance by iodine (I_2) or solid CO_2. If molecules are asymmetric, like H_2O in ice, they form dipoles and they feature increased melting temperature of the solid in comparison to similar symmetrical molecules.

The lattice of metallic crystals is built of positive metal ions surrounded by the so–called electronic gas which provides their high electrical and thermal conductivities, as well as metallic luster.

Four basic types of bonds mentioned above represent ideal cases. Most solids form intermediate bonds.
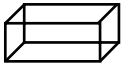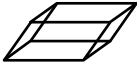
The atoms of molecules forming a crystal are arranged in an appropriate way and they are repeated in space usually forming 3-dimensional lattice. This lattice can be represented by an elementary cell which is a basic unit of crystalline structure. Different elementary cells differ in symmetry. There are 7 elementary cells (crystallographic systems): regular, tetragonal, trigonal, hexagonal, rhombic, monoclinic and triclinic. Each crystal can be assigned to one of the seven crystallographic systems. Elementary cells and selected minerals forming specific cells are shown in Table 1.2.

The elemental cell is a part of a three-dimensional net selected to feature the same symmetry as the crystal and to be possibly the smallest. The elementary cell contains all atoms at stoichiometric ratios resulting from the chemical formula of the material. A univocal description of an elementary cell is provided by the length of its edges and angles between the edges.

In the elementary cell, apart from lattice nodes, there can be also atoms, molecules or ions in its center, cell walls of edges. Taking this it into account we get 14 different structure lattices. Lattice P denotes a primitive cell without additional atoms, C is centered on the base of the elementary cell, I refers to space centering, while F means centering on the walls. Only few solids feature simple elementary lattice, like copper, which forms type P regular lattice. Most solids consist of two or more lattices. For instance, the structure of NaCl (halite) is a result of interpenetration of two regular nets, i.e. lattice F of sodium ions and the lattice F of chlorine ions. These lattices are shifted in relation to each other by half of the length of the elementary cell edge.

A description of the inner structure of crystals makes use of 7 crystallographic systems containing 32 elements of symmetry combined with 14 translation lattices. The combination of 32 classes of symmetry and 14 translation lattices makes 230 space groups. This means that a particular crystal, must belong to one of the 230 space groups. To distinguish between space groups there are used two different, international and the Schoenflies, notations. For example, the symbol of NaCl lattice in the international system is Fm3n while in the Schoenflies system is O_h^5.

Table 1.2. Crystallochemical classification of solid materials

System	Elemental cell (lattice)	Minerals
1	2	3
1. Regular (*C*)	$a = b = c$ $\alpha = \beta = \gamma = 90^\circ$	halite (NaCl) galena (PbS) fluorite (CaF$_2$) sphalerite (ZnS)
2. Tetragonal (*Q*)	$a = b \neq c$ $\alpha = \beta = \gamma = 90^\circ$	rutile (TiO$_2$) zircon (ZrSiO$_4$) hausmanite (Mn$_3$O$_4$) cassiterite (SnO$_2$)
3. Rhombic (*O*)	$a \neq b \neq c$ $\alpha = \beta = \gamma = 90^\circ$	sulfur (S) barite (BaSO$_4$) stibnite (Sb$_2$S$_3$) anhydrite (CaSO$_4$)
4. Hexagonal (*H*)	$a = b \neq c$ $\alpha = \beta = 90^\circ$, $\gamma = 120^\circ$	graphite (C) wurzite (ZnS) corundum (Al$_2$O$_3$) covellite (CuS)
5. Trigonal (*T*) (romboedric)	$a = b = c$ $\alpha = \beta = \gamma \neq 90^\circ$	α-quartz (SiO$_2$) calcite (CaCO$_3$) dolomite (MgCa(CO$_3$)$_2$) hematite (Fe$_3$O$_4$)
6. Monoclinic (*M*)	$a \neq b \neq c$ $\beta = \gamma = 90^\circ$, $\alpha \neq 120^\circ$	arsenopyrite (FeSAs) gipsum (CaSO$_4 \cdot$2H$_2$O) kriolite (Na$_3$AlF$_6$) diopside (CaMgSi$_2$O$_6$)
7. Triclinic (*A*)	$a \neq b \neq c$ $\alpha \neq \beta \neq \gamma \neq 90^\circ$	albite (NaAlSi$_3$O$_8$) microcline (KAlSi$_3$O$_8$) anorthite (CaAl$_2$Si$_2$O$_8$) kaolinite (Al$_4$Si$_4$O$_{10}$(OH)$_8$)

Detailed description of the international notation can be found in books on crystallography (Penkala, 1977).

Another classification of crystalline structures is based on chemical formula. Letter A refers to the structure of monoatomic elements, B – structures of diatomic compounds XY, C means two–component molecule of type XY$_2$ (e.g. CaF$_2$ and TiO$_2$), D designates the structures of X$_n$Y$_m$ compounds (e.g. Al$_2$O$_3$). Further letters cover still more complicated structures. In this classification the name of the structure originates

from its typical representative. For example structure A1 is the copper type, A2 – wolfram, A3 – magnesium, A4 – diamond, B1 – sodium chloride, B2 – cesium chloride, B3 – sphalerite, B4 – wurtzite, C1 – fluorite, C4 – rutile (Barycka. Skudlarski, 1993).

Sometimes crystallization of a solid does not take place and then we deal with amorphous or glassy materials having not a far–reaching arrangement. Carbon black can serve as an example. It consists of graphite lamellas but they are not arranged completely in a parallel way like in graphite. In quartz glass SiO_2 tetrahedrons are arranged chaotically in contrast to a symmetric pattern in crystalline quartz.

Most often crystalline materials consists of many fine, randomly oriented crystals which form a polycrystalline structure. This results from the history of a mineral, i.e. chemical system and parameters of crystallization. To determine possible forms of substances crystallizing from a liquid phase, the so-called phase diagrams can be plotted indicating pure components, their solutions and so-called eutectic mixtures. Co-crystallization is one of the reasons for a particle to form intergrowths which later, during mineral processing, require comminution. The size reduction of solids and liberation of useful components is one of the most important activity in mineral processing.

1.5. Minerals

Mineral can be defined as natural material featuring strictly determined internal structure, chemical composition, as well as chemical and physical properties, which was formed as a result of geological or cosmic processes. In terms of chemistry, mineral is a collection of molecules of the same chemical compound or, less frequently, mixture of compounds. Thus, the term minerals does not cover synthetic substances produced in laboratories and by industry. Sometimes the difference between mineral and chemical compound is elusive, especially when the substance is formed due to human activities and the forces of nature. Water is not a mineral while ice formed during geological processes is a mineral.

There are different classifications of minerals. The way they are classified depends on the aim of the classification. Usually (Bolewski and Manecki, 1993) minerals are classified according to their chemical composition:

  I. Native elements, alloys and intermetallic compounds
 II. Carbides, nitrides, phosphides and silicides
III. Sulfides and related minerals
IV. Halides
 V. Oxides and hydroxides

VI. Salts of oxy-acids (nitrates, iodates, carbonates, selenates, tellurates, borates, sulfates, chromates, molybdates, tungstates, phosphates, arsenates, antimonates, vanadates, uranates, geramanates, silicates and aluminosilicates)

VII. Ammonium minerals

VIII. Organic compounds and their derivatives.

The alteration of minerals takes continuously place on the Earth since it is a highly dynamic body in terms of geology and mineralogy. Cycle of processes taking place in the Earth crust, after Serkies (1970), is shown in Fig. 1.4. The cycle distinguishes the following processes: magmatic, post–magmatic, weathering, transportation, sedimentation, diagenesis, metamorphosis, anatexis, and palingenesis.

In the magmatic process sulfides and silicates are formed. Mineral composition of silicates depends on the composition of the initial magma and the conditions of a particular silicate precipitation. Subsequently formed minerals from magma are described by the so-called Bowen series. The anorthite arm of the Bowen series consists of bytownite, labrador, andesine, oligoclase and alkaline feldspars, while the olivine part consists of pyroxene, hornblende, biotite and alkaline feldspars. Crystallization of minerals described by the Bowen series can be stopped at each stage in the series or it can reach final stage and result in quartz or muscovite crystallization.

After the magmatic period, complicated post-magmatic processes including pegmatite, pnematolitic and hydrothermal take place.

In pegmatite processes, potassium-sodium feldspars, quartz, monazite, beryl and minerals of light elements such as Li, Ta, Nb, Br, Mn as well as minerals of rare earths chemical elements are formed.

In the pnematolitic processes, the following minerals are typically formed: quartz, muscovite, molybdenite, cassiterite, wolframite, bismuthinite, and minerals of F, B, Mo, W, and Sn. In the process of forming hydrothermal minerals a characteristic feature is the presence of quartz, sericite, albite, chlorite, calcite, dolomite and the compounds of Cu, S, As, Sb, Zn, Pb, Ag, Au, Hg, F, and Ba.

The chemicals which are active on the Earth surface, i.e. atmospheric oxygen, carbon dioxide, water and organic compounds cause diverse alterations in the mineral matter. These changes are called weathering and can lead to leaching and transforming some rocks, decreasing their cohesion and, in consequence, disintegration. The main weathering processes are: dissolution, hydration, hydrolysis, carbonatization, and oxidation.

Dissolving is a long lasting process of a high importance since it leads to the destruction of rocks and shifting mineral mass.

Hydration is the process of alteration of anhydrous minerals into hydrated ones. This process can cause transformation of mineral mass but it does not lead to its destruction. The best example of hydration is alteration of anhydrite into gypsum. Hydration usually occurs together with other processes, and it will be discussed later.
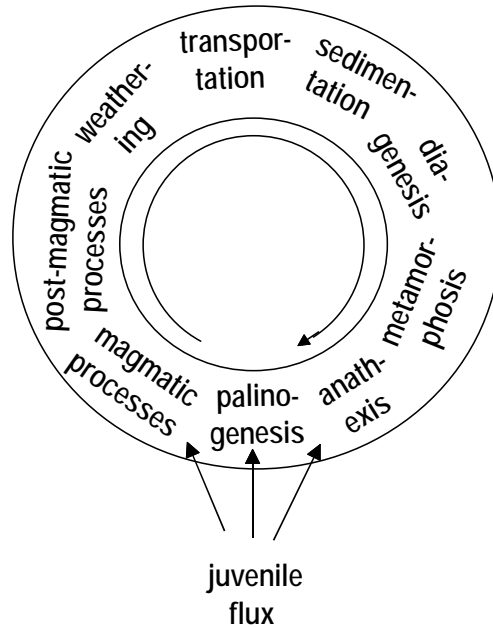
Fig. 1.4. Cycle of processes in the Earth crust

Hydrolysis is a process which results in destructive rock transformation. The products of hydrolytic disintegration, in some part soluble, are removed while the remaining sediment undergoes transportation. The process of hydrolysis leads to formation of new, secondary minerals and some other components pass into the solution in the ionic form (e.g. Na^+). Such a process leads to disintegration of main components of the original rocks, i.e. aluminosilicates turn into silicon dioxide and aluminum hydroxide. In a moderate climate hydrolysis is partial and its final product is usually kaolinite. In tropical climate feldspar hydrolysis can be complete resulting in gibbsite formation.

Carbonatization is the process of eliminating silicate anions from mineral material by CO_2 or by carbonate CO_3^{2-} and HCO_3^- anions (Polański, 1988). This process leads, for instance, to dolomitization of original silicate rocks and it is often accompanied by hydrolysis. Another example of cooperation between water and carbon dioxide in weathering is transformation of copper sulfides into alkaline copper carbonate - malachite $Cu_2[(CO_3)(OH)_2]$. Carbonatization can affect, for example, serpentine and the result is talc and magnesite (Borkowska, Smulikowski, 1973).

Oxidation is of a crucial meaning for weathering processes. It leads, within a wide range, to transformation of sparingly soluble compounds into easily soluble ones, for example sulfides become sulfates, ions featuring lower degree of oxidation into highly oxidized ions. Oxidation, combined with dissolution, causes advanced destruction and damage of original rocks. The mechanism of sulfides oxidation is quite complex.

The final stage is usually formation of sulfate. In the case of iron sulfides, iron(III) sulfate ($Fe_2(SO_4)_3$), is created which undergoes hydrolysis to more stable limonite, whose main component is goethite (FeOOH) (limonite contains more water than goethite) (Bolewski, Manecki, 1993).

Red, brown and yellow colors of oxidized deposits of iron ores result from the presence of different oxidized and hydrated iron compounds. Other examples of oxidation include: $S^{2-} \rightarrow S^{6+}$, $Mn^{3+} \rightarrow Mn^{4+}$, and $Cr^{3+} \rightarrow Cr^{6+}$.

In weathering an important role is played by biosphere which contributes to the formation of bitumen deposits. Biosphere also causes the decay of organic matter and it can induce reduction processes leading to the formation of uranium- and copper-bearing shales or sulfur deposits. Biodegradation, hydration, carbonatization, oxidation, and reduction can take place at different places of the same deposit, causing its diversification. Weathering can also be of a chemical character. Chemically weathered deposits are made from ions and marine colloidal particles (Serkies, 1970). Sedimentation can take place all over the water basin and the chemistry of the products depend on salinity, pH, and redox potential of the solution, as well as temperature and pressure. It happens quite often that remains of organic life, with slow water movement in the water pool, settle and decay creating in the bottom zones specific pH and redox potential environment. This usually leads to formation of low redox potential sediments.

Diagenesis covers a number of processes taking place in already formed sediments. Diagenesis makes both alterations of chemical composition and changes in the sediment structure. The alterations of the chemical composition can result from long-term effects of original solutions and it initiates transformation of physicochemical conditions within the sediment (e.g. decrease in pH, alterations of redox potential as well as composition of solution above the sediment), and local diversity of sediment environment. Long-term effects of the original solution on the sediment results in equilibrium state of all the reactions possible to take place in the solution–sediment system. This process is very important for the so-called dolomitization in which dolomite is formed as a result of the reaction between calcium carbonate of the sea sediment with magnesium ions present in the sea water. This phenomenon often leads to a complete dolomitization of the sediment. In an analogous way, iron(II) ions present in the sea water react with copper sulfide to form chalcopyrite. Similarly, sediment transformation, due to diffusion of ions from upper layers of the original solution can take place. For instance precipitated zinc, lead, and copper sulfides can be turned into copper sulfide due to copper ions, transported by diffusion from the upper layers of the solution.

Changes in solution composition above the sediment, resulting from the inflow of foreign components from other, either close or distant geochemical environments, can also cause alterations in the sediment. Then, sideritization can take place which relies on eliminating Ca^{2-} ions from calcium carbonate by Fe^{2+} ions and forming siderite. Sediment phosphatization results from substitution of carbonates by phosphates, sedi-

ment silicification results from replacing carbonates by silica, sediment pyritization…
etc.

The alterations in sediment structure are caused, first of all, by recrystallization.
The aggregates of larger crystals replace fine crystals and they bind the sediment into
a monolithic rock. Carbonate fines are transformed into compact limestone. Aragonite,
a calcium carbonate, turns into a more stable variety calcite. Colloidal particles are
transformed into crystalline aggregates. Also a considerable dehydration of the sedi-
ment and binding takes place. For instance opal becomes quartz. In consequence the
original, loose and fine sediment becomes homogenous, compact, crystalline rock.

In metamorphic processes the most important role is played by temperature and
pressure. Mineral composition is also of no lesser meaning. Another considerable fac-
tor is duration of the process. Metamorphic processes take place at high temperature.
It accelerates chemical reactions between rock components. Under high temperature
and pressure conditions carbonate rocks react with silica, which results in formation of
diopside ($CaMgSi_2O_6$) and carbon dioxide. In metamorphic processes a significant
role is played by the CO_2 and water vapor pressure. Higher pressure leads to formation
of minerals of higher density. This results from the LeChaterlier principle. Higher
pressure in metamorphic rock is favorable for forming the minerals whose sum of mo-
lar volume is lower than the sum of molar volumes of original minerals. This can be
exemplified by the reaction (Beres, 1992):

$$2CaSiO_3 + Ca(Al_2Si_2O_8) \rightarrow Ca_3Al_2(SiO_4)_3 + SiO_2 \qquad (1.1)$$

wollastonite   anorthite   garnet   quartz
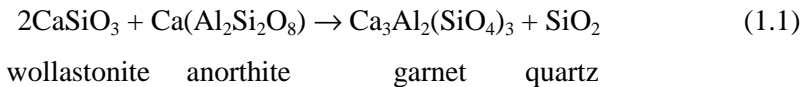
Molar volume, resulting from the quotient of molecular weight and specific gravity
for the left hand side of the equation amounts 180.1, while for the right one equals
150.5.

The metamorphic processes in the Earth crust lead to the formation of common
minerals of silicon and aluminum as well as small quantities of rare earths elements
compounds. So far, about four thousand minerals have been discovered and described
in details (Bolewski, Manecki, 1993; Manecki, 2004). Each mineral has its specific
chemical and crystallographic composition.

Minerals can occur as monocrystals and also, most commonly, as a cluster (adher-
ing monocrystals) grains. Crystals feature their own characteristic internal and exter-
nal structure. Their external form is determined by their internal structure which
causes that a crystal can have strictly determined planes and their combinations lead-
ing to certain external shape (habit) of a mineral.

The theory of crystalline solids is based on the so-called group theory. It is com-
plete and it has been confirmed by observations. The theory predicts the existence of
48 simple forms, including simple open forms (dihedron, prism, pyramid) and simple
closed forms (rhombohedron, trapezohedron, scalenohedron, cube, octahedron, deltoid
tetracosahedron (Beres, 1992). Real crystals, even of a very complicated shape, are

combinations of simple forms. Simple closed forms can occur separately, while simple open forms have to remain in combination with closed forms to close their space.

Internal structure of minerals is the same or, if they have admixtures of other minerals, similar to respective chemical compounds. This has been discussed in subchapter 1.4 regarding solids. The composition of some minerals can change within certain limits of chemical composition. The series from forsterite (Mg_2SiO_4) to fayalite (Fe_2SiO_4) with olivine ($Mg,FeSiO_4$) as transit mineral can serve as an example. They form isomorphic series.

Isomorphism (similarity in shape or structure) occurs when two different minerals feature identical crystalline lattice. Isomorphism results from similarity of the size of ions forming isomorphic minerals.

Crystallochemical similarity also allows some elements to co-occur in minerals. Rubidium can be present in minerals with potassium, gallium with aluminum, hafnium with zirconium, germanium with silicon. Crystallochemical dissimilarity of elements also plays an important role in forming mineral aggregates. Many heavy metals, although their average content in the Earth crust is low, occur in a native form (silver, mercury, antimony, bismuth and copper).

1.6. Deposits, mining and mineral processing

Geological processes take place in the Earth's crust and lead to accumulation of certain minerals. Any accumulation of minerals can be treated as mineral raw material. However, the value of a mineral or rock deposit is determined by economical, environmental, and technological factors. According to Gruszczyk (1972), environmental and technological factors refer to geological and environmental properties of deposits, the kind and quality of raw material, its physical and mechanical properties, as well as its structure. Economical factors involve geography and climate, deposit size, mining accessibility, availability of water, heat, gas, geotechnological conditions, as well as mining and processing technology.

The Earth consists of the atmosphere, hydrosphere, and lithosphere, silicate zone, oxide–sulfide zone, and metallic core. The hydrosphere is the source of vast amount of water soluble salts, including halite (kitchen salt), kieserite, etc. According to Gruszczyk (1972), the lithosphere is the most interesting Earth part in terms of raw materials since its upper part (SiAl) is in 95% built of magmatic and metamorphic rocks.

The rocks are usually classified into groups: magmatic, sedimentary and metamorphic. The rocks form deposits and deposits are divided into magmatic, post-magmatic and sedimentary.

Magmatic deposits are connected with magmatic rocks. The deposits of copper and nickel sulfides, native platinum, chromite, titanomagnetite, apatite and corundum are usually of this type. Magmatic rocks are used as building materials.

Scarn (metamorphic) deposits formed at the contact of magma and surrounding rock are a result of magma penetration. The scarn deposits may contain iron, copper, wolfram, zinc, lead, graphite, apatite, asbestos, and boron.

Pneumatolitic and hydrothermal deposits are also connected with magmatic processes of rock formation. This processes are the source of tin ores, wolfram, molybdenum, copper, gold, silver, zinc, lead, nickel, cobalt, bismuth, arsenic, antimony, mercury, iron, manganese, magnesium ores and barite, fluorite, topaz, and quartz deposits.

Sedimentary deposits are formed due to sedimentation processes. Deposits of coal, sandstones, silts, gravels, crude oil, natural gas, limestone, dolomites, marls, iron ores, manganese, bauxite, phosphates belong to this category. Sedimentary deposits are a source of copper, zinc, lead, uranium ores and pyrite, sulfur, clay, and rock salt deposits.

Weathering deposits constitute a separate group. They are formed as a result of deposit disintegration by atmospheric factors. Typical weathering deposits are platinum, gold, zirconium, scheelite, silicate, nickel, iron, manganese ores, and nickel hydroxides, and kaolinite deposits.

A deposit, after the approval by geologists as to its size and content, becomes a documented deposit, and after initiation of exploitation it becomes mined material. Mined materials can be classified into industrial rocks and minerals, ores, and energy raw materials. Industrial minerals include for instance: fluorite, barite, rock salt, kaolin while industrial rocks include granite, basalt, and limestone. Typical ores are copper, lead, tin, iron, and nickel ores, while energy raw materials are crude oil, natural gas, brown coal, hard coal and peat.

Useful minerals are the subject of interest of mining and mineral processing. The are open pit and underground mines. In the latter ones mines useful minerals are mined down to about 1000 meters. If the temperature at that depth is not too high, i.e. the so-called geothermal degree is near the typical value of 3°C per 100 meters of depth, exploitation is possible at a considerable depth. There are known examples of exploitation down to 3000 meters under the ground surface, like Oragun gold mine in India operating at the depth of 2835 m.

The run-of-mine material requires processing in order to make it a marketable product and therefore it is directed for mineral processing. Mineral processing treatments are based on separation processes. Sometimes it is simple separation process which depends on, for example, removing moisture or classification according to grain size. Usually transformation of a mined material into a marketable product requires many separation processes. For example, copper ore has to be ground, screened, subjected to hydraulic classification, flotation, filtration and drying before a final product

in the form of copper concentrates is achieved. The concentrates are next directed to metallurgy plants to produce metallic copper.

Literature

Barycka I., Skudlarski K., 1993. Podstawy chemii, Wydawnictwo Politechniki Wrocławskiej, Wrocław.

Beres B., 1992. Zarys mineralogii i petrografii, Wydawnictwo Politechniki Wrocławskiej, Wrocław.

Bielanski A., 1999. Podstawy chemii nieorganicznej, PWN, Warszawa, s. 218.

Bolewski A., Manecki, 1993. Mineralogia szczegółowa, PAE, Warszawa.

Borkowska M., Smulikowski K., 1973. Minerały skałotwórcze, PWN, Warszawa.

Goerlich E., 1965. An electrostatic model of chemical bonding, Prace Komisji Nauk Technicznych PAN, Kraków, Ceramika, 4, 1–104.

Goerlich E., 1977. Stan szklisty, w: Chemia ciała stałego, J. Dereń, J. Haber, R. Pampuch, rozdz. 6, PWN, Warszawa.

Gorecki A., 1994. Klasyfikacja pierwiastków i związków nieorganicznych, WNT, Warszawa.

Gribbin J., 1998. Kosmologia, Prószyński, Warszawa.

Gruszczyk H., 1972. Nauka o złożach, Wydawnictwa Geologiczne, Warszawa.

Kane G., 1986. The particle garden, Addison-Wesley, Reading (Massach., USA).

Manecki A., 2004, Encyklopedia minerałów, Wyd. AGH, Kraków.

Pajdowski L., 1993. Chemia ogólna, PWN, Warszawa.

Penkala T., 1977. Zarys krystalografii, PWN, Warszawa.

Polanski A., 1988. Podstawy geochemii, Wyd. Geol., Warszawa.

Serkies J., 1970. Mineralogia, Wydawnictwo Politechniki Wrocławskiej, Wrocław.

Wiedza i Zycie, 1998, Historia kosmosu, nr 10.

Part II

Characterization of mineralurgical

processes

2. Delineation, analysis, and evaluation of separation

2.1. Principles of separation

Separation is commonly performed in industrial applications and laboratory experiments. It also takes place in nature. The occurrence of separation in different fields of life since remote past has resulted in the use of various terms, phrases, symbols and ways of description, analysis, and assessment of separation. Its frequently causes misunderstanding among specialists of different fields of science and technology dealing with separations. In this chapter an effort has been undertaken to show the philosophy of separation applying a new self consistent approach as well as well carefully defined terms and relations.

Separation relies on the division of certain amount of matter, usually called the feed, under the influence of ordering and disordering fields and splitting forces, into two or more products which differ quantitatively or qualitatively, or both, in at least one property (Fig. 2.1). The feed and the products consist of one or more components. The property of the component which was utilized in separation will be called the main feature and it can be any property including particle size, density, shape, hydrophobicity, capability of adhesion, magnetic properties, electric properties, ability of adsorbing chemical substances, etc.
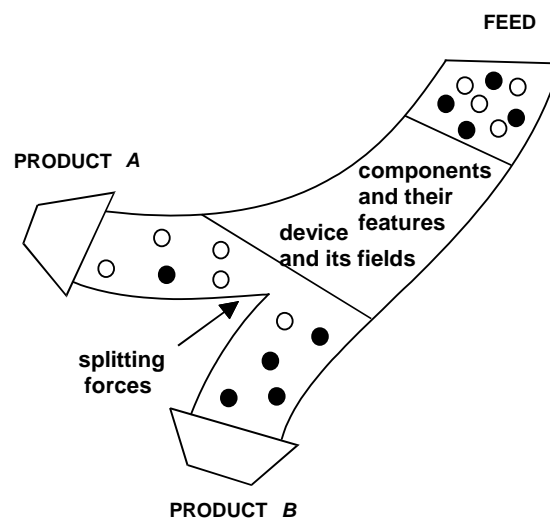
Fig. 2.1. Principle of separation

There can be distinguished three basic elements characterizing separation: delineation, analysis, and evaluation (Fig. 2.2). The description of separation provides physical and mathematical relations between the parameters of separation process, taking into account components, their features, fields, forces, space, time, etc. (Fig. 2.3). Delineation can be performed using physical, thermodynamic, mechanic, and mixed approaches and it will be discussed later.
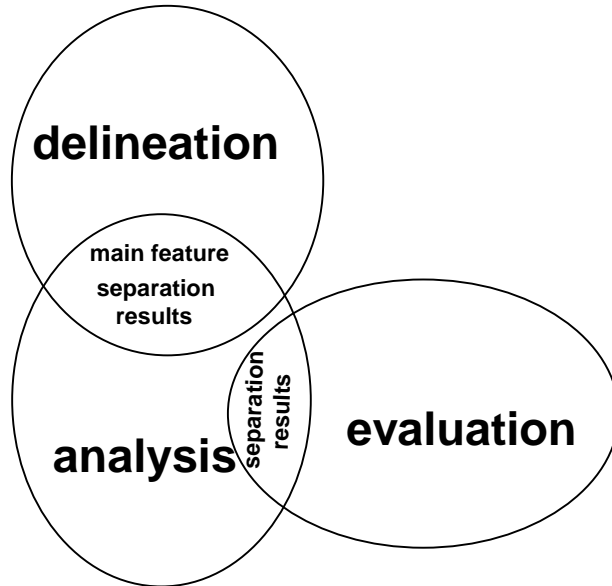
Fig. 2.2. Elements characterizing separation processes
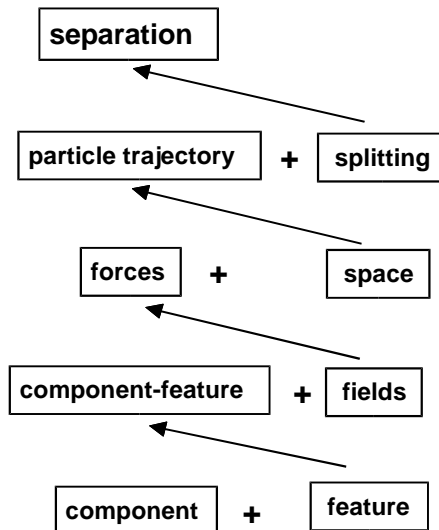
Fig. 2.3. The structure of separation

The analysis of separation deals with the parameters and the results of separation, especially quality and quantity of the feed and the products of separation as well as the main feature. To analyze separation, mass balances are usually calculated and utilized for plotting the so-called separation curves. The description and analysis have common elements, including the main feature utilized for separation.

The evaluation of separation allows to compare separation results with other separations and with ideal and no separation cases. Typically, evaluation is based on quality, quantity, and their combinations called indices, numbers, efficiencies, ratios, etc., and such elements as feature value and product name.

It should be added that separation is possible when the components provide suitable features for separation while the device provide fields (gravity and/or electromagnetic), space, and splitting forces, as well as other elements (time, etc.) (Fig. 2.2 and Fig. 2.4a). Thus, separation is an interactive system consisting of components, device and surroundings (Fig. 2.4b)
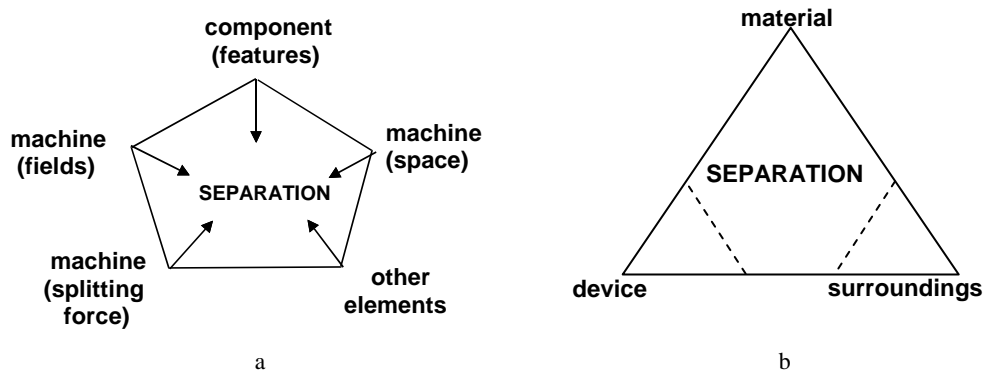
Fig. 2.4. Separation is a result of interaction of components providing features (material property) and machine providing fields, space, splitting forces, and other elements (a). Separation is an interactive system consisting of material (components), device and surroundings (b).

There are different possible components of separation systems. Their selection is arbitrary and therefore the number of possible component is great. Typical components are: deposit, ore, feed, product, subcomponent, fraction, class, group, analytical fraction, mineral, group of minerals, elements, quarks, etc, (Fig. 2.5). The example of chemical element is copper, of mineral is rutile, of a group of minerals is a collection of green mineral, of size fraction is collection of grains between 1 and 2 mm in size. A component is a part of the matter before separation (feed) and it is present in at least one separation product.

The term component has a broad meaning because considering the solar system as a starting material, the Earth is a component of the solar system, a deposit can be a component of the Earth, ore can be a component of a deposit, a mineral is a component of an ore, etc. The smallest (final) components are elementary particles such as quarks, electrons, neutrinos, etc.

initial component   **(feed)**

↓

main component   **(product)**

↓

primary component   **(analytical fraction)**

↓

secondary component   **(mineral)**

↓

elemental component   **(chemical element)**

↓

final component   **(quarks)**
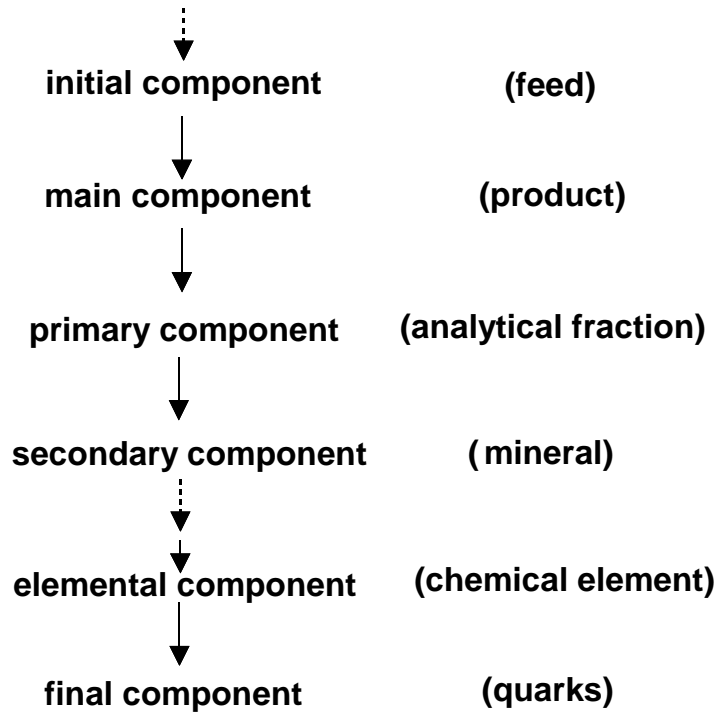
Fig. 2.5. Possible components of separation systems in mineral processing

The components have different features. For instance mass, volume, size, name, temperature, magnetic susceptibility, etc. They can be classified into different groups. The most useful in mineral processing seems to be classification into type (name, number, etc.), quantity (amount of component: mass, volume, etc.), quality (amount of a subcomponent in a component), separation parameters (including main and final separation features), and others. The main feature is the material property which determines the ordering force. For instance, in electric separation the main feature is charge of particle at the moment of separation Q_t. The ordering force in electric separation is the product of charge and electric field E, that is $F = Q_t E$. The main feature depends on other properties of the component and the parameters form a pyramid of parameters with the main feature (material constant) on the top (Fig. 2.6a). Sometimes there are more then one ordering force, as in the case of coagulation influenced by dispersion, electrostatic, hydrophobic and structural forces. The material properties are Hamaker constant A, surface potential ψ, contact angle θ, and air presence, respectively. In such a case the main parameters can be further combined into a single (final) parameter which in coagulation is called the stability ratio W (Fig. 2.6.b). The final parameter is a parameter which directly influences the results of separation (yield and content).
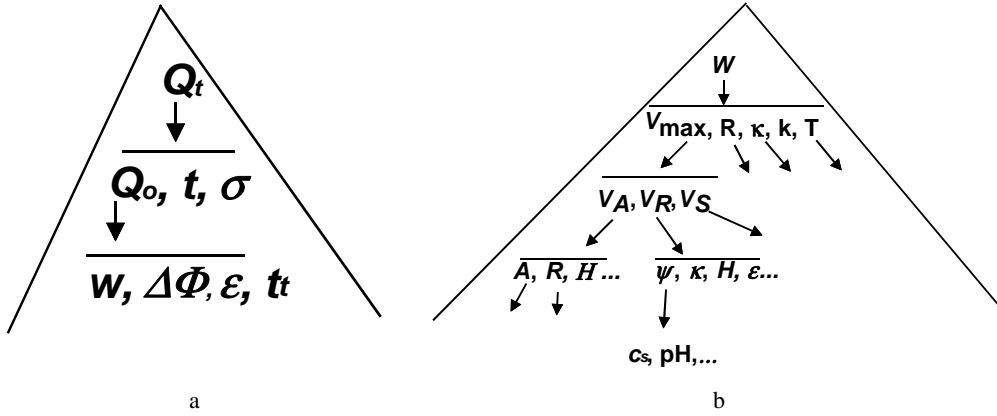
Fig. 2.6. The main feature depends on many other separation parameters. The parameters form a pyramid-like structure: a) material main feature is on the top (electric separation, main feature is surface charge at the moment of separation Q_t), b) when there are more than one material main features (coagulation: material features are Hamaker constant *A*, surface potential ψ, hydrophobicity/hydrophilicity…..), they can be combined into a single parameter (here stability ratio W).

The components and their features form a fractal-like structure which is shown in Fig. 2.7.
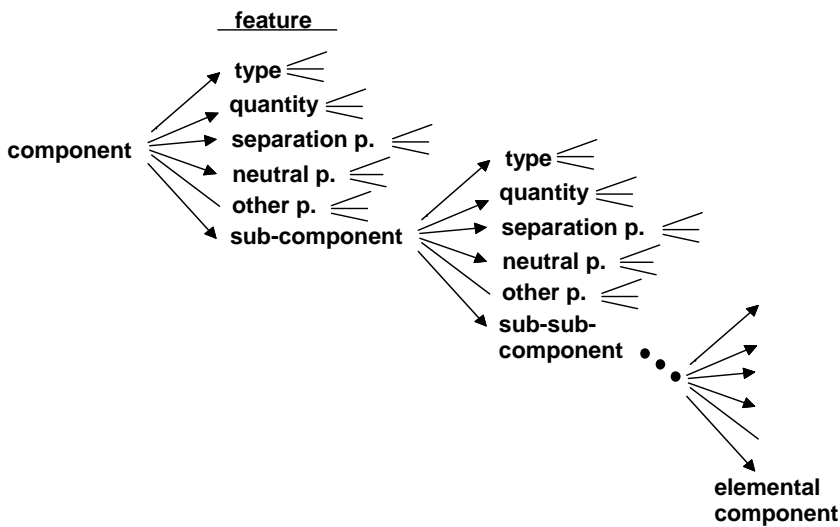
Fig. 2.7. Fractal-like structure of interrelated components and their features. Symbol *p* stands for parameters

To get full information about the results of separation, the data regarding the components and their features are needed. The first step of separation is forming the products of separation and next, depending on one's needs, determining the name, quality,

quantity, features, and other parameters of the components. In a typical separation process (Fig. 2.8) the feed *F* is selected from ore *O* and separated into products *P*, for instance into the concentrate and tailing. To determine the quantity (γ) of products one has to determine analytically (precisely) the amount of each product, and next, depending on one's needs, perform additional analytical (real or virtual) separation, to determine the quality (λ) of the product by establishing the amount of subcomponent *X* in products *P*. Running identical analytical separation for the feed to determine the content of subcomponent *X* in the feed *F* provides quality of the feed α. If necessary numerical values of the feature which was utilized for the separation can also be determined.

$$\ldots\ldots\ O\ \xrightarrow[2o]{n}\ F\ \xrightarrow[2o]{n}\ P\ \xrightarrow[2+]{i} X\ \ldots.$$
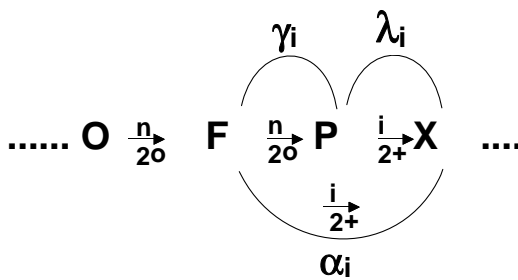
Fig. 2.8. Separation process. The separation of feed *F* taken from an ore *O* provides product *P*. Product (*P*) and the feed (*F*) contain subcomponent *X*. The quantity of the products (γ) is determined by an appropriate procedure while quality determination (λ) requires additional analytical (precise) separation for determination of the component content in the products. In the case the quality of the feed α is needed, additional analysis of the feed has to be done. Other symbols: *n* – nonideal separation, *i* – ideal separation, 2° - two products of separation, 2^+ - more than two products of separation

Having characterization of components and their features, further calculations can be performed to create mass balances of separation and plot separation curves. Figure 2.9 shows, in a pictorial form, the procedure of analyzing separation results.

Data on separation

1. Quantitative analysis of products

2. Qualitative analysis of products

3. Main feature, name, etc.

γ
– mass (weighing)
– volume
– amount (moles)

$\lambda,\ (\alpha)$
– density of particles (densimetric analysis)
– size of partilces (sieve analysis)
– chemical content (chemical analysis)
– mineral content (mineralogical analysis)

Separation balance

$\gamma,\ \lambda,\ (\alpha)$, separation feature, name

Evaluation of separation
1. Separation curves
2. Separtion indices

Fig. 2.9. Elements of analysis and evaluation of separation results

The data obtained on the considered separation system are schematically shown in Fig. 2.10.
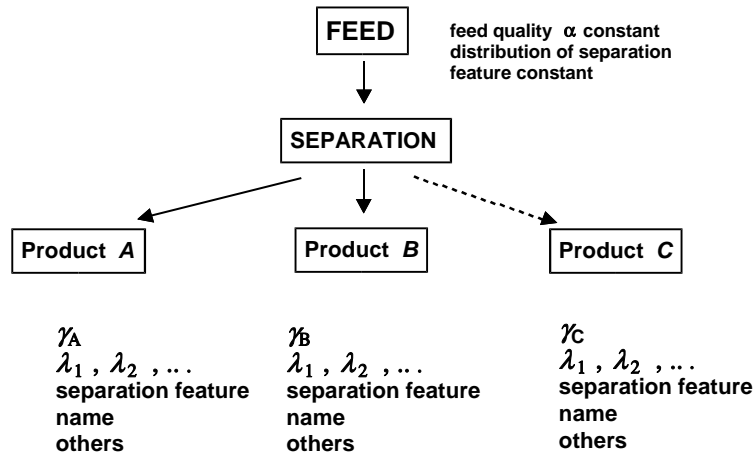
Fig. 2.10. General scheme of separation. α = component content in the feed, λ = component content in a product, γ = yield. Letters A, B, and C denote product name

In most cases the analysis and evaluation of separation performance requires much fewer data. Typical analysis uses two parameters of separation system. The most useful are such parameters as quality, quantity, feature, and component's name (Fig. 2.11).
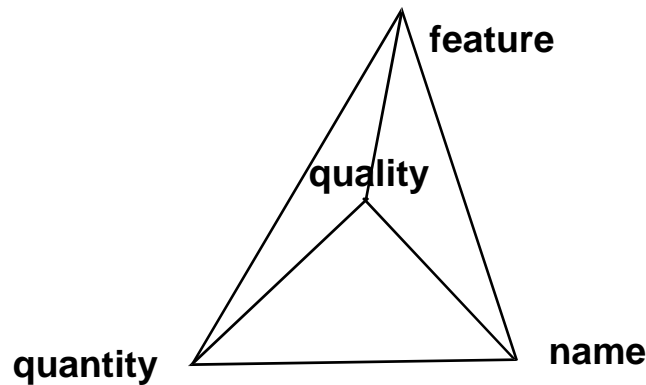
Fig. 2.11. The families of features of a considered component that can be utilized for the analysis of separation results. There are six possible pairs of these parameters

These parameters provide 6 two-parameter-ways of analysis of separation systems. Their proposed names are presented in Fig. 2.12.

**Types of analysis
of separation systems**

upgrading	distribution	classification	sorting	sampling portioning splitting	description
UP	**DI**	**CL**	**SO**	**SP**	**DE**
quantity vs quality	quantity vs feature	quality vs feature	quality vs name	quantity vs name	feature vs name

XY

others
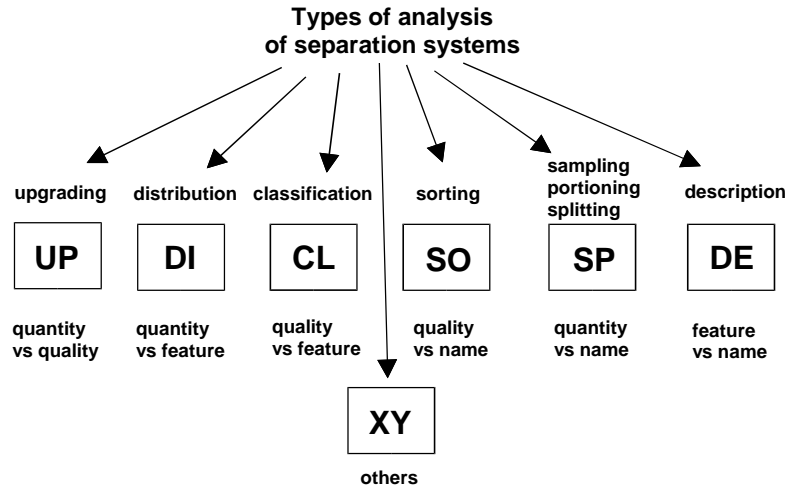
Fig. 2.12. Six simplest ways of analysis of separation results and their proposed symbols

All of them are used in mineral processing and will be discussed in more detail in the next chapters. Three of them: upgrading (quality versus quantity), classification (quantity versus main feature value) and splitting (quantity vs. name) are used most frequently (Table 2.1).

Table 2.1. Main features of selected separations utilized in mineral processing and typical ways of analysis of separation results

Technological Product	Typical way of analysis	Separation processes	Main feature
ore	upgrading	size reduction	surface energy and Young modulus
	classification	screening	grain size
	classification	classification in media	settling rate
feed	upgrading	separation in heavy media	grain density
	upgrading	separation in thin layers	stratification
	upgrading	flotation	hydrophobicity
	upgrading	flocculation	adsorption
	upgrading	coagulation	stability ratio
	upgrading	oil agglomeration	aquaoleophilicity and γ_0
	upgrading	magnetic separation	magnetic susceptibility
	upgrading	dielectric separation	dielectric constant
	upgrading	electric separation	electric charge
	upgrading	separation in eddy currents	electric conductivity
concentrate	splitting	dewatering	water flow rate
	splitting	drying	liquid vaporization
market product			

The yield is a good measure of component quantity. The yield can be measured as mass, volume, population, number of moles, etc. The most convenient way of expressing the yield is to use its relative form that is as a ratio of the mass (volume, number of moles, etc.) of a particular product to the same property (volume, number of moles, etc.) of the feed. This ratio indicates which part of the initial material is present in a particular product. The yield is often presented as streams, e.g. stream of mass in kg/min.

The parameter of quality is the content of a subcomponent in a component. The content determines quality and is usually given as fraction (in per cent) of one component in another component such as feed, fraction, product. It is obvious that component content of the feed in the feed, faction in the fraction, product in the product, is 100%. The symbol used for the content of a component in the feed is usually α, while for a component in products is λ. When two products are mixed together (cumulated) the content is represented by symbol β.

The yield, content, and the value of the main feature are enough for analysis of most separation processes. However, in mineral processing many other parameter resulting from a combination of quality and quantity parameters are used. One of many families of separation parameters characterizing results of separation that can be generated is based on the equation (Drzymala, 2001):

$$Z = \gamma^a \lambda^b \alpha^c \tag{2.1}$$

where:

Z - generated parameter characterizing separation results

γ - yield

λ - content of a component in a product

α - content of a component in the feed

a, b, c – integer numbers.

The most frequently generated parameters characterizing separation results which are based on formula $Z = \gamma^a \lambda^b \alpha^c$ are recovery (ε) and upgrading ratio (k).

Recovery indicates which part of a particular component was transferred, as a result of separation, from the feed to a particular product. Recovery is the parameter connecting the yield γ with content λ and quality of the material subjected to separation α through general relations:

$$\varepsilon = \gamma \lambda / \alpha \tag{2.2a}$$

that is generated with Eq. 2.1 for $a=1$, $b=1$, $c=-1$.

The recovery, for instance for a metal in a product is:

$$\varepsilon_{\text{metal in product}} = \gamma_{\text{product}} \, \lambda_{\text{metal in product}} / \alpha_{\text{metal in feed}}, \tag{2.2b}$$

and for a mineral in a fraction

$$\varepsilon_{\text{mineral in fraction}} = \gamma_{\text{fraction}} \, \lambda_{\text{mineral in fraction}} / \alpha_{\text{mineral in feed}}, \qquad (2.2c)$$

while for a fraction in a product:

$$\varepsilon_{\text{fraction in product}} = \gamma_{\text{product}} \, \lambda_{\text{fraction in product}} / \alpha_{\text{fraction in feed}}. \qquad (2.2d)$$

Table 2.2. Selected parameters used for characterizing results of separation. They can be generated by multiplying, dividing, subtracting or adding other parameters

Generated parameter	For instance used by:
$Z = \gamma^{\,a} \lambda^{\,b} \alpha^{\,c}$	
ε (recovery) (a=1, b=1, c=-1)	commonly used
k (enrichment ratio) (a=0, b=1, c=-1)	commonly used
γ/α (Dell's parameter) a=1, b=0, c=-1	Dell, 1953
$\lambda\gamma$ (Mayer's parameter) a=1, b=1, c=0)	Mayer, 1950
combination of recoveries	
$\dfrac{\varepsilon_{ij}}{\varepsilon_{ij}}$	$\dfrac{\varepsilon_{11}}{\varepsilon_{12}}$, Ulewicz et al., 2001
$\varepsilon_{ij}\varepsilon_{ij}$	$\varepsilon_{11}\varepsilon_{12}$, Fomenko, 1957; Barskij and Rubinstein, 1970
$\varepsilon_{ij} - \varepsilon_{ij}$	$\varepsilon_{11} - \varepsilon_{12}$, Schulz (1970), Barskij and Rubinstein (1970)[**]
$\varepsilon_{ij} + \varepsilon_{ij}$	$\varepsilon_{11} + \varepsilon_{22} - 100\%$, Sresty and Somasundaran, 1980; Gebhardt and Fuerstenau, 1986
$\varepsilon_{ij} - \varepsilon_{ij}^{*}$	$\varepsilon_{11} - \varepsilon_{11}^{*}$ (equivalent to $\varepsilon_{11} - \gamma_1$ because $\varepsilon_{11}^{*} = \gamma_1$), index used in ceramic industry (Myjkowski, 1999)
combination of contents	
$\dfrac{\lambda_{ij}}{\lambda_{ij}}$	Taggart, 1948; Sztaba, 1993
$\lambda_{ij}\lambda_{ij}$	
$\lambda_{ij} - \lambda_{ij}$	Taggart, 1948; Sztaba, 1993
$\lambda_{ij} + \lambda_{ij}$	
other combination (yields, contents, recoveries)	
$\gamma_{ij}\lambda_{ij} - \gamma_{ij}\lambda_{ij}$	$\gamma_1 \lambda_{11} - \gamma_1 \lambda_{12}$

* value of parameter when the process is non-selective
** equivalent to the Hancock index

The recovery is frequently used in mineral processing because it has an easy-to-grasp meaning and adds up to 100%. Therefore, it is often used in mass balances and curves plotting. Its simplest definition., as it has been alreadt discussed, is

$$\varepsilon_{of\ a\ component\ in\ the\ feed} = \frac{amount\ of\ a\ component\ in\ a\ \ product}{amount\ of\ that\ component\ in\ the\ \ feed} \qquad (2.2e)$$

The upgrading ratio is defined as a quotient of the component content in a product and the content in the feed. It can be generated with Eq. 2.1 for a=0, b=1, c=-1 and has a form

$$k=\lambda/\alpha. \qquad\qquad . (2.3)$$

Table 2.2 shows other families of generated separation parameters. Barskij and Rubinstein (1970) collected many of them. Some will be shown in the chapter dealing with separation curves.

The separation parameters are utilized for plotting separation (classification, upgrading, distribution, etc.) curves. The basic separation upgrading curve utilizes the yield and the content. Unfortunately, it is not attractive regarding its graphical form and mathematical usability, therefore other quality-quantity parameters are usually used for plotting upgrading curves. There does exist infinite number of separation parameters, and thus, separation curves.

The final stage of technological analysis of separation process is its evaluation, which aims at judging whether or not the process is efficient. The assessment of separation process can be accomplished using a pair of indices of separation results or in a graphical form. These issues are discussed in detail in the chapters on upgrading and classification.

2.2. Analysis and assessment of separation process

2.2.1. Division of feed into products (SP)

One of the results of separation is a division of the material into products. The material can be divided into two or more products. The separation may provide either identical or dissimilar products as to their quality and quantity (Fig. 2.13). The analysis of the separation process as division of the feed into products (SP) requires two parameters that is the quantity (yield, γ) and the identity (usually name) of the product. There is no need of using other separation parameters because, for instance, the recovery of a product is numerically equal to the yield of the product while the content of the product in the product is equal to 100%.
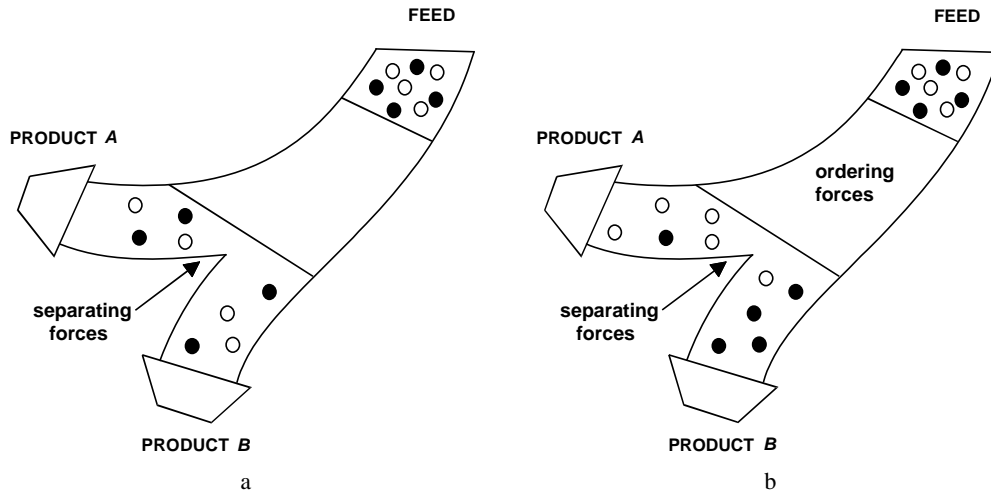
Fig. 2.13. Separation as division of material into products. a) nonselective: identical products, absence of net ordering forces, b) selective: product *A* is different from product *B*

Sometimes separation leads to the separation of phases, for instance in drying, filtration, and nonselective flotation. These separations rely on separation of the aqueous phase from the solid phase. Other examples of division into products are portioning and sampling.

An example of separation treated as division into products is given in Table 2.3 and Fig. 2.14.

Table 2.3. Material balance of separation leading to formation of concentrate and tailing.
* denotes yield expressed in real units (not in %), Mg stands for megagram

Product	Yield γ^* Mg/day	Yield γ %
Concentrate *C*	172	20.14
Tailing *T*	682	79.86
Feed *F*	854	100.00

Many separation processes provide products differing both in quality and quantity (Fig. 2.13b). Such a process can be characterized as a division into products (quantity versus product identity) by ignoring other parameters like content of components or the value of the feature utilized for separation. When we take into account these parameters we change the character of analysis into upgrading, classification, sorting, etc.

The yield, which characterizes the division of the material into products, can be expressed either directly in mass units (usually megagrams (Mg) which in equivalent to old unit ton) or in a relative form as per cent in relation to the mass of the feed. It

can be also expressed per time and then it is called flux or stream. It can be expressed not only per time but also per surface or surface-time unit.
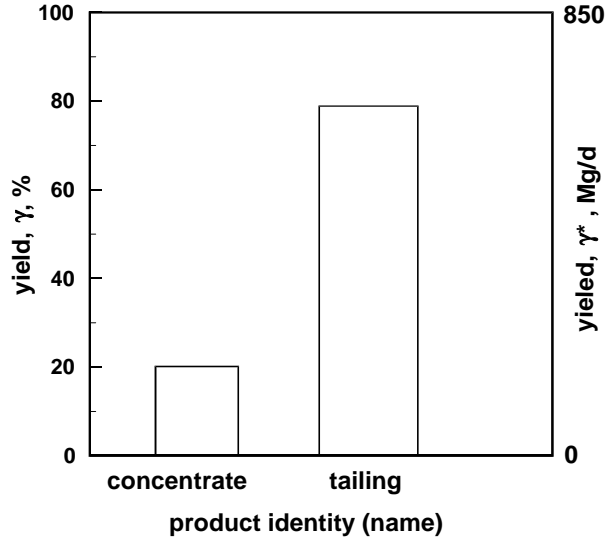
Fig. 2.14. Graphical representation of division of material into products (quantity versus identity), SP

The mass balance of the material division into products can be expressed as:

$$\Sigma\gamma_{products} = 100\% \ , \tag{2.4a}$$

and in the case of two products:

$$\gamma_{product\,A} + \gamma_{product\,B} = 100\%, \tag{2.4b}$$

where γ is the product yield expressed in percent.

2.2.2. Upgrading (UP)

2.2.2.1. Quantitative and qualitative analysis of upgrading

The separation of the initial material, called the feed, usually provides two products, most frequently called concentrate and tailing (Fig. 2.15). Sometimes, other products, semi-products, intermediate products, concentrates of lower quality, and so on, are obtained. The analysis of separation results from the upgrading perspective requires information about the quantity and quality of the products. The quantity of products in periodical processes can be expressed in mass units (gram, kilogram, megagram, gigagram, teragram, etc.) or other units including the volume or the num-

ber of moles. The quantity of products in continuous processes is given as stream (flux) in mass units or other units per time, e.g. hours, Mg/year, kg/min, m^3/h.

The quality of products is usually expressed as the content of useful component in the product. The useful component can be a chemical element, sum of several elements, a mineral or a sum of several minerals, a fraction, etc. On the basis of the balances of mass and contents of the considered component it is possible to prepare a complete mass balance of separation as upgrading process. It is, as a rule, a balance for one selected component. If we are interested in other components, their balances should be prepared separately.
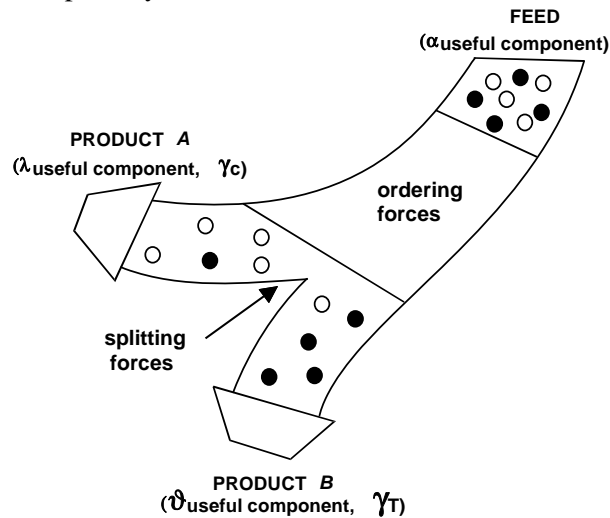
Fig. 2.15. A general scheme of upgrading

The mass balance of separation is based on the following considerations. If *F* megagrams (Mg) of the feed are subjected to separation and we obtain *C* Mg of the concentrate and *T* Mg of the tailing, the mass balance can be written as:

F megagrams of the material = *C* megagrams of the concentrate + *T* megagrams of the tailing (2.5a) or, briefly:

$$F = C + T \qquad (2.5b)$$

To get the mass balance in per cent, we divide both sides of the equation by *F* and, at the same time, multiply by 100%. The result is:

$$\frac{F}{F}100\% = \frac{C}{F}100\% + \frac{T}{F}100\% \ . \qquad (2.5c)$$

All the there parts of the equation are the yields and they are usually represented by the Greek letter γ, i.e.

$$\frac{F}{F}100\,\% \ = \gamma \ = 100\,\% \quad, \ \frac{C}{F}100\% = \gamma_c, \ \frac{T}{F}100\% = \gamma_T \qquad (2.5d)$$

Equations (2.5a-d), describing the mass balance of separation products and the sum of the yields of particular products provide the yield of the feed which is equal to 100%:

$$\gamma_C + \gamma_T = \gamma_F = 100\%. \qquad (2.6)$$

When there are more than two products, for instance two concentrates (C_1 and C_2), one semi-product P and two tailings T_1 and T_2, the feed yield is 100% and consists of the yields of all products:

$$\gamma_{C1} + \gamma_{C2} + \gamma_P + \gamma_{T1} + \gamma_{T2} = 100\%. \qquad (2.7)$$

As it was mentioned, another element needed for the calculation of the upgrading balance is the quality of the obtained separation product. The determination of the component content in a product or feed can be accomplished in many ways including chemical analysis, mineral analysis or by determination of other properties which are directly proportional to the content of the component under consideration. The analysis provides the content of the examined component in the separation products. The content of a component in a product will be denoted as λ. To distinguish the content in different product the following symbols will be used:

α - content of the considered component in initial material (feed), %,

λ - content of the considered component in concentrate, %,

β - content of the considered component in combined products, %,

ϑ - content of the considered component in tailing, %.

So far we have discussed the use of yield and contents for analysis of separation from the upgrading perspective. It was shown in the previous section that these parameters can be combined to form new parameters which can be equally good, and sometimes better, applied for characterizing upgrading.

One of the most frequently used quality-quantity parameters is recovery $\varepsilon = \dfrac{\lambda}{\alpha}\gamma$.

The recovery is the amount of the considered component, expressed in per cent in relation to the feed which was found in a particular product of separation process. The recovery of useful component in the concentrate is usually denoted as ε while in the tailing as η. Both ε and η are usually expressed in per cent.

The recovery of the component in the tailing is:

$$\eta = \gamma_T \, \frac{\vartheta}{\alpha}100\% \qquad (2.8)$$

where γ_T is the yield of tailing.

Thus, a following relation is valid:

$$\varepsilon + \eta = 100\%. \tag{2.9}$$

If there are more upgrading products, the sum of the recoveries of the component in all products is 100%.

$$\Sigma \varepsilon_j + \Sigma \eta_j = 100\%, \tag{2.10}$$

where *j* means a product and *j* = 1, 2, 3, 4….

Other relations resulting from the equations considered are:

$$\gamma_c = \frac{\alpha - \vartheta}{\beta - \vartheta} 100\% \tag{2.11}$$

$$\varepsilon = \frac{\alpha - \vartheta}{\beta - \vartheta} \frac{\beta}{\alpha} 100\% \tag{2.12}$$

$$\varepsilon = \frac{C\beta}{F\alpha} 100\% \tag{2.13}$$

To better understand the nature of the upgrading balance let us consider the example of a hypothetic upgrading plant processing 845 Mg of the ore per hour. The ore contained 15.4% of useful component. As a result of upgrading for 24 hours 172 Mg of concentrate, containing 60.4% of useful component and the tailing containing 4% of that component were obtained. The balance of upgrading is shown in Table 2.4.

Table 2.4. A balance of upgrading for two products of separation

Product	Concentrate yield γ_g Mg/day	Concentrate yield γ %	Useful component content λ %	Recovery of useful component ε %
Concentrate *C*	172	20.14	60.400 (= β)	79.0
Tailing *T*	682	79.86	4.045 (= υ)	21.0
Feed *F*	854	100.00	15.395 (= α)	100.0

Table 2.4 shows all the essential results of separation process, i.e. the yields and contents, as well as calculated recoveries. The balance is prepared correctly if the sum of the recoveries amounts 100%. To calculate the recovery, it was necessary to calculate the content of the useful component in the feed. The content of the useful component in the feed can be calculated by summing up $\gamma(\%) \cdot \lambda(\%)$ (mathematically products of $\gamma(\%)$ and $\lambda(\%)$) for all separation products and dividing the sum by 100%. Thus, the content of the useful component in the feed is the "weighted mean" of all products. This was shown in Table 2.5, prepared on the basis of Table 2.3 by adding

the numbers in column with "γ(%)·λ(%)" values. Table 2.5 additionally contains another upgrading parameter called the upgrading ratio (k) (Eq. 2.3).

Table 2.5. Procedure of calculation of content of useful component in feed (α).
(see the fifth column: $\alpha = \Sigma[\gamma(\%)\,\lambda\,(\%)]/100\%$.
Next, recovery ε of the useful component in the products was calculated

Product	Yield γ^* Mg/day	Yield γ %	Content λ %	γ(%)·λ(%)	Upgrading ratio $k = \lambda/\alpha$	Recovery ε, (%) $\varepsilon = \gamma\lambda/\alpha$
Concentrate C	172	20.14	60.40 (= β)	1216.456	3.92	79.0
Tailing T	682	79.86	4.045 (= υ)	323.034	0.26	21.0
Feed F	854	100.00	15.395 (= α)	1539.490 (1216.456+323.034)	1	100.0

The analysis of separation process becomes more complicated when more than two products are formed. Table 2.6 shows the balance of upgrading in which the upgrading of ore containing 15.4% of hypothetic metal sulfate (MeSO$_4$) compound resulted in two concentrates and two semi-products.

It is convenient to make calculation in columns up to the vertical thick black line for determining the content (α) of a component (here denotes as MeSO$_4$) in the feed. Then, the recoveries can be calculated. The recoveries in particular upgrading products were calculated, and subsequently, for cumulated products. The recoveries for combined products are called cumulated recoveries and they are calculated by adding the recoveries of products. For instance, the cumulated recovery for the two first products is the sum of their recoveries. The cumulated recovery, marked with symbol Σ, can also be calculated from the equation:

$$\Sigma\varepsilon = \frac{\beta}{\alpha}\Sigma\gamma, \tag{2.14}$$

that is by dividing the content of the considered component in combined products (β) by the content of this component in the material α and multiplying the result by cumulated yield of the combined products ($\Sigma\gamma$). Cumulated yield is marked with a Greek letter Σ while cumulated content of a component in combined products with the letter β. It is recommended to use the Greek symbol Σ for cumulating by simple addition while for other ways of cumulating capital letters are recommended, as in the case of upgrading ratio k and K. In the case of content λ, usually cumulated as weight average, it would be better to use character Λ rather than β, but usage of β is more popular.

From mathematical point of view a well calculated separation balance shows the agreement between the values in columns and rows. From a technological point of

view the balance is correct if the calculated content of the considered component in the feed agrees with the value determined directly by chemical analysis.

Table 2.6. Mass balance of upgrading for more-than-two products of separation

Product	Amount of product γ(Mg)	Yield of product γ(%)	Yield of products (cumul.) $\Sigma\gamma$(%)	Content of MeSO$_4$ λ (%)	$\gamma\lambda$	$\Sigma(\gamma\lambda)$	$\beta =$ $\Sigma(\gamma\lambda)/\Sigma\gamma$ %	Upgrading ratio $K = \beta/\alpha$	Recovery of MeSO$_4$ ε $=\gamma\lambda/\alpha$, %	Recovery of MeSO$_4$ $\Sigma\varepsilon$ $= K\Sigma\gamma$, %
Concentrate C_1	103	12.06	12.06	81.7	985.30	985.30	81.70	5.305	64.00	64.00
Concentrate C_2	69	8.08	20.14	28.6	231.09	1216.39	60.40	3.922	15.01	79.01
Semiproduct P_1	189	22.13	42.27	7.0	154.91	1371.30	32.44	2.106	10.06	89.07
Semiproduct P_2	238	27.87	70.14	5.48	152.73	1524.03	21.73	1.411	9.92	98.99
Tailing T	255	29.86	100.00	0.52	15.53	1539.56	15.40	1	1.01	100.00
Feed F (calculated)	854	100.00		15.40 (α)					100.00	
Feed (analytical): α = for instance 15.65										

Thick vertical line indicates the end of the first stage of α calculation

In Table 2.6 the upgrading ratio was calculated for cumulated products using the relation:

$$K = \frac{\text{component content in a cumulated product}}{\text{component content in the feed}} = \frac{\beta}{\alpha} \qquad (2.15)$$

The formula for calculating non-cumulative upgrading ratio k was given in Eq.2.3.

2.2.2.2. Upgrading curves

Mass balance is used for creation of upgrading parameters of separation. They are also a good base for graphical representation of separation results. In the case of two-product separation the interpretation of results and mass balance is simple. In other cases it is convenient to plot the so-called upgrading curves which are based on the upgrading balance.

The analysis of any separation from the upgrading point of view has to take into account three basic variables: yield γ, content (λ or β), and α. When dealing with the same material, the feed composition (α) is constant and then two variables are enough to describe the system. Since γ and β and α can be combined into unlimited number of new parameters (Eq. 2.1, Table 2.2) the number of upgrading curves is unlimited. The simplest upgrading parameter based on γ, λ, and α is recovery $\varepsilon(=\gamma\lambda/\alpha)$. The three ε, γ, and λ upgrading parameters provide (Fig. 2.16.) five most frequently used families of upgrading curves. Other families of upgrading curves are also possible (Table 2.7).

$$\gamma \longrightarrow \lambda$$

$$\varepsilon \qquad \alpha = const.$$
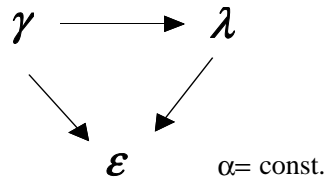
Fig. 2.16. Most frequently used upgrading curves are based on ε, γ, λ, and α

Table 2.7. Upgrading curves based on two, out of three (ε, γ, λ), upgrading parameters

Upgrading curves			
relation	name of curve	other names of curve	source
principal curve			
$\gamma = f(\beta$, or β^*, or λ, or υ) (* denotes cumulating starting from the richest product)	Henry's curve	principal upgrading curve yield-content curve	Henry, 1905 Reinhardt, 1911
ε curves			
ε (or η) $= f(\gamma)$	Mayer's curve*	recovery–yield curve modified M curve	Budryk and Stepinski, 1954; Laskowski and Luszczkiewicz, 1989
ε (or η) $= f(\beta$ or $\vartheta)$	Halbich's curve	recovery –content curve	Halbich, 1934
mirror curves			
$\varepsilon_{\text{component 1 in concentrate or tailing}}$ $= f(\varepsilon_{\text{component 2 in concentrate or tailing}})$	Fuerstenau's curve		Fuerstenau, 1979 Mohanty, 1999
$\beta = f(\vartheta)$	Stepinski's curve		Stepinski 1955, 1958
γ, α, ε, λ curves			
$\varepsilon = f(\gamma/\alpha)$	Dell's	release curve	Dell, 1953, 1969
$\gamma = f(\beta/\alpha$ or $\vartheta/\alpha)$	–	yield–upgrading ratio ($K = \beta/\alpha$) curve	
$\beta = f(\gamma/\alpha)$	–	content $= f(\gamma/\alpha)$ curves	
$\varepsilon = f(\beta/\alpha)$	–	recovery – upgrading ratio ($K = \beta/\alpha$) curve	
equal basis upgrading curves**			
	Hall's curve		Hall, 1971
$\varepsilon_1 - \varepsilon_2 = f(\varepsilon_1)$	Luszczkiewicz's curve		Luszczkiewicz, 2002
recovery index vs yield index	the Mayer–Drzymala–Tyson–Wheelock curve	modified Mayer's curve	Drzymala et al., 2007

**the original upgrading curve proposed by Mayer was in the form of γ vs. $\gamma\beta$ plot called the M curve,

*** lines of no and ideal upgrading are not sensitive to α variation (the Fuerstenau curve also belongs to this category)

When the concentrate and tailing are the only products of separation, there is no much sense to draw upgrading curves because such diagrams would have only one experimental point and comparing different sets of upgrading results would be actually not possible. The comparison of separation results requires at least a part of upgrading curve.

To have a more complete industrial separation upgrading curve, the feed has to be subjected to more detailed examination in the laboratory. It is useful to plot upgradeability curve which is the best upgrading curve one can obtain for a particular material. In the literature, there are procedures for creation of the upgradeability curves. The most popular is the method based on so-called multiple fractionation, which consists in collecting subsequent products of upgrading at different time of the process or changing intensity of the field (magnetic, electric, an so on) responsible for separation. The determination of floatability based on flotation tests is described in another chapter.

2.2.2.2.1. The Henry curve

The basic upgrading curve is the Henry plot. It represents the relationship between yield and content of a useful component in upgrading products. It can be also plotted in another mode, that is as content versus yield. It was proposed by Henry in 1905 (Czeczot, 1937, Rainhardt, 1911) The Henry plot for the mass balance presented in Table 2.6 is given in Fig. 2.17. The Henry plot in Fig. 2.17 is presented in a cumulative form $\Sigma\gamma = f(\beta)$. The lines of no separation, ideal separation, and ideal mixing, are also indicated.
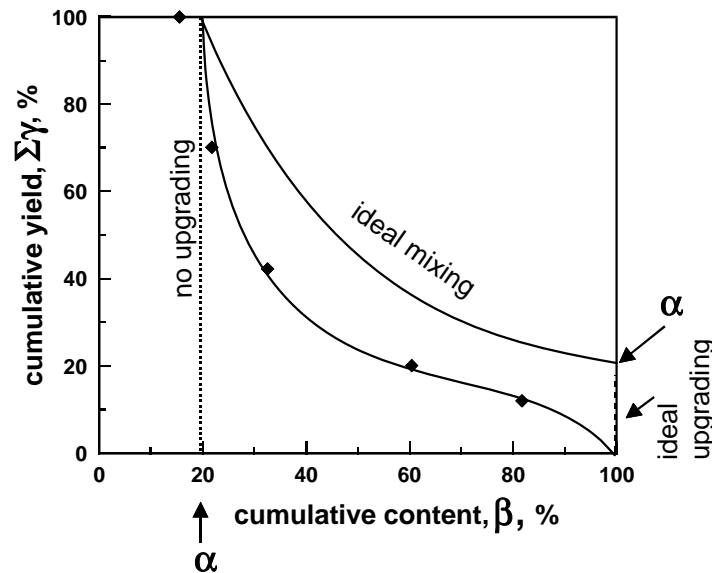
Fig. 2.17. The Henry upgrading curve

The Henry curves can also be plotted in a non-cumulative way $\gamma = f(\lambda)$, as well as in the form of $\gamma=f(\eta)$. Different Henry's plots ($\gamma = f(\lambda)$, $\gamma=f(\beta)$, and $\gamma= f(\eta)$ are called the Henry family of curves and are shown in Fig. 2.18. It should be noticed that the data for drawing the $\gamma=f(\beta)$ and $\gamma=f(\eta)$ curves can be taken directly from the upgrading balance, while plotting $\gamma=f(\lambda)$ curve (histogram) requires a special procedure to make the curve smooth. There are few ways of plotting histograms. The simplest ones involve a graphical and a mean–value smoothening. The first one relies on drawing histogram that is columns of λ values high and from γ_n to γ_{n+1} (where $n = 1, 2,3 ...$) wide and drawing a smooth line passing through the mean thickness of the columns. The procedure of plotting, based on the mean value γ, relies on marking the points $\gamma=\gamma_{n-1}+\gamma_n/2$ and λ_n. Figure 2.17 shows the non-cumulative $\gamma=f(\lambda)$ Henry plot drawn by the mean–value method. Other Henry's curves forming the Henry family of upgrading curves are also shown in Fig. 2.18.
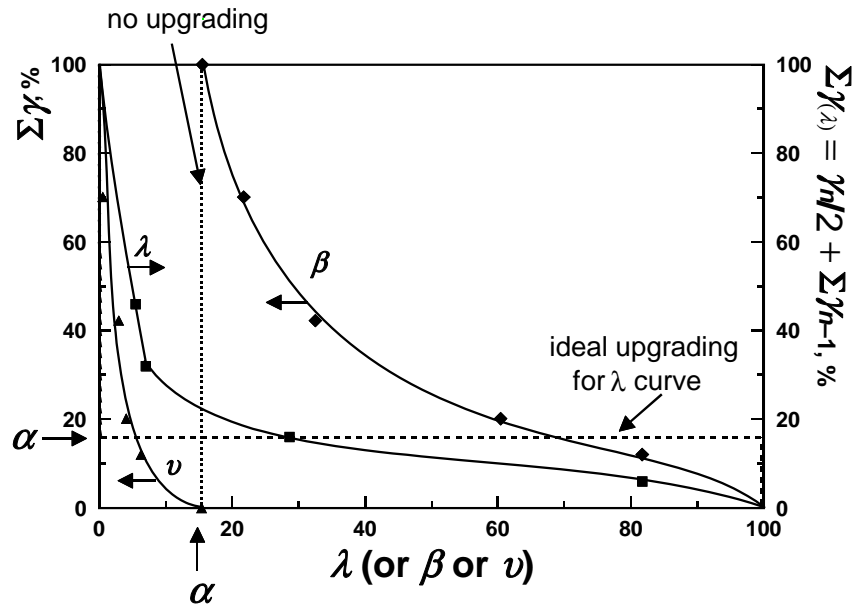
Fig. 2.18. Family of the Henry curves

To draw the relation $\gamma=f(\eta)$ it is advantageous to slightly modify the upgrading balance, adding a column on the content of the considered component in combined products starting from the tailing side as it was done in Table 2.8.

For the non-cumulative $\gamma=f(\lambda)$ Henry plot the no-upgrading line is vertical and it shows that for all upgrading products, regardless their yield, the content of useful component is constant and equals α. The ideal upgrading line for the non-cumulative $\gamma=f(\lambda)$ Henry plot is horizontal because the concentrate contains only pure (100%) useful component.

Table 2.8. Data for plotting the Henry curves

Product	γ %	$\Sigma\gamma$ %	λ %	$\gamma\lambda$	Product	$\Sigma\gamma\lambda$	β, % $\Sigma\gamma\lambda/\Sigma\gamma$	$\Sigma\varepsilon$ %	Product	$100-\Sigma\gamma$ %	$100\alpha-$ $-\Sigma\gamma\lambda$	υ, %
C_1	12.06	12.06	81.7	985.30	C_1	985.30	81.70	63.39	C_2+P_1+ $+P_2+T$	87.94	554.7	6.31
C_2	8.08	20.14	28.6	231.09	C_1+C_2	1216.39	60.40	78.99	P_1+P_2+T	79.86	323.61	4.05
P_1	22.13	42.27	7.0	154.91	$C_1+C_2+P_1$	1371.30	32.44	89.05	P_2+T	57.73	168.7	2.92
P_2	27.87	70.14	5.48	152.73	$C_1+C_2+P_1$ $+P_2$	1524.03	21.73	98.97	T	29.86	15.53	0.52
T	29.86	100.00	0.52	15.53	F	1539.56	15.40= α	~100	F	0	1540	15.4
F	100.00		15.4	1540								

$\upsilon = 100\alpha - \gamma_i\lambda_i/100 - \Sigma\gamma$, %.

If the upgrading balance is prepared not for a mineral, but for a chemical component (metal), the beginning of λ and β curves on the axis λ is not at the point of mineral content in the mineral, i.e. 100% but at the point of the content of considered chemical element in the mineral, which was shown in Fig. 2.19 for a hypothetic substance in which the metal content amounted 80%.
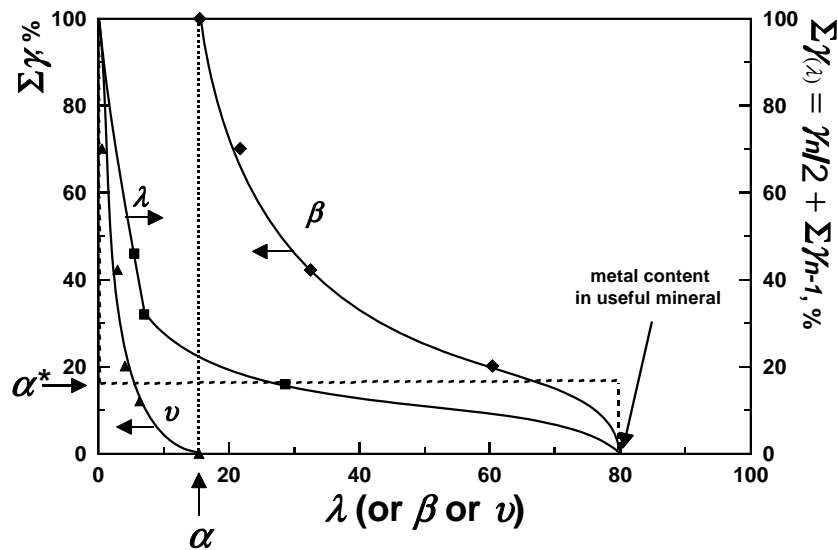
Fig. 2.19. The Henry curves when the mass balance is prepared for chemical element not for mineral. α^* denotes yield of ideally upgraded concentrate calculated from the content of metal in the feed taking into account the content of metal in mineral. At this point $\gamma=\alpha^*=\alpha\cdot$ molecular mass of mineral / molecular mass of metal

The Henry curves can be described by empirical mathematical equations (Brozek, 1996). Currently the Henry curves are seldom used in mineral processing.

2.2.2.2.2. The Mayer curve

The Mayer curve relates the yield of products and recovery of a component in products (ε=f(γ)). It was proposed by Mayer (1950, 1951, 1952) originally in the form of $\beta\gamma$=f(γ) relation and it was called the M curve. Soon after it was discovered by Budryk and Stepinski (1954) that the ε=$\gamma\beta/\alpha$=f(γ) curve had the same shape due to the constant value of α and presently the plot ε=$\gamma\beta/\alpha$=f(γ) is known as the Mayer curve. The ε=$\gamma\beta/\alpha$=f(γ) plot is more universal than the $\beta\gamma$=f(γ) curve. The Mayer curve represents a modification of the Henry plot and is much more convenient than the Henry curve because the area available for plotting is larger and also the plot itself is much less complicated since the line of no and ideal separation do not cross. The curve is drawn on the basis of upgrading balance. The Mayer curve is shown in Fig. 2.20 and its points were taken from the balance given in Table 2.6. The Mayer curve can also be drawn on the basis of the balance for several, separately conducted separations, in which only the concentrate and the tailing are produced. In each of these separations the concentrate yield has to be different, which can be regulated, for instance, by the time of separation.
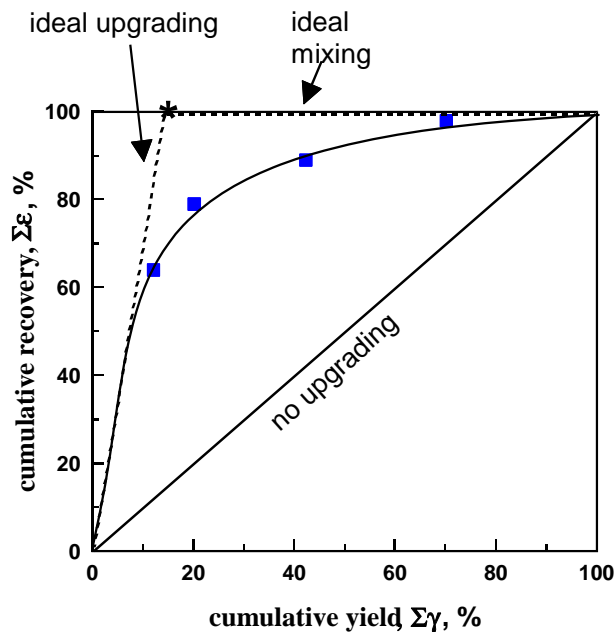
Fig. 2.20. The Mayer curve. The plot is based on data presented in Table 2.6. Asterisk denotes the point at which $\Sigma\gamma = \alpha$

The Mayer curve allows to evaluate separation results by comparing them with the ideal and no upgrading lines. The no upgrading line represents the collection of separation results for which yield is equal to recovery. This is synonymous to a mechanical

transfer of the material to the concentrate without any upgrading of the considered components. The line of ideal upgrading starts at 0,0 point and ends at the point representing separation in which only pure considered component is obtained. At this point the concentrate yield is numerically equal to the content of the considered component in the feed ($\gamma = \alpha$). If the balance of useful component is made for a chemical element while, in fact, during the upgrading a mineral is separated, the characteristic point of the ideal upgrading is not $\gamma = \alpha$, but it should be calculated taking into account the stoichiometry of the mineral.

The upgrading process is efficient when the upgrading Mayer curve is closed to the ideal upgrading line. If the upgrading curve is closed to the no upgrading line, the separation is poor.

The upgrading curves, including the Mayer plot can be used for generating other upgrading parameters. One of them, called the selectivity factor, defined as:

$$S = \frac{\varepsilon_r - \varepsilon_{i(\gamma = \alpha)}}{\varepsilon_{100} - \varepsilon_{i(\gamma = \alpha)}} = \frac{\varepsilon_r - \varepsilon_{i(\gamma = \alpha)}}{100 - \varepsilon_{i(\gamma = \alpha)}} \qquad (2.17)$$

is shown in Fig. 2.21.
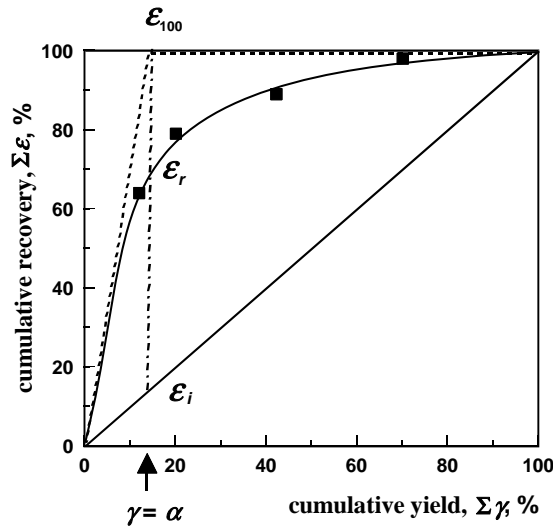
Fig. 2.21. Graphical determination, from the Mayer curve, the selectivity coefficient *S* defined by Eq. 2.17

The Mayer curves can be used for comparing upgrading of two components in the same feed (Fig. 2.22) containing two or more components. To accomplish that, separate quality-quantity mass balances for the two components should be calculated and the results plotted in the form of recovery of each component versus yield of the products. The separation of the two components is the better the bigger is the difference

between their separation curves. The best separation takes place when one of the components becomes enriched in the concentrate and the other concentrates in the tailing. In such situation the curve for the component which concentrates in the tailing is below the no upgrading line (Fig. 2.22). The figure shows the previous upgrading results for the ore containing hypothetic useful mineral $MeSO_4$ and other unwanted mineral, say MeF_2, which we want to transfer to the tailing. A measure of the separation selectivity of both components can be the difference in their recoveries calculated at a particular yield of the concentrate. This measure:

$$S = \varepsilon_{A,\, \gamma\, =\, \gamma_1} - \varepsilon_{B,\, \gamma\, =\, \gamma_1}, \tag{2.18}$$

was proposed by Schulz (1970) but in fact it represents one of many forms of the Hancock index (Sztaba, 1993). It should be noticed that the Hancock index, similarly to any other index, is valid for a given yield, and it changes with the yield. Therefore, it must be remembered that a correct evaluation of selectivity of separation cannot be based on one parameter, but it has to be a two-parameter approach.
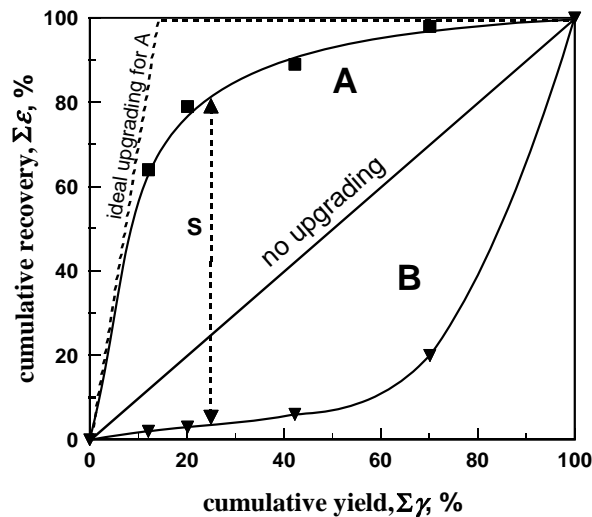
Fig. 2.22. The Mayer curve for two considered components *A* and *B* in a multicomponent feed. The difference between recoveries of two components is the Hancock index (Eq. 2.18)

The Mayer curve can be supplemented with content of a useful component in the products (Fig. 2.23). To accomplish this the content of the component under consideration is to be plotted on the recovery axis. Appropriate scaling of the content axis (point α at the height of $\varepsilon=100\%$) enables graphical reading of the content of the considered component at any arbitrary point of the upgrading curve, i.e. for any arbitrary concentrate yield or recovery. More details regarding the use of additional information contained in the Mayer curve of upgrading can be found in many works including the monograph by Tarjan (1981).
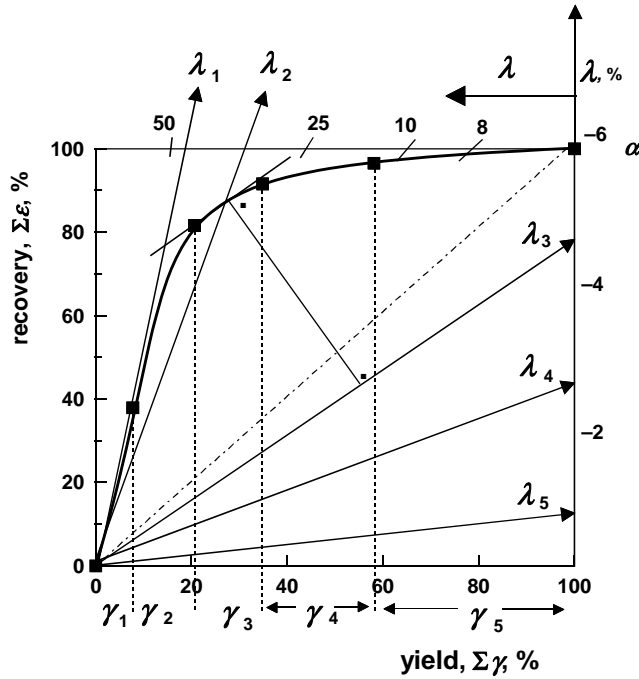
Fig. 2.23. Procedure of determining content of a considered component from the Mayer curve at any point of the upgrading curve (after Tarjan, 1981; Laskowski and Luszczkiewicz, 1989)
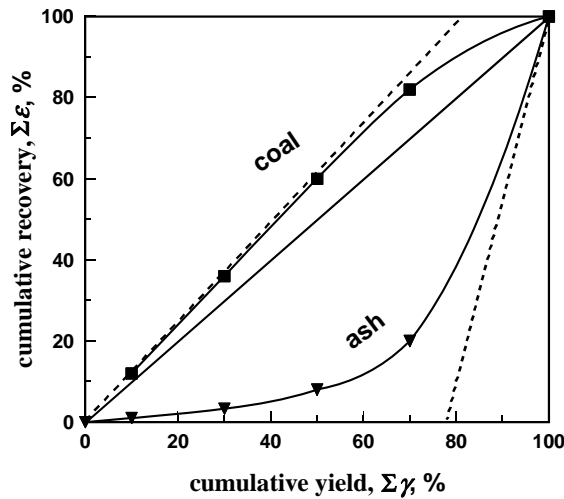
Fig. 2.24. The Mayer curve are not suitable for analysis of upgrading when the content of useful component in the feed is high. Then, recovery of the remaining material (here ash) vs yield should be plotted

The Mayer curve is very useful for the analysis and assessment of the upgrading of ores and raw materials of low useful component content. If the content of a useful

component is high, like in coal, the Mayer curve becomes very compressed because the no upgrading and the ideal upgrading lines are situated close to each other. Then, instead of plotting the yield of the combustible matter in coal vs concentrate yield, it is better to draw the ash yield in the concentrate as the function of yield, which is shown in Fig. 2.24. The Mayer curves have usually a hyperbolic shape and, therefore, either second degree polynomial, power or exponential relations can be used for their approximation (Brozek, 1996).

2.2.2.2.3. The Dell curve

The Dell curve is a modification of the Mayer plot in which the yield scale has been replaced by the parameter which is the ratio of yield and content of useful component in the feed multiplied by 100, i.e.

$$w = \frac{\gamma}{\alpha} 100 \quad .$$

(2.19)

The second axis, showing useful component recovery, is the same for both the Dell and the Mayer curves. Parameter w represents concentrate yield per 100 units of useful component in the feed. It is claimed that the substitution of yield γ by w that is by γ/α makes the upgrading curves of a conic shape, most often hyperbolic, which can be described by a formula: $ax^2 + 2fy + by^2 + 2gx + 2hxy + c = 0$ (Jowett, 1969). In this equation, the factors a, b, c, f, g, and h are constants of the curve and they do not have any physical sense, while x and y are the variables.

Table 2.9. Mass balance of hypothetical ore upgrading, useful for plotting the Dell upgrading curve

Produkt	product yield			w	Σw	Content MeSO$_4$			$\beta =$	Recovery MeSO$_4$
	γ	γ	$\Sigma\gamma$	$100\gamma/\alpha$	$\Sigma(100\gamma/\alpha)$	λ	$\gamma\lambda$	$\Sigma(\gamma\lambda)$	$\Sigma(\gamma\lambda)/\Sigma\gamma$	$\Sigma\varepsilon = K\Sigma\gamma$
	Mg	%	%			%			%	%
Concentrate C_1	103	12.06	12.06	78.31	78.31	81.7	985.30	985.30	81.70	64.00
Concentrate C_2	69	8.08	20.14	52.46	130.77	28.6	231.09	1216.39	60.40	79.01
Semiproduct P_1	189	22.13	42.27	143.70	274.47	7.0	154.91	1371.30	32.44	89.07
Semiproduct P_2	238	27.87	70.14	180.98	455.45	5.48	152.73	1524.03	21.73	98.99
Tailing T	255	29.86	100.0	193.90	649.35	0.52	15.53	1539.56	15.40	100.00
Feed F (calculated)	854	100.00		649.35		$\alpha=\beta=$ =15.40	1540			

Mathematical formulas used to delineate the Dell curve allow to calculate and modify upgrading with the use of computers. The Dell curve (Fig.2.25) is drawn on the basis of the upgrading balance, in which, additional columns representing $100\gamma/\alpha$ and $\Sigma(100\gamma/\alpha)$ are included (Table 2.9.). The balance is based on the one used for drawing other upgrading curves (Table. 2.6.) The Dell, similarly to the other upgrad-

ing curves, contains the no and ideal upgrading as well as ideal mixing lines. The no upgrading line has the slope of α while the ideal upgrading line reaches 100% recovery at $w=100$.
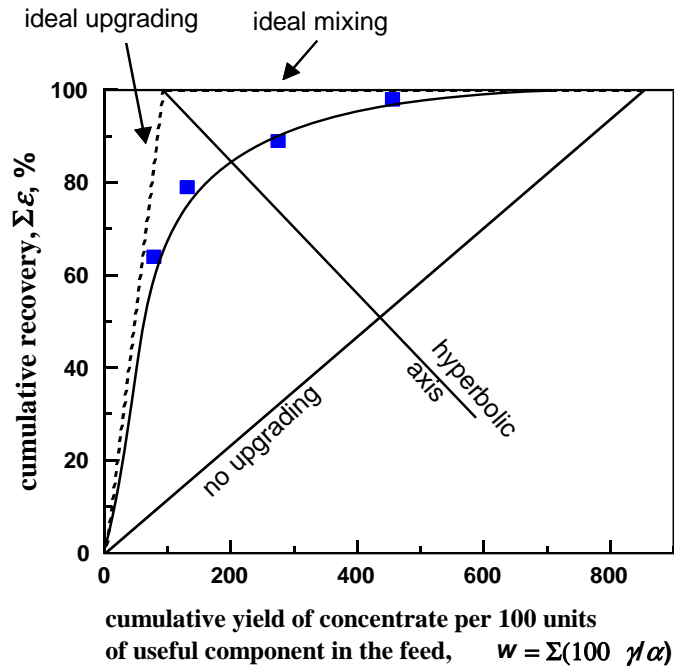
Fig. 2.25. The Dell upgrading curve

The Dell, like Mayer, curve enables comparing the results of upgrading of the same ore (α=const.) obtained under different separation conditions. Comparing the shape of the curves or their mathematical formulas allows to determine which process is better. Different Dell's upgrading curves can be compared by calculating different factors. The factors can be the same as shown in Fig. 2.21 for the Mayer plot. It is important, however, to compare the curves at the same w value, i.e. for a constant yield. Both the Mayer and Dell curves are not suitable for comparing upgrading results for the materials with variable content of the considered component α. Detailed discussion of the construction principles and the properties of the Dell curve can be found in the original works by Dell (1953, 1961, 1969, 1971) and in Polish by Luszczkiewicz and Laskowski (1989), as well as Laskowski and Lupa (1970).

2.2.2.2.4. The Halbich curve

The Halbich (1934) curve is obtained by drawing, on the basis of the upgrading balance, the recovery of a component in products of separation as a function of the content of the considered component in the products. The Halbich curve can also be

drawn in a reversed way, i.e. as the content in relation to the recovery. Usually the Halbich curves are plotted in a cumulative form. The Halbich curve has two characteristic points, which involve the final and the initial point of the curve. For the balance made for the mineral as useful component, the point at 100 per cent recovery is equivalent to mineral content in the feed and the point at zero recovery corresponds to β=100%. Figure 2.26 shows the Halbich curve based on the data given in Table 2.6.
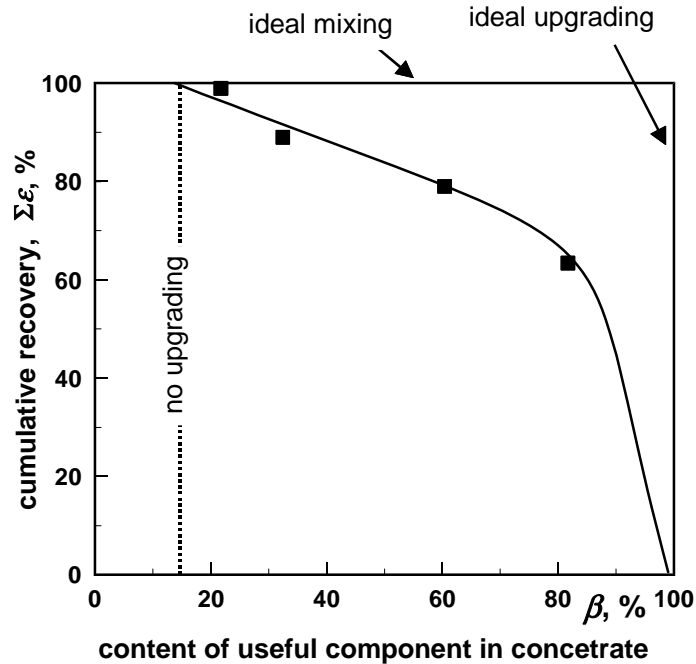
Fig. 2.26. The Halbich upgrading curve

When the balance is made for chemical element as the useful component, the point 100% recovery of the Halbich curve corresponds to the content of chemical element in feed and the final point for ε=0% and β=100% corresponds to the content (in per cent) of chemical element in pure mineral (Fig. 2.27). According to Kelly and Spottiswood (1982), to find the point of the best upgrading one should plot on the Halbich diagram selectivity index f lines defined as:

$$f = \varepsilon\beta/100\%. \qquad (2.20)$$

There usually exists only one point which represents the highest selectivity. It is worth noticing that it does not mean that the upgrading process should be conducted at this point since economical analyses may indicate that another point of the upgrading curve is optimal.
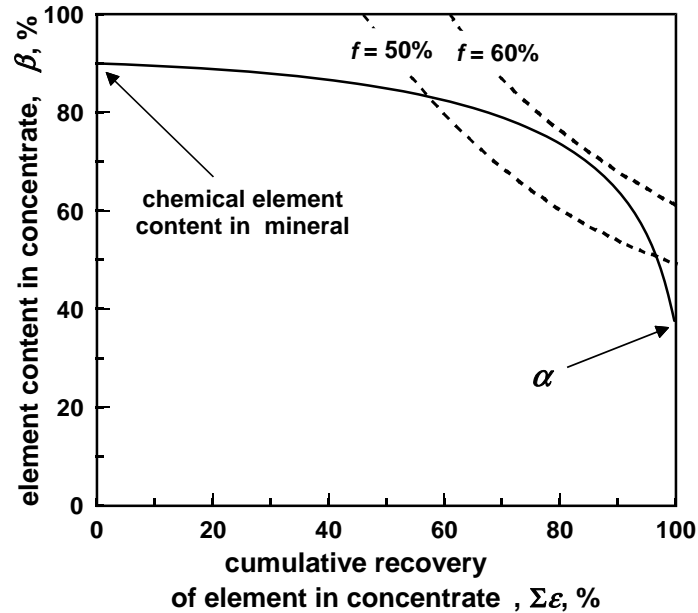
Fig. 2.27. The Halbich curve with lines of selectivity index *f* allowing to determine the best point of up-grading

2.2.2.2.5. Equal basis upgrading curves

The Henry, Mayer, Dell, and Halbich curves are very helpful for the assessment of the upgrading process when the ore features constant quality of the feed (α=const.). When the content of component separated from the feed is not constant, these upgrading curves are not very useful as the position of both ideal and no upgrading lines change.

All the previous upgrading curves have their either no and ideal upgrading lines dependent on the feed quality, that is the content of components in the feed (α). As a result the comparison of the separation results for two feeds of different useful component content is not possible. In such a case there is a need to use upgrading curves which provide equal base for comparison, that is having their no and ideal separation lines insensitive to α variation There are known several such curves. Three of them will be discussed here in more detail.

2.2.2.2.5.1. The Fuerstenau curve

The Fuerstenau upgrading curve relates recoveries of a component or components in products (Fig. 2.28). The variation of the feed quality does not effect the area of plotting. The curve was extensively used by D.W. Fuerstenau and his coworkers (1992, 1997, 2002) in their research on coal beneficiation, that is for the assessment of

coal upgrading in relation to ash. To compare separation results, the mass balances of the two components has to be calculated. In the case of plotting the recovery of one component in the concentrate and another component in the tailing, a column in the mass balance has to be added in which the recovery of each considered component in the tailing is calculated. This can be done by subtracting from 100% component recovery in the concentrate, since the sum of a particular component recovery in the concentrate and in the tailing is equal to 100%. The mass balances are shown in Tables 2.10 and 2.11. Since the Fuerstenau curve tends to be symmetric in the vicinity of the maximum curvature, this point can be used as a characteristic point suitable for comparisons of different results of separation. This point generally characterizes the process and it is referred to as the point *F* and it represents the crossing point of the upgrading curve with the straight line linking points 0,0 and 100,100. The *F* point assumes the values from 0,0 to 100,100. Figure 2.29 shows that for the considered separation the *F* point is equal to *F*=89/89.
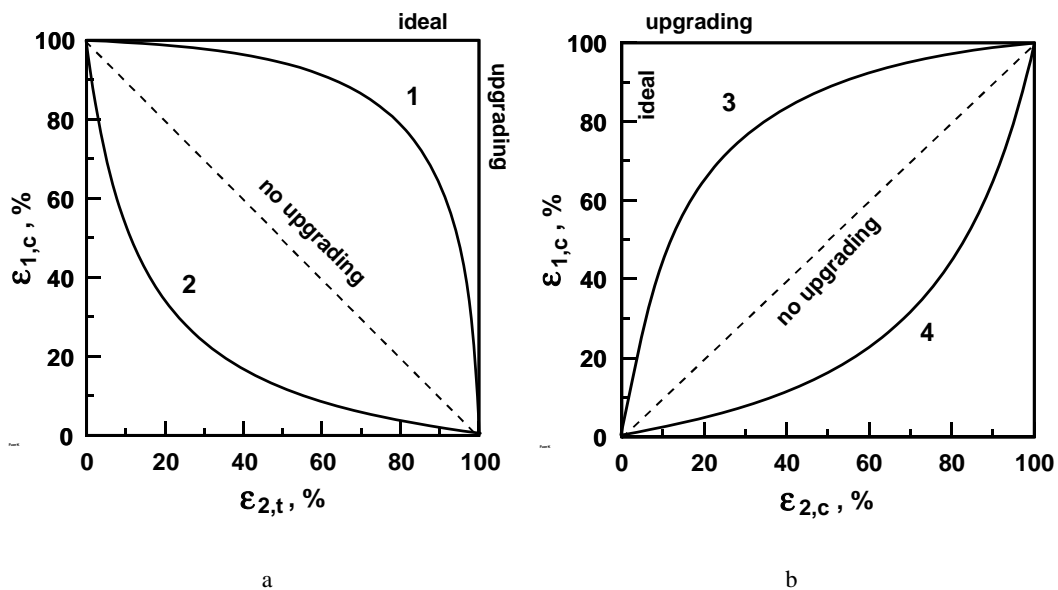
Fig. 2.28. The Fuerstenau upgrading curves: a) relationship between recovery of a component 1 in concentrate $\varepsilon_{1,c}$ and recovery of a second component in the tailing $\varepsilon_{2,t}$: 1 - recovery of component 1 in concentrate is greater than recovery of component 2 in concentrate, 2 - recovery of component 2 in concentrate is greater than recovery of component 1 in concentrate, b) relationship $\varepsilon_{1,c}$ vs $\varepsilon_{2,c}$: 3 - recovery of component 1 in concentrate is greater than recovery of component 2 also in concentrate, 4 - recovery of component 1 is smaller than recovery of component 2 in the same concentrate.
After Drzymala and Ahmed, 2005.

Table 2.10. Mass balance of carbonaceous matter in products of coal beneficiation

Product	product yield γ %	cum. product yield $\Sigma\gamma$ %	combustible matter content λ %	$\gamma\lambda$	$\Sigma(\gamma\lambda)$	$\beta = \Sigma(\gamma\lambda)/\Sigma\gamma$ %	combustible matter cum. recovery in concentrate $\Sigma\varepsilon$ %	combustible matter cum. recovery in tailing $100-\Sigma\varepsilon$ %
Concentrate C_1	52	52	98	5096	5096	98.0	64.1	35.9
Concentrate C_2	19	71	96	1824	6920	97.5	87.1	12.9
Semiproduct P_1	8	79	93	744	7664	97.0	96.4	3.6
Semiproduct P_2	6	85	42	252	7916	93.1	99.6	0.4
Tailing T	15	100	2.2	33	7949	79.49	100	0
Feed F (calculated)	100		$\alpha = 79.49$	7949				
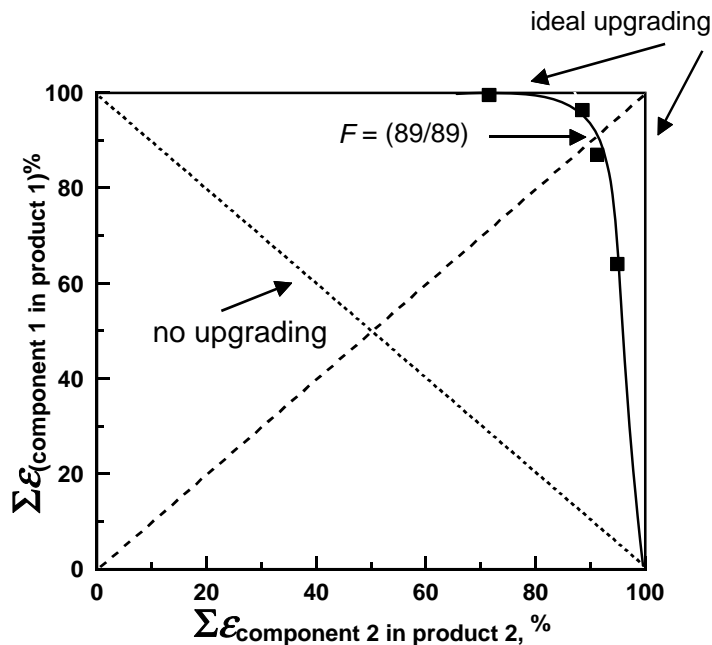
Fig. 2.29. The Fuerstenau upgrading curve

The F factor between $F = 0,0$ and 50,50 indicates upgrading of component A in the concentrate and component B in the tailing, while between 50,50 and 100,100 upgrading of component B in the concentrate and component A in the tailing. The point 50/50 indicates the lack of upgrading. The selectivities equal to 70/70 and 30/30 are the same because it is not important for the selectivity of the process whether component A was present in the concentrate and B in the tailing or vice versa.

Table 2.11. Mass balance of ash in coal beneficiation products

Product	product yield γ %	cumulative product yield $\Sigma\gamma$ %	ash content λ %	$\gamma\lambda$	$\Sigma(\gamma\lambda)$	$\beta = \Sigma(\gamma\lambda)/\Sigma\gamma$ %	ash cumulative recovery in concentrate $\Sigma\varepsilon$ %	ash cumulative recovery in tailing $100-\Sigma\varepsilon$ %
Concentrate C_1	52	52	2.0	104	104	2.00	5.07	94.93
Concentrate C_2	19	71	4.0	76	180	2.54	8.78	91.22
Semiproduct P_1	8	79	7.0	56	236	2.99	11.51	88.49
Semiproduct P_2	6	85	58.0	348	584	6.87	28.47	71.53
Tailing T	15	100	97.8	1467	2051	20.51	100	0
Feed F (calculated)	100		$\alpha = 20.51$	2051				

Table 2.12 presents the scale of separation selectivity based on factor *F*.

Table 2.12. Relative scale of selectivity of separation of two components of an ore based on the Fuerstenau upgrading curves. Seleivity index F consists of two numbers

Generation of separation	Selectivity index	Degree of separation
upgrading in concentrate of component *A* in relation to component *B*		
VI	0/0	ideal separation
V	1/1–10/10	very good separation
IV	10/10–20/20	good separation
III	20/20–30/30	medium separation
II	30/30–40/40	weak separation
I	40/40–50/50	negligibleseparation
0	50/50	lack of separation
upgrading in concentrate of component *B* in relation to component *A*		
I	50/50–60/60	negligibleseparation
II	60/60–70/70	weak separation
III	70/70–80/80	medium separation
IV	80/80–90/90	good separation
V	90/90–99/99	very good separation
VI	100/100	ideal separation

The Fuerstenau curve can be used for comparing upgrading results not only for the materials of varying composition of the feed but also for different materials upgraded by various methods. It is well illustrated in Fig. 2.30 which presents laboratory results of separation by flotation of copper from lead minerals present in industrial concentrates. It can be seen that some reagents cause depression of lead minerals while others depress copper minerals. The separation with some reagents is better than separation of the feed into products by screening according to the particle size. There is some accumulation of the lead minerals in the fine products of separation resulting from galena tendency to overgrinding. The Fuerstenau curves, in spite of their universality, are rather seldom used in mineral processing but they certainly deserve promotion. Recently, they have been used by Mohanty and Honaker (1999) and Drzymala (2005b).

Mathematical equations that can be used for approximation of the Fuerstenau curve were presented by Drzymala and Ahmed (2005).
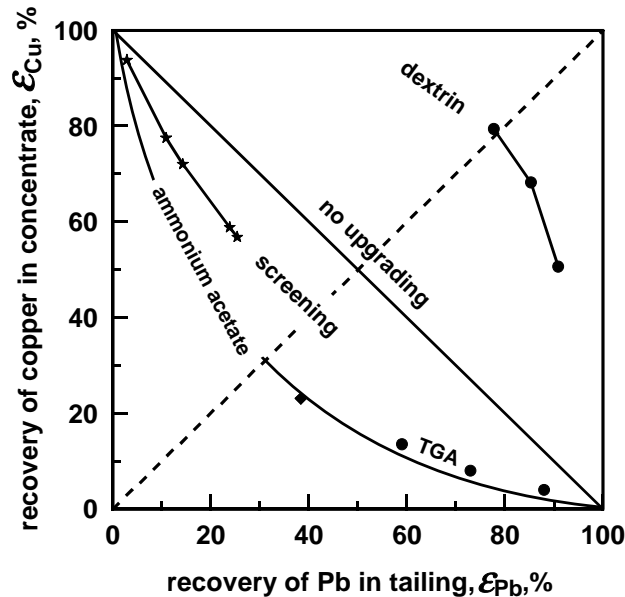
Fig. 2.30. Application of the Fuerstenau curves for comparison of selectivity of removal of lead minerals from industrial copper concentrates by flotation (Drzymala et al., 2000), leaching with ammonium acetate (Sanak-Rydlewska et al., 1999 and by screening (Luszczkiewicz and Drzymala, 1995/6). TGA denostes thioglycolic acid.

2.2.2.2.5.2. The Mayer-Drzymala-Tyson-Wheelock curve

The Fuerstenau curve provide only half of the graph area for plotting. It also takes into account the changes of α in a specific for the plot way. To create an upgrading curve having larger area (the whole square for plotting) and also to be able to compare the upgrading results on equal basis, Drzymala, Tyson and Wheelock (1990, 2006) modified the Mayer curve which fulfils these requirements. The Mayer-Drzymala-Tyson-Wheelock upgrading curve will be referred to as the MDTW upgrading curve. The MDTW upgrading curve is created by "opening" the Mayer plot like a Chinese fan (Fig. 2.31) and by further appropriate normalization of the obtained plot. Since there are different possible normalizations, variations of the MDTW upgrading curves are available. Two of them will be discussed here and presented in Fig. 2.32.
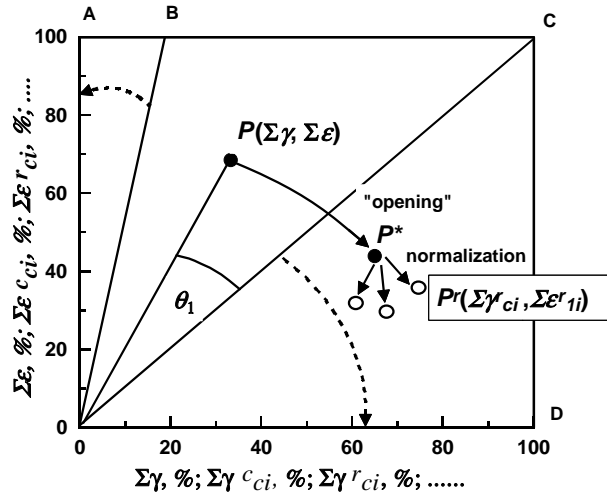
Fig. 2.31. Graphical representation of the Mayer curve transformation into the MDTW upgrading curve. The region OBC is transformed into OACD region. Point P ($\Sigma\varepsilon$, $\Sigma\gamma$) is first transformed into P^* and then normalized to have axes from 0 to 100
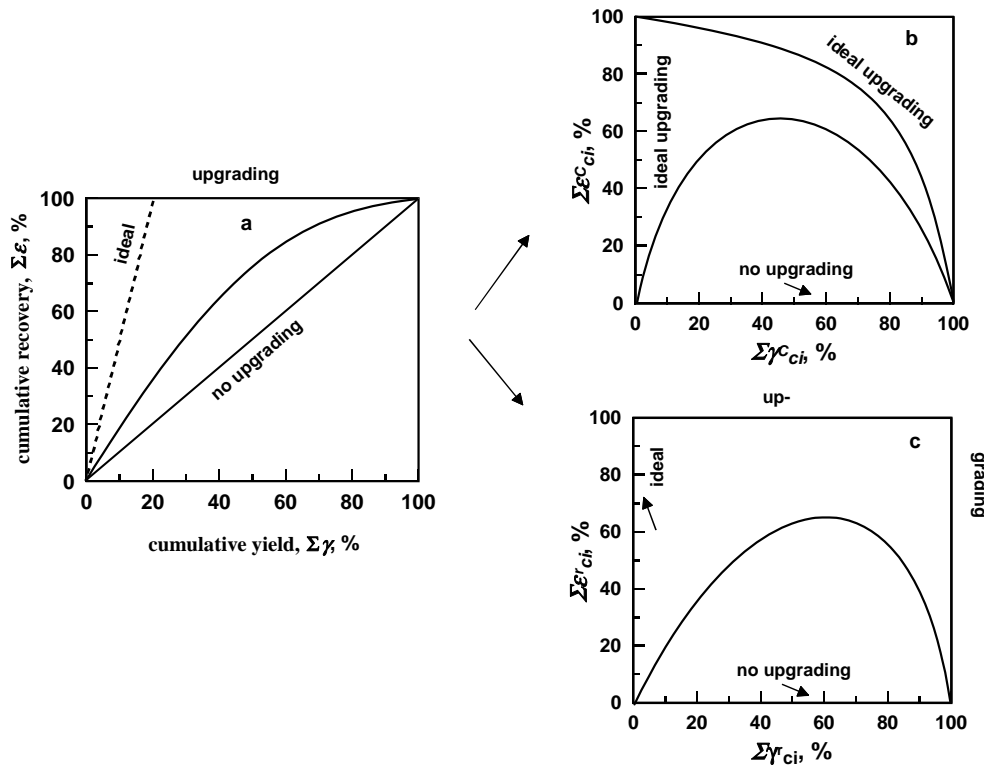
Fig. 2.32. Possible transformations of the Mayer upgrading cure (a) into circular MDTW plot, b) and rectangular MDTW plot (c). A third type of the MDTW curve is shown later in Fig. 2.33.

After "opening" the Mayer curve the measurement points change their positions. The new points obtained are not, however, the yield and recovery but specific indices of yield and recovery. An example of calculation of the values of both indices is shown in Tables 2.13a-b.

The circular MDTW upgrading curve provides more than half of the area for plotting with a circular shape of the limiting ideal separation line while the rectangular MDTW upgrading curve provides total square for plotting. The procedure of plotting of both curves is summarized in Tables 2.13a-b.

Table 2.13a. Calculation procedure summary (after Drzymala et al., 2006). The needed equations are given in Table 2.13b. $\Sigma\gamma_{ci}$ denotes cumulative yield of while $\Sigma\varepsilon_{1i}$ stands for cumulative recovery of component 1 in concentrate.

1. Use equation 10 to calculate θ_o for each test.

2. Use $\tan\theta_i = \sum\varepsilon_{1i}/\sum\gamma_{ci}$ to calculate θ_i for each experimental point.

3. Use equation 9 to calculate θ_i^T for each experimental point.

4. Use equations 6 and 7 to determine $\sum\gamma_{ci}^T$ and $\sum\varepsilon_{1i}^T$, respectively.

5. Given $\sum\varepsilon_{1i}^e = 100$, calculate $\sum\varepsilon_{1i}^{eT}$ by using equation 16.

6. Calculate $\sum\gamma_{ci}^{eT}$ by using the following combination of equations 11, 13 and 15:

7. $\sum\gamma_{ci}^{eT} = 100\cos\theta_i^T/\sin\theta_i$

8. For circular normalization apply equations 22 and 23 to determine $\sum\varepsilon_{1i}^c$ and $\sum\gamma_{ci}^c$, respectively.

9. For rectangular normalization and $\theta_i^T > 45^o$, use equations 26 and 27 to determine $\sum\varepsilon_{1i}^r$ and $\sum\gamma_{ci}^r$, respectively.

10. For rectangular normalization and $\theta_i^T < 45^o$, use equations 28 and 29 to determine $\sum\gamma_{ci}^r$ and $\sum\varepsilon_{1i}^r$, respectively.

As it has been mentioned, the MDTW curves feature constant position of the ideal and no upgrading regardless of the quality content of the feed and are suitable for comparing different upgrading results for different ores. They take into account the changes of α in a specific for them ways. Therefore, they can be tried when other "equal basis" upgrading curves fail. Further details on of the MTDW upgrading curves are available in ref. (Drzymala, et al., 2006).

Table 2.13. Equation needed for calculations of parameters for the MDTW upgrading curves

$$\sum \gamma_{ci}^T = \sum \gamma_{ci} \frac{\cos \theta_i^T}{\cos \theta_i} \qquad\qquad \sum \varepsilon_{1i}^T = \sum \varepsilon_{1i} \frac{\sin \theta_i^T}{\sin \theta_i} \qquad (6,7)$$

$$\theta_i^T = \frac{90^o \left(\theta_i - 45^o\right)}{\theta_o} \qquad (9)$$

$$\tan\left(\theta_o + 45^o\right) = \frac{100}{\alpha_1} \qquad (10)$$

$$\sum \gamma_{ci}^e = R_i^e \cos \theta_i \qquad\qquad \sum \varepsilon_{1i}^e = R_i^e \sin \theta_i \qquad (11,12)$$

$$R_i^e = \sum \varepsilon_{1i}^e / \sin \theta_i = 100 / \sin \theta_i \qquad (13)$$

$$\sum \gamma_{ci}^{eT} = \frac{\sum \gamma_{ci}^e \cos \theta_i^T}{\cos \theta_i} \qquad\qquad \sum \varepsilon_{1i}^{eT} = \frac{\sum \varepsilon_{1i}^e \sin \theta_i^T}{\sin \theta_i} \qquad (15,16)$$

$$\sum \varepsilon_{1i}^c = \frac{R_i^c \sin \theta_i^T \sum \varepsilon_{1i}^T}{\sum \varepsilon_{1i}^{eT}} = \frac{100 \sin \theta_i^T \sum \varepsilon_{1i}^T}{\sum \varepsilon_{1i}^{eT}} \qquad (22)$$

$$\sum \gamma_{ci}^c = \frac{R_i^c \cos \theta_i^T \sum \gamma_{ci}^T}{\sum \gamma_{ci}^{eT}} = \frac{100 \cos \theta_i^T \sum \gamma_{ci}^T}{\sum \gamma_{ci}^{eT}} \qquad (23)$$

$$\sum \varepsilon_{1i}^r = \sum \varepsilon_{1i}^{er} \frac{\sum \varepsilon_{1i}^T}{\sum \varepsilon_{1i}^{eT}} = 100 \frac{\sum \varepsilon_{1i}^T}{\sum \varepsilon_{1i}^{eT}} \qquad (26)$$

$$\sum \gamma_{ci}^r = \frac{\sum \varepsilon_{1i}^{er} \left(\sum \gamma_{ci}^T\right)^2}{\sum \varepsilon_{1i}^T \left(\sum \gamma_{ci}^{eT}\right)} = \frac{100 \left(\sum \gamma_{ci}^T\right)^2}{\sum \varepsilon_{1i}^T \left(\sum \gamma_{ci}^{eT}\right)} \qquad (27)$$

$$\sum \gamma_{ci}^r = \sum \gamma_{ci}^{er} \frac{\sum \gamma_{ci}^T}{\sum \gamma_{ci}^{eT}} = 100 \frac{\sum \gamma_{ci}^T}{\sum \gamma_{ci}^{eT}} \qquad (28)$$

$$\sum \varepsilon_{1i}^r = \frac{\sum \gamma_{ci}^{er} \left(\sum \varepsilon_{1i}^T\right)^2}{\sum \gamma_{ci}^T \left(\sum \varepsilon_{1i}^{eT}\right)} = \frac{100 \left(\sum \varepsilon_{li}^T\right)^2}{\sum \gamma_{ci}^T \left(\sum \varepsilon_{1i}^{eT}\right)} \qquad (29)$$

The third MDTW upgrading curve is not as universal as the previous two because its ideal separation line, after pseudo-circular normalization still slightly depends on the feed quality (α), contrary to the claims made during first presentation of the curve (Drzymala, 2001)

Table 2.14. Way of recalculating recovery and yield into recovery ε^T and yield γ^T indices for plotting the pseudo-circular MDTW upgrading curves. The arrows indicate the data useful for plotting. Calculations for α=50%.

Expression	Calibration points		Real point as example	
$\rightarrow\varepsilon$	100%	100%	70.7	63.3
$\rightarrow\gamma$	50%	100%	69.7	39.6
ε/γ	2	1	1.014	1.5985
$\mathrm{tg}^{-1}(\varepsilon/\gamma)$	63.43^o	45°	45.408^o	57.97^o
$\theta_1 = \mathrm{tg}^{-1}(\varepsilon/\gamma) - 45°$	18.43^o	0°	0.408^o	12.97^o
$k\theta_1$ (for α=50% k=4.8833) $(k = 90^o/[\mathrm{tg}^{-1}(100/\alpha)-45^o])$	90°	0°	1.992^o	63.336^o
$\sin k\,\theta_1$	1	0	0.0348	0.8936
$\sin \mathrm{tg}^{-1}(\varepsilon/\gamma)$	0.8944	0.707	0.71212	0.8477
$A = \sin(k\theta_1)/\sin \mathrm{tg}^{-1}(\varepsilon/\gamma)$	1.118	0	0.04886	1.10541
$A\varepsilon$	111.8	0	3.45	66.726
$\rightarrow\varepsilon^T =A\varepsilon/z$ $(z= \sin k\,\theta_1/[\sin \mathrm{tg}^{-1}(100/\alpha)]$	100	0	3.09	59.68
$\cos k\theta_1$	0	1	0.9994	0.44875
$\cos \mathrm{tg}^{-1}(\varepsilon/\gamma)$	0.4472	0.707	0.70205	0.53036
$B = \cos k\theta_1/\cos \mathrm{tg}^{-1}(\varepsilon/\gamma)$	0	1.4142	1.42235	0.84613
$B\gamma$	0	141.42	99.22	33.507
$\rightarrow\gamma^T = B\gamma/n$ (n=1.4142=const)	0%	100%	70.16	23.69
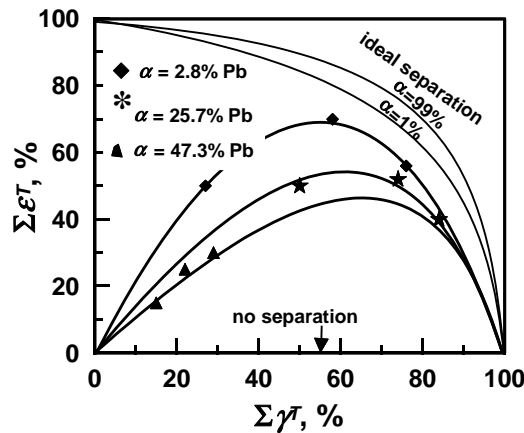
Fig. 2.33. The pseudocircular MTDW upgrading curves for the case considered by Bigosiński (1989)

The example of application of the pseudocircular MDTW upgrading curve is presented after Bigosiński (1989) in Fig. 2.33. It shows the results of flotation of lead minerals from different copper products. The upper line in Fig. 2.33 shows the results for the industrial concentrates of the Lubin processing plant, while the remaining two

for the concentrates with added galena. According to Figure 2.33 the increased Pb content in the copper-lead products makes the separation worse.

The discussed MDTW upgrading curves can also be useful for comparing upgrading of more than one ore component. To do this, separate upgrading balances for these components should be calculated and the data obtained plotted in the same diagram.

2.2.2.2.5.3. Other upgrading curves

There are more upgrading curves which provide the comparison of separation results on an equal basis with their area of plotting not sensitive to the feed quality. The list of plots includes the Hall, Luszczkiewicz, and Stepinski curves. The curves are briefly presented in Fig. 2.34.
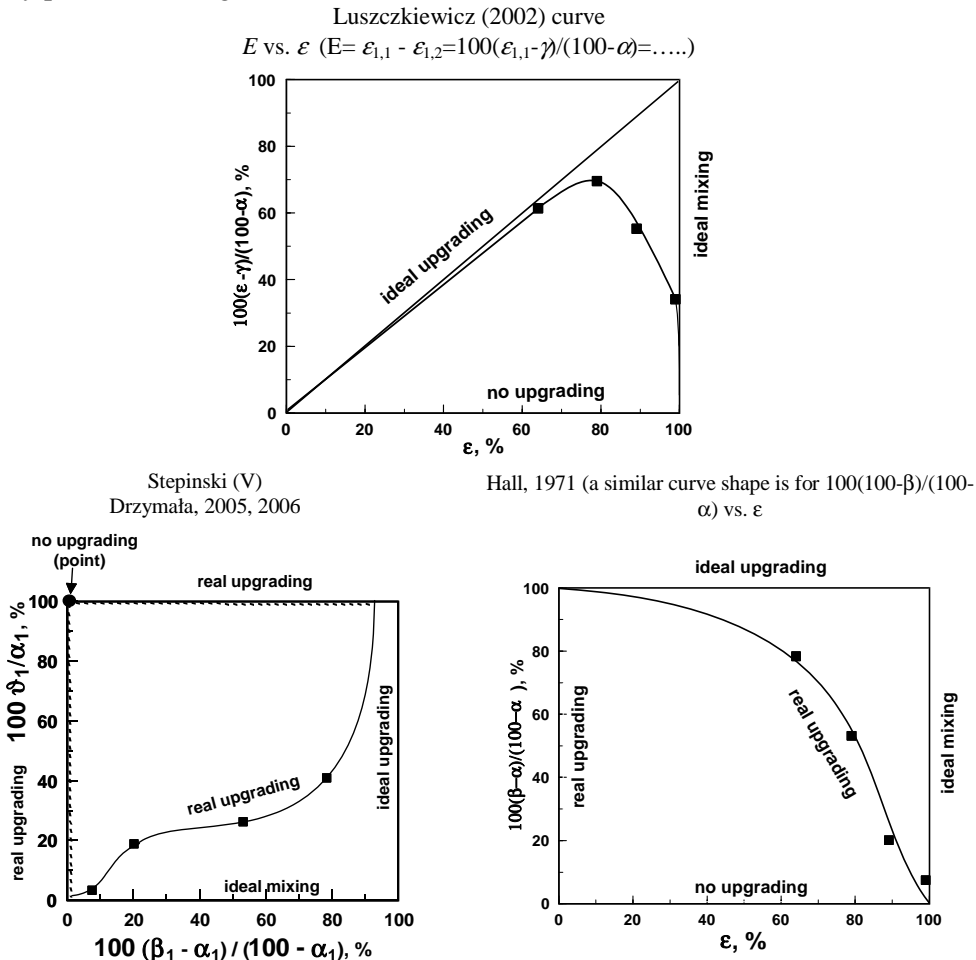
Fig. 2.34. Additional useful upgrading curves

2.2.2.3. Upgradeability

The results of upgrading depend on the properties of feed, the work of the upgrading device, as well as on other factors including human factor (Fig. 2.35). Sometimes there is a need of determining possible separation results which would depend only on the property of the feed, without any disturbances originating from the separator and its crew. Such property is called upgradeability (Fig. 2.35). Theoretically, it is also possible to establish the ability of a separation device for separation which would not be affected by the material subjected to separation.

influence of ore

upgradeability

upgrading

**influence of
separating device**

**other
influences**
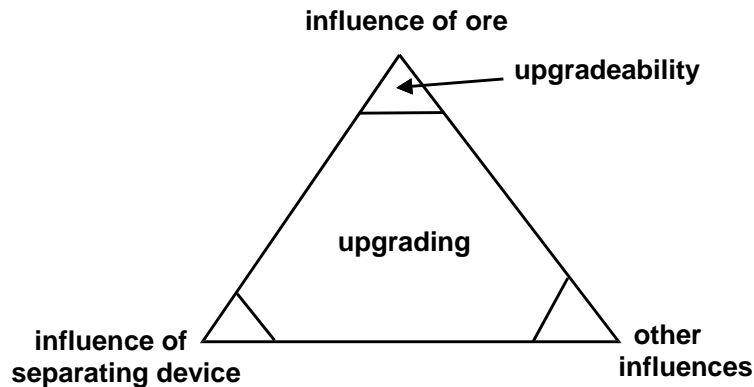
Fig. 2.35. Difference between upgrading and upgradeability

So far, there have not been any normalized and commonly accepted procedures for determining upgradeability, however, there are some approximate approaches. The procedures described in the literature are usually very specific for method of separation. The Dell (1972) procedures are often applied for determining floatability of materials. One of them is based on fractionated flotation of ore or raw material, while another involves multiple re-flotation of the upgrading products. The re-flotation procedure is most often used as it is simple and allows to introduce various modifications of testing. The Dell method is schematically shown in Fig. 2.36. The method of multiple re-flotation (cleaning), used for determining floatability, consists of main flotation with an excess of the collector conducted until every particle capable of flotation reports to the concentrate. The main flotation provides concentrate and tailing I. Next, the concentrate is subjected to a cleaning flotation without any addition of reagents and tailing II is obtained, while the concentrate is subjected to a fractionated flotation. The subsequent concentrates are obtained through changing flotation conditions, which involve gradual increase of the air supply and the slurry stirring rate. The tailing I, III, and III can be additionally, after combining them together, subjected to a control flotation, which results in the final tailing and a semi-product. The produced products are weighted to determine their yields and analyzed to determine the content of useful component or components. On the basis of these data, upgrading mass balance is

made and then appropriate upgrading curves are plotted, which provide the assessment of feed upgradeability. It should be noticed that different types of flotation in the method shown in Fig. 2.36 are used including the main, cleaning, fractionated, and control flotations.

Feed

MAIN FLOTATION
– excess of collector
– long time of flotation

Tailing I

CLEANING FLOTATION
– no addtion of reagents

Tailing II

CONTROL FLOTATION

FRACTIONATED FLOTATION
– increasing air supply
– increasing stirrer speed

Tailing III

Tailing

Semiproduct

C I   *C II*   *C III*   *C IV*
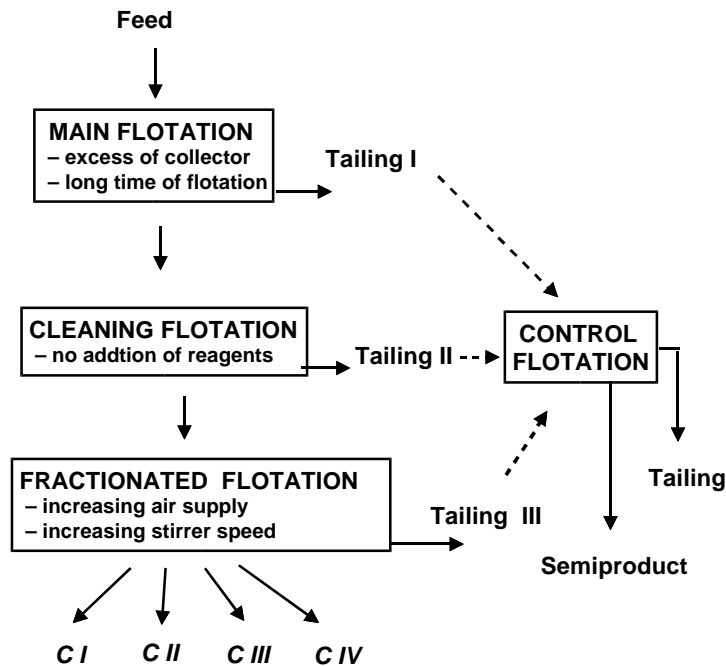
Fig. 2.36. Scheme of conducting flotation tests for determination of floatability of material subjected to separation of valuable components

Another method of determining floatability of the feed is based exclusively on fractioned flotation, which involves mixing concentrates from the previous flotation. This method is shown in Fig. 2.37.

Another method of determining upgradeability is to separate the feed into products by the method not based on the main feature of separation but by another parameter dependent on the main feature. A good example is the so-called washability curve. To determine the floatability of coal, a sample of the feed is separated into products by means of gravity separation in heavy liquids of varying densities. The density fractions (products) can be subjected to chemical analysis to determine the content of ash and the washability curve, relating the yield of the products (density fractions) and their ash content is drawn (Fig. 2.38). Since in the case of coal the hydrophobicity of particles is related to their density, the washability curves can be compared with separation data (curve) obtained by flotation. Since the washability curve is determined by the analytical (densimetric) method it indicates coal floatability. A comparison of the washability for the feed and the real separation curve indicates how much particular

separation is different from potential separation. Other types of washability curves are also available (Jacobsen et al., 1990).
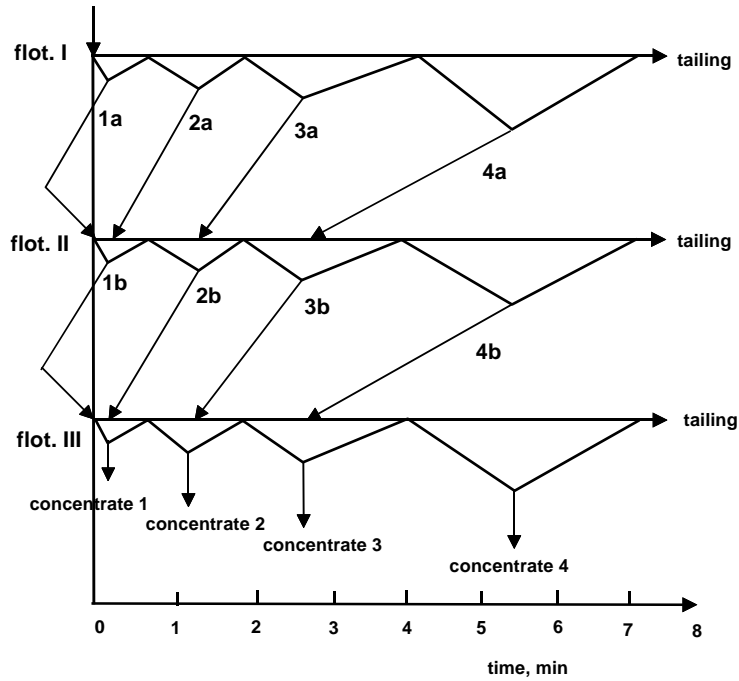
Fig. 2.37. Scheme of fractionated flotation used for determination of upgradeability (floatability) (after Laskowski and Luszczkiewicz, 1989)
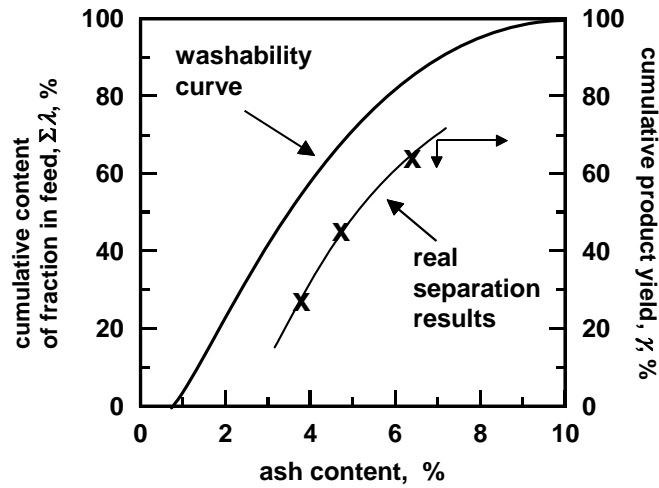
Fig. 2.38. A comparison of washability (upgradeability) curve (gravity separation) with results of coal cleaning by flotation (upgrading curve)

Upgrading results and upgradeability curves can be plotted on any upgrading diagram. Ideal and no upgrading curves should also be added. The ideal separation can be achieved only for a full liberation of valuable components and lack of other disturbances. The upgradeability represents a separation process for a given partial liberation of valuable component and influence of other factors which cannot be eliminated. The real upgrading curve reflects the existence of intergrowths (middlings) in the feed and influences of other factors such as imperfect work of the upgrading device.

Sometimes we observe degrading of the feed (Fig. 2.39). It occurs when the useful component, instead of reporting to the concentrate, stays in the tailing.

Similar procedures of upgradeability determination can be used for processes treated as classification or sorting. These issues will be discussed in other chapters.
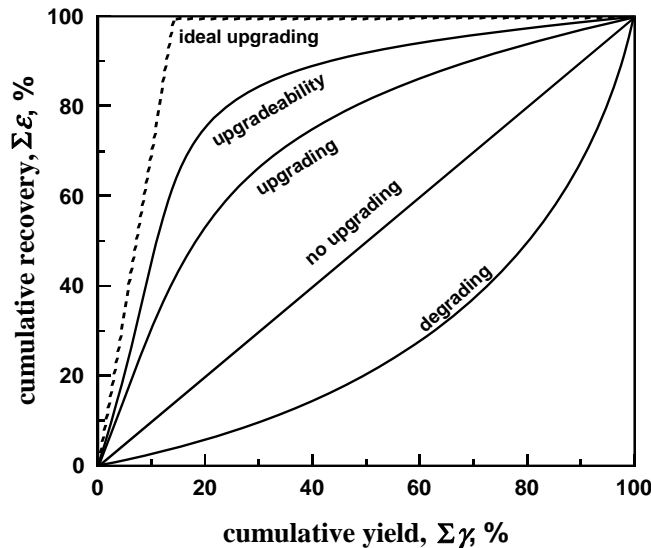
Fig. 2.39. Comparison of possible upgrading curves plotted in the Mayer diagram

2.2.2.4. Upgrading indices and evaluation of separation treated as upgrading

The assessment of separation results from the upgrading perspective consists of comparing real with ideal upgrading, lack of upgrading, while comparison relies on comparing the results with other separation outcomes. A proper evaluation and comparison from the upgrading perspective always requires two separation parameters: one representing quality and one quantity (or their combinations). Therefore, the results of separation in one region of parameters values can be very good while in other poor. Figure 2.40 shows the Mayer curves, which indicate, that up to a certain yield γ the recovery according to procedure A is greater while above that point of yield, the separation procedure B is better. If one would use only one parameter, the results of evaluation would be simply incorrect.
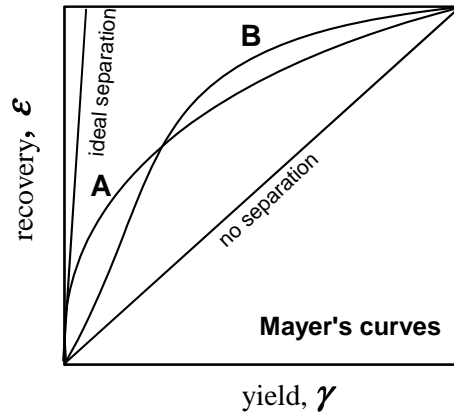
Fig. 2.40. Evaluation of separation results requires two upgrading parameters. An example of upgrading of the same ore when efficiency of separation depends on yield. Recovery indicates that procedure A is better than that of B only at low yields

The list of parameters which can be used for evaluation and comparison of separation results is infinite and the parameters are called factors, indices, numbers, ratios, efficiencies (qualitative E, quantitative E'', general E*, Sztaba, 1993), etc. Some of them are shown in Table. 2.15. It should be stressed that a comparison and evaluation of a separation process from an upgrading perspective is impossible by using only one parameter, except for very limited cases.

Table 2.15. Selected upgrading parameters. They are based on principal parameters γ, λ (or β), α

Index	Formula	Source
k, upgrading ratio	λ/α	
$\gamma\lambda$, partial yield	$\gamma\lambda$	
ε, recovery	$\gamma\lambda/\alpha$	
w, Dell's parameter	γ/α	
Hancock's parameter	$E_1^s = 10000\dfrac{(\alpha-\vartheta)(\lambda-\alpha)}{\alpha(\lambda-\vartheta)(100-\alpha)}$	
S, selectivity	$S = \dfrac{\varepsilon_r - \varepsilon_{i(\gamma=\alpha)}}{\varepsilon_{100} - \varepsilon_{i(\gamma=\alpha)}} = \dfrac{\varepsilon_r - \varepsilon_{i(\gamma=\alpha)}}{100 - \varepsilon_{i(\gamma=\alpha)}}$	See Fig. 2.21
Schulz's index = Hancock's parameter	$E = \varepsilon - \varepsilon_2 = 100(\varepsilon-\gamma)/(100-\alpha)$	
f, optimum index	$f = \varepsilon\beta/100\%$	Kelly and Spottiswood, 1982
H, Hall's parameters	$H_1 = 100(100-\beta)/(100-\alpha)$ $H_2 = 100(\beta-\alpha)/(100-\alpha)$ $\beta-\alpha$	Hall, 1971 Wieniewski, 1988; 1990
Stepinski's parameters	$\lambda/\alpha,\ \vartheta/\alpha$	Stepinski, 1958; Pudlo, 1971

More upgrading factors can be found in literature starting with classic book on mineral processing by Taggart (1948) as well as by Barski and Rubinstein (1970). It is very important to remember that for evaluation and comparing upgrading results it is necessary to have a pair of upgrading factors. The simplest upgrading pair of factors is yield γ and content λ. These parameters combined with the feed quality α provide many new parameters including the simplest, recovery $\varepsilon = \gamma\lambda/\alpha$, which plays of role of both quality and quantity parameter. Having three parameters (ε, γ, λ) we can use three pairs of upgrading factors to assess upgrading process, that is yield-content, yield-recovery and recovery-content. Creating another upgrading parameter, for instance upgrading ratio, provides more pairs of separation parameters. And so on, until infinite number of pairs of parameters is created.

The results of upgrading are compared using pairs of upgrading parameters obtained either from the mass balance of separation or from appropriate upgrading curves. If one of the parameters is constant, the evaluation procedure is limited to comparing numerical values of the second factor.

Evaluation and comparing upgrading results should be performed for separation results involving constant feed quality, that is for identical content of useful component in the feed (α) because separation depends on the quality of feed. Otherwise appropriate upgrading curves (Fuerstenau, MDTW, Hall, Stepinski, Luszczkiewicz) plots have to be used but the results of comparison will depend on the curve used.

In mineral processing the basic upgrading factors used are not yield and content but rather content and recovery. The information that separation leads to concentrates with 95% recovery of useful component at the content of useful component in the concentrate equal 30% is understandable for everyone dealing with mineral processing.

It is interesting to note that the selectivity factors for two components in one product and for one component in two products can be equivalent. For instance the Hancock formula (Budryka and Stępiński, 1954; Sztaba, 1993):

$$E_1^S = 10000 \frac{\left(\lambda_{s1,F} - \lambda_{s1,T}\right)\left(\lambda_{s1,C} - \lambda_{s1,F}\right)}{\lambda_{s1,F}\left(\lambda_{s1,C} - \lambda_{s1,T}\right)\left(100 - \lambda_{s1,F}\right)} \, , \tag{2.21}$$

in which:
C – concentrate
F – feed
T – tailing
s_1 – component 1
s_2 – component 2
λ - content
is equivalent with the Schultz (1970) index:

$$E_1^S = \varepsilon_{s1} - \varepsilon_{s2}, \tag{2.22}$$

where:

E_1^S – selectivity index (general efficiency)

ε_{s1} – recovery of component 1 in concentrate

ε_{s2} – recovery of component 2 in the same concentrate.

It is very important for each selectivity factor used for the assessment of upgrading to provide its range, i.e. the values for the lack of selectivity and ideal selectivity. It is also necessary to indicate at what recovery or other upgrading parameters its value was determined.

There are other approaches to evaluation of the upgrading data including integration of the upgrading curves (Mahanty et al., 1999). It should be stressed that the new selectivity factors do not provide any new information on separation system in relation to the contribution of the principal upgrading factors γ and λ. They create only new pairs of upgrading parameters presented in a new form. Sometime they may have advantages over the Henry curve when mathematical formula of separation is needed and only this particular upgrading curve is suitable.

2.2.2.5. Summary

Upgrading represents a certain way of analysis and evaluation of separation results.
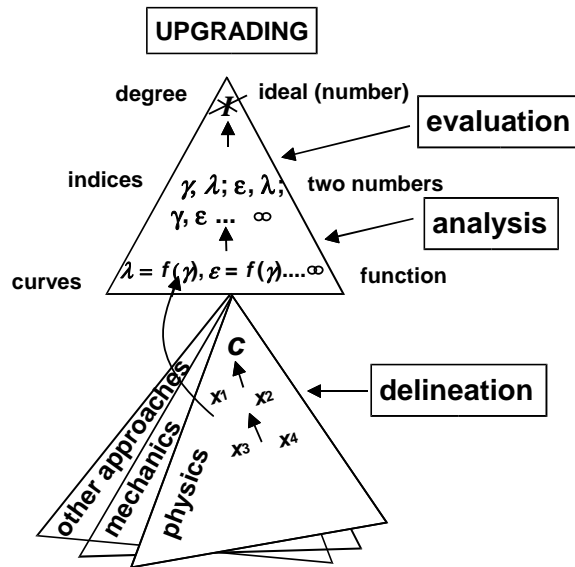
Fig. 2.41. Schematic summary of analysis of separation as upgrading

It is based on two principal parameters of separation that is the yield (γ) of products and the content of components (λ) in the products and in the feed (α, usually constant). The quantity γ and quality λ parameters (and α) can be combined to provide

infinite number of new parameters which can be also used for the analysis of separation from the upgrading perspective. Other parameter of separation such as the value of the main feature utilized for separation is not used. The main feature value is important for analysis of separation as classification. For a meaningful evaluation of separation results two parameters are necessary. The delineation of separation for such analysis as upgrading, classification, sorting, etc. is the same. Schematic summary of upgrading is presented in Fig. 2.41.

2.2.3. Classification (CF)

Classification is a way of analyzing separation results. Classification takes into account two parameters that is the quality of the products of separation and the numerical value of the feature utilized for separation. Classification usually takes into account fraction as a component, but it can be any kind of component. Each fraction features minimum and maximum value of the property determining the fraction. The fraction can be also characterized by mean value which is usually calculated as an arithmetic mean of the minimum and maximum value. The number of fractions in the feed and in the separation products depends on the way they are defined. There often exist appropriate standards which specify the size of fractions. Different branches of science and practice usually have different standards regarding the size of fraction. If the fraction is based on particle size, the fraction is called the size fraction. The minimum number of fractions in a separation system is two.

There are different ways of presenting fractions in writing. In the case of size fraction we can say that fraction containing particles from 2 to 5 mm is size the 2-5 mm size fraction. This size fraction can be also written as 2-5mm, 2/5 mm, -5+2 mm, 2÷5mm, 2+5mm, or >2<5mm. The term "fraction" can be applied for any property including density, magnetic susceptibility, hydrophobicity, etc.

The products of separation, which are analyzed from the classification perspective, can be named as upper and lower, chamber and froth, sandy and fine, overflow and underflow, concentrate and tailing, etc. products. It should be stressed that when analyzing results of separation either as classification or upgrading the same terms (recovery, yield, content, and their combinations) can be used.

2.2.3.1. Analysis of separation process as classification

Separation results to be analyzed as classification, similarly to the upgrading procedure, are subjected to weighting the products of separation in order to determine their yields. The definition of yield (γ) in classification is the same as in upgrading and it was described earlier. Next, samples of separation products and the feed are collected to analyze their quality, that is the content (λ) of each fraction in the products. The method of analysis of fractions content depends on the fraction property. It is ob-

vious, that the contents of hydrophobicity fractions will be determined in a different way than, for instance, magnetic susceptibility fractions.

The determination of the content of fractions in products and the feed usually consists of two stages. First, a product sample is analytically divided into fractions and then the amount (mass, volume, etc.) of the fractions is determined. The second stage is mostly performed by weighing. Therefore, it often happens that the content of a size fraction in a product is called yield of the fraction. In this work we will use the term yield for quantity of the product produced in a real separation process while the term content will be used to characterize the quality of the product which was determined by analytical separation to determine the amount of the component under consideration in the product. This follows the recommendations of Sztaba (1993), who suggested to use the term yield in relation to the products when the feed is divided in physical sense into several parts (products) as a result of e.g. screening, separation in heavy liquids, flotation, etc., and these parts (products) are used for other purposes (e.g. quality determination). On the other hand, the content expresses relations between the components of particular material and their separation is not a technological operation but an analytical procedure. Such definitions of yield and content allow to use the same expressions for separations treated as upgrading and classification.

Table 2.16. Output and relative (in %) yield of material subjected to separation and analyzed as classification

Product	Mass yield Mg/day	Yield, %
Coarse product	276	32.1
Fine product	584	67.9
Feed	860	100.0

Table 2.17. Results of analysis of separation as size classification. Coarse product is denoted as *G* and fine product as *D*

Size fractions		Content of size fractions k_i in product		
Size fraction, μm	Average particle size, μm	Feed	Coarse product	Fine product
$k_i = d_{i-1} \div d_i$	$d = 0.5(d_{i-1} + d_i)$	α_i, %	$\lambda_{i\,G}$, %	$\lambda_{i\,D}$, %
0–125	62.5	0.01	0	0.015
125–160	142	2.45	0	3.61
160–200	180	12.32	2.51	16.96
200–250	225	24.05	8.39	31.45
250–320	285	21.16	16.21	23.50
320–400	360	13.12	16.02	11.75
400–500	450	11.45	19.66	7.57
500–630	565	7.78	16.54	3.64
630–800	715	3.86	9.42	1.23
800–1000	900	3.80	11.25	0.28

Let us consider a hypothetical example in which certain material was subjected to separation leading to classification of particles according to their size. Two products were obtained which were named fine (D) and coarse (G) products. After weighing (Table 2.17) the output of the fine and coarse products per day and their yields were calculated. The samples of the separation products were subjected to particle size analysis using analytical laboratory screens. The content of each particle size fraction in the feed, coarse and fine products is shown in Table 2.18. The calculated fine and coarse yields of the product and the content of different size fractions in the products provide complete characteristics of separation. Having the yields and contents, other parameters such as recovery of a component in a product can be calculated (Table 2.18).

Table 2.18. Mass balance of separation analyzed as classification
Yield of coarse product $\gamma_G = 32.1\%$, yield of fine product $\gamma_D = 67.9\%$

Size fraction, μm	Average particle size, μm	Feed	Content of size fraction k_i in product		Recovery of size fraction k_i in product	
			coarse product	fine product	coarse product ε_{iG} ($\gamma_G \lambda_{iG}/\alpha_i$)	fine product
k_i	d	α_i, %	λ_{iG}, %	λ_{iD}, %	ε_{iG}, %	ε_{iD}, %
0–125	62	0.01	0	0.0147	0	100
125–160	142	2.45	0	3.608	0	100
160–200	180	12.32	2.51	16.96	6.54	93.46
200–250	225	24.05	8.39	31.45	11.20	88.80
250–320	285	21.16	16.21	23.50	24.59	75.41
320–400	360	13.12	16.02	11.75	39.20	60.80
400–500	450	11.45	19.66	7.57	55.11	44.89
500–630	565	7.78	16.54	3.64	68.24	31.76
630–800	715	3.86	9.42	1.23	78.34	21.66
800–1000	900	3.80	11.25	0.28	95.00	5.00

The recovery of the i-th size fraction in a product, e.g. coarse product G is calculated from a general equation already provided when discussing upgrading:

$$\varepsilon_{iG} = \gamma_G \lambda_{iG}/\alpha_i \qquad (2.23)$$

where α is the content of i-th class in the feed.

The same formula is used for calculating recovery in the fine product, but then symbol G in Eq. (2.23) should be replaced by another symbol, for instance D.

In the literature and in mineral processing practice dealing with classification, instead of recovery, other terms, including partition coefficient (Wills, 1981) separation number (Laskowski and Luszczkiewicz, 1989; Sztaba, 1993), separation efficiency (Laskowski et al., 1977), probability of separation (Brozek, 1996) are used. The recovery of fraction i in product j (ε_{ij}) can be also calculated directly taking into account

the definition of recovery. The recovery represents a ratio of produced amount of matter to its possible amount. In our case it will be a ratio between the mass of a component in a product and the mass of the same component in the feed:

$$\varepsilon_{ij} = Q_{i\,P}/Q_{i\,F}, \qquad (2.24)$$

where:

Q_{iP} – amount of fraction i in a product $j=P$, usually in the mass unit

Q_{iF} – amount of the same fraction i in the feed, in the same unit as Q_{iP}.

It should be noticed that classification balance has a slightly different layout than that of upgrading. If there is a need to make classification and upgrading balance similarly, each fraction should be balanced separately. Once we have yields, contents, and eventually other (derived) parameters such as recovery or enrichment ratio, as well as the sizes of fractions, analysis of separation from the classification perspective can be accomplished. The best for this purpose are graphical relations. Graphical analysis of separation from the classification perspective, when the composition of the feed is constant (α=const), at a constant product yield (γ_D = const, γ_G = const, $\gamma_G + \gamma_D = \gamma_F = 100\%$), is possible on the basis of two parameters: quality of the product (content of components in a product) and the value of property used for separation. If the content is used for analysis and then for the assessment of separation results as classification, the data involving two or more products should be used.

For analyzing separation as classification, apart from the principal content vs separation feature curve, many other plots can be used. The division of the classification curves is given in Fig. 2.42.

The figure shows that classification curve can be non-cumulative, cumulative and modified. Their systematics is shown again in Table 2.19 along with their names.
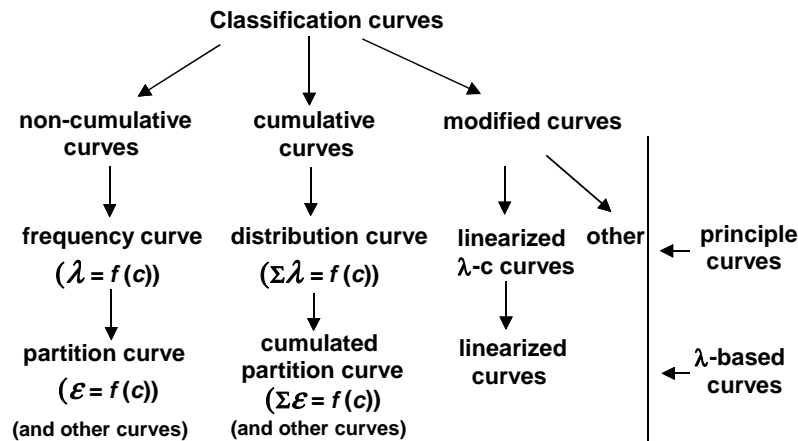
Fig. 2.42. Types of classification curves

Table 2.19. Systematics of classification curves

Classification curves		
Relation	curve name	other names of the curve
noncumulative curves		
principle curve $\lambda = f(c)$	frequency	content–feature curve, noncumulative feature distribution curve, histogram
λ-based curves, e.g. $\varepsilon = f(c)$	partition	$\varepsilon = f(c)$ curve is also called Tromp, partition, distribution, efficiency, action, classification curve
cumulative curves		
$\Sigma\lambda = f(c)$	distribution	cumulative content–feature, feature distribution
$\Sigma\lambda$-based curves e.g. $\Sigma\varepsilon = f(c)$	cumulative partition	cumulative recovery–feature
modified classification curves		
$f(\Sigma\lambda) = f(c/c^x)$	linearized distribution	Gates–Gaudin–Schumann, Gaudin–Meloy, Rosin–Rammler–Sperling, Kolmogorov curves (equations in Table 2.21)
	logarithmic scale curves	
	reduced partition	
E (probable error), d_{50}	–	–

c – selected feature of material

c^x – reference state for the selected feature of material.

2.2.3.2. Classification curves

2.2.3.2.1. Frequency curves

The component content λ vs separation feature c, or shortly $\lambda = f(c)$ curve, is one of two (frequency and distribution) basic classification curves. It represents the relationship between the contents of subsequent fractions in a product of separation as a function of the value of the feature utilized for separation. When plotted in a noncumulative way it is called the frequency curve while a cumulative version ($\Sigma\lambda = f(c)$) is called the distribution curve. The frequency curves of are also called histograms.

A correct graphical way of constructing the frequency curves is presented in Fig. 2.43 for the coarse product from Table 2.19 as an example. The plot consists of columns representing fractions. Each fractions has average value equal $0.5(c_{i-1}+c_i)$. $i=1$ denotes the first fraction. Symbols c_{i-1} and c_i stand for the fraction limits. When the fraction feature is the size of particle, as in Fig 2.43, the general symbol c denoting the feature of a component can be replaced with symbol d meaning particle size. The

curve should cross, if possible, each column in the middle of the top and provide simi-
lar areas to the left and the right of the column center of the top.
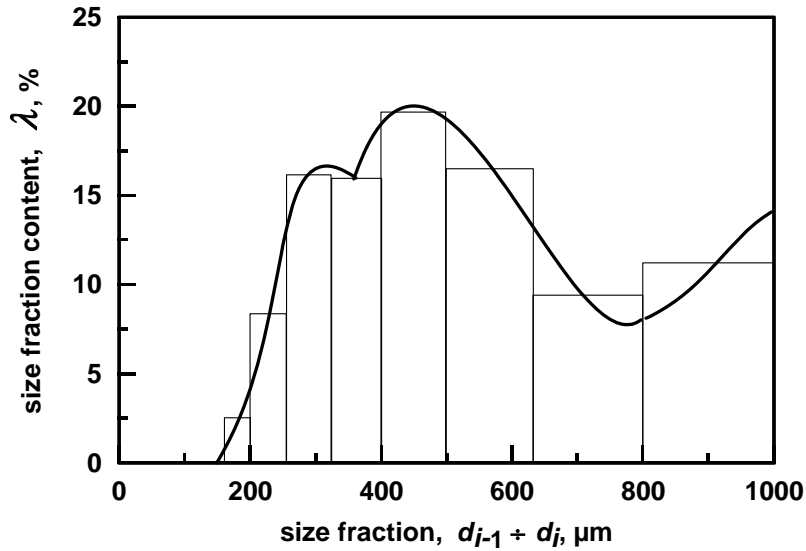
Fig. 2.43. Graphical construction of the frequency curves (histograms)

To analyze properly separation as classification using the λ=f(c) function, the dia-
gram should contain the histograms for the feed and at least one product of separation,
or be plotted for the two products of separation. Both the feed and the two products
can also be plotted (Fig. 2.44).
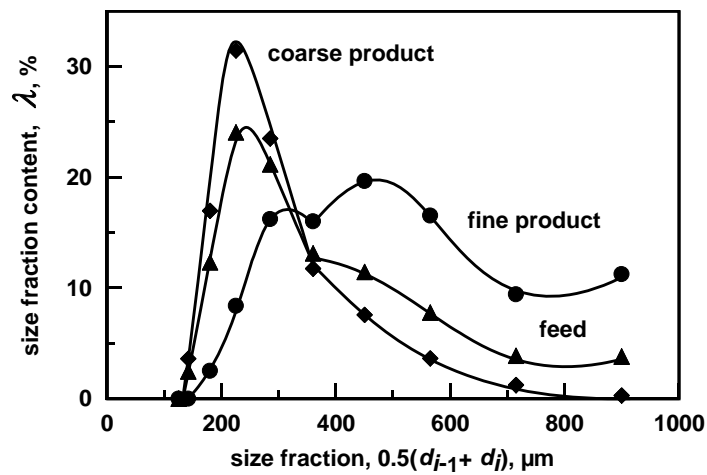
Fig. 2.44. Frequency curves characterizing separation process. The columns (bars) are not plotted
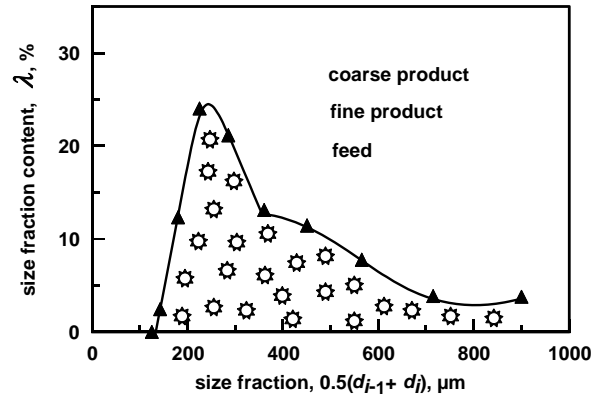
a
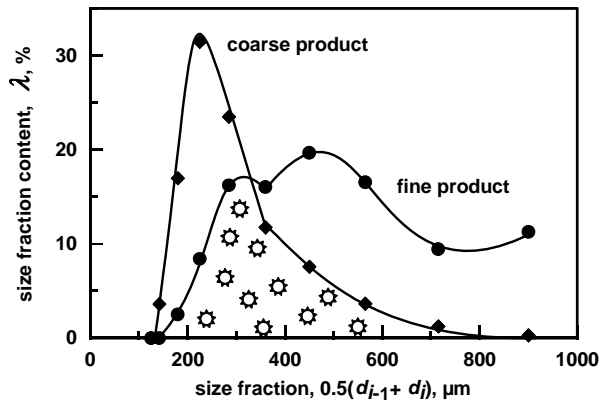
b
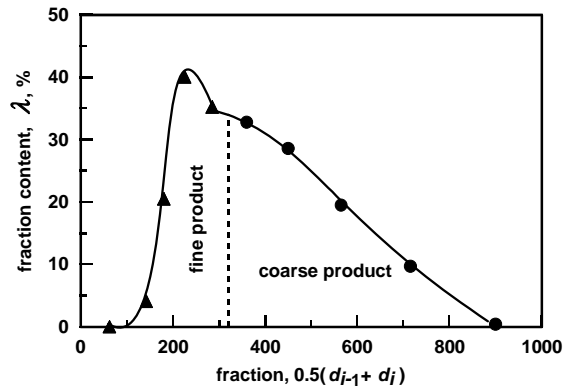
c

Fig. 2.45. Evaluation of separation treated as classification by means of frequency curves. a) no separa-
tion, b) partial separation, c) ideal separation (data from Table 2.19)

The frequency curves as basic classification curves contain all needed information about considered separation. Their shape allows to evaluate the examined process in comparison to the lack of classification and ideal classification. For instance the degree of superposition of curves can be used as a measure of separation (Fig. 2.45b). When separation does not take place the frequency curves for the feed and two products are identical (Fig. 2.45a). In the case of partial separation, the area of superposition of the curves for the coarse and fine products (marked with the asterisks) is smaller than that for the lack of separation (Fig. 2.45b). Thus, the selectivity of separation is the higher the lower degree of superposition of the frequency curves. For ideal classification the curves do not overlap (Fig. 2.45c) and the line for the second product starts at a certain feature value c when the frequency curve for the first product comes to its end.

In some cases, especially when analyzing screening and hydraulic separation, the frequency curves are deformed due to the use of the analytical sieves changing their size in a geometrical progress due to screen module, the points representing small particles becomes considerably compact on the abscissa. Then, it is better to drawn the frequency curves in a semi logarithmic form, i.e. to plot the size of particle on the logarithmic scale.

There are several disadvantages of frequency curves. The most obvious is the dependence of the curve shape of the on the size (width) of the fractions. Therefore, the comparison of different frequency curves requires the use of the same fraction sizes. Another difficulty results from the necessity of considering two frequency curves for one separation test. It makes the frequency curves unpopular and therefore they are seldom applied.

2.2.3.2.2. Distribution curve

The distribution curves are cumulated frequency curves. They express a relation between cumulated content of the component and the value of the feature used for separation, i.e. $\Sigma\lambda$=f(c). If the feature is the particle size, the distribution curve is called the particle size distribution curve. It should be noticed that in some works, the term fraction yield is used instead of fraction content in a product, especially when the content is determined using particle size analysis based on weighing the fraction. This is not recommended (Sztaba, 1993) and the problem has already been explained in subchapter 2.2.3.1.

In order to draw a distribution curve one should plot on the diagram the cumulated contents of subsequent fractions, starting from the smallest one, using as the feature value the upper value of the considered fraction. In the same way we plot the data for the feed and for other products on the same diagram. This means that distribution and frequency curves do not have the same x axis since the frequency curves is based on the mean value of the considered fraction feature while the distribution curve uses the upper value of the fraction feature. Table 2.21 shows the data needed for drawing dis-

tribution curves for the discussed example of screening in which the yield of the fine product was 67.9%.

Table 2.20. Data for drawing distribution curve.
Yield of the coarse product was $\gamma_G = 32.1\%$ and yield of fine product was $\gamma_D = 67.9\%$

Size fraction μm	Content of fraction in feed	Cumulated content of fraction in feed	Content of fraction in coarse product G	Cumulated content of fraction in coarse product G	Content of fraction in fine product D	Cumulated content of fraction in fine product, D
k_i	α_i, %	$\Sigma\alpha_i$, %	λ_{iG}, %	$\Sigma\lambda_{iG}$, %	λ_{iD}, %	$\Sigma\lambda_{iD}$, %
0–125	0.01	0.01	0	0	0.015	0.010
125–160	2.45	2.46	0	0	3.61	3.62
160–200	12.32	1478	2.51	2.51	16.96	20.58
200–250	24.05	3883	8.39	10.90	31.45	52.03
250–320	21.16	59.99	16.21	27.11	2350	75.53
320–400	13.12	73.11	16.02	43.13	11.75	87.28
400–500	11.45	84.56	19.66	62.79	7.57	94.85
500–630	7.78	92.34	16.54	79.33	3.64	98.49
630–800	3.86	96.20	9.42	8875	1.23	99.72
800–1000	3.80	100.00	11.25	100.00	0.28	100.00

Figure 2.46 shows the distribution curves for the considered example for the feed and for both products of separation. However, for assessment of the results it is enough to plot either the curves for one product and the feed or for the two products.
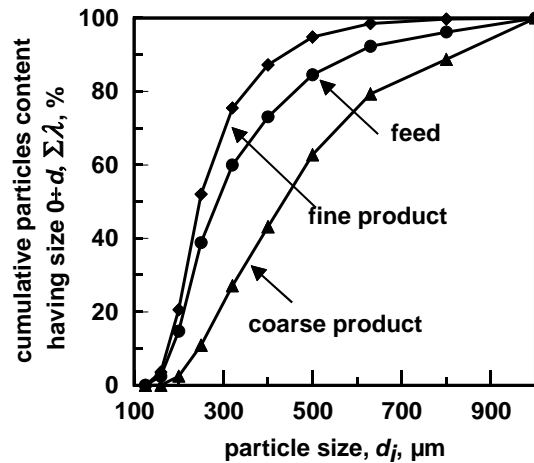
Fig. 2.46. Distribution curves. In this case the curves represent particle size, therefore they can be called the particle size distribution curves. The curves are cumulative. They can also be plotted as descending lines by cumulating, starting from the coarsest product
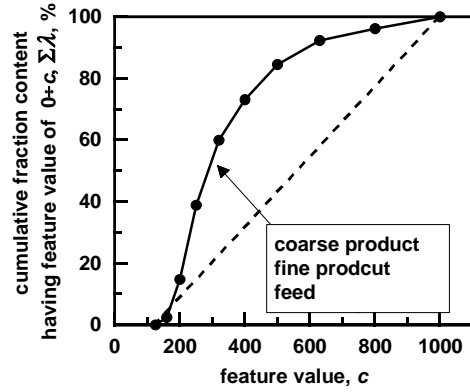
a
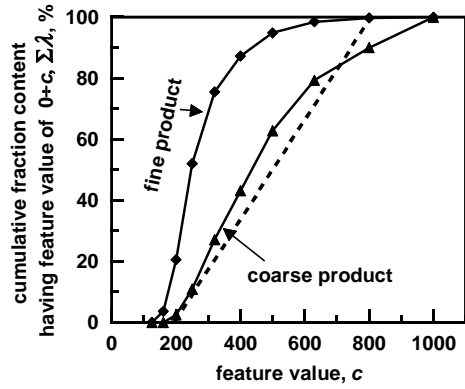
b
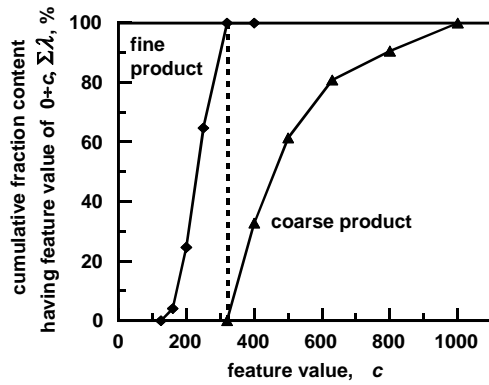
c

Fig. 2.47. Evaluation of separation treated as classification relies for instance on comparing either the shape of distribution curves for two products or the slope of line connecting the last fraction of the fine product with the first fraction of the second product. a) no separation, b) real separation, c) ideal separation. For cumulative curves c is represented by the upper value of the fraction range

Evaluation of separation on the basis of the distribution curves is done by comparing the shape of the product curve with the curve for the feed and with ideal and no separation lines (Fig. 2.47). When the separation does not take place, the distribution curves for the products are the same as for the feed. In the case of ideal classification, one of the products contains only particles up to a certain feature value and another product contains particle having greater feature value. It should be noticed that the measure of separation can be the slope of the line linking the last fraction of the first product with the first fraction of the second product. It was shown in Fig. 2.47 in the form of a broken line.

Sometimes the distribution curves are modified by plotting them on graphs having one or two logarithmic axes. The logarithmic plotting is useful when the points reflecting the feature in the range of low values are very close (Kelly and Spottiswood, 1982).

The distribution curves can also be presented in a linearized form. To make them linear different mathematical functions can be used. There are many available functions and some of them are shown in Table 2.21. More details on linearizing distribution curves can be found in the works by Sztaba (1993), Malewski (1981), Laskowski et al. (1977), and Kelly and Spottiswood (1985).

Table 2.21. Selected functions applied for linearization of size distribution curves. c denotes value of the feature, n is a constant ($n = 1+6/s$). s denostes a constant of the linearized equation of particle size distribution according to Weibull. After Kelly and Spottiswood, 1985

Name	$\Sigma\lambda$ (%)/100% = (cumulative content (%)/100% of fraction for a given c)	Meaning of $c*$
Rosin–Rammler or Weibull	$1 - \exp[-(c/c*)^s]$	c value at $\Sigma\lambda = 0.632$
Gates–Gaudin–Schumann	$[c/c*]^n$	maximum c value
Broadbent–Callcott	$1 - \exp[-(c/c*)]/(1 - \exp(-1))$	maximum c value
Gaudin–Meloy	$1 - [1 - (c/c*)]^n$	maximum c value
Log-probability	erf $[\ln(c/c*)/\sigma]$, erf – error function, σ – geometric standard deviation	median c value
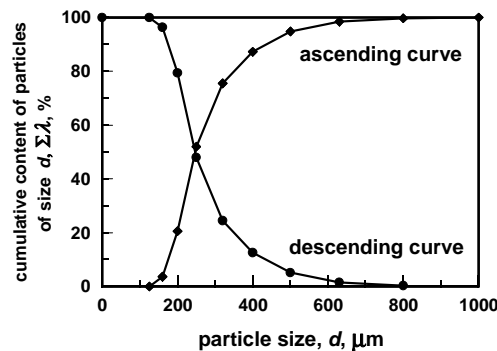
Fig. 2.48. The distribution curve can be plotted either as ascending or descending function

The distribution curves can be drawn either as ascending or decreasing lines (Fig. 2.48). To have then in an descending form the content of particular fractions should be cumulated starting from the last, that is largest, fraction.

2.2.3.2.3. Partition curve

The partition curve is another kind of classification curves. It expresses the relation between recovery of a particular fraction and the value of property which is the basis of separation or the quantity proportional to it. Generally, separation curve can be written as: $\varepsilon = f(c)$. It is also called the recovery–property, Tromp, distribution, affectivity, performance, probability, and classification curve. The example of the partition curve for the coarse product from Table 2.18 was drawn in Fig. 2.49 where both ideal separation and lack of separation lines were added. The particle curve for the fine product is a mirror image of the curve for the coarse product and therefore it is usually not plotted.
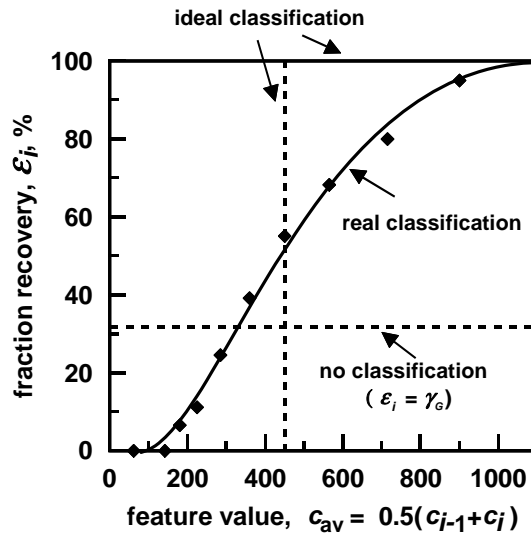
Fig. 2.49. Partition curve

The easiest way of making the partition curves is drawing them on the basis of classification mass balance. The partition curve can also be drawn starting from the frequency curves, since both partition and frequency curves are non-cumulated and have common x axis, that is c_{av}. The recovery of a particular fraction can be calculated using the well known expression:

$$\varepsilon_{ci\ av} = \gamma \lambda_{ci\ av} / \alpha_{ci\ av} \qquad (2.25)$$

where i denotes a fraction, reading off from the frequency curve the values of content $\lambda_{ci\ av}$ of fraction i in the product as well the values of the content of the same fraction in the feed $\alpha_{ci\ av}$. γ values should be taken from the mass balance.

Calculation of the partition curve from the distribution curves is not easy because both curves have different scales. The distribution curve, being cumulative, is based on the upper value of the feature utilized for separation of a particular fraction, while the partition curve, as non-cumulative, utilizes the mean value of the fraction feature. Then, it is convenient to plot both scales (Fig. 2.50) of feature value, i.e. the mean and upper value of the fraction feature and properly read from them the λ and α values (Sztaba, 1993).

The partition curves usually deal with one classification product. The partition curves shown in Fig. 2.49 and Fig. 2.50 represent the data for the coarse product, based on the balance shown in Table 12.18. When the partition curve is plotted for the second (here fine) product, one obtains a reversed (decreasing) curve which is shown in Fig. 2.51. It results from the figure, that the partition curves feature specific property: they cross at a location called the cut point, which indicates at which feature value the probability of particle (phase, drop, etc.) transition to one of the two separation product is the same and is equal to 50%. In the case of particle size, the point is called the cut size. Partition curves are simple in construction and easy to use, therefore they are widely applied in mineral processing.
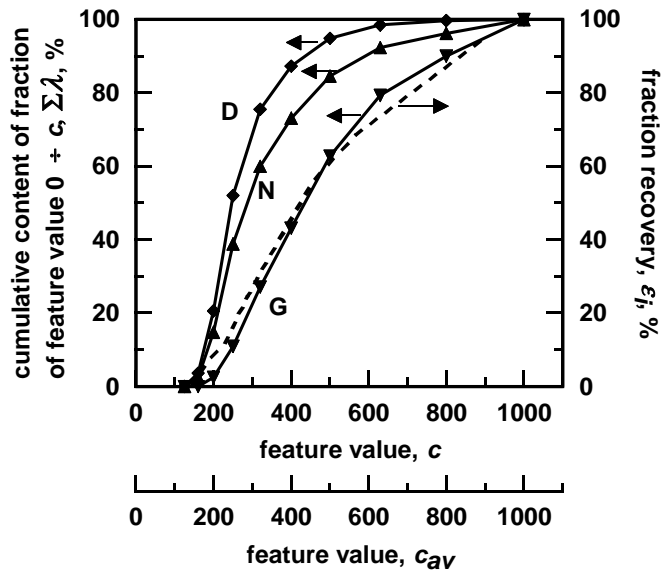
Fig. 2.50. Partition curve (solid line) and distribution line (dashed line) plotted in the same graph. The partition curve is a function of c_{av}
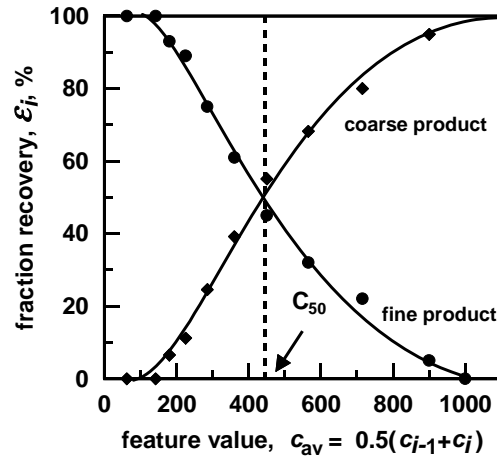
Fig. 2.51. The partition curve can be plotted for one product only because the curve for the remaining material is its mirror image (in relation to line ε=50%)

2.2.3.2.4. Modified classification curves

Sometimes the shape of the partition curve is complex, as it is shown in Fig. 2.52.
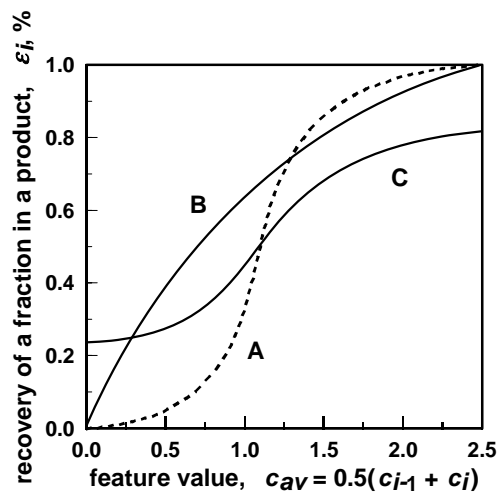
Fig. 2.52. Partition curves for normal (A) ineffective (B) and disturbed (C) separation processes

Unusual shape of the partition curve may result from either the nature of the process or inadequate performance of the separation device. Screening deals with particles having sizes similar to the screen openings which can blind them. The particle with sizes from 3/4 to 3/2 of the sieve or screen (Sztaba, 1993) are considered as difficult-to-screen particles. For hydraulic classification in hydrocyclones there exists a phe-

nomenon called imperfection, caused by grains, especially the finest and the largest, which pass through the device without any separation. This makes the partition curves flat which does not asymptotically approach zero at the far end of the *x* axis. Instead it reaches a plateau at a finite value of the recovery. In order to take this phenomenon into account the partition curves are corrected (Fig. 2.53) to obtain modified partition curves.

The real and modified partition curves can be presented in a reduced form by expressing the feature value in a relative form, for instance in relation to the cut point (c_{50}). A reduced partition curve is shown in Fig. 2.53c. The modification of the complex partitions curves allow to compare different separation systems.

a

b

c
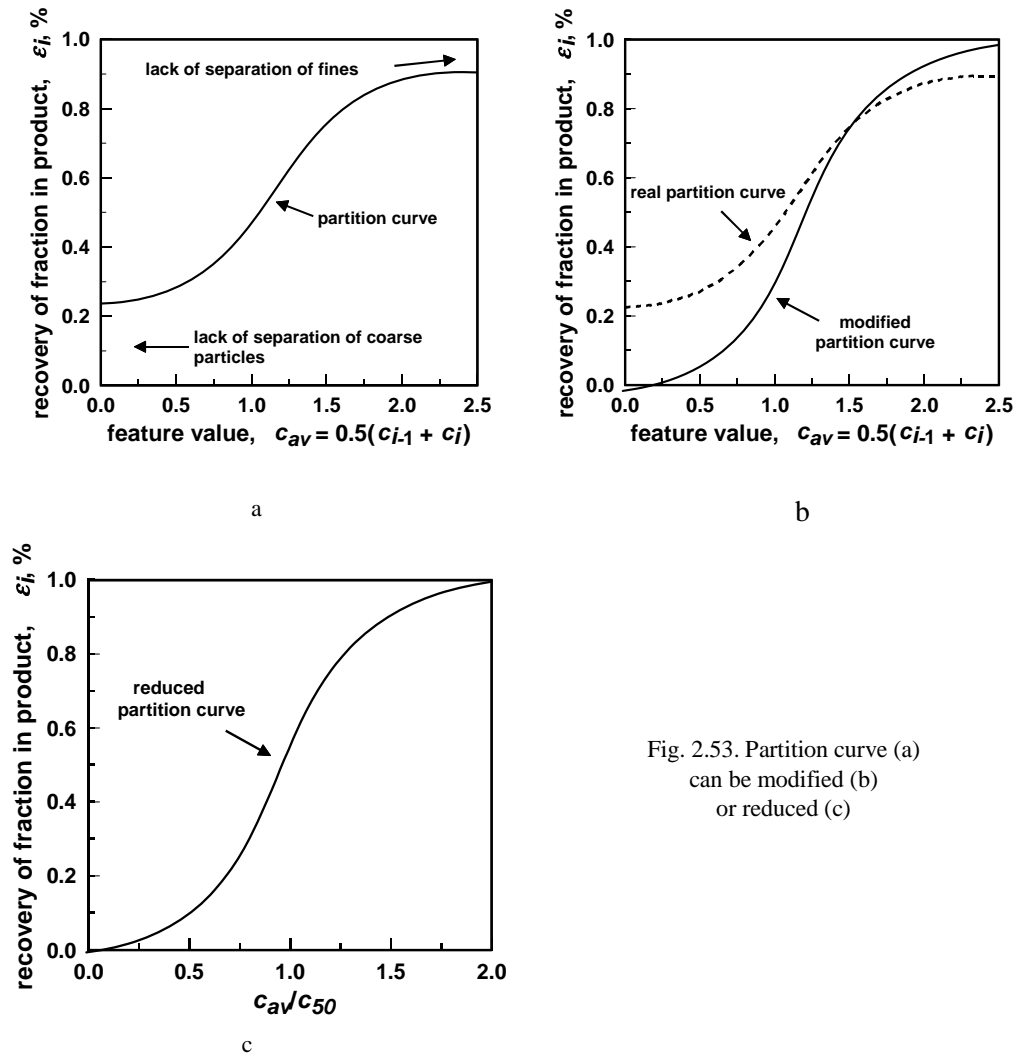
Fig. 2.53. Partition curve (a)
can be modified (b)
or reduced (c)

2.2.3.2.5. Other classification curves

There is infinite number of classification curves based on λ, taking into account also γ and α. They can be generated in a similar way as the upgrading curves. One of the families of the classification curve can is generated by means of the formula $\gamma^a \lambda^b / \alpha^c$, where a, b, c are equal to ....2, 1, 0, -1, -2.... Some of them, after Konapacka and Drzymala (2002), are presented in Fig. 2.54.

a) $\lambda\gamma/100$

b) $\Sigma\lambda(\gamma)/100$

c) λ/γ

d) $\Sigma\lambda/\gamma$

e) λ/α
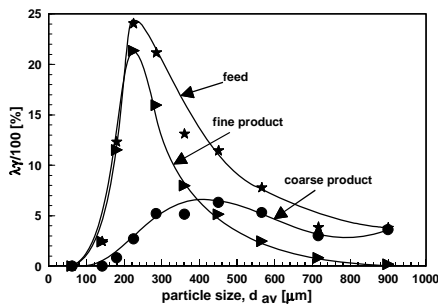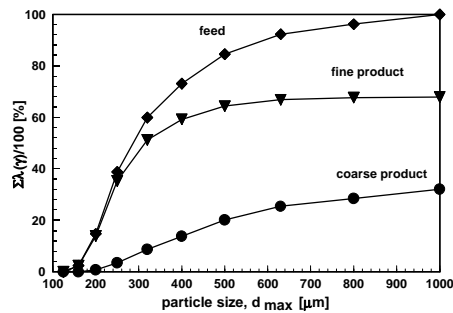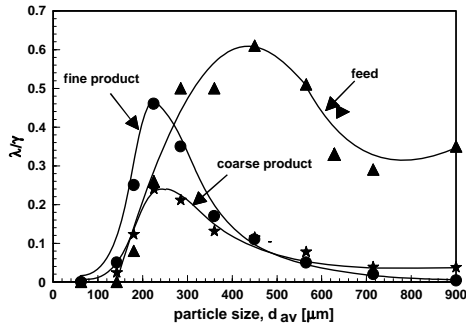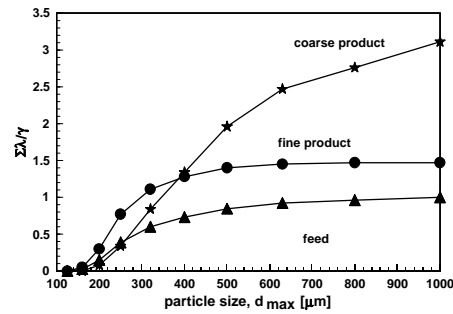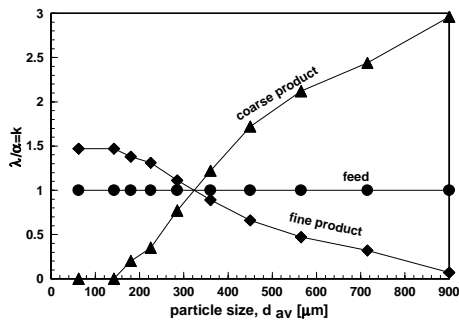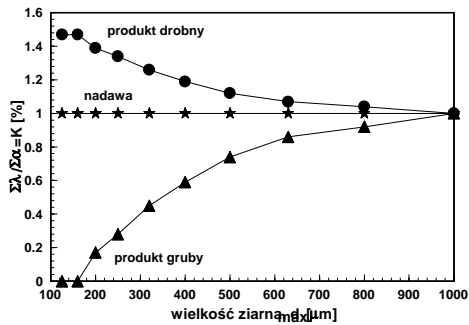
f) $\Sigma\lambda/\Sigma\alpha$
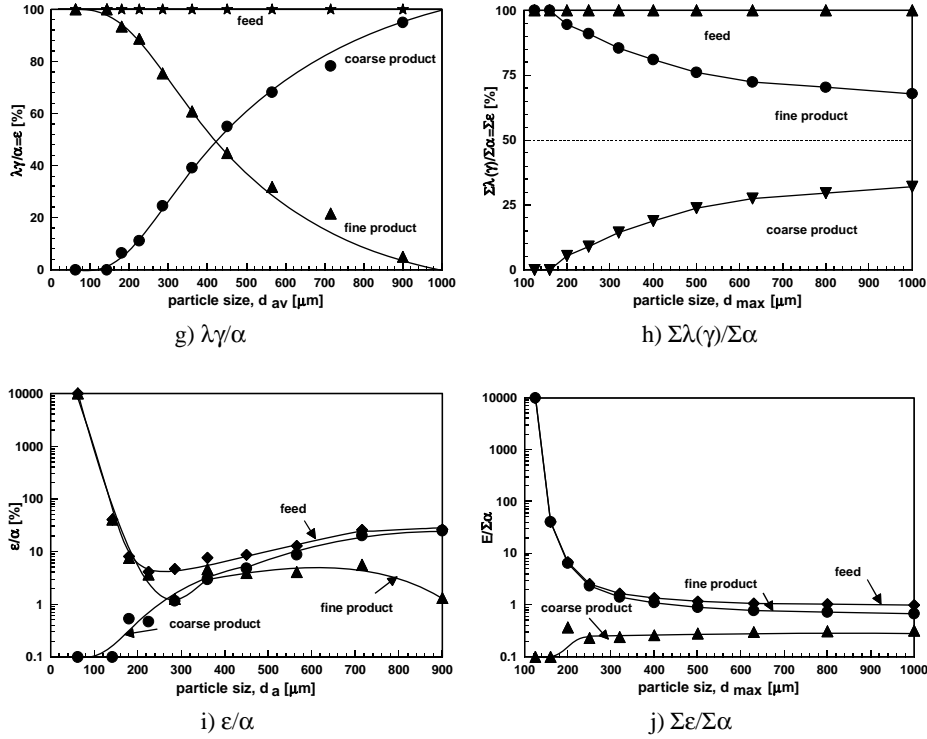
Fig. 2.54. Selected classification curves based on parameters generated by formula $\gamma^a \lambda^b / \alpha^c$. Figures a, c, e, g and i are non-cumulative plotted against d_{av} and b, d, f, h, and j cumulative plotted against d_{max}. After Konopacka and Drzymala (2002).

2.2.3.3. The assessment of separation considered from classification

point of view

The classification curves represent, in a graphical form, separation results. The graphs are very useful because they can be used for prediction of the results situated between the experimental points. Although the classification curves well characterize separation, sometimes it is not easily to compare different sets of data especially when they assume complex shape. Therefore, different methods have been worked out, such as mathematical formulas and procedures, which help to approximate the curves with appropriate formulas, including linearization of the curves. Other approaches consist in calculating different parameters of the separation, usually called indicators. In the case of the partition curves, usually different mathematical functions are used. One of them is the Weibull function (Wills, 1985):

$$y(x) = 100(y_0 + a \exp (-(x - x_0)^{b/c})), \tag{2.26}$$

where: x_0, y_0, a, b, c are constants which have to be determined separately for each curve.

A disadvantage of this function is that it has too many constants. Its advantage is that it can be used for approximation of any partition curve, a feature desired for separation modeling. Another, much easier and simpler method is a direct approximation of the partition curve with a straight line passing through the cut point (ε=50%) and determining the parameters of the line. Still another procedure involves determination of the so-called probable error or E_p, which is the measure of the partition curve slope in the vicinity of c_{50}, where the partition curve can be easily approximated by a straight line. The E_p factor is expressed by the relation:

$$E_p = (c_{\varepsilon = \text{usually } 75\%} - c_{\varepsilon = \text{usually } 25\%})/2. \tag{2.27}$$

Probable error is of the dimension of the analyzed property, which has been used for separation. For ideal separation E_p is equal to zero while for lack of separation it is infinite. The E_p values for normal separation depend on the method applied. A complete characteristics of the separation curve requires two factors and in the case of using E_p from the partition curve the second one can be the cut point value c_{50}.

Instead of the probable error one can determine separation sharpness also called the separation factor, which is defined as:

$$O = \text{sharpness of separation} = c_{\varepsilon = \text{usually } 75\%}/c_{\varepsilon = \text{usually } 25\%}. \tag{2.28}$$

Thus, mathematically the partition curve is usually described with two or more parameters, though theoretically one-fitting-parameter equations also exist. It should be noticed that a meaningful analysis, and then assessment of separation results treated as classification, requires at least two parameters. One parameter may be based on the partition curve (E_p, d_{50}, linearization constants, fitting constants, etc.) while the second can one is yield or a parameter based on yield. Using smaller-than-necessary number of parameters of separation makes the characteristics of a separation system incomplete. Thus, similarly to upgrading, more than one parameter is needed for full characterization of separation results and any hypothetical ideal one-parameter factor (classification degree I_k) does not exist. In the case we somehow find a one-adjustable parameter equation combining the two used for separation characterization parameters (for instance d_{50} and γ), we still need two elements for characterization of separation, that is the new one-adjustable parameter and the equation itself.

In some works the result of separation are presented in such a way that they suggest that a certain one-parameter factor is sufficient. In fact such works contain a second hidden factor, whose role is omitted. It is usually the yield of the considered product.

In the case of the frequency curves, different classification factors can be determined from them. One is the degree of superposition of the frequency curves for both products. From the distribution curves it is possible to calculate a factor characterizing

the slope of the straight line connecting the last fraction of the first product with the first fraction of the second product. If distribution curves are subjected to mathematical processing, the parameters of the equations are also classification factors. In the case of partition curves the factors are the following pairs: probable error E_p and c_{50}, separation sharpness O and c_{50} or other pairs. The modified classification curves also have their own factors and thus the number of pairs which can be used for characterization of separation as classification is unlimited. Selected classification factors are shown in Table 2.23. They are the factors determined from the classification curves. Additional factor is either yield or yield-based parameter.

Table 2.22. Selected indices (besides yield or equivalent) of separation treated as classification

Type of classification curve	Indices of separation	Remarks
Frequency $\lambda = f(c)$	S, x	S – degree of superposition of the curves for products x – index to be determined
Distribution $\Sigma\lambda = f(c)$	M, x k, c^*	M – slope of line connecting last fraction of first product and first fraction of the second product x – index to be determined k – constants s, n or σ from Table 2.21 c^* – constant equal to a selected feature value
Partition $\varepsilon = f(c)$	E_p, c_{50} O, c_{50}	E_p – probable error c_{50} – cut point O – sharpness of separation

2.2.3.4. Classificability and ideal classification

Separation processes are not ideal as their results are effected by the property of the material, the design and performance of the separating device, and other factors such as the skills of people operating the device (Fig. 2.55). Sometimes we want to know what would be the separation if the separation considered as classification depended only on the properties of the feed. Such a property can be called classificability. The term classificability, is analogous to the pair of terms upgrading and upgradeability. In spite of logical correctness of the term classificability, it is not frequently used.

 Ideal classification is when not only the device and operating procedure but also the material subjected to separation itself do not affect the separation analyzed as classification. Usually it requires a full liberation of particles. In the case of separation according to the size of particles there usually takes place full liberation of particles. However, when the particles stick to each other, due to, for instance, moisture or oil present in oil agglomerates, the classificability and ideal separation are different.

There are many features utilized for separation, and therefore there are many methods which can be used to determine classificability and ideal classification. In the subsequent subchapters particle size and densimetric analyses will be discussed. The particle size analysis is the most often used technique for determining classificability of

particles when size as the separation feature is involved. Densimetric analysis allows to determine classificability in relation to particle density.

Fig. 2.55. Schematic explanation of the difference between classification and classificability
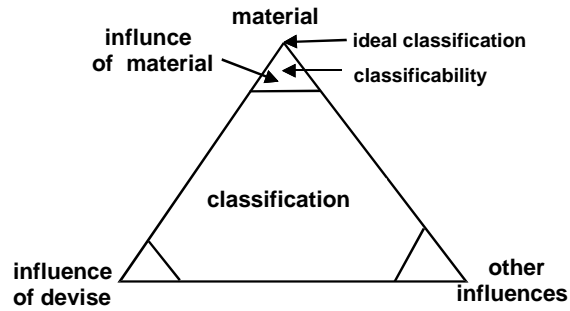
2.2.3.4.1. The particle size analysis

Particle size analysis is an analytical procedure for determination of particles distribution according to their size. The procedure is useful for evaluation of size classificability of particulate materials subjected to separation into products in different screening devices, as well as for comparing the results of different separations. The particle size analysis, the procedure which should be based on approved testing standard methods, relies on screening a sample of grainy material through a set of the laboratory analytical sieves (Fig. 2.56a). The sieves are arranged as a column according to the increasing size of the sieve openings with the largest mesh on the top (Fig. 2.56b). To facilitate classification according to particle size the sieves are shaken.

a   b

Fig. 2.56. Analytical sieves a) individual sieves, b) stock of sieves

The particle size analysis for the particles up to about 75μm is usually conducted as a wet classification. In order to standardized the tests to be able to compare directly the resulting particle size frequency curves (histograms), which are based on the particle size analysis, the sieves having appropriate mesh size should be used. In Polish mineral processing industry it is recommended for particle size analysis to use square mesh sieves which ratio of the openings of the neighboring sieves is $\sqrt[10]{10} = 1.259$ *or* $\sqrt[20]{10} = 1.122$, which is also called the sieve modulus. The two numbers represent two series of sieves and are termed R-10 and R-20, respectively (Sztaba, 1993). The sieve mesh sizes (aperture), for both series, are presented in Table 2.23.

Table 2.23. Aperture of analytical sieves according to Polish Standards (PN-86/M-94001) for particle size analysis

APERTURE mm		APERTURE mm		APERTURE mm		APERTURE mm	
Modulus ~1,26	Modulus ~1,12 / Modulus ~1,26	Modulus ~1,26	Modulus ~1,12 / Modulus ~1,26 cont.	Modulus ~1,26	Modulus ~1,12 / Modulus ~1,26 cont.	Modulus ~1,26	Modulus ~1,12 / Modulus ~1,26 cont.
0.025		0.25		2.5		25	
	0.028		0.28		2.8		28
0.032		0.32		(3.0), 3.2		(30), 32	
	0.036		0.36		3.6		36
0.040		0.40		4.0		40	
	0.045		0.45		4.5		45
0.050		0.50		5.0		50	
	0.056		0.56		5.6		56
0.063		0.63		(6.0), 63		(60), 63	
	0.071, (0.075)		0.71		7.1		71
0.080		0.80		8.0		80	
	0.090		0.90		9.0		90
0.10		1.0		10.0		100	
	0.11		1.1, 1.2		11.2		112
0.12		(1.25)		12.0, 13.5		(120), 125	
	0.14 (0.15)		1.4		14.0		140
0.16		1.6		16.0		160	
	0.18		1.8		18.0		180
0.20		2.0		20.0		200	
	0.22		2.2		22.0, (224)		

Table 2.24. Results of particle size analysis of a sample

Size fraction μm	Average particle size μm	Size fraction content in the sample	cumulative content of size fractions in the sample
$k_i = d_{i-1} \div d_i$	$d = 0.5(d_{i-1} + d_i)$	λ_i, %	$\Sigma\lambda_i$, %
0–125	62.5	0.01	0.01
125–160	142	2.45	2.46
160–200	180	12.32	14.78
200–250	225	24.05	38.83
250–320	285	21.16	59.99
320–400	360	13.12	73.11
400–500	450	11.45	84.56
500–630	565	7.78	92.34
630–800	715	3.86	96.20
800–1000	900	3.80	100.0

a   b
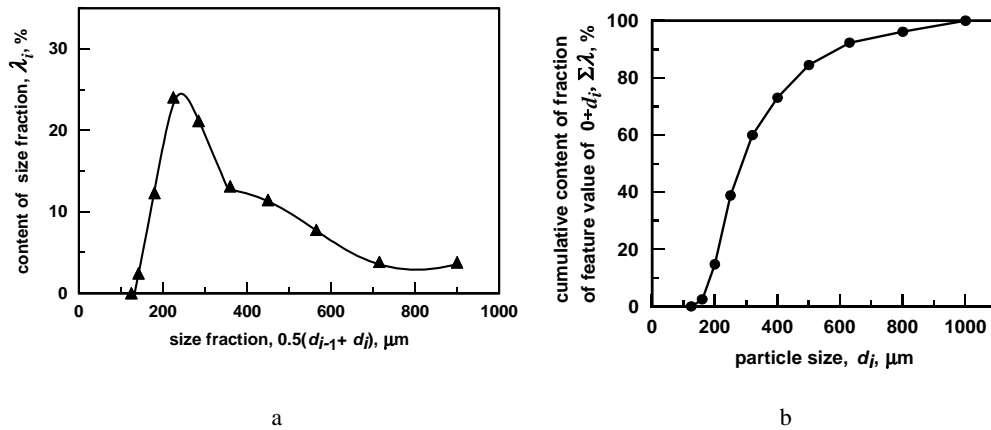
Fig. 2.57. a) Frequency curve (histogram) of particle size distribution for a sample subjected to sieve analysis described in Table 2.24 and b) distribution curve (cumulative histogram) of particle size distribution for a sample subjected to sieve analysis described in Table 2.24

Different standards are recommended in various fields of industry. In civil engineering, according to the Polish standard PN-78/B-06714/15, determination of composition of aggregates requires the following sieves, 0.063; 0.125; 0.25; 0.50; 1.0; 2.0; 4.0; 8.0; 16.0; 31.3 (or 32), and 63.8 mm (Grzelak, 1995). It can be noticed that the sieve module i.e. the ratio of the neighboring sieves size is 2. For road and railway construction slightly different mesh size, namely: 0.75; 0.15; 0.18; 0.25; 0.15; 1.0; 2.0; 4.0; 6.3; 10.0; 12.8; 16.0; 20.0; 31.5; 63.0 mm should be used (Grzelak, 1985).

The results of the particle size analysis can be presented either as tables or diagrams. Typical tabular sieving results are shown in Table 2.24. The results of particle size analysis can also be presented in a graphical form using various particle size distribution curves. Fig. 2.57a shows the frequency curves while Fig. 2.57b shows cumulated frequency curves, that is the distribution curves. The curves representing particle

size distribution can also be plotted in a logarithm form with one or both axes with logarithmic scale. The curves can be also made linear by using appropriate equations discussed in detail in another chapter (Tab. 2.21).

On the basis of particle size distribution for a particular sample it is possible to determine the content of all particle size fractions in the sample, as well as compare the classificability with real classification results obtained in a separator.

Evaluation of the results of separation can be accomplished by plotting the ideal classification curves for the feed based on the content of all fractions in the feed determined by particle size analysis and inserting the points representing the yields of products of separation, e.g. for fine product (0-$d_{\text{sieve in the screening device}}$) and the coarse product ($d_{\text{sieve in the screening device}} - d_{max}$) and the size of screen openings d (Fig. 2.58). The shift of the ideal separation curves in relation to the yield points forming a real separation curve is the measure of the degree of difference between real and ideal screening. The lack of ideal results of screening when using industrial screening devices results from the presence of oversized particles in the fine product and the occurrence of undersized grains in the coarse product.
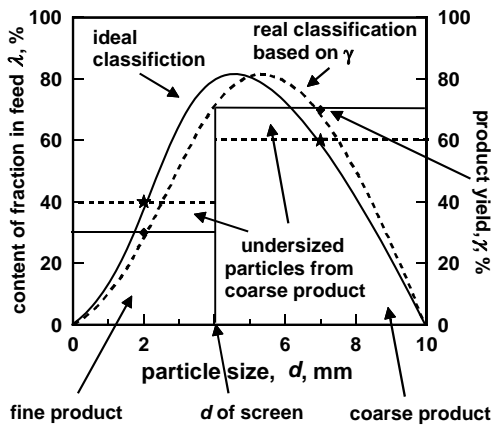
Fig. 2.58. Comparison of frequency classification curve with ideal classification based on particle size analysis for feed and results of real separation in an industrial separator. Only presence of undersized particles in the coarse product was taken into account (oversize particles in the fine product were absent).
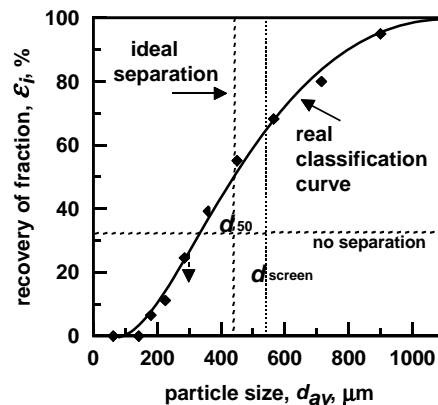
Fig. 2.59. Comparison of real classification curve with ideal one using partition curve as an example

If the feed and selected separation products are subjected to particle size analysis, it is possible to draw the partition curve for this product as well as the no and ideal separation lines, as it has been done in Fig. 2.59. The shift of the partition curve in relation to the vertical line of ideal separation indicates a departure from ideality. Additionally,

there is usually a shift of the d_{50} of the partition curve in relation to the opening size of the screen d_{sieve} used for separation (Banaszewski, 1990).

2.2.3.4.2. Densimetric analysis

In the case of separation based on particle density, the determination of the classificability requires densimetric analysis. It is based on placing samples of the feed and product or products of separation in liquids of different densities. Depending on the density of the liquid the particles will either float or sink. After separation of the floating and sinking fractions, the content of the density fractions in the sample is determined. Having analytical data, appropriate classification curves (see chapter 7.2) can be plotted. Most often the densimetric curves are drawn in the form of the partition curve which for density data usually are called the Tromp curve.

More detail on densimetric analysis is given in another chapter.

2.2.3.5. Summary

The classification mass balance and classification curves, the essence of analysis of separation results in separation systems, combined with the evaluation of separation results, as well as with delineation of the process, provide a meaningful picture of separation as it is schematically shown in Fig. 2.60.
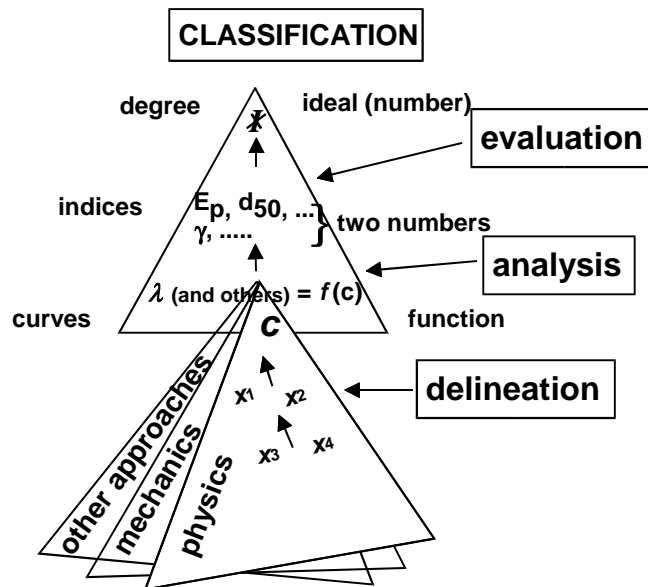
Fig. 2.60. Pictorial summary of separation considered as classification. Classification is based on qualities of products and features of components subjected to separation. The elements of complete characterization of separation as classification include delineation, analysis, and evaluation of separation

2.2.4. Other approaches to separation

As it has been discussed earlier, there are other upgrading approaches that can be used for analysis of separation results than product separation, classification, and upgrading. It can be, for instance, sorting and distribution. They are rarely used in mineral processing, and therefore, they will not be presented in this book. Information on the principles of upgrading analyzed as sorting can be find in Drzymala's paper (2003).

Different approaches to analysis of separation can be combined and considered in sequence or together. Examples of such treatment are classification and upgrading which can be easily combined with the separation-into-product analysis. The classification can be combined with upgrading. The presentation of classification data at different yields of classification products would be an example of combination of classification and upgrading approaches to the analysis of separation data. There is a need for working out the methodology, terminology and symbolism of such complex approaches to separation.

2.3. Delineation of separation

2.3.1. Role of material and separator

Separation takes place when a component of the feed has suitable properties while the separating device provides adequate environment for the process including space, time, and fields. Other factors may also influence separation (Fig. 2.61).
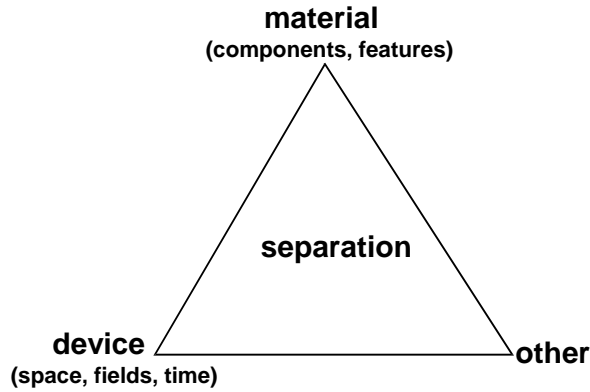
Fig. 2.61. Material provides suitable components and their features for separation while device provides space, time, and fields. Influence of other parameters is also possible

The main task of delineation of separation is to characterize phenomena occurring during separation (Fig. 2.62) as a result of interactions between material and separation device, as well as to determine relationships between process parameters and results of separation. The delineation can be divided into many steps. In this work three steps are distinguished: ordering, stratification, and splitting.
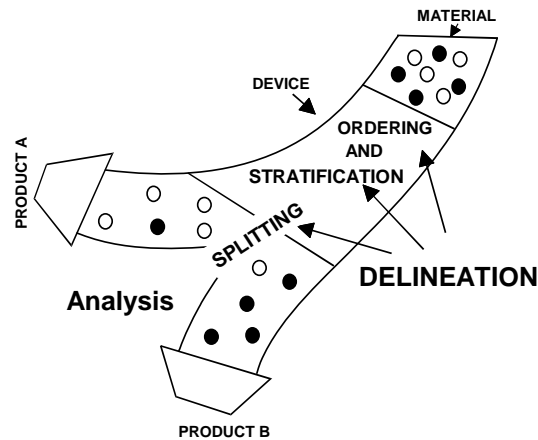
Fig. 2.62. A detailed characteristics of separation requires delineation of phenomena leading to separation and analysis of separation results followed by evaluation

Usually many parameters are needed for meaningful characterization of the material subjected to separation. These parameters are also mutually interrelated. It is possible and convenient to define a parameter, called the main feature (c_m), which is responsible, together with the devise, for creation of ordering forces leading to stratification and splitting forces needed for products formation. Sometimes there are more than one ordering feature (c_o) and force in the considered separation system. Then, it is

convenient to combine the ordering features into one general parameter (main feature) c_m of separation which can be related to the results of separation such for instance recovery and yield.
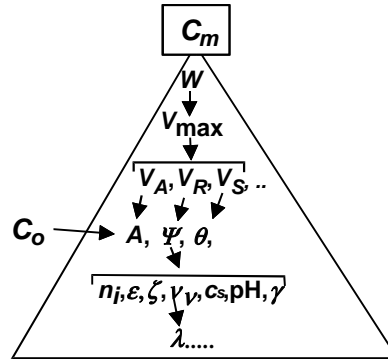
Fig. 2.63. The main parameter c_m of separation is based on other parameters of separation system including ordering features (c_o). They form a pyramid. Meaning of symbols is given in the text on coagulation

A well defined main feature c_m depends on other parameters forming a pyramid–like structure (Fig. 2.63). The main parameter can be a simple factor, like surface charge per unit mass, but it can also be a complex parameter as the stability ratio W important for coagulation of fines in water. The stability ratio depends on energy barrier V_{max} between particles, which, in turn, depends on dispersion (A), electrostatic (R) and structural (S) interactions (forces) between particles resulting from the ordering features (c_o): Hamaker constant (A) electrostatic potential (Ψ) and hydrophobicity θ which depend on still other factors (Fig. 2.63). The way of combining parameters into main feature results from the specificity of the separation system.

As it has been already mentioned, separation process is possible only when particles differ in properties. The features utilized for separation can be natural or it can be induced by special treatment of particles. The categorization of features of particles according to their ability of modification is shown in Table 2.26.

Table 2.25. Categorization of features of particles according to their ability to modification

	Typical particle feature	Class	Property
Modifiability	size	I	completely modifiable, does not or seldom exists as natural feature
	hydrophobicity aquaoleophilicity electrical charge coagulation index size reduction index	II	partially modifiable, exist as natural feature
	volatility dielectric constant density magnetic susceptibility	III	unmodifiable without deep chemical change, feature usually natural

For a meaningful delineation of separation we need to know the main feature, important mutual relations between features of the material, reaction of the material to the space, time, and fields provided by the separator, and finally the characteristics of the splitting forces. These issues will be discussed in the subsequent chapters.

2.3.2. Ordering

The requirement for separation is the appearance of a force which leads to particles ordering. The ordering force is a result of interaction of features of components of the feed and the fields provided by the separating device. The ordering force acts on the components of the feed creating their movement leading to ordering of particles in the separator. Usually, there are more than one force acting in the separation system. Therefore, the first step in delineation of separation is making inventory and balance of the essential forces acting in the system.

The balance of forces can be performed using not only forces (mechanics) but also parameters related to the force such as energy (thermodynamics) and probability (Fig. 2.64). Other approaches and their combinations are also possible.
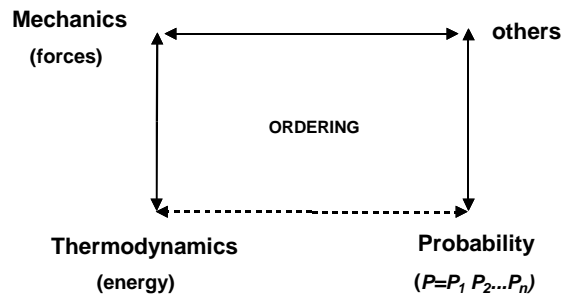
Fig. 2.64. Typical approaches to delineation of separation include mechanics, thermodynamics and probability

In the following chapter the mechanics, thermodynamic, and probability of particles ordering as a part of delineation of separation are presented.

2.3.2.1. Mechanics of ordering

Mechanical description of separation processes is based on the balance of forces acting in the system and resulting trajectory of a particle in a separator. For instance, Urvantsev (2000) considered the movement of electrically charged particles in electrical field. No force ($F_g = 0$) was acting on particles along the y axis and the particle was falling with a constant speed V_y presumably due to equality of the gravity force and resistance forces. In the horizontal direction (x) there was an electrical force $F_{el,x}$ acting on the particle due to electric field E_{el} because $F_{el} = qE_{el}$. As a result of forces action, the trajectory of the falling particle was parabolic, as is shown in Fig. 2.65.
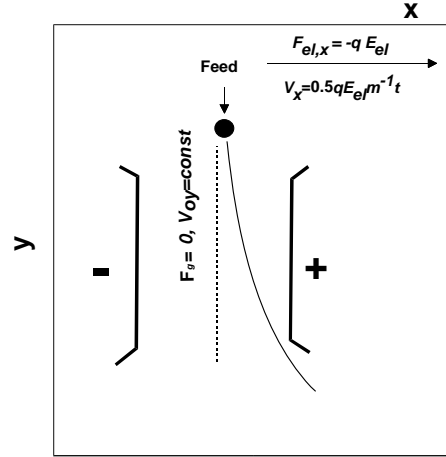
Fig. 2.65. Trajectory of charged particles in electrical field. Case considered by Urvantsev (2006)

The balance of forces indicates that a falling particle will change its position in relation to the *x* and *y* axis with the time of movement *t* according to the equations:

$$x = \frac{1}{2}at_x^2 = \frac{1}{2}\frac{qE_{el}}{m}t_x^2 \qquad (2.29)$$

$$y = V_y t_y \qquad (2.30)$$

Elimination of time ($t_x = t_y$) from Eq. 2.29 provides parabolic trajectory of the particle:

$$x = \frac{1}{2}\frac{q}{m}\frac{y^2}{V_y^2}E_{el} \qquad (2.31).$$

The ordering feature utilized for separation is electrical charge of particle *q* because $F_{el} = qE_{el}$, while the main feature is charge of particle per particle mass that is *q/m* (Eq. 2.29). The separator facilitates electrical field E_{el} and constant V_{oy} speed of the falling particle, as well as the space (*x, y*). More details on ordering of particles are provided in Table 2.26.

Table 2.26. Force balance, condition of separation and trajectory of a particle, and other details of the case of electrical separation considered by Urvantsev (2000) (*g* - gravity, *o* – resistance, *el* – electrical, *F* – force, *E* – field, *x*– distance, *y* – distance, *V* – velocity, *m* – mass, *q* – electrical charge, *t* – time)

Step	Equations
Force balance	$F_{g,y}=F_{o,y}$; $F_{el,x}$ ($V_y=y/t_y=$ cont; $V_x=x/t_x=0.5qE_{el}m^{-1}t_x$)
Condition of separation	$t_y = t_x$

Ordering equation (trajectory of particle)	$x = \dfrac{1}{2}\dfrac{q}{m}\dfrac{y^2}{V_y^2}E_{el}$
Ordering force Ordering feature Main feature	$F_{el,x}=qE_{el}$ electrical charge q electrical charge per unit mass, q/m
Fields	gravity (E_g), electromagnetic (E_o, E_{el})
Space and time	x, y, t

Separation into floating and non-floating particles by a procedure called flotometry (Drzymala and Lekki, 1989; Drzymala, 1999) can serve as another example of balancing forces for calculation of particles ordering. The flotometry is designed to provide the maximum size of floating particles needed for determination of their hydrophobicity. Thus, it is based on separation of particles into floating and non-floating products. The balance of forces is made for the moment when the particle is too heavy for flotation and starts to detach from the gas bubble (Figs. 2.26, 2.27):
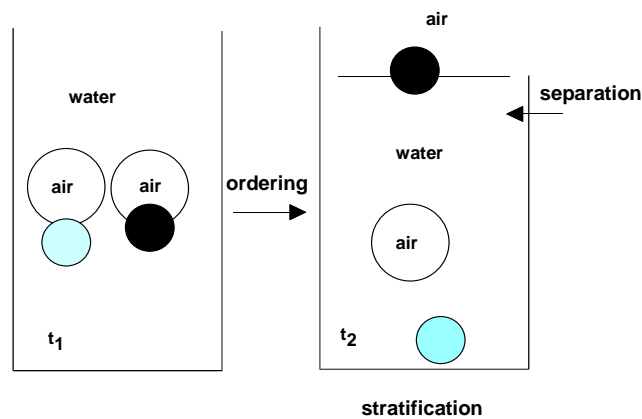
Fig. 2.66. Ordering of particles in flotometry
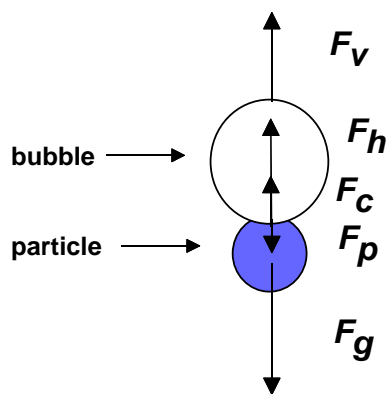
Fig. 2.67. Balance of forces in flotometry

$$F_{c\,(max)} - F_g + F_v - F_p + F_h + F_x = 0, \tag{2.32}$$

where:

$F_{c(max)}$ – maximum capillary force at the moment of particles detachment from bubble
F_g – weight force of particle in the air
F_v – buoyancy force (weight of particle in water is : $F_g - F_v$)
F_h – hydrostatic pressure force acting on grain at the point of bubble attachment
F_p – additional pressure inside bubble
F_x – additional external force if such a force is acting in the system.

After substitution appropriate expressions for each force (Drzymala, 1999), that is:

$$F_{c\,(max)} = \pi\, r_p \gamma_{lv}\,(1 - \cos\,\theta_d), \tag{2.33}$$

$$F_g = (4/3)\pi\, r_p^{\,3}\rho_p\, g, \tag{2.34}$$

$$F_v = \pi\, r_p^{\,3}\rho_w\, g\{(2/3) + \cos\,(\theta_d/2) - (1/3)\cos^3\,(\theta_d/2)\}, \tag{2.35}$$

$$F_p - F_h = \pi\, r_p^{\,2}(1 - \cos\,\theta_d)\,(\gamma_{lv}/R - R\rho_w\, g, \tag{2.36}$$

the flotometric equation is obtained:

$$\pi\, r_p\, \gamma_{lv}\,(1 - \cos\,\theta_d) - [(4/3)\pi\, r_p^{\,3}\rho_p\, g - \pi\, r_p^{\,3}\rho_w\, g\{(2/3) + \cos\,(\theta_d/2) - (1/3)\cos^3\,(\theta_d/2)\}] -$$

$$-\pi\, r_p^{\,2}(1 - \cos\,\theta_d)\,(\gamma_{lv}/R - R\rho_w\, g) - F_x = 0, \tag{2.37}$$

which, after measuring the maximum radius of floating particle, can be used for determination of the hydrophobicity θ_d of a particle. In Eq. 2.37:

r_p – particle radius
γ_{lv} – liquid surface tension
ρ_p – particle density
ρ_w – water density
g – acceleration due to gravity
θ_d - the angle of detachment of particles from bubble (a measure of hydrophobicity called the contact angle)
R – bubble radius
π =3.14.

Equation 2.37 determines the trajectory of particles. It contains the main parameter (a complex combination of θ_d, γ_{lv}, r_p, and ρ_p), fields provided by the device (g, γ_{lv}, R) and space parameter y (not explicit). For the left hand term greater than zero, the particle will float wile for the left hand term smaller than zero the particle sinks.

2.3.2.2. Thermodynamics of ordering

The ordering of a particle can also be described using energies and related thermodynamic parameters instead of forces. The transition between mechanical and thermodynamic descriptions of ordering sometimes is simple because energy is a multiplication product of force and distance. An example of equivalence of ordering descriptions using mechanics and thermodynamics is the DLVO theory. The theory was developed by Derjaguin and Landau and independently by Verwey and Overbeek. Derjaguin and Landau used a balance of forces for delineation of coagulation while Verwey and Overbeek used energy. In many cases the transition between mechanical and thermodynamic descriptions of ordering is difficult.

Different thermodynamic parameters can be used for delineation of ordering. Most frequently energy is used. It depends on the specificity of separation and is best represented by one of many thermodynamic energies, including internal energy, surface energy, Gibbs energy, Helmholz energy. The balance of energies transferred to a particle determines its trajectory of movement in a separation device leading to ordering of the particle and subsequent reporting to products of separation. The energy transferred to the particles can come from four possible natural fields: weak, strong, gravity, and electromagnetic. The mechanical energy (force) frequently encountered in separation systems is a form of the electromagnetic field (force). The energy transferred to a particle can be recalculated into forces acting on a particle with suitable equations, and then the delineation of ordering can be done by means of forces.

As an example of energy approach to ordering delineation, separation of a surfactant from surface of its aqueous solution (Fig. 2.68) will be considered. Essential elements of ordering in this separation system are presented in Table 2.27.
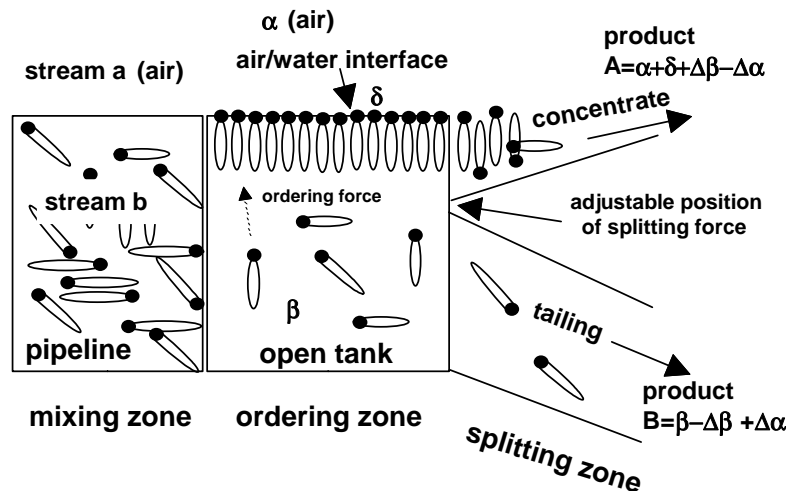
Fig. 2.68. Sketch of hypothetical separation system. $\Delta\beta$ indicates that some of phase β is transferred to concentrate A. Remaining phase β forms tailing B, while $\Delta\alpha$ denotes air. Not to scale. Drzymala (2005a)

Table 2.27. Energy balance, condition of ordering and trajectory of a particle for the case considered by Drzymala (2005a). G – Gibbs energy (free enthalpy), σ – surface tension, Γ - surface adsorption, μ – chemical potential, y - distance, t – time, a –activity (=c f), c - concentration, f –activity coefficient, R - gas constant, T – absolute temperature)

Step	Equations
Energy balance	$\Delta G = \Delta\sigma$
Condition of separation	$t > t_{relaxation}$
Ordering equation (trajectory of particle)	top layer: $$(d\sigma)_T = -\Gamma^s_{surfactant} d\mu_{surfactant} = -RT\,\Gamma^s_{surfactant} d(\ln a_{surfactant})$$ bulk solution: $c_{initial}$ - amount adsorbed $= c_{final} =$ const
Ordering feature	surface equilibrium concentration of surfactant, $\Gamma^s_{surfactant}$
Fields	electromagnetic *(chemical potential, dµ)*
Space and time	surface layer + height of vessel y, equilibrium thermodynamics (time is not a parameter if $t > t_{relaxation}$)

2.3.2.3. Probability of ordering

Some separations are complex due to the presence of many different forces in the system. In such systems not only ordering and neutral forces but also disordering forces, forces preventing some particles from ordering, and forces which send some non-ordered particle into re-ordering exist. Moreover, the ordering forces can be very sensitive to any change of the value of parameters of the system. In such a case, the delineation of particles ordering using either force or energy approach is difficult. Instead, the probability approach can be used. In the probability approach the ordering process is evaluated taking into account disordering forces which make ordering not ideal. For instance adhesion of a bubble to a particle during flotation does not always occur but takes place with a certain probability. It is frequently assumed that this probability is equal to:

$$P_a = \exp\left(-\frac{E_l}{E_k}\right) \tag{2.38}$$

where
P_a - probability of adhesion of a bubble to a particle
E_l – energy barrier for adhesion of bubble and particle
E_k – kinetic energy of collision.

It means that for $E_l = E_k$ there will be only 37 successful attachments per 100 attempts (for $E_l = E_k$, $P_a = 0.367879$).

The probability approach is very useful for complicated separation systems for which the whole ordering and stratification can be split into subprocesses. Each subprocess is usually based on different fields, ordering features, and resulting forces or

group of forces. The probability of the whole ordering process P leading to stratification is the product of probabilities of sub-processes:

$$P = P_1 \cdot P_2 \cdot P_3 \cdot P_n \tag{2.39}$$

The number of subprocesses can be from two to many. For complex separation systems three the most influential subprocesses are usually considered assuming that the probability of remaining subprocesses is 1.

The probability approach is very useful because it can be easily transformed into physical description.

2.3.3. Stratification

Stratification occurs when the separation system contains more than one particle which have different values of the main feature. The approach used for delineation of stratification depends on the system. Considered in the previous chapter 2.3.2.2 the case of ordering of surfactant molecules at the air-water interface, the stratification is simple because there were two different layers: top containing 4.5 μmol/m² of n-octanol (determined by surface tension) and the solution with n-octanol concentration equal to 1 mmol/dm³. In the separation system considered by Urvantsev (2000) (chapter 2.3.2.1) the stratification is much more complex and results from the variation of the sign and value of the main feature (q/m). He assumed that the variation of the feature followed the normal distribution law. The distribution of mineral A (denoted as *h* meaning hematite) in an electrostatic separator, having a tendency to be positively charged and having q/m value near a_h, is shown in Fig. 2.69. The probability density function f_i of the random variable q/m is equal to:

$$f_h = \frac{1}{\delta_h \sqrt{2\pi}} e^{-\frac{\left(\frac{q}{m} - a_h\right)^2}{2\delta_h^2}} \tag{2.40}$$

where:
δ_h^2 – variance for a given distribution curve,
a_h – mean value (expected value of q/m for hematite)
q – surface echarge
m – mass of particle .

Having the number of particles for each q/m value and the position of the splitter it is possible to predict the results of separation. This issue will be discussed in the next chapter.
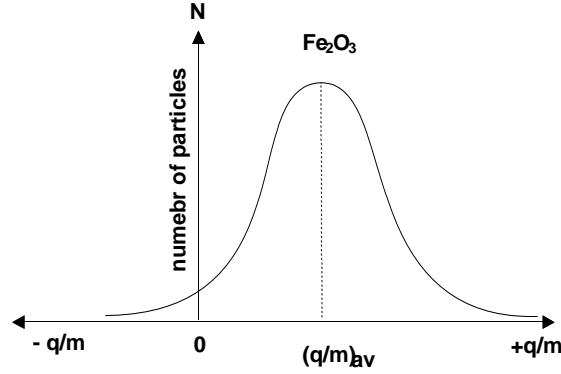
Fig. 2.69. Normal distribution curve for hematite considered by Urvantsev (2000)

Thus, for calculation of the stratification of particles information on distribution of the feature of particles is needed.

2.3.4. Splitting

The stratified particles or molecules can be subjected to splitting into products. In the considered by Drzymala (2005a) case of separation of a n-octanol accumulated at the water-air interface (Fig. 2.68) the amount of surfactant in the concentrate z is a function of the splitter position g:

$$z = \Gamma_{\text{surfactant}}^{\text{H}_2\text{O}} + \frac{c_i V}{P} \frac{g}{h} \qquad (2.41)$$

where:

z – total amount of surfactant per cross section area of tank in concentrate
c_i – concentration of surfactant in bulk solution
V – tank volume
P – tank cross section
h – tank height
Γ – surface concentration of surfactant at water-air interface
g – position of splitter
$g/h = r$, where r is the fraction of tank height at which splitter is located (assumes values from 0 to 1)
ε – recovery (%),
γ – yield (%).

For the considered separation c_i was 10^{-3} mol/dm^3, $V = 1$ dm^3, $P = 1$ m^2, $\Gamma = 4.5$ µm/m^2, $h = 1$ mm (g is a variable) and Eq. 2.41 was reduced to:

$$z = 4.5 + 1.0 \cdot 10^{-3} \cdot r \left(\frac{\mu mol}{m^2} \right). \tag{2.42}$$

The recovery of the surfactant in the concentrate is:

$$\varepsilon = \frac{z}{1004.5} 100\% \tag{2.43}$$

while the yield is:

$$\gamma = r \cdot 100\% . \tag{2.44}$$

Having the result of splitting, the separation (upgrading, sorting, classification, etc.) curves can be plotted. An upgrading curve $\varepsilon/\gamma(=\beta/\alpha)$ vs yield γ of the concentrate in which γ is a measure of splitter position is shown in Fig. 2.70.

In the case considered by Urvantsev (2000) there was separation between quartz and hematite due to electric field. After establishing the trajectory of particle (ordering), then stratification of quartz and hematite, changing the splitter position provides separation results. The equation for recovery of component 1 (quartz) and component 2 (hematite) for a given splitter position K is:
for hematite:

$$\varepsilon_{h,c} = \frac{1}{\delta_h \sqrt{2\pi}} \int\limits_{\left(\frac{q}{m}\right)_K}^{+\infty} e^{-\frac{\left(\frac{q}{m}-a_h\right)^2}{2\delta_h^2}} d\left(\frac{q}{m}\right) \tag{2.45}$$

and for quartz:

$$\varepsilon_{k,c} = \frac{1}{\delta_k \sqrt{2\pi}} \int\limits_{\left(\frac{q}{m}\right)_K}^{+\infty} e^{-\frac{\left(\frac{q}{m}-a_k\right)^2}{2\delta_k^2}} d\left(\frac{q}{m}\right) \tag{2.46}$$

The position (x, y) of the splitter K can be calculated from the equation:

$$x = \frac{1}{2} \left(\frac{q}{m}\right)_K \frac{y^2}{V_y^2} E_{el} \tag{2.47}$$

Having recovery for quartz and hematite, the separation curves, for instance the Fuerstenau plot can be drawn.

Other examples of the influence of the splitter position on separation of stratified materials can be found in the literature. The relations are usually complicated.

○ **ordering force = const, splitting force = const**
● **ordering force = const, splitting force - variable**
∗ **ordering, splitting, mixing, ect. forces - variable**
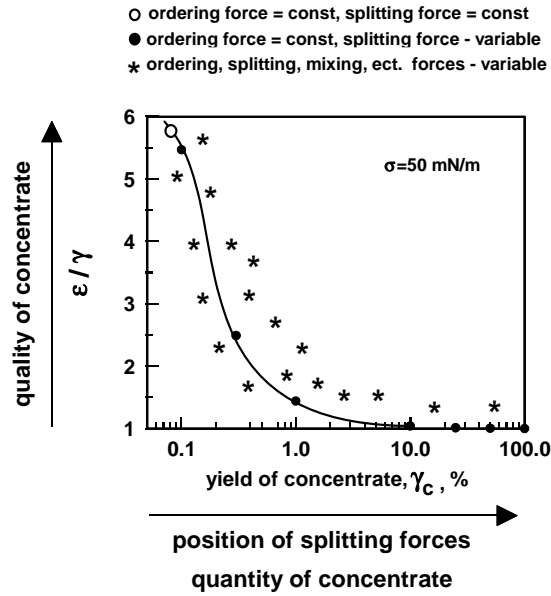
Fig. 2.70. Influence of splitter position on separation results plotted as upgrading curve. For more details see Fig. 2.68

2.3.5. Total physical delineation of separation

Having the balance of forces (or equivalent), the relationships between forces and parameters including the main feature, as well as the relations between fields and space, stratification of particles can be calculated. Additional information on the procedure of splitting the stratified particles into products provides physical delineation of separation process. The elements of physical delineation of separation have been already presented using the examples considered by Urvantsev (2000) and Drzymala (2005a) (Fig. 2.68). Figure 2.71 presents total physical delineation of the case considered by Urvantsev (2006).
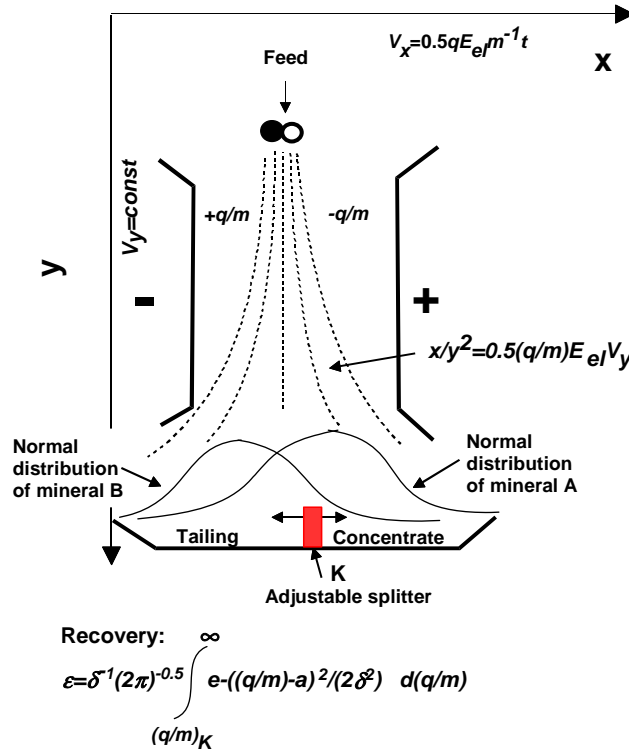
Fig. 2.71. Physical delineation of separation leading to products of separation. The picture shows ordering (trajectory) of particles, stratification (according to the normal distribution law) and splitting into products by changing the position of splitter K

In many papers delineation of a separation and its results is not considered in a systematic heuristic way as it has been discussed in the previous chapters but rather empirically. There are many empirical equations relating operational variables with the results of separation. Some of them will be presented in Chapter 4 regarding screening.

2.3.6. Time aspects of separation

Time is one of many parameters influencing separation. Time can be considered in any stage of separation, starting with ordering. However, in more complex separation systems when a particle tries several times to reach final stratification, the time of ordering is not the same as the time of separation. The time of separation is usually investigated as kinetics of the process. Kinetics describes the behavior of separation systems as a function of time. The rate of the separation is described by general equation:

$$v = dN/dt = -kN^m,$$ (2.48)

where:

v – speed of the process, l/s

N – number of grains undergoing the process at particular time *t*,

k – process speed constant, l/s

m –constant, dimensionless

t - time.

The value of constant *m* is usually one (*m* = 1), therefore after integrating, a general expression for the rate of the process is obtained:

$$N = N_0 \exp(-t\,k_i), \tag{2.49}$$

where N_0 is the initial number of particles subjected to separation.

There are many modifications of the so-called first order kinetic equation which result from specificity of the process. If the particles are of different properties, constant *k* assumes different values. The kinetic equations can be applied either to the whole material subjected to separation or to particular components.

Almost all parameters characterizing the results of separation can be relate to the time of separation. For instance, the recovery ε of a particular particle size fraction in a product of screening, as a function of time *t*, can be written as:

$$\varepsilon_i = 1 - \exp[-t\,k_i], \tag{2.50}$$

and constant *k* depends on the parameters of the separating system (Malewski, 1990).

$$k_i = 3600\ VBW\varphi sCd_t\,[2(1 - d/d_t)]^{\delta}/Q_o]\ 100\%, \tag{2.51}$$

where:

V – rate of movement of material on screen, m/s

B – sieve width, m

W – function of moisture influence on screening (for dry material W=1)

φ – constant dependent on the scale of screening also called the scale factor

s –screen openings size factor ($s = [d_t/(d_t + a_d)]^2$)

C – constant determined empirically, dependent on sieve inclination

d_t – screen opening size, m

Q_o – intensity of material stream, m³/h

a_d – thickness of screen wire, m

d – mean particle size, m.

2.3.7. Summary

A complete characterization of separation requires its delineation, analysis and evaluation. The delineation provides mathematical relations between parameters of separation and makes prediction of separation results possible. A precise delineation of separation reveals the nature of the process as well as provides foundations for influencing the separation results. The delineation of separation can be based on me-

chanical, thermodynamic, probability, etc., and mixed foundations. These approaches should provide the same final relationships between parameters of separation because they characterize the same reality and the force, probability, and energy are interrelated quantities. The main purpose of delineation of separation is relating parameters of separation system resulting from the separation material, device, and environment as well as and their combinations.
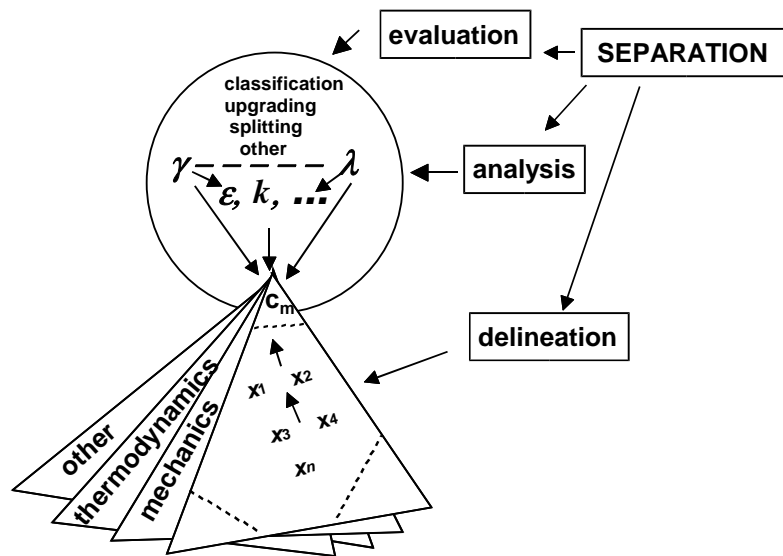
Fig. 2.72. Characterization of separation is based on delineation, analysis and evaluation of separation

  The results of a separation process can be analyzed as separation into products, classification, upgrading, and others. The combination of these approaches is also possible. If there is separation but the process for any reason does not provide real products, separation can still be delineated, analyzed and evaluated, but as a virtual process in which typical components (fraction, minerals, elements, etc.) are distinguished. The methodology of characterization of virtual and real processes is the same. The virtual separation can be treated as a real system in which the products of separation were combined after separation. Fig. 2.72 presents the main elements characterizing separation.

Literature

Barskij L.A., Rubinstein J.B., 1970. Cybernetic methods in mineral processing, Nedra, Moscow, 1970, in Russian.

Bigosiński J., 1998. Wpływ zawartości rozdzielanych składników na wzbogacanie metodą flotacji, Ph.D. thesis, J. Drzymala, supervisor, Instytut Górnictwa Politechniki Wrocławskiej, Poland.

Brozek M., 1984. Ocena stopnia uwolnienia frakcji mineralnej węgla na podstawie krzywej separacji Halla, Przegląd Górniczy, nr 11, 384–387.

Brozek M., 1996. Analiza wzbogacalności i wzbogacania surowców z uwzględnieniem ich właściwości fizycznych oraz oddziaływań między ziarnami, Rozprawy, Monografie, 51, Wyd. AGH, Kraków.

Buchowski H., Ufnalski W., 1998. Podstawy termodynamiki, WNT, Warszawa.

Budryk W., Stepinski W., 1954. Teoria przeróbki mechanicznej kopalin, skrypty uczelniane AGH, PWN, Kraków.

Dell C.C., 1953. Release analysis – a new tool for ore-dressing research, in: Recent developments in mineral dressing, London, IMM, 75-84.

Dell C.C., 1961. The analysis of flotation test data, Quarterly of the Colorado School of Mines, Vol. 56, No. 3, 113-127.

Dell C.C., 1969. An expression for the degree of liberation of an ore, Trans. Inst. Min. Metal., Sec., C, Mineral Process Extr. Metal., 78, C152-C153.

Dell C.C., Bunyard M.J., Rickelton W.A., Young P.A., 1972. Release analysis – a comparison of techniques, Trans. Inst. Min. Metal., Sec., C, Mineral Process Extr. Metal., 81, C89-C96.

Drzymala J., 1994. Characterization of materials by Hallimond tube flotation, Int. J. Miner. Process., part 1 – 42 (139–152), part 2 – 42 (153–167), part 3 – 55 (203–218, 1999).

Drzymala J., 2001. Generating upgrading curves for characterizing separation processes, Journal of Polish Mineral Engineering Society-Inzynieria Mineralna, 2(4), pp. 35-40.

Drzymala J., 2003. Sorting as a procedure of evaluating and comparing separation results, Physicochemical Problems of Mineral Processing - Fizykochemiczne Problemy Mineralurgii, 37, 19-26.

Drzymala J., 2005a. Derivation of a separation curve based on thermodynamic considerations and variation of splitting force, Prace Naukowe Instytutu Górnictwa Politechniki Wrocławskiej 31, Studia i materiały 113, 35-45.

Drzymala J., 2005b. Evaluation and comparison of separation performance for varying feed composition and scattered separation results, Int. J. Miner. Process., 75, 189-196.

Drzymala J., Kapusniak J., Tomasik P., 2000. Sposób wytwarzania koncentratów miedziowych bogatych w chalkozyn, Polish Patent P 337953, PL 195693 BI, 2007.

Drzymala J., Lekki J., 1989. Flotometry – another way of characterizing flotation, J. Colloid Interface Sci., 130(1), 205–210.

Drzymala J., Tyson D., Wheelock T.D., 2007. Presentation of Particle Beneficiation Test Results on an Equal Basis When Yield and Recovery are Involved, Minerals and Metallurgical Processing, 24(3), 145-151.

Drzymala, J., Ahmed, H. A. M., 2005. Mathematical equations for approximation of separation results using the Fuerstenau upgrading curves, Int. J. Miner. Process., 76, pp. 55-65.

Drzymala, J., Kapusniak, J., and Tomasik, P., 2003. Removal of lead minerals from copper industrial flotation concentrates by xanthate flotation in the presence of dextrin, Int. J. Miner. Process., 70, pp. 147-155.

Fomenko T. G., 1957, Determination of optimal indices of upgrading, USSR Magadanskij NII 1, chapter IV, Upgrading and metallurgy, 24, Severostoc-zoloto, 1957 (in Russian).

Fuerstenau D.W., et al., 1988-1992, Coal surface control for advanced fine coal flotation, Final Report, University of California, Berkeley, Final Report DOE/PC/88878-T13, DE92 015625 for U.S. Dept. of Energy. Prepared by Univ. California, Columbia Univ., Univ. of Utah, and Praxis Engineers Inc.

Gaudin, A.M., 1963, Flotation, Slask, Katowice, (Polish edition).

Gebhardt J.E., Fuerstenau D.W., 1986. Flotation behavior of hematite fines flocculated with polyacrylic acid, Minerals and Metallurgical Processing, 164-170.

Grzelak E., 1998. Kruszywa mineralne, Poradnik, Wyd. COIB, Warszawa.

Guminski K., 1982. Termodynamika, PWN, Warszawa.

Halbich W., 1934. Über die Anwendungsmöglichkeiten einiger Netzmittel in der Flotation, Kondrad Triltsch, Würzburg.

Hall W.B., 1971. The mathematical form of separation curves based on two known ore parameters and a single liberation coefficient, Trans. IMM., Sec.C, 80, C213–C222.

Henry, 1905. Le lavage des charbons, Revue Universelle, ser. 4, vol. V, p.274 (Information after H. Czeczott, Przeróbka mechaniczna użytecznych ciał kopalnych, Kraków, 1937).

Holland-Batt A.B., 1985, Analysis of mineral separation system by means of recovery functions, Trans. IMM, Section C., 94, C17-29.

Hu Vejbaj, 1975. How to calculate separation efficiency, Non-ferrous Metals (Mineral Processing), 6, 40-50.

Jacobsen P.S., Killmeyer P., Hucko R.E., 1990. Interlaboratory comparison of advanced fine coal beneficiation process, in: Processing and utilization of high sulfur coals, III, R. Markuszewski, T.D. Wheelock (eds.), Elsevier, Amsterdam, 109–118.

Jia R., Harris G. H., Fuerstenau D. W., 2002. Chemical Reagents for Enhanced Coal Flotation, Coal Preparation, 22, pp. 123-149.

Jierong Li, 1982. The practice of concentration and the way to increase grade and recovery of the graphite concentrate in Nanshu Graphite Mine, Shandong, China, Proc. IMPC, Canada, V-91 – V-9-10

Jowett A., 1969. A mathematical form of minerals separation curves, Trans. Inst. Min. Metal., Sec., C, Mineral Process Extr. Metal., 78, C185.

Kelley E. G., and Spottiswood D. J. 1982. Introduction to Mineral Processing. John Wiley & Sons, New York, pp. 46-61.

Konopacka Z., Drzymała J., 2002. Generowanie krzywych klasyfikacji stosowanych do opisu procesów separacji, Prace Naukowe Instytutu Górnictwa Politechniki Wrocławskiej 96, Konferencje 32, 25-43, 2002.

Laskowski J., Lupa Z., 1970. Krzywe wzbogacalności Della, Prace Naukowe Instytutu Górnictwa Politechniki Wrocławskiej, nr 3, Studia i Materiały nr 3, 229–249.

Laskowski J., Luszczkiewicz A., Malewski J., 1977. Przeróbka kopalin, Oficyna Wydawnicza Politechniki Wrocławskiej, Wrocław.

Laskowski J., Luszczkiewicz A., 1989. Przeróbka kopalin. Wzbogacanie surowców mineralnych, Wydawnictwo Politechniki Wrocławskiej, Wrocław.

Luszczkiewicz A., Drzymala J., 1996. Określenie możliwości zmniejszenia zawartości ołowiu w koncentracie miedziowym metodami flotacyjnymi przy wykorzystaniu najnowszych osiągnięć z fizykochemii powierzchni, Raporty I-11 Politechniki Wrocławskiej, cz. I, 1995, cz. II.

Luszczkiewicz, A., 2002, Ocena skuteczności wydzielania wieloskładnikowych koncentratów pierwiastków rozproszonych, Prace Naukowe Instytutu Politechniki Wroclawskiej, nr 101, Konference 35, 87-103

Malewski J., 1990. Modelowanie i symulacja systemów wydobycia i przeróbki skał, Prace Naukowe Instytutu Górnictwa nr 60, Monografie nr 27, Wydawnictwo Politechniki Wrocławskiej, Wrocław.

Mayer F.W, 1951. Krzywe średniej wartości (krzywe „M"), cz. I, Metoda krzywych średniej wartości w przeróbce mechanicznej, Przegląd Górniczy, 11, 446–452.

Mayer F.W, 1952. Przemysłowe badania przeróbcze krzywymi „M". A. Mieszanina dwu węgli, Przegląd Górniczy, 3, 109–111.

Mayer F.W, 1952. Przemysłowe badania przeróbcze krzywymi „M". B. Mieszanina trzech i więcej węgli, Przegląd Górniczy, 4, 148–153.

Mayer F.W., 1950. Die Mittelwertkurve, eine neue Verwacksungskurve, Glückauf, 26, 498–509.

Michałowski S., Wankiewicz K., 1999. Termodynamika procesowa, WNT, Warszawa.

Mohanty M.K., Honaker R.Q, Govidarajan B., 1999. Development of a characteristic flotation cleaning index for fine coal, Int. J. Miner. Process, 55, 231–243.

Mohanty M.K., Honaker R.Q., 1999. A comparative evaluation of the leading advanced flotation technologies, Minerals Engineering, Vol. 12 (1), 1–13.

Myjkowski, M., 1999, Master thesis, Wroclaw Technical University, W-6, Poland

Newton I., 1687. Philosophiae naturalis principia mathematica.

PN-86/M-94001, Sita tkane kontrolne o oczkach kwadratowych.

Pudlo W. 1971, O pewnej metodzie aproksymacji krzywych wzbogacalności, Zeszyty Problemowe Górnictwa PAN, Zeszyt 2, Vol., 9, 83-103.

Reinhardt K., 1911. Charakteristik der Feinkohlen und ihre aufbereitung mit Rücksicht auf der grösste Ausbringen, Glückauf, 47(6–7), 221, 257–264.

Salama A.I.A., 1996. Separation data balancing utilizing the maximum entropy approach, Int. J. Miner. Process., 47, 231–249.

Sanak-Rydlewska S., Małysa E., Spalińska B., Ociepa Z., Konopka E., Kamiński S., 1999. Obniżanie zawartości ołowiu w koncentracie miedzi, materiały V międzynarodowej konferencji „Przeróbka rud metali nieżelaznych", Szklarska Poręba, 25–27.10.1999, KGHM Polska Miedź S.A., CBPM Cuprum, IMN, Wrocław.

Schulz N.F., 1970. Separation efficiency, Trans. Soc. Min.Eng., AIME, 247, 81–87.

Schuster H.G., 1993. Chaos deterministyczny – wprowadzenie, PWN, Warszawa.

Sotillo F.J., Fuerstenau D.W., Harris G., 1997. Surface chemistry and rheology of Pittsburgh No.8. coal-water slurry in the presence of a new pyrite depressant, Coal Preparation, 18, 151-183.

Sresty G.C., Somasundaran P., 1980. Selective flocculation of synthetic mineral mixtures using modified polymers, Inter. J. Min. Process., 6, 303-320.

Stepinski W., 1955. Teoria Przeróbki Mechanicznej Kopalin, II, PWN, Kraków.

Stepinski W., 1958, Ekonomika przeróbki rud i węgla, AGH, Kraków.

Stepinski W., 1965. Krzywe średnich wartości, Rudy i Metale Nieżelazne, R9, nr 10, 532–535, 1964; R10, nr 3, 117–120.

Sztaba K., 1993. Przesiewanie, Śląskie Wydawnictwo Techniczne, Katowice, 1993.

Sztaba K., 1993. Przesiewanie, Śląskie Wydawnictwo Techniczne, Katowice, 1993

Taggart, A.F., 1948, Handbook of Mineral Dressing - Ores and Industrial Minerals, New York, Wiley.

Tarjan G., 1981. Mineral Processing, Vol. 1, Akademiai Diado, Budapest, pp. 83-142.

Ulewicz M., Walkowiak W., Kozłowski C., 2001. Selective flotation of zinc(II) and cadmium(II) ions from dilute aqueous solutions in the presence of halides, Physicochemical Problems of Mineral Processing, 35, 21-29.

Urvantsev, A.I., 2000. On efficiency of electrical separation with triboelectric charging of particles. Obogashcheniye Rud, Special issue: 31, Flotation.

Wieniewski A., 1988; 1990, IMN, Reports of Investigations, 4097/88, 4463/II/90, Gliwice, Poland.

Wills B.A., 1979. Mineral processing technology. Pergamon Press, Oxford.

Part III

Separation processes

3. Comminution

3.1. Principles of size reduction

Comminution is performed for the reduction of particle size. The process requires application of forces. It can be accomplished in a mechanical or chemical way (Fig. 3.1). Mechanical comminution is a result of operation of external (Fig. 3.2a) or special forces (Fig. 3.2b) while chemical size reduction is based on the removal of certain particles or their fragments by dissolution or leaching with or without precipitation of other substances (Fig. 3.3). Chemical comminution is different in character from physical size reduction, therefore it is a part of extraction metallurgy rather than mineral processing.

COMMINUTION

MECHANICAL

CHEMICAL

external forces

- smashing
- breaking
- attrition
- pealing
- cutting
- crushing
- other

special forces

- thermal shock
- pressure change
- bombing with
  photons and other
  elemental particles
- other

chemical forces

- leaching
- dissolution
- burning
- bioleaching
- other
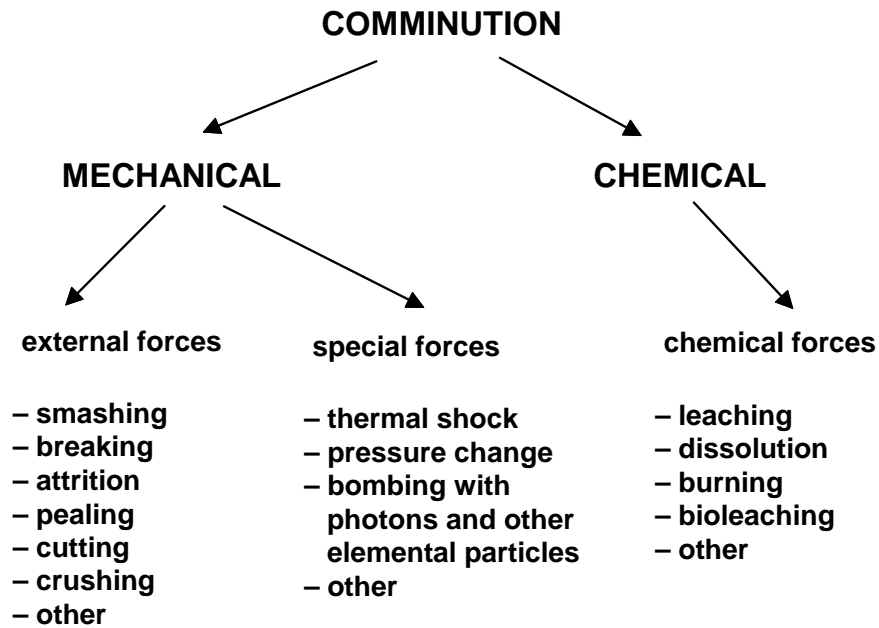
Fig. 3.1. Methods of particle comminution
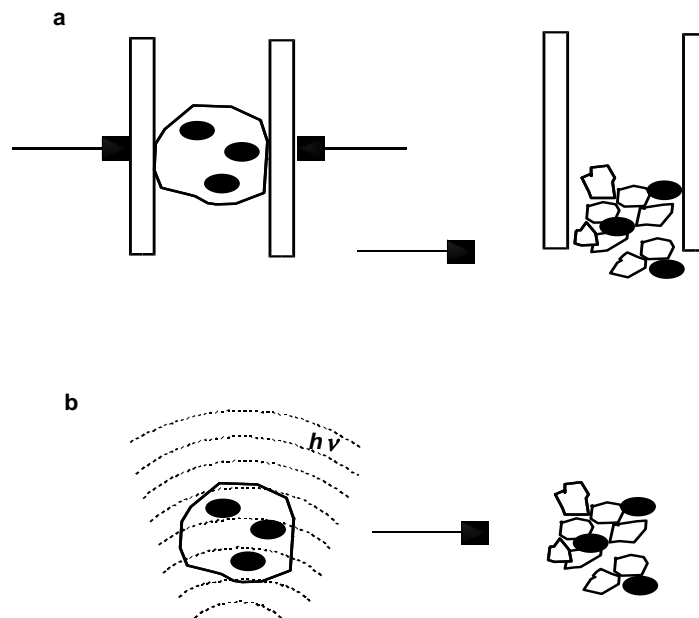
Fig. 3.2. Mechanical comminution with external (a) and internal (b) forces
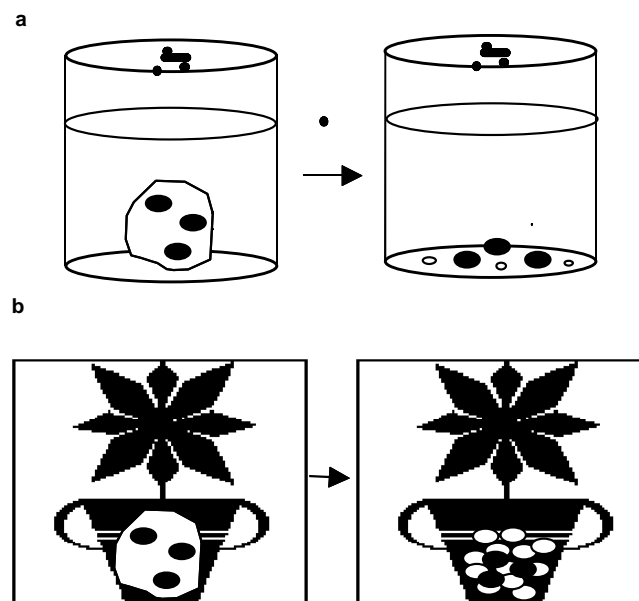
Fig. 3.3. Illustration of comminution by chemical leaching (a) and bioleaching (b)

Mechanical comminution can be accomplished in many different ways which are shown in Fig. 3.4.
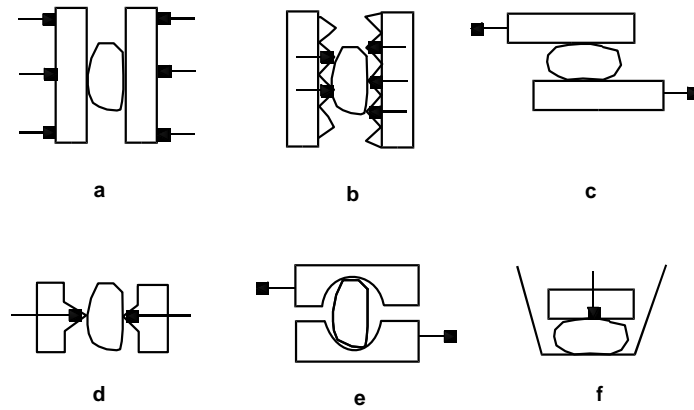
Fig. 3.4. Modes of size reduction:
a – compression, b – fracture, c – abrasion, d – splitting, e – cutting, f – shattering
(after Mokrzycki et al., 1981)

Abrasion consists in tearing off small portions of a solid body as a result local low energy forces. Cleaving takes place when the force applied is not too big but sufficient for dividing particles into several smaller particles. Shattering leads to a higher number of smaller partices under the influence of a considerable force. There are other possible modes of grinding including torsion, twisting, stretching, compressing, and so on. In comminution devices all kinds of grinding modes can take place simultaneously, but to a different degree. Comminution machines are usually constructed in such a way that one kind of grinding prevails.

The material subjected to size reduction may be a mineral, rock or ore which contains both useful and gangue minerals. The goal of comminution of rock and ore material is to release useful particles from the gangue. If liberation is not complete, the product of comminution contains intergrowths. Typical shapes of intergrowths are shown in Fig. 3.5.
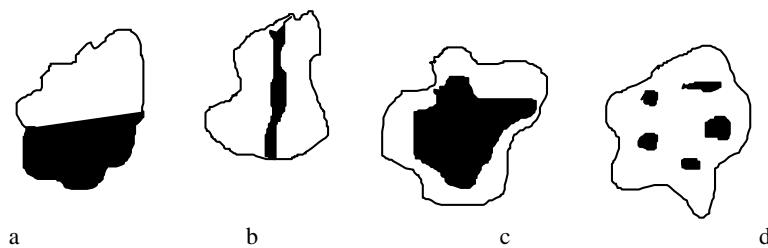
Fig. 3.5. Typical intergrowths of valuable and gangue minerals:
a – regular, b – vain, c – frame, d – occlusion (Kelly and Spottiswood, 1982)

Comminution can be accomplished by crushing or grinding. Crushing is performed on large particles while grinding on particles smaller than about 50 mm (Table 3.1).

Table 3.1. Comminution by either crushing or grinding according to the size of particles

comminution type	Maximum particle size, mm	
	feed	product
Primary crushing	1500	500
Secondary crushing	500	150
Tertiary crushing	150	50
Coarse (primary) grinding	50	5
Secondary grinding	5	0.5
Fine grinding	0.5	0.05
Ultrafine (colloidal) grinding	0.05	<0.005

Grinding deals with particles smaller than about 50 mm and is performed in mills containing the feed, water and grinding media. Balls, cylindrical pebbles (cylpebs), bars, pebbles, as well as lumps of the same material are used as grinding media. The grinding media can be metallic or ceramic.

Grinding consumes considerable amount of energy, therefore effective carrying out of the process is very important. Excessive grinding (overgrinding) should be avoided because of its high cost and fine grinding usually makes further upgrading difficult.

Each method of separation requires optimal range of particle size (Fig. 3.6). To meet this requirement the size reduction, as a rule, is coupled with either mechanical or hydraulic classification for the removal of proper size particles from comminution environment.
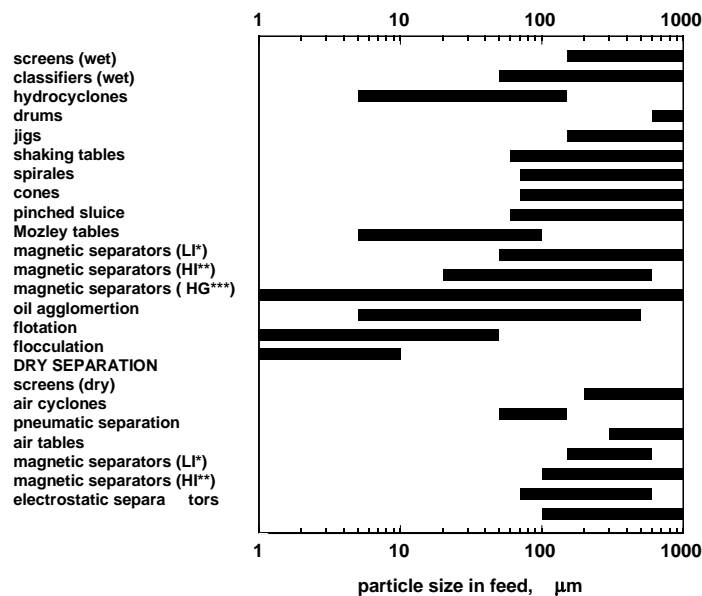
Fig. 3.6. Optimal range of particle size for separation by different separation methods.
(* low intensity (LI), ** high intensity (HI), *** high gradient magnetic field (HG))

$F << F_{cr}$ $F < F_{cr}$ $F = F_{cr}$

F_r F_r

F_s
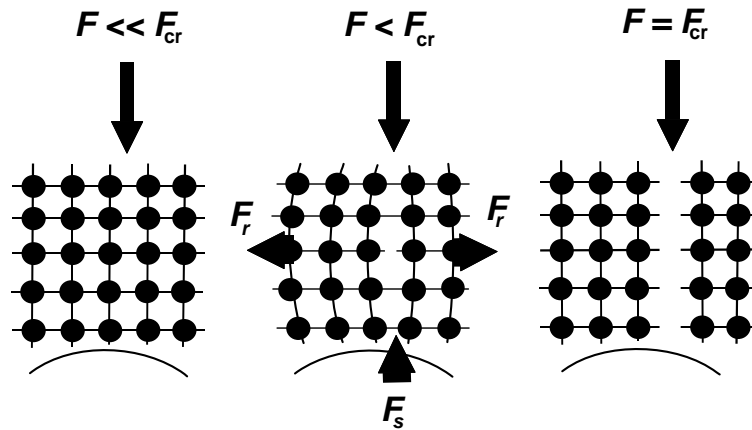
Fig. 3.7. Compressive F_s and tensile forces F_r leading to disintegration of brittle particles

To break a particle the application of one force or several forces is needed. When the force is week, the result is particle deformation leading to stress, which is proportional to the load force and inversely proportional to cross section of the material. The stress causes stretching the atoms forming particles which, in turn, causes the tensile forces in the material (Fig. 3.7). The increase in the load force transfers higher amount of energy to particles until the stress exceeds the adhesion forces within the material and this leads to breaking particle bonds and particle disintegration.

A different mechanism of comminution is valid for flexible particles, including metals, rubber and plastics for which there takes place shifting of atoms and layers (Fig. 3.8). Therefore grinding of these materials is difficult.

$F < F_{cr}$ $F = F_{cr}$
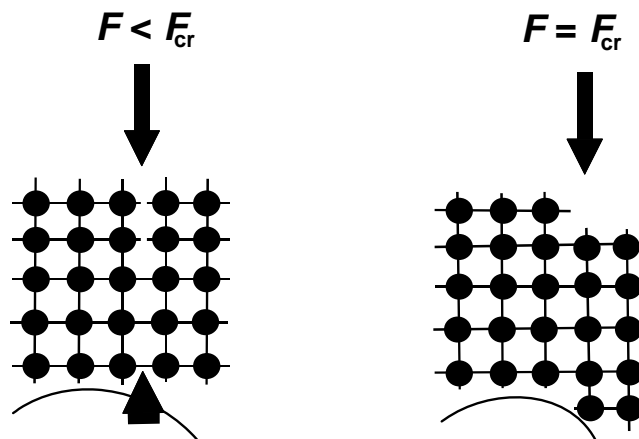
Fig. 3.8. Behavior of flexible particles influenced by grinding forces

3.2. Physicomechanical description of particle disintegration

Application of one force or forces is necessary to break a piece of matter (Fig. 3.7). The simplest delineation of breaking can be based on the Hook law relating the force applied to the sample material and the change of its lengths without changing its cross section area:

$$F = E \, S \, \Delta l/l_o \qquad (3.1)$$

where:

F – applied force, N

E – constant also known as Young's modulus, modulus of elasticity, elastic modulus or tensile modulus, N/m^2

S – cross section area of the sample , m^2

Δl – increase or reduction of lengths of the tested material, m

l_o – original length of the sample, m.

The force needed to break the tested material is:

$$F_{cr} = E \, S \, \Delta l_{cr} /l_o \qquad (3.2)$$

where:

F_{cr} – critical force needed to rupture the sample, N

Δl_{cr} – increase or reduction of lengths of the tested material needed for breaking, m.

Thus, at least two parameters are needed to characterize breaking of materials having identical l and S, that is the Young modulus E and characteristic critical lengths increase Δl_{cr}. Additional parameters are needed for odd shape objects, and for the samples which do not obey well the Hook law. Typical values of the Young modulus are given in Table 3.2. It should be noticed that the Young modulus, because of stresses and defects in the materials, can be different for different samples of the same material, i.e. it depends on sample history. It is obvious that defected particles easier disintegrate than the ideal ones. Moreover, particles can posses a highly diversified distribution of defects, number of cracks and different size of cracks, which also effects the value of the Young modulus and grinding. It should be also added that not all accumulated strain remains in the particles at the moment of disintegration because it disappears, leading to the emission of energy in the form of vibration, sounds, heat and other.

The Hook law can also be written in an abbreviated form:

$$F_{cr} = G_{cr} \, S \qquad (3.3)$$

where:

G_{cr} - critical tensile stress or Griffith (1921) stress, that is $G_{cr} = E \, \Delta l_{cr}/l_o$, (N/m^2),

For spherical and of other shape particles the Hook law can be written in a general form:

$$F_{kr} = G_{cr} \, d^2 /k_i \qquad (3.4)$$

where

d – diameter of particle, m

k_i – dimensionless constant characterizing the shape of a particle and its cross section area, $k_i = d^2/S$.

Table 3.2. The Young modulus and surface energy as two principal parameters of comminution. The Young modulus after Lipczyński and co-workers (1984), surface energy after Drzymala (1994)

Material	Young modulus $GN/m^2 = 10^9$ Pa=GPa	Surface energy* $mN/m = 10^{-3}$ J/m^2
Water	~0	72.8
Ice	9.5 (at 268K)***	90–120
KCl (silvinite)	29.6*[6]	97(780 °C)
CaF$_2$ (fluorite)	75.8*[6]	450 (plane 111)
CaCO$_3$ (calcite)	56.5(marble)	230 (100)
Al$_2$O$_3$ (corundum)	390****	580 (2050 °C)
C (diamond)	1050-1200**	~3700
Ag	83	923 (995 °C)
Au	78*****	1128 (1120 °C)
Cu	120	1120 (1140 °C)
Pb	16.2	442 (350 °C)
SiO$_2$	50–78 (glass)	230 (1400 °C)
Granite	51.5–61.4	–
Sand stone	34–50	–
Diabase	61–69	–

* Undisputable values of surface energy for solids at ambient temperature are difficult to determine and therefore are not available in the literature, ** http://en.wikipedia.org, 2006, ***Prensky, S.E., 1995, A review of gas hydrates and formation evaluation of hydrate-bearing reservoirs, presented at the meeting of the Society of Professional Well Log Analysts, Paris, France, June 26-29, 1995 (based on Davidson, D., 1983, Gas hydrates as clathrate ices, in Cox, J., Ed., Natural gas hydrates--properties, occurrence and recovery: Butterworth, Woburn, MA, p.1-16), ****http://web.mit.edu/course/3/3.11/www/modules/ /props.pdf,   *****http://www.allmeasures.com/Formulae/static/formulae/youngs_modulus/16.htm,   *6- http://www.almazoptics.com

According to different theories critical tensile stress can be given by different equations shown in Table 3.3.

Table 3.3. Formulas use for the critical tensile stress

Formula	Source
$\sigma_{cr} = E \, \Delta l_{cr} / l_o$	Hook's law
$\sigma_{cr} = (\gamma_s E / c)^{0.5}$ (c = crystalline translation lattice constant, m)	Cortel, 1964
$\sigma_{cr} \cong (2\gamma_s E / l_{cr})^{0.5}$ (l_c = crack length, m)	Kelly and Spottiswood, 1982
$\sigma_{cr} = \dfrac{1-2\nu}{3} \dfrac{F_{cr}}{2\pi} \left[\dfrac{4E}{3F_{cr}(1-\nu^2)d/2} \right]^{2/3}$ (ν = Poisson number, d =particle size, m)	Hertz (Brożek, et al., 995)
$\sigma_{cr} = k_p \, \rho^{0.67}$ (ρ = particle density, g/cm^3, k_p = a constant of varying dimension)	Protodyakonov and Voblikov (Brożek et al., 1995)

Different formulas that can be used to delineate breaking of particles indicate that there is no single and simple theory of size reduction of particles. There are also many parameters which are needed even for approximate delineation of particle disintegration. One of them can be the Poisson number (reciprocal of the Poisson ratio) given in Table 3.4. The Poisson ratio is the ratio of relative contraction strain or transverse strain (normal for the applied load), divided by relative extension strain (in the direction of the applied load).

Table 3.4. The Poisson number ν of selected materials. After Sokolowski, 1995

Material	Poisson number, ν
Steel	0.25–0.30
Concrete	0.16–0.20
Glass	0.23

Another approach is the use of energy balance. The surface energy of a particle is:

$$E_p = \gamma_s \Delta S \tag{3.5}$$

where

E_p – total surface energy of a particle, J
γ_s – surface energy (specific) of material, J/m^2
ΔS - area of particle, m^2.
    The surface energy of selected materials was presented in Table 3.2.
    If the grinding process followed the pattern that all grinding energy E_r (J) would be transformed into local strain energy E_n (J), and then into surface energy E_p (J) forming new smaller particles with new surfaces, then:

$$E_r = E_n = E_p, \tag{3.6}$$

In such an ideal case (Oka and Majima, 1970; Kelly and Spottiswood, 1982):

$$E_r = 1.23 K_v \, \mathcal{G}_{cr}{}^2 d^3/E = \gamma_s \Delta S \tag{3.7}$$

where:
V – volume of particle (or particles after disintegration), m^3
E – Young modulus, N/m^2
K_v – dimensionless constant.
    In reality, breaking of particles remains a highly complicated process since particles are not ideal in structure and do not follow any ideal pattern of disintegration. This observation is also valid for the materials which look like ideal ones, i.e. monocrystalls, metals or glass. It results from the fact that particles have different defects, inclusions, cracks, shifts, accumulated strain energy. They are usually polycrystalline, i.e. clusters of smaller particles. Additionally, comminution energy is used not only to increase particle surface, but also to form stresses, cracks and other defects all

over particle volume, i.e. for increasing internal volumetric energy. Therefore, critical tensile stresses of particle disintegration are usually lower than that of ideal particles.

Thus, the breaking energy E_r is used for forming new surface (E_p) as well as for creation of cracks, stress, sound, heat, and other effects (E_x):

$$E_r = \gamma_s \Delta S + E_x \tag{3.8}$$

3.3. Empirical evaluation of size reduction

According to Hukki (1975) empirical relationship between size reduction and energy can be approximated with general differential equation (Fig. 3.9):

$$dE_o = -C \, d \, d/d^{\,f(d)}, \tag{3.9}$$

where:

dE_o – increase of specific (per unit mass) energy of comminution
C – constant
$f(d)$ – function dependent on particle size d
dd – change in particles size.

The relation between size reduction energy E_r and specific energy E_o is:

$$E_o = E_r / m = E_r / (\rho V) = 6 E_r / (\rho \pi d^3), \tag{3.10}$$

where:

E_r – comminution energy, J
E_o – specific comminution energy, J/kg
m – mass of material subjected to comminution, kg
d – size (diameter) of particle, m
V – particle volume, m3
$\pi = 3.14$.

Equation (3.9) is general in which mathematical form of the term $f(d)$ has not been established. Therefore, it is usually used in a simplified form (Walker, 1937):

$$dE_o = -C \, d \, d/d^{\,n}, \tag{3.11}$$

in which $f(d)$ is replaced by a constant n valid for a certain range of particle size.

When n =1, integration of Eq. (3.11) leads to the relation:

$$K_K \ln (D/d) = E_o = E_r/m = E_r/(\rho V), \tag{3.12}$$

or

$$E_r = \rho V K_K \ln (D/d) \tag{3.13}$$

where:

d – average size of particles after grinding, m

D – average size of particles before grinding, m
K_K – the Kick constant, J/kg (a second, besides n, size reduction constant).
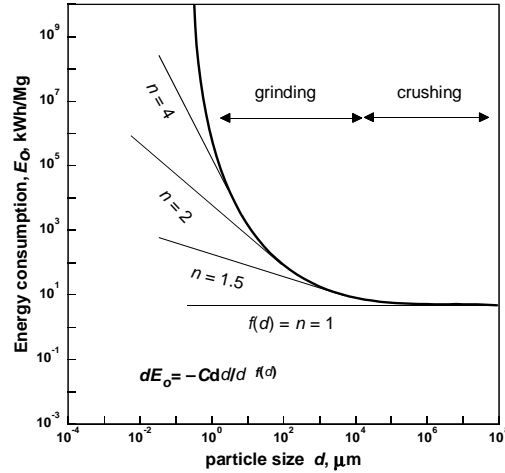
Fig. 3.9. Graphical form of the general formula for energy of size reduction

Equation (3.13) is also called the Kick (1885) hypothesis which says that size reduction energy E_r, at constant size reduction ratio (D/d), is proportional to the volume of ground material V. Determination of size reduction energy of a particle size fraction requires appropriate mean value of the size fraction before (D) and after (d) comminution. Following the approach of Sokolowski (1995; also Récents progrés en génie des procédés, v.10, Ed. Tec&Doc, Lavoisier, Paris, 1996), based on the so-called equienergetics of ground particles, the following equations for d and D can be used for the Kick region of the size reduction (n=1):

$$d = \left(\frac{1}{\sum_i \frac{g_i}{d_i^{n-1}}} \right)^{\frac{1}{n-1}}, \quad D = \left(\frac{1}{\sum_i \frac{g_i}{D_i^{n-1}}} \right)^{\frac{1}{n-1}} \quad \text{(for Kick's region no n=1 but n≅1.0001 should be used)}$$

(3.14)

$$\text{or} \quad \ln d = \sum_i g_i \ln d_i, \quad \ln D = \sum_i g_i \ln D_i \quad (3.14b)$$

where:
g_i – mass fraction of particles with size d_i (for the feed of size D)
i – number of the size fraction.
Both formulas provide practically the same results.
    Integration of Equation 3.11 for n = 2 provides the following formula:

$$E_o = K_R (1/d - 1/D), \tag{3.15}$$

which is equivalent to the Rittinger (1857) equation:

$$E_r = K^*_R \, \Delta S = K^*_R \, S_d - K_C, \qquad (3.16)$$

because $E_r = E_o \, m = K_R \, (1/d - 1/D) \, \rho V = K_R \, \rho \, (V/d - V/D) = K_R \, \rho \, (K_a S_d - K_b S_D) = K^*_R S_d - K_c$, where K_R, K^*_R, K_a, K_b, and K_c are constant with appropriate dimensions. K_R is expressed in J·m/kg while K^*_R in J/m^2.

Thus, according to the Rittinger hypothesis, the grinding energy E_r is dependent on the newly formed surface area S_d.

Integration of Eq. 3.11 for n = 1.5 leads to the equation:

$$E_o = K_B \, (1/d^{\,0.5} - 1/D^{\,0.5}), \qquad (3.17)$$

in which K_B is a constant expressed in J·m$^{0.5}$/kg.

Formula (3.17) is also called the Bond equation (1952). For the average particle size representing the whole ground sample (*d*) Bond used the size of sieve opening through which 80% of sample mass passed while *D* was determined in the same way but for the feed. Sokolowski (1995), taking for *d* and *D* the values calculated with more universal Eq. 3.14, determined the size reduction constant K_B for selected rocks at *n* = 1.5, which are shown in Table 3.5.

Table 3.5. Comminution energy constants K_B (Bond constant) for selected rocks determined by Soko-lowski (1995) for free shatter comminution according to Eq. (3.11) for *n* = 1.5

Material	Rock type	K_B J·mm$^{0.5}$/kg
Dolomite (Pisarzowice)	sedimentation	2100
Granite (Borów)	magmatic	2600
Granite (Graniczna)	magmatic	2900
Granite (Strzegom)	magmatic	3000
Dolomite (Ołdrzychowice)	sedimentation	3900
Granite (Strzelin)	magmatic	4200
Marble (Biala Marianna)	metamorphic	4700
Limestone (Morawica)	sedimentation	5000
Dolomite (Dubie and Jaźwica)	sedimentation	5050
Grey rock (Klodzko)	sedimentation	6600
Gabro (Slupiec)	magmatic	7000
Melaphyre (Czarny Bór and Grzedy)	magmatic	7600
Gneiss (Doboszowice)	Metamorphic	8050
Melaphyre (Borówko A)	Magmatic	8200
Serpentinite (Nasłowice)	metamorphic	8400
Quartzite	Sedimentation	9000
Basalt Gracze	Magmatic	9650
Amphibolite Ogorzelec	Metamorphic	10300

Other size reduction relations can be derived from the Walker equation (Eq. 3.11), for instance the Rebinder equation for *n* = 2.5 and the Brach equation for *n* between 1

and 2. According to Hukki (1961) and his diagram shown in Fig. 3.9 appropriate description of energy of size reduction requires suitable equation which depends on the size of particles produced by comminution. For large particles the Kick equation is suitable, for middle size the equation Bond is appropriate, while for fine particles the Rittinger equation should be used.

Another, more universal approach to the description of comminution energy was proposed by Malewski (1990), who showed that n can assume any values. He used two parameters n and K_M for characterizing energy of comminution E_o which was measured in a double pendulum device. Starting with general empirical equation of Walker for specific size reduction energy E_o integrated for $n = 1$ and for other n values and written in the form:

$$E_o(d,D) = K_M\left(\frac{1}{d^{n-1}} - \frac{1}{D^{n-1}}\right) \text{ for } n \neq 1; \ E_o(d,D) = K_M \log(D/d) \text{ for } n = 1 , \quad (3.18)$$

he calculated E_0 using a matrix:

			Feed: particle size					
		$i \setminus j$	0	1	2	...	m	
		0	0	0	0	0	0	$f(D_0)$
	Products:	1	$E^*(d_1, D_0)$					$f(D_1)$
$E_0 =$	particle	2	$E^*(d_2, D_0)$	$E^*(d_2, D_1)$				$f(D_2)$
	size	:	...	...	...	...	...	$f(D_{...})$
		m	$E^*(d_m, D_0)$	$E^*(d_m, D_1)$	$E^*(d_m, D_2)$		0	$f(D_m)$

where:

$E^*(d, D)$ is defined as $E_0(d, D) \cdot f(d, D)$

$E_o(d,D)$ – specific energy (energy per mass) used up for size reduction of a sample having initial size D and final size d

E_o – total specific energy needed for comminution

$f(d,D)$ – size distribution of the product of comminution produced from disintegration of particles of initial size D (frequency function that is a non-cumulative function characterizing particle size distribution)

$i, j = 0, 1, 2 ,..., m$ – number of size fraction starting from the largest size.

The matrix calculation were based on the equation:

$$E_O = \sum_i \sum_j E_O(d_i, D_j) f(d_i, D_j) f(D_j) = \sum_i \sum_j E^*(d_i, D_j) f(D_j) , \quad (3.19)$$

resulting from a general equation:

$$E_O = \int\limits_{0}^{D_0} \int\limits_{0}^{d_0} E_O(d,D)dF(d,D)dF(D) \quad , \tag{3.20}$$

where:

d_0 – maximum size of particles after comminution

D_0 – maximum size of particles before comminution

$F(d, D)$ – particle size distribution for product of comminution resulting from particles
           of initial size D (function delineating cumulative size distribution curve).

The results of his investigation are presented in Table 3.6. It should be noticed that constant K_M does not bear constant dimension.

Table 3.6. Values of constants K_M and n in Eq. (3.18) for energy of comminution expressed in J/cm^3.
Measurements in double pendulum comminution device (Malewski, 1990)

Material	Comminution constant K_M	Comminution constant n
Basalt	616	1.91
Granite	239	1.76
Limeston	261	1.617

There are other empirical equations relating comminution energy and the size of particles. For instance, correlating equation proposed by Oka and Majimy (1970) is:

$$E_0 = K_O(d^{-6/s} - D^{-6/s}) \quad , \tag{3.21}$$

where:

K_O – constant

s – constant of linearized equation of particle size distribution according to Weibull
     (Kelly and Spottiswood, 1982) (Table. 2.22).

Among other equations the one by Rumpf et al. (1973) is worth mentioning. They delineated size reduction using the dimensional analysis.

All discussed so far empirical models describe size reduction using two constants that is constant K_B (or K_K, K_R, K_M, ect.) which is dependent on the properties of particles subjected to breaking and constant n. Constant n indicates the point of energy-particle size curve at which the process takes place and which indicates if the grinding energy is roughly proportional to particle volume (n = 1), surface (n = 2) or is situated in between. This is fully analogous to the description of grinding using mechano-physical models in which energy of comminution depends on the surface energy γ_s and additional parameters such as Young modulus and (or) other parameters characterizing material (Poisson number, length of microcracks), i.e., also two constants.

It should be added that comminution energy constants K are not strictly constant. This results not only from assuming certain round value of constant n, but also from stochastic character of comminution. This means that achieving more complete agreement between experimental and calculated data is possible by taking into account additional parameters being a function of process probability distribution (Brożek et al., 1993).

The size distribution of particles of the feed and comminution products can be presented either graphically or by means of mathematic functions. Particle size distribution can be plotted as frequency curves (histogram) or distribution (cumulated) curves which have been already discussed in detail while a general mathematical function, describing particle size distribution, called the Fagerholt equation (1945) has the form:

$$F(x) = A\ x^m e^{-B\ x^n},\qquad\qquad (3.22)$$

where:

x – variable, ratio of particle size d of product of comminution and arithmetic mean of borders of the sizes of the feed D_0, that is $x = d/D_0$

A, B, m, n – constant.

The Fagerholt and similar equations (Brożek et al., 1995) provide other relations presented in Table 2.21.

Particle size distribution can also be characterized with statistical functions, including the normal, log–normal, and other distribution. Their application, due to poor fitting, is limited (Kelly, Spoittiswood, 1982).

3.4. Other descriptions of grinding

To relate better the effects of grinding with particle properties, expressed not as mean values but as distributions, there have been worked out mathematical models of comminution of different degrees of complication (Brożek et al., 1995; Lunch, 1997). One of them is the matrix model. It is based on the following general matrix equation:

$$\mathbf{p} = \mathbf{U}\,\mathbf{f},\qquad\qquad (3.23)$$

where:

$\mathbf{p}$ – vector of particle size distribution of the product of size reduction expressed as matrix ($n{\times}1$)

$\mathbf{f}$ – feed particle size distribution expressed as ($n{\times}1$) matrix

$\mathbf{U}$ – ($n{\times}n$) matrix where n denotes the number of matrix lines providing quantitative description of size reduction in a given device.

If single size reduction process is repeated many (x) times in the same way, matrix equation assumes the form:

$$\mathbf{p} = \mathbf{U}^x \, \mathbf{f}. \tag{3.24}$$

When the subsequent regrinding is identical, it should be taken into account by the use of appropriate equations (Lynch, 1977). Application of the matrix calculation for the delineation of size reduction has already been described and showed in Table 3.6. Those interested in the application of mathematical models to comminution can consult the works by Brożek et al. (2005) and Lynch (1997).

3.5. Kinetics of grinding

Different functions can be used for delineation of kinetics of comminution. The most useful are simple kinetic equations of the first order (Kelly and Spottiswood, 1982; Lynch 1977; Manlapig et al., 1979)

$$dW(d)/dt = -k(d) \; W(d), \tag{3.25}$$

where:
$W(d)/dt$ – mass of particles of size d
$k(d)$ – constant for particles of size d.

The are also „matrix" equivalents of Eq. 3.25 (Lynch, 1977, Horst and Freeh, 1970). A precise description of the size reduction kinetics, taking into consideration particle size distribution in the feed and its products is quite complicated. This problem was discussed in details in the monograph by Brożek et al. (1995).

3.6. Analysis of grinding process

Mechanical comminution is a very important and useful mineral processing operation since nearly each raw material, before upgrading, is subjected to size reduction. The size reduction can be conducted either as a process in which only particle size is altered (Fig. 3.10a) or, apart from particle size reduction, as separation of one type of particles from the other (Fig. 3.10b), i.e. liberation. Comminution leading to liberation can be called selective comminution. We always deal with non-selective comminution when single mineral is subjected to size reduction (Fig. 3.11). Grinding and crushing of rocks and ores can be either selective or non-selective (Fig. 3.11).
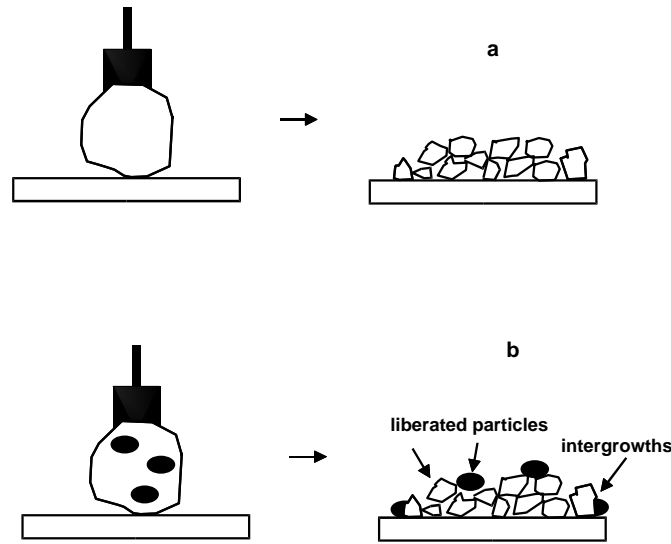
Fig. 3.10. Mechanical comminution:
a – nonselective, b – selective, leading to liberation of either all or certain number of particles
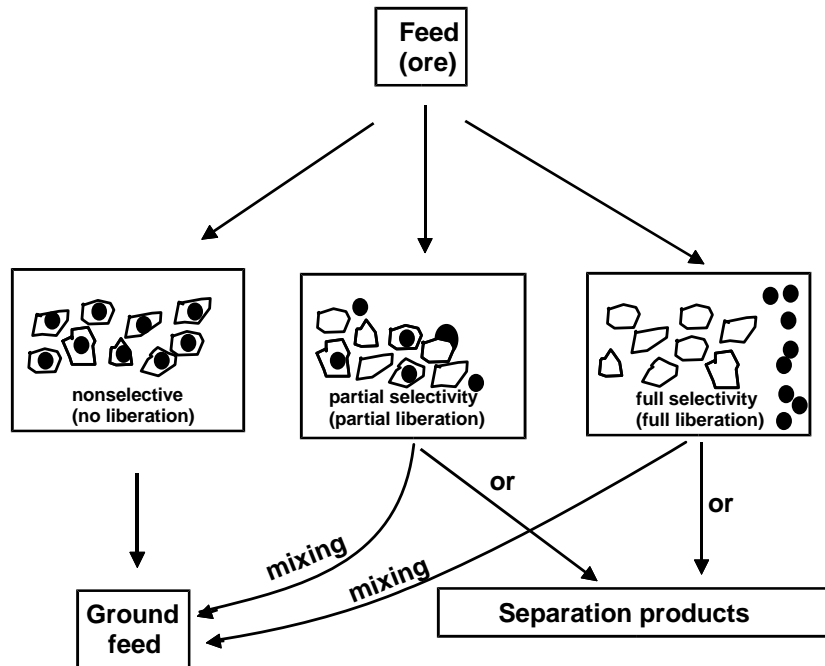
Fig. 3.11. Comminution can be selective, partially selective and nonselective and can provide either separation products or modified feed

In general sense, size reduction is a separation process similar to any other concentration separation. It has its main parameter, which can be generally termed as the susceptibility to comminution. The susceptibility to comminution has not been precisely defined so far, but we know that it is based on at least two parameters. One of them can be surface energy γ_s and/or the Young modulus E, as well as their equivalents.

The constants K and n can be treated as substitute parameters for γ_s and E in empirical delineation of comminution energy vs. particle size. Making use of the differences in susceptibility to size reduction one can, at least partially, create separation of components of the feed, i.e. separation into a collection of particles of different sizes or of different compositions. The evidence of particles separation according to their susceptibility to grinding can be observed in many crushing and grinding devices as pointed out by Lynch (1977). Figure 3.12. schematically shows a tendency of white particles to faster disintegration and separation in a jaw crusher.
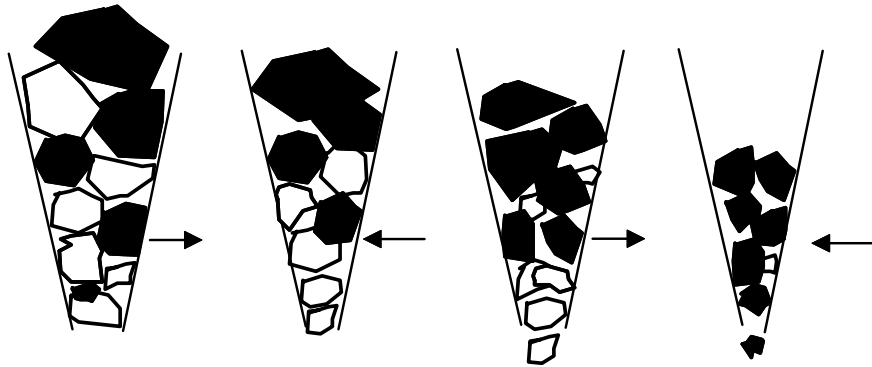
Fig. 3.12. Partial separation in a jaw crusher (after Lynch, 1977)

Size reduction, as a rule, does not provide separate products of separation even though some minerals have tendency to accumulate in different sites of the grinding device. In majority of cases the comminution provides modified feed (Fig. 3.13). Typical crushing and grinding leads to considerable reduction of particle size and liberation of certain components, but, at the same time mixes the products of the process. The reason of conducting comminution as a nonselective process is that the stratification forces are very week while other forces are significant. This lack of selectivity is overcome by subjecting the modified feed to another separation process (for instance flotation) in which separating forces are of considerable values.

Uniqueness of comminution in comparison to other methods of separation does not prevent considering the results of grinding as either classification or upgrading, which will be demonstrated in the next chapter.
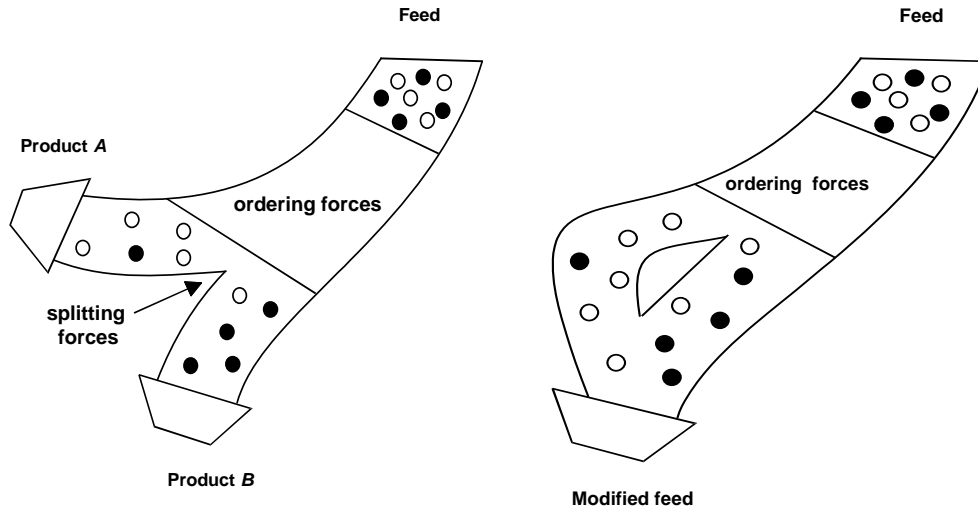
Fig. 3.13. Possible ways of performing crushing and grinding, a) selective, with separation, b) nonselective, leading to modified feed

3.6.1. Grinding as classification process

The analysis of any separation process from the classification perspective (quantity vs. value of the feature utilized for separation) requires monitoring these properties. In the case of size reduction the main feature is susceptibility to comminution determined by the surface energy and Young modulus of the ground material. Unfortunatelly, the surface energy of solids, due to the difficulties with measurement, is not always available. Therefore, empirical constants K and n (equations (3.10—3.17)) are used to analyze comminution and to predict its results.

Empirical grinding constants K and n are accessible from experimental tests. They usually depend on the device in which the tests are conducted and the procedure applied. When the process is conducted in such a way that the results do not depend on the way of grinding, obtained parameters K and n are grindibility constants in a particular device (Sokołowski, 1995 – Table 3.4; Malewski, 1990 – Table 3.5; Mölling, 1960 – Table 3.6). The grinding constants, regardless of the device and procedure of performance are constants of ideal grinding or grindability constants.

In practice, a special procedure proposed by Bond, based on determining the energy needed for grinding of an appropriate sample to a certain size is used. The energy needed for grinding a sample according to the Bond procedure is called the grinding index, work index or W. Its typical values are shown in Tables 3.7 and 3.8. The Bond grinding index is expressed as energy per mass (J/g) or equivalent (kWh/Mg, $m^{2.5}/s^2$) units while the Bond constant K_b in $Jm^{0.5}/kg$.

Table 3.7. Values of comminution constant K_B for various materials
(data after Mölling, 1960, cited by Koch and Noworyta, 1992)
$n = 1.5$. Constant K_B in J/(kg·m$^{-0,5}$) recalculated into m$^{2.5}$/s^2 (J = kg·m^2/s^2)

Material	Wet grinding K_B, m$^{1.5}$/s^2	Dry grinding K_B, m$^{2.5}$/s^2
Clay	227	303
Gypsum	243	324
Boxite	317	422
Phosphorite	358	477
Raw cement	379	505
Limestone	459	613
Hematite	463	617
Coal	469	625
Clinker (cement)	485	647
Quartz	489	653
Granite	546	728
Clay shale	572	763
Gravel	579	772

The Bond procedure is a comparative empirical method based on the Bond equation (Eq. 3.17) for which $n = 1.5$. For this method the Bond equation is written in the form:

$$E_0 = 10W_i \left(\frac{1}{\sqrt{d_{80}}} - \frac{1}{\sqrt{D_{80}}} \right),$$
(3.26)

where:

10Wi – differently written work index and comminution constant in the Bond equation ($K_B = 10Wi$). For $d_{80} = 100$ μm and $D_{80} = \infty$: $10W_i = K_B$.

d_{80}, D_{80} – the size of sieve opening allowing 80% of particles mass to pass the screen for a given material d_{80} for product of grinding, D_{80} for feed).

The constant W_i, called the grinding index, is defined as the work of grinding of a mass unit of a particular material from an infinitely large size to the size of 100 μm, because:

$$W_i = E(\infty \rightarrow 100) = 10W_i \left(\frac{1}{\sqrt{100}} - \frac{1}{\sqrt{\infty}} \right).$$
(3.27)

Table 3.8. Selected Bond index values for different materials (after Wills, 1985)

Material	comminution index W_i kWh/short US tonne	Material	comminution index W_i kWh/short US tonne
Barite	4.73	limestone	12.74
Bauxite	8.78	coal	13.00
Fluorite	8.91	quartz	13.57
Quartzite	9.58	granite	15.13
Ferrosilicon	10.01	graphite	43.56
Dolomite	11.27	emery	56.70

In the original work by Bond, *W* is expressed in kWh per short American tonne, i.e., per 907 kg.

Table 3.9. Bond (grindibility) index for selected materials. Dane taken from Lowrison (1979) and Soko-łowski (1995)

Material	Grindibility index W_i kWh/short US tone	Material	Grindibility index W_i kWh/short US tone
Marble	4–12	Lead ore	13
Gypsum	7	Glass	14
Bauxite	10	Hematite	14
Granite	11	Limestone	14
Magnetite	11	Clinker	15
Quartzite	11	Quartz	15
Sandstone	11	Shale	16
Slag	11	Basalt	19
Feldspar	12	SiC	29
Magnesite	12	Corundum	33
Dolomite	13		

The Bond procedure is complicated and time consuming. Therefore, there are many modifications in use. Sometimes the energy needed for grinding vs. degree of size reduction is used to characterize grinding (Table 3.10).

Table 3.10. Energy consumption in different crushers along with the size reduction factor (after Mokrzycki, 1981)

Crusher	Size reduction factor	Energy consumption, MJ/Mg
Jaw	from 3 to 4 (max. 8)	1.1–4.7
Cone (primary crushing)	from 3 to 4 (max. 8)	0.4–4.7
Cone (secondary crushing)	from 4 to 7 (max. 15)	1.8–9.0
Roll	from 3 to 4	1.3–4.7
Hammer	from 10 to 30 (max. 40)	2.2–5.4
Jet	from 20 to 50 (max. 60)	2.2–7.9

If the feed consists of particles of different susceptibility to grinding, it is possible to describe the size reduction process in a more complete way, that is as classification, by determining and drawing the relations between yield (or recovery) of a size fractions vs grindibility, for instance vs *K* at a constant *n* value.

3.6.2. Grinding as upgrading process

Grinding is a separation process and therefore it can be treated from upgrading, classification, and other perspectives. In the case of analyzing grinding process in terms of upgrading it is not important what the main feature of the process is, but imortant is the information on quality and quantity of the feed and separation products. When grinding is non-selective, only smaller particles are produced, and only one

product is generated that is a ground (modified) feed. Then, grinding can be characterized by the degree of the size reduction, defined as:

$$I = \text{degree of size reduction} = \frac{D}{d} = \frac{\text{particles size before size reduction}}{\text{particles size after size reduction}} \qquad (3.28)$$

where:

D – average size of particles in the initial feed

d – average size of particles in the modified feed.

Average particle size can be given as mean, modal, harmonic, maximum, minimum, d_{50}, d_{80}, etc. Thus, the degree of size reduction also depends on the procedure used for determining average particle size, that is d and D. Average value of particle size can also be taken from size distribution curves which are shown in Figs 3.14a, b.

In the case of selective grinding providing liberation of certain particles, the liberated particles can be treated as a virtual grinding product even though the particles remain physically not separated into products. The expression for the degree of liberation is:

$$L = \varepsilon_L = \text{liberation degree} = \frac{\text{mass of free particles of considered component}}{\text{mass of considered component in feed}} 100\% \qquad (3.29)$$

This definition is often used for measuring liberation. The degree of liberation is the recovery ε of free particles of a particular component in a virtual product of liberated particles. Since in the modified feed two components (considered component and the rest) and two products (free particles of the examined component and the remaining particles) can be distinguished, thus the yield of the liberated particles will be the mass of the liberated particles of the examined component divided by the mass of the remaining particles in the material multiplied by 100%. The content of the examined component in the feed (α) is calculated as the ratio of liberated component mass to the mass of the whole material multiplied by 100%, while the total amount of pure mineral in the product (λ) containing pure mineral is equal to 100%. Aiming at making more familiar the notions of recovery, yield and content in grinding with liberation we are considering the following example. Let us assume that a lump of mineral was ground. The lump mass was 120g and it contained 50g of hematite while the rest was quartz. The grinding resulted in 30g of liberated hematite particles, 25 g of free quartz particles and the remaining part was in the form of intergrowths. The yield of liberated hematite particles was $\gamma = (30/120) \cdot 100\% = 25\%$. The content of hematite in the feed was $\alpha_{hematite} = (50/120) \cdot 100\% = 41.7\%$. Hematite recovery as free particles, i.e. liberation degree was $\varepsilon = (30/50) \cdot 100\% = 60\%$. The recovery of hematite as liberated particles can be also calculated on the bases of known equation for the recovery that is $\varepsilon = (\lambda/\alpha)\gamma = 100\% / 41,7\%) \cdot 25\% = 60\%$, where $\lambda = 100\%$ because the content of hematite in free particles is 100%.

Grinding provides particles of different sizes. When liberation is considered as a function of particle size, the degree of liberation L, i.e. ε_L can be determined for each size fraction.

To determine liberation, different methods can be used but they have to be very accurate to play the role of analytical methods. Flotation, magnetic, gravity separations as well as microscopic analysis can be used for this purpose. Then, appropriate liberation relations are used in order to present and determine particle liberation. The relation should present the state of liberation (yield, recovery, content) of a component or their combination, as a function of particle size. These quantities can be used for liberated particles and their intergrowths, i.e. all particles in the feed except for the liberated gangue particles and treated as a function of particle size. For example, Fig. 3.14c-d shows two diagrams describing grinding process providing information on liberation.

Figure 3.14c gives upgrading results for modified feed subjected to flotation in the form of component recovery in concentrate ε_i as a function of the yield of the concentrate (expressed as γ/α ratio), depending on the size of particles regulated by the extent of grinding. The time of grinding can also serve as the parameter regulating particle size. It should be noticed that ε_i in Fig. 3.14c is not the degree of liberation since it deals with the concentrate containing intergrowths as well. It is ε_L which refers to the product containing only pure particles. The best liberation is obtained when the enrichment curve, in this case the Dell upgrading curve, reaches maximum curvature.

Figure 3.14d shows the relationship between the content of iron in concentrate and average size of particles in iron ore determined by magnetic separation. Each point represents a different test. The beginning of liberation occurs when the curve starts to go up as particles size decreases. A complete liberation takes place when the concentrate contains solely pure component under examination (pure iron minerals). It is also possible to use other upgrading curves or their elements related to the size of particles produced in the course of grinding.

Liberation has been theoretically considered by many researchers. Among them the models by Gaudin (1939), Bodziony (1965), Wiegel (1976), and King (1965) should be mentioned. There are also theoretical equations determining the degree of liberation (recovery) in relation to the size of ground particles and the size of mineral particles and their content in the ore (Wiegel, 1967).

It can be concluded that grinding can be delineated as upgrading using such terms as yield, recovery, content, as well as their combinations. In the case of grinding without liberation, the process is best described by the size distribution curves (frequency, distribution, linear functions, and so on), while grinding with liberation by liberation curves in the form of the degree of liberation related to particle size or similar parameters.
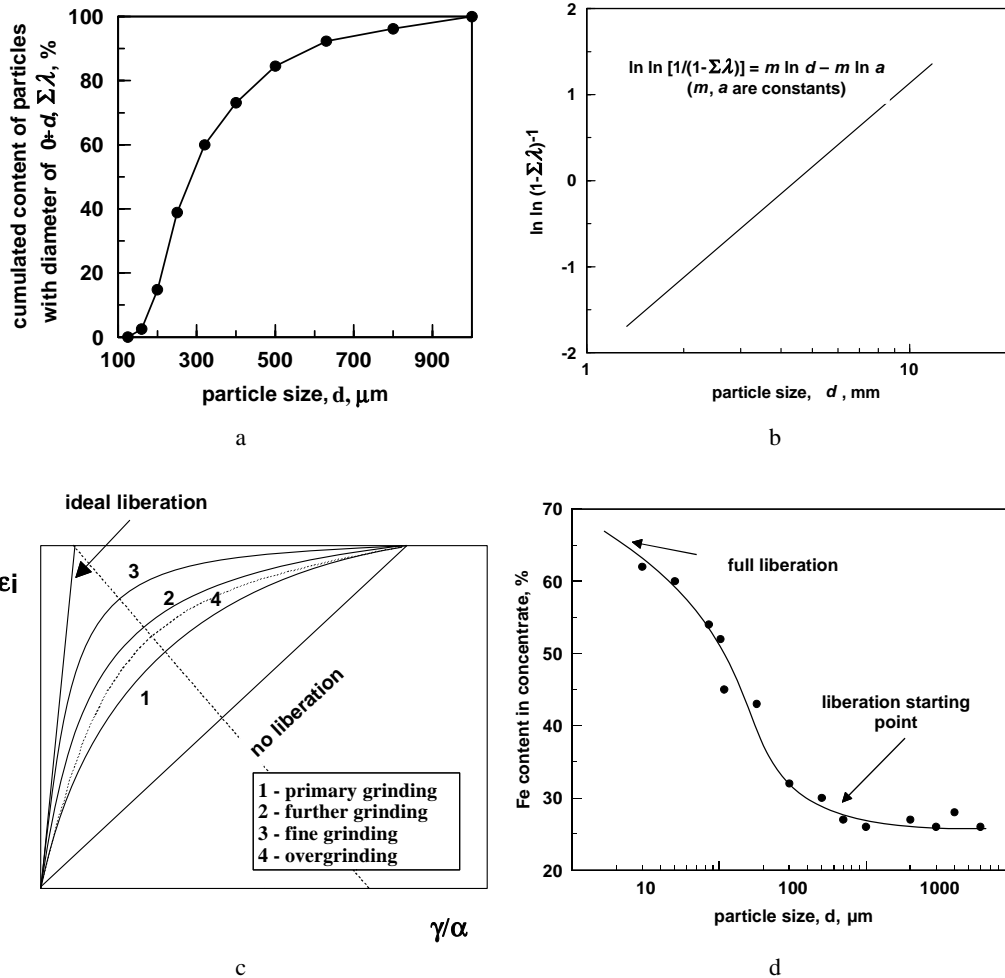
Fig. 3.14. Comminution results without taking into account liberation can be characterized by particle size distribution curves such as : a – distribution curve, b – Rosin–Rammler curve. Comminution with liberation can be characterized by means of separation curves , e.g. floatability curve of Dell (c) or concentrate quality curve containing intergrowths and free particles of the considered component as a function of particle size of the ground feed (d)

3.7. Devices used for grinding

Grinding is conducted in crushers and mills. Crushing reduces the size of particles greater than about 50-150 mm. Jaw, cone, and gyratory crushers are used for initial size reduction. Comminution of medium size grains requires jaw, cone, and gyratory

crushers as well as roll crushers. Smaller particles are ground in cone, roll and hammer crushers as well as in disintegrators an rotary breakers.

Milling is conducted in mills. Tumbling mills, rotary breakers and pendulum mills can be used for grinding. Crushing is done dry, while milling is performed wet. Wet milling is more advantageous than the dry one because it requires lower energy input (Table 3.7). Additionally, the consumption of grinding energy can be regulated by the use of chemical reagents.

Milling can be influenced by the *Rebinder effect* (1928, 1948). It predicts that grinding energy is minimum at pH of the point of zero electrical charge of the material surface. Another effect is called *mechanical activation* (Balaz, 1997; Ficeriova and Balaz, 1998). It appears that the best chemical reactivity is offered by particles having highly stressed and fresh surface resulting from grinding.

Simplified schemes of grinding devices are presented in Fig. 3.15 and Table 3.11. Each device features its own specificity and therefore the description of their operation, as well as the course of grinding is analysed in a different way. In the literature one can find detailed descriptions of the operation of different devices. Figure 3.16 shows photographs of two laboratory tumbling ball mills.
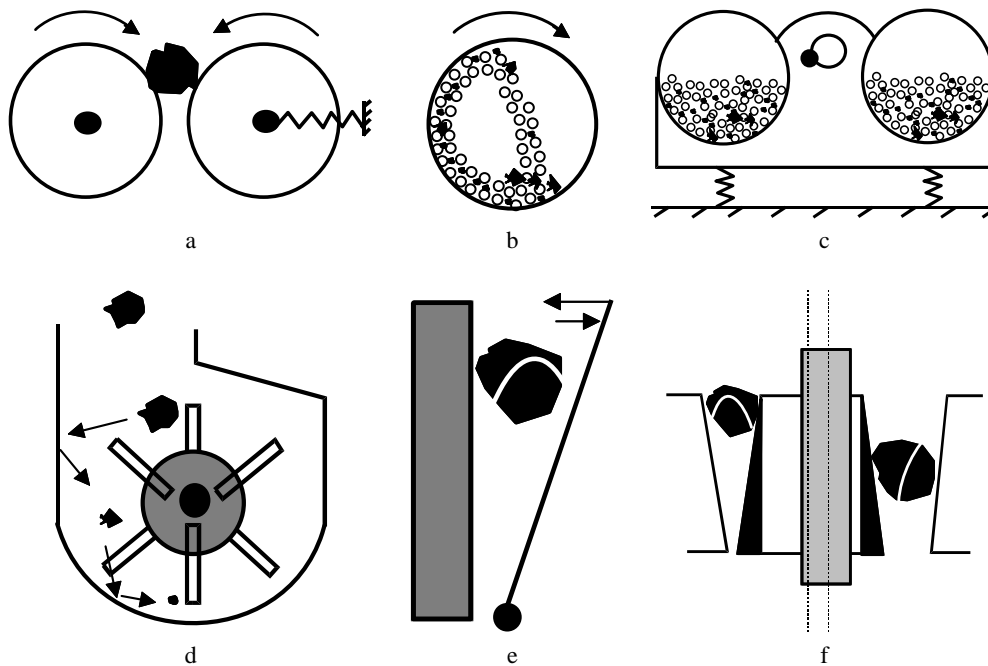
Fig. 3.15. Selected comminution devices: a – roll crusher, b – tumbling (ball) mill,
c – pendulum mill, d – hammer crusher, e – jaw crusher, f – cone crusher
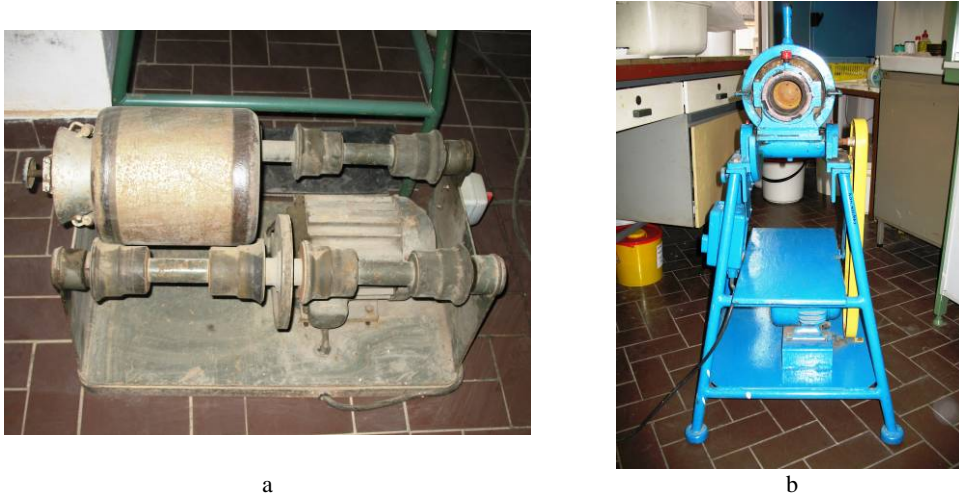
a   b

Fig. 3.16. Photographs of selected laboratory tumbling ball mills of different design and capacity,
a) 5 dm^3, b) 1 dm^3

a   b

Fig. 3.17. Laboratory cone crusher (a) and laboratory finger disintegrator (b)

Table 3.11. Dominant ways of disintegration in different size reduction devices

Grinding device	Dominant mode of size reduction	Dominant mode of size reduction
Jaw crusher	crushing	breaking, abrasion
Cone crusher	crushing	breaking , abrasion
Roller crusher	crushing	
Rotary breaker	crushing with abrasion	
Dezintegrator	free fall hitting	
Hammer crusher	free fall pitting	
Ball crusher	hitting by balls	abrasion

The mills can be filled with different grindings aids including balls, cylpebbs, rods (Fig. 3.18a), and pieces of ore (Fig. 3.18 b)

a

b

Fig. 3.18. Grindings aids: a) balls, cylpebbs, and rods, b) pieces of ore

Literature

Balaz P., 1997. Mechanical activation in processes of extractive metallurgy, Veda, Bratislava.

Bodziony J., 1965. Application of integral geometry methods to problems in mineral liberation, Bullein de l'Academie Polonise des Sciences, Series des Sciences Techniques, Vol. XIII, No. 9 (459–469); No. 10 (513–519).

Bond F.C., 1952. The third theory of comminution, Trans. AIME/SME, 193, 484–494.

Brożek M., Mączka W., Tumidajski T., 1995. Modele matematyczne procesów rozdrabniania, Wydawnictwo AGH, Kraków.

Cortel A.H., 1964. The mechanical properties of matter, Wiley, New York.

Drzymala J., 1994. Hydrophobicity and collectorless flotation of inorganic materials, Advances in Colloid and Interface Sci., 50, 143–185.

Fagerholt B., 1945. Particle size distribution of products ground in a tube mill, VI Int. Min. Proc. Congr., Cannes, 87–114.

Ficeriova J., Balaż P., 1998. Influence of mechanical activation on leaching of gold and silver from sulphidic minerals, Fizykochem. Prob. Mineralugii, XXXV Sympozjum, 53–60.

Gaudin A.M., 1939. Principles of mineral dressing, McGraw-Hill Book Company, New York.

Griffith A.A., 1921. Phenomena of rupture and flow in solids, Phil. Trans. Roy. Soc. London A., 222, 163–198.

Horst H., Freeh J., 1970. Mathematical modelling applied to analysis and control of grinding circuits, AIME Annual Meeting, Salt Lake City, paper 75-B-322.

Hukki R.T., 1961. Proposal for a solomonic settlement between the theory of von Rittinger, Kick and Bond, Trans. AIME/SME, 220, 403–408.

Kelly E.G., Spottiswood D.J., 1982. Introduction to mineral processing, Wiley, New York.

Kick F., 1885. Das Gesetz der Proportionalen Widerstande und seine Anwendung, Leipzig.

King R.P., 1975. A quantitative model for mineral liberation, J. South Afr. Inst. Mining and Metallurgy, 76, special issue.

Koch R., Noworyta A., 1992. Procesy mechaniczne w inżynierii chemicznej, WNT, Warszawa.

Lipczyński J., Okołowicz M., Olczak S., 1984. Tablice fizyczne, chemiczne i astronomiczne, Wydawnictwa Szkolne i Pedagogiczne, Warszawa.

Lowrison G.C., 1979. Crushing and grinding, Butterworths, London.

Lynch A.J., 1977. Mineral crushing and grinding circuits, Developments in Mineral Processing, 1, Elsevier, Amsterdam.

Malewski J., 1990. Modelowanie i symulacja systemów wydobycia i przeróbki skał, Prace Naukowe Instytutu Górnictwa, nr 60, Seria Monografie 27, Wyd. PWr., Wrocław.

Manlapig E.V., Seitz R.A., Spottiswood D.J., 1979. Analysis of breakage mechanism in autogenous grinding, XIII Int. Min. Proc. Congress, J. Laskowski (ed.), V. 1, PWN, 677–694.

Mokrzycki E., 1981. Rozdrabnianie, w: Blaschke Z., Brożek M., Mokrzycki E., Ociepa Z., Górnictwo, cz. V, Zarys technologii procesów przeróbczych, skrypt AHG, Kraków, s. 768.

Mölling H.A., 1960. Grundfragen der Grobzerkleinerung, Aufber. Techn. 7, 287–298.

Oka Y., Majima W., 1970. A theory of size reduction involving fracture mechanics, Can. Met. Quarterly, 9, 429–439.

Rebinder P.A., 1928. On the effect of surface energy changes on cohesion, hardness, and other properties of crystals, Proc. 6th Phys. Congress, State Press, Moscow.

Rebinder P.A., Schreiner L.A., Zhigach K.F., 1948. Hardness reducers in drilling, Trans. Counc. Sci. Ind. Res., Melbourne, 163ff.

Rittinger P.R., 1857. Lehrbuch der Aufbereitungskunde, Berlin.

Rumpf H., 1973. Physical aspects of comminution and new formulation of a law of comminution, Powder Technology, 7, 145–159.

Sokołowski M., 1995. Energia rozdrabniania, IMBiGS, Warszawa.

Walker W.H., 1937. Principles of chemical Engineering, McGraw-Hill, New York.

Wiegel R.L., Li K., 1967. A random model for mineral liberation by size reduction, Trans. SME/AIME, Vol. 238, No. 7, 179.

Wills B., 1985. Mineral Processing Technology, Pergamon Press, Oxford.

Wroblewski A.K., Zakrzewski J.A., 1984. Wstęp do fizyki, t. 1, PWN, Warszawa.

4. Screening

4.1. Principles

Screening, also called mechanical classification, is a separation process which utilizes the differences in particle size. The particles which are smaller than screen opening pass through the screen while larger particles either remain on the screen or fall off at a designated place (Fig. 4.1).
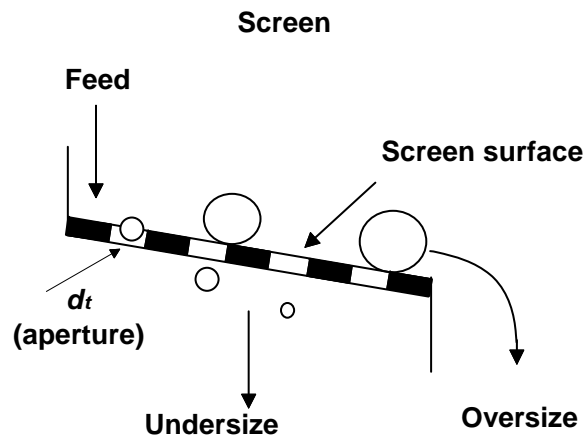
Fig. 4.1. Screening. Main parameter of screening is particle size

The purpose of screening is splitting the feed into two or more, differing in size, products. The main parameter, due to which separation takes place, is the particle size. Screening is a continuous process performed on a large scale while sieving is performed on sieves on a small batch laboratory scale (Kelly and Spottiswood, 1982). Each screen usually provides two products. To obtain more products it is necessary to use additional screens. Particles going through the screen form a product usually called undersize, minus, or lower product, while the ones remaining on the screen are known as oversize, plus, or upper product. Other names are also used including concentrate and waste. Intermediate product is the material passing through one and retained on a subsequent screen. Screening is frequently used as the method of separation, and is applied both as a single operation or in combination with other processes.

Each separation product and the feed represent a collection of particles differing in size. Therefore, the feed and separation products can be analyzed for the content of particles of strictly limited sizes, i.e. the content of particular fractions of particles.

Each separation product has its own, characteristic particle composition, which can be presented as table, histogram, distribution curves and other plots. On the basis of two histograms or one partition curve it is possible to characterize any separation process in terms of classification into fractions according to the main feature, which for screening is the particle size (Fig. 4.1). One of the size fractions can be considered as a characteristic component of the screening system and used for analysis of screening as upgrading. The mass of a selected size fraction can be balanced in the feed and the products of separation by determining the yield of the products, the content of the selected size fraction in the products and other parameters such as recoveries. The upgrading approach uses quality vs. quantity parameters and the results can be presented in a graphical form. The curves and indicators of upgrading do not express the behavior of many particle size fraction, as it takes place in the case of classification, but only one selected size fraction.

4.2. Particle size and shape

Particles undergoing separation are rarely spherical. Non-spherical particles (Fig. 4.2) require more detailed description of their shape and size. The ways of defining and determining particles size and shape are presented in Table 4.1. and some of them are demonstrated in Fig. 4.3.

a   **b**
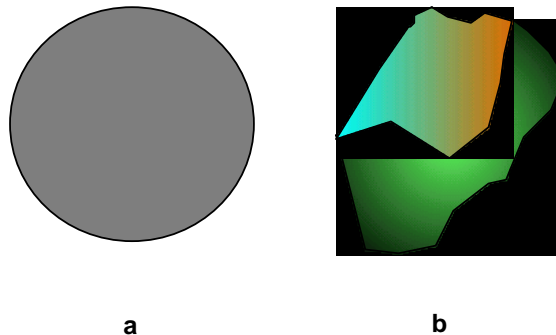
Fig. 4.2. Spherical (a) and irregular (b) particles

The particle shape can be described using words and numbers. Table 4.2 shows classification of particles into spherical, column-like, flat and flat-column in shape. The division is based on the length, width, and height of particles. The factors characterizing particle shape are shown in Table 4.3.
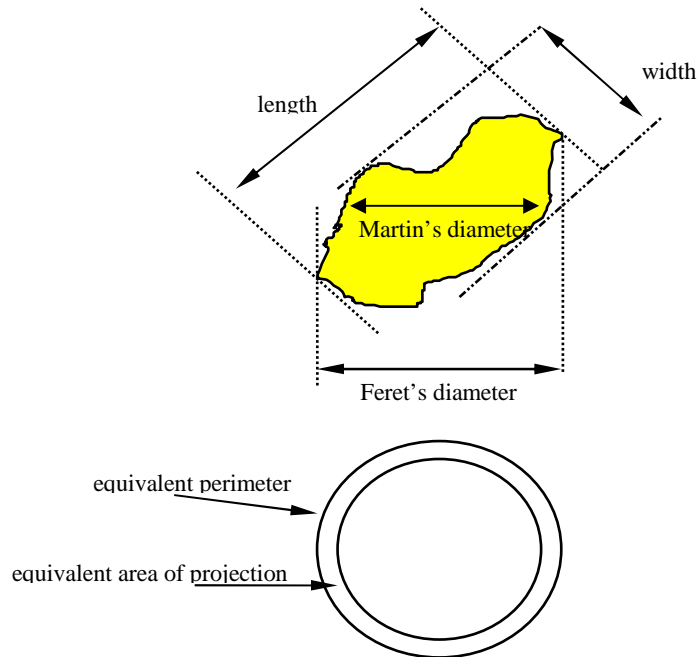
Fig. 4.3. Selected ways of size delineation of irregular particles (after Kaye, 1966)

Table 4.1. Diameter of irregular particles

Name	Details
Arithmetic diameter	Arithmetic mean of three sizes (length, width and height) of particle $((a+ b +c)/3))$
Geometric diameter	Geometric mean of three sizes of particle $(abc)^{1/3}$
Harmonic	Harmonic mean of three sizes of particle $\{1/3(1/a+1/b+1/c)\}^{-1}$
Screen diameter	With of a minimum square opening through which particle will pass
Screen diameter	Arithmetic mean of two screen apertures: through which a particle will not pass and through which particle the particle will pass
Surface diameter	Diameter of a sphere having the same surface area as the particle
Volume diameter	Diameter of a sphere having the same volume as the particle
Projected area diameter	Diameter of a sphere having the same projected area as the particle when viewed in a direction perpendicular to a plane of stability
Drag diameter	Diameter of a sphere having the same resistance to motion as the particle in a fluid of the same viscosity and velocity when Re is small
Fee-falling diameter	Diameter of a sphere having the same falling speed as the particle in the same fluid
Stokes' diameter	Free-falling diameter in the laminar flow regime, $Re_{partilce} < 0.2$
Specific surface diameter	Diameter of a sphere having the same ratio of surface area to volume as the particle
Feret's diameter	Microscopy calculation to determine particle size by measuring distance between theoretical parallel lines that are drawn tangent to the particle profile and perpendicular to the ocular scale
Martin's diameter	Microscopy calculation to determine particle size by measuring the dimension that severs a randomly aligned particle into two identical projected halves parallel to the ocular scale

Table 4.2. Shape of irregular particles (*a* – length, *b* – width, *c* – height). According to Zingga

Particle shape	Indices
Spherical	*b/a* > 2/3; *c/b* > 2/3
Column-like	*b/a* < 2/3; *c/b* < 2/3
Flat-like	*b/a* > 2/3; *c/b* < 2/3
Flat- and column-like	*b/a* < 2/3; *c/b* <2/3

Applicability of the particle size and shape measures depends on the nature of the process and, sometimes, personal preferences. These issues are important when precise description of separation processes based on screening is needed.

Table 4.3. Selected shape factors

Shape factors	Description	Formula
Superficial λ_s	ratio of surface area of particle and area calculated from nominal particle diameter	$\lambda_s = \pi d_s^2/\pi d_n^2$ d_s – diameter of sphere having the same area as the particle
Volumetric λ_v	ratio of volume of particle and its volume calculated from nominal particle diameter	$\lambda_v = (\pi/6)d_v^3/(\pi/6)d_n^2$ d_v – diameter of sphere having the same volume as the particle
Spherical Ψ	ratio of sphere surface area having the same volume as the particle and the surface area of particle	$\Psi = (d_v/d_s)^2$
Krumbein's sphericity, Ψ_k	ratio of volume of ellipsoid (triaxial) to volume of sphere outlining the ellipsoid	$\Psi_k = \{(\pi/6)abc/(\pi/6)a^3\}^{1/3}$
Schiel's sphericity Ψ_S	ratio of average particle determined with circular opening screens ($d_o = d_{o\,0,5}$) to average particle determined by squared opening screens ($d_k = d_{k\,0,5}$), that is ($k = d_o/d_k$)	$\Psi_S = (1 - \log k/\log\sqrt{2}\,)$

Sometimes there is a need to calculate average diameter of a collection of particle. In such a case, depending on application, arithmetic, geometric, and harmonic averaging can be used. There are other approaches based on the formulas used by Bond (Eq. 3.14) and Sauter ($d_{30} = \sqrt[3]{\dfrac{\Sigma n_i d_i^3}{\Sigma n_i}}$ -mean volume–quantitative diameter and

$d_{32} = \dfrac{\Sigma n_i d_i^3}{\Sigma n_i d_i^2}$ mean volume-area diameter where d_{ij} is appropriate average diameter, d_i diameter of a particle, *n* number of particles of size d_i).

4.3. Description of screening process

Screening, like other separation processes, can be described in many different ways. The description depends on what is to be stressed and which parameters of the process is important. In this work it has been assumed that each separation process can be described in terms of thermodynamics, mechanics, probability, and others (Fig. 4.4).
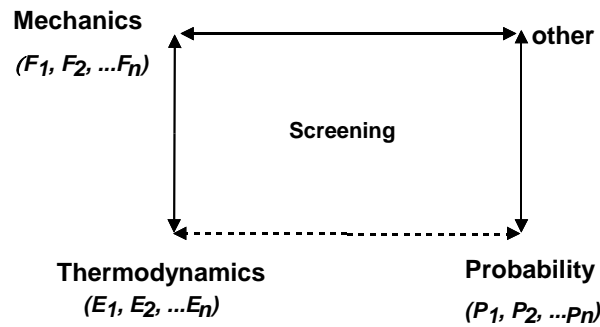
Fig. 4.4. Possible ways of delineation of screening as separation process

The current knowledge on screening does not allow to describe fully this process. Thermodynamics of screening is especially poorly developed because the equilibrium and linear thermodynamics cannot be applied for this purpose. The description of the mechanics of screening, based on force balance has been quite satisfactorily worked out. Other types of delineations are fragmentary. In the subsequent chapters basic relations necessary for describing screening from the point of view of mechanics, probability of its occurrence and the formulas combing different physical parameters of this operation and, finally, selected equations for screening kinetics have been presented. The analysis and assessment of screening can be found in another chapter.

4.3.1. Mechanics of screening

Many different forces influence screening. A particle sitting on a vibrating screen is effected by the gravity G, inertia P and friction T forces. Each force can be split into normal (y) and tangent (x) components (Fig. 4.5). The basic requirement for initiation of screening is the movement of a particle. In the case of screening on flat horizontal screen surface this condition is fulfilled when the particle starts to slide. It happens when maximum inertia force P is larger than the friction force T operating between a particle and the screen surface. This is expressed by the force balance (Fig. 4.5a).

$$P = \mu_o G > T \tag{4.1}$$

where μ_0 is the friction coefficient.

This equation can be applied to batch screening (sieving).
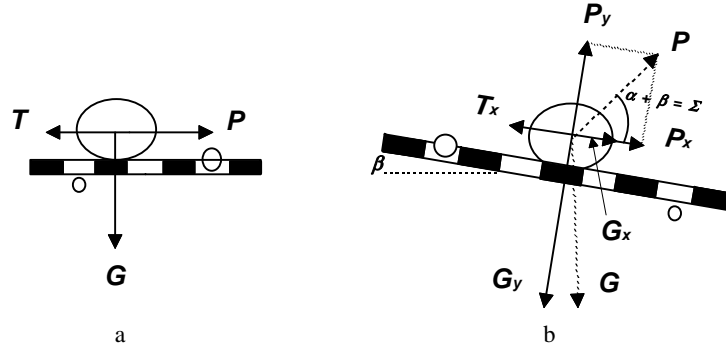
Fig. 4.5. Forces acting on a particle present on a screen surface: a) horizontally vibrating screen, b) inclined screen surface with angle β and vibrating with angle α (based on Banaszewski, 1990)

In the course of screening it is important to ensure smooth transportation of particles all over the screen for efficient removal of the oversized particles. This can be obtained by vibrating the screens. Most often harmonic vibrations are applied at an angle in relation to the screen surface. The screens can also be positioned at a certain angle β in relation to the horizontal level. The force balance for such a case has a form of (Banaszewski, 1990) (Fig. 4.5b):

$$P_x + G_x > T_x. \tag{4.2}$$

Inequality (4.2) shows that the condition of particle movement is when the sum of the tangent forces of inertia (P_x) and gravity (G_x) is greater than the friction T_x.

When the inertia force operates at an angle in relation to the screen, the particle detaches and moves above the screen surface. This phenomenon is called the particle movement with casting. The condition for particle ejection is that the normal component of the inertia force is greater than the normal component of gravity force, i.e. (Fig. 4.5b):

$$P_y > G_y. \tag{4.3}$$

Other forces may participate in screening. When they are significant, they should be taken into consideration.

On the basis of the force balance, appropriate equations describing physics of the process can be derived. In the case of screening with transportation in the absence of particle casting ($P_x + G_x > T_x$), after substitution of the forces with the following expressions (Banaszewski, 1990):

$$P_x = P \cos(\alpha + \beta) = ma \cos(\alpha + \beta), \tag{4.4}$$

$$G_x = G \sin \beta = mg \sin \beta, \tag{4.5}$$

$$T_x = \mu_o (G_y - P_y) = \mu_o [mg \cos \beta - ma \sin(\alpha + \beta)], \tag{4.6}$$

it is possible to obtain the so-called particle shift factor u_s:

$$u_s = \frac{u_o \left[\cos (\alpha + \beta) + u_o \sin (\alpha + \beta) \right]}{u_o \cos \beta - \sin \beta} > 1 \, , \tag{4.7}$$

where u_o is the dynamic screening factor defined as the ratio between the maximum screen acceleration and acceleration due to gravity:

$$u_o = \frac{A \omega^2}{g} \, . \tag{4.8}$$

Screen acceleration a was replaced with maximum acceleration which is $a = A\omega^2$ for harmonic vibrations.

In Eqs (4.4)-(4.7) the used symbols denote:

A – amplitude of harmonic vibration
ω – angular speed
G_x – tangent component of the gravity force
G_y – normal component of the gravity force
P_x – tangent component on the inertia force
P_y – normal component on the inertia force
m – particle mass
g – gravity
a – shifting acceleration
β – screen inclination
α – direction of inertia force resulting from harmonic vibration of inclined screen.

When one considers particle movement with casting (Fig. 4.5b), the condition determined by Eq. (4.3), i.e. $P_y > G_y$ has to be fulfilled. After substituting P_y and G_y with appropriate expressions for the forces:

$$P_y = P \sin (\alpha + \beta), \tag{4.9}$$

$$G_y = G \cos \beta, \tag{4.10}$$

the expression for the casting factor is obtained:

$$u_p = \frac{A\omega^2 \sin(\alpha + \beta)}{g \cos \beta} => \frac{A\omega^2 \sin(\Sigma)}{g \cos \beta} > 1 \, , \tag{4.11}$$

because $G = mg$, $P = ma$, and $a = A\omega^2$.

In equation (4.11) Σ is the casting angle and it represents the sum of the angle of screen surface inclination β and the angle of action of the inertia force α. Maximum value of the casting factor does not exceed 3.3 (Sztaba, 1993). The casting factor is

determined by the construction and operation of the screen because it depends on *A*, ω and β.

Particle movement with casting is more effective because screening with casting facilitates better loosening of the particles layer and detachment of fine particles from the large ones. There are better conditions for particles to pass through the screen surface and removal of the so-called blinding particles which block the screen (Fig. 4.6). The blinding particles are of the size between 3/4 d_t and 3/2 d_t, where d_t is the size of the screen opening (Sztaba, 1993). The extent of casting depends on the screening system including the properties of particles. The mode of casting depends on the angle of fall, particle and screen relative speed at the moment of particle falling.

As a result of a movement or casting the particles fall into the screen aperture. When particle movement is the main mechanism of screening, the shift indicator u_s is a very useful factor describing screening from the mechanical point of view. When casting accompanies particle movement, the casting factor is a better measure, namely, the angle of casting Σ as it determines the angle of particle fall on the screen. The angle of fall, in addition to the particle size in relation to the screen size, are the most important parameters governing particles screening. This results from the fact that the angle of particle fall decides about the probability of its screening. More details are provided in the section on the probability of screening. Thus, the angle of casting and the angle of fall belong to those few parameters which combine mechanics and probability aspects of the screening.
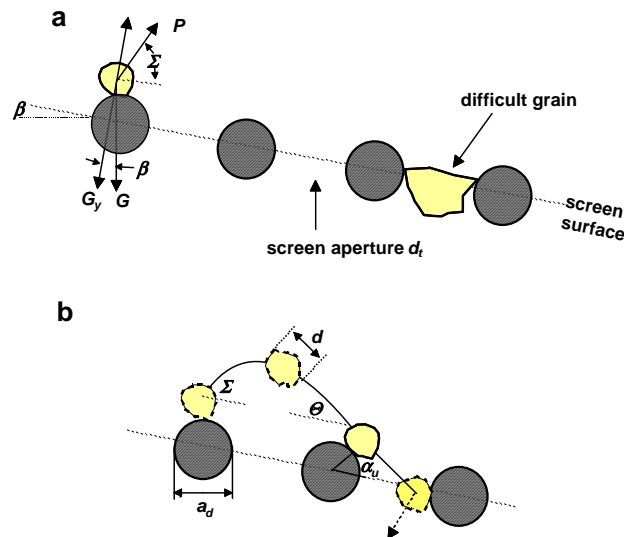
Fig. 4.6. Steps of particle movement on the surface of screen: a – step I and step II – movement of particle and screen together and beginning of the movement of particle against the surface, b – step III and IV – flight of particle, falling of particle, sliding, bouncing and passing through the screen. Σ– casting angle, θ – falling angle, α – inertia force angle , β – screen surface inclination angle, a_d - diameter of woven wire screen

According to Czubak (1964) and Banawszewski (1990) the process of screening consists of four phases. The first one covers mutual movement of the particle and screen. The second phase deals with particle sliding, the third one consists in particle flight, and the fourth phase is particle fall. In the latter phase several phenomena can take place: particle falling into a screen mesh, particle sliding on the screen or on other particles, or particle bouncing from the screen surface.

4.3.2. Probability of screening

The screening process can be also be treated as a random process. The probability of particle screening $P_{screening}$ depends on many factors and it can be written as:

$$P_{screening} = P_1 \, P_2 \, P_3 \, ... \, P_n \, ,$$

(4.12)

where symbols P_1, P_2 ..., P_n refer to probability of components of the process.

The probabilities of any process can be combined into groups. In our case they can be gathered into three groups, i.e. probability reflecting the size and shape of particle (P_z), probability referring to screen geometry P_s, and probability P_r dealing with the mode of screen movement in which the screen surface is installed, i.e.:

$$P_{screening} = P_z P_s P_r,$$

(4.13)

which was schematically shown in Fig. 4.7.
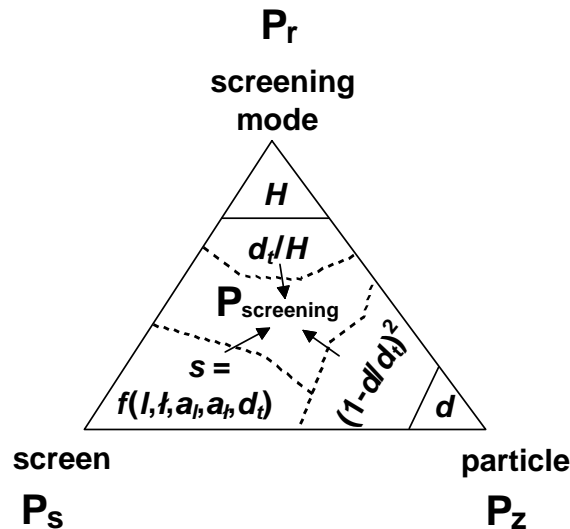
Fig. 4.7. Influence of different parameters on probability of screening for a layer of particles

When considering each of those probabilities, it is advantageous to make them dependent on the size of screen aperture d$_t$. Then, the probability of screening, connected with the particle size P$_z$, can be written as:

$$P_z = \left(1 - \frac{d}{d_t}\right)^2,$$ (4.14)

where:
d – particle diameter, mm
d_t – screen aperture, mm.

Equation 4.14 is valid for spherical particles. According to Sztaba (1993) it can be adopted for real particles because the particles on a screen tend to assume stable positions. Then, their diameter becomes best characterized by a projection diameter (d_p). It is connected with the equivalent diameter d_z through shape factor C_{AN}:

$$d_p = \frac{d_z}{\sqrt{C_{AN}}}.$$ (4.15)

In Eq. 4.15, as it has been shown in Table 4.1, d_p is the diameter of a circle which has the same surface area as particle perpendicular projection on the plane situated as close as possible to the plane. Equivalent diameter d_z, is a diameter of a sphere of the same volume as the considered particle. The equivalent diameter can, according to Sztaba (1993) be made dependent on the arithmetic mean of particle size fraction borders d_A and constants a and b, which can be experimentally determined. For quartz they are equal to: $a = 1.08967$, $b = -0.0003$, for limestone: $a = 0.9228$, $b = 0.1578$, for galena: $a = 0.9490$, $b = 0.1885$ and for ferrosilicon: $a = 0.9541$, $b = 0.1166$. Screening probability of a real particle is, therefore, connected with its size and shape and can be expressed by the dependence (Sztaba, 1993):

$$P_z = \left(1 - \frac{ad_A + b}{\sqrt{C_{AN}} d_t}\right)^2.$$ (4.16)

Probability connected with the screen design P$_s$ can be written in the form:

$$P_s = s = \frac{rd_t^2}{(rd_t + a_l)(d_t + a_l)},$$ (4.17)

where:
s – the so-called screen transparency coefficient
r – coefficient of rectangularity of screen aperture, $r = l/ł$
l – lengths of screen opening

ł – width of screen opening

a_l – thickness of bridge between two neighboring screen openings dividing sides *l* of the aperture

a_t – thickness of bridge between two neighboring screen openings dividing sides *ł* of the aperture (Sztaba, 1993).

The probability connected with the screening mode P_r depends on the way screening is conducted. For screening involving thick layer of the material on the screen, probability P_r will be expressed by the relation:

$$P_r = \frac{d_t}{H} \ ,$$ (4.18)

where *H* is the thickness of particle layer on a screen surface (Fig. 4.7).

Finally, general expression for the probability of particle screening can be expressed by the equation:

$$P_{screening} = P_z P_s P_r = \left(1 - \frac{a d_A + b)}{\sqrt{C_{AN}} \ d_t}\right)^2 \frac{r d_t^2}{(r d_t + a_l)(d_t + a_t)} \frac{d_t}{H} \ .$$ (4.19)

According to Sztaba (1993) Eq. (4.19) determines minimum probability of particle screening on the screen, and its calculation is extremely complicated. The delineation of this process can be found in other works (e.g. Sztaba, 1993).
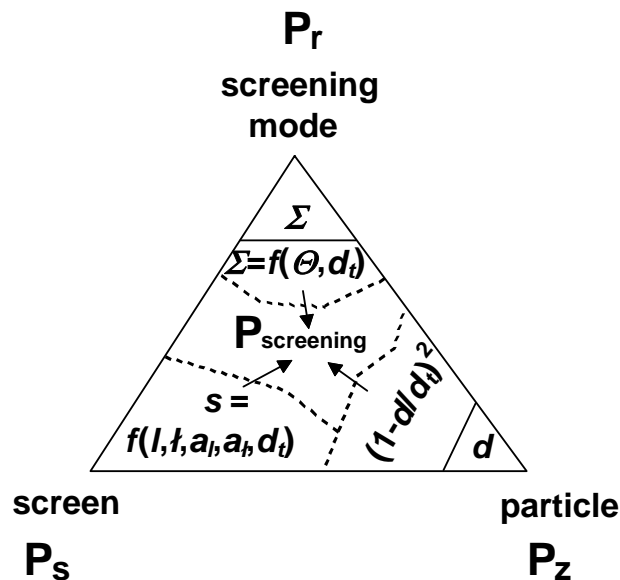
Fig. 4.8. Influence of parameters on probability of screening with particle casting

Various expressions for probability of screening for other cases, especially for different modes of screen movement are offered in the literature. Probability of screening of a free single particle which is ejected during screening (Fig. 4.6 and Fig. 4.8) is expressed by the relation (Sztaba, 1993; Gaudin, 1946):

$$P_g = \left[\frac{(d_t + a) - (a + d)\cos\alpha_0}{d_T + a} \right] \left[\frac{(d_t + a) - \left(\dfrac{a+d}{2}\right)\left(\dfrac{\sin(\theta + \alpha_1) + \sin(\theta - \alpha_1)}{\sin\theta}\right)}{d_t + a} \right] \quad (4.20)$$

where:
θ – angle of particle fall or angle of approach
α_0 – critical angle is determined by the relation:

$$\cos\alpha_0 = \frac{1 + \sqrt{1 + 8m^2}}{4m}, \quad (4.21)$$

and α_1 and α_2 are positive roots of the equation

$$4m^2(k^2 + 1)\cos^4\alpha - 4mk(k^2 + 1)\cos^3\alpha - (4m^2 - 1)(k^2 + 1)\cos^2\alpha + \\ + 2m(k^2 + 2)\cos\alpha + m^2k^2 - 1 = 0,$$

in which $k = \text{tg}\,\alpha_u$ and α_u is the angle formed with the screen plane by the line connecting the center of particle gravity with the cross-section centre of a wire forming the screen at the moment of particle touching the wire (screen bridge) ($\alpha_0 \leq 90^0$) and:

$$m = \frac{2d_t + a - d}{a + d} . \quad (4.22)$$

According to Sztaba (1993) there is a considerable difference between the probability formulas and the results of actual screening. Therefore they are seldom used in practice.

4.4. Kinetics of screening

Usually it is assumed that the kinetics of screening conducted in a periodical way can be described with the first order differential equation:

$$v_{p\,i} = -d\lambda_i/dt = k_i\,\lambda_i, \quad (4.23)$$

where v_{pi} determines the speed of passing of certain particles having certain properties through the screen.

Screening involves only the particles smaller than the screen aperture and it will not be a great error to assume that a particle of given properties can be represented by

a narrow size fraction *i* of the feed. In Eq. (4.23) λ_i represents the content of fraction *i* in the product on a screen surface at particular moment of screening time *t*.

For periodical processes at $t = 0$, fraction *i* content on the screen is equal to the content of this fraction in the feed, i.e. α_i. For a long time of screening λ_i assumes constant low value, while in the case of ideal screening this value equals zero. In equation (4.23) k_i is the constant of screening rate of particular class of particles. Negative sign in this equation means that the screening rate decreases as the content of particles capable of being screened decreases. In Eq. (4.23), instead of the content of particular size fraction of particles, one can use particle *i* mass, the number of particles or their volume, but then constant *k* value will be different. After solving differential equation (4.23) one obtains general relation describing concentration of the fraction on the screen surface at particular moment of periodical process:

$$\lambda_{i,t} = \alpha_i \exp(-k_i t), \tag{4.24}$$

where α_i denotes content of *i* size fraction in the feed.

For the description of a continuous screening, Eqs (4.23) and (4.24) should be modified because screening efficiency also depends on location of particle on the screen surface, as well as on the speed of feeding, but not on the time which has passed since the initiation of screening took place.

For a continuous screening, when particle movement is not restricted by other particles, the speed of free screening v_s expressed as a change of flow of material mass subjected to screening on a screen surface per unit time and per screen unit width at a particular place at a distance *L* from the point of feed addition per unit length *L* change, has the following form (Kelly, Spottiswood, 1982):

$$v_s = -dI_L/dL = k_s I_L, \tag{4.25}$$

where:

I_L – specific rate, i.e. the flow of material mass per unit time and screen unit width at a particular place

L – distance between considered place on the screen and the point of material feeding for screening

k_s – rate constant of the process.

The constant of the process rate k_s depends on the kind of particle size fraction *i*. Therefore, introducing the content of the size fraction λ_i in the feed, leads to the following equation:

$$-d\,(I_L\lambda_{iL})\,/dL = k_s\,I_L\lambda_{iL}, \tag{4.26}$$

where λ_{iL} is the size fraction content *i* on the screen at place *L* measured as the distance from the front of the screen towards the movement of the screened material. After integrating, one can obtain:

$$I_L\lambda_{iL}/I\lambda_i = \exp(-k_s L). \tag{4.27}$$

Since $I_L/I_{L=0} = I_L/I = \lambda_s$, the ratio of the stream of material on the screen at a particular point of screen length and the stream of material at the initial point of the stream, i.e. the feed stream, it is the yield of the material on the screen γ_s. As $\lambda_i = \alpha_i$, i.e. the content of particular size fraction in the feed and since $\gamma_s \lambda_{iL}/\alpha_i = \varepsilon_{-i}$, as well as since the recovery on the screen in the product passing through the screen is $\varepsilon_{+i} = 100\% - \varepsilon_{-i}$, the following relation is obtained (Kelly, Spottiswood, 1982):

$$(100\% - \varepsilon_{+i})/100\% = \exp(-k_{si}L). \tag{4.28}$$

When a large amount of particles is subjected to screening, they can mutually interact, e.g. when the particle layer is very thick, only the particles close to the screen surface undergo screening. The particles which become screened are immediately replaced by similar particles from higher layers. Then, screening can be determined with the use of equation of zero order kinetics (Kelly, Spottiswod, 1982):

$$-dI_L/dL = k_c, \tag{4.29}$$

in which k_c is constant of moving particle for a hindered screening.

Since, like in the previous case, each size fraction of particle has its own rate constant, therefore:

$$-d(I_L\lambda_{iL})/dL = k_{ci}\,\lambda_{iL}. \tag{4.30}$$

To calculate the yield of particular size fraction of particles in the screened product up to a selected location on the screen, the following formula can be applied:

$$-\ln(100\% - \varepsilon_{+i}/100\%) = k_{ci}\int_0^L \frac{dL}{I_L}, \tag{4.31}$$

which requires integrating expression dL/I_L within L ranging vales from zero to the point on the screen length where the screening is hindered. For a continuous screening, very often the initial part of separation can be described using equation for the hindered screening, while in the lower part of the screen with the formula for a non-hindered screening.

From the so far presented equations a strong relation between the yield of a particular size fraction and the screening rate is visible. It is also called the output. The output can be expressed as the quantity of screened feed, component or particular fraction. The screening speed can be expressed not only in terms of mass per unit time or per mass unit or even per screen width unit, but also per time and surface. Sztaba (1993) calls it the unit output.

According to Malewski (1990), the rate constant for selected size fraction and for non-hindered, periodical screening can be expressed by the relation:

$$k_{si} = k_{0.5}\left[2\left(1 - \frac{d_i}{d_t}\right)\right]^{\delta}, \qquad (4.32)$$

where:

$k_{0.5}$ – constant of screening rate for particle size equal half the size of the screen mesh
δ – constant.

The constant of the screening rate $k_{0.5}$ depends on many parameters of screening:

$$k_{0.5} = 3600\ VBW\varphi sCd_s/Q_o, \qquad (4.33)$$

where:

V – speed of material moving on the screen, m/s
B – screen width, m
W – moisture function effecting screening (for dry material $W=1$)
φ – constant dependent on the scale on which screening takes place, also called the
       scale factor
s – clearance factor ($s = [d_t/(d_i + a_d)]^2$)
c – constant determined empirically, is dependent on screen inclination
d_i – screen opening diameter, m
Q_0 – intensity of the stream of feed, m³/h
a_d – screen wire thickness (size)
d – particle diameter.

The final formula for the recovery of selected size fraction i of screening as a function of screening time, has the form:

$$\varepsilon_i = 1 - \exp[-t\,k_i] = 1 - \exp\left[-t\,3600\ VBW\varphi sCd_s\,[2(1 - d/d_t)]^{\delta}/Q_o\right]100\%. \qquad (4.34)$$

There are numerous empirical equations describing screening for particular screens and material (Malewski, 1990); Banaszewski, 1990; Sztaba, 1993). For a continuous screening screens most often the equation involves the intensity of the stream in the form of feed stream or stream of selected products or components (fractions) as a function of the recovery of selected particles, also called the screening efficiency. Selected approximate formulas of these relations are shown in Table 4.4.

Table 4.4. Selected approximate formulas for mass yields of continuous screening

Author	Formula	Source
Nawrocki	$Q = 900Fn^{0.5}sd_t\rho_u v_m\,C/Sb$ (Mg/h)	Banaszewski, 1990
Kluge	$Q = FQ_jW_gW_d\,SHM$ (Mg/h)	Banaszewski, 1990
Olewski	$Q = 2.23\cdot10^{-4}(100 - \varepsilon)\,d_t\,p_c\,\rho_u$ (Mg/h)	Sztaba, 1993

Q – effective efficiency (mass stream) of the feed at a given recovery.

The Nawrocki formula: n – frequency of vibration, min⁻¹, s – coefficient of openings area, d_t – side size of square screen opening, m, ρ_u – bulk density of screening

material (feed), Mg/m^3, v_m– velocity of material on the screen, m/s, C– screening difficulty coefficient, S – screening efficiency coefficient, b – material viscosity coefficient.

```
                        ┌──────────────┐
                        │   SCREENS    │
                        └──────────────┘
              ┌───────────────┴───────────────┐
         ┌─────────┐                     ┌─────────┐
         │  mesh   │                     │   bar   │
         └─────────┘                     └─────────┘
        ┌────┴────┐                    ┌─────┴──────┐
   ┌────────┐ ┌────────┐          ┌────────┐  ┌──────────┐
   │  drum  │ │  flat  │          │ static │  │ dynamic  │
   └────────┘ └────────┘          └────────┘  └──────────┘
```
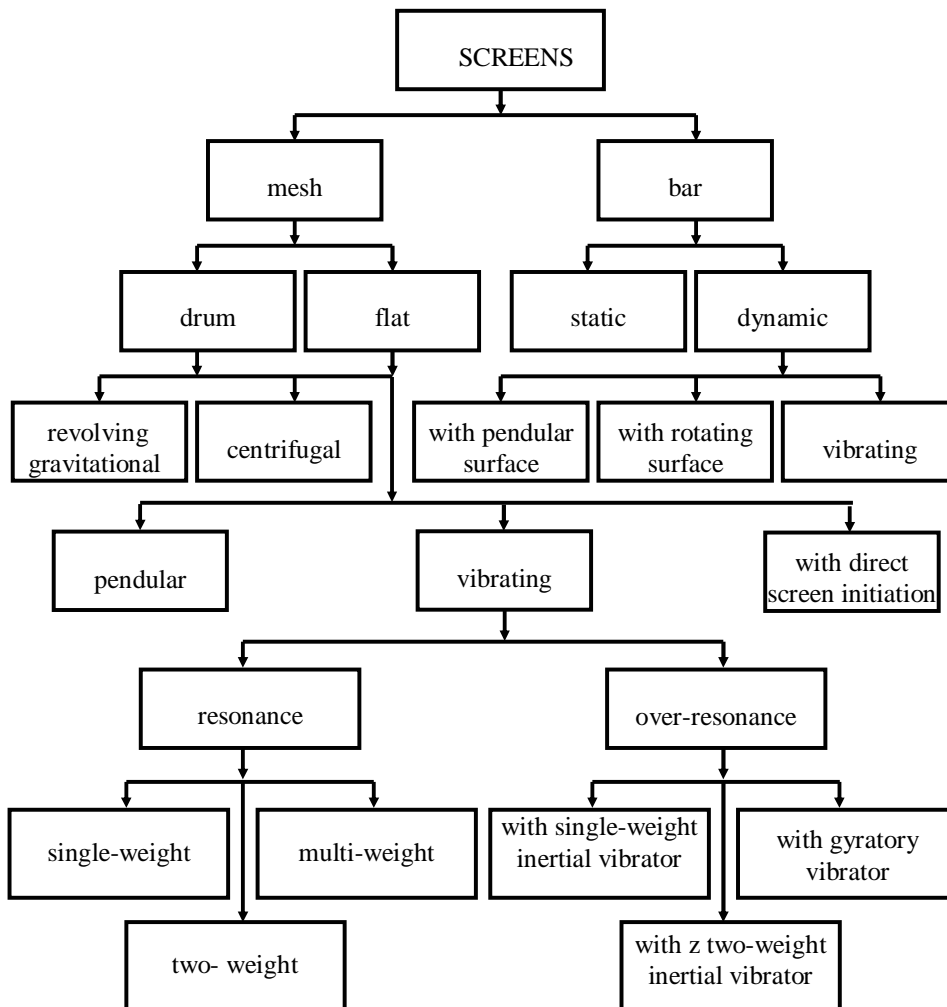

Fig. 4.9. Classification of screens according to their type (after Banaszewski, 1990; with permission of the Śląskie Wydawnictwo Techniczne)

The Kluge formula: F – screen surface area, Q_j – unit output depending on the screening surface opening and type of screened material, Mg/(h·m^2), W_g– coefficient depending on content (in %) of particles greater that the screen openings, W_d – coefficient dependent on the content (in %) of particles smaller than the half size of the screen aperture, S – coefficient depending on requested efficiency of screening; H – coefficient depending on type of screening (wet or dry) and appropriate size of screen openings d_t; M – taking into account number of decks in one riddle, for the first deck $M = 1$, for a second $M = 0.9$, while for third $M = 0.75$. Coefficients W_g, W_d and S can be determined using nomograms available from Banaszewski (1990).

The Olewski formula: p_c – surface area of working part of screen, m^2, ε – recovery of undersize product, d_t – screen surface opening, ρ_u– bulk density of the material.

The formulas given in Table 4.4 are often complicated, although they represent only approximate versions. According to Banaszewski (1990) a correct determination of the screening output can be done only by experienced specialists who are skillful in estimating the influence of many parameters on the process. Classification of screeners, after Banaszewski (1990) is shown in Fig. 4.9, and after Kelly and Spottiswood (1982) in Fig. 4.10.
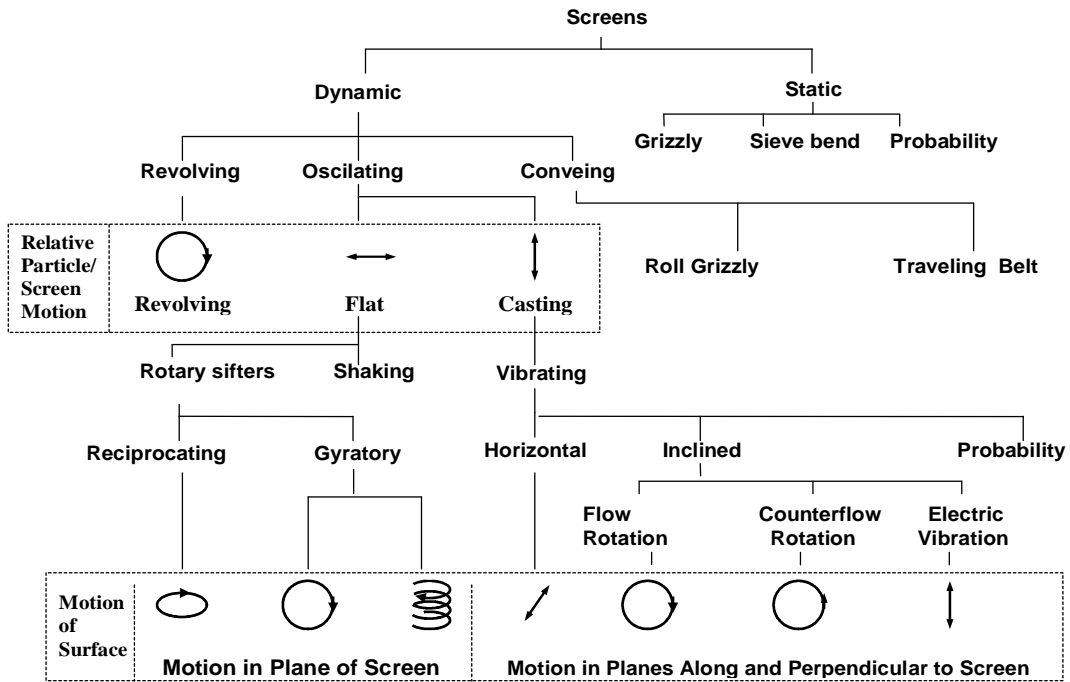
Fig. 4.10. Classification of screen according to their mode of work (after Kelly and Spottiswood, 1982, with permission of the authors)

4.5. Other parameters of screening

There are many other parameters used for delineation of screening including transport efficiency, screen load, etc. Detailed discussion of these issues are presented in monographs of Sztaba (1993), Banaszewski (1990).

4.6. Analysis and evaluation of screening

Screening is mostly applied as the method for separation of the feed into size fractions. The results of screening of particles is most often analyzed as classification that is the content of size fractions (their quantities) as a function of their name or size numerical value. In order to perform such an analysis, a mass balance of selected size fractions has to be made. A selected size fraction can be treated as a component and its behavior in the screening system can be analyzed from the upgrading perspective. In the upgrading approach the quality and quantity of a selected size fraction is taken into account and balanced. A third approach, splitting, takes into account only the amount of products produced by screening and its name.

Screening is one of few processes which can be easily described in those three ways. The details of analysis and assessment of screening in the view of division into products (splitting), classification and upgrading have been described in a previous chapter.

Literature

Banaszewski T., 1990. Przesiewacze, Śląsk, Katowice.

Czubak A., 1964. Przenośniki wibracyjne, Śląsk, Katowice.

Gaudin A.M., 1946. Principles of mineral dressing, Metallurgizdat, Moskva, in Russian.

Kaye B.H., 1966. Determination of the characteristics of particles, Chem Eng. 73, 239–246.

Kelly E.G., Spottiswood D.J., 1982. Introduction to Mineral Processing, Wiley, New York.,

Laskowski J., Łuszczkiewicz A., Malewski J., 1977. Przeróbka kopalin, Wydawnictwo Politechniki Wrocławskiej, Wrocław.

Malewski J., 1990. Modelowanie i symulacja systemów wydobycia i przeróbki skał, Prace Naukowe Instytutu Górnictwa nr 60, Monografie nr 27, Wydawnictwo Politechniki Wrocławskiej, Wrocław.

Sztaba K., 1993. Przesiewanie, Śląskie Wydawnictwo Techniczne, Katowice.

5. Hydraulic and air separation

5.1. Principles

Hydraulic and air separations are usually called hydraulic and air classifications. They utilize the differences in velocity of settling of particles. The use of "*hydraulic*" or "*air*" words before the term "*classification*" is very important as it allows to distinguish the two separations from a general term "*classification*" meaning, in this work, the way of analyzing the results of separation.

The product of hydraulic separation, containing fast settling particles, is usually called "underflow", while the second product, containing slowly settling particles, is called "overflow". Hydraulic and air separators can be used to remove very fine particles from the feed, separate larger and heavier particles from lighter and smaller, divide the feed into narrow size fractions, limit lower and upper range of particles size because of requirements by the applied technology, as well as to regulate the size reduction during grinding.

There are many ways of hydraulic and air separations. They can be carried out in stationary media, in the media moving vertically, horizontally, sideward, and in a pulsating or spiral stream. Fig. 5.1. shows schematically typical devices applied for hydraulic separation in the media.

The initial point for analyzing any hydraulic and air separation is the free vertical fall of particles due to gravity. The equation, which determines the relation between the velocity of settling of spherical particles v (m/s) and their density in the medium $\Delta\rho$ (kg/m^3) having diameter d (m) and resistance factor ζ (dimensionless factor which characterizes the resistance of the medium to a moving particle) is as follows:

$$v \cong \sqrt{\frac{4}{3}\frac{\Delta\rho\, d}{\zeta\rho_c}}\ ,\qquad\qquad (5.1)$$

where:

$\Delta\rho$ -difference between densities of particle in vacuum ρ_z (kg/m^3) and medium ρ_c (kg/m^3), i.e. $\rho' = \Delta\rho = \rho_z - \rho_c$ (kg/m^3).

Equation (5.1) is based on the balance of the forces taking part in the process, that is the weight of particle in the medium F_c, resistance force F_o which oposes particle falling down and the force of inertia F_b. At any moment of settling the sum of forces should equal zero:

$$F_c + F_o + F_b = 0\qquad\qquad (5.2)$$
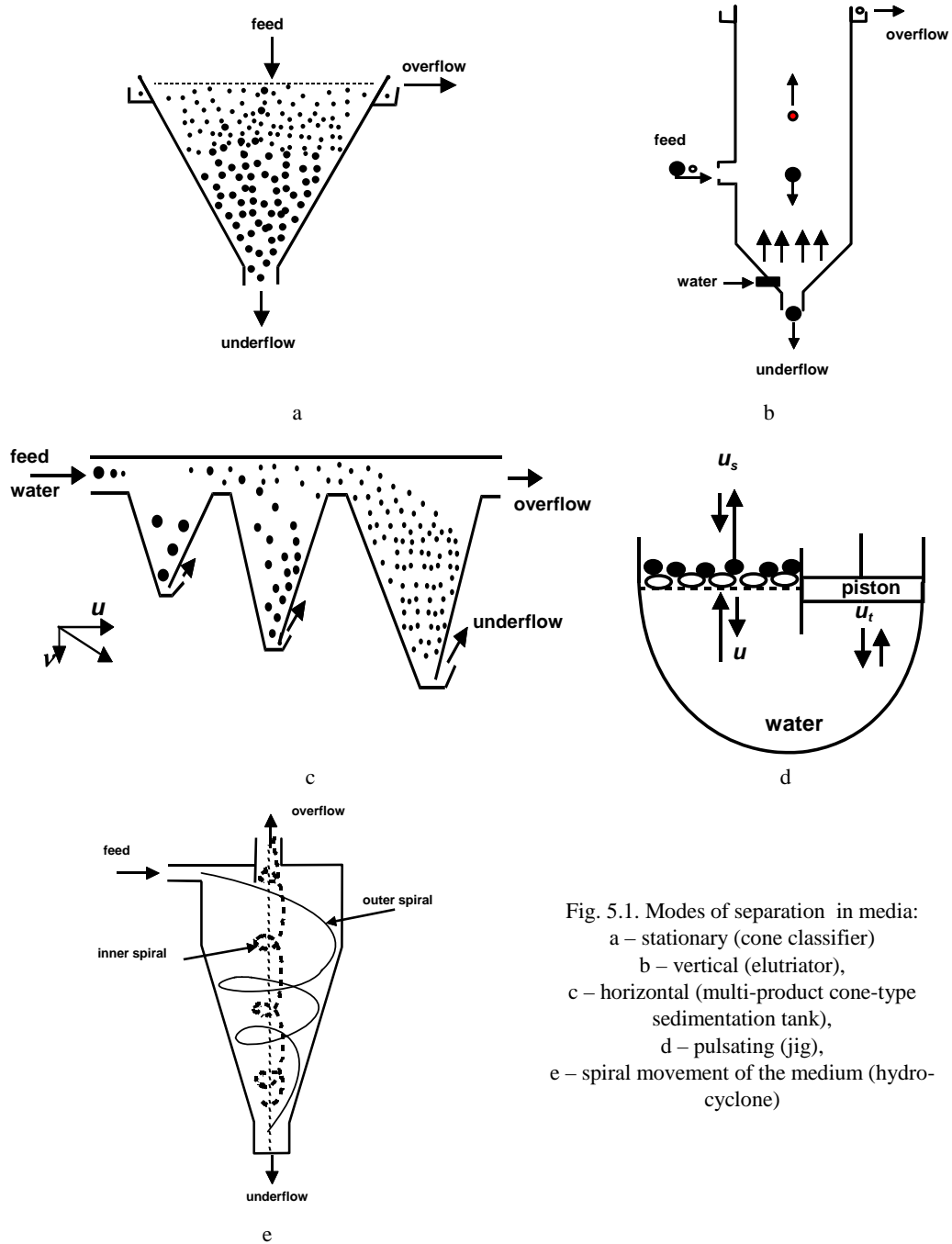
Fig. 5.1. Modes of separation in media:
a – stationary (cone classifier)
b – vertical (elutriator),
c – horizontal (multi-product cone-type sedimentation tank),
d – pulsating (jig),
e – spiral movement of the medium (hydro-cyclone)
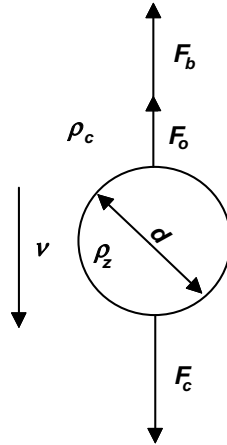
Fig. 5.2. Forces acting on a particle settling in a medium

The forces are determined by the relations:

$$F_c = V_d \Delta\rho\, g, \tag{5.3}$$

$$F_o = 0.5\ \zeta\,\rho_c\, v^2\, A, \tag{5.4}$$

$$F_b = V_d(\rho_z + a_d\rho_c)\, dv/dt, \tag{5.5}$$

where:

A – surface of the largest projection of the cross section of dispersed elements in the direction perpendicular to particle movement, m^2

V_d – particle volume, m^2

a_d – acceleration factor (dimensionless, 0.5 for spheres and 0.75 for a cylinders)

t – time, s

g – acceleration due to gravity, m/s^2.

After rearrangement, one obtains a general equation for particles of any shape:

$$V_d\Delta\rho\, g + 0.5\zeta\,\rho_c v^2 A + V_d(\rho_z + a_d\rho_c)\frac{dv}{dt} = 0. \tag{5.6}$$

For spherical particles Eq. (5.6) can be simplified by introducing the relation:

$$A = \pi d^2/4,\ V_d = \pi d^3/6\ \text{ and }\ a_d = 0.5.$$

After the initial period of acceleration, the velocity of settling particles reaches constant value, and then $dV/dt = $ const. The equation, determining the velocity of spherical particles falling down as a function of their density in the medium and particle size, takes the form shown in Eq. (5.1).

There are other forms of Eq. (5.1). For instance, it can be written as a combination of the dimensionless Reynolds (Re) and Archimedes (Ar) numbers (Koch and Noworyta, 1992):

$$4/3 \, \text{Ar} = \zeta \, \text{Re}^2, \tag{5.7}$$

where:

$$\text{Re} = \frac{vd \, \rho_c}{\eta_c}, \tag{5.8}$$

$$\text{Ar} = \frac{d^3 \Delta \rho \rho_c g}{\eta_c^2} \tag{5.9}$$

and η_c denotes liquid viscosity.

Particle resistance factor ζ depends on hydrodynamics of the system characterized by the Reynolds number. Table 5.1 shows the expressions for the resistance factor which can be applied to Eq. (5.1) in order to calculate the velocity of particle settling. With reasonable accuracy Eq. (5.1) can be also be used for the determination of settling velocity of non-spherical particles. It requires however, introducing an appropriate function for the resistance factor which depends not only on the Reynolds number but also on the shape of the particle. Selected relations for ζ for non-spherical particles are shown in Table 5.1.

Table 5.1. Dimensionless resistance factor for particles of different shapes and for various modes of settling

Mode of particle settling	Reynolds number (for particles)	Resistance factor, ζ	
		spherical particles	non-spherical particles
Laminar (Stokes)	$\text{Re} < 0.2$	$24/\text{Re}$	$28.46/[\text{Re} \, \lg(\Phi/0.065)]$*
Intermediate (Allen)	$0.2 < \text{Re} < 5 \cdot 10^2$	$18.5 \text{Re}^{-0.6}$	–
Turbulent Newton (Rittinger)	$5 \cdot 10^2 < \text{Re} < 3 \cdot 10^5$	0.44	0.44–1.9**

* Φ is the sphericity of particle
** Values for different shapes and mode of settling are given in Koch and Noworyta (1992)

The relationship between the resistance factor and the Reynolds number for $\text{Re} < 3 \cdot 10^5$ is given by the Yilmaz equation (Koch and Noworyta, 1992):

$$\zeta = \frac{24}{\text{Re}} + \frac{3.73}{\sqrt{\text{Re}}} - \frac{0.00483 \, \sqrt{\text{Re}}}{1 + 3 \cdot 10^{-6} \, \text{Re}^{1.5}} + 0.49. \tag{5.10}$$

The equations for the velocity of settling presented so far do not directly show the relation between the velocity of settling and particle density and its size. It can be done

separately for each range of the Reynolds numbers shown in Table 5.1. For Re<0.2, i.e. for spherical particles with diameter approximately from 0.1 mm to 0.1 mm (exact range of particle size depends on their density and shape) one can use the equation:

$$v = 0.0556 \frac{\Delta \rho \, g d^2}{\eta} = f\left(\Delta \rho^{0.5} d\right). \tag{5.11}$$

This is the so-called Stokes range of particle settling, also known as laminar settling.

For the Reynolds numbers $0.2 < Re < 5 \cdot 10^2$ (also called the Allen or transition range) the resistance factor vs. the Reynolds number is $\zeta = 18.5 Re^{-0.6}$ (Table 5.1). The presentation of a simple formula describing the settling velocity in the Allen range is not an easy task. It is so because the settling velocity depends on the Reynolds number, which, in turn, depends on the same velocity we use for calculations. Various approximations have been used in different works. They usually are incomplete as they contain the constants for which the values are not provided (Laskowski and Luszczkiewicz 1989; Bogdanov, 1972; Malewski, 1981). The best seems to be diagrams, presented for instance by Kelly and Spottiswood (1982). It should be added that when it is not important to have the equation but only the values of the settling velocity, they can be calculated by introducing the expression $\zeta = 18.5 \, Re^{-0.6}$ to Eq. (5.1). To approximately write the relationship between velocity of falling and particle density and its size for the Allen range, i.e. for the particles of diameter from 0.1 mm to 1 mm, one can make use of the formula (Laskowski and Luszczkiewicz (1989):

$$v = k_A d \sqrt[3]{\frac{\Delta \rho^2}{\eta \rho_c}} = f\left(\Delta \rho^{2/3} d\right), \tag{5.12}$$

where k_A is a dimensionless constant.

This is an approximate formula as it has been derived by assuming that ζ is proportional to $Re^{-0.5}$ instead of $Re^{-0.6}$.

For a turbulent movement of the liquid around a settling particle (the Rittinger or Newton range of settling for $5 \cdot 10^2 < Re < 3 \cdot 10^5$ and approximate particle diameter d > 1 mm) the particle sedimentation velocity is:

$$v = 1.74 \sqrt{\frac{\Delta \rho \, d g}{\rho_c}} = f(\Delta \rho \, d). \tag{5.13}$$

It results from formula (5.13) that the particle density increasingly effects the settling velocity and the hydraulic or air separation, because as the Reynolds number increases the density exponent also increases. For the analysis of settling of free falling particles of different sizes and densities one can apply the so called free-settling ratio, ie. the ratio of particle size required for two minerals to fall at equal rates (Wills,

1985). They are obtained by dividing the expression for settling velocity for one kind of particles by velocity of another kind of particles. For example, for a turbulent flow and spherical particles, when the falling velocity of particle A and B are identical, it is possible to obtain a relation for free-settling ratio *C*.

$$C = \frac{d_A}{d_B} = \frac{\Delta \rho_B}{\Delta \rho_A} \, . \qquad (5.14)$$

The value of the free-settling ratio determines the susceptibility to separation.

The main material parameter of separation in the media is the settling velocity of particle (Fig. 5.3), which depends, first of all, on particle density and size. If separation in the media involves materials of similar particle density or size, the main parameter of hydraulic or air separation becomes the other variable parameter.
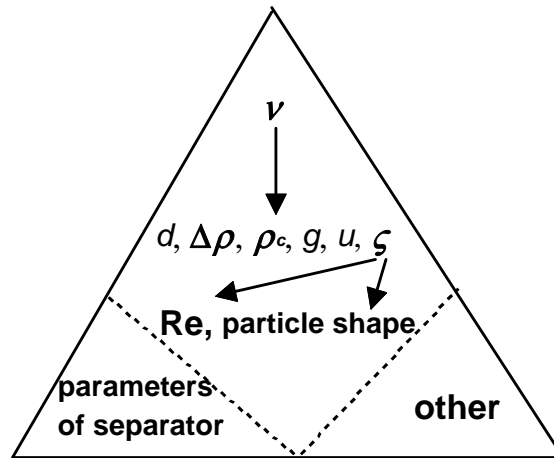
Fig. 5.3. General characteristics of hydraulic and air separations.
The main material parameter is settling velocity v. Meaning of other parameters is given in the text

Additional forces, for example resulting from medium flow, can influence the settling. In such a case it should be taken into account when calculating particle movement. Additional obstacle in determination of particle movement in real suspensions is their hindered settling, occurring at high concentrations of the particles in the classifier. For such cases the presented above formula for free settling of particles must be modified. Appropriate formulas can be found in literature.

5.2. Classification by sedimentation

In sedimentation classifiers the feed is supplied from the upper part of the container and particles fall down in water or air vertically or nearly vertically. Particle separa-

tion takes place according to the difference in their velocity of settling. Fine and light particles, i.e. those which settle slowly, are removed from the classifier together with water as overflow. The particles settling rapidly are removed either as an underflow at the bottom of the vessel, or with the use of appropriate mechanical devices. Therefore, sedimentation separators can be divided into mechanical and non-mechanical ones. Non-mechanical cone separator is shown in Fig. (5.1a), while Fig. (5.4) presents typical mechanical separator also called coil classifier. In these devices the particles settling rapidly are removed upwards from the container bottom with the use of a spiral while slowly settling particles are removed as an overflow in the upper part of classifier (Fig. (5.4)).
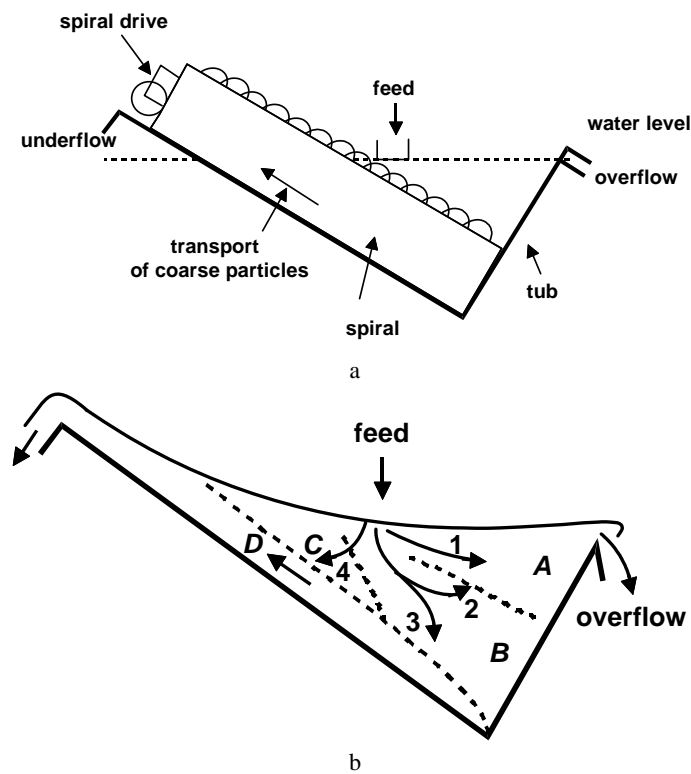
Fig. 5.4. Coil classifier: a – elements, b – regions and direction of particles movement
(after Steward and Restarick, 1967)

In a small model coil classifier (Steward and Restarick, 1967) the particles of the feed move in four directions, assigned with numbers 1-4, forming regions A-D. In region A, situated above the spiral, particle concentration is low and particles move towards the overflow. In region B, fine particles pass towards the overflow, while the larger ones towards the underflow. In region C, most particles pass to the large parti-

cles fraction, commonly called the sandy fraction, while in region D large particles are transported with the use of a coil device (spiral) to the underflow.

There are many types of mechanical sedimentation separators in which spirals are replaced with rakes of blades. In some classifiers rakes direct large particles to the underflow at the container bottom (Kelly and Spottiswool, 1982).

One of the most important classification parameters (for a particular concentration of particles) is d_{50}. For low solids concentrations, when free sedimentation of particles takes place, d_{50} can be estimated from Eq. (5.1). When hindered settling occurs and also when there is some movement of the medium, determining d_{50} becomes more difficult.

A full description of coil classifier operation does not exist due to considerable number of parameters effecting the process. Sztaba and Nowak (2000) defined and systematized a significant number of those parameters.

5.3. Fluidizing classification

In fluidizing classifiers (elutriators) (Fig. 5.1b) a stream of water beneath the tank is additionally introduced into the classifier with settling particles. Then, calculation of the forces balance and velocity of sedimentation require taking into account the flow of the medium. The rule of separation in those devices is simple. For ideal separation the particles whose sedimentation velocity is lower than the velocity of up going medium flow, are carried by the medium to the overflow, while a particle having higher sedimentation velocity is directed to the overflow (Fig. 5.5). The particle of size d_{50} has zero or close to zero velocity of settling in relation to the separator and therefore it has the same chance to report, after suitable period of time, either to underflow or overflow of the classifier.
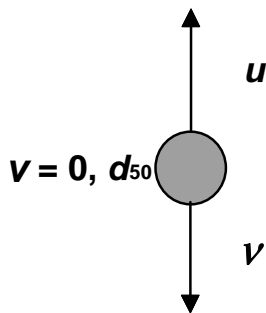
Fig. 5.5. In fluidized classifiers particle of size d_{50} has the same chance to move upward and downward: u – velocity of upward movement of medium, v – velocity of free falling of particle in medium, v = ($v - u$) – velocity of particle movement in relation to classifier

The d_{50} value for a particular separator can be estimated from the equations for free sedimentation. One of the equations taking into account the hindered settling is the relation (Kelly and Spottiswood, 1982):

$$v_h = v(\varepsilon)^n,$$ (5.15)

where:

v – particle velocity during free sedimentation

v_h – velocity of hindered settling

ε – porosity of fluidized layer $(\rho_z - \rho_m)/(\rho_z - \rho_c)$

n – constant depending on the Reynolds number

ρ_z – particle density

ρ_m – suspension density

ρ_c – medium density.

Irregular flow of the medium in fluidizing columns can also considerably effect the change of separation d_{50}.

5.4. Classification in horizontal stream of medium

The feed consisting of medium and particles can be also supplied from one of the sides of the classifying vessel. In such a case additional horizontal force acting on particles, together with the remaining forces (gravity, buoyancy, resistance) create diagonal settling of particles.
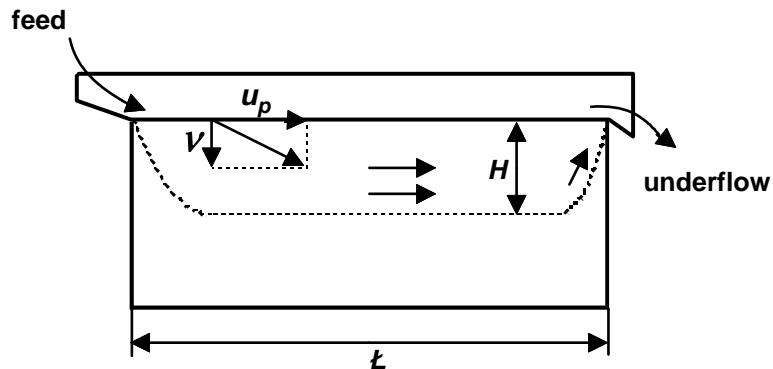
Fig. 5.6. Principle of particles separation of in a horizontal stream of liquid
(after Laskowski et al., 1977)

In the separator, the feed is supplied from one side and the overflow is removed from the other side. The stream of liquid moving in the separators reaches H depth, the length of the separator is $Ł$ and the stream of suspension moves at velocity u_p. The time necessary for horizontal movement of the suspension is:

$$t_{\text{vertical}} = Ł/u_p,$$ (5.16)

and the relation between vertical particle falling time t_{pion} at depth H takes the following form:

$$t_{horizontal} = H/v. \tag{5.17}$$

For the cut size particles (d_{50}), which will be present at the corner of the classifier and still having a change to report to the overflow $t_{\text{horizontal}} = t_{\text{vertical}}$. Thus:

$$v_{d_{50}} = H \, u_p/Ł. \tag{5.18}$$

There are many designs of hydraulic classifier utilizing horizontal movement of the medium stream. A scheme of a multiproduct classifier is shown in Fig. 5.1c.

5.5. Classification in pulsating stream

Classification with the use of pulsating medium stream is performed in jigs. The feed is supplied onto a jig screen and then it is treated with a pulsating stream of the medium, which is usually water. Water going upwards through a screen loosens the sediment, while a downward movement of the stream causes sedimentation and stratification of the sediment (Fig. 5.7). Medium pulsation is achieved due to the movement of a piston or air pressure, movement of membrane, movement of the screen surface, as well as due to other procedures.
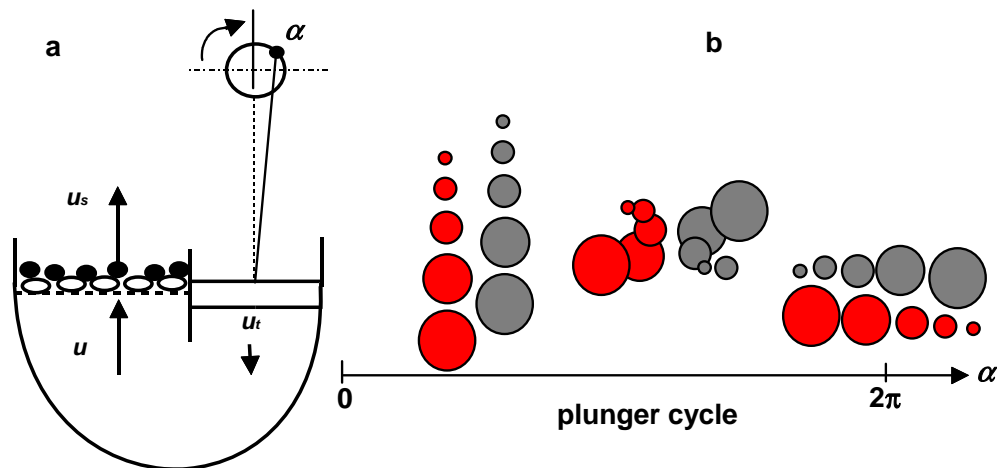
Fig. 5.7. Operation principles of jig: u_s – velocity of upward stream of water,
u – velocity of water under screen surface, u_t – piston velocity

Jigs work continuously and they are used, first of all, for hydraulic separation of coarse particles according to the difference in their densities. Separation into the particles settling slowly and those settling fast is obtained due to appropriately situated

dam and gate. More detailed description of jigs operation and the effect of different parameters on sedimentation can be found in scientific literature.

5.6. Hydrocyclones

Classification can be also conducted in a medium passing through the classifier with a spiral-type particle movement. This kind of the movement takes place in air cyclones, centrifuges, and hydrocyclones and it results from a cylindrical shape of the separator (Fig. 5.1e), as well as from pushing the feed stream tangent to the classifier wall. As a result of the spiral movement, the particles are subjected to centrifugal force which is the main separating force. The operation principle of a hydrocyclone and its design is shown in Fig. 5.8.
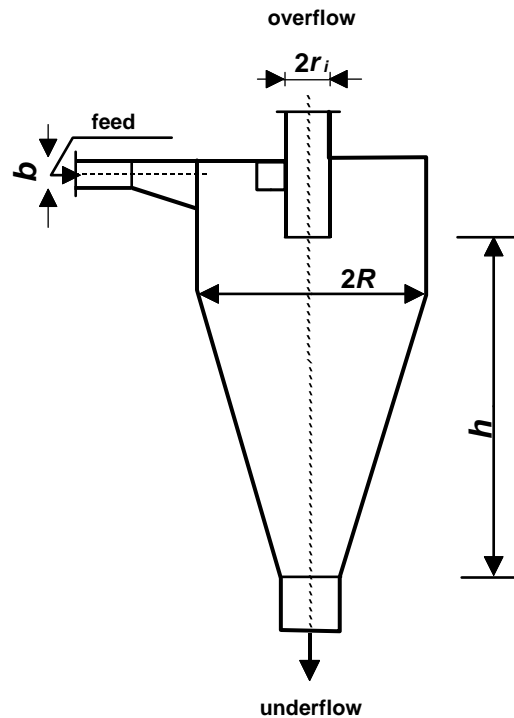
Fig. 5.8. Selected parameters of hydrocyclone

Particle movement in the hydrocyclone results from the force balance in the system. Resultant force F_w effecting the particles is the difference between the centrifugal force $F_{cent.}$ causing particle movement towards hydrocyclone walls and medium resistance force F_R directed to the cyclone axis:

$$F_w = F_{\text{cent.}} + F_R. \tag{5.19}$$

After inserting physical expression for particular forces to Eq. (5.19), one obtains a general equation describing particles movement in a hydrocyclone:

$$m\frac{dv}{dt} = \frac{\pi d^3}{6}(\rho_z - \rho_c)\frac{v_t^2}{R} - \zeta\frac{\rho_c}{2}v_w^2\frac{\pi d^2}{4}, \tag{5.20}$$

where:
m – particle mass ($\pi d^3 \rho_z / 6$)
t – time
v – relative velocity of particle movement in the suspension in hydrocyclone
v_t – liquid tangent velocity in the suspension depending on inlet pressure
ρ_z – particle density
ρ_c – liquid density
R – hydrocyclone radius in the consideration site
d – particle diameter
ζ – particle resistance factor.

As the description of particle movement is quite complicated, empirical relations are used for hydrocyclone design. Koch and Nowaryta (1992) provided, for example, an equation for determining the cut-size (d_{50}) of the hydrocyclone:

$$d_{50} = \sqrt{\frac{18\eta_c V_o R \rho_m}{2\pi d_i h (\rho_z - \rho_c)\Delta p}}, \tag{5.21}$$

where:
η_c – suspension viscosity
V_o – suspension stream (volume per unit time)
$d_i = 2r_i$ – overflow outlet diameter
h – hydrocyclone height from underflow to the overflow pipe
g – acceleration due to gravity
ρ_c – suspension density
R – hydrocyclone radius
Δp – pressure drop in hydrocyclone.

The principle of hydrocyclone operation was schematically shown in Fig. 5.1e.

The suspension pumped tangent to hydrocyclone walls, due to its variable diameter, forms a spiral, directed downwards the stream around the walls of hydrocyclone. Since large particles are more strongly subjected to centrifugal force, the spiral carries mostly large particles. Specific design of hydrocyclone causes that around its axis there is an air core, close to which there is a second spiral stream of the liquid, directed upwards. The secondary spiral stream carries fine particles to the overflow.

There are many types of hydrocyclones. Generally, they can be divided into cylindrical, conic and cylindrical–conic hydrocyclones. They are applied in grinding cir-

cuits for removal of fine particle from the systems. The main advantage of hydrocyclones is simplicity of their operation, small size and low price. Hydrocyclones do not possess movable parts. They can work under different angles, although vertical position is recommended to create gravitation discharge of the underflow. Separation time in these classifiers is short. Hydrocyclones, however, have some disadvantages. One of them is not always precise particle classification. The devices are not suitable for extremely fine particles, especially of a micron size. They also require stable composition of feed.

Literature

Bogdanov O.S., 1972. Handbook of mineral processing, t. 1, Nedra, Moskva, 22, in Russian.

Kelly E.G., Spottiswood D.J., 1982. Introduction to Mineral Processing, Wiley, New York.

Koch R., Noworyta A., 1992. Procesy mechaniczne w inżynierii chemicznej, PWN, Warszawa.

Laskowski J., Luszczkiewicz A., 1989. Przeróbka kopalin. Wzbogacanie surowców mineralnych, Wydanictwo Politechniki Wrocławskiej, Wrocław.

Laskowski J., Luszczkiewicz A., Malewski J., 1977. Przeróbka kopalin, Wydawnictwo Politechniki Wrocławskiej, Wrocław.

Malewski J., 1981. Przeróbka kopalin. Zasady rozdrabiania i klasyfikacji, Politechnika Wrocławska, Wrocław.

Steward P.S.B., Restarick C.J., 1967. Dynamic flow characteristics of a small spiral classifier, Trans. IMM Sec.C., 76, C225-C230.

Sztaba K., Nowak A., 2000. Assumptions for modeling separation in coil classifiers, Physicochemical Problems of Mineral Processing, 34, 2000, 77–94.

Wills B., 1985. Mineral Processing Technology, 3rd edition, Pergamon Press, Oxford.

6. Thin stream separation

6.1. Introduction

Separation in a thin stream of liquid utilizes stratification of particles during their movement in a suspension (Fig. 6.1).

a

b
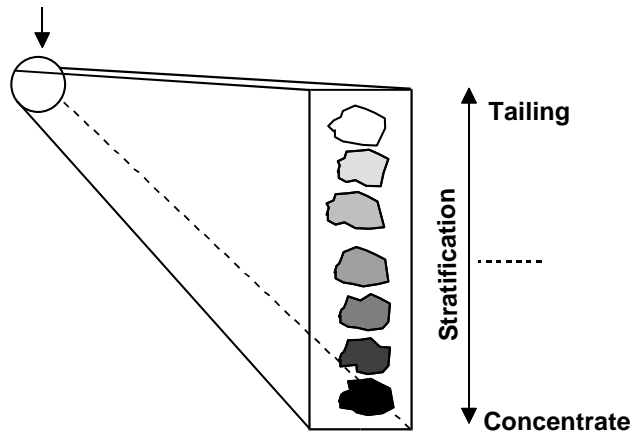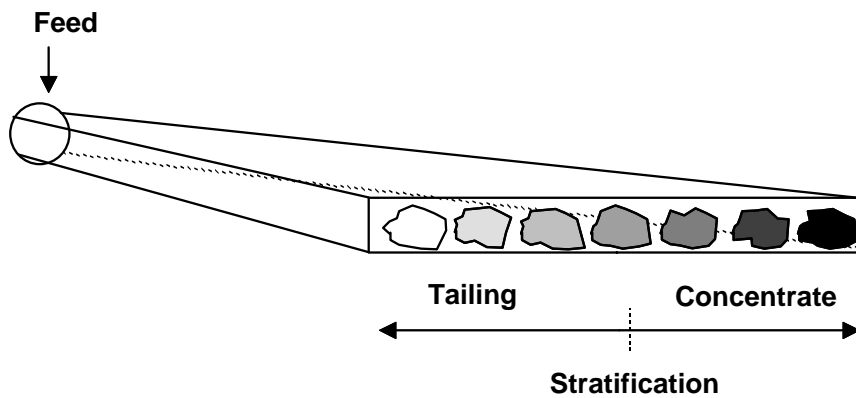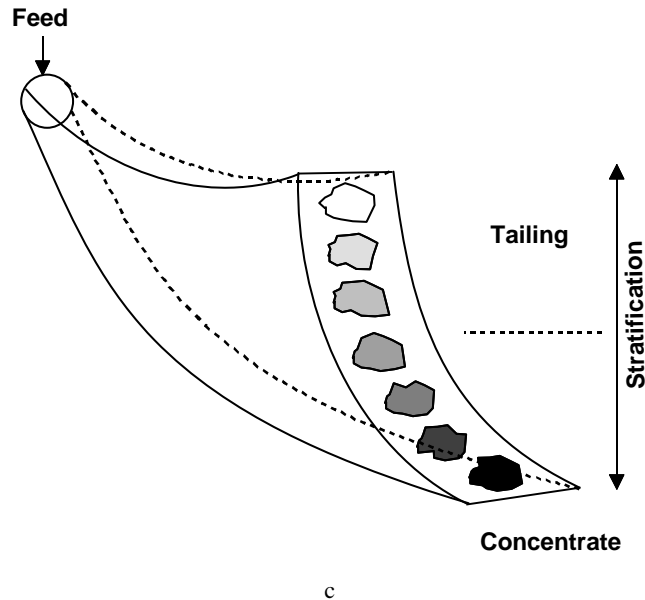
c
Fig. 6.1. Stratification of particles traveling in a thin layer of medium:
a – vertical separation, b – horizontal separation, c – other

The stream of liquid can be of different shape and thickness. The stratification can be horizontal, vertical, bend, spiral, etc. The ability of particle stratification depends on a property based on particle size, its density and shape, friction between particles, and walls shape of the separator. These properties form the main feature of separation which can be called stratification ability (Fig. 6.2). This parameter, however, so far has not been defined.
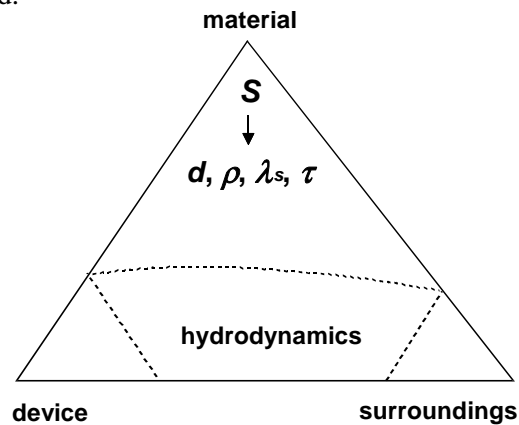
Fig. 6.2. Main parameter of separation in a thin layer of medium is ability of stratification *S*, which depends on particle size *d*, its density ρ, shape λ_s
and friction of particles against themselves and walls of separator τ

In the stratified material one can distinguish zones of particles which occupy central part of stratification fan, "heavy" particles at the one end of the fan and "light" particles at the opposite side. This can be a base for delineation of stratification. After appropriate calibration, stratification for "heavy" particles would be equal, for instance 1 and for the "light" ones - 1.

The list of devices used for the thin layer separation includes, for instance, Reichert cones, concentration tables, as well as stream, coil, and Bartles-Mozley separators.

6.2. Stream separators

They are the oldest and simplest separators which have been applied since the beginnings of mineral processing. Agricola (1494-1555), in one of his illustrations dealing with mining and mineral processing, presented a stream separator. A general scheme of the stream separator and the mode of its operation is shown in Fig. 6.3. Stream separators do not possess movable parts. Their performance is based on hindered falling of particles and their friction against the walls of the separator in the course of particle moving together with the liquid. A precise description of particles separation in stream separators is more difficult for very thin streams. When the stream is thick, approximate description of particles separation can be performed on the basis of the relations valid for hydraulic separation in horizontal stream of water (subchapter 5.3) with inclination taken into account.
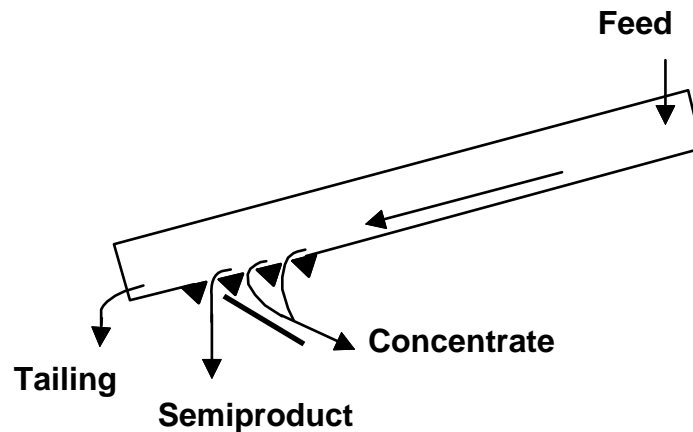
Fig. 6.3. Stream separator

For proper operation of the stream separator, it is important to ensure, for a particular feed, appropriate speed of the liquid flow and position of openings through which the concentrate and intermediate products are collected.

6.3. Reichert cones

The advantage of the Reichert cones is also the lack of movable parts. Although separation in Reichert cones is similar to that in stream separators, the design of the Reichert cones is different (Fig. 6.4).
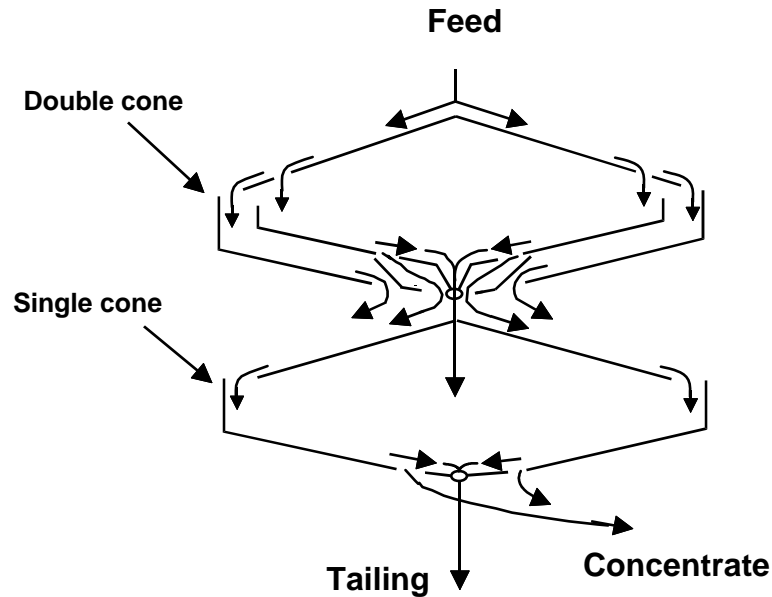
Fig. 6.4. Reichert cones

The feed, containing water and particles, flows evenly on the surface of flattened cones of diameter about two meters. Heavy particles concentrate in the lower zone of the stream and therefore fall into the openings, while light particles, together with water are transported down wards in the device. Heavier particles are subjected to multiple separation on the subsequent cones, which results in diversified products.

One separating device contains from several to a dozen of stacked cones and its height can be up to 6 m. The Reichert cones are very efficient and can process about 100 Mg of the feed per hour. They can be used for all kinds of ores and raw materials.

6.4. Humphrey spiral concentrator

Spiral separators operate similarly to stream separators, but additionally, a centrifugal force is present in the system (Fig. 6.5). The centrifugal force is a result of the shape of the separator. The material travels down through a stationary spiral with many turns of mean radius (20 cm) with a fall per turn of about (28 cm). The forces

effecting particles in the spiral separator are shown in Fig. 6.6. They involve: centrifugal (F_o), gravity (F_c), friction (F_t), and liquid pressure (F_n) forces. The forces which determine separation are F_t , F_n , and they operate in the same direction as horizontal component of the gravity forces $F_{c(x)}$, as well as the horizontal component of the centrifugal force $F_{o(x)}$.
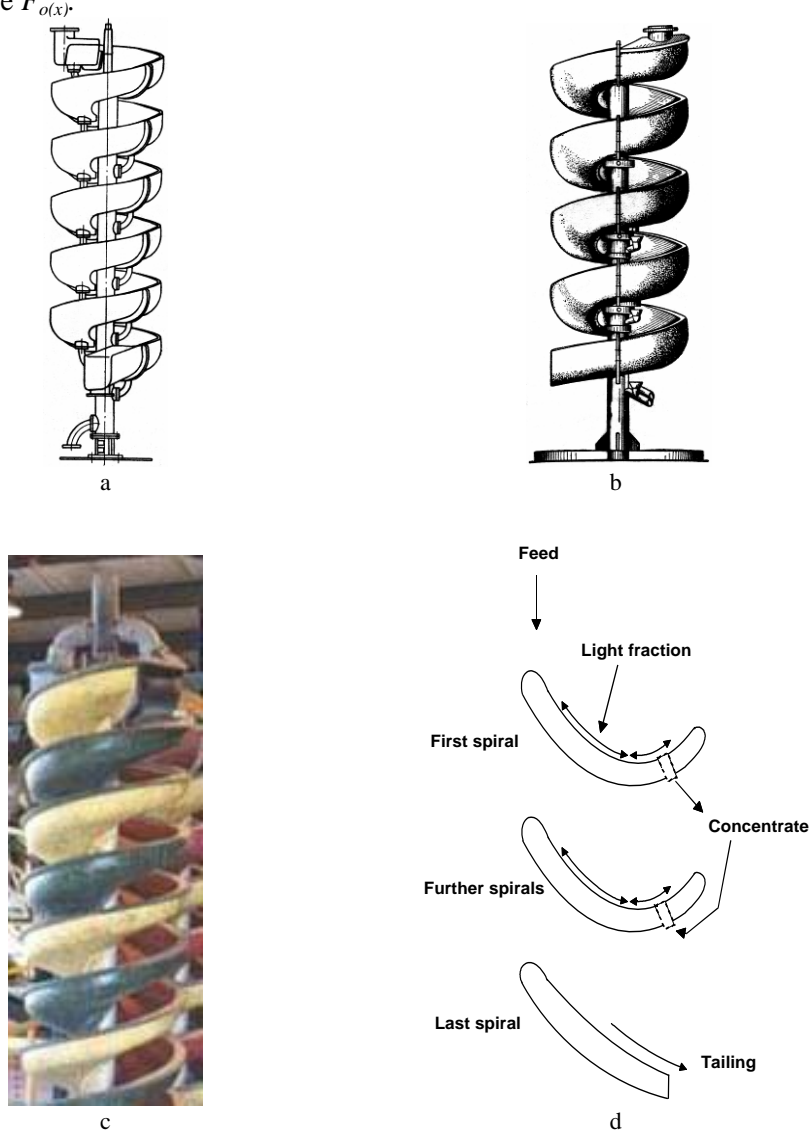
Fig. 6.5. Spiral separators: a) VIMCa-645, b) SVM-1200 (Anikin, et al., 1970),
a photo of spiral separator (c) and principle of its operation (d). In figures a-c the spiral of separator is wound right while in figure d left

HEAVY PARTICLES **LIGHT PARTICLES**
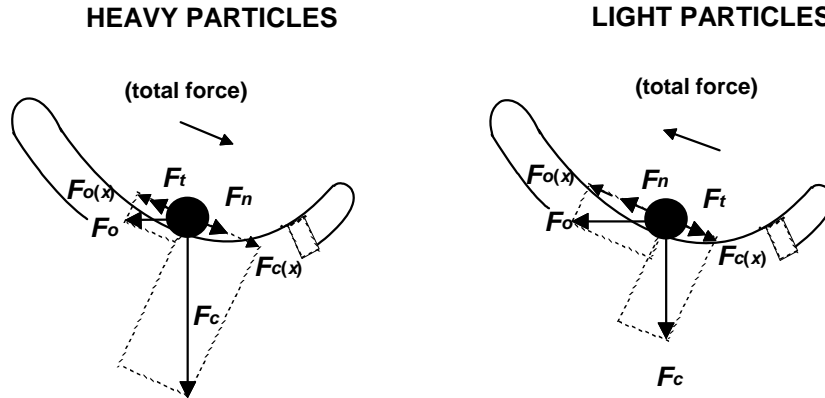
Fig. 6.6. Forces effecting a particle in a spiral separator

The force pushing particles towards the side of "light" and low friction particles or towards heavy and high friction particles is the excess force F_w resulting from the force balance. For "light" particles:

$$F_n + F_{o(x)} > F_t + F_{c(x)} . \tag{6.1}$$

It means that the separating force F_w is:

$$F_w = F_n + F_{o(x)} - (F_t + F_{c(x)}). \tag{6.2}$$

The same relations for "heavy" particles is:

$$F_n + F_{c(x)} > F_t + F_{o(x)} \tag{6.3}$$

and

$$F_w = F_n + F_{c(x)} - (F_t + F_{o(x)}). \tag{6.4}$$

The particles are stratified in the stream until they reach a proper place in the fan and the excess force F_w disappears.

In the Humphrey spiral separator the tailing containing light particles is collected in the lowest coil. The concentrate is collected from the neighbouring 2-3 coils through the holes in coil surface bottom. Particles larger than about 0.05 mm in diameter are suitable for separation.

6.5. Concentrating tables

Concentrating tables spread particles on their surface as shown in Fig. 6.7. The formation of stratified particles on the concentrating table, like in the coil separator, is the result of many forces including gravity forces, the friction forces between particles

and the table which are caused by the table plate movement and liquid movement, the force of liquid pressure on particles, and the force of inertia. The ordering force acting on particles is the sum of vectors representing the forces. This stratification force for heavy particles has a slightly different direction than that for light particles. This is caused by the fact that stratification force for heavy particles is mainly determined by the inertia force, while other forces (friction, gravity and water pressure force) are of low values. For light particles it is otherwise (Laskowski and Luszczkiewicz, 1989).
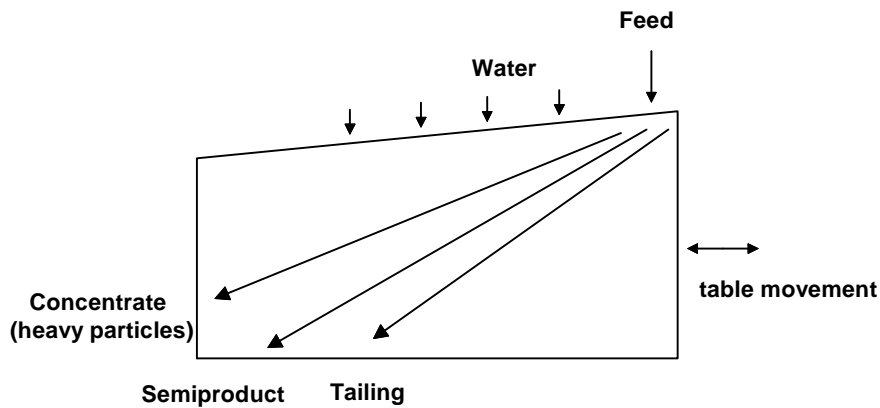
a

b

Fig. 6.7. Concentrating table (top view) (a) and a photograph (b)

The output of concentrating tables is not high. The yield, table oscillation frequency, and table shift can be calculated using empirical equations. The expression for the mass yield W (kg/h) has the form (Krukowiecki, 1979; Koch and Noworyta, 1992):

$$W = 0.1\rho_m\{Ad_d(\rho_1 - 1000)/(\rho_2 - 1000)\}^{0.6}, \tag{6.5}$$

where:

ρ_m – mixture density, kg/m^3

ρ_1 – density of light fraction, kg/m^3

ρ_2 – density of heavy fraction, kg/m^3

A – table surface area, m^2

d_d – average size of particles, mm.

To calculate the frequency of the table n (1/s) the following formula can be used:

$$n = 4.17(d_{d\,max})^{-0.2}, \tag{6.6}$$

where $d_{d\,max}$ is maximum particle size.

For determination of the shift of the concentrating table plate l (mm) one can use the formula:

$$l = 18(d_{d\,max})^{0.25}. \tag{6.7}$$

The concentrating tables can be used to process nonferrous metals ores containing particles smaller than about 3 mm. In the case of coal, because of its considerably lower density, larger particles (up to 6 mm in diameter) should be used. For fine particles of about 0.1 mm in size smooth surfaces of the concentrating table are recommended. In other cases the surface of the concentrating table is modified by grooves and strips. Additional factor improving separation is the use of asymmetric shaking of the concentrating table.

6.6. Other separators

There are also other devices for separation in thin stream of water including the Bartles-Mozley table (Burt and Ottley, 1974) and Bartles Crossbelt separator (Burt, 1975a, b). The Bartles-Mozley separator operates periodically. In the first cycle the feed is transported through the separator, consisting of 40 plates 1.1 m x 1.4 m in size and inclined at the angle of 3°-4° to the level This stage lasts for about 36 minutes and heavy particles sediment on the plate surfaces, while light particles, together with water, flow out of the separator. In the second stage, the supply of feed is stopped, the separator is inclined at the angle of 45° to the level and water is used to remove heavy particles from the separator. When the particle settle, the whole separator vibrates, due to oscillation of a special unbalanced load. The separator output is about 2.5-4.0 Mg per minute (Burt, 1975a, 1975b). In the Bartles-Mozley separator it is possible to process the material consisting of particles from 5 to 100 micrometers.

Literature

Anikin M.F., Ivanov V.D, Pievzner M.L., Spiral separators for upgrading of ores, Nedra, Moscow, 1970, in Russian.

Burt R.O., 1975a. Development of the Bartles cross-belt concentrator for the gravity concentration of fines, Int. J. Mineral Process., 2, 219–234.

Burt R.O., 1975b. Gravity concentration of fine minerals, Chemistry and Industry, 18, 64–69.

Burt R.O., Ottley D.J., 1974. Fine gravity concentration using the Bartles–Mozley concentrator, Int. Journal of Mineral Processing, 1, 347–366.

Koch R., Noworyta A., 1992. Procesy mechaniczne w inżynierii chemicznej, WNT, Warszawa.

Krukowiecki W., 1979. Przeróbka mechaniczna rud, węgla, soli i innych kopalin, PWN, Warszawa.

Laskowski J., Luszczkiewicz A., 1989. Przeróbka kopalin – wzbogacanie surowców mineralnych, Wydawnictwa Politechniki Wrocławskiej, Wrocław.

7. Gravity separation

7.1. The basis of gravity separation in water and heavy liquids

During gravity separation the particles denser than the liquid, in which particles are suspended, sink, while particles of lower density float (Fig. 7.1). When gravity separation is carried out slowly, separation is effected only by the gravity (F_c) and buoyancy forces (F_w) and the resulting ordering force is:

$$F = F_c - F_w = m_p\, g - m_c\, g = v\, \rho_p\, g - v\, \rho_c\, g = (\rho_p - \rho_c)\, v\, g, \qquad (7.1)$$

where:
m_p – particle mass
ρ_p – particle density
m_c – mass of liquid displaced by particle
ρ_c – liquid density
g – gravity constant
v – particle volume.

Thus, the main material feature of static gravity separation is $\rho' = (\rho_p - \rho_c)$ that is the density of material in the medium in which separation takes place (Fig. 7.2a).
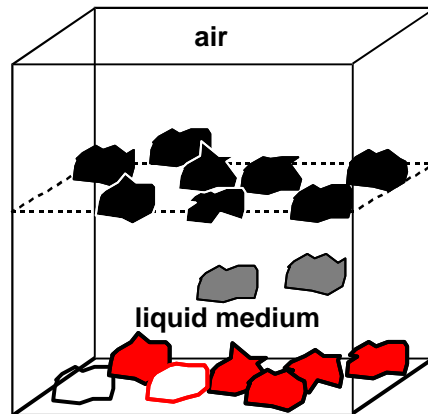
Fig. 7.1. Principle of gravity separation

When density separation takes place as a dynamic process, the result of separation will be effected by additional parameters, mostly the friction force F_T, which depends on particle diameter d, velocity of moving particle w, and liquid viscosity η (Fig. 7.2b):

$$F_T = 3\pi d\eta w. \tag{7.2}$$
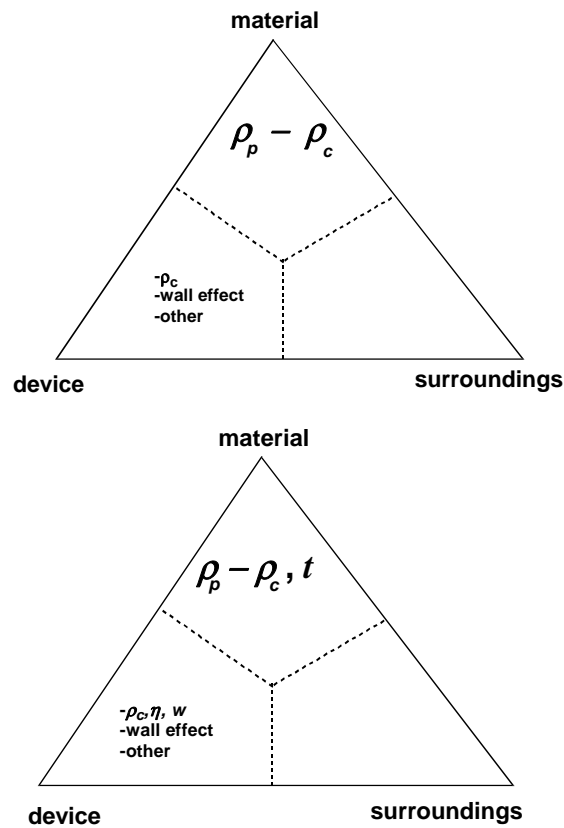
Fig. 7.2. The principle feature of gravity separation in liquids is: a) difference between densities of particle and liquid ($\rho_p - \rho_c$) (static process), while in dynamic processes is: b) difference between densities of particle and liquid as well as the time of separation

The viscosity results from friction occurring between moving molecules of the liquid as well as moving particles. When viscosity does not depend on the movement of particles and molecules and is constant at particular temperature, the liquid or suspension are called newtonian. However, viscosity of suspensions containing mineral particles is usually not constant. Their viscosity depends on particles content in the liquid and such suspensions are termed nonnewtonian. The viscosity of a nonnewtonian suspensions is described by general equation (Kelly and Spottiswood, 1982):

$$\tau_s = \eta_{\text{app}}\, q \tag{7.3}$$

where:

τ_s – shear stress

q – shear rate

η_{app} – apparent viscosity (dependent on shear stress).

For many nonnewtonian liquids the relation between the shear rate and shear stress can be described by an approximate equation (Laskowski, 1969):

$$\tau_s \approx \tau_d + \eta_{\text{plas}}\, q, \tag{7.4}$$

where:

τ_d – dynamic shear stress,

η_{plas} – plastic viscosity measured at the shear stress range when the liquid is newtonian.

Thus, Eq. (7.4) describes a system in which at low shear stress there is no movement of liquid (or the liquid moves very slowly). At a certain shear stress τ_d the liquid starts to flow. Taking into account the friction force F_T in the balance of forces acting on a particle leads to the following relation:

$$F = F_c - F_w - F_T \tag{7.5}$$

Equation (7.5) indicates that at a high resistance force a rapid separation of particles cannot take place as the difference in liquid and particle densities is apparently reduced by particle friction against molecules of the suspending liquid.

The gravity separation is usually performed in water. The density of water is 0,99823 g/cm^3 at 293 K (20 $^\circ$C) (CRC, 1986). However, except for ice and some polymers having densities lower than 1 g/cm^3, solid materials are denser than water. Therefore, liquids denser than water, called heavy liquids, have to be used for gravity separation. The heavy liquids can be homogeneous or heterogeneous (containing two or more phases and forming suspensions). The homogeneous liquids can be divided into organic and inorganic liquids. The homogeneous inorganic heavy liquids usually consist of water and water soluble salts. Figure 7.3 shows classification of heavy liquids and their typical representatives.

Homogeneous organic liquids are seldom applied for gravity separation, though many technologies and patents are available for this purpose. Heavy organic liquids presented in Fig. 7.3 are most often mentioned in the literature. Other liquids can also be used, but special attention should be paid to their potential toxicity, reactivity with particles, and harmful ability to penetrate pores of the particles.

```
                          ┌──────────────────┐
                          │  heavy liquids   │
                          └──────────────────┘
                          ╱                    ╲
        ┌──────────────────────┐          ┌──────────────────────┐
        │ homogeneous liquids  │          │     suspenions       │
        └──────────────────────┘          └──────────────────────┘
          ╱              ╲
┌────────────────────┐  ┌──────────────────┐
│ aqueous solutions  │  │ organic liquids  │
└────────────────────┘  └──────────────────┘
```

• quartz	1.4
• barite	1.8
• magnetite	2.0
• ferrosilicon	2.3

aqueous solutions

• Clerici*	5.0
• Klein**	3.19
• $ZnCl_2$	2.07
• $CaCl_2$	1.65

organic liquids

• methylene iodide	3.31
• bromoform	2.89
• methylene bromide	2.48
• pentachloroethan	1.67
• carbontetrachloride	1.59

magnetic liquids

dielectric liquids
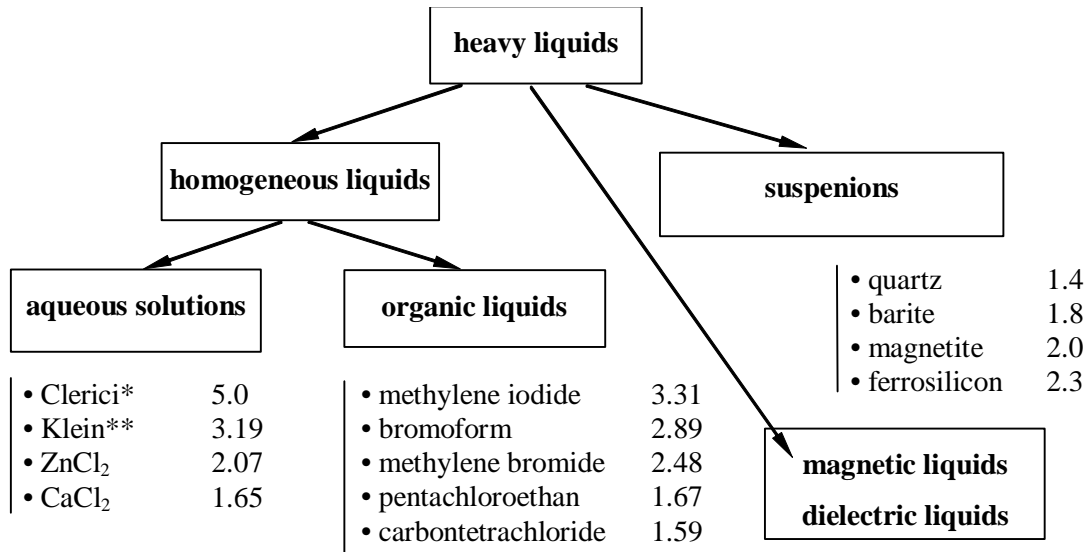
Fig. 7.3. Classification of liquids applied for gravity separation in heavy liquids.
* Mixture of thallium formate and thallium malonate $(COOTl)_2CH_2$ + HCOOTl,
** contains $HgI_2 \cdot 2KI \cdot H_2O$.
Numbers denote density in g/cm^3 or in Mg/m^3

Homogeneous liquids in the form of inorganic salts solutions, especially $ZnCl_2$ and $CaCl_2$ dissolved in water are much more advantageous for application than organic liquids. They also are seldom used by industry. In practical applications heavy liquids in the form of suspension are most often applied. The substances which are used in suspension are also called the dead weights. Typical dead weights are: magnetite, ferrosilicon, quartz, barite, clay minerals (Fig. 7.3). In heavy suspension liquids are used for the cleaning of coal and other materials, including ores and raw materials (Laskowski et al., 1979; Stepinski, 1964). Heavy suspension liquids featuring high dynamic shear stress τ_d and low values of plastic viscosity η_{plas} are best suited for separation because they are more stabile when the τ_d is high. To improve the stability of heavy suspension, the same dispersing agents as in flotation are used, including polyphosphates, short chain polyelectrolytes, modified carbohydrates, and water glass. Typical values of viscosity of heavy liquids, after Laskowski et al. (1979) as well as Laskowski and Luszczkiewicz (1984) are shown in Table 7.1.

Different devices are used for separation in heavy liquids. Laboratory scale separators are known under the names of Gross, Salzman, Jewsionowicz and Humboldt. The details of their design can be found elsewhere, for instance Laskowski et al., (1979). There are also large laboratory heavy liquids devices, for instance conic and drum separators (Laskowski et al., 1979). Special separators and washers are used on the industrial scale. The washers are used for upgrading coal using heavy homogeneous

liquids under static conditions. Among the washers there can be distinguished devices designed by Lessing, Bertrand, and du Pont.

Table 7.1. Dynamic viscosity (newtonian or plastic) of different liquids

Liquid	Viscosity cP (10^{-3} N·s/m^2)	Density g/cm^3	Remarks
Water	1.002	0.99823	293 K (20 °C)
Bromoform	1.89	2.89	298 K (25 °C)
Methylene bromide	1.09	2.48	288 K (15 °C)
CaCl$_2$ in water	1.21	1.043	299.8 K (26.8 °C), 5% CaCl$_2$
	4.88	1.33	299.8 K (26.8 °C), 35% CaCl$_2$
	33.20	1.52	299.8 K (26.8 °C), 51% CaCl$_2$
ZnCl$_2$ in water	1.94, 298 K (25 °C)	1.18, 293 K (20 °C)	20% ZnCl$_2$
	4.04, 298 K (25 °C)	1.55, 293 K (20 °C)	50% ZnCl$_2$
	137, 298 K (25 °C)	2.07, 293 K (20 °C)	75% ZnCl$_2$
Fe$_3$O$_4$ in water	100	2.3	0.017 mm particles
	45	2.3	0.026 mm particles
	45	2.6	0.038 mm particles
	30	2.6	0.051 mm particles

The devices used for separation in heavy suspensions under dynamic conditions are called separators. There are many kinds and types of them (Laskowski et al., 1979): Wemco, Cyanamid, Humbolt, Neldco, Tromp, Menzis, CRRS, Potasse d'Alsace, Bac Static, SM, JGPSz, KKN, Ridley-Scholes, Vogel, Link-Belt, Nelson-Davis, HRS, Norwalt, Teska, Hardinge, SKB, Rheinhausen, Don-Ugi, Krupp, Tromp, Drew-Boy, de Voys, Disa, Huntington, Teska, Chance, IWAR, SWS.

The operation principle of one of separator containing heavy suspension, a drum separator is shown in Fig. 7.4.
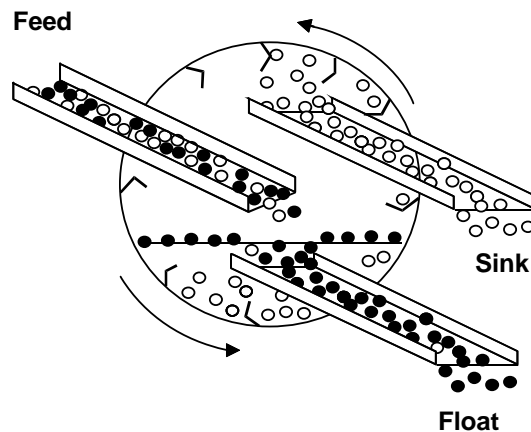
Fig. 7.4. Gravity separation in a drum separator

Usually separators are coupled with other devices which recover the dead weight. The heavy liquid is next subjected to regeneration which consists of removing unwanted circulating substances (ghost particles) and restoring desired quality parameters including density and viscosity. Separation in heavy liquids also has found its application as the analytic method called densimetric analysis.

7.2. Densimetric analysis

The densimetric analysis allows to determine the content of different fractions in the feed and separation products. The analysis can be conducted in either organic or inorganic heavy liquids. The results of densimetric analysis are tabled and usually plotted as the content of each particular density fraction as a function of either average, lower or upper boundary of fraction density.

The densimetric analysis of the feed and separation products is a good base for analysis of separation as classification. It can also be used for determining upgradeability. For this purpose an additional chemical analysis of selected component content in different densimetric fractions of the feed has to be performed. The densimetric analysis is usually performed for coal to establish its upgradeability. A typical way of conducting densimetric analysis is shown in Fig. 7.5.
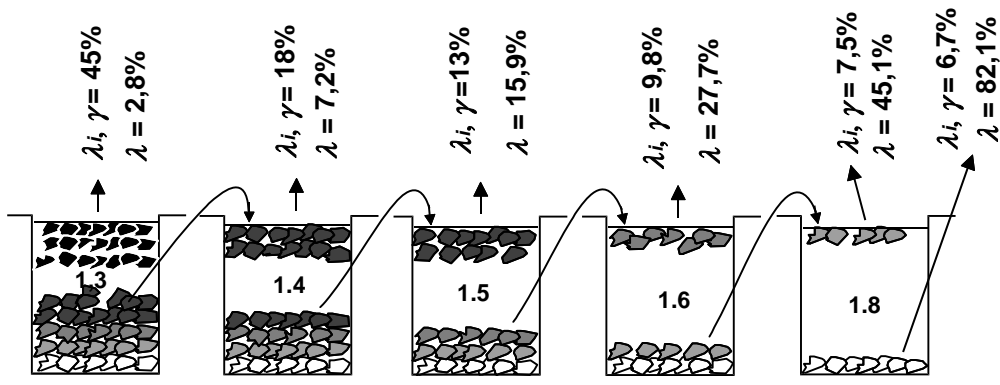
Fig. 7.5. Densimetric analysis of coal can be used to determine its upgradeability. It provides content λ_i of different density fractions in the sample. The density of heavy liquid (g/cm^3) is given as a number on the container. After ash content (λ) determination in all density fractions it is possible to determine the upgradeability of the sample Then, the content of each fraction (λ_i) has to be treated as yield (γ) of potential products of ideal separation

In order to conduct densimetric analysis, heavy liquids of increasing density have to be prepared. For coal they can be solutions of ZnCl$_2$ of density ranging from 1.3 to 1.8 g/cm^3 as coal density is from 1.17 to 1.35 while for ash forming minerals from 1.8

(shale) to 5.2 (pyrite) g/cm^3. The sample of the material is first immersed in the lightest liquid. The lightest material having density below 1.3 is gathered on the heavy liquid surface. According to Fig. 7.5, the content of the lightest coal fraction was 45% of the sample mass while ash content was 2.8%. The sinking particles (their content was 55%) were directed to another container of higher density (1.4 g/cm^3) and a subsequent density fraction was obtained. It contained the particles within density range from 1.3 to 1.4 g/cm^3. The procedure is repeated until the last separation provides two fractions: floating particles having density from 1.6 to 1.9g/cm^3 and sinking particles with density higher than 1.8 g/cm^3.

As it has already been mentioned, on the basis of the densimetric analysis one can draw the relationship between the content of different density fractions in the sample and their densities in the form of the frequency or cumulated distribution curves. These curves characterize one product of separation. When either the other separation product or the feed are the subject to densimetric analysis, one can do draw pairs of frequency, distribution, and other separation curves.

As it has already been mentioned the fractions obtained by the densimetric analysis of feed can be subjected to chemical analysis for the content of selected component, which in the case of coal can be ash. Then, the densimetric analysis becomes the method of ideal separation and the density fractions are products of separation. Well conducted density tests represent the analytical method. The results can be a good base for drawing upgradeability curves in the form of yield (content) of particular density fraction in the feed versus the component content. Figure 7.6 represents the Henry's diagram. The obtained upgradeability curves can be the reference for separation results obtained by other methods or in different devices. The upgrading curves based on densimetric analysis and chemical analysis are also called washability curves.
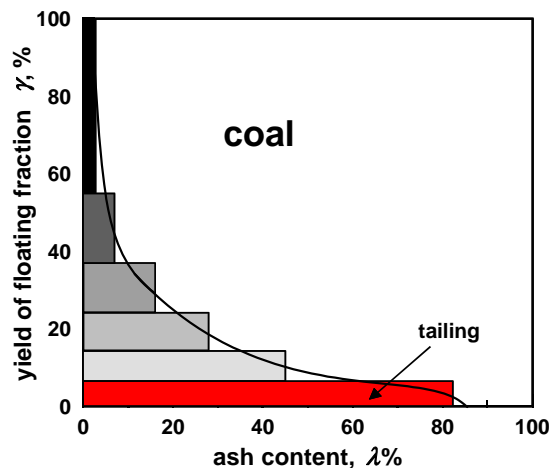
Fig. 7.6. Washability (upgradeability, Henry) curve. The coal sample was first separated into products (density fraction) by densimetric analysis and then subjected to chemical analysis to determine the ash content in all the products (fractions). Data taken from Fig. 7.5

On the basis of the results of the two mentioned analyses of the examined material density fractions, it is possible to produce other relations, including correlation curves combining the content of a component (ash) in different density fraction and density of the fraction. This type of the curve, for coal, is shown in Fig. 7.7.
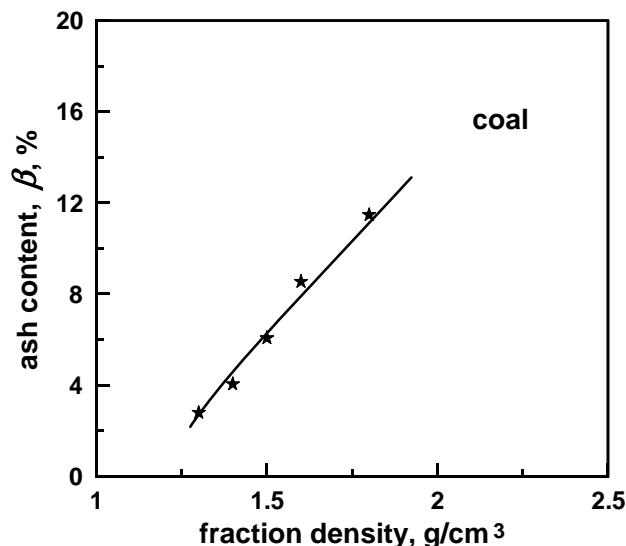
Fig. 7.7. Correlation curve showing ash content in different density fractions of coal as a function of their mean density. Based on data from Fig. 7.5

Density of selected materials is given in Tables 7.2. The density of substances depends on temperature.

Table 7.2. Metallic minerals. After http://webmineral.com, with permission of David Barthelmy (dbarthelmy@webmineral.com).

Density g/cm^3	Mineral Name	Mohs Hardness	2.82	Patronite	2
			2.88	Coyoteite	1.5
1.45	Abelsonite	2-2.5	2.94	Yushkinite	1
1.96	Vyalsovite	-	2.98	Tochilinite	1-1.5
2.16	Graphite	1.5-2	3.00	Birnessite	1.5
2.30	Erdite	2	3.08	Klyuchevskite	2.5
2.51	Cronusite !	1.5	3.08	Klyuchevskite-Duplicate	3.5
2.55	Melanovanadite	2.5			
2.57	Hydrobiotite	2.5-3	3.10	Rasvumite	4-5
2.58	Oldhamite	4	3.12	Valleriite	1-1.5
2.69	Metavivianite	1.5-2	3.15	Siderazot	-
2.70	Schollhornite	1.5-2	3.17	Annite	2.5-3
2.70	Bariandite	-	3.18	Fluorannite !	3
2.78	Fernandinite	2-3	3.21	Caswellsilverite	1-2

3.22	Moissanite	9.5	4.03	Orthopinakiolite	6
3.26	Norrishite	2.5	4.05	Greigite	4-4.5
3.30	Doloresite	-	4.08	Nagashimalite	6
3.31	Bartonite	3.5	4.10	Heideite	3.5-4.5
3.38	Chaoite	1-2	4.11	Arsenosulvanite	3.5
3.40	Steenstrupine-(Ce)	4	4.11	Grimaldiite	3.5-4.5
3.42	Takanelite	2.5-3	4.12	Brookite	5.5-6
3.46	Hauerite	4	4.15	Uhligite	5.5
3.50	Bannermanite	-	4.17	Tivanite	5.5
3.54	Wicksite	4.5-5	4.17	Dolerophanite	3
3.55	Jianshuiite	1.5-2	4.18	Magnesiohulsite	5.5-6.5
3.56	Realgar	1.5-2	4.20	Chalcopyrite	3.5
3.58	Haapalaite	1	4.20	Idaite	2.5-3.5
3.58	Rhonite	5-6	4.20	Colusite	3-4
3.60	Julgoldite-(Fe+++)	4.5	4.20	Gallite	3-3.5
3.60	Julgoldite-(Fe++)	4.5	4.20	Sedovite	3
3.65	Chiluite	3	4.20	Magnesiochromite	5.5
3.70	Arseniosiderite	1.5	4.21	Ericssonite	4.5
3.72	Chlorbartonite !	4	4.21	Orickite	3.5
3.80	Viaeneite !	3.5-4.5	4.22	Sternbergite	1-1.5
3.80	Stanekite !	4-5	4.23	Galaxite	7.5
3.80	Pseudorutile	3.5	4.25	Argentopyrite	3.5-4
3.80	Vrbaite	3.5	4.29	Vinciennite	4.5
3.81	Daubreelite	4.5-5	4.29	Talnakhite	4-4.5
3.84	Hibonite	7.5-8	4.29	Stannoidite	4
3.84	Ernienickelite	2	4.30	Hulsite	3
3.86	Ziesite	-	4.30	Magnesiocoulsonite	6-6.5
3.88	Kraisslite	3-4	4.30	Schneiderhohnite	3
3.90	Cafarsite	5.5-6	4.30	Heterogenite-2H	3-4
3.91	Chalcophanite	2.5	4.30	Schafarzikite	3.5
3.92	Laihunite	6	4.30	Berthierite	2-2.5
3.93	Isocubanite	3.5	4.30	Nukundamite	3.5
3.93	Takeuchiite	6	4.32	Smythite	4.5
3.94	Jeppeite	5-6	4.34	Yimengite	4
3.95	Aurorite	2-3	4.35	Haycockite	4.5
3.96	Blossite	-	4.35	Manganite	4
4.00	Alabandite	3.5-4	4.36	Mooihoekite	4
4.00	Armalcolite	6	4.36	Cryptomelane	6-6.5
4.00	Montroseite	5.5-6.5	4.37	Ramsdellite	3
4.00	Paramontroseite	-	4.38	Renierite	4-5
4.00	Sulvanite	3.5	4.39	Imhofite	2
4.00	Lepidocrocite	5	4.40	Stannite	3.5-4
4.00	Geikielite	6	4.40	Titanium *	4
4.00	Perovskite	5.5	4.40	Latrappite	5.5
4.02	Ilvaite	5.5-6	4.41	Loveringite	7.5
4.02	Gillulyite	2-2.5	4.42	Landauite	7.5
4.03	Qandilite	7	4.44	Manganese-shadlunite	4

4.45	Vaesite	4.5-5.5		4.70	Tranquillityite	-
4.45	Enargite	3		4.70	Cubanite	3.5
4.47	Hemusite	4		4.70	Blatterite	6
4.48	Olkhonskite	8		4.72	Ilmenite	5-5.5
4.48	Putoranite	4.5		4.73	Pyrolusite	6-6.5
4.50	Briartite	3.5-4		4.74	Umohoite	2
4.50	Luzonite	3.5		4.75	Jacobsite	5.5-6
4.50	Duranusite	2		4.77	Hocartite	4
4.50	Germanite	3		4.77	Braunite-II *	6-6.5
4.52	Pyrophanite	5		4.77	Braunite-I	6-6.5
4.52	Villamaninite	4.5		4.77	Hausmannite	5.5
4.55	Psilomelane ?	5-6		4.78	Cernyite	4
4.56	Kuramite	5		4.78	Fingerite	-
4.56	Katoptrite	5.5		4.78	Owensite	3.5
4.57	Kesterite	4.5		4.80	Chromite	5.5
4.57	Famatinite	3-4		4.80	Cattierite	4.5
4.57	Lenaite	4.5		4.80	Linnaeite	4.5-5.5
4.60	Fetiasite	5		4.80	Pentlandite	3.5-4
4.60	Mathiasite	7.5		4.80	Polybasite	2.5-3
4.60	Loranskite-(Y)	5		4.81	Selenium	2
4.60	Hutchinsonite	1.5-2		4.81	Rebulite	-
4.61	Petrukite	4.5		4.82	Pirquitasite	4
4.62	Pyrrhotite	3.5-4		4.84	Ottemannite	2
4.62	Troilite	3.5-4		4.85	Iwakiite	6-6.5
4.62	Nekrasovite	4.5-5		4.86	Livingstonite	2
4.62	Graeserite !	5.5		4.86	Manganochromite	5.5
4.63	Neltnerite	6		4.86	Mohite	4
4.63	Lindsleyite	7.5		4.87	Karelianite	8-9
4.63	Stibnite	2		4.87	Hawleyite	2.5-3
4.64	Ilmenorutile	6-6.5		4.88	Chalcostibite	3.5
4.64	Vuorelainenite	6.5		4.89	Yarrowite	3.5
4.64	Hydrohetaerolite	5-6		4.89	Marcasite	6-6.5
4.64	Marokite	6.5		4.90	Fukuchilite	6
4.65	Carrollite	4.5-5.5		4.90	Lautite	3-3.5
4.65	Violarite	4.5-5.5		4.90	Tetrahedrite	3.5-4
4.65	Siegenite	5-5.5		4.90	Maghemite	6
4.65	Polydymite	4.5-5.5		4.90	Smithite	1.5-2
4.65	Tennantite	3.5-4		4.91	Langbanite	6.5
4.65	Magnesioferrite	6-6.5		4.93	Freibergite	3.5-4
4.66	Mawsonite	3.5-4		4.94	Toyohaite	4
4.66	Clerite !	3.5-4		4.95	Bixbyite	6-6.5
4.66	Watanabeite	4-4.5		4.95	Goldfieldite	3-3.5
4.67	Indite	5		4.96	Abswurmbachite	6.5
4.68	Dessauite !	6.5-7		4.96	Stoiberite	-
4.68	Covellite	1.5-2		4.97	Lapieite	4.5-5
4.69	Murataite	6-6.5		4.97	Pierrotite	3.5
4.69	Nolanite	5-5.5		4.97	Stalderite	3.5-4

5.00	Chatkalite	4.5	5.33	Apuanite	4-5
5.00	Crednerite	4-5	5.33	Cuboargyrite !	3
5.00	Donathite ?	6.5-7	5.33	Ramdohrite	2
5.01	Bravoite ?	6.5	5.33	Baumstarkite !	2.5
5.01	Pyrite	6.5	5.33	Baumhauerite	3
5.02	Hetaerolite	6	5.35	Bismutoplagionite *	2.5
5.04	Magnesiocolumbite	6.5	5.35	Eskebornite	3-3.5
5.04	Parapierrotite	2.5-3	5.36	Hongquiite *	5-6
5.05	Ferdisilicite *	6.5	5.39	Geffroyite	2.5
5.05	Fergusonite-(Y)	5.5-6	5.40	Osbornite	8.5
5.07	Skinnerite	3.5-4	5.41	Delafossite	5.5
5.08	Jankovicite	2	5.41	Cylindrite	2.5
5.10	Cuprospinel	6.5-7	5.41	Andorite	3-3.5
5.10	Bornite	3	5.41	Seligmannite	2.5-3
5.10	Sartorite	3	5.41	Rathite	3
5.10	Chabourneite	3-3.5	5.42	Stilleite	5
5.12	Versiliaite	5	5.44	Arsenolamprite	2
5.13	Spionkopite	2.5-3	5.44	Coronadite	4.5-5
5.15	Franklinite	5.5-6	5.44	Strontiochevkinite	5-6
5.15	Magnetite	5.5-6	5.45	Horobetsuite *	2
5.15	Zoubekite	3.5-4	5.45	Jaipurite *	-
5.16	Uchucchacuaite	3.5	5.45	Velikite	4
5.16	Ianthinite	2.5-3	5.46	Koragoite	4-5
5.17	Trevorite	5	5.48	Tintinaite	2.5-3
5.18	Eskolaite	8-8.5	5.48	Parajamesonite	2.5-3
5.19	Coulsonite	4.5-5	5.49	Mcconnellite	5.5
5.20	Herzenbergite	2	5.50	Aktashite	3.5
5.20	Miargyrite	2-2.5	5.50	Petscheckite	5
5.20	Picotpaulite	2	5.50	Millerite	3-3.5
5.20	Sinnerite	5	5.50	Plagionite	2.5
5.21	Paakkonenite	2	5.50	Molybdenite	1
5.22	Fuloppite	2-2.5	5.51	Brunogeierite	4.5
5.22	Cochromite	7	5.51	Samsonite	2.5
5.24	Zinkenite	3-3.5	5.52	Magnetoplumbite	6
5.24	Nichromite	6-6.5	5.52	Sorbyite	3.5-4
5.24	Jentschite !	2-2.5	5.53	Lorandite	2-2.5
5.26	Thalfenisite	1-1.5	5.54	Vigezzite	4.5-5
5.26	Twinnite	3.5	5.55	Proustite	2-2.5
5.27	Godlevskite	4-5	5.56	Fizelyite	2
5.27	Roshchinite	2.5-3.5	5.56	Dufrenoysite	3
5.28	Manganocolumbite	6	5.57	Jamesonite	2.5
5.29	Cesarolite	4.5	5.57	Zincite	4-5
5.30	Paxite	3.5-4	5.60	Aramayoite	2.5
5.30	Senaite	6-6.5	5.60	Digenite	2.5-3
5.30	Liveingite	3	5.60	Benavidesite	2.5
5.30	Hematite	6.5	5.63	Melanostibite	4
5.31	Guettardite	4	5.63	Djurleite	2.5-3

5.64	Garavellite	4	6.07	Laffittite	3.5
5.64	Bambollaite	3	6.10	Diaphorite	2.5
5.65	Chalcocite	2.5-3	6.12	Gersdorffite	5.5
5.68	Anilite	3-4	6.15	Thalcusite	2.5-3
5.69	Nezilovite !	4-5	6.15	Stibarsen	3-4
5.70	Robinsonite	2.5-3	6.15	Pearceite	3
5.70	Arsenic	3.5	6.15	Stromeyerite	2.5-3
5.70	Franckeite	2.5	6.17	Chameanite	4.5
5.70	Yttrotantalite-(Y)	5-5.5	6.17	Alloclasite	5
5.71	Ferrorhodsite	4.5	6.19	Fangite	2-2.5
5.71	Suredaite !	2.5-3	6.19	Kentrolite	5
5.72	Dadsonite	2.5	6.20	Argyrodite	2.5
5.73	Heteromorphite	2.5-3	6.20	Bursaite	2.5-3
5.73	Melanotekite	6.5	6.20	Potosiite	2.5
5.75	Launayite	3.5-4	6.20	Umangite	3
5.75	Giraudite	3.5-4	6.20	Vozhminite	4.5-5
5.76	Lindqvistite	6	6.20	Tellurium	2-2.5
5.79	Weissbergite	1.5	6.21	Arsenpolybasite	3
5.80	Playfairite	3.5-4	6.22	Gratonite	2.5
5.80	Bournonite	3	6.23	Marrite	3
5.82	Heazlewoodite	4	6.25	Stephanite	2-2.5
5.83	Lengenbachite	1-2	6.25	Drysdallite	1-1.5
5.83	Routhierite	3.5	6.28	Canfieldite	2.5
5.85	Pyrargyrite	2.5	6.30	Kobellite	2.5-3
5.88	Gruzdevite	4.5	6.30	Ferrocolumbite	6
5.88	Cechite	4.5-5	6.30	Hakite	5
5.88	Antimonselite	3.5	6.30	Murdochite	4
5.88	Muckeite	3.5	6.30	Freieslebenite	2.5
5.90	Carlsbergite	7	6.31	Falkmanite	2-3
5.92	Billingsleyite	2.5	6.32	Balkanite	3.5
5.92	Veenite	3.5-4	6.33	Cobaltite	5.5
5.93	Yttrocolumbite-(Y)	5-6	6.34	Antimonpearceite	3
5.95	Pararsenolamprite !	2-2.5	6.35	Arsenohauchecornite	5.5
5.95	Semseyite	2.5	6.36	Hauchecornite	5
5.95	Jordanite	3	6.37	Owyheeite	2.5
5.95	Fersilicite *	6.5	6.39	Meneghinite	2.5
5.96	Glaucodot	5	6.40	Raguinite	-
5.96	Kamiokite	4.5	6.40	Emplectite	2
5.98	Madocite	3	6.40	Teallite	1.5-2
6.00	Weissite	3	6.40	Geocronite	2.5-3
6.00	Plumboferrite	5	6.40	Rynersonite	4.5
6.00	Boulangerite	2.5	6.42	Qitianlingite	5.5
6.00	Sterryite	3.5	6.43	Wolframoixiolite *	5-6
6.01	Betekhtinite	3	6.45	Aikinite	2-2.5
6.05	Brackebuschite	4-5	6.45	Xifengite	5.5
6.06	Miharaite	4	6.45	Romanechite	5-6
6.07	Arsenopyrite	5	6.45	Hodrushite	4-5

6.47	Cuprobismutite	-		6.91	Stistaite	3
6.47	Izoklakeite	3.5-4		6.91	Paderaite	4
6.50	Nickel-skutterudite	5.5-6		6.92	Oregonite	5
6.50	Wittichenite	2.5		6.92	Barringerite	-
6.50	Skutterudite	5.5-6		6.96	Gladite	2.5-3
6.50	Jaskolskiite	4		6.98	Friedrichite	4
6.52	Paradocrasite	3.5		6.99	Laurite	7.5
6.53	Achavalite *	2.5		7.00	Lillianite	2-3
6.60	Cosalite	2.5-3		7.00	Galenobismutite	2.5-3
6.60	Chalcothallite	2-2.5		7.00	Bismuthinite	2
6.60	Paraguanajuatite	2.5-3		7.01	Lindstromite	3-3.5
6.61	Ashanite ?	6-6.5		7.01	Nuffieldite	3.5-4
6.61	Mckinstryite	1.5-2.5		7.01	Gustavite	3.5
6.62	Guanajuatite	2.5-3.5		7.02	Neyite	2.5
6.62	Polkovicite	3.5		7.03	Daomanite *	3.5-4
6.62	Morozeviczite	3.5		7.03	Bellidoite	1.5-2
6.64	Mummeite	4		7.05	Zinc	2
6.64	Xingzhongite	6		7.06	Weibullite	2-2.5
6.65	Ullmannite	5.5		7.08	Suessite	-
6.66	Penroseite	2.5-3		7.08	Xilingolite	3
6.67	Antimony	3-3.5		7.09	Ixiolite	6-6.5
6.69	Vysotskite	1.5		7.10	Eskimoite	4
6.70	Berryite	3.5		7.10	Vulcanite	1-2
6.70	Cannizzarite	2.5		7.10	Jolliffeite	6-6.5
6.70	Benjaminite	3.5		7.10	Safflorite	4-5
6.70	Novakite	3-3.5		7.10	Rammelsbergite	5.5
6.70	Makovickyite	3.5		7.10	Ellisite	2
6.70	Magnesiotantalite !	5.5		7.11	Ourayite	2
6.70	Berzelianite	2		7.12	Proudite	2-2.5
6.72	Kullerudite	5.5-6.5		7.12	Wittite	2-2.5
6.72	Gudmundite	5.5-6		7.14	Peterbaylissite	4-5
6.73	Hammarite	3-4		7.15	Heyrovskyite	3.5-4
6.74	Cuprorhodsite	5-5.5		7.15	Gupeiite	5
6.74	Furutobeite	3		7.15	Hubnerite	4.5
6.74	Schirmerite	2		7.19	Kitkaite	3.5
6.76	Willyamite	5.5		7.20	Chromium	7.5
6.77	Junoite	3.5-4		7.20	Pararammelsbergite	5.5
6.80	Gortdrumite	3.5-4		7.20	Kieftite	5-5.5
6.80	Pavonite	2		7.21	Roaldite	5.5-6.5
6.82	Vincentite	5		7.21	Ferroselite	6-6.5
6.82	Jalpaite	2-2.5		7.22	Hastite	6
6.83	Zenzenite	5.7		7.24	Cuproiridsite	5-6
6.85	Eclarite	3-3.5		7.25	Treasurite	-
6.89	Costibite	6		7.25	Naumannite	2.5
6.90	Crookesite	2.5-3		7.27	Aschamalmite	3.5
6.90	Paracostibite	7		7.28	Wodginite	5.5
6.90	Matildite	2.5		7.30	Wolframite *	4.5

7.30	Melonite	1-1.5		7.87	Bohdanowiczite	3
7.30	Argentite *	2-2.5		7.89	Kochkarite	2-2.5
7.30	Acanthite	2-2.5		7.90	Borodaevite	3.5
7.31	Tin	2		7.90	Kamacite	4
7.31	Indium	3.5		7.91	Hollingworthite	6-6.5
7.34	Dzharkenite	5		7.92	Oenite !	5-5.5
7.36	Bukovite	2		7.98	Platynite ?	2-3
7.36	Danbaite	4		8.00	Platarsite	7.5
7.38	Telargpalite	2-2.5		8.00	Nisbite	5
7.38	Tsnigriite	3.5		8.00	Stutzite	3.5
7.40	Malanite	5		8.00	Awaruite	5
7.40	Galena	2.5		8.00	Nickel	4-5
7.40	Lollingite	5		8.01	Volynskite	2.5-3
7.40	Schreibersite	6.5-7		8.01	Taenite	5-5.5
7.43	Cohenite	5.5-6		8.06	Frohbergite	3-4
7.45	Ferberite	4.5		8.07	Coloradoite	2.5
7.45	Giessenite	2.5		8.09	Babkinite !	2
7.46	Clinosafflorite	4.5-5		8.10	Joseite	2
7.50	Orcelite	-		8.10	Baksanite !	1.5-2
7.50	Nagyagite	1.5-2		8.10	Telluronevskite	3.5
7.54	Rickardite	3.5		8.10	Manganotantalite	6-6.5
7.55	Empressite	3.5		8.10	Sylvanite	1.5-2
7.55	Hessite	1.5-2		8.12	Borovskite	3
7.55	Tetradymite	1.5-2		8.12	Laitakarite	2
7.56	Bismutocolumbite	5.5		8.15	Monteponite	3
7.60	Soucekite	4		8.15	Altaite	2.5
7.60	Iron !	4-5		8.16	Tsumoite	2.5-3
7.61	Prassoite !	5-6		8.17	Langisite	6-6.5
7.65	Domeykite	3-3.5		8.17	Tapiolite *	6-6.5
7.70	Eucairite	2.5		8.20	Clausthalite	2.5
7.70	Haxonite	5.5-6		8.20	Ferrotantalite	6-6.5
7.70	Hematophanite	2-3		8.21	Zlatogorite !	4.5
7.71	Petrovicite	3		8.23	Breithauptite	3.5-4
7.72	Manganotapiolite	6		8.26	Kotulskite	4-4.5
7.74	Rucklidgeite	2.5		8.28	Tetrataenite	3.5
7.75	Sorosite !	5-5.5		8.30	Palladseite	4.5-5
7.75	Metacinnabar	3		8.30	Joseite-B	2
7.78	Kharaelakhite	-		8.31	Chrisstanleyite !	5
7.78	Rohaite	3-3.5		8.33	Tiemannite	2.5
7.79	Nickeline	5.5		8.38	Kutinaite	4.5
7.79	Kawazulite	1.5		8.41	Pilsenite	1.5-2.5
7.80	Ikunolite	2		8.42	Cuprostibite	4
7.82	Tellurobismuthite	1.5-2		8.43	Kostovite	2-2.5
7.82	Ferrotapiolite	6		8.44	Osarsite	6
7.83	Maucherite	5		8.48	Oosterboschite	5
7.85	Imiterite	2.5-3		8.48	Koutekite	3.5
7.86	Henryite	3.5		8.50	Protojoseite *	-

8.50	Kusachiite	4-5		10.20	Atheneite	5
8.50	Parkerite	3		10.22	Polkanovite !	-
8.53	Krennerite	2.5		10.25	Telluropalladinite	5
8.55	Imgreite ?	4		10.25	Niobocarbide !	8
8.55	Algodonite	4		10.27	Oulankaite !	3.5-4
8.60	Cadmium	1-2		10.33	Isomertieite	5.5
8.60	Jedwabite !	7		10.40	Stillwaterite	4.5
8.72	Shandite	4		10.40	Arsenopalladinite	4
8.73	Uraninite	5-6		10.42	Palladoarsenide	5
8.79	Vasilite	5-5.5		10.50	Tolovkite	7.5
8.80	Horsfordite	4-5		10.50	Silver	2.5-3
8.83	Genkinite	5.5-6		10.58	Sperrylite	6-7
8.91	Hedleyite	2		10.60	Mertieite-I	5.5
8.91	Wattersite	4.5		10.70	Cabriite	4-4.5
8.92	Petzite	2.5		10.75	Eugenite	2.5-3
8.94	Hexatestibiopanickelite	2		10.86	Palladobismutharsenide	5
8.95	Copper	2.5-3		10.90	Iridarsenite	5-5.5
8.99	Testibiopalladite	3.5-4		10.95	Damiaoite !	5
9.04	Calaverite	2.5		10.97	Geversite	4.5-5
9.05	Fischesserite	2-2.5		11.20	Omeiite	7
9.07	Plattnerite	5.5		11.29	Mertieite-II	6
9.10	Kashinite	7.5		11.30	Rhodarsenide !	4-5
9.14	Kolarite	-		11.32	Paolovite	5
9.33	Majakite	6		11.37	Lead	2-2.5
9.50	Temagamite	2.5		11.50	Auricupride	2-3
9.50	Cooperite	4-5		11.55	Palladium	4.5-5
9.50	Stibiopalladinite	4-5		11.80	Yuanjiangite	3.5-4
9.50	Michenerite	2.5		11.88	Sobolevskite	4
9.52	Hanawaltite	4		12.12	Changchengite !	3.5
9.57	Avicennite	2		12.20	Ruthenium	6.5
9.59	Erlichmanite	4.5-5.5		12.40	Plumbopalladinite	5
9.66	Urvantsevite	2.5		12.50	Luanheite	2.5
9.67	Sudovikovite !	2-2.5		12.51	Polarite	3.5-4
9.70	Dyscrasite	3.5-4		12.55	Froodite	2.5
9.72	Cherepanovite	6		12.72	Mayingite	4
9.75	Bismuth	2-2.5		12.80	Insizwaite	5-5.5
9.94	Montbrayite	2.5		12.98	Paraschachnerite	4
9.97	Gaotaiite	3		13.00	Kolymite	4
9.98	Aurostibite	3		13.02	Luberoite	5-5.5
10.00	Ruthenarsenite	6-6.5		13.20	Belendorffite	2.5-4
10.00	Allargentum	4		13.32	Zvyagintsevite	4.5
10.00	Braggite	1.5		13.44	Niggliite	3
10.00	Moncheite	2-3		13.52	Stumpflite	5
10.00	Thorianite	6		13.60	Moschellandsbergite	3.5
10.01	Khamrabaevite	9-9.5		13.60	Mercury	0
10.14	Shuangfengite	3		13.93	Amalgam *	3-3.5
10.20	Stannopalladinite	5		14.27	Bilibinskite	5

14.30	Tetraferroplatinum	4-5		16.30	Bezsmertnovite	4.5
14.50	Tantalcarbide !	6-7		16.50	Isoferroplatinum	5
14.88	Potarite	3.5		16.51	Rhodium	3.5
14.90	Atokite	5		17.65	Gold	2.5-3
14.90	Tulameenite	5		18.00	Platinum	4-4.5
15.03	Tetra-auricupride	4.5		18.27	Yixunite !	6
15.39	Ferronickelplatinum	5		19.30	Chengdeite	5
15.46	Maldonite	1.5-2		20.00	Osmium	6-7
15.47	Goldamalgam *	3		21.03	Rhenium *	-
15.60	Taimyrite	5		22.70	Iridium	6-7
15.63	Hongshiite *	5				
16.00	Hunchunite !	3.5				

cont. Table 7.2. Non-metallic minerals. After http://webmineral.com,with permission of David Barthelmy (dbarthelmy@webmineral.com.)

Density g/cm³	Mineral Name	Mohs Hardness		1.69	Lonecreekite	2-3
1.01	Dinite *	1		1.70	Lansfordite	2.5
1.05	Hartite !	1		1.70	Boussingaultite	2
1.09	Flagstaffite	-		1.70	Struvite	1.5-2
1.10	Amber *	2-2.5		1.71	Qilianshanite	2
1.11	Ravatite	1		1.71	Borax	2-2.5
1.24	Idrialite	1.5		1.71	Sborgite	-
1.33	Phosphammite	-		1.72	Alunogen	1.5-2
1.35	Karpatite	1.5		1.72	Antarcticite	2-3
1.45	Natron	1		1.72	Natrophosphate	2.5
1.49	Mirabilite	1.5-2		1.73	Phosphorrosslerite	2.5
1.50	Oxammite	2.5		1.73	Sodium-alum	3
1.50	Sal-ammoniac	1.5-2		1.73	Tinnunculite *	-
1.51	Hydroglauberite	-		1.75	Lecontite	2-2.5
1.55	Stercorite	2		1.75	Mendozite	3
1.56	Bischofite	1.5-2		1.76	Potassium-alum	2
1.58	Nitromagnesite	-		1.76	Hexahydrite	2-2.5
1.58	Teschemacherite	1.5		1.76	Kalinite	2
1.60	Carnallite	2.5		1.76	Nepskoeite !	1.5-2
1.60	Mellite	2-2.5		1.76	Redingtonite	2
1.60	Indigirite	2		1.77	Mascagnite	2-2.5
1.65	Cattiite !	2		1.77	Gwihabaite !	5
1.65	Tschermigite	1.5-2		1.77	Charlesite	2.5
1.66	Cadwaladerite	-		1.79	Ikaite	-
1.66	Tachyhydrite	2		1.79	Jurbanite	2.5
1.67	Chloraluminite	-		1.79	Korshunovskite	2
1.68	Epsomite	2-2.5		1.80	Magnesioaubertite	2-3
1.68	Aluminite	1		1.80	Apjohnite	1.5-2
1.69	Stepanovite	2		1.80	Ettringite	2-2.5
1.69	Zhemchuzhnikovite	2		1.80	Inderite	2.5
1.69	Svyazhinite	2-3		1.80	Canavesite	-
				1.80	Dietrichite	2

1.81	Sinjarite	1.5		1.93	Faujasite-Na	5
1.81	Wattevillite	-		1.93	Faujasite-Ca !	5
1.82	Aubertite	2-3		1.93	Faujasite-Mg !	5
1.82	Megacyclite	2		1.93	Ferrohexahydrite	2
1.83	Pickeringite	1.5-2		1.94	Revdite	2
1.83	Schertelite	-		1.94	Sanjuanite	3
1.83	Kurnakovite	3		1.95	Fullerite !	3.5
1.83	Letovicite	1-2		1.95	Gutsevichite ?	2.5
1.83	Bazhenovite	2		1.95	Evansite	3.5-4
1.83	Mohrite	2-2.5		1.95	Jouravskite	2.5
1.84	Halotrichite	1.5-2		1.96	Ulexite	2.5
1.84	Nesquehonite	2.5		1.96	Vashegyite	2-3
1.84	Chvaleticeite	1.5		1.96	Gaylussite	2.5
1.85	Mallardite	2		1.97	Hellyerite	2.5
1.85	Sturmanite	2.5		1.97	Brianroulstonite !	5
1.85	Caoxite !	2-2.5		1.97	Moorhouseite	2.5
1.85	Hydrochlorborite	2.5		1.98	Koenenite	1.5
1.87	Mcallisterite	2.5		1.98	Boggsite	3.5
1.87	Lesukite !	-		1.99	Sylvite	2.5
1.87	Hexahydroborite	2.5		1.99	Xitieshanite	3
1.87	Bilinite	2		2.00	Richellite	2-3
1.87	Inyoite	2		2.00	Slavikite	3.5
1.87	Pascoite	2.5		2.00	Goslarite	2-2.5
1.88	Wardsmithite	2.5		2.00	Gmelinite-K !	4
1.88	Tincalconite	2		2.00	Gowerite	3
1.89	Thaumasite	3.5		2.00	Hydroboracite	2
1.89	Barberiite	1		2.00	Morenosite	2-2.5
1.90	Melanterite	2		2.00	Sepiolite	2
1.90	Wupatkiite	1.5-2		2.00	Inderborite	3.5
1.90	Orschallite	4		2.01	Kuzelite !	1.5-2
1.90	Nitrocalcite	1-2		2.01	Starkeyite	2-3
1.90	Fibroferrite	2		2.01	Zaherite	3.5
1.90	Bieberite	2		2.01	Bolivarite	2.5-3.5
1.90	Formicaite !	1		2.01	Cryptohalite	2.5
1.90	Allophane	3		2.02	Pentahydroborite	2.5
1.90	Pentahydrite	2.5		2.02	Artinite	2.5
1.90	Delvauxite	2.5		2.02	Meta-aluminite	1-2
1.91	Rivadavite	3.5		2.02	Zinc-melanterite	2
1.91	Kernite	2.5-3		2.02	Weddellite	4
1.91	Kanonerovite !	2.5-3		2.02	Tschernichite	4.5
1.91	Chelyabinskite *	3		2.02	Roggianite	-
1.91	Swaknoite	1.5-2		2.03	Bentorite	2
1.92	Behoite	4		2.03	Dickthomssenite !	2.5
1.93	Nickelbischofite	1.5		2.03	Mitryaevaite !	-
1.93	Rosslerite	2-3		2.03	Ameghinite	2-3
1.93	Clinobehoite	2-3		2.03	Aristarainite	3.5
1.93	Kribergite	-		2.03	Picromerite	2.5

2.03	Minasragrite	1-2		2.10	Tschortnerite !	4.5
2.03	Bianchite	2.5		2.10	Kainite	3
2.03	Jokokuite	2.5		2.10	Newberyite	3-3.5
2.03	Hannayite	2-3		2.10	Rosenbergite	3-3.5
2.04	Chlormagaluminite	1.5-2.5		2.10	Barbertonite	1.5-2
2.04	Biphosphammite	1-2		2.10	Lindbergite !	2.5
2.04	Tsaregorodtsevite	6		2.10	Satimolite	1-2
2.05	Luneburgite	2		2.10	Ferricopiapite	2.5-3
2.05	Sturtite *	3-3.5		2.10	Copiapite	2.5
2.05	Melanophlogite	6.5-7		2.11	Niter	2
2.05	Melanophlogite-beta !	6.5-7		2.11	Mazzite	4-5
2.05	Mundrabillaite	1-2		2.11	Paracoquimbite	2.5
2.05	Nastrophite	2		2.11	Sjogrenite	2.5
2.05	Manasseite	2		2.11	Erionite-Na	3.5-4
2.05	Coquimbite	2		2.11	Erionite-K !	3.5-4
2.05	Bayleyite	-		2.11	Erionite-Ca !	3.5-4
2.05	Iquiqueite	2		2.11	Peisleyite	3
2.05	Botryogen	2		2.12	Kaliborite	4-4.5
2.05	Ezcurrite	3-3.5		2.12	Minguzzite	-
2.06	Terranovaite !	-		2.12	Meyerhofferite	2
2.06	Tamarugite	3		2.12	Herschelite ?	4-5
2.06	Hydrotalcite	2		2.12	Carboborite	2
2.06	Amicite	5-5.5		2.12	Mountkeithite	2
2.06	Hotsonite-VII	2.5		2.12	Basaluminite	1.5
2.06	Hotsonite-VI	2.5		2.13	Mordenite	5
2.06	Woodallite !	1.5-2		2.13	Levyne-Na !	4-4.5
2.07	Walkerite !	3		2.13	Levyne-Ca	4-4.5
2.07	Nickelhexahydrite	2		2.13	Stellerite	4.5
2.07	Sulfur	1.5-2.5		2.13	Magnesiocopiapite	2.5-3
2.07	Pyroaurite	2.5		2.13	Cuprocopiapite	2.5-3
2.07	Retgersite	2.5		2.13	Desautelsite	2
2.07	Makatite	-		2.13	Offretite	4-4.5
2.07	Rosickyite	2-3		2.13	Barrerite	3-4
2.08	Teepleite	3-3.5		2.14	Trona	2.5
2.08	Ginorite	3.5		2.14	Quenstedtite	2.5
2.09	Paulingite-Ca !	5		2.14	Quintinite-3T	2
2.09	Zabuyelite	3		2.14	Cowlesite	5-5.5
2.09	Nobleite	3		2.14	Gottardiite !	-
2.10	Uralolite	2.5		2.14	Probertite	3.5
2.10	Chabazite-K !	4		2.14	Mutinaite !	-
2.10	Chabazite-Ca	4		2.14	Quintinite-2H	2
2.10	Chabazite-Na !	4		2.14	Brugnatellite	2
2.10	Iowaite	1.5		2.14	Frolovite	3.5
2.10	Opal	5.5-6		2.14	Perlialite	4-5
2.10	Gmelinite-Na	4.5		2.15	Ferrierite-Na !	3-3.5
2.10	Gmelinite-Ca !	4.5		2.15	Ferrierite-Mg	3-3.5
2.10	Boothite	2-2.5		2.15	Ferrierite-K !	3-3.5

2.15	Gobbinsite	4		2.20	Heulandite-K !	3-3.5
2.15	Teruggite	2.5		2.20	Heulandite-Na !	3-3.5
2.15	Romerite	3-3.5		2.20	Phillipsite-Na	4-5
2.15	Chrysocolla	2.5-3.5		2.20	Phillipsite-Ca !	4-5
2.15	Vertumnite	5		2.20	Heulandite-Ca	3-3.5
2.15	Weinebeneite	3-4		2.20	Heulandite-Sr !	3-3.5
2.15	Micheelsenite !	3.5-4		2.20	Phillipsite-K !	4-5
2.15	Hydrocalumite	3		2.20	Viseite	3-4
2.15	Dypingite	-		2.20	Caichengyunite !	1.5-2
2.15	Beidellite	1-2		2.20	Rosieresite	3-3.5
2.15	Clinoptilolite-K	3.5-4		2.20	Ilmajokite	1
2.15	Garronite	4-5		2.20	Diadochite	3-3.5
2.15	Palygorskite	2-2.5		2.20	Leonite	2.5-3
2.15	Clinoptilolite-Na !	3.5-4		2.20	Zincobotryogen	2.5
2.15	Stilbite-Ca	3.5-4		2.20	Darapskite	2.5
2.15	Stilbite-Na !	3.5-4		2.21	Merlinoite	4.5
2.15	Clinoptilolite-Ca !	3.5-4		2.21	Lishizhenite	3.5
2.15	Siderotil	2.5		2.21	Pringleite	3-4
2.15	Bararite	2.5		2.21	Paranatrolite	5-5.5
2.16	Phosphovanadylite !	-		2.21	Nahcolite	2.5
2.16	Nabesite !	5-6		2.21	Olshanskyite	4
2.16	Chabazite-Sr !	4-4.5		2.21	Goosecreekite	4.5
2.16	Dachiardite-Na	4-5		2.21	Ruitenbergite	3-4
2.16	Douglasite	-		2.21	Rapidcreekite	2
2.16	Paulingite-K	5		2.21	Tuzlaite	2-3
2.16	Paulingite-Na !	5		2.21	Chalcanthite	2.5
2.17	Loughlinite	-		2.21	Chessexite	-
2.17	Hydrodelhayelite	4		2.21	Grumantite	4-5
2.17	Kalicinite	1-2		2.22	Whewellite	2.5-3
2.17	Kremersite	-		2.22	Mcauslanite	3.5
2.17	Halite	2.5		2.22	Lannonite	2
2.18	Dachiardite-Ca	4-4.5		2.22	Hydrophilite	-
2.18	Hydromagnesite	3.5		2.22	Lanmuchangite !	3-3.5
2.18	Willhendersonite	3		2.22	Calciocopiapite	2.5-3
2.18	Fluellite	3		2.22	Cyanochroite	2-2.5
2.18	Zincocopiapite	2		2.23	Rhomboclase	2
2.19	Tyretskite	5		2.23	Portlandite	2.5-3
2.19	Dittmarite	5		2.23	Gordonite	3.5
2.19	Amarillite	2.5-3		2.23	Yugawaralite	4.5
2.20	Bobierrite	2-2.5		2.23	Alumohydrocalcite	2.5
2.20	Rozenite	2-3		2.23	Nekoite	-
2.20	Beryllite	1		2.24	Amarantite	2.5
2.20	Stichtite	1.5-2		2.24	Endellite !	1-2
2.20	Hohmannite	3		2.24	Canaphite	2
2.20	Bellbergite	5		2.24	Silinaite	4.5
2.20	Berborite	3		2.25	Volkonskoite	1.5-2
2.20	Spadaite	2.5		2.25	Strontioginorite	2-3

2.25	Natrolite	5.5-6	2.31	Griffithite *	1
2.25	Epistilbite	4-5	2.31	Studenitsite	5.5-6
2.25	Sideronatrite	1.5-2	2.31	Varennesite	4
2.25	Humberstonite	2.5	2.31	Chlormanganokalite	2.5
2.26	Thermonatrite	1	2.32	Okenite	5
2.26	Wairakite	5.5-6	2.32	Buddingtonite	5.5
2.26	Gismondine	4-5	2.32	Hydroxycancrinite	6
2.26	Penobsquisite !	3	2.32	Misenite	-
2.26	Cavansite	3-4	2.32	Matveevite ?	2.5
2.26	Ilesite	2-3	2.32	Natroxalate !	3
2.27	Nitratine	1.5-2	2.33	Kalifersite !	2
2.27	Wheatleyite	1-2	2.33	Jennite	3.5
2.27	Macdonaldite	3.5-4	2.33	Brushite	2.5
2.27	Sinkankasite	4	2.33	Hydrowoodwardite !	-
2.27	Cristobalite	6.5	2.33	Nikischerite !	2
2.28	Hydrobasaluminite	-	2.33	Matulaite	1
2.28	Sergeevite	3.5	2.33	Mercallite	-
2.28	Phaunouxite	-	2.33	Lovdarite	5-6
2.28	Pahasapaite	4.5	2.33	Aplowite	3
2.28	Bikitaite	6	2.33	Pentagonite	3-4
2.28	Tetranatrolite ?	5	2.34	Quadridavyne	5
2.28	Humboldtine	1.5-2	2.34	Chukhrovite-(Y)	3
2.28	Scolecite	5-5.5	2.34	Montesommaite	-
2.29	Tacharanite	5	2.34	Wegscheiderite	2.5-3
2.29	Ungemachite	2.5	2.34	Arnhemite *	-
2.29	Sodalite	6	2.34	Bukovskyite	5
2.29	Pinnoite	3.5	2.34	Tatarskite	2.5
2.29	Vitimite !	1.5	2.35	Metavauxite	3
2.29	Ammonioleucite	5.5-6	2.35	Wavellite	3.5-4
2.29	Lemoynite	4	2.35	Gibbsite	2.5-3
2.29	Chalcoalumite	2.5	2.35	Thomsonite-Ca	5-5.5
2.30	Laumontite	3.5-4	2.35	Apophyllite *	4-5
2.30	Nabaphite	2	2.35	Fluorapophyllite	4-5
2.30	Rinneite	3	2.35	Natroapophyllite	4-5
2.30	Analcime	5	2.35	Hydroxyapophyllite	4-5
2.30	Saponite	1.5-2	2.35	Nosean	5.5-6
2.30	Gypsum	2	2.35	Vanalite	-
2.30	Mesolite	5	2.35	Felsobanyaite	1.5
2.30	Gonnardite	4-5	2.35	Giuseppettite	6-7
2.30	Thomasclarkite-(Y) !	2-3	2.35	Sigloite	3
2.30	Vantasselite	2-2.5	2.35	Heulandite-Ba !	3.5
2.30	Nontronite	1.5-2	2.35	Ertixiite	5.8-6.5
2.30	Ardealite	1-1.5	2.35	Pirssonite	3
2.31	Tridymite	6.5-7	2.35	Vlodavetsite !	-
2.31	Volkovskite	2.5	2.35	Truscottite	-
2.31	Kornelite	-	2.35	Montmorillonite	1.5-2
2.31	Mantienneite	3	2.35	Kastningite !	1-2

2.36	Belyankinite	2-3	2.42	Priceite	3-3.5
2.36	Paravauxite	3	2.42	Partheite	4
2.36	Mangangordonite	3	2.42	Intersilite !	3-4
2.36	Nifontovite	3.5	2.43	Petalite	6-6.5
2.36	Zorite	3-4	2.43	Juonniite !	4-4.5
2.36	Mountainite	-	2.43	Sulphohalite	3.5
2.36	Tugtupite	4	2.43	Munirite	1-2
2.36	Rhodesite	3-4	2.43	Bystrite	5
2.36	Foshagite	-	2.43	Tobermorite	2.5
2.36	Mereiterite !	2.5-3	2.44	Sulfoborite	4-4.5
2.36	Paulkerrite	3	2.44	Kolbeckite	5
2.37	Loweite	2.5-3	2.44	Haigerachite !	2
2.37	Pitiglianoite	5	2.44	Ekaterinite	1
2.37	Vishnevite	5-6	2.44	Ferristrunzite	4
2.37	Erythrosiderite	-	2.45	Fairchildite	2.5
2.37	Hambergite	7.5	2.45	Metarossite	1-2
2.38	Coalingite	1-2	2.45	Rossite	2-3
2.38	Ushkovite	3.5	2.45	Manganbelyankinite	2-2.5
2.38	Northupite	3.5-4	2.45	Alvanite	3-3.5
2.38	Novgorodovaite !	2.5	2.45	Cancrinite	6
2.38	Monohydrocalcite	2-3	2.45	Carletonite	4-4.5
2.39	Gravegliaite	-	2.45	Searlesite	1-2
2.39	Huemulite	2.5-3	2.45	Brewsterite-Sr	5
2.40	Brucite	2.5-3	2.45	Stevensite	4
2.40	Lazurite	5.5	2.45	Sauconite	1-2
2.40	Vauxite	3.5	2.45	Hauyne	5-6
2.40	Amstallite	4	2.45	Brewsterite-Ba !	5
2.40	Cancrisilite	5	2.46	Despujolsite	2.5
2.40	Camgasite	2	2.46	Smolianinovite	2
2.40	Tunellite	2.5	2.46	Uklonskovite	-
2.40	Ammonioalunite	2-3	2.46	Minyulite	3.5
2.40	Benyacarite	2.5-3	2.46	Zemkorite	2
2.40	Koninckite	3.5-4	2.46	Girvasite	3.5
2.40	Glaucocerinite	1	2.46	Pseudolaueite	3
2.40	Satpaevite	1.5	2.47	Laueite	3
2.41	Marinellite !	5.5	2.47	Tuperssuatsiaite	-
2.41	Boyleite	2	2.47	Harmotome	4-5
2.41	Liebigite	2.5-3	2.47	Eriochalcite	2.5
2.42	Mitscherlichite	2.5	2.47	Metaborite	5
2.42	Santabarbaraite !	-	2.47	Mooreite	3
2.42	Tosudite	1-2	2.47	Leucite	6
2.42	Nordstrandite	3	2.47	Natrolemoynite !	3
2.42	Colemanite	4.5	2.47	Thomsonite-Sr !	5
2.42	Monteregianite-(Y)	3.5	2.48	Davyne	6
2.42	Tiettaite	3	2.48	Microsommite	6
2.42	Dawsonite	3	2.48	Lithiophosphate	4
2.42	Sacrofanite	5.5-6	2.48	Krohnkite	2.5-3

2.48	Gyrolite	2.5		2.53	Chrysotile !	2.5
2.48	Ankinovichite !	2.5-3		2.53	Godovikovite	2
2.48	Ussingite	6.5		2.53	Calcioferrite	2.5
2.48	Doyleite	2.5-3		2.53	Chalcophyllite	2
2.48	Aerinite	3		2.54	Switzerite	2
2.49	Ferrosaponite !	2		2.54	Nevadaite !	3
2.49	Franzinite	5		2.54	Elpidite	7
2.50	Montgomeryite	4		2.54	Parafransoletite	2.5
2.50	Lovozerite	5		2.54	Vimsite	4
2.50	Charmarite-2H	2.5		2.54	Natrite	3.5
2.50	Charmarite-3T	2		2.54	Falcondoite	2-3
2.50	Ferrostrunzite	4		2.54	Metavariscite	3.5
2.50	Metahewettite	-		2.54	Arsenuranospathite	2
2.50	Changoite !	-		2.54	Tvedalite	4.5
2.50	Hanksite	3		2.54	Natrofairchildite	2.5
2.50	Tychite	3.5		2.55	Gerasimovskite	2
2.50	Bakhchisaraitsevite !	2-2.5		2.55	Lutecite *	6
2.50	Machatschkiite	2-3		2.55	Schrockingerite	2.5
2.50	Eugsterite	1-2		2.55	Georgeite	1-2
2.50	Defernite	3		2.55	Hisingerite	3
2.50	Sphaerobertrandite !	5		2.55	Hewettite	-
2.50	Pimelite	2.5		2.55	Epididymite	5.5
2.50	Kalborsite	6		2.55	Ralstonite	4.5
2.50	Hectorite	1-2		2.55	Swinefordite	1
2.50	Parasibirskite !	3		2.55	Kvanefjeldite	5.5-6
2.50	Zykaite	2		2.55	Antigorite	3.5-4
2.50	Vermiculite	1.5-2		2.55	Steigerite	2.5-3
2.50	Pitticite	2-3		2.55	Parabutlerite	2.5
2.50	Metavoltine	2.5		2.55	Butlerite	2.5
2.51	Fedorite	-		2.55	Senegalite	5.5
2.51	Henmilite	1.5-2		2.55	Eudidymite	6
2.51	Kingsmountite	2.5		2.56	Ferrinatrite	2.5
2.51	Lithosite	5.5		2.56	Tounkite	5-5.5
2.51	Poudretteite	5		2.56	Reyerite	3-4
2.51	Indialite	7-7.5		2.56	Navajoite	1.5
2.51	Variscite	4-5		2.56	Marialite	5.5-6
2.51	Solongoite	3.5		2.56	Liottite	5
2.52	Pokrovskite	3		2.56	Barentsite	3
2.52	Strunzite	4		2.56	Orthoclase	6
2.52	Shomiokite-(Y)	2-3		2.56	Fransoletite	3
2.52	Sanidine	6		2.56	Microcline	6
2.52	Milarite	6		2.56	Charoite	5-6
2.52	Hannebachite	3.5		2.57	Varlamoffite *	6-6.5
2.52	Gaultite	6		2.57	Ashcroftine-(Ce) *	-
2.52	Theresemagnanite	1.5-2		2.57	Hornesite	1
2.52	Carobbiite	2-2.5		2.57	Ansermetite !	3
2.53	Overite	3.5-4		2.57	Leifite	6

2.57	Kieserite	3.5		2.61	Lanthanite-(La)	3
2.57	Burkeite	3.5		2.61	Sazhinite-(Ce)	2.5
2.58	Lechatelierite *	6.5		2.61	Litvinskite !	5
2.58	Howlite	2.5-3.5		2.61	Ashcroftine-(Y)	5
2.58	Picropharmacolite	1-2		2.61	Kittatinnyite	4
2.58	Kaliophilite	5.5-6		2.61	Zakharovite	2
2.58	Karpinskite	2.5-3		2.62	Avogadrite	-
2.58	Clinotobermorite	4.5		2.62	Afwillite	3
2.58	Megakalsilite !	6		2.62	Thornasite	-
2.58	Caresite	2		2.62	Veatchite	2
2.58	Syngenite	2.5		2.62	Borocookeite !	3
2.58	Tobelite	2		2.62	Oyelite	5
2.58	Nahpoite	1-2		2.62	Albite	7
2.58	Nalipoite	4		2.62	Griceite	4.5
2.58	Whiteite-(CaFeMg)	4		2.62	Naujakasite	2-3
2.58	Wilhelmvierlingite	4		2.63	Veatchite-p !	2
2.59	Rabbittite	2.5		2.63	Quartz	7
2.59	Anorthoclase	6		2.63	Gordaite !	2.5
2.59	Tungusite	2		2.63	Osumilite-(Mg)	5-6
2.59	Orthochrysotile	2.5-3		2.63	Fahleite	2
2.59	Paraumbite	4.5		2.63	Carlosturanite	2.5
2.59	Clinochrysotile	2.5-3		2.63	Trikalsilite	6
2.59	Parachrysotile	2.5-3		2.63	Penkvilksite	5
2.59	Parsettensite	1.5		2.63	Whiteite-(CaMnMg)	3.5
2.60	Bertrandite	6-7		2.63	Ransomite	2.5
2.60	Afghanite	5.5-6		2.64	Donbassite	2-2.5
2.60	Nepheline	6		2.64	Osumilite-(Fe)	5-6
2.60	Halloysite	2		2.64	Simplotite	1
2.60	Odinite	2.5		2.64	Perhamite	5
2.60	Zaratite	3-3.5		2.64	Ehrleite	3.5
2.60	Dickite	1.5-2		2.64	Berlinite	6.5
2.60	Nacrite	1		2.64	Riversideite	3
2.60	Wightmanite	5.5		2.64	Chiavennite	3
2.60	Bulachite	2		2.65	Cordierite	7
2.60	Uralborite	4		2.65	Tiptopite	3.5
2.60	Shortite	3		2.65	Jaffeite	-
2.60	Spodiophyllite ?	3-3.5		2.65	Clinochlore	2-2.5
2.60	Roedderite	5-6		2.65	Schaurteite	2.5
2.60	Albrechtschraufite	2-3		2.65	Whiteite-(MnFeMg)	4
2.60	Kaolinite	1.5-2		2.65	Oligoclase	7
2.60	Zirklerite	3.5		2.65	Vivianite	1.5-2
2.60	Mcnearite	-		2.66	Altisite	6
2.60	Kimuraite-(Y)	2.5		2.66	Sudoite	2.5-3.5
2.60	Coeruleolactite	5		2.66	Carbonate-cyanotrichite	2
2.60	Keckite	4.5		2.66	Dozyite	2.5
2.61	Kalsilite	6		2.66	Bigcreekite !	2-3
2.61	Schairerite	3.5		2.66	Glagolevite !	3-4

2.66	Lunokite	3-4	2.70	Edingtonite	4-5
2.66	Berezanskite !	2.5-3	2.70	Augelite	4.5-5
2.66	Zincsilite	1.5-2	2.70	Huntite	1-2
2.66	Zincowoodwardite-3R !	1	2.70	Kankite	2-3
2.66	Chkalovite	6	2.70	Aluminum	1.5
2.66	Arcanite	2	2.70	Franklinphilite	4
2.67	Hieratite	2.5	2.70	Voltaite	3-3.5
2.67	Scapolite *	6	2.70	Aphthitalite	3
2.67	Pharmacolite	2-2.5	2.70	Polylithionite	2-3
2.67	Torreyite	3	2.70	Manganotychite	4
2.67	Montroyalite	3.5	2.70	Narsarsukite	7
2.67	Manganonaujakasite !	3-4	2.70	Xonotlite	6.5
2.67	Eucryptite	6.5	2.70	Bassanite	-
2.67	Rimkorolgite !	3	2.70	Voggite	-
2.67	Andesine *	7	2.70	Kulkeite	2
2.67	Rouvilleite	3	2.70	Yagiite	5-6
2.67	Eifelite	5-6	2.70	Shkatulkalite !	3
2.67	Segelerite	4	2.70	Hillebrandite	5.5
2.67	Cookeite	2.5	2.70	Nafertisite !	2-3
2.68	Glauconite	2	2.70	Bavenite	5.5
2.68	Szaibelyite	3-3.5	2.70	Turquoise	5-6
2.68	Kogarkoite	3.5	2.70	Hydronium-jarosite	4-4.5
2.68	Frankamenite !	5.5	2.71	Armstrongite	4.5
2.68	Englishite	3	2.71	Canasite	-
2.68	Guerinite	1.5	2.71	Callaghanite	3-3.5
2.68	Pyatenkoite-(Y) !	4-5	2.71	Spheniscidite	1-1.5
2.68	Calciohilairite	4	2.71	Creedite	3.5
2.68	Planerite	5	2.71	Calcite	3
2.68	Zodacite	4	2.71	Bytownite *	7
2.68	Metasideronatrite	1.5-2.5	2.71	Strontiodresserite	2-3
2.68	Suolunite	3.5	2.71	Terskite	5
2.69	Plagioclase *	6-6.5	2.71	Karupmollerite-Ca !	5
2.69	Caminite	2.5	2.71	Zincowoodwardite-1T !	1
2.69	Thenardite	2.5	2.71	Jahnsite-(CaMnMg)	4
2.69	Sabieite	2	2.72	Ershovite	2.5-3
2.69	Zincowoodwardite !	1	2.72	Lennilenapeite	3
2.69	Liberite	7	2.72	Hilairite	4.5
2.69	Tisinalite	5	2.72	Franconite	4
2.69	Tinsleyite	5	2.72	Walentaite	3
2.69	Hilgardite	5	2.72	Chaidamuite	2.5-3
2.69	Sazykinaite-(Y)	5	2.73	Veatchite-A	2
2.69	Kaluginite *	3.5	2.73	Manaksite	5
2.69	Lopezite	2.5	2.73	Tsepinite-Ca !	-
2.69	Vanthoffite	3.5	2.73	Telyushenkoite !	6
2.70	Svyatoslavite	6	2.73	Guildite	2.5
2.70	Meionite	5-6	2.73	Bradleyite	3-4
2.70	Labradorite *	7	2.73	Malladrite	3

2.74	Anorthite	6	2.77	Borcarite	4
2.74	Eitelite	3.5	2.77	Fukalite	4
2.74	Kostylevite	5	2.77	Epistolite	1-1.5
2.74	Lisitsynite !	5-6	2.77	Paravinogradovite !	5
2.74	Tsepinite-Na !	5	2.77	Calcium-catapleiite	4.5-5
2.74	Murmanite	2.5-3	2.78	Polyhalite	2.5-3.5
2.74	Sugilite	6-6.5	2.78	Glauberite	2.5-3
2.74	Tarapacaite	-	2.78	Reedmergnerite	6-6.5
2.74	Fenaksite	5-5.5	2.78	Kapustinite !	6
2.75	Alunite	3.5-4	2.78	Ponomarevite	2.5
2.75	Orlymanite	4-5	2.78	Goldquarryite !	3-4
2.75	Catapleiite	6	2.78	Rorisite	2
2.75	Lunijianlaite	2	2.78	Tumchaite !	4.5
2.75	Saliotite	2-3	2.78	Cryolithionite	2.5
2.75	Talc	1	2.78	Paragonite	2.5
2.75	Gearksutite	2	2.78	Jahnsite-(CaMnMn)	4
2.75	Illite *	1-2	2.78	Hendersonite	2.5
2.75	Natroalunite	3.5-4	2.79	Sodium-pharmacosiderite	3
2.75	Silvialite !	5.5			
2.75	Litidionite	5-6	2.79	Stoppaniite !	7.5
2.75	Tancoite	4-4.5	2.79	Ferrotychite	4
2.75	Heidornite	4-5	2.79	Umbite	4.5
2.76	Pyrophosphite *	-	2.79	Zektzerite	6
2.76	Zeophyllite	3	2.80	Villiaumite	2.5
2.76	Zincovoltaite	3	2.80	Takovite	2
2.76	Eggletonite	3-4	2.80	Barium-zinc-alumopharmacosiderite *	2.5
2.76	Lanthanite-(Ce)	2.5			
2.76	Phosphosiderite	3.5-4	2.80	Sherwoodite	2
2.76	Davanite	5	2.80	Neotocite	3-4
2.76	Emeleusite	5-6	2.80	Yukonite	2-3
2.76	Armenite	7.5	2.80	Voglite	-
2.76	Katoite	5-6	2.80	Guarinoite	1.5-2
2.76	Zanazziite	5	2.80	Phlogopite	2-2.5
2.76	Alluaivite	5-6	2.80	Beryllonite	5.5-6
2.76	Seidite-(Ce) !	3-4	2.80	Olympite	4
2.76	Tokkoite	4-5	2.80	Bakerite	4.5
2.76	Denisovite	4-5	2.80	Lemmleinite-K !	5
2.76	Manganosegelerite	3-4	2.80	Hydrodresserite	3-4
2.77	Rusakovite	1.5-2	2.80	Minamiite	3-4
2.77	Beryl	7.5-8	2.80	Bazzite	6.5
2.77	Shafranovskite	2-3	2.80	Ferripyrophyllite	1.5-2
2.77	Namuwite	2	2.81	Sakhaite	5
2.77	Amesite	2.5-3	2.81	Anapaite	3-4
2.77	Sekaninaite	7.5	2.81	Strontioborite	-
2.77	Scawtite	4-5	2.81	Bandylite	2.5
2.77	Lintisite	5-6	2.81	Hyalophane	6-6.5
2.77	Fabianite	6	2.81	Zharchikhite	4.5

2.81	Lanthanite-(Nd)	2.5-3	2.85	Tamaite !	4
2.81	Boromuscovite	2.5-3	2.85	Nacaphite	3
2.81	Rittmannite	3.5	2.85	Mineevite-(Y)	4
2.82	Wycheproofite	4-5	2.85	Aheylite	5-6
2.82	Corvusite	2.5-3	2.85	Nepouite	2-2.5
2.82	Vonbezingite	4	2.86	Brammallite *	2.5-3
2.82	Tinaksite	6	2.86	Jahnsite-(CaMnFe)	4
2.82	Gjerdingenite-Fe !	5	2.86	Carlhintzeite	-
2.82	Ikranite !	5	2.86	Sheldrickite !	3
2.82	Kuzmenkoite-Mn !	5	2.86	Manganokukisvumite !	5.5-6
2.83	Kuzmenkoite-Zn !	-	2.86	Sitinakite	4.5
2.83	Karlite !	5.5	2.86	Pectolite	5
2.83	Muscovite	2-2.5	2.86	Furongite	2-3
2.83	Andersonite	2.5	2.86	Nenadkevichite !	5
2.83	Kamaishilite	-	2.87	Clinophosinaite !	4
2.83	Tuscanite	5.5-6	2.87	Stilpnomelane	3
2.83	Langbeinite	3.5-4	2.87	Whitmoreite	3
2.83	Laplandite-(Ce)	2-3	2.87	Feklichevite !	5.5
2.83	Gutkovaite-Mn !	5	2.87	Caryopilite	3-3.5
2.83	Yoshiokaite	-	2.87	Cianciulliite	2
2.83	Bottinoite	3.5	2.87	Merrihueite	5-6
2.84	Bannisterite	4	2.87	Chiolite	3.5-4
2.84	Bermanite	3.5	2.87	Strengite	3.5
2.84	Reevesite	2	2.87	Tinticite	2.5
2.84	Khaidarkanite !	2.5	2.88	Prehnite	6-6.5
2.84	Ronneburgite !	3	2.88	Hurlbutite	6
2.84	Zircosulfate	2.5-3	2.88	Vinogradovite	4
2.84	Dalyite	7.5	2.88	Tsepinite-K !	5
2.84	Wardite	5	2.88	Ferrisymplesite	2.5
2.84	Krausite	2.5	2.88	Chromphyllite !	3
2.84	Reinhardbraunsite	5-6	2.88	Paratsepinite-Ba !	5
2.84	Kazakovite	4	2.88	Neskevaaraite-Fe !	5
2.84	Ganophyllite	4-4.5	2.88	Organovaite-Mn !	5
2.84	Jungite	1	2.88	Zunyite	7
2.85	Cyanotrichite	2	2.88	Grossite	-
2.85	Lepidolite	2.5-3	2.88	Labuntsovite-Mg !	5
2.85	Cuspidine	5-6	2.88	Organovaite-Zn !	5
2.85	Chantalite	-	2.88	Petarasite	5-5.5
2.85	Crandallite	4	2.88	Yavapaiite	2.5-3
2.85	Pyrophyllite	1.5-2	2.89	Miserite	5.5-6
2.85	Dolomite	3.5-4	2.89	Prosopite	4-5
2.85	Wollastonite-1A	5	2.89	Xanthoxenite	2.5
2.85	Wollastonite-2M *	5	2.89	Agrellite	5.5
2.85	Wollastonite-3A-4A-5A-7A *	5	2.89	Manandonite	2.5-3.5
2.85	Cacoxenite	3-3.5	2.89	Fluoborite	3.5
2.85	Wallkilldellite	3	2.90	Hochelagaite	4
2.85	Eveslogite !	5	2.90	Sogdianite	7

2.90	Phosphofibrite	4		2.94	Gainesite	4
2.90	Beraunite	2		2.94	Spodiosite ?	5
2.90	Earlshannonite	3-4		2.94	Labuntsovite-Fe !	5
2.90	Chromceladonite !	1-2		2.94	Grantsite	1-2
2.90	Pharmacosiderite	2.5		2.94	Ktenasite	2-2.5
2.90	Datolite	5.5		2.94	Selwynite	4
2.90	Tainiolite	2.5-3		2.94	Hydroxylherderite	5-5.5
2.90	Zirsinalite	5		2.94	Holtedahlite	4.5-5
2.90	Sorensenite	5.5		2.94	Dellaite	-
2.90	Kukisvumite	5.5-6		2.94	Aminoffite	5.5
2.90	Pollucite	6.5		2.94	Chudobaite	2.5-3
2.90	Boracite	7		2.94	Masutomilite	2.5
2.90	Sidorenkite	2		2.94	Maricopaite	1-1.5
2.90	Eudialyte	5-5.5		2.94	Akermanite	5-6
2.90	Alsakharovite-Zn !	5		2.95	Leucophosphite	3.5
2.90	Malinkoite !	5		2.95	Gorgeyite	3.5
2.90	Carpholite	5.5		2.95	Panethite	-
2.90	Braitschite-(Ce)	-		2.95	Liroconite	2-2.5
2.91	Rosenhahnite	4.5-5		2.95	Mapimite	3
2.91	Poldervaartite	5		2.95	Metaswitzerite	2.5
2.91	Moskvinite-(Y) !	5		2.95	Steacyite	5
2.91	Katayamalite	3.5-4		2.95	Collinsite	3-3.5
2.91	Suanite	5.5		2.95	Haidingerite	2-2.5
2.91	Reederite-(Y) !	3-3.5		2.95	Leightonite	3
2.92	Isoclasite	1.5		2.95	Raslakite !	5
2.92	Sodium-betpakdalite	-		2.95	Stronalsite	6.5
2.92	Rauvite	-		2.95	Sterlinghillite	3
2.92	Darapiosite	5		2.95	Vuoriyarvite-K !	4.5
2.92	Gatumbaite	4-5		2.95	Melilite	5-5.5
2.92	Baratovite	3.5		2.95	Ternovite !	3
2.92	Lokkaite-(Y)	-		2.95	Amakinite	3.5-4
2.92	Faustite	5.5		2.96	Labuntsovite-Mn !	6
2.92	Karnasurtite-(Ce)	2		2.96	Harkerite	-
2.93	Monetite	3.5		2.96	Ternesite !	4.5
2.93	Greifensteinite !	4.5		2.96	Dusmatovite	4.5
2.93	Mandarinoite	2.5		2.96	Winchite	5.5
2.93	Ferro-aluminoceladonite !	2-2.5		2.96	Lepkhenelmite-Zn !	5
2.93	Bostwickite	1		2.96	Cebollite	5
2.93	Eakerite	5.5		2.96	Odintsovite	5-5.5
2.93	Minehillite	4		2.96	Weberite	3.5
2.93	Aragonite	3.5-4		2.96	Leucophanite	4
2.93	Coesite	7.5		2.96	Dresserite	2.5-3
2.93	Latiumite	5.5-6		2.96	Preiswerkite	2.5
2.93	Imandrite	5-5.5		2.96	Ajoite	-
2.94	Roweite	5		2.96	Meurigite !	3
2.94	Sarcolite	6		2.96	Morinite	4-4.5
2.94	Aluminobarroisite !	5-6		2.97	Anhydrite	3.5

2.97	Sincosite	1-2	3.00	Coombsite !	-
2.97	Vlasovite	6	3.00	Akaganeite	-
2.97	Phosinaite-(Ce) !	3.5	3.00	Xiangjiangite	1-2
2.97	Althausite	3.5	3.01	Gonyerite	2.5
2.97	Pezzottaite !	8	3.01	Chladniite	4
2.97	Roscoelite	2.5	3.01	Nefedovite	4.5
2.97	Melkovite	3	3.01	Minnesotaite	1.5-2
2.98	Cryolite	2.5-3	3.01	Cascandite	4.5-5.5
2.98	Grandidierite	7.5	3.01	Olenite !	7
2.98	Thomsenolite	2	3.01	Woodhouseite	4.5
2.98	Brazilianite	5.5	3.02	Betpakdalite	3
2.98	Brannockite	5-6	3.02	Ogdensburgite	2
2.98	Pachnolite	3	3.02	Heneuite	5
2.98	Rankinite	5.5	3.02	Bromellite	9
2.98	Symplesite	2.5	3.02	Meliphanite	5-5.5
2.98	Mcgillite	5	3.02	Hydroxylellestadite	4.5
2.98	Bementite	6	3.02	Sieleckiite	3
2.98	Ephesite	3.5-4.5	3.02	Thorosteenstrupine	4
2.99	Gehlenite	5-6	3.02	Hubeite !	5.5
2.99	Phenakite	7.5-8	3.02	Arthurite	3-4
2.99	Hsianghualite	6.5	3.02	Liddicoatite !	7.5
2.99	Jeffreyite	5	3.02	Clinojimthompsonite	2-2.5
2.99	Kurgantaite !	6-6.5	3.02	Kurchatovite	4.5
3.00	Elpasolite	2.5	3.02	Manganolangbeinite	2.5-3
3.00	Danburite	7	3.02	Ammoniojarosite	3.5-4.5
3.00	Orientite	4-5	3.03	Montebrasite	5.5-6
3.00	Wallkilldellite-(Fe) !	2-3	3.03	Szmikite	1.5
3.00	Greenalite	2.5	3.03	Edenite	6
3.00	Siderophyllite	2.5	3.03	Sobolevite	4.5-5
3.00	Monsmedite ?	2	3.03	Jimthompsonite	2-2.5
3.00	Orthoserpierite	-	3.03	Gugiaite	3-4
3.00	Phosphoellenbergerite !	6.5	3.03	Caysichite-(Y)	4.5
3.00	Zinnwaldite	3.5-4	3.03	Neighborite	4.5
3.00	Brianite	4-5	3.03	Jasmundite	5
3.00	Hopeite	3	3.03	Lemmleinite-Ba !	-
3.00	Wawayandaite	1	3.03	Berthierine	2.5
3.00	Magnesite	4	3.03	Balangeroite	-
3.00	Spurrite	5	3.03	Mansfieldite	3.5-4
3.00	Clinoholmquistite ?	5-6	3.04	Bokite	3
3.00	Schlossmacherite	3-4	3.04	Margarite	4
3.00	Parakuzmenkoite-Fe !	5	3.04	Boehmite	3
3.00	Rossmanite !	7	3.04	Georgeericksenite !	3-4
3.00	Herderite	5	3.04	Sainfeldite	4
3.00	Bityite	5.5	3.04	Kotoite	6.5
3.00	Koashvite	6	3.04	Actinolite	5.5
3.00	Campigliaite	-	3.04	Natromontebrasite	5.5
3.00	Celadonite	2	3.04	Werdingite	7

3.04	Ferrocarpholite	5.5		3.07	Kellyite	2.5
3.04	Kidwellite	3		3.08	Glaucophane	6-6.5
3.04	Euclase	7.5		3.08	Cuprorivaite	5
3.05	Leucosphenite	6-6.5		3.08	Messelite	3.5
3.05	Amblygonite	5.5-6		3.08	Hydroxylapatite	5
3.05	Comblainite	2		3.08	Trabzonite	-
3.05	Fluorocannilloite !	6		3.08	Ekanite	4.5
3.05	Ferro-edenite	5-6		3.08	Eosphorite	5
3.05	Tetra-ferri-annite	2.5-3		3.08	Potassic-carpholite !	5
3.05	Clintonite	4-5		3.08	Cyrilovite	4
3.05	Annabergite	2		3.09	Kentbrooksite !	5-6
3.05	Ferroceladonite !	2-2.5		3.09	Eckermannite	5-6
3.05	Lazulite	5-6		3.09	Souzalite	5.5-6
3.05	Elbaite !	7.5		3.09	Dravite !	7-7.5
3.05	Szomolnokite	2.5		3.09	Richterite	6
3.05	Ankerite	3.5-4		3.09	Trolleite	5.5-6
3.05	Tremolite	5-6		3.09	Irhtemite	-
3.05	Wulfingite	3		3.09	Trembathite	6-8
3.05	Mullite	6-7		3.09	Lawsonite	7.5
3.05	Simmonsite !	2.5-3		3.09	Fluoro-magnesio-arfvedsonite	5.5
3.05	Yuksporite	4.5-5		3.09	Ferrobustamite	6
3.05	Geigerite	3		3.09	Yaroslavite	4.5
3.05	Fluorellestadite	4.5		3.10	Holmquistite	5.5
3.06	Znucalite	-		3.10	Biotite *	2.5-3
3.06	Bonshtedtite	4		3.10	Jarosite	2.5-3.5
3.06	Christelite !	2-3		3.10	Natrojarosite	2.5-3.5
3.06	Ferrokentbrooksite !	5-6		3.10	Cyanophyllite	2
3.06	Sellaite	5-6		3.10	Blakeite *	2-3
3.06	Wadalite	-		3.10	Cassidyite	3.5
3.06	Mikasaite	2		3.10	Rancieite	2.5-3
3.06	Boralsilite !	-		3.10	Spangolite	2.5-3
3.06	Pennantite	2-3		3.10	Camerolaite	-
3.06	Hauckite	2-3		3.10	Alumoklyuchevskite	2
3.06	Inesite	6		3.10	Delrioite	2
3.07	Nagelschmidtite	-		3.10	Chalcosiderite	4.5
3.07	Crawfordite	3		3.10	Phosphophyllite	3-3.5
3.07	Banalsite	6		3.10	Bertossaite	6
3.07	Nasledovite	2		3.10	Reddingite	3.5
3.07	Polyphite-VIII	5		3.10	Takedaite	4.5
3.07	Polyphite-VII	5		3.10	Fairfieldite	3.5
3.07	Rodolicoite !	-		3.11	Wagnerite	5-5.5
3.07	Friedelite	4-5		3.11	Haiweeite	3.5
3.07	Parasymplesite	2		3.11	Erlianite	3.5
3.07	Manganocummingtonite	6-6.5		3.11	Gladiusite !	4-4.5
3.07	Chlorellestadite	4.5		3.11	Leakeite	6
3.07	Parvowinchite	5-6		3.11	Scholzite	4
3.07	Serpierite	3.5-4		3.11	Saryarkite-(Y)	3.5-4

3.11	Nanpingite	2.5-3	3.15	Barnesite	-
3.11	Kutnohorite	3.5-4	3.15	Tuliokite	3-4
3.12	Devilline	2.5	3.15	Merwinite	6
3.12	Wadeite	5.5-6	3.15	Zirsilite-(Ce) !	5
3.12	Quadruphite-VII	5	3.15	Natisite	3-4
3.12	Quadruphite-VIII	5	3.15	Ludlamite	3.5
3.12	Mcguinnessite	2.5	3.15	Andalusite	6.5-7
3.12	Erythrite	1.5-2	3.15	Davreuxite	2-3
3.12	Nyboite	6	3.15	Hydroastrophyllite	3-4
3.12	Carbonate-fluorapatite	5	3.15	Tyrolite	1.5-2
3.12	Mccrillisite	4.5	3.15	Schorl !	7.5
3.12	Parascholzite	4	3.15	Uvite !	7.5
3.12	Arctite	5	3.15	Chondrodite	6-6.5
3.12	Sussexite	3	3.15	Fluorapatite	5
3.12	Spencerite	3	3.15	Humite	6-6.5
3.12	Tengerite-(Y)	-	3.15	Norbergite	6-6.5
3.12	Sidwillite	2.5	3.15	Chlorapatite	5
3.12	Paranatisite	5	3.15	Spodumene	6.5-7
3.13	Ferropyrosmalite	4.5	3.15	Autunite	2-2.5
3.13	Pargasite	6	3.15	Viitaniemiite	5
3.13	Orthochamosite !	2	3.16	Garyansellite	4
3.13	Manganpyrosmalite	4.5	3.16	Crossite ?	6
3.13	Widgiemoolthalite	3.5	3.16	Cahnite	3
3.13	Gormanite	4-5	3.16	Harstigite	5.5
3.13	Magnesiocummingtonite	5-6	3.16	Hillite !	3.5
3.13	Whitlockite	5	3.16	Kinoite	5
3.13	Hibschite	6.5	3.17	Gotzenite	5.5-6
3.13	Manganokhomyakovite !	5-6	3.17	Magnesio-arfvedsonite	5-6
3.13	Hydroxylclinohumite !	6.5	3.17	Robertsite	3.5
3.13	Fluorite	4	3.17	Brindleyite	2.5-3
3.13	Seamanite	4	3.17	Serrabrancaite !	3.5
3.13	Moydite-(Y)	1-2	3.17	Foitite !	7
3.13	Vuonnemite	2-3	3.17	Lourenswalsite	-
3.13	Shabaite-(Nd)	2.5	3.18	Muskoxite	3
3.14	Lomonosovite	3-4	3.18	Nierite	9
3.14	Ferroglaucophane	6	3.18	Cualstibite	2
3.14	Mahnertite !	2-3	3.18	Kambaldaite	3
3.14	Semenovite	3.5-4	3.18	Baileychlore	2.5-3
3.14	Vladimirite	3.5	3.18	Hureaulite	5
3.14	Krauskopfite	4	3.19	Ellenbergerite	6.5
3.14	Carbokentbrooksite !	5	3.19	Ferri-clinoholmquistite !	6
3.14	Chernykhite	3-4	3.19	Magnesioriebeckite	5
3.15	Zussmanite	-	3.19	Holdawayite	3
3.15	Hainite	5	3.19	Kamphaugite-(Y)	2-3
3.15	Mongolite	2	3.19	Nchwaningite	5.5
3.15	Stanfieldite	4-5	3.19	Apatite *	5
3.15	Sodic-ferripedrizite !	6	3.19	Kosnarite	4.5

3.20	Gunningite	2.5
3.20	Vayrynenite	5
3.20	Shirozulite !	3
3.20	Straczekite	1-2
3.20	Yvonite !	3.5-4
3.20	Enstatite	5.5
3.20	Chamosite	3
3.20	Torbernite	2-2.5
3.20	Serandite	4.5-5.5
3.20	Oneillite !	5-6
3.20	Monticellite	5
3.20	Kalistrontite	2
3.20	Stokesite	6
3.20	Villyaellenite	4
3.20	Simonkolleite	1.5
3.20	Pumpellyite-(Fe++)	5.5
3.20	Pumpellyite-(Fe+++)	5.5
3.20	Pumpellyite-(Mn++)	5.5
3.20	Pumpellyite-(Mg)	5.5
3.20	Wesselsite !	4-5
3.20	Sampleite	4
3.20	Scorodite	3.5-4
3.20	Sabugalite	2.5
3.21	Fedotovite	2.5
3.21	Karasugite	-
3.21	Feruvite !	7
3.21	Anthophyllite	5-6
3.21	Abenakiite-(Ce)	4
3.21	Mopungite	3
3.21	Nimite	3
3.21	Parascorodite !	1-2
3.22	Kupletskite	4
3.22	Fianelite !	3
3.22	Childrenite	4.5-5
3.22	Goyazite	4-5
3.22	Clinotyrolite	-
3.22	Pararobertsite	2
3.22	Palermoite	5.5
3.22	Svanbergite	5
3.22	Jervisite	6-7
3.22	Ericaite	7-7.5
3.22	Magnesiodumortierite	7.5
3.22	Weloganite	3.5
3.22	Cobaltarthurite !	3.5-4
3.23	Tritomite-(Y)	3.5-6.5
3.23	Magnesiohastingsite	5-6
3.23	Vuagnatite	6

3.23	Metakirchheimerite	2-2.5
3.23	Mangan-neptunite	5-6
3.23	Neptunite	5-6
3.23	Natrodufrenite	3.5-4.5
3.23	Chesterite	2-2.5
3.24	Ferrohornblende	5-6
3.24	Magnesiohornblende	5-6
3.24	Scandiobabingtonite !	6
3.24	Shuiskite	6
3.24	Kaersutite	5-6
3.24	Mitridatite	3.5
3.24	Sillimanite	7
3.24	Esperanzaite !	4.5
3.24	Taseqite !	-
3.25	Tschermakite	5-6
3.25	Richelsdorfite	2
3.25	Papagoite	5-5.5
3.25	Potassicpargasite !	6-6.5
3.25	Arsenocrandallite	5.5
3.25	Manganogrunerite	5-6
3.25	Celsian	6-6.5
3.25	Jonesite	3-4
3.25	Nitrobarite	3
3.25	Thadeuite	3.5-4
3.25	Uranosilite	-
3.25	Zellerite	2
3.26	Lithiophorite	2.5-3
3.26	Sursassite	-
3.26	Povondraite !	7
3.26	Clinohumite	6
3.26	Pyrochroite	2.5-3
3.26	Tikhonenkovite	3.5
3.26	Helvite	6-6.5
3.27	Churchite-(Y)	3
3.27	Hiortdahlite	5.5
3.27	Deliensite !	2
3.27	Wroewolfeite	2.5
3.27	Potassic-magnesiosadanagaite	6
3.27	Scorzalite	5.5-6
3.27	Isokite	5
3.27	Forsterite	6-7
3.27	Panasqueiraite	5
3.27	Loseyite	3
3.27	Iraqite-(La)	4.5
3.27	Saleeite	2.5
3.28	Slawsonite	5.5-6.5

3.28	Jacquesdietrichite !	2	3.31	Fuenzalidaite	2.5-3
3.28	Schulenbergite	2	3.31	Chalcomenite	2-2.5
3.28	Schubnelite	-	3.32	Dioptase	5
3.28	Clinochalcomenite	2	3.32	Paracelsian	6
3.28	Burtite	3	3.32	Lithiomarsturite	6
3.28	Samfowlerite	2.5-3	3.32	Bernalite	4
3.28	Cafetite	4-5	3.32	Vanadiumdravite !	7.5
3.28	Larnite	6	3.32	Kornerupine	7
3.28	Shcherbinaite	3-3.5	3.32	Kochite !	5
3.28	Ferroaxinite	6.5-7	3.32	Magnesiumastrophyllite	3
3.28	Manganaxinite	6.5-7	3.32	Niocalite	6
3.28	Magnesio-axinite	6.5-7	3.32	Perloffite	5
3.29	Tavorite	5	3.32	Olivine *	6.5-7
3.29	Tienshanite	6-6.5	3.32	Gorceixite	6
3.29	Tinzenite	6.5-7	3.33	Niobokupletskite !	3-4
3.29	Potassic-chloropargasite !	5.5	3.33	Kottigite	2.5-3
3.29	Mosandrite	4	3.33	Gillespite	4
3.29	Phosphoferrite	3-3.5	3.33	Laubmannite ?	3.5-4
3.29	Lacroixite	4.5	3.33	Clinohedrite	5.5
3.30	Jeremejevite	7	3.33	Burpalite	5-6
3.30	Acuminite	3.5	3.34	Olmsteadite	4
3.30	Magnesium-zippeite	5-5.5	3.34	Alarsite !	3
3.30	Sadanagaite	6	3.34	Henritermierite	-
3.30	Kozulite	5	3.34	Zircophyllite	4-4.5
3.30	Dufrenite	3.5-4	3.34	Shcherbakovite	6.5
3.30	Zeunerite	2.5	3.34	Londonite !	8
3.30	Kolfanite	2.5	3.34	Dickinsonite	3.5-4
3.30	Donnayite-(Y)	3	3.34	Balipholite	5-5.5
3.30	Dilithium *	5	3.34	Dwornikite	2-3
3.30	Ashoverite	-	3.34	Arsenogoyazite	4
3.30	Parahopeite	3.5	3.34	Lithiophilite	4-5
3.30	Kristiansenite !	5.5-6	3.34	Omphacite	5-6
3.30	Diaoyudaoite	7.6	3.34	Prismatine !	6.5-7
3.30	Zoisite	6.5	3.35	Cronstedtite	3.5
3.30	Rosenbuschite	5-6	3.35	Astrophyllite	3-3.5
3.30	Jadeite	6.5	3.35	Dumortierite	8.5
3.30	Paraotwayite	4	3.35	Khibinskite	4.5-5.5
3.30	Poitevinite	3-3.5	3.35	Clinozoisite	7
3.30	Delindeite	-	3.35	Katophorite	5
3.30	Na-komarovite ?	4	3.35	Claraite	2
3.30	Keldyshite	3.5-4.5	3.35	Johnsomervilleite	4.5
3.30	Okayamalite !	5.5	3.35	Talmessite	5
3.30	Kinoshitalite	2.5-3	3.35	Pekovite !	7
3.30	Taneyamalite	5-6	3.35	Pushcharovskite !	-
3.31	Komkovite	3-4	3.35	Metahaiweeite	3.5
3.31	Kryzhanovskite	3.5-4	3.35	Cummingtonite	5-6
3.31	Santaclaraite	6.5	3.35	Lindackerite	2-2.5

3.35	Paramendozavilite	1	3.40	Diaspore	6.5-7
3.35	Samuelsonite	5	3.40	Diopside	6
3.36	Donpeacorite	5-6	3.40	Johnwalkite	4
3.36	Warwickite	3-4	3.40	Lorenzenite	6
3.36	Wiluite !	6	3.40	Clinoenstatite	5-6
3.36	Sabinaite	-	3.40	Augite	5-6.5
3.36	Turkestanite !	5.5-6	3.40	Vesuvianite	6.5
3.36	Niedermayrite !	-	3.41	Heterosite	4-4.5
3.36	Gedrite	5.5-6	3.41	Ferrisicklerite	4
3.37	Magnesium-chlorophoenicite	3-3.5	3.41	Ferrotschermakite !	5-6
3.37	Schallerite	4.5-5	3.41	Otwayite	4
3.37	Fluoro-ferroleakeite	6	3.41	Giniite	3-4
3.37	Ahlfeldite	2-2.5	3.41	Cymrite	2-3
3.37	Johachidolite	7.5	3.41	Magbasite	5
3.37	Uzonite	1.5	3.41	Gageite	-
3.38	Bustamite	5.5-6.5	3.41	Petersite-(Y)	3-4
3.38	Howieite	-	3.41	Gerenite-(Y) !	5
3.38	Santafeite	-	3.41	Eylettersite	3-4
3.38	Homilite	5	3.41	Natrophilite	4.5-5
3.38	Hastingsite	6	3.41	Lonsdaleite	7-8
3.38	Potassic-chlorohastingsite !	6	3.41	Leisingite !	3-4
3.38	Rouaite !	-	3.41	Metazellerite	2
3.38	Pigeonite	6	3.42	Gerhardtite	2
3.38	Krinovite	6-7	3.42	Niobophyllite	3-4
3.39	Ramsbeckite	3.5	3.42	Buttgenbachite	3
3.39	Cobaltomenite	2-2.5	3.42	Euchroite	3.5-4
3.39	Yoderite	6	3.42	Carlosruizite	2.5-3
3.39	Parakeldyshite	5.5-6	3.42	Kassite	5
3.39	Ojuelaite	3	3.42	Wohlerite	5.5-6
3.40	Rockbridgeite	4.5	3.43	Gaudefroyite	6
3.40	Kanonaite	6.5	3.43	Sicklerite	4
3.40	Griphite	5.5	3.43	Alacranite	1.5
3.40	Veszelyite	3.5-4	3.43	Moolooite	-
3.40	Posnjakite	2.5-3	3.43	Macfallite	5-5.5
3.40	Babingtonite	5.5-6	3.43	Remondite-(Ce)	3-3.5
3.40	Riebeckite	4	3.43	Roeblingite	3
3.40	Chromdravite !	7-7.5	3.43	Fillowite	4.5
3.40	Johannite	2	3.43	Danalite	5.5-6
3.40	Connellite	3	3.43	Batisite	5.9
3.40	Purpurite	4-5	3.43	Kirschsteinite	5.5
3.40	Piemontite	6-7	3.44	Potassicferrisadanagaite !	5.5-6
3.40	Serendibite	6-7	3.44	Rhodizite	8.5
3.40	Bredigite	-	3.44	Lamprophyllite	2.5
3.40	Bergslagite	5	3.44	Fersmanite	5.5
3.40	Glaucochroite	6	3.44	Kalipyrochlore	4-4.5
3.40	Hardystonite	3-4	3.44	Ferropargasite	5-6
3.40	Sassolite	1	3.44	Abernathyite	2-3

3.45	Arfvedsonite	5.5-6		3.50	Aegirine-augite *	6
3.45	Hydrougrandite ?	-		3.50	Meta-autunite	1
3.45	Manganbabingtonite	5.5-6		3.50	Tangeite	3.5
3.45	Grunerite	5-6		3.50	Kazakhstanite	2.5
3.45	Sapphirine	7.5		3.50	Langite	2.5-3
3.45	Hemimorphite	5		3.50	Thortveitite	6.5
3.45	Minrecordite	3.5-4		3.50	Taramite	5-6
3.45	Nacareniobsite-(Ce)	5		3.50	Volborthite	3
3.45	Calcioburbankite	3-4		3.50	Vajdakite !	-
3.45	Peprossiite-(Ce)	2		3.50	Yttrocerite *	4-5
3.45	Epidote	7		3.50	Kainosite-(Y)	5-6
3.45	Uranospinite	2-3		3.50	Junitoite	4.5
3.45	Lazarenkoite	1		3.50	Burbankite	3.5
3.46	Nordite-(La)	5-6		3.50	Ferronordite-(Ce) !	5-5.5
3.46	Ferrorichterite	5-6		3.50	Hydrozincite	2-2.5
3.46	Nelenite	5		3.50	Remondite-(La) !	3
3.46	Fluorvesuvianite !	6		3.50	Protomangano-ferro-anthophyllite !	5-6
3.46	Marsturite	6		3.50	Triphylite	4-5
3.46	Uranocircite	2-2.5		3.50	Goudeyite	3-4
3.47	Ferritaramite	5-6		3.50	Phuralumite	3
3.47	Bechererite !	2.5-3		3.50	Rinkite !	5
3.47	Saneroite	6-7		3.51	Tombarthite-(Y)	5-6
3.47	Seidozerite	4-5		3.51	Natronambulite	5.5-6
3.47	Trimerite	6-7		3.51	Sclarite	3-4
3.48	Frondelite	4.5		3.51	Pellyite	6
3.48	Springcreekite !	4-5		3.51	Metanovacekite	2.5
3.48	Bederite !	5		3.51	Nambulite	6.5
3.48	Dundasite	2		3.52	Diamond	10
3.48	Baghdadite	6		3.52	Fermorite	5
3.48	Wiserite	2.5		3.52	Ottrelite	6-7
3.48	Weilite	-		3.52	Aegirine	6-6.5
3.48	Titanite	5-5.5		3.52	Verplanckite	2.5-3
3.48	Akatoreite	6		3.52	Wendwilsonite	3-4
3.48	Kamchatkite	3.5		3.52	Florencite-(La)	5-6
3.48	Johninnesite	5-6		3.52	Ungarettiite	6
3.48	Metakahlerite	2.5		3.52	Pararealgar	1-1.5
3.48	Schoenfliesite	4-4.5		3.53	Florencite-(Nd)	5-6
3.49	Bornemanite	3.5-4		3.53	Mckelveyite-(Nd) *	3-3.5
3.49	Sinhalite	6.5-7		3.53	Mckelveyite-(Y)	3.5-4
3.49	Grenmarite !	4.5		3.53	Orpiment	1.5-2
3.49	Hematolite	3.5		3.53	Carbocernaite	3
3.49	Chambersite	7		3.53	Lavenite	6
3.49	Zalesiite !	2-3		3.54	Lavendulan	2.5
3.49	Natrochalcite	4.5		3.54	Bobfergusonite	4
3.49	Normandite !	5-6		3.54	Fraipontite	2.5
3.50	Gottlobite !	4.5		3.54	Esseneite	6
3.50	Manganonordite-(Ce) !	5-5.5		3.54	Ferronordite-(La) !	5

3.54	Koritnigite	2		3.60	Fluorcaphite !	5
3.54	Sigismundite !	-		3.60	Rosemaryite	4-4.5
3.54	Sklodowskite	2-3		3.60	Wyllieite	4-4.5
3.54	Meta-ankoleite	2-2.5		3.60	Stottite	4.5
3.55	Effenbergerite	4-5		3.61	Magnesiotaaffeite-2N2S	8-8.5
3.55	Chloritoid	6.5		3.61	Mottanaite-(Ce) !	-
3.55	Chlorophoenicite	3-3.5		3.61	Protoferro-anthophyllite !	-
3.55	Lulzacite !	5.5-6		3.61	Heinrichite	2.5
3.55	Trogerite	2-3		3.61	Juanitaite !	1
3.55	Natalyite	7		3.61	Jinshajiangite	4.5-5
3.55	Lehnerite	2-3		3.62	Kyanite	4-7
3.55	Topaz	8		3.62	Dietzeite	3.5
3.55	Parabrandtite	3-4		3.62	Strontio-orthojoaquinite	5.5
3.55	Hedenbergite	5-6		3.62	Gerstleyite	2.5
3.55	Magnesiochloritoid	6.5		3.62	Genthelvite	6-6.5
3.55	Hypersthene ?	5.5-6		3.62	Bamfordite !	2-3
3.56	Pseudosinhalite !	-		3.62	Vanuralite	2
3.56	Nullaginite	1.5-2		3.63	Benstonite	3-4
3.56	Arrojadite	5		3.63	Azoproite	5.5
3.56	Johannsenite	6		3.63	Palenzonaite	5-5.5
3.57	Ferrogedrite	5.5-6		3.63	Bussenite !	4
3.57	Grossular	6.5-7.5		3.63	Kemmlitzite	5.5
3.58	Gageite-2M	-		3.63	Bassetite	2.5
3.58	Congolite	6.5-7.5		3.64	Plumbojarosite	1.5-2
3.58	Nabalamprophyllite !	3		3.64	Decrespignyite-(Y) !	4
3.58	Horvathite-(Y) !	4		3.64	Barytolamprophyllite	2-3
3.58	Varulite	5		3.64	Chapmanite	2.5
3.58	Florencite-(Ce)	5-6		3.64	Manganarsite	3
3.58	Sodium meta-autunite !	2-2.5		3.64	Mozartite	6
3.58	Sodium-autunite	2-2.5		3.64	Strontiowhitlockite	5
3.59	Janggunite	2-3		3.64	Metazeunerite	2-2.5
3.59	Dimorphite	1.5		3.65	Spinel	8
3.60	Uvarovite	6.5-7		3.65	Vochtenite	3
3.60	Barbosalite	5.5-6		3.65	Melonjosephite	5
3.60	Umbozerite	5		3.65	Chalcocyanite	3.5
3.60	Janhaugite	5		3.65	Johnbaumite	4.5
3.60	Ferrowyllieite	4		3.65	Svabite	4-5
3.60	Kosmochlor	6-7		3.65	Tetrawickmanite	3.5-4.5
3.60	Vanadomalayaite	6		3.65	Arsenogorceixite !	4
3.60	Namansilite	6-7		3.65	Benauite !	3.5
3.60	Benitoite	6-6.5		3.65	Beusite	5
3.60	Turneaureite	5		3.65	Barytocalcite	4
3.60	Paralstonite	4-4.5		3.65	Vitusite-(Ce)	4.5
3.60	Rhodonite	6		3.66	Todorokite	1.5
3.60	Sverigeite	6.5		3.66	Franklinfurnaceite	3
3.60	Boltwoodite	3.5-4		3.66	Kanoite	6-7
3.60	Ilimaussite-(Ce)	4		3.66	Jarosewichite	4

3.66	Maricite	4-4.5	3.71	Geminite	3-3.5
3.66	Zippeite	2	3.71	Perraultite	4
3.66	Argentojarosite	3.5-4.5	3.71	Traskite	5
3.67	Stringhamite	-	3.71	Staurolite	7-7.5
3.67	Triplite	5	3.71	Gaspeite	4-5
3.67	Brandtite	3.5	3.71	Roselite-beta	3.5-4
3.67	Walstromite	3.5	3.71	Pretulite !	5
3.67	Chrysoberyl	8.5	3.71	Clinoatacamite !	3
3.67	Vistepite	4.5	3.72	Qingheiite	5.5
3.67	Cejkaite !	-	3.72	Pyroxferroite	4.5-5.5
3.67	Oursinite	3-3.5	3.72	Mcgovernite	-
3.68	Synadelphite	4.5	3.72	Chestermanite	6
3.68	Kupletskite-(Cs)	4	3.72	Redledgeite	6-7
3.68	Strontiojoaquinite	5.5	3.72	Agardite-(La) !	3-4
3.68	Orthojoaquinite-(Ce)	5.5	3.72	Agardite-(Nd) !	3-4
3.68	Magnesiotaaffeite-6N3S	8-8.5	3.72	Agardite-(Ca) !	3-4
3.68	Diversilite-(Ce) !	5	3.72	Agardite-(Dy) !	3-4
3.68	Akdalaite	7	3.72	Agardite-(Ce) !	3
3.68	Gerstmannite	4.5	3.74	Paratacamite	3
3.68	Petedunnite	6	3.74	Sanbornite	5
3.68	Satterlyite	4.5-5	3.74	Goldmanite	6-7
3.69	Komarovite	4	3.74	Kapitsaite-(Y) !	5.5
3.69	Graftonite	5	3.74	Gatehouseite	4
3.69	Sarcopside	4	3.75	Pyrope	7.5
3.69	Ardennite	6-7	3.75	Kyzylkumite	6-6.5
3.69	Ferrokinoshitalite !	3	3.75	Dussertite	3.5
3.69	Strontiopiemontite	6	3.75	Allanite-(Y)	5.5
3.69	Roselite	3.5	3.75	Allanite-(Ce)	5.5
3.69	Rhodochrosite	3	3.75	Morimotoite	7.5
3.69	Petersenite-(Ce)	3	3.75	Metatorbernite	2.5
3.69	Agardite-(Y)	3-4	3.75	Dissakisite-(Ce)	6.5-7
3.70	Asbecasite	6.5-7	3.75	Holtite	8.5
3.70	Seelite-2	3	3.75	Poughite	2.5
3.70	Seelite-1	3	3.76	Averievite !	4
3.70	Hellandite-(Y)	5.5-6	3.76	Knorringite	6-7
3.70	Plancheite	5.5	3.76	Adelite	5
3.70	Yttropyrochlore-(Y)	4.5-5.5	3.76	Eveite	4
3.70	Arsenolite	1.5	3.77	Atacamite	3-3.5
3.70	Krasnovite !	2	3.77	Tilasite	5
3.70	Alstonite	4-4.5	3.77	Aurichalcite	2
3.70	Triploidite	4.5-5	3.77	Welshite	6
3.70	Olekminskite	3	3.77	Manganlotharmeyerite !	3
3.70	Tundrite-(Nd)	3	3.78	Glaukosphaerite	3-4
3.70	Tundrite-(Ce)	3	3.78	Flinkite	4.5
3.70	Uramphite	2-2.5	3.78	Strontianite	3.5
3.70	Medaite	-	3.78	Maleevite !	7
3.70	Novacekite	2.5	3.79	Periclase	6

3.79	Hentschelite	3.5	3.85	Khanneshite	3-4
3.79	Penikisite	4	3.85	Metatyuyamunite	2
3.79	Wolfeite	4.5-5	3.85	Hogtuvaite	5.5
3.80	Tadzhikite-(Y) !	6	3.85	Uranopilite	-
3.80	Aenigmatite	5-6	3.85	Ludwigite	5.5
3.80	Tadzhikite-(Ce)	6	3.85	Herbertsmithite !	3-3.5
3.80	Leucophoenicite	5.5-6	3.85	Bogvadite	4
3.80	Joaquinite-(Ce)	5-5.5	3.85	Wickenburgite	5
3.80	Haradaite	4.5	3.85	Dorallcharite	3-4
3.80	Montanite	-	3.85	Mendozavilite	1.5
3.80	Kipushite	4	3.86	Priderite	7
3.80	Shattuckite	-	3.86	Strakhovite	5-6
3.80	Feitknechtite	-	3.86	Muirite	2.5
3.80	Grischunite	5	3.86	Stenonite	3.5
3.80	Goethite	5-5.5	3.86	Waylandite	4-5
3.80	Turtmannite !	-	3.87	Noelbensonite !	4
3.80	Malachite	3.5-4	3.87	Jarlite	4-4.5
3.80	Libethenite	4	3.87	Yanomamite	5.5-6
3.80	Mixite	3.5-4	3.88	Pinakiolite	6
3.80	Strashimirite	2.5-3	3.88	Ancylite-(La) !	4-4.5
3.80	Strontiopyrochlore *	4	3.88	Schwertmannite	2.5-3.5
3.80	Pyroxmangite	5.5-6	3.89	Cabalzarite !	5
3.80	Astrocyanite-(Ce)	2-3	3.89	Jorgensenite !	3.5-4
3.80	Cuprosklodowskite	4	3.89	Wickmanite	3-4
3.80	Tyuyamunite	1.5-2	3.90	Cuzticite	3
3.81	Magnesiohogbomite-2N3S	6.5	3.90	Graulichite-(Ce) !	-
3.81	Magnesiohogbomite-6N6S	6.5	3.90	Brockite	3-4
3.81	Magnesiohogbomite-2N2S	6.5	3.90	Calcio-andyrobertsite-2O !	3-4
3.81	Gaitite	5	3.90	Radovanite !	-
3.81	Hyalotekite	5.5	3.90	Rollandite !	4-4.5
3.81	Daqingshanite-(Ce)	5	3.90	Antlerite	3
3.82	Sonolite	5.5	3.90	Maxwellite	5-5.5
3.82	Bazirite	6-6.5	3.90	Ribbeite	5
3.83	Allactite	4.5	3.90	Andradite	6.5-7
3.83	Azurite	3.5-4	3.90	Ancylite-(Ce)	4.5
3.83	Joesmithite	5.5	3.90	Anatase	5.5-6
3.83	Manganhumite	4	3.90	Althupite	3.5-4
3.83	Goedkenite	5	3.90	Uranophane	2.5
3.84	Norsethite	3.5	3.90	Durangite	5.5
3.84	Strontium-apatite	5	3.90	Chenevixite	4
3.84	Fredrikssonite	6	3.90	Bijvoetite-(Y)	2
3.84	Lautenthalite	2.5	3.90	Uranophane-beta	2.5-3
3.84	Tiragalloite	-	3.91	Hodgkinsonite	4.5-5
3.84	Surkhobite !	-	3.91	Taramellite	5.5
3.84	Iriginite	1-2	3.91	Galileiite !	4
3.85	Schorlomite	7-7.5	3.91	Kulanite	4
3.85	Sodium-uranospinite	2.5	3.92	Reppiaite	3-3.5

3.92	Getchellite	1.5-2	4.00	Rhabdophane-(Nd)	3-4
3.92	Byelorussite-(Ce)	5.5-6	4.00	Legrandite	4-5
3.93	Nanlingite	2.5	4.00	Metalodevite	2-2.5
3.93	Spertiniite	-	4.00	Swamboite	2.5
3.93	Kamotoite-(Y)	-	4.00	Hancockite	6-7
3.93	Nantokite	2-2.5	4.00	Ferrisurite	2-2.5
3.94	Deloneite-(Ce) !	5	4.01	Piretite !	2.5
3.94	Olgite	4.5	4.01	Woodruffite	4.5
3.94	Rhabdophane-(La)	3-4	4.01	Brianyoungite	2-2.5
3.94	Anandite	3-4	4.01	Jagowerite	4.5
3.95	Zwieselite	5-5.5	4.01	Calcio-andyrobertsite-1M !	3
3.95	Ferrosilite	5-6	4.01	Andyrobertsite !	3
3.95	Meta-uranocircite	2-2.5	4.02	Painite	8
3.95	Sonoraite	3	4.02	Hejtmanite	4.5
3.95	Hercynite	7.5	4.02	Yuanfuliite	6-6.5
3.95	Celestine	3-3.5	4.02	Vyuntspakhkite-(Y)	6-7
3.96	Innelite	4.5-5	4.02	Bjarebyite	4
3.96	Yftisite-(Y) ?	3.5-4	4.02	Blatonite !	2-3
3.96	Bario-orthojoaquinite	5-5.5	4.02	Meymacite	-
3.96	Kinichilite	2	4.02	Harrisonite !	4-5
3.96	Siderite	3.5	4.03	Synchysite-(Ce)	4.5
3.96	Hidalgoite	4.5	4.03	Kurumsakite	-
3.97	Pseudomalachite	4-5	4.03	Wurtzite	3.5-4
3.97	Kolwezite	4	4.03	Marecottite !	3
3.97	Brochantite	3.5-4	4.03	Pabstite	6
3.97	Lukechangite-(Ce) !	4.5	4.04	Natanite	5
3.97	Clinobarylite !	6.5	4.04	Osarizawaite	3-4
3.97	Lepersonnite-(Gd)	-	4.04	Thorbastnasite	4-4.5
3.98	Wakabayashilite	1.5	4.04	Mushistonite	4-4.5
3.98	Jimboite	5.5	4.04	Srebrodolskite	5.5
3.99	Margarosanite	2.5-3	4.04	Metaheinrichite	2.5
4.00	Synchysite-(Y)	6-6.5	4.05	Barylite	6-7
4.00	Alleghanyite	6-5	4.05	Zemannite	-
4.00	Tristramite	3-4	4.05	Johntomaite !	4.5
4.00	Grayite	3-4	4.05	Sengierite	2.5
4.00	Moluranite	3-4	4.05	Vesignieite	3.5-4
4.00	Kimzeyite	7	4.05	Corundum	9
4.00	Henrymeyerite !	5-6	4.05	Willemite	5.5
4.00	Theophrastite	3.5	4.05	Sphalerite	3.5-4
4.00	Suzukiite	4-4.5	4.06	Peretaite	3.5-4
4.00	Jerrygibbsite	5.5	4.06	Francoisite-(Nd)	3
4.00	Majorite	7-7.5	4.07	Clinoferrosilite	5-6
4.00	Claudetite	2.5	4.07	Grattarolaite !	-
4.00	Bariopyrochlore	4.5-5	4.07	Philipsburgite	3-4
4.00	Bario-olgite !	4-4.5	4.07	Ferrotaaffeite-6N3S	8-8.5
4.00	Surite	2-3	4.07	Vismirnovite	4
4.00	Rhabdophane-(Ce)	3.5	4.08	Melanothallite	-

4.08	Khristovite-(Ce)	5	4.20	Tritomite-(Ce)	5.5
4.08	Cornwallite	4-5	4.20	Nordenskioldine	5.5-6
4.08	Ilinskite !	1.5-2	4.20	Gilmarite !	3
4.08	Berzeliite	4.5-5	4.20	Atlasovite	2-2.5
4.08	Calderite	-	4.20	Gadolinite-(Ce)	6.5-7
4.10	Arsenoflorencite-(Ce)	3.5	4.20	Thalenite-(Y)	6-6.5
4.10	Orthojoaquinite-(La) !	5	4.20	Carnotite	2
4.10	Franciscanite-III	4	4.21	Androsite-(La) !	-
4.10	Franciscanite-VIII	4	4.21	Vonsenite	5
4.10	Cornetite	4.5	4.21	Synchysite-(Nd)	4.5
4.10	Rosasite	4	4.21	Gagarinite-(Y)	4.5
4.10	Zdenekite	1.5-2	4.22	Magnesionigerite-2N1S	8-8.5
4.10	Conichalcite	4.5	4.22	Ferriallanite-(Ce) !	6
4.10	Sphaerocobaltite	3-4	4.22	Magnesionigerite-6N6S	8-8.5
4.10	Arsenoflorencite-(Nd) *	3.5	4.22	Phurcalite	3
4.10	Zincrosasite	4.5	4.23	Lotharmeyerite	3
4.10	Rabejacite	3	4.23	Mourite	3
4.10	Haynesite	1.5-2	4.24	Tooeleite	3
4.10	Fontanite	3	4.24	Bruggenite	3.5
4.10	Weeksite	1-2	4.24	Fluorthalenite-(Y) !	4-5
4.10	Strelkinite	2.5	4.25	Rutile	6-6.5
4.10	Phosphuranylite	2.5	4.25	Britholite-(Y)	5
4.11	Bafertisite	5	4.25	Tephroite	6.5
4.11	Holdenite	4	4.25	Gadolinite-(Y)	6.5-7
4.12	Brezinaite	3.5-4.5	4.25	Olivenite	3
4.13	Melanocerite-(Ce)	5-6	4.25	Pseudocotunnite	-
4.13	Ceriopyrochlore-(Ce)	5-5.5	4.25	Minasgeraisite-(Y)	6-7
4.13	Austinite	4-4.5	4.25	Tengchongite	2-2.5
4.13	Sarkinite	4-5	4.25	Ferrimolybdite	2.5-3
4.14	Tarbuttite	4	4.25	Ferrilotharmeyerite	3
4.14	Groutite	5.5	4.26	Arseniopleite	3.5
4.15	Downeyite	-	4.26	Szenicsite	3.5-4
4.15	Johillerite	3	4.26	Lindgrenite	4.5
4.15	Retzian-(Ce)	4	4.27	Romanite	6.5-7
4.15	Arsenoflorencite-(La) *	3.5	4.27	Reinerite	5-5.5
4.16	Arsenoclasite	5-6	4.27	Uranotungstite	2
4.16	Tomichite	6	4.28	Yttrobetafite-(Y)	4.5-5.5
4.16	Belkovite !	6-7	4.28	Mannardite	7
4.17	Kolicite	4.5	4.29	Swedenborgite	8
4.18	Nabokoite	2-2.5	4.29	Manjiroite	7
4.18	Usovite	3.5	4.29	Caryinite	4
4.18	Spessartine	6.5-7.5	4.30	Corkite	3.5-4.5
4.19	Belovite-(La) !	5	4.30	Clinoclase	2.5-3
4.19	Belovite-(Ce)	5	4.30	Kintoreite	4
4.20	Almandine	7-8	4.30	Cobalt-zippeite	5-5.5
4.20	Beudantite	4	4.30	Sodium-zippeite	5-5.5
4.20	Dixenite	3-4	4.30	Zinc-zippeite	5-5.5

4.30	Nickel-zippeite	5-5.5	4.44	Davidite-(Ce)	6
4.30	Heterogenite-3R	4-5	4.44	Ankangite	6.5
4.30	Freudenbergite	-	4.44	Lueshite	5.5
4.30	Gahnite	8	4.44	Cordylite-(Ce)	4.5
4.30	Nickelaustinite	4	4.45	Britholite-(Ce)	5.5
4.30	Metadelrioite	2	4.45	Retzian-(Nd)	3-4
4.30	Witherite	3-3.5	4.45	Cesbronite-x	3
4.30	Kuliokite-(Y)	4-5	4.45	Cesbronite	3
4.30	Magnussonite	3.5-4	4.45	Keiviite-(Y)	4-5
4.30	Fleischerite	2.5-3	4.45	Smithsonite	4.5
4.30	Zhonghuacerite-(Ce)	4.5	4.46	Nsutite	6.5-8.5
4.30	Betafite	5-5.5	4.46	Crichtonite	5-6
4.31	Leiteite	1.5-2	4.47	Bracewellite	5.5-6.5
4.31	Prosperite	4.5	4.47	Welinite-III	4
4.31	Curetonite	3.5	4.47	Bismutoferrite	6
4.31	Babefphite	3.5-4	4.47	Welinite-VIII	4
4.32	Abhurite	2	4.47	Iimoriite-(Y)	5.5-6
4.33	Philipsbornite	4.5	4.48	Barite	3-3.5
4.33	Palmierite	2	4.48	Radiobarite	3-3.5
4.34	Manganberzeliite	4.5-5	4.49	Wilhelmkleinite !	4.5
4.34	Powellite	3.5	4.49	Retzian-(La)	3-4
4.35	Calciobetafite	4.5-5.5	4.49	Greenockite	3.5-4
4.35	Reichenbachite	3.5	4.50	Zajacite-(Ce)	3.5
4.35	Okanoganite-(Y)	4	4.50	Chevkinite-(Ce)	5-5.5
4.35	Mroseite	4	4.50	Rankachite	2.5
4.35	Plumalsite ?	5-6	4.50	Lermontovite	-
4.35	Stishovite	7.5-8	4.50	Laphamite	1-2
4.35	Parisite-(Nd)	4-5	4.50	Bernardite	2
4.36	Zincohogbomite-2N2S !	7	4.50	Chernovite-(Ce) *	4-4.5
4.36	Parisite-(Ce)	4.5	4.50	Plumbogummite	4-5
4.36	Beaverite	3.5-4.5	4.50	Berndtite	1-2
4.37	Perrierite-(Ce)	5.5	4.50	Kegelite	-
4.37	Zairite	4.5	4.51	Ferronigerite-6N6S	8.5
4.38	Ludlockite	1.5-2	4.51	Ferronigerite-2N1S	8.5
4.39	Ludlockite-(Pb) *	1.5-2	4.52	Lautarite	3.5-4
4.39	Fayalite	6.5	4.53	Emmonsite	2-2.5
4.39	Fritzscheite	2-3	4.54	Yingjiangite	3-4
4.40	Cappelenite-(Y)	6	4.55	Derbylite	5
4.40	Keystoneite	-	4.55	Kermesite	1.5-2
4.40	Pseudobrookite	6	4.55	Paradamite	3.5
4.40	Adamite	3.5	4.55	Francevillite	3
4.41	Macaulayite	-	4.57	Baotite	6
4.41	Jeanbandyite	3.5	4.58	Gallobeudantite !	4
4.42	Davidite-(La)	6	4.59	Stillwellite-(Ce)	6.5
4.42	Esperite	5	4.59	Huanghoite-(Ce)	4.7
4.43	Malayaite	3.5-4	4.59	Juabite !	3-4
4.43	Fresnoite	3-4	4.59	Hashemite	3.5

4.60	Kobeite-(Y)	5.5		4.78	Trechmannite	1.5-2
4.60	Liebenbergite	6		4.79	Jachymovite !	-
4.60	Hydrotungstite	2		4.80	Trippkeite	4
4.62	Gamagarite	4.5-5		4.80	Cebaite-(Nd) !	4.5-5
4.62	Calciouranoite	4		4.80	Yttrocrasite-(Y)	5.5-6
4.62	Parwelite	5.5		4.80	Sarabauite	4.5
4.62	Klebelsbergite	3.5-4		4.80	Leningradite	4.5
4.63	Soddyite	3-4		4.80	Anthoinite	1
4.64	Plumbobetafite	4.5-5.5		4.80	Uranpyrochlore	5
4.65	Tlapallite	3		4.80	Schoepite	2.5
4.65	Sabelliite !	4.5		4.81	Cebaite-(Ce)	4.5-5
4.65	Zircon	7.5		4.82	Aeschynite-(Nd)	5-6
4.65	Hinsdalite	4.5		4.82	Gysinite-(Nd)	4-4.5
4.66	Kukharenkoite-(Ce) !	4.5		4.83	Hingganite-(Yb)	6-7
4.66	Fluorbritholite-(Ce)	5		4.83	Hingganite-(Y)	6-7
4.66	Hingganite-(Ce)	6-7		4.85	Hollandite	4-6
4.67	Cumengite	2.5		4.85	Euxenite-(Y)	6.5
4.67	Metastudtite	-		4.85	Calcioaravaipaite !	2.5
4.69	Ashburtonite	-		4.86	Cerite-(Ce)	5.5
4.69	Wyartite	3-4		4.86	Mackayite	4.5
4.70	Zirconolite-2M	5.5		4.86	Chadwickite !	2
4.70	Zirconolite-3O	5.5		4.87	Chernovite-(Y)	4-5
4.70	Zirconolite-3T	5.5		4.87	Angelellite	5.5
4.70	Zirkelite	5.5		4.88	Brizziite-III	2
4.70	Molybdophyllite	3-4		4.88	Brizziite-VII	2
4.70	Mathewrogersite	2		4.88	Tausonite	6-6.5
4.70	Cerite-(La) !	5		4.88	Curienite	3
4.72	Taikanite	6-7		4.89	Bellingerite	4
4.72	Brabantite	5.5		4.89	Frankdicksonite	3
4.72	Molybdite	3-4		4.90	Tornebohmite-(Ce)	4.5
4.72	Isolueshite !	5.5		4.90	Mrazekite	2-3
4.73	Tusionite	5-6		4.90	Deloryite	4
4.73	Alforsite	5		4.93	Polhemusite	4.5
4.73	Vicanite-(Ce)	5.5-6		4.94	Tornebohmite-(La)	4.5
4.74	Scheteligite ?	5.5		4.95	Manganostibite	-
4.74	Fersmite	4-4.5		4.95	Boleite	3-3.5
4.75	Hydroxylbastnasite-(Ce)	4		4.95	Stibiconite	4-5
4.75	Ningyoite	3-4		4.95	Lewisite !	5.5
4.75	Hydroxylbastnasite-(La)	4		4.95	Bastnasite-(Y)	4-4.5
4.75	Polyakovite-(Ce) !	5.5-6		4.95	Rouseite	3
4.75	Xenotime-(Y)	4-5		4.96	Burckhardtite	2
4.76	Wakefieldite-(Ce)	4.5		4.97	Yeatmanite	4
4.76	Jensenite	3-4		4.97	Bismutopyrochlore !	5
4.77	Srilankite	6.5		4.98	Bastnasite-(Ce)	4-5
4.77	Loparite-(Ce)	5.5		4.98	Bastnasite-(La)	4-5
4.77	Orebroite-III	4		4.98	Schieffelinite	2
4.77	Salesite	3		4.99	Aeschynite-(Y)	5-6

5.00	Pseudoboleite	2.5	5.33	Utahite !	4-5
5.00	Trimounsite-(Y)	7	5.34	Fergusonite-beta-(Ce)	5.5-6.5
5.01	Polycrase-(Y)	5-6	5.35	Thorite	5
5.01	Spiroffite	3.5	5.38	Pyrobelonite	3.5
5.01	Calzirtite	6-7	5.38	Stetefeldtite	3.5-4.5
5.01	Tazheranite	7.5	5.39	Artroeite	2.5
5.02	Roubaultite	3	5.40	Thorogummite	5.5
5.03	Otavite	3.5-4	5.40	Linarite	2.5
5.04	Niobo-aeschynite-(Ce)	5.3-5.6	5.40	Galkhaite	3
5.04	Plumbopyrochlore	4.5-5.5	5.43	Brannerite	4-5
5.05	Denningite	4	5.43	Jagoite	3
5.05	Phosphogartrellite !	4.5	5.44	Frankhawthorneite	3-3.5
5.05	Romeite	5.5-6	5.45	Metavandendriesscheite	3
5.08	Masuyite	-	5.45	Vandendriesscheite	3
5.08	Vandenbrandeite	4	5.46	Nasonite	4
5.09	Hyttsjoite !	-	5.46	Orthobrannerite	5.5
5.10	Pyrostilpnite	2	5.48	Fergusonite-(Ce) *	5.5-6.5
5.10	Jamesite	3	5.49	Macquartite	3.5
5.10	Coffinite	5-6	5.50	Bayldonite	4.5
5.10	Fergusonite-(Nd) *	5.5-6.5	5.50	Mawbyite	4
5.10	Rodalquilarite	2-3	5.50	Rankamaite	3-4
5.10	Caracolite	4.5	5.50	Tungstite	2.5
5.10	Hugelite	2.5	5.55	Yafsoanite	5.5
5.11	Ferritungstite	-	5.55	Cotunnite	1.5-2
5.12	Stibivanite	4	5.55	Drugmanite	-
5.14	Becquerelite	2.5	5.55	Chlorargyrite	1-1.5
5.15	Monazite-(La)	5-5.5	5.55	Xanthoconite	2.5-3
5.15	Monazite-(Ce)	5-5.5	5.56	Roxbyite	2.5-3
5.15	Monazite-(Nd)	5-5.5	5.57	Winstanleyite	4
5.17	Bonaccordite	7	5.59	Yecoraite	3
5.18	Bahianite	9	5.60	Barstowite	3
5.18	Manganosite	5-6	5.60	Asselbornite	3
5.18	Lammerite	3-4	5.60	Plumbotsumite	2
5.19	Aeschynite-(Ce)	5-6	5.60	Iodargyrite	1.5-2
5.20	Schuilingite-(Nd)	3-4	5.60	Paratellurite	1
5.22	Carminite	3.5	5.64	Miersite	2.5-3
5.25	Struverite	6-6.5	5.65	Tanteuxenite-(Y)	5-6
5.25	Mammothite	3	5.66	Agrinierite	-
5.25	Senarmontite	2	5.66	Cadmoselite	4
5.26	Phyllotungstite	2	5.68	Bariomicrolite	4.5-5
5.28	Billietite	-	5.70	Samarskite-(Y)	5-6
5.30	Cheralite-(Ce)	5	5.70	Embolite *	1.5-2
5.30	Helmutwinklerite	4.5	5.70	Valentinite	2.5-3
5.30	Stibiobetafite	5	5.70	Rutherfordine	-
5.30	Pyrochlore	5-5.5	5.74	Ganomalite	3
5.30	Microlite	5-5.5	5.75	Uranopolycrase	5-6
5.32	Morelandite	4.5	5.75	Baddeleyite	6.5

5.75	Marshite	2.5	6.15	Phosgenite	2.5-3
5.80	Iranite	3	6.19	Capgaronnite	-
5.81	Hedyphane	4-5	6.20	Christite	1-2
5.82	Uranmicrolite	5.5	6.20	Zimbabweite	5-5.5
5.82	Thorutite	4.5-5.5	6.23	Kasolite	4
5.82	Penfieldite	3-4	6.24	Laurionite	2.5-3
5.82	Tripuhyite	7	6.25	Pucherite	4
5.83	Protasite	-	6.25	Dreyerite	2-3
5.85	Yedlinite	2.5	6.27	Fornacite	2-3
5.88	Wustite	5-5.5	6.27	Bideauxite	3
5.88	Nealite	4	6.29	Fettelite !	3.5-4
5.88	Fiedlerite	3.5	6.30	Heyite	4
5.89	Nealite-(H2O) *	-	6.30	Anglesite	2.5-3
5.90	Fourmarierite	3-4	6.30	Georgiadesite	3.5
5.90	Bromargyrite	1.5-2	6.30	Ishikawaite	5-6
5.90	Tellurite	2	6.33	Dugganite	3
5.90	Larsenite	3	6.36	Uranosphaerite	2-3
5.90	Medenbachite !	4.5	6.37	Scotlandite	2
5.91	Philolithite !	3-4	6.39	Clarkeite	4-4.5
5.93	Fluocerite-(La)	4-5	6.39	Hallimondite	2.5-3
5.94	Tantalaeschynite-(Y)	5.5-6	6.40	Chervetite	2-2.5
5.94	Schultenite	2.5	6.40	Duftite-alpha	3
5.95	Diaboleite	2.5	6.40	Duftite-beta	3
5.95	Bindheimite	4-5	6.40	Choloalite	3
5.95	Mottramite	3.5	6.41	Leadhillite	2.5
5.95	Keiviite-(Yb)	4-5	6.42	Barysilite	3
5.95	Walpurgite	3.5	6.42	Hemihedrite	3
5.96	Yttrotungstite-(Y)	1	6.45	Wherryite	-
5.97	Parabariomicrolite	4	6.45	Fergusonite-beta-(Nd)	5.5-6.5
5.98	Chenite	2.5	6.45	Calomel	1.5-2
5.98	Stibiocolumbite	5.5	6.45	Embreyite	3.5
5.99	Klockmannite	2-2.5	6.46	Nordite-(Ce)	5
6.00	Vauquelinite	2.5-3	6.46	Arsentsumebite	4-5
6.00	Crocoite	2.5-3	6.48	Changbaiite	5.5
6.00	Gebhardite	3	6.49	Alamosite	4.5
6.00	Elyite	2	6.50	Daubreeite	2-2.5
6.01	Parsonsite	2.5-3	6.50	Tenorite	3.5-4
6.01	Scheelite	4-5	6.50	Cesstibtantite	6.5
6.04	Jixianite	3	6.50	Macphersonite	2.5-3
6.05	Paralaurionite	3	6.50	Cervantite	4-5
6.05	Caledonite	2.5-3	6.50	Orthowalpurgite	4.5
6.07	Queitite	4	6.52	Cannonite	4
6.10	Cuprite	3.5-4	6.52	Feinglosite !	4-5
6.11	Paramelaconite	4.5	6.54	Arsenbrackebuschite	4.5
6.13	Fluocerite-(Ce)	4.5-5	6.55	Olsacherite	3-3.5
6.15	Descloizite	3.5	6.55	Susannite	2.5-3
6.15	Natrobistantite	-	6.56	Beyerite	2-3

6.57	Arsendescloizite	4		6.97	Hafnon	7.5
6.57	Cliffordite	4		7.00	Bismutite	4
6.58	Cerussite	3-3.5		7.00	Radtkeite	2-3
6.59	Iltisite !	-		7.00	Sundiusite	3
6.60	Bunsenite	5.5		7.00	Pseudograndreefite	2.5
6.60	Eulytite	4.5		7.00	Lithiotantite	6-6.5
6.60	Plumbomicrolite	5		7.00	Freedite	3
6.60	Trigonite	2-3		7.00	Pottsite	3.5
6.60	Molybdofornacite	2-3		7.00	Ecdemite	2.5
6.62	Monimolite	4.5-6		7.01	Phoenicochroite	2.5
6.62	Krasnoselskite	4		7.02	Nadorite	3.5-4
6.62	Krasnogorite	4		7.03	Formanite-(Y)	5.5-6.5
6.63	Mcalpineite	3		7.03	Irtyshite	7
6.64	Ordonezite	6.5		7.06	Cuprotungstite	4-5
6.67	Gabrielsonite	3.5		7.07	Plumbonacrite	3.5
6.67	Itoite	-		7.07	Molybdomenite	3.5
6.69	Tungstibite	2		7.08	Kerstenite *	3.5
6.70	Sanmartinite	4-4.5		7.10	Kuzminite	1.5
6.70	Simpsonite	7-7.5		7.10	Mendipite	2.5-3
6.70	Stibiotantalite	5.5		7.10	Huttonite	5
6.71	Kuranakhite	4-5		7.10	Grandreefite	2.5
6.73	Foordite	6		7.12	Matlockite	2.5-3
6.75	Wulfenite	3		7.15	Tantalowodginite *	5-5.5
6.76	Chloroxiphite	2.5		7.16	Grechishchevite	2.5
6.76	Kenhsuite !	2-3		7.17	Sphaerobismoite	4
6.80	Wolsendorfite	5		7.17	Mimetite	3.5-4
6.80	Hydrocerussite	3.5		7.19	Curite	4-5
6.80	Liandratite	3.5		7.24	Preisingerite	3-4
6.82	Atelestite	4.5-5		7.24	Thorikosite	3
6.83	Brendelite !	4.5		7.27	Finnemanite	2.5
6.83	Bismutomicrolite	5		7.30	Symesite !	4
6.84	Quenselite	2.5		7.32	Parkinsonite	2-2.5
6.85	Pyromorphite	3.5-4		7.35	Blixite	3
6.86	Titanowodginite	5.5		7.36	Clinomimetite	3.5-4
6.86	Rooseveltite	4-4.5		7.38	Bismutostibiconite	4-5
6.87	Hechtsbergite !	4.5		7.38	Tvalchrelidzeite	3
6.88	Schmitterite	1		7.39	Schwartzembergite	2.5
6.88	Chekhovichite	4		7.40	Tungstenite	2.5
6.89	Widenmannite	2		7.41	Mereheadite !	3.5
6.89	Heliophyllite	2		7.43	Hypercinnabar	3
6.90	Sosedkoite	6		7.45	Fairbankite	2
6.90	Cassiterite	6-7		7.46	Calciotantite	6.5
6.90	Schumacherite	3		7.48	Aguilarite	2-3
6.92	Lanarkite	2-2.5		7.50	Lithiowodginite	5-6
6.95	Vanadinite	3.5-4		7.64	Arzakite	2-2.5
6.95	Paulmooreite	3		7.65	Laurelite	2
6.96	Rosiaite !	5.5		7.69	Lorettoite ?	3

7.70	Comancheite	2		8.44	Zavaritskite	2-2.5
7.71	Natrotantite	7		8.45	Tantite	7
7.72	Bismoclite	2-2.5		8.47	Raspite	2.5-3
7.72	Mosesite	3-4		8.54	Pingguite	5.5-6
7.75	Thoreaulite	5.5-6		8.68	Bismutotantalite	5
7.78	Smirnite	3.5-4		8.70	Terlinguaite	2-3
7.82	Macedonite	5.5-6		8.73	Kuznetsovite !	2.5-3
7.86	Behierite	7-7.5		9.00	Bismite	4-5
8.00	Kleinite	3.5		9.06	Chursinite	3-4
8.00	Sahlinite	2-3		9.25	Litharge	2
8.05	Stolzite	2.5-3		9.31	Shannonite !	3-3.5
8.10	Carlinite	1		9.40	Edgarbaileyite	4
8.10	Cinnabar	2-2.5		9.50	Petrovskaite	2-2.5
8.16	Perite	3		9.56	Poyarkovite	2-2.5
8.20	Minium	2.5-3		9.64	Massicot	2
8.26	Koechlinite	-		9.80	Chrombismite !	3-3.5
8.30	Eglestonite	2-3		11.20	Montroydite	1.5-2
8.34	Stannomicrolite	4.5-5.5				

Symbols:

* - Mineral name not approved by the IMA

! - New Dana classification number has been added or changed

? - IMA Discredited Mineral Species Name

7.3. Gravity separation in magnetic liquids

The gravity separation of particles can also be accomplished in magnetic liquids. This approach is applied for separation of materials of high density. The magnetic liquids change their apparent density depending on the intensity of the magnetic field. Their apparent density can be changed from about 1.3 (no magnetic field) to about 20 g/cm^3 at high intensity of the magnetic field. The magnetic liquid usually contains nanoparticles (~10 nm) of magnetite which are suspended in such liquids as water, oil, esters, naphtha which also contain surfactants which provide stability of the magnetic suspension. Fine magnetic particles are produced by precipitation from aqueous solutions containing Fe(II) and Fe(III) salts (Odenbach, 1998). Separation in magnetic liquids can be applied for nonmagnetic material of significantly different densities, especially non-ferrous metals and plastics from car scraps.

Literature

CRC, 1986/87. Handbook of Chemistry and Physics, 67th ed., CRC Press, Boca Raton, Florida, USA.

Kelly E.G., Spottiswood D.J., 1982. Introduction to mineral processing, Wiley, New York.

Laskowski J., 1969. Chemia fizyczna w procesach mechanicznej przeróbki kopalin, Wydawnictwo Śląsk, Katowice.

Laskowski J., Luszczkiewicz A., 1989. Przeróbka kopalin – wzbogacanie surowców mineralnych, Wydawnictwo Politechniki Wrocławskiej, Wrocław.

Laskowski J., Luszczkiewicz A., Malewski J., 1977. Przeróbka kopalin, Wydawnictwo Politechniki Wrocławskiej, Wrocław.

Laskowski T., Blaszczynski S., Slusarek M., 1979. Wzbogacanie w cieczach ciężkich, Wydawnictwo Śląsk, Katowice.

Odenbach S., 1998. Ferrofluids – magnetisable liquids and their application in density separation, Magnetic and Electric Separation, 9, 1–25.

Stepinski W., 1964. Wzbogacanie grawitacyjne, PWN, Łódź.

8. Magnetic separation

8.1. Magnetic properties of materials

A particle placed in a magnetic field interacts with this field. As a result, the particle moves in the field. This phenomenon is utilized in separation of particles of different materials and it is termed magnetic separation. The utilized feature of the material is magnetic susceptibility. For particles pulled into stronger magnetic fields magnetic susceptibility is positive (paramagnetics) and for those which are pushed out is negative (diamagnetics). Magnetic separation is possible for particles of different signs or susceptibilities (Fig. 8.1).
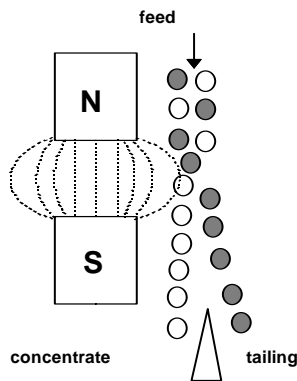
Fig. 8.1. Magnetic separation. Paramagnetic (white) particles are directed towards denser lines of magnetic field, while diamagnetic (black) ones outside the field

When the magnetic field of intensity H (A/m) is generated in vacuum, induced magnetic filed is B_0 (Vs/m^2=T):

$$B_0 = \mu_0\, H, \tag{8.1}$$

where:

μ_0 – magnetic permeability of vacuum, $\mu_0 = 4\pi 10^{-7}$ V·s/(A·m) $= 4\pi 10^{-7}$ H/m

A – ampere

V – volt

s – second

m – meter

H – henry (it should not be mistaken with symbol H which denotes intensity of the magnetic field (in A/m)),

Wb – weber

T – tesla,

$$T = \frac{V\cdot s}{m^2} = \frac{Wb}{m^2} = \frac{H\cdot A}{m^2}.$$

When a particle is placed in vacuum in the same magnetic field *H*, generated magnetic induction will be different from that of vacuum due to a different magnetic permeability of the particle μ (Ibach and Lüth, 1996)

$$B = \mu H, \tag{8.2}$$

where μ is particle magnetic permeability which, like magnetic permeability in vacuum μ_0, is expressed as henry per 1 meter.

Generated magnetic induction *B* depends both on magnetic field *H* and on the substance magnetization *M*. Thus:

$$B = \mu_0 (H + M) = B_0 + \mu_0 M, \tag{8.3}$$

where *M* is magnetization expressed, like magnetic field *H*, in A/m.

As the vector of magnetic induction *B*, in the presence of a particle in a magnetic field, is different from the vector of induction in vacuum, i.e., in the original field, the increment of magnetic induction over that in vacuum can be expressed as:

$$\chi = (B - B_0)/B_0 = (\mu - \mu_0)/\mu_0 = \mu_0 M/B_0, \tag{8.4}$$

where χ is volumetric magnetic susceptibility, which is a dimensionless quantity, either positive or negative. When χ is negative, induced magnetic polarization has an opposite sign to the applied field *H*.

Materials having negative values of magnetic susceptibility are called *diamagnetics*, while the ones with positive magnetic susceptibility are called *paramagnetics*. Thus, susceptibility characterizes magnetic properties of substances and is the main material parameter of magnetic separation. The values of magnetic susceptibility for different substances can be found in many handbooks e.g. CRS Handbook of Chemistry and Physics (CRS, 1986/87; Gupta, 1986/87, Smith, 1986/87) or in the monograph by Svoboda (1987). While reviewing literature one should pay attention to the units system of magnetic susceptibility. There are three kinds of magnetic susceptibility: volumetric, mass (also called specific), and molar susceptibility. However, they can be expressed in different units (SI or obsolete electromagnetic cgs system). Transformation of dimensionless volumetric magnetic susceptibility χ expressed in cgs system into a SI unit can be done using the relation:

$$\chi = \chi^{SI} = 4\pi \chi^{cgs}. \tag{8.5}$$

The specific (gram) susceptibility χ_w in both systems of units can be obtained by taking into account material density, i.e. calculating it from the relation:

$$\chi_w = \chi / \rho, \tag{8.6}$$

where:

χ – volume magnetic susceptibility (dimensionless), defined in Eq. (8.4)
χ_w – specific susceptibility, cm^3/g

ρ – material density, g/cm^3.

Molar (atomic) susceptibility χ_M is expressed in cm^3/mole. It is obtained by multiplying specific (gram) susceptibility by molecular mass (g/mol). Frequently, especially older sources, do not disclose the unit system used for characterizing the three (volumetric, specific and molar) magnetic susceptibility of materials. This means that χ_0, χ_W, χ_M can be either in SI or cgs systems. Table 8.1 presents magnetic susceptibility for quartz SiO_2 (diamagnetic) (Laskowski and Luszczkiewicz, 1989) and for paramagnetic metallic titanium (Ti) (Svoboda, 1987).

Table 8.1. Comparison of magnetic susceptibility in SI and cgs units for silicon dioxide and titanium. To get a desired form of magnetic susceptibility in the cgs system the quantity in the SI units should be divided by 4π, because $\chi^{SI} = 4\pi\chi^{cgs}$, $\chi_w^{SI} = 4\pi\chi_w^{cgs}$, and $\chi_M^{SI} = 4\pi\chi_M^{cgs}$

	SiO_2 ($M = 60.08$ g/mol, $\rho = 2.65$ g/cm³)		Ti ($M = 47.9$ g/mol, $\rho = 4.5$ g/cm³)	
Magnetic susceptibility	SI	cgs	SI	cgs
Dimensionless, χ	$-16.4 \cdot 10^{-6}$	$-1.306 \cdot 10^{-6}$	$180.9 \cdot 10^{-6}$	$14.4 \cdot 10^{-6}$
Specific, χ_w (cm³/g)	$-6.19 \cdot 10^{-6}$	$-0.493 \cdot 10^{-6}$	$40.12 \cdot 10^{-6}$	$3.19 \cdot 10^{-6}$
molar, χ_M (cm³/mol)	$-372 \cdot 10^{-6}$	$-29.6 \cdot 10^{-6}$	$1921,7 \cdot 10^{-6}$	$153 \cdot 10^{-6}$

For easy calculation of the data in the SI units from the cgs magnetic units, Table 8.2 provides fundamental relations between the systems.

Table 8.2. Comparison of units of magnetic field for the SI units and the cgs emu (electromagnetic units) system (after Frederikse, 1997/98 and Svoboda, 1987)

Quantity	Symbol	SI unit	emu units (cgs)	Factor f
Intensity of magnetic field	H	A/m	Oe (oersted)	$10^3/(4\pi)$
Magnetic induction	B	T (tesla)	G (gauss)	10^{-4}
Magnetization (specific, spontaneous, saturation)	M	A/m	emu/cm³	10^3
Magnetic flux	Φ	Wb (weber)	Mx (maxwell)	10^{-8}
Magnetic moment	μ_m	T·m³	emu	$4\pi \cdot 10^{-10}$
Magnetic susceptibility (volume)	χ	dimensionless	dimensionless	$1/(4\pi)$
Magnetic permeability	μ	H/m (henry/metr)	1, dimensionless	$4\pi \cdot 10^{-7}$
Vacuum magnetic permeability	μ_0	H/m; $4\pi \cdot 10^{-7}$ H/m	dimensionless	$4\pi \cdot 10^{-7}$
Specific polarization	σ	T·m³·kg⁻¹	emu·g⁻¹	10^{-7}
Magnetic polarization	J	T (tesla)	emu·cm⁻³	$4\pi \cdot 10^{-4}$
Curie temperature	T_C	K (kelvin)	K	1
Néel temperature	T_N	K	K	1

Remark: To get a quantity in SI, the same quantity in cgs should be multiplied by factor f (SI = cgs × f). For instance 100 gauss gives 0.01 tesla, because 100 G × f = 100 × 10^{-4} T = 0.01 T. Aberration emu denotes electromagnetic units in cgs system, 1 emu/cm³ = 10^3 A/m.

Magnetic properties of substances result from magnetic properties of their chemical elements. In turn, magnetic properties of elements depend on their structure, especially of the outer electrons, and is characterized by magnetic moment of an atom. The magnetic moment is resultant of magnetic moments of valence electrons, other electrons present in the atom, and, to a small extent, the nucleus.

The resultant magnetic moment of diamagnetics is negative while that of paramagnetics is positive. They can be recognized by placing them in a non-uniform magnetic field. Paramagnetic substances are attracted towards more denser lines of magnetic field forces, while diamagnetic ones are pushed out of the field. It results from the appearance of force *F* which acts on a particle in magnetic field *H*. It is described by a general equation (Svoboda, 1987, Hopstock, 1985):

$$\vec{F}_m = \nabla \int_V (\vec{J}\,\vec{H})dV \,, \tag{8.7}$$

where:

F_m – magnetic force (newton)
J – magnetic polarization (tesla)
H – intensity of magnetic field (A/m)
∇ – gradient operator
V – volume of particle (m^3) having mass *m,*
and symbol $\rightarrow$ stands for vector.

A proper transformation of Eq. (8.7) for small particles (point dipoles) gives:

$$\vec{F}_m = (\vec{\mu}\ \nabla)\vec{H} \,, \tag{8.8}$$

where μ is magnetic susceptibility.

For a weakly magnetic spherical particle placed in the external magnetic field it can be written:

$$\vec{F}_m = 1/2\mu_0\chi\, V(\vec{H}\nabla)\vec{H} = 1/2\mu_0\chi\, V\, \nabla(\vec{H})^2 \,. \tag{8.9}$$

Taking into account that $m/V=\rho$ and that $\chi_w = \chi/\rho,$ assuming that the change of *H*, connected with the change of volume, is relatively small, Eq. (8.9) takes a differential form:

$$F_m = \mu_0\,\chi_w\, mH\, \text{grad}\, H \tag{8.10}$$

or, in a detailed version:

$$F_x = \mu_0 \chi_w m \left(H_x \frac{\partial H_x}{\partial x} + H_y \frac{\partial H_y}{\partial x} + H_z \frac{\partial H_z}{\partial x} \right),$$

$$F_y = \mu_0 \chi_w m \left(H_x \frac{\partial H_x}{\partial y} + H_y \frac{\partial H_y}{\partial y} + H_z \frac{\partial H_z}{\partial y} \right),$$ (8.11)

$$F_z = \mu_0 \chi_w m \left(H_x \frac{\partial H_x}{\partial z} + H_y \frac{\partial H_y}{\partial z} + H_z \frac{\partial H_z}{\partial z} \right).$$

Depending on geometry of magnetic field Eq. (8.10) can be less complicated. It depends mainly on the structure of the separator (Nesset and Fingh, 1980). An approximated formula for the force acting on a particle in direction x is as follows:

$$F_x = \mu_0 \chi_w m \left(H_x \frac{\partial H_x}{\partial x} \right).$$ (8.12)

The magnetic force acting on a molecule is expressed in newtons. It results from the dimensional analysis of Eq. (8.11) or (8.12).

$$F_x = \frac{\mathrm{Vs}}{\mathrm{Am}} \frac{\mathrm{m}^3}{\mathrm{g}} \mathrm{g} \frac{\mathrm{A}}{\mathrm{m}} \frac{\mathrm{A}}{\mathrm{m}} \frac{1}{\mathrm{m}} = \frac{\mathrm{VAs}}{\mathrm{m}} = \frac{\mathrm{J}}{\mathrm{m}} = \mathrm{N}.$$ (8.13)

After placing a material in a magnetic field, it undergoes magnetization. The degree of substance magnetization M (A/m) in a magnetic field of intensity H depends on dimensionless (volumetric) magnetic susceptibility χ:

$$M = \chi H,$$ (8.14)

and magnetic polarization I (in teslas) is defined as:

$$J = \mu_0 \chi H.$$ (8.15)

As it has already been stated, substances can be divided into diamagnetics and paramagnetics. Paramagnetics however, do not form a homogenous group and can be divided into: genuine paramagnetics, ferromagnetics, ferrimagnetics and antiferromagnetics. This classification results from their diversified behaviour in magnetic field as the intensity of magnetic filed increases (Fig. 8.2).
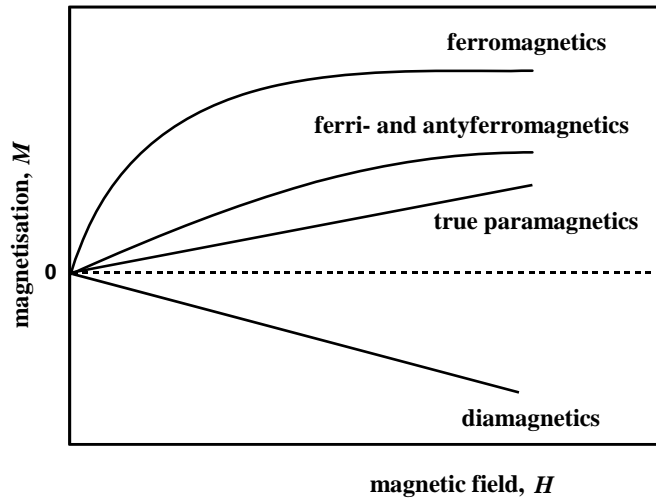
Fig. 8.2. Influence of magnetic field on magnetization of substances
allowing classification of paramagnetics into subgroups (after Svoboda, 1987)

Magnetic susceptibility, except for diamagnetics (Fig. 8.3), depends on the Néel temperature for antiferromagnetics and the Curie temperature for ferromagnetics (Fig. 8.3). This relation is descirbed by the Curie-Weiss law,

$$\chi = C'/(T - \Delta), \tag{8.16}$$

where:
C' i Δ – constants depending on material type
T – absolute temperature, K.
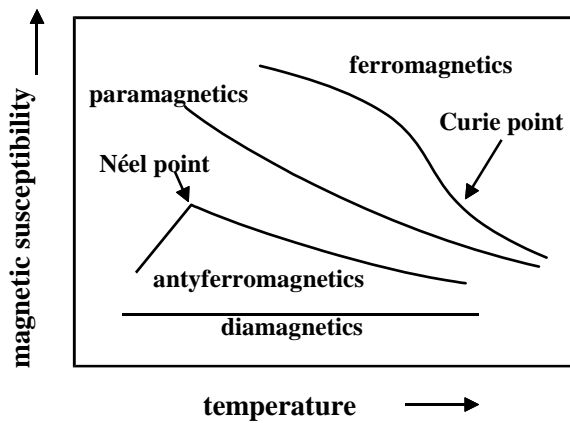
Fig. 8.3. Influence of temperature on magnetic susceptibility of substances
(after Svoboda, 1987)

For metals and semiconductors (Pauli paramagnetics) the relation between magnetic susceptibility and the temperature is more complicated (Encyklopedia Fizyki, 1973).

8.2. Diamagnetics

As it has already been mentioned, diamagnetics posses negative magnetic susceptibility in the order of 10^{-4} cm^3/g, which is dependent neither on temperature (Fig. 8.3) nor intensity of magnetic field (Fig. 8.2). Their negative susceptibility value result from screening of the external magnetic field by oppositely directed fields formed in diamagnetics. The list of selected diamagnetics and their specific magnetic susceptibility in SI units is presented in Table 8.3.

Table 8.3. Specific magnetic susceptibility of diamagnetic materials
(293 K, after Hopstock, 1985)

Mineral and its chemical formula	$-\chi_w (10^{-6}$ cm^3/g) (SI)	Mineral and its chemical formula	$-\chi_w (10^{-6}$ cm^3/g) (SI)
Elements			
Diamond, C	6.17	Silver, Ag	2.41
Graphite, C	44	Gold, Au	1.79
Sulfur, α-S	6.09	Bismuth, Bi	16.8
Copper, Cu	1.08		
Sulfides			
Sphalerite, ZnS	3.27	Stibnite, Sb$_2$S$_3$	3.17
Molybdenite, MoS$_2$	6.05	Cinnabar, HgS	2.99
Argentite, Ag$_2$S	3.71	Galena, PbS	4.40
Oxides			
Water (ice), H$_2$O	9,07	Cuprite, Cu$_2$O	1.76
Corundum, Al$_2$O$_3$	3.80	Zincite, ZnO	4.29
Quartz, SiO$_2$	6.20	Cassiterite, SnO$_2$	2.33
Halogens			
Halite, NaCl	6.49	Fluorite, CaF$_2$	4.51
Sylvite, KCl	6.54		
Carbonates			
Magnesite, MgCO$_3$	4.83	Cerusite, PbCO$_3$	2.88
Calcite, CaCO$_3$	4.80		
Sulfates			
Anhydrite, CaSO$_4$	4.47	Barite, BaSO$_4$	3.84
Gypsum, CaSO$_4$·2H$_2$O	5.33	Anglesite, PbSO$_4$	2.89
Smitsonite, ZnSO$_4$	3.41		

Magnetic susceptibility values of pure diamagnetics can be estimated on the basis of magnetic susceptibility of their ions (Table 8.4).

Table 8.4. Molar magnetic susceptibility of diamagnetic ions at w 293 K (20 °C)
(after Hopstock, 1985). For H^+ it can be assumed that $-\chi_M \cong 1 \cdot 10^{-6}$ cm^3/mol

Diamagnetic anions			
Anion	$-\chi_M(10^{-6}$ cm^3/mol) (SI)	Anion	$-\chi_M(10^{-6}$ cm^3/mol) (SI)
F^-	140	OH^-	150
Cl^-	330	NO_3^-	250
Br^-	450	CO_3^{2-}	430
I^-	650	SiO_3^{2-}	450
O^{2-}	150	SO_4^{2-}	500
S^{2-}	480	PO_4^{3-}	590
Diamagnetic cations			
cation	$-\chi_M(10^{-6}$ cm^3/mol) (SI)	cation	$-\chi_M(10^{-6}$ cm^3/mol) (SI)
Li^+	8	B^{3+}	3
Na^+	70	Al^{3+}	30
K^+	160	C^{4+}	1
Cu^+	150	Si^{4+}	20
Ag^+	300	Ti^{4+}	60
Au^+	500	Sn^{4+}	200
Mg^{2+}	40	N^{5+}	1
Ca^{2+}	100	P^{5+}	10
Sr^{2+}	190	V^{5+}	50
Ba^{2+}	300	S^{6+}	10
Zn^{2+}	130	Cr^{6+}	40
Cd^{2+}	280	Mo^{6+}	90
Hg^{2+}	460	W^{6+}	160
Pb^{2+}	350	V^{6+}	240
Ni^{2+}	140		

For example, molar magnetic susceptibility of quartz (SiO$_2$) is -20·10^4 cm^3/mol (Si^{4+}) + 2·(-150·10^{-4} cm^3/mol) (2 O^{2-})= -320·10^4 cm^3/mol, while specific magnetic susceptibility -320·10^{-4} cm^3/mol : 60g/mol = -5.33.10^{-4} cm^3/g. The calculated value of χ_w is similar to the experimental value of -6.20.10^{-6} cm^3/g presented in Table 8.3.

When diamagnetic substance contains paramagnetic impurities, its magnetic susceptibility can be positive and it can depend on the temperature and the intensity of magnetic field. Dolomite or cassiterite can serve as an example (Svoboda, 1985).

8.3. Paramagnetics

8.3.1. True paramagnetics

True paramagnetics feature positive magnetic susceptibility in the order of 10^{-3} cm^3/g which is not dependent on magnetic field. Such a relatively low value of magnetic susceptibility results from a negligible orientation of magnetic moments of elec-

trons in crystalline lattice of a particle placed in magnetic field. In the absence of magnetic field true paramagnetics do not store any magnetization. Their magnetic susceptibility decreases as the temperature decreases according to the Curie-Weiss equation (Eq. 8.16). True paramagnetics are also dielectrics. For metals of high number of conductivity electrons the dependence between magnetic susceptibility and the temperature is not significant. For conductors the relation between magnetic susceptibility and temperature is determined by other equations.

Some paramagnetic minerals and their magnetic susceptibility at room temperature are shown in Table 8.5.

Table 8.5. Magnetic susceptibility of selected true paramagnetics at room temperature

Paramagnetics	Susceptibility, χ_w (SI) cm^3/g*	Paramagnetics	Susceptibility, χ_M (SI) cm^3/mol**
$FeCO_3$	$1000 \pm 200 \cdot 10^{-6}$	UO_2	$29657 \cdot 10^{-6}$
$CuSO_4 \cdot 5H_2O$	$76.7 \cdot 10^{-6}$	$KMnO_4$	$251,3 \cdot 10^{-6}$
$FeSO_4$	$844 \cdot 10^{-6}$	Pt	$2537 \cdot 10^{-6}$
$NiSO_4 \cdot 7H_2O$	$201 \cdot 10^{-6}$	NiS	$2388 \cdot 10^{-6}$
MnO	$860 \cdot 10^{-6}$	MoO_3	$37,7 \cdot 10^{-6}$
CoS	$2827 \cdot 10^{-6}$	Al	$207,3 \cdot 10^{-6}$

* χ_w after Svoboda (1986/87)
** χ_M after CRC (1987)

8.3.2. Antiferromagnetics

In antiferromagnetics neighbouring elementary magnetic moments (magnetic domains) are arranged antipararelly. It means that there are two sub-lattices which compensate each other. As a result antiferromagnetics have, in relation to the ferromagnetics (strongly magnetic substances), low magnetic susceptibility. In weak magnetic fields ($H \leq 10^4$ A/m) magnetic susceptibility of antiferromagnetics practically does not depend on the field intensity H. Yet such dependence does occur at H from 10^4 to 10^5 A/m and usually equals from 10^{-3} to 10^{-5}. As the temperature increases, magnetic susceptibility of antiferromagnetics slowly increases due to disturbance of the magnetic structure, but this dependence cannot be described by the Curie-Weiss equation. Antiferromagnetics exist only up to a certain temperature, called the Néel point or Néel temperature T_N, above which antiferromagnetics become true paramagnetic and its dependence of magnetic susceptibility on the temperature decreases and then can be determined by the Curie-Weiss relation. Table 8.6 presents the susceptibilities of antiferromagnetics above their Néel temperature. More detailed list of antiferromagnetics is available in literature (CRS, 1986/87; CRS, 1997/98; Encyklopedia fizyki, 1972).

Table 8.6. Selected antiferromagnetics and their Néel point (temperature) θ_N, when they become true paramagnetics having constant magnetic susceptibility χ at a given temperature and obeying the Curie–Weiss equation $\chi = C/(T + \theta_p)$) (after CRC, 1986/87)

Antyferromagnetics	χ_M(cgs)	θ_N (K)	θ_p (K), for $T > \theta_N$
Hematite, Fe_2O_3	$3586 \cdot 10^{-6}$ (1033 K)	953	2940
Bunsenite, NiO	–	533–650	~2000
Pirrhotite, FeS*	$1074 \cdot 10^{-6}$ (293 K)	613	857
Cr_2O_3	$1960 \cdot 10^{-6}$ (300 K)	318	–
Tenorite, CuO	$238.6 \cdot 10^{-6}$ (289 K)	230	–
Alabandite, MnS	$3850 \cdot 10^{-6}$ (293 K)	165	528
Pirolusite, MnO_2	$2280 \cdot 10^{-6}$ (293 K)	84	–
Ilmenite, $FeTiO_3$		68	–
Siderite, $FeCO_3$	$11300 \cdot 10^{-6}$ (293 K)	57	–

* FeS is a bertolid (non-stoichiometric) compound and its properties depend on composition. $FeS_{1.10}$ and $FeS_{1.14}$ are ferromagnetic material

Hematite is an example of antiferromagnetism. At room temperature its magnetic susceptibility depends on the magnetic field and changes form 500 to $760 \cdot 10^{-6}$ cm^3/g, but above 950 K it becomes true paramagnetic featuring constant dependence of magnetic susceptibility on temperature. Information on the type of minerals is very important because it allows to predict the behavior of ore components at selected for separation magnetic fields.

8.3.3. Ferrimagnetics

Ferrimagnetics, similar to antiferromagnetics, contain oppositely oriented magnetic sub-lattices, which are not compensated and therefore in zero magnetic field they can show some magnetization. The name "ferrimagnetics" originates from oxides of ferrite type having a general formula of $MeO \cdot Fe_2O_3$ which belong to a wider group of spinels. A representative of ferrimagnetics is magnetite, i.e. ferric ferrite.

Table 8.7. Magnetic susceptibility of ferrimagnetic magnetite and antiferromagnetic pyrrhotite as a function of field intensity (after Svoboda, 1986/87)

Intensity of magnetic field H, kA/m	Specific (mass) magnetic susceptibility, χ_w (SI), cm^3/g	Intensity of magnetic field H, kA/m	Specific (mass) magnetic susceptibility, χ_w (SI), cm^3/g
Magnetite		Pyrrhotite	
2	1.40	1	$3.8 \cdot 10^{-2}$
4	1.65	8	$5.0 \cdot 10^{-2}$
8	2.75	16	$6.2 \cdot 10^{-2}$
16	2.25	24	$6.8 \cdot 10^{-2}$
24	1.80	32	$6.2 \cdot 10^{-2}$
32	1.53		
48	1.11		

Magnetic susceptibility of ferrimagnetics depends on the applied magnetic field. Above certain temperature, called the Néel temperature, magnetic susceptibility does not strictly follow the Curie-Weiss law. Ferrimagnetics are used in microwave ovens, permanent magnets, and transformers.

A change of the magnetic susceptibility for magnetite is related to the intensity of the magnetic field and is shown in Table 8.7.

8.3.4. Ferromagnetics

Ferromagnetics display certain magnetization even when the external magnetic field is not present. This phenomenon either occurs spontaneously or is a remnant of previous magnetization in the magnetic field. The most known representative of ferromagnetic substance is iron. Nickel and cobalt also belong to that group. Their magnetization exceeds several times that of other paramagnetics. Magnetization of ferromagnetics results from a spontaneous parallel positioning of magnetic moments of electrons. Above certain temperature, called the Curie temperature, the areas of spontaneous magnetization of ferromagnetics undergo destruction. In the case of iron it occurs above 1041 K while for nickel above 638 K. Then, ferromagnetics become true paramagnetic and they fulfil the Curie-Weiss law. Ferromagnetics are used for construction of magnetic separators equipped with either electromagnets or permanent magnets. In permanent magnet magnetic separators a high remnant magnetization B_r is utilized. The effect of the magnetic field on the magnetic induction and the presence of hysteresis and remnant magnetization B_r in ferromagnetics are shown in Fig. 8.4.
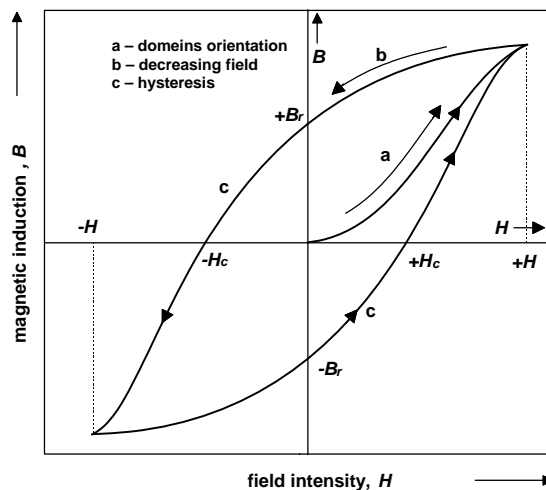
Fig. 8.4. Relationship between intensity of magnetic field and magnetic induction for ferromagnetics (after Frederikse, 1997/98)

Table 8.8. lists selected ferromagnetics of high value of remnant magnetization and high magnetic energy determined by integral B_rH.

Table 8.8. Selected ferromagnetic materials with significant remnant (B_r)
and energy product (BH)

Material	B_r (Tesla)	$(BH)_{max}$ (kJ·m^{-3})
Alnico 12 (13.5Ni; 8Al; 24.5Co; 2Nb)	1.20	76.8
PrCo$_5$	1.20	286
NdCo$_5$	1.22	295
Sm(Co$_{0.65}$Fe$_{0.28}$Cu$_{0.05}$Zr$_{0.02}$)$_{7.7}$	1.20	264
Fe; 23Cr; 15Co; 3V; 2Ti	1.35	44

8.4. Separation

The questions discussed so far involved the properties of diamagnetics and pa-ramagenetics (true paramagnetics, ferrimagnetics, antiferromagnetics, ferromagnetics). From a practical point of view substances are divided into magnetic and non-magnetic materials. Non-magnetic particles are characterized by zero or negative value of magnetic susceptibility while magnetic particles by positive values taking into account actual magnetic properties resulting from impurities which can considerably alter magnetic susceptibility of particles. SnO_2 or $(Ca, Mg)CO_3$ can serve as an example, which as pure chemical substances are non-magnetic, while their mineral equivalents, cassiterite and dolomite, always show some positive magnetism. Magnetic impurities can cause that magnetic susceptibility of contaminated material depends on the intensity of magnetic field. Magnetic susceptibilities of selected minerals (the previous Tables contained the values of magnetic susceptibility of pure substances) are shown in Tables 8.9 and 8.10. It should be added that the same minerals, originating from different sources, can feature different magnetic susceptibility.

Table 8.9. Specific (mass) magnetic susceptibility of selected magnetic minerals at ambient temperature. The values significantly depends on the mineral origin and impurities content (after Svoboda, 1987)

Paramagnetics	Susceptibility χ_w (SI), cm^3/g	Paramagnetics	Susceptibility χ_w (SI), cm^3/g
Goethite, FeOOH	250–380·10^{-6}	Malachite, Cu$_2$(OH)$_2$CO$_3$	100–200·10^{-6}
Hausmanite, Mn$_3$O$_4$	500–760·10^{-6}	Monacite, (Ce,La,Dy)PO$_4$	120–250·10^{-6}
Ilmenite, (Fe, Mn)TiO$_3$	200–1500·10^{-6}	Siderite, FeCO$_3$	380–1500·10^{-6}
Limonite, Fe$_2$O$_3$·H$_2$O	250–760·10^{-6}	Wolframite, (MnFe)WO$_4$	380–1200·10^{-6}

For a successful separation of minerals their magnetic susceptibility must be significantly different. According to Dobby et al. (1979) the ratio of magnetic susceptibility of particles undergoing separation should be at least as 20 to 1. The selectivity of separation depends not only on the differences in magnetic susceptibility but also on the changes of the susceptibility with magnetic field, as well as on particles size. Therefore, each raw material can be subjected only to a carefully chosen type of sepa-

rator. Figure 8.5 shows different devices that can be used for magnetic separation, depending on particle size and the method of separation (dry or wet). Within each kind of separation there do exist many varieties of devices produced by different manufactures as typical ones or as the equipment made on request.

Table 8.10. Specific (mass) magnetic susceptibility of minerals (after Hopstock, 1985)

Mineral	Chemical formula	χ_w $(10^{-3}$ cm^3/g) (SI)
Sulfides		
Pyrite	FeS_2	0.004–0.013
Markasite	FeS_2	0.004–0.013
Millerite	NiS	0.003–0.048
Chalcopyrite	$CuFeS_2$	0.011–0.055
Bornite	Cu_5FeS_4	0.092–0.100
Arsenides		
Nickeline	$NiAs$	0.005–0011
Oxides		
Goethite	$FeOOH$	0.38–0.46
Manganite	$MnOOH$	0.36–0.50
Pyrolusite	MnO_2	0.30–0.48
Wolframite	$(Fe, Mn)WO_4$	0.40–0.53
Chromite	$FeCr_2O_4$	0.32–0.38
Carbonates		
Siderite	$FeCO_3$	1.06–1,30
Rodochrosite	$MnCO_3$	1,31–1,34
Silicates		
Olivine	$(Mg, Fe)_2SiO_4$	0,11–1,26
Orthopiroxene	$(Mg, Fe)SiO_3$	0,04–0,92
Clinopiroxene	$Ca(Mg, Fe)(SiO_3)_2$	0,08–0,80
Amphiboles	Hydrated silicates	0,08–1,13
Biotite	$K(Mg, Fe)_3AlSi_3O_{11} \cdot H_2O$	0.05–0.98
Cordierite	$(Mg, Fe)_2Al_4Si_5O_{18}$	0.08–0.41
Garnet	$(Ca, Mg, Fe, Mn)_3(Al, Fe, Cr)_2$ $(SiO_4)_3$	0.14–0.95
Rodonite	$(Mn, Ca)SiO_3$	0.67–1.10
Dioptase	$CuSiO_3 \cdot H_2O$	0.106–0.111
Garnierite	$(Ni, Mg)SiO_3 \cdot H_2O$	0.38–0.39

It was shown in Fig. 8.5 that separators can be divided into the devices working in dry or wet environment. This classification results from the fact that separation of fine magnetic particles can be conducted exclusively wet. Another classification is based on the parameters which influence the magnetic force acting on a particle. It was shown in Eq. (8.12) that the magnetic force acting on a particle is proportional to $\chi_w H \cdot dH/dx$, thus the following separators can be distinguished:

- low intensity magnetic separator (low *H* values) – abbreviation: LIMS,
- high intensity magnetic separator (high *H* values) – HIMS,

- high gradient magnetic separator (high d*H*/d*x* values) – HGMS,
- isodynamic (constant *H* d*H*/d*x* values),
- other, e.g. high intensity low gradient magnetic separator (Svoboda, 1987).

 The principle of separation in low intensity magnetic field devices, operating both in air and water, are shown in Fig. 8.6. Among the wet separators there can be distinguished not only parallel current, but also counter–current, counter–rotary and other types of separators (Svoboda, 1987). LIMS separators are applied for strongly magnetic particles.
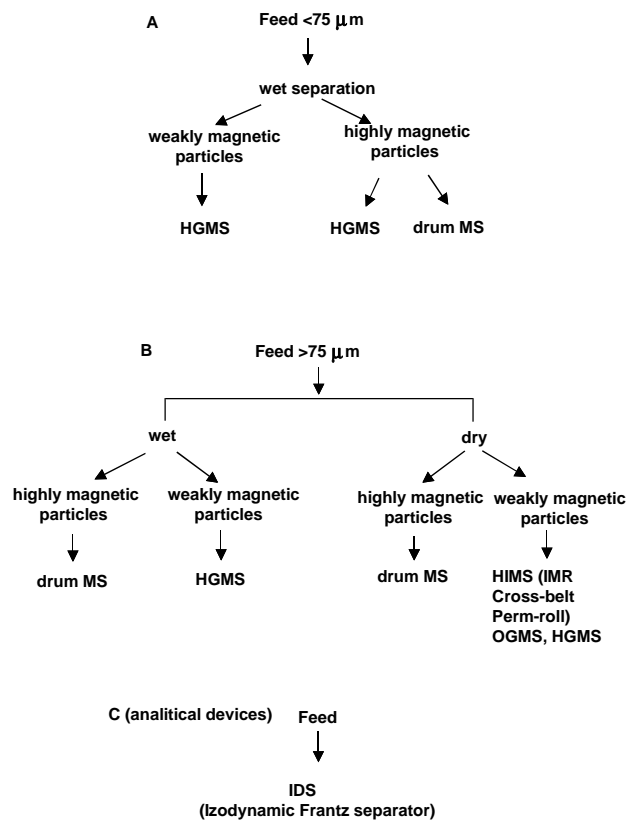
Fig. 8.5. Types of magnetic separations classified according to particle size and way of separation: drum MS – separation in a field of low intensity of magnetic field (or shortly LIMS), HIMS – separation in high intensity magnetic field, e.g. IMR (induced magnetic roll), HGMS – separation in high gradient magnetic field, OGMS – separation in an open gradient field in superconducting devices, IDS – separation in isodynamic magnetic field
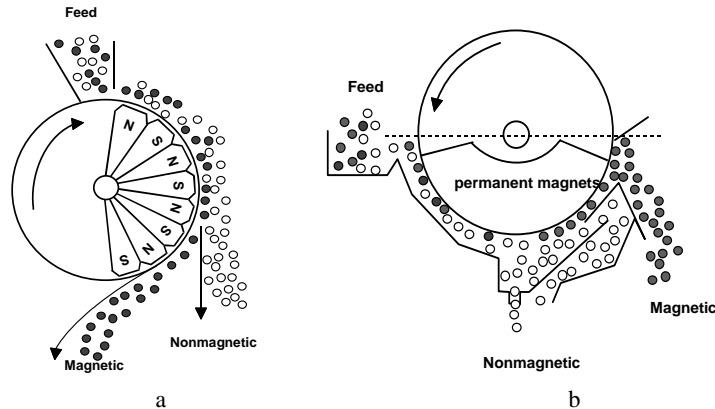
Fig. 8.6. Operating principle of low intensity magnetic field separators
(LIMS = drum MS): a – drum separator for dry separation , b –drum (parallel current type) for wet sepa-
ration (after Svoboda, 1987)

For separation of coarse particles of low magnetic susceptibility high intensity
separators (HIMS) are used and the principles of separation are shown in Fig. 8.7. One
of them is the separator in which strong magnetic fields are achieved due to supercon-
ductivity of electrical coils at low temperatures. There are numerous types of the
HIMS separators. Some of them, described by Svoboda (1987) are: Cross-belt, Perm-
roll (Ore Sorters), induction magnetic separator (Eriez Magnetics, Carpco, Inc.),
Laurilla, wet belt conveyor (Hyland), Ferrous Wheel).

Magnetic separation can be also conducted in the devices featuring considerable
gradient of the magnetic field (HGMS). This kind of separation is applied both for fine
and coarse particles. The latter separation is usually conducted in water.

Typical representative of the HGMS separators family is the Jones separator whose
operation principle is shown in Fig. 8.8. Variation of the magnetic field can be ob-
tained due to filling the spaces between magnet or electromagnet poles with magnetic
material. The filling can be metal wool or metal inserts shaped in a special way, which
guarantees a high dH/dx value, i.e. significant curvature of magnetic field lines. In
these separators the process of separation is performed in a cyclic mode. In the first
stage, the feed is passing through a separator while the magnetic particles are arrested
by the filling of the separator. In the second stage the magnetic field is turned off or
the filling removed and then, magnetic particles are washed out by water.

In order to obtain a continuous process, carousel type devices are applied, whose
special mechanisms turn batch processes into a cyclic process. The separator possesses
many sections which gather magnetic particles in one cycle, i.e. provide non-magnetic
product. In the second cycle, they provide magnetic particles. Both types of sections
work simultaneously. Therefore, the whole separator works as a continuous device.
The scheme of the continuous Jones separator is shown in Fig. 8.9.

A completely different type of magnetic separator is the Frantz isodynamic separator. It is built in such a way that the force acting on a particle is constant within the whole area of magnetic field. It is used in laboratories for determining magnetic properties of particles, including magnetic susceptibility and the potentials of separation. It represents analytical type of devices. Figure 8.10 shows the Frantz separator and forces effecting the particles.

Sometime an ore requires special preparation for a successful separation by magnetic methods. The preparation consists of:

- selective covering of diamagnetic particles with magnetite (Parsonage, 1984),
- magnetite hydrophobization with the use of silanes, enabling adhesion of fine particles such as gold to magnetite (Gray et al., 1994),
- roasting of weakly magnetic minerals (limonite, siderite, Laskowski and Luszczkiewicz, 1989) to convert them into ferrimagnetic magnetite,
- magnetizing leaching e.g. siderite with sodium hydroxide (Krukiewicz and Laskowski, 1973).
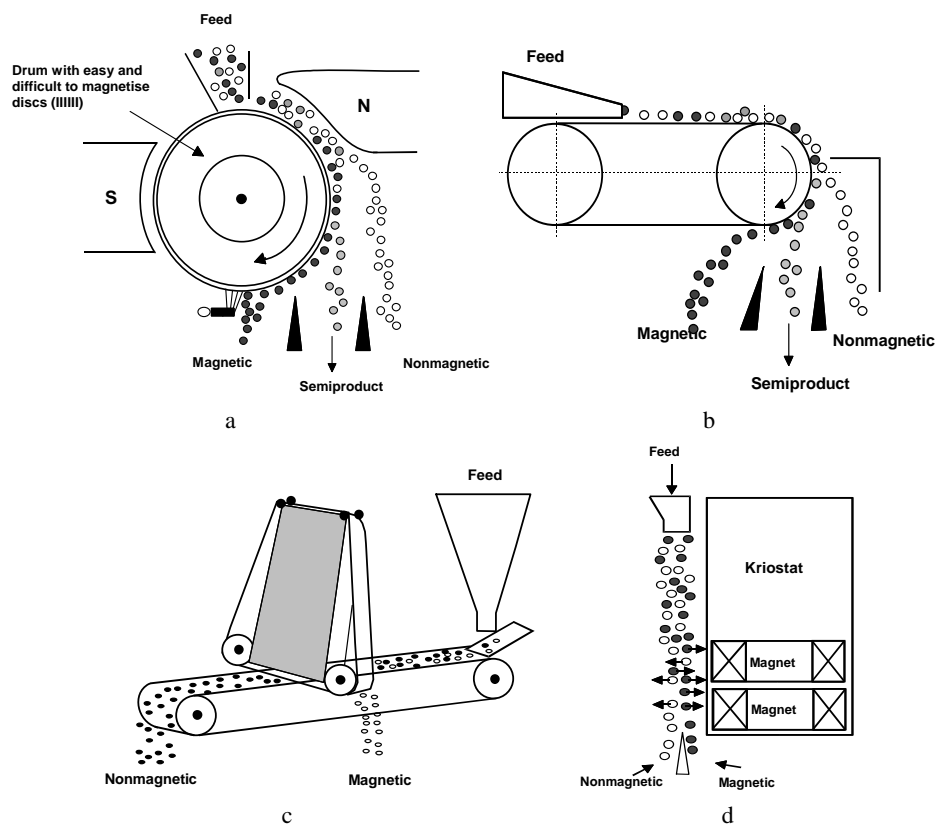
Fig. 8.7. Operating principle of the HIMS separators: a – IMR (induced magnetic roll),
b – Cross-belt, c – Permroll, d – separation in an open gradient superconducting separator (OGMS)
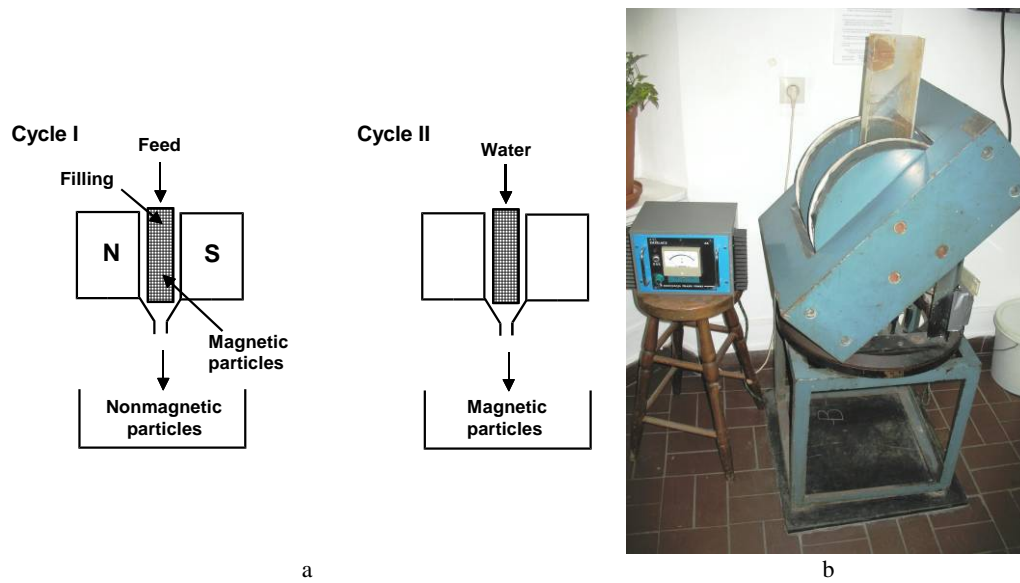
Fig. 8.8. Operating principle of the Jones HGMS separator (a) and a photograph of a laboratory Jones separator (b)
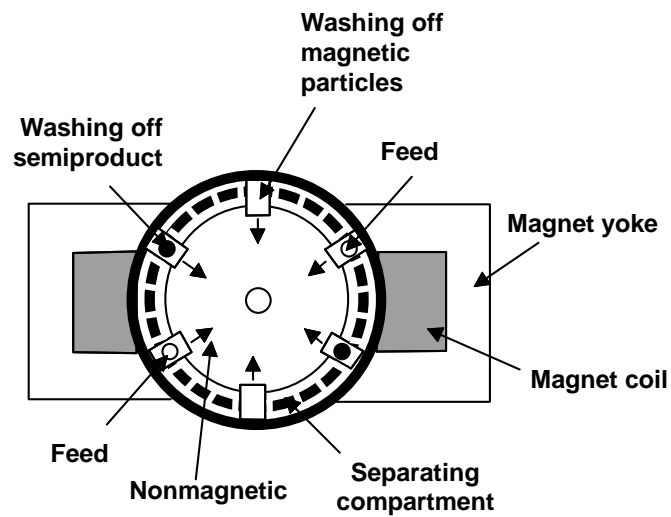
Fig. 8.9. Operating principle of the HGMS carousel type Jones separator which works continuously
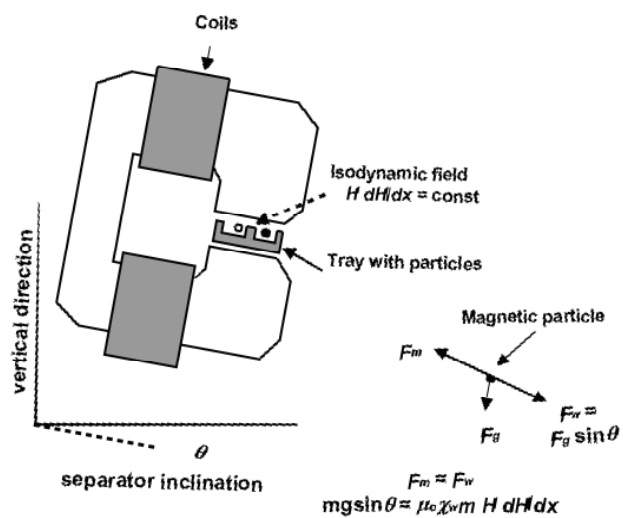
Fig. 8.10. Operating principle of the Frantz isodynamic separator
(IDS) (after Svoboda, 1987 with modifications) (a) and its photograph (b)

Literature

CRC, 1986/87. Handbook of Chemistry and Physics, 67th Edition, CRC Press, Boca Raton, Florida, USA, E-119–E-124.

CRC, 1997/98. Handbook of Chemistry and Physics, 78th Edition, CRC Press, Boca Raton, Florida, USA, 12–117.

Dobby G., Nesset J., Finch J.A., 1979. Mineral recovery by high gradient magnetic separation, Canadian Metallurgical Quarterly, 18, 293–301.

Encyklopedia fizyki, 1972. Praca zbiorowa, PWN, Warszawa.

Frederikse H.P.R., 1997/98. CRC Handbook of Chemistry and Physics, 78th Edition, CRC Press, Boca Raton, Florida, USA, s. 12–115.

Gray S.R., Langberg D.E., Gray N.B., 1994. Fine mineral recovery with hydrophobic mag-netite, Int. J. Min. Process., 41, 183–200.

Gupta R.R., 1986/87. Diamagnetic susceptibility data of organosilicon compounds, in: CRC, Handbook of Chemistry and Physics, 67th Edition, CRC Press, Boca Raton, Florida, USA, E-132–E-135.

Hopstock D.M., 1985. SME Mineral Handbook, L.Weiss ed., SME/AIME, New York, 6.19.

Ibach H., Lüth H., 1966. Fizyka ciała stałego, PWN, Warszawa.

Laskowski J., Luszczkiewicz A., 1989. Przerobka kopalin. Wzbogacanie surowcow mineralnych, Wydawnictwo Politechniki Wrocławskiej, Wrocław.

Krukiewicz P., Laskowski J., 1973. Development of a magnetizing alkali leaching process for a concentration of siderite ores, Xth Int. Mineral. Proc. Cogress, London, 391.

Nesset J.E., Finch J.A., 1980. Determination of magnetic parameters for field-dependent susceptibility minerals by Frantz isodynamic magnetic separator, Trans. IMM, Sec.C., 89, C161–C166.

Parsonage P., 1984. Selective magnetic coating for mineral separation, Trans. IMM, 93, C37-C44.

Smith G.W., 1986/87. Diamagnetic susceptibility of organic compounds, in: CRC, Handbook of Chemistry and Physics, 67th Edition, CRC Press, Boca Raton, Florida, USA, E-124–E-132.

Svoboda J., 1987. Magnetic methods for the treatment of minerals, Developments in Mineral Processing, 8, D.W. Fuerstenau (series Ed.), Elsevier, Amsterdam.

9. Eddy current separation

Materials conducting electric current can be separated from non-conductors utilizing eddy currents. Eddy current is induced in electric conductors placed in the alternating magnetic field. Eddy currents create the force called the Lorentz force, which moves the particles.

The force F acting on a particle which conducts electric current in an electric field *E* is:

$$F = \mathbf{U} \int_V \sigma E \ \mathbf{B} \mathrm{d}E \ ,$$ (9.1)

where:
V – particle volume
U – matrix of location of a particle in relation to the separator
σ – electrical conductivity of particle, $\Omega^{-1} \cdot \mathrm{m}^{-1}$
E – electric field
d*E* – electric field gradient
B – electric field vector.

Typical values of the electric conductivity (in $\Omega^{-1}\mathrm{m}^{-1}$) at 293 K are: aluminium $3.77^{.}10^{7}$, coppers $5.96^{.}10^{7}$, silica glass (Clear, at 623 K) from $2.5^{.}10^{-4}$ to $3.3^{.}10^{-9}$ quartz ~0, plastic ~0. The values of electrical conductivity for other substances and minerals can be found, for instance, in the form of electrical resistance being a reciprocal of conductivity (CRC, 1986/87). It results from Eq. (9.1) that the Lorentz force (Fig. 9.1) does not depend on the magnetic properties of particles because the eddy currents occur both in paramagnetic (aluminium) and diamagnetic (copper) conductors.

The principle of particles separation in eddy currents separators utilizing eddy currents induced in conductors is shown in Fig. 9.2. The eddy currents separator usually consists of a belt conveyor which transports the material subjected to enrichment and a drum placed at the belt end. The drum is covered with magnets placed alternatively as to their N-S poles and it moves independently and faster than the belt. Fluctuating magnetic poles of the rotating drum induce eddy currents in the objects conducting electric current. The Lorentz force of the eddy currents accelerates conducting particles along the direction of the rotation drum pushing the particles to fall much further than the non-conductive particles falling just behind the drum.
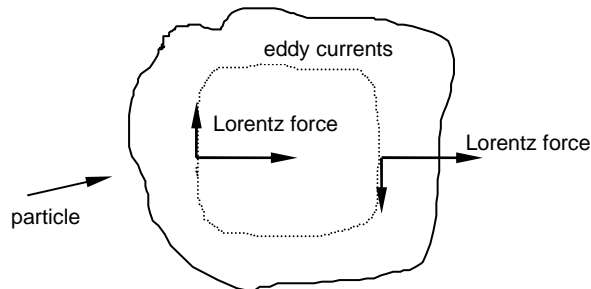
Fig. 9.1. The Lorentz forces operating in a particle in the presence of eddy currents

belt conveyor
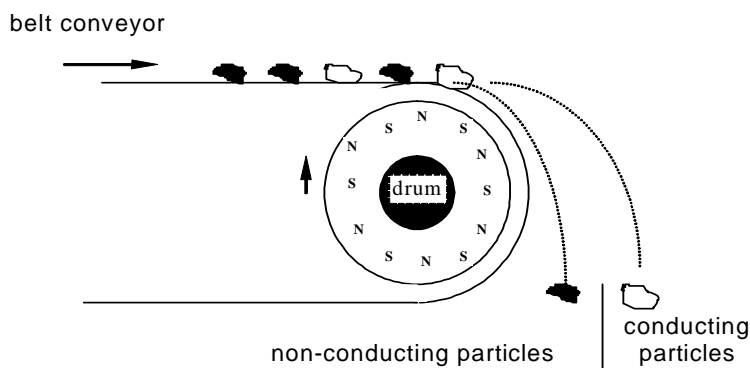
Fig. 9.2. Principle of separation by mean of eddy currents (after Rem et al., 1997)

Separation with eddy currents is applied for removing non-ferrous metals, mainly copper and aluminium and their alloys, from car scraps, as well as for separating metals from glass or plastic in plants processing municipal garbage (Dalmijn, 1990). The technology of separation using eddy currents has been known for a long time. It was patented by Edison in 1889. Eddy currents separators are produced for instance by Bakker Magnitics Company. There are also wet eddy current separators (Rem et al., 2000).

Literature

CRC, 1986/87. Handbook of Chemistry and Physics, 67th Edition, CRC Press, Boca Raton, Florida, USA.

Dalmijn W.L., 1990. Practical applications of eddy current in the scrap recycling, in: Second International Symposium Recycling of Metals and Eng. Materials, the Minerals, Metals and Materials Society.

Edison T.A., 1889. US Patent 400, 317.

Rem P.C., Leest P.A., van den Akker A.J., 1997. A model for eddy current separation, Int. J. Miner. Process, 49, 193–200.

Rem P.C., Zhang S., Forssberg E., de Jong T.P.R., 2000. The investigation of separability of particles smaller than 5 mm by eddy-current separation technology, part II, Novel design concept, Magnetic and Electrical Separation, 1, 85–105.

10. Dielectric separation

There are at least three important electric properties of the materials: conductivity, dielectric constant, and surface electrification. Differences in particles conduction are utilized in eddy current separation, differences in electric charges in electric separation, while differences in dielectric constants in dielectric separation. The dielectric separation is based on the principle stating that particles, in the presence of a non-homogeneous electric field, having dielectric constant (ε_{p1}) higher than that of the nonconducting medium (ε_m) in which they are immersed, move from low to high field strength zone, while particles of lower dielectric constant (ε_{p2}) than the medium are directed into a zone of low field strength (Fig. 10.1.).
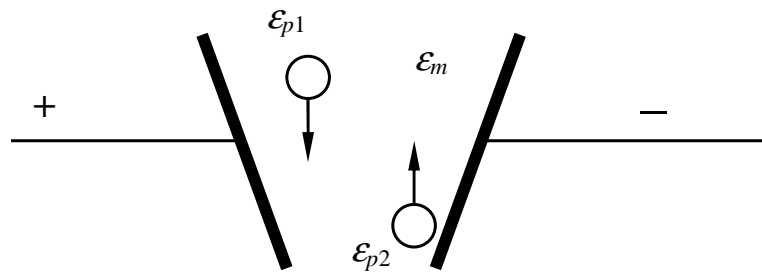
Fig. 10.1. Dielectric separation. The case when $\varepsilon_{p1} > \varepsilon_m > \varepsilon_{p2}$. The electric field in the upper part of separator, due to inclination of the electrodes, is lower than that in the bottom part. Arrows indicate direction of particles movement

The dielectric constant represents the proportionality constant between the electric field **D** (Ibach and Lüth, 1996) and electric field induction **E**:

$$\mathbf{D} = \varepsilon_o \varepsilon \mathbf{E} \tag{10.1}$$

where:
D – electric field induction vector also called the electric shift ($C \cdot m^{-2}$)
E – electric field vector (niuton·kulomb^{-1}, that is N C^{-1} or V m^{-1}),
ε – dielectric constant (dimensionless) also called relative dielectric constant or relative permittivity
ε_0 – electric constant (permittivity of free space sometimes also called vacuum permittivity) ($8.854 \cdot 10^{-12}$ C^{2}N^{-1}m^{-2} or As^{-1} m^{-1}).
Vectors **D, E** are marked in bold.

The dielectric constant ε is relative because it is determined by comparing dielectric static permittivity of the material ε_s to the electric constant ε_0 (Jaworski et al., 1971):

$$\varepsilon = \frac{\varepsilon_s}{\varepsilon_0} \qquad (10.2)$$

There is one more dielectric quantity called electric susceptibility(κ_e). It is defined as the constant of proportionality (a tensor binding vectors of the electric field **E** and induced dielectric polarization density **P):**

$$\mathbf{P} = \varepsilon_o \kappa_e \mathbf{E} \qquad (10.3)$$

The susceptibility of a medium is related to its relative permittivity (dielectric constant) ε by:

$$\kappa_e = \varepsilon\text{-}1 \qquad (10.4)$$

For vacuum $\kappa_e = 0$. It is based on the fact that when we place dielectric material in the electric field, polarization of electric domains occurs and their values are characterized by the polarization vector **P** which can be written as:

$$\mathbf{D} = \varepsilon_0 \, \mathbf{E} + \mathbf{P}. \qquad (10.5)$$

Since the vector of polarization is proportional to **E**, therefore:

$$\mathbf{D} = \varepsilon_0 \, \mathbf{E} + \varepsilon_0 \, \kappa_e \, \mathbf{E} = \varepsilon_0 \, (1 + \kappa_e \,)\mathbf{E} \qquad (10.6)$$

The electric susceptibility (κ_e), like magnetic susceptibility, can be expressed as specific (κ_g) and as molar (κ_M). The specific electric susceptibility κ_g (cm^3/g) is obtained by dividing the dimensionless dielectric constant κ_e by material density while κ_M (cm^3/mol) is a result of multiplying κ_g by substance molar mass (m$_M$, g/mol).

The dielectric separation is based on the dielectric constant (electric susceptibility) of materials. The values of dielectric constants for different materials, including vacuum and water, are given in Table 10.1.

The dielectric separation is based on the principle that a particle having dielectric dipoles characterized by the dielectric constant $\varepsilon = \varepsilon_p$ inserted in a medium of dielectric constant $\varepsilon = \varepsilon_m$ and effected by nonhomogenous electric field E (N C^{-1}) with field gradient dE/dx (N C^{-1} m^{-1}), is subjected to an electric ordering force F_p (N), expressed by the formula:

$$F_d = 4\pi \varepsilon_0 \varepsilon_p r^3 \frac{\varepsilon_p - \varepsilon_m}{\varepsilon_p + 2\varepsilon_m} E \frac{dE}{dx} , \qquad (10.7)$$

where:

F_p – (ponderomotoric) electric force acting on particle in an electric field

r – particle radius, m,

ε_p and ε_m – dimensionless dielectric constants for particle and medium, respectively.

Table 10.1. Dielectric constants for different materials at room temperature (after Young and Frederikse, 1973). For anisotropic materials three values are given: ε_{11}, ε_{22}, and ε_{33} for *x*, *y*, and *z* directions, respectively

Substance	ε	Field frequency Hz	Substance	ε	Field frequency Hz
Fluorite, CaF_2	6.81		sphalerite, ZnS	$\varepsilon_{11} = 8.3$	10^4
Calcite, $CaCO_3$	8.6	$9.4 \cdot 10^{10}$	cuprite, Cu_2O	7.6	10^5
Ice, H_2O (243K)	99 (0 kbar) 117 (3 kbar)	static* static	beryl, $Be_3Al_2Si_6O_{18}$	$\varepsilon_{33} = 5.95$	$7 \cdot 10^3$
Halite, NaCl	5.9	10^2–10^7	scheelite, $CaWO_4$	$\varepsilon_{11} = \varepsilon_{22} = 11.7$ $\varepsilon_p = 9.5$	$1.59 \cdot 10^3$ $1.59 \cdot 10^3$
Sulfur, S	3.75; 3.95; 4.44	10^2–10^3	gypsum, $CaSO_4 \cdot 2H_2O$	5.1; 5.24; 10.30	
Cyclohexane	2.023	static	galena, PbS	200 ± 35	infrared
CCl_4	2.238	static	carborundum, SiC	9.72	infrared
Benzene	2.284	static	quartz , SiO_2	4.42; 4.41; 4.60	$9.4 \cdot 10^{10}$
1,2–dichloroethane	10.65	static	barite, $BaSO_4$	11.4	10^8
Methanol	33.62	static	Al_2O_3	$\varepsilon_{11} = \varepsilon_{22} = 9.34$	10^2–$8 \cdot 10^9$
Water	78.36 5.2	0 upper limit	diamond, C	5.87	10^3
Vacuum	1		asphalt	2.68	$< 3 \cdot 10^6$

* values extrapolated to zero field frequency

    The expression for the ponderomotoric force depends on the geometry of the system. Lin et al. (1981) presented the expression for polarized particles interacting with the electric field formed by the a conductor of circular cross section.

    It results from Eq. 10.7 that the conditions under which the ponderomotoric force occurs is the existence of not only the electric field but also electric field gradient dE/dx. As it was presented at the beginning of the chapter, a particle will be effected by a positive force when its dielectric constant is higher than that of the medium and it will be pulled into electric field. The particles having dielectric constant lower than that of the medium will be pulled out of the electric field. The so called cut-value of the dielectric constant ($\varepsilon_{50} = \varepsilon_m$) of particles subjected to separation is regulated by the use of liquids featuring appropriate dielectric constant.

The dielectric separators are rarely used on a larger scale since the forces effecting the particles are of low values. Dielectric separation has been tried for the enrichment of chromite ores (Kelly and Spotiiswood, 1982).

It can be added that the electric constant (vacuum permittivity ε_0) is connected with the magnetic permeability according to the following relation:

$$\varepsilon_0 = \frac{1}{\mu_0 c^2},$$

(10.8)

where:

μ_0 – magnetic permeability of vacuum ($4\pi\ 10^{-7}$ V s A^{-1} m^{-1})

c – speed of light ($2.997925 \cdot 10^8$ m/s).

The dielectric constants can be affected by such parameters as temperature, intensity of the electric field and its frequency (Table 10.1). The substances for which the dielectric constant does not depend on the field intensity are called paraelectrics. For paraelectrics the temperature does not strongly effects the values of the dielectric constant. The substances whose dielectric constant depends on the electric field intensity are called ferroelectrics. The list of selected ferroelectrics is given in Table 10.2. A characteristic feature of the ferroelectric materials is their hysteresis. Ferroelectrics considerably alter their relative dielectric permeability as the temperature changes. There also exists a certain temperature, called the Curie point or temperature above which ferroelectrics become paraelectrics. Ferroelectrics are used for the production of high capacity and small size condensers, as well as for modulation of the frequency of electromagnetic oscillation.

Table 10.2. Selected ferroelectrics and antiferroelectrics and their Curie temperature (T_C)
(after CRC, 1998)

Ferroelectrics		Antiferroelectrics	
substance	T_C, K	substancje	T_C, K
KH$_2$PO$_4$ ($\varepsilon = 46$)	123	NH$_4$H$_2$PO$_4$ ($\varepsilon_{11,22} = 57,1$)	148
NH$_4$HSO$_4$ ($\varepsilon = 165$)	397	NaNO$_2$ ($\varepsilon_{11} = 7,4$)	437
BaTiO$_3$ ($\varepsilon_{11} = 3600$)	406	PbZrO$_3$ ($\varepsilon = 200$)	503
NaNO$_3$ ($\varepsilon = 6,85$)	548	NaNbO$_3$ ($\varepsilon_{33} = 670$)	911
PbTiO$_3$ ($\varepsilon = {\sim}200$)	765	WO$_3$ ($\varepsilon = 300$)	1010

Another group is formed by antiferroelectrics. The structure of these materials consists of permanent dipoles located on adherent planes but they are arranged opposite to each other which partially causes their compensation. Examples of antiferroelectrics are shown in Table 10.2. Their Curie temperature above which they become paraelectrics is also included.

Literature

CRC, 1997/98. Handbook of Chemistry and Physics, 78th Edition, CRC Press, Boca Raton, Florida, USA.

Ibach H., Lüth H., 1996. Fizyka ciała stałego, PWN, Warszawa.

Jaworski B., Dietlaf A., Milkowska L., 1971. Elektryczność i magnetyzm. Kurs fizyki, t. II, wyd. III, PWN, Warszawa.

Kelly E.G., Spottiswood D.J., 1982. Introduction to mineral processing, Wiley, New York.

Laskowski J., Luszczkiewicz A., 1989. Przeróbka kopalin. Wzbogacanie surowców mineralnych, Wydawnictwo Politechniki Wrocławskiej, Wrocław.

Lin I.J., Yaniv I., Zimmels Y., 1981. On the separation of minerals in high-gradient electric fields, XIII IMPC, PWN, Warszawa, 1168–1194.

Rao C.N.R., Rao K.J., 1992. Ferroics, in: Solid state chemistry, A.K. Cheetham and P. Day (eds.), Clarendon Press, Oxford, 1992.

Young K.F., Frederikse H.P.R., 1973. J. Phys. Chem. Ref. Data, 2, 313, 1973 or CRC, Handbook, 1998.

11. Electric separation

The electric separation is based on interaction of electrically charged particles with the electric field. The ordering electric force $\mathbf{F}_{el}$ appearing in the separation system is a result of the electric field $\mathbf{E}$ (V/m) and the electric charge of particle Q_t at the moment of separation.

$$\mathbf{F}_{el} = Q_t \, \mathbf{E} = A \, q \, \mathbf{E} \qquad (11.1)$$

where
A – surface area of particle, m^2
q - surface electric charge of particle, (C/m^2)
Q_t –electric charge of particle (it can be negative or positive and of different magnitude).

The bold-faced symbols F and E are vectors.

A general scheme of the electric separation is shown in Fig. 11.1.
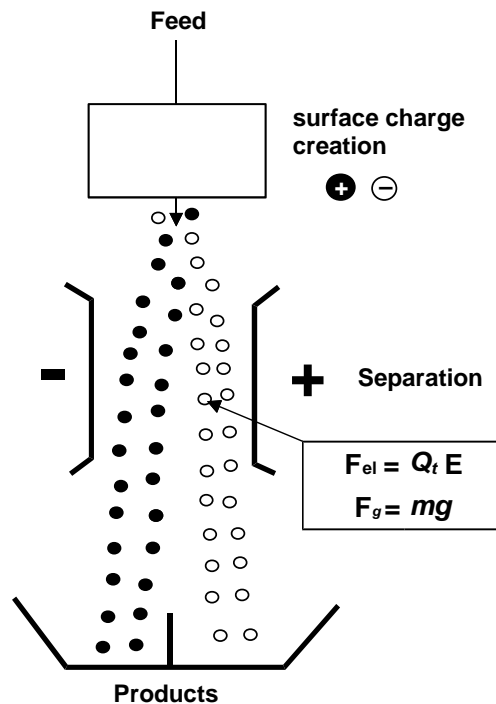
Fig. 11.1 General scheme of electric separation. There are different methods of electrification and different ways of separation. The symbol are explained in the text

The electric force acting on a particle in an electric separator results from the Coulomb law which describes the force of interaction between two elemental charges Q_1 and Q_2. When the charges are immobile in relation to each other and to the observer and are situated at a distance h from each other (Nussbaum, 1985):

$$F_{el} = -\frac{1}{4\pi\varepsilon_0}\frac{Q_1 Q_2}{h^2}, \tag{11.2}$$

where:
Q_1, Q_2 - elemental charges
h – distance between charges
ε_o - electric constant (permittivity of free space) ($8.854\cdot10^{-12}$ $C^2N^{-1}m^{-2}$)
$\pi = 3.14$.

Equations 11.1 and 11.2 are equivalent because charges Q_1 and Q_2 generate the electric field E.

There are other forces which can be present in electric separation systems including gravity, centrifugal, and ponderomotoric forces. The gravity force is expressed by the equation:

$$F_g = mg = (1/6)\,\pi\,d^3\rho\,g \tag{11.3}$$

where:
m - mass of particle
ρ - density of particle
d - size (diameter) of particle
g - acceleration due to gravity
$\pi = 3.14$.

The centrifugal force is characterized by the relation:

$$F_o = (1/6)\pi\,d^3\rho\,\omega^2 R, \tag{11.3}$$

where:
R – movement radius
ω - angular velocity.

Appropriate combination of the forces acting in the separation system (Fig. 11.1) create stratification of particles which then are split into products (Urvancev, 2000).

The surface static electric charge can be created on any particle. Its value and sign depend on the mode of electrization. The electrification results from the transfer of electrons from one particle to another or to particle environment as a result of a direct or indirect contact. Although the surface charge can be created on any substance, not all materials are capable of keeping the charge on their surface long enough for sepa-

ration to be successful. The magnitude of real surface charge of a particle is a function of time (Simorda and Stanoba, 1970; Nussbaum, 1985):

$$Q_t = Q_0 \exp(-t/\tau), \tag{11.4}$$

where:
Q_o – electric charge at the moment of its creation (t=0)
Q_t – electric charge at a time t
τ – relaxation time
t – time since the electrization.

Equation 11.4 can be modified into a more practical form (Olofinskij, 1970; Nussbaum, 1985):

$$Q_t = Q_0 \exp(-\sigma t/\varepsilon\varepsilon_0), \tag{11.5}$$

where:
σ – conductivity ($\Omega^{-1}\mathrm{m}^{-1}$)
ε – dielectric constant of particle (dimensionless)
ε_0 – permittivity of free space ($8.854 \cdot 10^{-12}$ $\mathrm{C}^2\mathrm{N}^{-1}\mathrm{m}^{-2}$)
t - time.

The conducting materials, for instance metals, do not keep their electric charge long on their surface, while non-conductive substances (non-conductors) maintain the surface charge relatively longer. The stability of particle surface charge is effected by air humidity and temperature which also alters the particle conductivity. The influence of humidity on particle charge is usually described by the empirical equation (Laskowski and Luszczkiewicz, 1989):

$$\log \sigma = a + b\,c \tag{11.6}$$

where:
a, b – constants
c – relative humidity of air.

The above considerations indicate that the main parameter of electric separation is the electric charge present on the particle surface at the moment of acting of the electric field which creates the stratification force. The parameters affecting particle charge Q_t are initial charge Q_o, time t which elapsed from the charging to the moment of separation, and the conductivity σ (both volumetric and superficial) (Fig.11.2). The initial charge, in turn, depends on the way of electrization and the kind of substance, which is characterized by such parameters as work function, dielectric constant, contact potential, and others. The values of work function, that is the energy needed to remove the electron from the surface of material are given in Tables 11.1.

Table 11.1. Work function (work to remove electron), w, eV

Material	Work function, eV	Source
CS_2	0.99 - 1.117	1
BaO	1.10	1
$(Ba,Sr)CO_3$	1.25	1
SrO	1.27	1
CaO	1.60 ±0.20	1
Y_2O_3	2.00	1
Gd_2O_3	2.10	1
Tb_2O_3	2.10	1
Dy_2O_3	2.10	1
Ho_2O_3	2.10	1
Nd_2O_3	2.30	1
Er_2O_3	2.40	1
ThO_2	2.54	1
Eu_2O_3	2.60	1
La_2O_3	2.80	1
Pr_6O_{11}	2.80	1
Sm_2O_3	2.80	1
UO_2	3.15	1
CeO_2	3.21	1
U	3.63 - 3.90	4
BeO	3.80 - 4.70	1
FeS_2	3.8	2
FeO	3.85	1
graphite	4.00	1
Al	4.06 - 4.41	4
MoO_3	4.25	1
Pb	4.25	4
Ag	4.26 - 4.74	4
Pyrex	4.48	3
Hg	4.49	4
Fe	4.50 - 4.81	4
Cu	4.53 - 4.94	4
Al_2O_3	4.70	1
MgO	4.70	1
Si	4.85n	4
SiO_2	5.00	1
Ni	5.04 - 5.15	4
Co	5.00	4
Au	5.10 - 5.47	4
Pt	5.70	4
ZrO_2	5.80	1
TiO_2	6.21	1

Sources: 1-V.S.Fomienko, NTIS, US Dep. of Commerce Report, No.JPRS-56579, 1972 or Gupta et al., Powder technology, 75 (1993) 79-87, 2 - Lewowski, Coal Preparation Journal, 1993, 13, 97-105, 3 – unknown source , 4. CRC Handbook, 67th ed., 1986-87
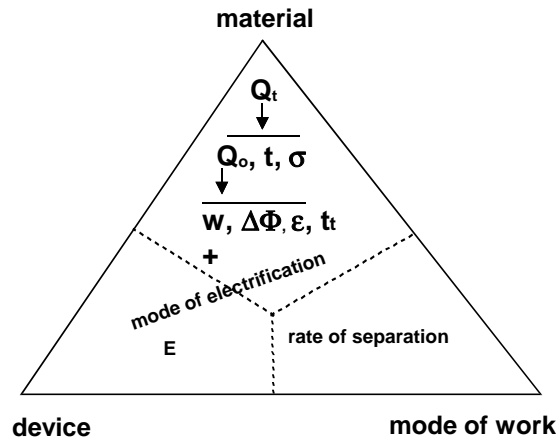
Fig. 11.2. The main feature of material utilized in separation is particle surface charge Q_t at the moment of separation. Dependent parameters : Q_o initial charge, t time, σ conductivity (surface and volume), w – work function, $\Delta\Phi$ - contact potential difference, ε - dielectric constant , electric field **E,** and ways of electrification and separation

There are different ways of electrification of particle surface. It can be accomplished by rubbing (tribocharging), ionization, induction and contact with electrically charged particles. There are also different ways of separation, therefore there are many devises used for electric separation. Fig. 11.3a presents the scheme of triboelectric separator in which the surface charge (positive or negative) results from the friction of particles with the metal plate while separation takes place in the air. Figure 11.3b shows ionization separator in which electrization provides negative charge on all particles and is a result of bombarding particles with a stream of electrons and ions formed from the air molecules due to the electrical discharge called the corona discharge. Next figure (11.3c) shows inductive-conductive separator in which electrization takes place as a result of particle contact with electrically charged separator surface. Finally, due to charge polarization, the non-conductive particles acquire a positive charge. When the particles are in the vicinity of the electrode, induction takes place and it leads to polarization of both conductive and non-conductive particles.

Ionization separators are also called electrodynamic or high tension separators and the separators in which electrization occurs through rubbing or induction are called electrostatic separators. Apart from typical triboelectric, ionization and induction–conduction separators shown in Fig.11.3 there are other separators (Kelly and Spotiswood, 1982). There are different classifications of separators. Taking into account the method used for conveying granular material separators are divided into: plate, rotary roll, free fall and vibrating table, while according to electrode type into wire, needle, and blade separators.
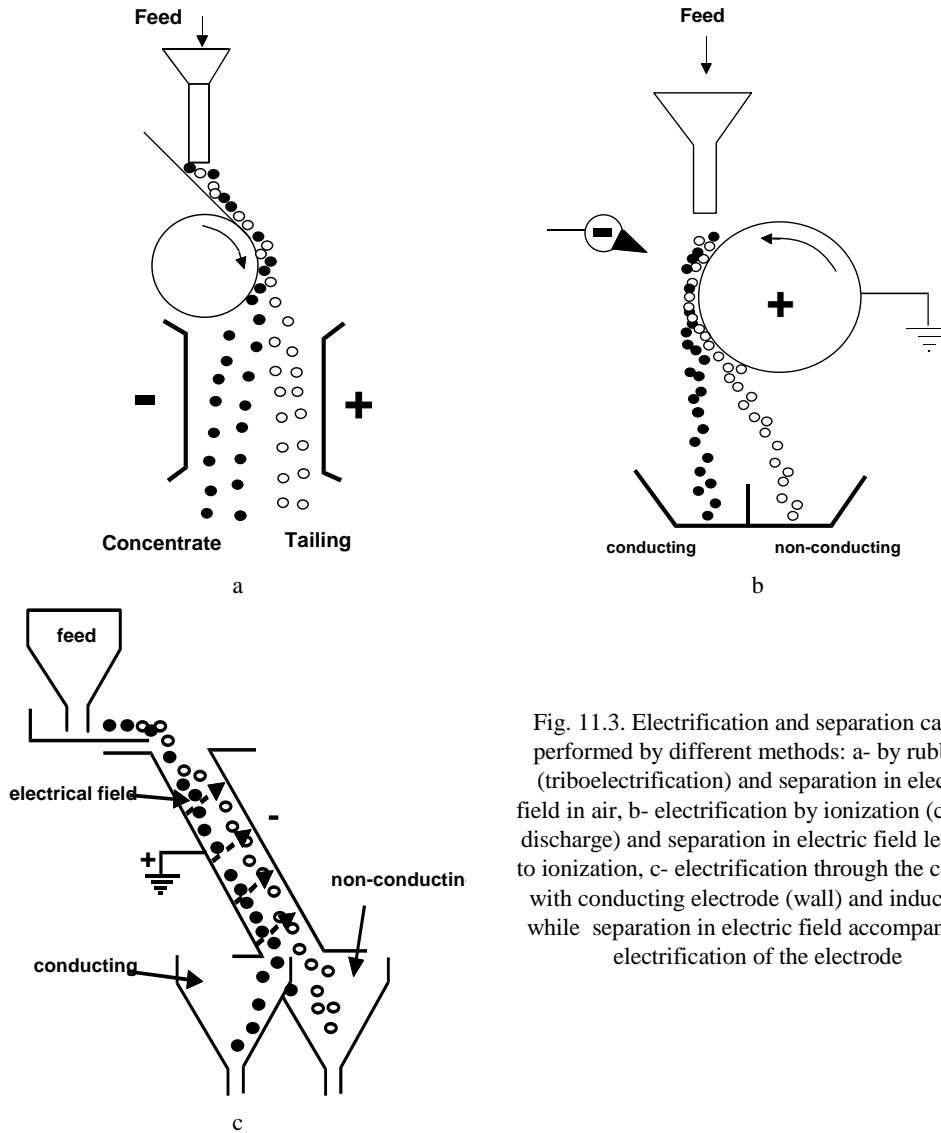
Fig. 11.3. Electrification and separation can be performed by different methods: a- by rubbing (triboelectrification) and separation in electric field in air, b- electrification by ionization (corona discharge) and separation in electric field leading to ionization, c- electrification through the contact with conducting electrode (wall) and induction, while separation in electric field accompanying electrification of the electrode

Triboelectrization is used for separation between non-conductive particles while electrification through induction, contact and ionization for separating the conducting ones from non-conducting particles. Is not easy to theoretically predict the results of electrical separation. The most practical approach is to use laboratory tests (Bogdanov, 1983). Extremely fine particles are not suitable for electric separation.

The electric separation can be applied for various ores and raw materials (Olefinskij, 1970). Figure 11.4 shows the upgrading curves for sea sand containing garnets and ilmenite.
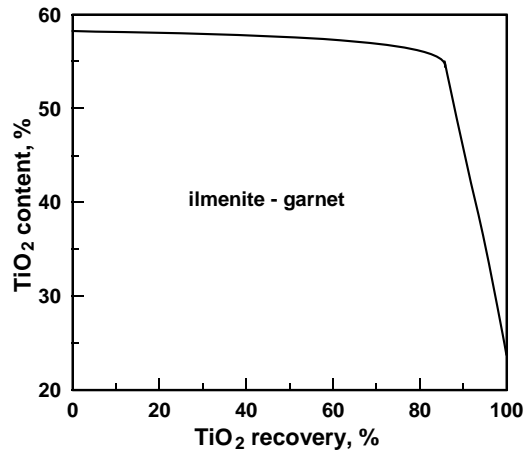
Fig. 11.4. Results of electric separation of sea sand containing ilmenite and garnets in a laboratory separator LTH with negative polarization of the exit electrode at 50 kV (after Luszczkiewicz and Kurzyca, 1986)

The separation can be modified by drying the feed. Figure 11.5 shows the effect of the temperature of the sample heated before triboelectric separation on selectivity of the process.
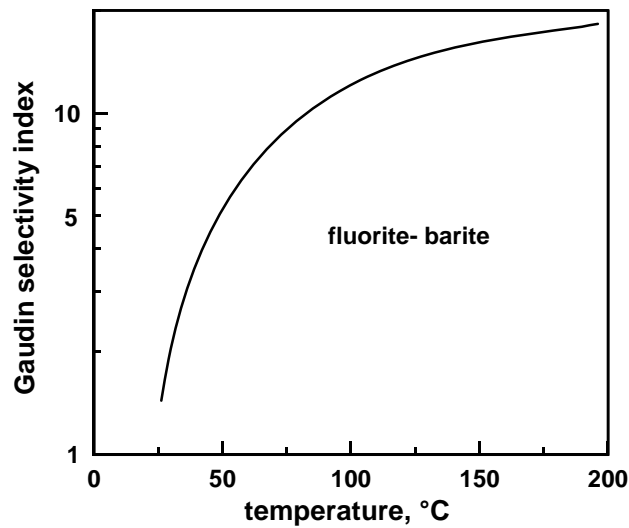
Fig. 11.5. Influence of temperature of feed on selectivity of separation of 1:1 mixture of barite and fluorite (after Carta et al., 1974)

The list of minerals adhering and rejected from the drum surface during electrostatic separator which can be used as an initial guide for electric separation of minerals is provided in Table 11.2.

Table 11.2. List of minerals adhering and rejected from the drum surface of electrostatic separator

Nonconducting, adhearing to the drum surface		Conducting, rejected from the drum surface	
anorthite	hyperstene	bismutite	magnetite
apatite	kyanite	brucite	manganite
baddeleyite	magnesite	cassiterite	pyrite
barite	monazite	chromite	rutile
bastnäsite	quartz	diamond	stibnite
beryl	scheelite	ferberite	tantalite
celestine	serpentinite	fluorite	tungstenite
corundum	silimanite	galena	wolframite
diopside	sphalerite	gold	
epidote	spinel	graphite	
feldspar	staurolite	hematite	
garnet	turmaline	hübnerite	
gypsum	wollanstonite	ilmenite	
hornblende	zircon	limonite	

Literature

Bogdanov O.S. (ed.), 1983. Handbook of mineral processing, izd. 2, Nedra, Moscow, in Russian.

Carta M., Cicccu R., Delfa C., Ferrara G., Ghiani M., Massacci P., 1974. Improvement in electric separation and flotation by modyfication of energy levels in surface layers, XIMPC., M.J. Jones (ed.), IMM, 1974.

Kelly E.G., Spottiswood D.J., 1982. Introduction to mineral processing, Wiley, New York.

Laskowski J., Łuszczkiewicz A., 1989. Przeróbka kopalin – wzbogacanie surowców mineralnych, Wydawnictwo Politechniki Wrocławskiej, Wrocław.

Luszczkiewicz A., Kurzyca M., 1986. Wydzielanie ilmenitu z półproduktów przeróbki piasków drogą wzbogacania elektrycznego, Fizykochemiczne Problemy Mineralurgii, 18, 179–191.

Nussbaum A., 1985. Electrostatic fundamentals and elementary theory of electrical properties of solids, in: SME Mineral Processing Handbook, SME/AIMM, New York, 6-2–6-5.

Olofinskij N.F., 1970. Electrical methods of mineral processing, Nedra, Moscow, in Russian.

Simorda J., Staroba J., 1970. Elektryczność statyczna w przemyśle, WNT, Warszawa.

Urvantsev, A.I., 2000. On efficiency of electrical separation with triboelectric charging of particles. Obogashcheniye Rud, Special issue: 31, Flotation.

Wroblewski K., Zakrzewski J.A.,1984. Wstęp do fizyki, t. 1, PWN, Warszawa.

12. Flotation

12.1. Theoretical basis

Flotation is one of many methods of separation and can be used for separation of phases, for instance to remove solid particles or oil drops from water. More frequently flotation is used for separation of particles having different hydrophobicities. Hydrophobicity is a feature of material characterizing its ability to be wetted with a liquid in the presence of a gas phase. In mineral processing, solids which can be easily wetted with water are called hydrophilic, while solids with limited affinity for wetting are called hydrophobic. As a result of hydrophobicity, particles adhere to a gas bubble forming a particle-air aggregate which is lighter than water, and travels upwards to the surface of water (Fig. 12.1). Hydrophilic particles do not adhere to the bubbles and fall down to the bottom of a flotation tank.
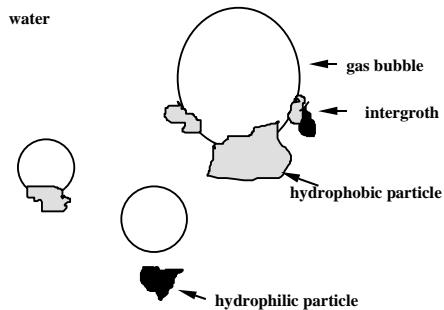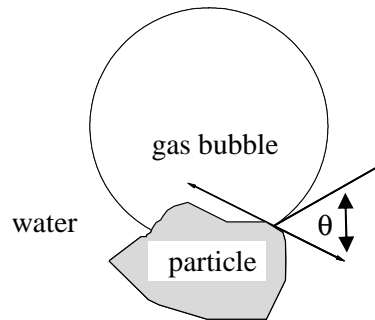
Fig. 12.1. Flotation   Fig. 12.2. Contact angle in flotation

Substances can be hydrophobic to a different degree and the measure of their hydrophobicity is contact angle. The contact angle (Fig. 12.2) is determined by straight lines drawn from the point of contact between a particle, gas and water which are tangent to the solid–gas, gas–water, and solid–water interfaces. Commonly, contact angle is expressed and measured as an angle between gas and solid phases, through the water phase. The contact angle can be also defined as the angle between solid and water phases, through the gas phase. Both ways of expressing contact angle are equally

valid, since the sum of contact angle measured through the water phase, as well as the angle expressed through a gas phase is 180^0. To avoid misunderstanding, information which phase contact angle is expressed through should be clearly stated.

The contact angle for hydrophilic materials is zero, while for hydrophobic substances is more than zero. Maximum value of contact angle for materials in contact with water and air is about 110^0 (paraffin, Teflon). Table 12.1 presents contact angles for selected materials measured by flotometry (Drzymała and Lekki 1989a, 1989b).

Table 12.1. Hydrophobicity of materials. Contact angle is based on flotometric measurements expressed in degrees

Strongly hydrophobic*		hydrophobic		weakly hydrophobic		hydrophilic** $\theta = 0$
Material	θ	Material	θ	Material	θ	Material
Paraffin C_nH_{2n+2}	90+	sulfides	44–0	fluorite, CaF_2	10–13	gypsum $CaSO_4 \cdot 2H_2O$
Teflon, C_2F_4	90+	silicon carbide SiC	27.6	arsenic, As_2O_3	9.3	ferrosilicon
Sulfur, S	63.2	coal	26–0	perovskite, $CaTiO_3$	9	dolomite $CaMg(CO_3)_2$
Mercury, Hg	45.6	indium, In	25	scheelite, $CaWO_4$	9	magnetite Fe_3O_4
Germanium, Ge	39.7	iodargyrite, AgI	23.5	diamond, C	7.9	halite, NaCl
Silicon, Si	35.4	cassiterite, SnO_2	22–	tin, Sn	7.5	brawn coal
Talc	35.2	silver, Ag	14	boric acid, H_3BO_3	64	kaolinite
		ilmenite, Fe	14	graphite, C	6.2+	hematite, Fe_2O_3
		molybdenite, MoS_2	5.9+	PbJ_2	6	quartz, SiO_2
				gold, Au	5	calcite, $CaCO_3$
				barite, $BaSO_4$	5	anhydrite, $CaSO_4$
				corundum, Al_2O_3	4	bones
				HgO	3,3	tourmaline
				HgJ_2	3	vegetables
				copper, Cu	3	iron, Fe
						amber
						ice, D_2O

* Flotometric method is able to measure contact angles smaller than 90°.

** Other hydrophilic materials: chromite, malachite, smithsonite, azurite, rutile, zircon, mica.

Contact angles measured on polished plates made of different naturally hydrophobic minerals are usually higher than the flotometric ones. Contact angles of different materials on smooth plates are presented in Table 12.2.

Numerous measurements of contact angle revealed that most minerals are hydrophilic. Hydrophilic materials can be rendered hydrophobic with appropriate reagents. Artificially made hydrophobic materials acquire surface properties similar to those of naturally hydrophobic substances.

Table 12.2. Advancing contact angle (in degrees) measured on polished plates
(after Adamson, 1967; data from other sources are denoted as *)

Substance	Advancing contact angle	Substance	Advancing contact angle
Teflon	112	sulfur	86*
Paraffin	110	graphite	86
Polystyrene	103	stibnite (Sb_2S_3)	84
Human skin	90	iodargyrite (AgI)	17
Naphthalene	88	calcite ($CaCO_3$)	~0*
Stearic acid	80	glass	~0

The simplest method of contact angle determination relies on a direct measurement of an angle of bubble attachment to a mineral surface immersed in water. It is called the captive bubble method (Fig. 12.3a). When using this method it is important for an air bubble not to stick to particle edges because both different hydrophobicity of the edge and additional forces cause distortion of the results. Additionally, to avoid hysteresis of contact angle resulting from surface roughness, the surface should be well polished. Occurrence of hysteresis of contact angle can be detected when contact angle, measured through a water phase, after slight increase in bubble size, shows lower values than the angle after releasing the gas from a bubble. Minimum angle obtained during such measurements is called receding or retreating angle, while maximum one the advancing contact angle. The hysteresis of contact angle can also take place due to other reasons, for instance surface energy heterogeneity. From a theoretical point of view the hydrophobicity is best characterized by equilibrium contact angle which can be rarely determined experimentally. Approximately equilibrium angles can be calculated by taking arithmetic mean of the advancing and receding angles.
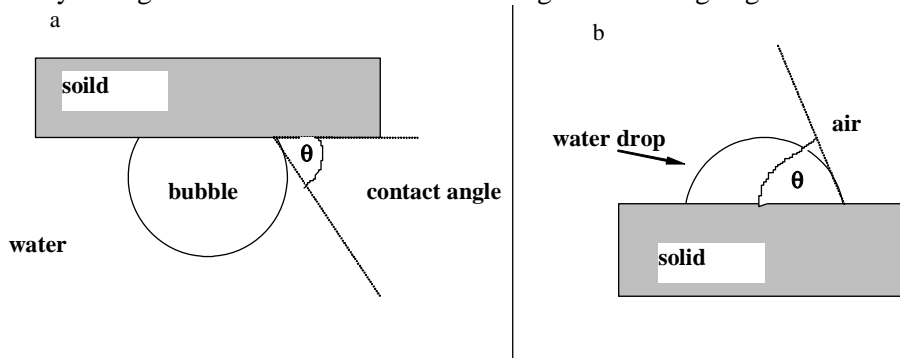
Fig. 12.3. Contact angle θ can be measured by the captive bubble (a) and sessile drop (b) methods

The contact angle can be also measured using the sessile drop method (Fig. 12.3b). The sessile drop contact angle usually disagrees with the results obtained by the captive bubble procedure.

The contact angle depends not only on the method of measurement, physical or chemical heterogeneity of the surface, but also on such parameters as drop and bubble

size. The value of a contact angle can be also effected by the so-called line tension, which is an analogue of a surface tension, but characterizing the energy of contact lines of phases. Therefore, each measuring system of contact angle is specific in some respect, which, if taken into account, can provide the equilibrium contact angle. Unfortunately, exact procedures for recalculating the measured contact angles into equilibrium contact angles is not known. A list of methods used for measurement of contact angle on smooth surfaces and particles is presented in Table 12.3.

Table 12.3. Methods of contact angle measurements

Smoothly polished surfaces	Source*	Particles	Source
Captured bubble	Adamson, 1967	heat of immersion	Neumann and Good, 1979
Sessile drop	Adamson, 1967	flotometry	Drzymała and Lekki, 1989a,b Drzymała, 1995; 1999a,b,c
Tilted plate in liquid	Hiemenz, 1986	shape of border between phases	Aveyard and Clint, 1995
Force of detachment	Hiemenz, 1986	levitation	Li and współ., 1993
Wetting of plate	Adamson, 1967	pressed disc	Heertjes and Kossen, 1967, He and Laskowski, 1992
Drop on a tilte plate	Hiemenz, 1986	rate of penetration of a thin layer of particles	van Oss and współ., 1992
Drop shape	Ralson i Newcombe, 1992	rate of penetration of a column of particles	Washburn, 1921, Crowl and Wooldridge, 1967
Drop size	Ralson i Newcombe, 1992	captured bubble for particles	Hanning and Rutter, 1989
		Langmuir through	Clint and Tylor, 1992; Aveyard and współ., 1944
		centrifuge	Huethorst and Leenaars, 1990
		capillary rise without probe liquid	White, 1982
		capillary rise in column of particles with probe liquid	Bartell and Whitney, 1933

*Additional source: Neumann and Good (1979)

There are many theories binding hydrophobicity (contact angle) with the properties of multi-phase systems. The principal is the Young formula (1805) which correlates the contact angle with the interfacial energies (γ) of three-phase system including solid (s), gas (g), and liquid (c).

$$\gamma_{sg} = \gamma_{sc} + \gamma_{cg} \cos \theta, \qquad (12.1)$$

where:

θ – equilibrium contact angle,

γ_{sg}, γ_{sc}, γ_{cg} – interfacial energy for solid-gas, solid liquid, and liquid-gas phase boundaries, respectively.

Graphical expression of the Young equation is presented in Fig. 12.4.

$$\gamma_{sg} = \gamma_{sc} + \gamma_{cg}\cos\theta$$

$$\gamma_s - \pi = \gamma_{sc} + \gamma_{cg}\cos\theta$$
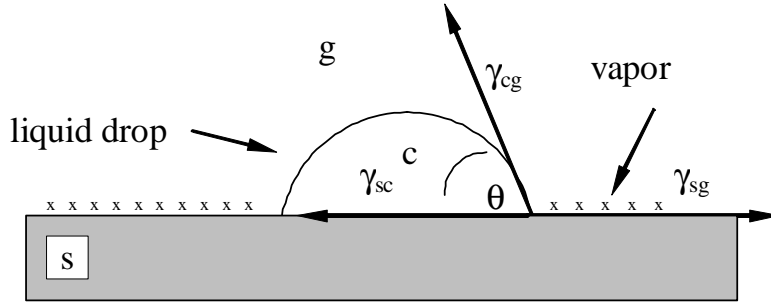
Fig. 12.4. Graphical representation of the Young equation

Interfacial energy of a solid–gas system should be expressed for gas saturated with vapor of the liquid forming the measurement system. It means it should take into account liquid adsorption on the solid surface. A relation between surface energy of the material γ and its energy in the presence of liquid vapor γ_{sg} is determined by the equation:

$$\gamma_{sg} = \gamma_s - \pi, \tag{12.2}$$

in which π is the so-called film pressure. It is commonly assumed that π is equal zero for solids having surface energy lower than surface energy of a liquid. In the case of water it should be lower than 72 mN/m. The so-called low-energy surfaces have surface energy lower than about 70mN/m. For liquids surface energy is measured by surface tension determination. For solids surface energy, i.e. energy necessary to form a unit surface, is not an equivalent of surface tension (Adamson, 1967). The unit of surface energy is mJ/m^2, while equivalent unit is mN/m (1mN/m=1mJ/m^2).

The Young equation, although very simple, is not often applied, due to lack of full data for particular systems. Table 12.4 presents materials for which existing data provide contact angle using the Young equation. As one can see, this list is very short, therefore there is a need of carrying out further investigation aiming at determining surface energy of solids in vacuum and in water, as well as the data regarding water adsorption on these bodies, which is crucial for determination of the film pressure π. The π value can be, for instance, evaluated following the relation (Adamson, 1967):

$$\pi = \gamma_s - \gamma_{sg} = -\int d\gamma = RT \int_P^{P_0} \Gamma\, d\ln P, \tag{12.3}$$

where:

Γ – surface excess

P – vapor pressure

P_o – saturation vapor pressure.

According to Adamson (1967) typical π values for solids are up to 100 mN/m.

Table 12.4. Contact angle determined directly from the Young equation
Contact angle in degrees (Drzymała, 1994)

Substance	γ_s, mN/m	π_e, mN/m	γ_{sw}, mN/m	γ_{cg}, mN/m	$\theta_{calculated}$	$\theta_{measured}$*
Ice	90–120	~0	22–33	72.8	0	0
Quartz	120–135	~small	46	72.8	~0	0
Paraffin	50– 68	0	51	72.8	77– 91	110
Mercury	484	~75	415	72.8	95	43–110

* Some works indicate that contact angle of ice (van Oss i współ., 1992) and quartz (Jańczuk i współ., 1986) can be more than zero

Surface energy of solids is difficult to determine and, therefore the data available in the literature can include a considerable error. Surface energy of solids can be estimated on the basis of surface tension of the substance melted at higher temperature and linear extrapolation to a desired temperature, without taking into account possible non-linear alterations of surface energy during crystallization. Usually, the coefficient of surface tension changes with temperature $d\gamma/dT$ is about –0.1 mN/mK (Hutner, 1987). The values of surface energy for some solids are presented in Table 12.5.

Table 12.5. Surface energy of selected crystalline materials.
(Crystallographic planes are given in parenthesis)

Solid	γ_{cg}, mJ/m^2 (Dereń et al., 1977)	Solid	γ_{cg}, mJ/m^2 (Kitchener, 1992)
$CaCO_3$ (100)	230	paraffin	45
LiF (100)	340	polyethylene	55
CaF_2 (111)	450	mica	300
MgO (100)	1200	halite	400
Si (111)	1240	fluorite	500
		diamond	4000–9000

The literature provides numerous data dealing with surface tension of liquids. The values of surface tension for selected substances at the temperature of their liquid state are shown in Table 12.6, while surface tension for selected liquids at room temperature are presented in Table 12.7.

Table 12.6. Surface tension (γ) of selected liquids at different than ambient temperature s (after various sources including Gaudin, 1963; CRC, 1986/87)

Liquid	Temperature, °C	γ, mN/m
Elements		
Nitrogen	–193	8.27
Bromine	0	45.5
Chlorine	–61.5	31.61
Fluorine	–20316	17.9
Argon	–188	13.2
Helium	–270	0.24
Iodine	130	53.1
Neon	–248	5.5
Platinum	2000	1819
Sulfur	112.8 (melting point)	60.9
Sodium	100	206.4
Silver	970	480.3
Oxygen	–193	15.7
Hydrogen	–255	2.31
Organic compounds		
Ethyl alcohol	0	24.05
Benzene	30	27.56
Carbon tetrachloride	200	6.53
Glycerol	150	51.9
Ethylene oxide	–20	30.8
Inorganic compounds		
Sodium bromide	747 (melting point)	102.8
Sodium chloride	803	113.8
Sodium fluoride	1010	199.5
Cesium iodide	654	73.1
Rubidium iodide	673	79.4
Sodium iodide	661 (melting point)	93.9
Water	20	72.75

Table 12.7. Surface tension of various liquids in contact with their vapors at room temperature (after CRC, 1986/87)

Liquid	γ_{cg}, mN/m	Liquid	γ_{cg}, mN/m
Mercury	484 (vacuum)	Styrene	32.14
Hydrazine	91.5	Benzene	28.89
Water	72.8	Acetic acid	27.80
Sulfuric acid (98,5%)	55.1	Carbon tetrachloride	26.95
Glycerol	47.7	Acetone	23.70
Aniline	42.9	Ethyl alcohol	22.75
Pyridine	38.0	Oleic acid	32.50

Table 12.8. Interfacial solid-water energy at room temperature. Data collected by Söhnel and Garside, 1992. Data after Stumm and Morgan (1970) are marked as *

Compound	Interfacial energy mJ/m^2	Compound	Interfacial energy mJ/m^2
AgBr	65, 110, 140	KNO$_3$	29, 30, 54
AgBrO$_3$	55	K$_2$SO$_4$	23, 29, 41
AgCH$_3$COO	39, 113	MgC$_2$O$_4$·2H$_2$O	100
AgCl	57, 88, 92, 103	Mg(OH)$_2$	123
Ag$_2$CrO$_4$	107	MnCO$_3$	104
Ag$_2$SO$_4$	96	MnC$_2$O$_4$·2H$_2$O	95
Al(OH)$_3$	25 (pseudo-boehmit); 67(gibbsite)	NaCl	38
BaCO$_3$	96, 109, 115	Na$_2$SiF$_6$	52
BaC$_2$O$_4$·2H$_2$O	110	Na$_2$S$_2$O$_3$	16
BaCl$_2$	22	NH$_4$Br	14
BaCrO$_4$	120	NH$_4$Cl	27, 30, 32, 60
BaF$_2$	86	(NH$_4$)$_2$Cr$_2$O$_7$	53
BaMoO$_4$	103	NH$_4$H$_2$PO$_4$	4, 8, 12
BaSeO$_4$	88	NH$_4$I	13
BaSO$_4$	117, 135	NH$_4$NO$_3$	27
BaWO$_4$	116	NH$_4$SCN	34
CaC$_2$O$_4$	123	Ni(NH$_4$)$_2$(SO$_4$)$_2$·12H$_2$O	8, 12
CaC$_2$O$_4$·3H$_2$O	135	Ni(OH)$_2$	110
CaCO$_3$	58, 68, 97	PbCO$_3$	125
CaF$_2$	167	PbC$_2$O$_4$	139, 145
Ca(OH)$_2$	66, 79, 86	PbCrO$_4$	170, 194
CaSO$_4$·2H$_2$O	76, 92, 95, 117	Pb(NO$_3$)$_2$	3
CaMoO$_4$	118	PbSeO$_4$	71
CaWO$_4$	151	PbSO$_4$	100, 104
CaHPO$_4$·2H$_2$O	46, 68	SrCO$_3$	116
Ca$_4$H(PO$_4$)$_3$·2H$_2$O	59	SrC$_2$O$_4$	76
Ca$_5$OH(PO$_4$)$_3$	45	SrMoO$_4$	100
CdI$_2$	19	SrSO$_4$	82, 92
CuCl$_2$	12	SrWO$_4$	62
FeC$_2$O$_4$·2H$_2$O	90	TlBr	92
KAl(SO$_4$)$_2$·2H$_2$O	2, 5	TlCl	40, 92
KBr	15, 23, 24	Tl$_2$CrO$_4$	108
KBrO$_3$	14, 44	TlO$_3$	87
KCl	22, 27, 30	TlSCN	65
KClO$_3$	49	SiO$_2$ (amorphic)	46*
K$_2$Cr$_2$O$_7$	33, 47, 66	glycine	29*
KH$_2$PO$_4$	12, 14, 16	ZnO 0,2MNaClO$_4$	770*
KI	17	CuO 0,2MNaClO$_4$	690*
KIO$_3$	14, 44	Cu(OH)$_2$ 0,2MNaClO$_4$	410*

There are also available data on interfacial energy for solid–water systems, especially for salts (Table 12.8). The interfacial energy for such systems is usually determined utilizing the solubility measurements for different particle sizes, speed of nucleation, critical supersaturation indispensable for homogenous nucleation, or kinetics of crystal growth (Söhnel and Graside, 1992).

Another way of determining interfacial energy was proposed by Fowkes (1964):

$$\gamma_{12} = \gamma_1 + \gamma_2 - D - N, \tag{12.4}$$

where:

γ_1, γ_2, γ_{12} – surface energy of phase 1, phase 2 (both in vacuum) and interfacial energy
  of phase 1 and 2.
D – dispersion interactions (London-van der Waals),
N – other interactions.

The dispersion interactions D are determined by the relationship:

$$D = 2\left(\gamma_1^d \, \gamma_2^d\right)^{1/2}, \tag{12.5}$$

in which γ_1^d and γ_2^d denote dispersion component of surface energy of phase 1 and 2, respectively. The non-dispersion contribution N can be divided into metallic, hydrogen, and other interactions.

After combining the Fowkes and the Young equations, one can obtain the relation:

$$\cos\theta = \frac{2\,\sqrt{(\gamma_s^d \gamma_c^d)} - N - \pi}{\gamma_{cg}} - 1. \tag{12.6}$$

Although a number of formulas were proposed for determining N, all of them were disqualified by Fowkes et al. (1990). Therefore Eq. (12.6) is useful for calculation of contact angle for substances interacting with water only due to their dispersion forces, since then $N=0$.

As it has already been stated the dispersion component for water is 21.8 mN/m, while for the non-dispersion component is 51mN/m. For other substances they can be determined from contact angle measurement using certain standard liquids or estimated according to the so-called Hamaker constants and relation (Drzymała, 1994c):

$$\gamma^d = \frac{A_{11} \cdot 10^{13}}{0.20527} \, . \tag{12.7}$$

The values of the Hamaker constant are known for many substances and some selected ones are presented in the chapter dealing with flocculation. Table 12.9 presents hydrophobicity of materials for which contact angle can be calculated from the Fowkes-Young equation.

Table 12.9. Contact angle for nonpolar materials calculated by means of the Fowkes–Young equation (12.6). γ^d for water is 21.8 mN/m, $N = 0$ (Drzymała, 1994c)

Solid	γ^d, mN/m	π, mN/m	$\theta_{calculated}$	$\theta_{measured}$
Paraffin	25.5	~0	110	110
Teflon	21.7	~0	113	112
Mercury	200	~75	112	43–110
Graphite	115–132	19	81	86 (plane 0001)
Silver	194.9	0 (?)	38	57–62

There are other possible ways of contact angle calculation. Among them there is the so-called equation of state of Neumann (1974), which, after several modifications, has the form (Spelt and Li, 1996):

$$\cos \theta = -1 + 2 \sqrt{\frac{\gamma_{sg}}{\gamma_{cg}}} \; e^{-\beta(\gamma_{cg} - \gamma_{sg})^2} , \qquad (12.8)$$

where β is a constant equal to 0.000115 while *cg* and *sg* denote liquid-gas and solid-gas interfaces, respectively.

This equation has been frequently criticized (Fowkes et al. 1990; Johson and Dettre, 1989) and therefore it is not often used, except by Neumann and his team. Another equation has been proposed by van Oss et al. (1988; van Oss and Good 1996).

$$(1 + \cos \theta)\gamma_c = 2[(\gamma_c^{LW}\gamma_s^{LW})^{1/2} + (\gamma_s^+\gamma_c^-)^{1/2} + (\gamma_s^-\gamma_c^+)^{1/2}], \qquad (12.9)$$

where: c – liquid , s – solid, γ^{LW}, γ^+ and γ^- stand for Lifshitz–van der Waals, electron-accepting, and electron-donor components, respectively.

It has been assumed that for water γ_c^{LW}=21.8 mJ/m², γ_c^+=25.5 mJ/m², γ_c^-=25.5 mJ/m². However, some works suggest that these constants should have other values (Lee, 1996). The values of γ^{LW}, γ^+, and γ^- can be determined with the use of standard liquids and contact angle measurements. The van Oss et al. equation has been the subject to experimental verification and criticized (Lyklema, 1999; Kwok, 1999). In Table 12.10, the values of γ^{LW}, γ^+ and γ^- were presented for several liquids. They are presently considered as standard liquids.

Table 12.10. γ^{LW}, γ^+ and γ^- values for selected liquids (Chibowski et al., 1996)

Liquid	γ	γ^{LW}	γ^+	γ^-
Water	72.8	21.8	25.5	25.5
Diiodomethane	50.8	50.8	0	0
α-bromonaphthalene	44.4	44.4	0	0
Formamide	58	39	2.28	39.6
Glycerol	64	34	3.92	57.4
Ethylene Glycol	48	29	1.92	47.0
Decane	23.8	23.8	0	0

According to Gaudin et al. (1957), solids build of molecular (iodine, sulfur, realgar, paraffin), chain (Ag, selenium), and layered (molybdenite, graphite, talc, boric acid)

structures are hydrophobic. In these structures molecules, chains, and layers are bound together with the van der Waals-London forces. The rule is not entirely correct, since there are solids, for example iodargyrite (AgI), which has an ionic-covalent structure of zinc blende and its contact angle is not zero but about 17^0. On the other hand $SnCl_2$ has a chain-like structure but is, according to flotometric tests, hydrophilic. Gaudin's rule does not say anything about substances having metallic bond. The metals can be either hydrophilic (Fe, Al, Au) or hydrophobic (Ag, Cu, In). On the bases of existing data it can be said that hydrophilic are those substances on whose surfaces absorbed water becomes chemically bound. Non-ionic surface structures (layer, chain or molecular nets) usually prevent water form being chemically bound, which provides hydrophobicity of the substance. It should be noticed that hydrophilic substances are capable to form hydrates (Drzymała, 2001). Therefore, oxides are mostly hydrophilic as they form hydroxides. Hydrophilic are many salts since they can form hydrates. For instance, NaCl or $CaCO_3$ are hydrophilic because they form hydrates $NaCl^.2H_2O$ (hydrohalite) and $CaCO_3^.H_2O$ (monohydrocalcite) (Bolewski and Manecki, 1993; Wells, 1993), respectively. Thus, the salts which do not form hydrates can be hydrophobic, for instance, barite ($BaSO_4$) or iodargyrite (AgI) (Drzymała 1994c). Following this hypothesis, hydrophilic can also be the substances of molecular, chain or layer structure if, when reacting with water, they form hydrophilic hydrates. This rule, although varying in its form, also is valid for metals, since metals, on whose surfaces reaction with water takes place leading to the formation of surface -OH and –H groups, are hydrophilic (Drzymała (1994c).

12.2. Hydrophobicity modification

Hydrophobicity of the materials is effected by reagents (acids, bases, salts, organic compounds) added to the solid-water system. Their action can be explained with the Young equation, since they modify all three interfaces. As a rule, however, one of the interfaces is mostly effected. The compounds modifying hydrophobicity and floatability of naturally and rendered hydrophobic materials can be classified into four groups: collectors, hydrophilization reagents, electrolytes (potential determining substances and salts), and modifiers (activators, depressors, frothers). Each of these groups differently effects hydrophobicity.

Collectors increase surface hydrophobicity and contact angle mainly through the decrease in surface energy of the treated material, i.e. γ_{sg}. This fact was proved experimentally by Smolders (1961) and theoretically by de Bruyn, Overbeek and Schumann in 1954 (de Bruyn and Agar, 1962). Hydrophilization compounds decrease hydrophobicity mostly by decreasing surface tension of the liquids, whereas electrolytes can either increase or decrease contact angle by effecting mainly the solid-water inter-

face. The effect of modifiers (activators, depressors, frothers) on properties of inter-faces is not well established. It is schematically presented in Fig. 12.5.
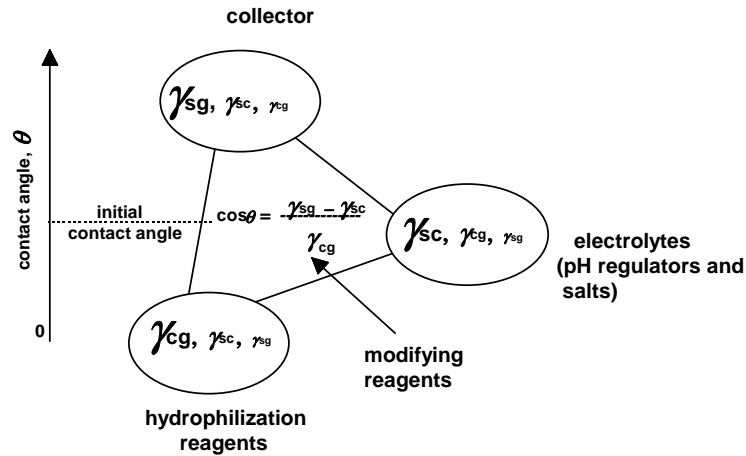
Fig. 12.5. Flotation is influenced by reagents modifying the interfaces. Collectors strongly change the solid-gas, surfactants water–gas, and electrolytes (pH reagents and salts) solid–water interfaces. The extent of modification is expressed by the height of symbol

When hydrophobicity is regulated with the concentration of the collector, the inter-facial energies of the solid-gas, solid–water, and water-gas interfaces decrease. How-ever, the most significant is the drop in the interfacial energy of the solid-gas interface (Fig.12.6). According to the Young equation it leads to the increase in hydrophobicity and improves flotation. This is well visible in Fig. 12.6 for mercury.

Hydrophobizing substances, i.e. collectors, can increase the contact angle up to 110^0, which is the value characteristic for paraffin. Generally high values of contact angles can be obtained with increased concentrations of collectors and collectors with larger hydrocarbon chain are more powerful.
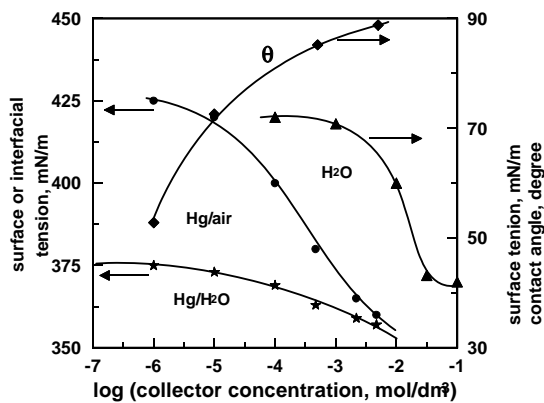
Fig. 12.6. Dependence of contact angle and the state of mercury at interfaces on concentration of collector Data by Smolders (1961) taken from various sources: contact angle in dodecyl sulfate solution and $\gamma_{H_2O \text{ (dodecyl sulfate)}}$ (Leja, 1982), $\gamma_{Hg/H_2O\text{(decyl sulfonate)}}$ and $\gamma_{Hg \text{ (decyl sulfonate)}}$ (de Bruyn i Agar, 1962))

Investigation relating hydrophobicity and surface tension of the liquid was initiated by Zisman (1964). The relation between contact angle of a solid and surface tension of the liquids is called the Zisman plot. It is used in film flotation process, which relies on placing fine particles on liquid surface and collecting floating particles. The surface tension of the flotation medium is regulated by adding the liquid of lower-than-water surface tension. The so-called gamma flotation is similar to the film flotation. In gamma flotation particles are floated with gas bubbles passing through the aqueous solution whose surface tension is regulated with low surface tension liquid. The film flotation method was widely investigated by Fuerstenau et al. (1988) and Sablik, (1998). It is applied for determination of the so-called surface tension of wetting or critical surface tension (γ_c). This parameter allows to compare flotation properties of different substances. Gamma flotation in aqueous solutions of alcohols (usually ethyl) was initiated by Yarar and his co-workers (Yarar and Kaoma, 1984).

It should be stressed that γ_c is not equivalent to the surface energy. It is easy to prove by determining γ_c for a high surface energy hydrophobic material such as mercury. Its γ_c is below 72.8 mN/m while it surface tension is 484 mN/m. Fig. 12.7 shows an agreement of contact angle (Zisman's diagram) with surface flotation as a function of surface tension of the solution.
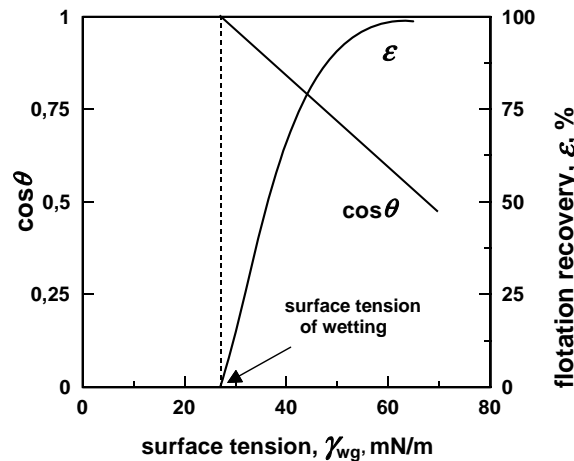
Fig. 12.7. Typical shape of the cos $\theta = f$ (surface tension of liquid) relationship also called the Zisman plot, and flotation of naturally hydrophobic materials

Electrolytes effect mostly the solid–water interface. Their action is complex and depends on concentration and properties of the electrical double layer. As a result of adding electrolytes the flotation can increase or decrease. If acid, or base, is used as electrolyte and the pH regulation medium, change of hydrophobicity depends on the electric properties of the solid–water interface. It appears that any deviation from pH at which the interface is electrically neutral, causes a decrease in the hydrophobicity and flotation. The relation between contact angle (or flotation) and pH can be called

the electrocapillary curve of a second kind. For example, Fig. 12.8 shows a decrease in germanium flotation, which occurs above and below pH 2.8. At that pH the interface is electrically neutral.
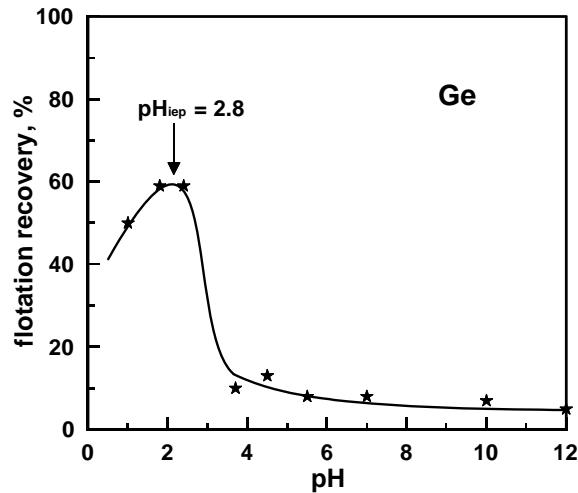
Fig. 12.8. Influence of pH on germanium flotation
(after Drzymala et al., 1987)

If salt is applied as the electrolyte, hydrophobicity and flotation decrease or increase, depending on the flotation system environment. This question will be discussed in details in a next chapter. Figure 12.9 shows changes of coal flotation as a function of NaCl concentration.
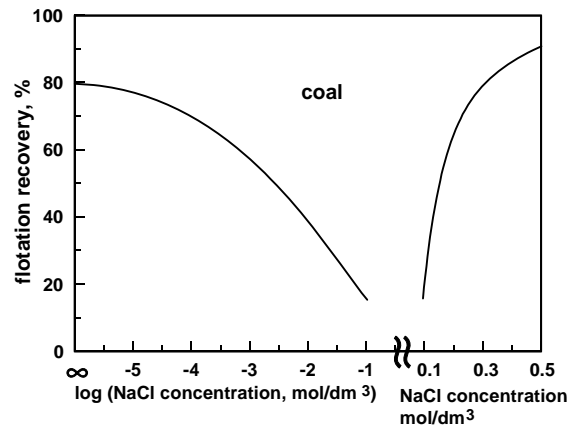
Fig. 12.9. Coal flotation containing 80.65% C as a function of sodium chloride concentration in aqueous solution(based on data of Li and Somasundaran, 1993)

To make the reader more familiar with the terms used in different fields Fig. 12.10 presents schematically the influence of the factors discussed on hydrophobicity and flotation.
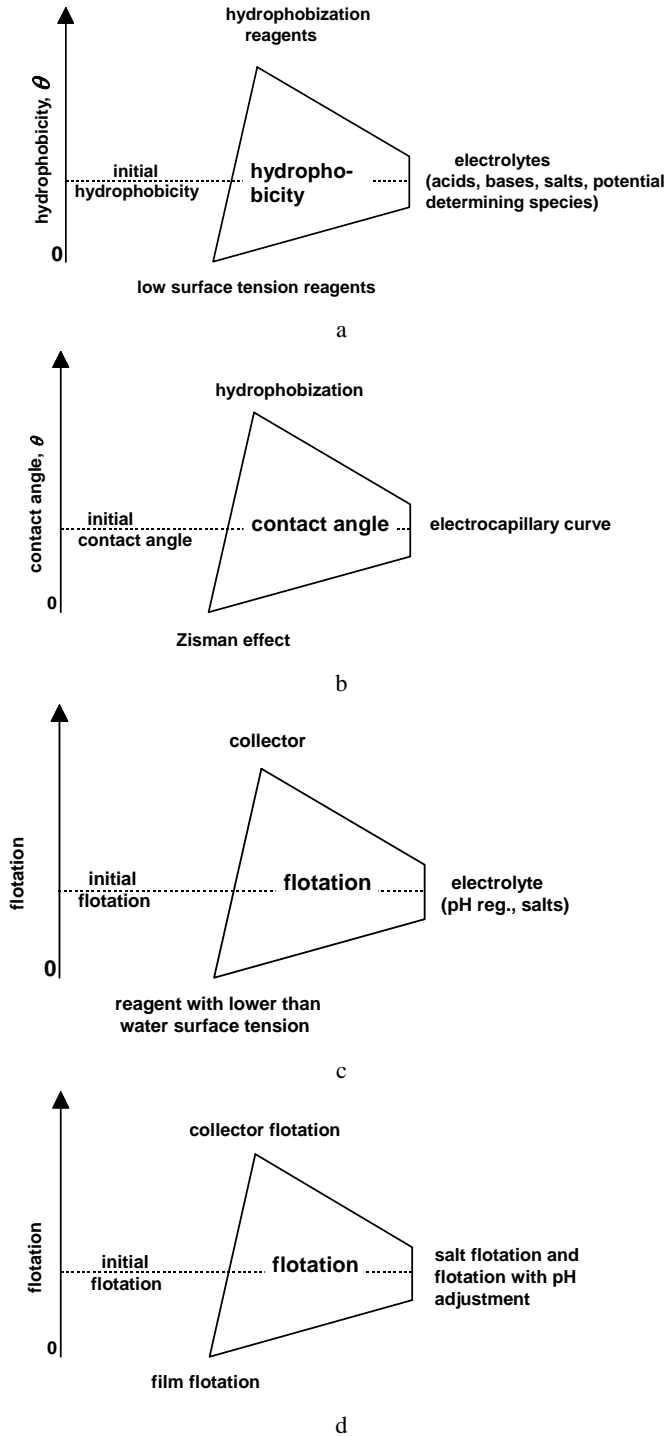
Fig. 12.10. Influence of various factors on hydrophobicity, contact angle, and flotation along with terms used in different fields:
a – colloidal physical chemistry (delineation of hydrophobicity),
b – colloidal physical chemistry (phenomena),
c – flotation (applied reagents),
d – in practice (type of flotation)

12.3. Electrical phenomena at interfaces

Interactions between two separated or being in contact objects can be described as a sum of different, including electrical, interactions. The theory and practice indicate that electrical interactions are significant in the processes taking place in different systems including flotation. Therefore, this question will be discussed in more details.

Introduction of any liquid, solid, or gas as a phase into water causes creation of an interface and formation of electrical double layer. The term electrical double layer reflects the situation that the electrical charge present within or close to one phase is neutralized in the second phase. Together they form electrical double layer (Fig. 12.11) which is often abbreviated to edl.

There are many models of edl and they differently express electrical properties of the interface. The main purpose of the models is to relate parameters of edl, especially surface electrical charge and surface potential. Figure 12.2 presents the mostly used edl models.

Description of electrical properties of interfaces can be based on the Helmholz (flat capacitor) or Gouy-Chapman (one plate of the capacitor is diffused) models, or their combinations. A simple combination of the Helmholz and Gouy-Chapman models results in the Stern model while two rigid and one diffuse layer is the essence of the Graham model. Unfortunately, the simplest Helmholz model is capable to describe only a few systems with a very low surface electrical charge. Otherwise the Gouy-Chapman model is used as in the case of the AgI/H_2O interface. Metal oxides in water usually require more complex edl models such as the Graham and more complex theories. Among them is the site bonding model (SBM) and its modifications such as surface complexation model (SCM) which incorporate the Helmholz and Gouy-Chapman models. More details regarding the edl models can be founds in a number of works including a review work by Janusz (1999).

The Helmholz model considers edl as a flat capacitor, for which the equation relating the electrical charge (σ0) and potential (ψ0) has the following form:

$$\sigma_o = \varepsilon \varepsilon_o \kappa \psi_o, \tag{12.10}$$

where:
ε – dimensionless dielectric constant
ε_o – permittivity of free space ($8.854 \cdot 10^{-12}$ C^2 N^{-1} m^{-2})
$1/\kappa$ – electrical double layer thickness.
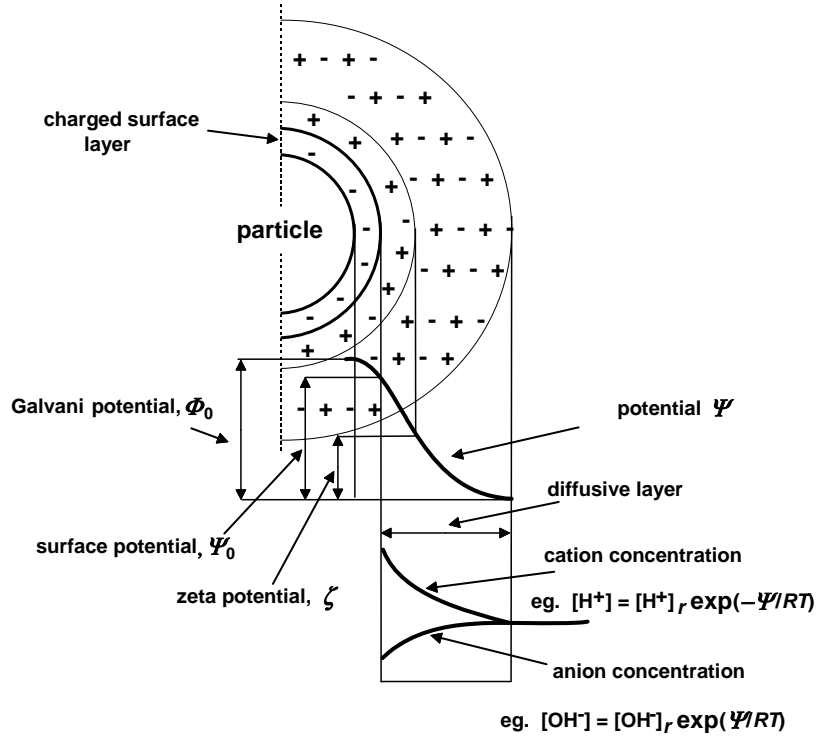
Fig. 12.11. Electrical double layer (edl) model consisting of a charged surface layer within the solid and neutralizing it diffused layer in the solution. The Galvani potential between two phased is also shown as well as location of the slipping plane determining the zeta potential. H_r and OH_r symbols denote concentration of H^+ and OH^- ions in the solution H and OH without subscript r stand for concentration of the ions at the surface
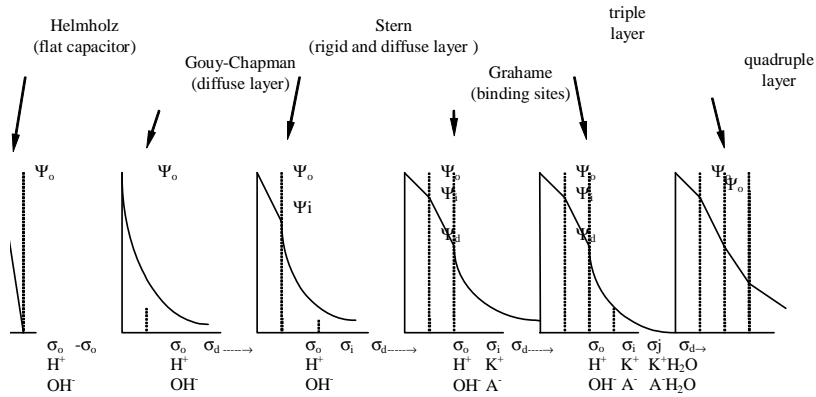
Fig. 12.12. Models of electrical double layer (edl). The layers $i, j, ...,$ form flat capacitors and can be treated as connected consequently or parallel. $\sigma_0 = -\sigma_i - \sigma_j - \sigma_d$. K^+ – cation, A^- – anion

The Gouy–Chapman model assumes that the electrical charge σ_d is gathered in the solution to neutralized the electrical surface charge within or near the surface, does not form a uniform layer but is diffused. It is given by (Hunter, 1987):

$$\sigma_d = \frac{-2\kappa \; kT\varepsilon_0\varepsilon}{ze}\sinh\left(\frac{ze_0\psi_0}{2kT}\right),$$ (12.11)

where:
k – Boltzmann constant
T – absolute temperature
e_o – elemental charge
z – valence of potential determining ions (positive number)
ψ_d – electrical potential of diffuse layer
σ_d – charge in the solution $(\sigma_s = -\sigma_d)$.

For a symmetric electrolyte in water at 250C (298K) the electrical charge in the Gouy-Chapman diffuse layer can be calculated from the relation:

$$\sigma_d = -11.74\; c^{0.5}\sinh\,(19.46\; z\,\psi_o),$$ (12.12)

where c is the concentration of electrolyte in solution, expressed in mol/dm^3 and ψ_o is the surface potential (in volts).

The Gouy-Chapman edl model is shown in Fig. 12.11 with marked potential differences between the interior of the solid phase and the liquid phase, called the Galvani potential (Φ_o), as well as surface potential (Ψ_o). The Galvani potential is equal to the sum of surface potential and the potential drop transition between surface and bulk solution, called the χ potential. Figure 12.11 also shows the zeta potential which plays an important role not only in mineral processing. The zeta potential (ζ) is an electrical potential at the place called the slipping plane, where a particle moving in water leaves a part of its edl behind. A moving particle renews its edl very soon and the time needed to achieve it is called the relaxation time. If edl renewal is impossible, as e.g. during the fall of melting hail balls, then electrification takes place, in this case of the Earth and clouds, leading to lightning (Drzymala, 2001).

The structure of the electrical double layer in water depends on the mechanism of formation. In the case of metals whose surface does not react with water (precious metals and mercury), their edl is formed due to electrons gathered at the interface on the side of metal. This phenomenon results from either transition of some amount of metal to the solution in the form of cations, or application of external potential to the metal. Then, the metal surface becomes negatively charged. A positive charge on metal surface occurs when electrons are removed from metal. The formation of electrical charge in edl on metal surface is shown Fig. 12.13.
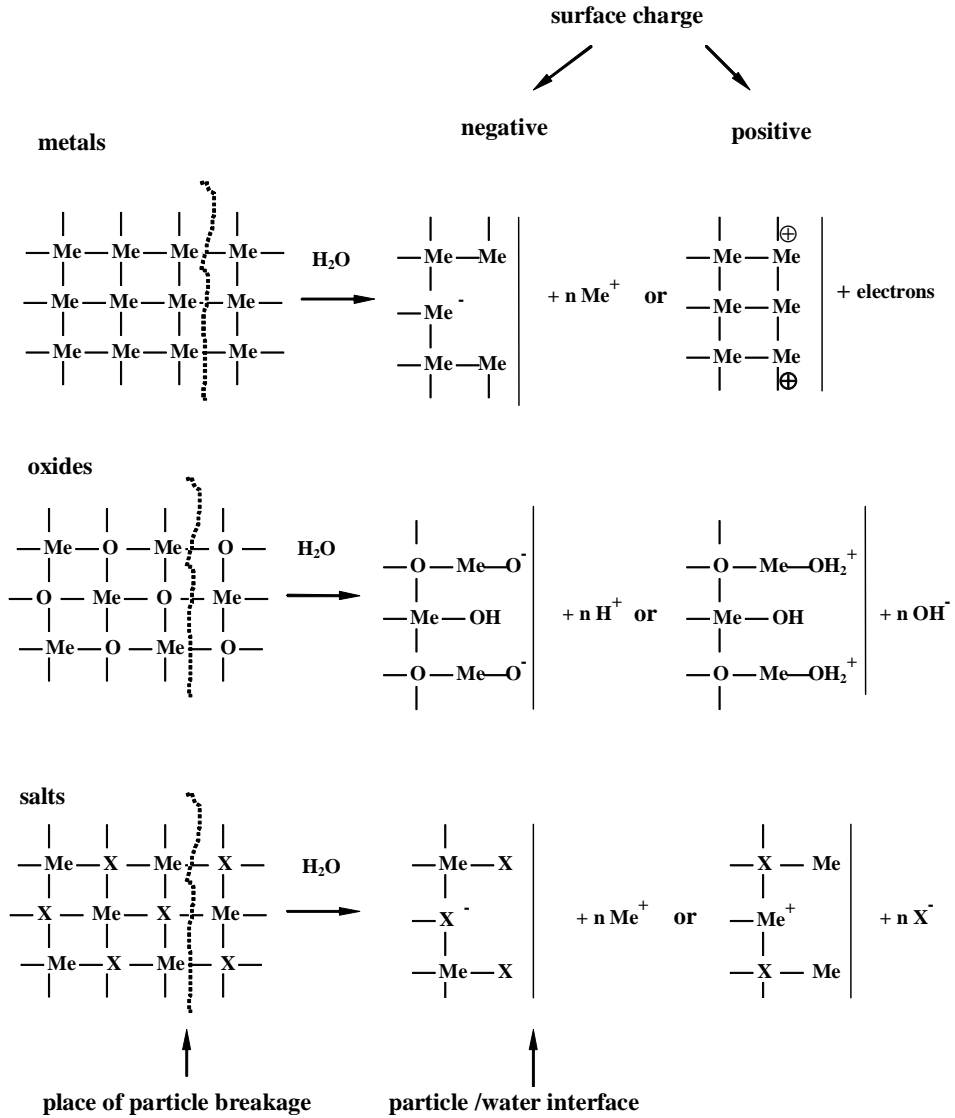
Fig. 12.13. Formation of surface charge on metal, oxide and salt

A different electrical double layer is formed on particles which do not conduct electrical current (Fig. 12.13). The cause of electrical charge on the surface of salts are ions passing from the salt into the solution. For instance, for NaCl they will be Na^+ and Cl^- ions. The more ions of one kind pass into the solution, the higher the surface electrical charge. The electrical charge can be further increased by adding to the solution another soluble salt having at least one identical ion as the solid particle. The ions

which form the salt and regulate the electrical charge are called the potential determining ions.

$$
\begin{array}{ccccc}
| & | & | & | & \\
-Me-S-Me & \cdot & S- & & \\
| & | & | & | & \\
-S-Me-S & - & Me- & \xrightarrow{\ H_2O\ } & \\
| & | & | & | & \\
-Me-S-Me & - & S- & & \\
| & | & | & | & \\
\end{array}
$$

$$
\begin{array}{l}
| \\
-S-Me-OH \\
| \\
-Me-SH \\
| \\
-S-Me-OH \\
|
\end{array}
$$

other

$$
\begin{array}{l}
| \\
-S-Me-OH_2^{+} \\
| \\
-Me-SH \qquad + n\,OH^{-} \\
| \\
-S-Me-OH_2^{+} \\
|
\end{array}
\qquad
\begin{array}{l}
| \\
-S-Me-OH \\
| \\
-Me-S^{-} \qquad + H^{+} \\
| \\
-S-Me-OH \\
|
\end{array}
$$
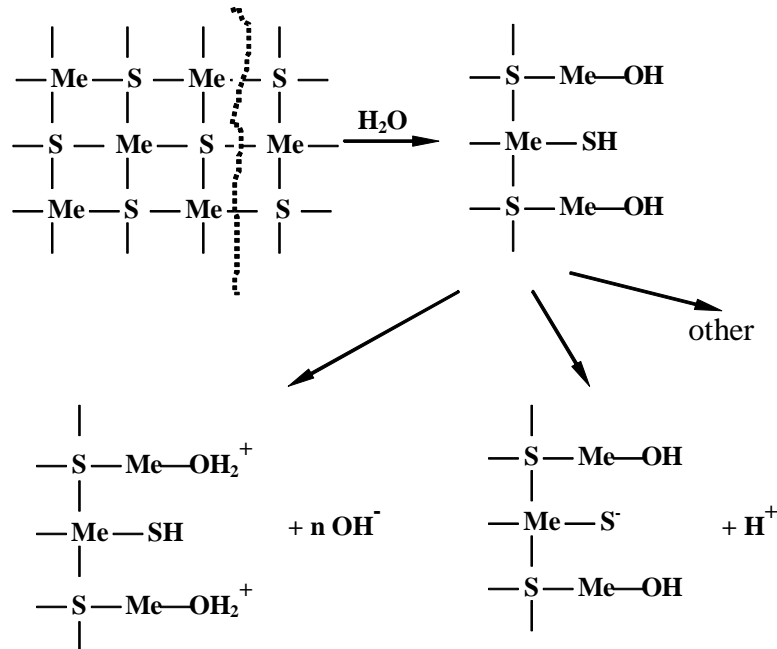
Fig. 12.14. Formation of surface charge on sulfide

In the case of oxides the edl forming is more complicated than on salt type minerals. This is so because the original (primary) potential determining ions are Me (Me^{+}, Me^{2+}, Me^{3+}) cations and O^{2-} anions. However, the O^{2-} ions are not present in the solution. Instead, OH^{-} ions are present as a result of reactions between O^{2-} surface ions and water. Therefore, OH^{-} ions, as well as related to them (due to water molecules dissociation) H^{+} cations, are the secondary potential determining ions for metal oxides. The OH^{-} and H^{+} ions are the secondary potential determining ions for all substances whose surfaces undergo reaction with water. This refers also to sulfides (Fig. 12.14) for which the original potential determining ions are S^{2-} and Me^{n+}, while the secondary potential determining ions are OH^{-} and H^{+}. Figure 12.15 shows a diagram for zinc sulfide indicating the areas of dominance of different surface species as function of concentration of H^{+} and HS^{-} ions. For some solid–water systems the potential determining ions can be still other species, for example ions introduced to the solution to regulate pH and ionic strength of the system, that is sodium, potassium, halide, and other ions. The potential determining ions can be also ions present in water as contaminants.
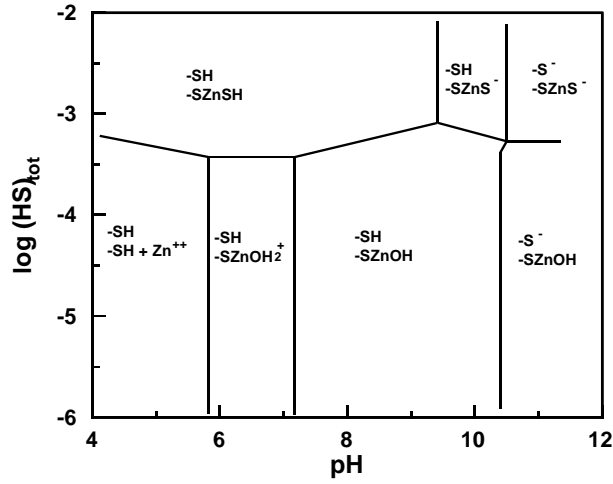
Fig. 12.15. Diagram of dominance of surface species on zinc sulfide (sphalerite) depending on total amount of HS^- and pH. Assumptions: $(-SZn)_{tot} = 1.0$ mmol/dm^3 (after Rönngren et al., 1994)

Potential determining ions regulate the electrical surface charge of materials in water. The net charge can be either positive or negative, or sometimes zero. Fig. 12.16. presents a typical shape of electrical charge plotted as a function of pH of the solution.
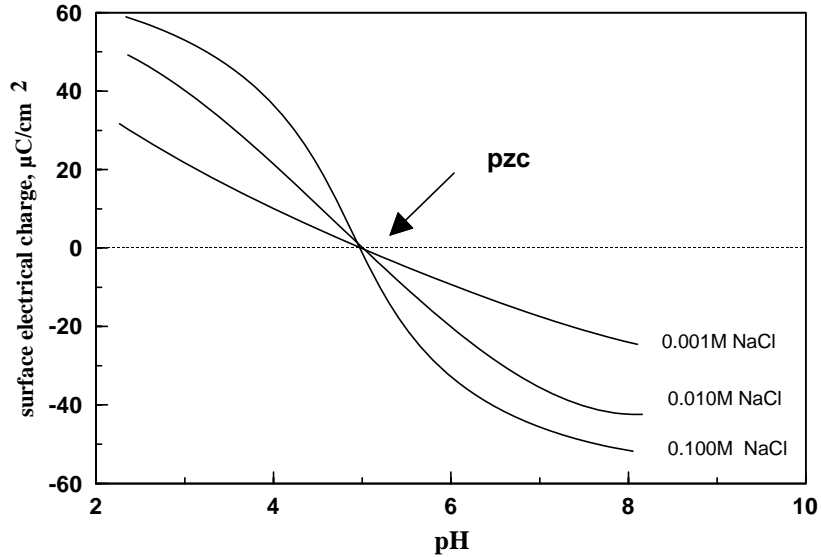
Fig. 12.16. Surface charge vs. pH of solution and concentration of electrolyte in solution. The pzc is also shown

The point at which the electrical surface charge equals zero is a very important property of the system and is called the point of zero charge or shortly pzc. Table 12.11 presents pzc values for different substances. Fig. 12.16 shows that the charge depends on the concentration of salts (ions) present in the solution. It should be noticed that for a particular pH the higher electrolyte concentration in the solution, the higher values of electrical charge.

Table 12.11. Point of zero charge (pzc) and isoelectric point (iep)
for selected substances in aqueous solution. The values of pzc and iep
for a great number of solids were collected by Parks (1965) and Kosmulski (2001)

Substance	pH_{pzc}	pH_{iep}
Quartz, SiO_2	<5	1.54
Oleic acid, $C_{17}H_{33}COOH$		2.0
Cassiterite, SnO_2	<5.5	2.0–55
Sulfur, S	–	2.1
Sulfides, MeS	–	2.1–7.0
Ice, D_2O	7.0 ±0.5	3.0–3.5
Hydrocarbons, C_nH_{2n+2}	6.3	3.3
Air, $O_2+N_2+CO_2$	–	3.5
Diamond, C	–	3.5
Bacteria (Nocardia)	–	3.5
Rutile, TiO_2	4.8–5.3	
Ilmenite, $FeTiO_3$	5,6	
Hematite, Fe_2O_3	6.5–8.5	4.8–8.7
Barite, $BaSO_4$	–	6.0–8.1
Tenorite, CuO	6.5–8.5	6.0–7.6
Dolomite, $(Ca,Mg)CO_3$	–	7.5
Magnesite, $MgCO_3$		7.5
Corundum, Al_2O_3	9.1	
Periclase, MgO		12.0

The electrical state of the surface can also be determined by measuring either surface potential or zeta potential. Fig. 12.17 shows a typical pattern of the relation between zeta potential and pH at different concentrations of an electrolyte in the solution. The point at which the surface assumes zero potential is called the isoelectric point or iep. Typical pzc and iep values for different substances are presented in Table 12.11. It can be concluded from the table, the iep not always is equal to the pzc. It results from difference in the adsorption of cations and anions in the edl coming from the electrolyte used, especially close to the pzc.
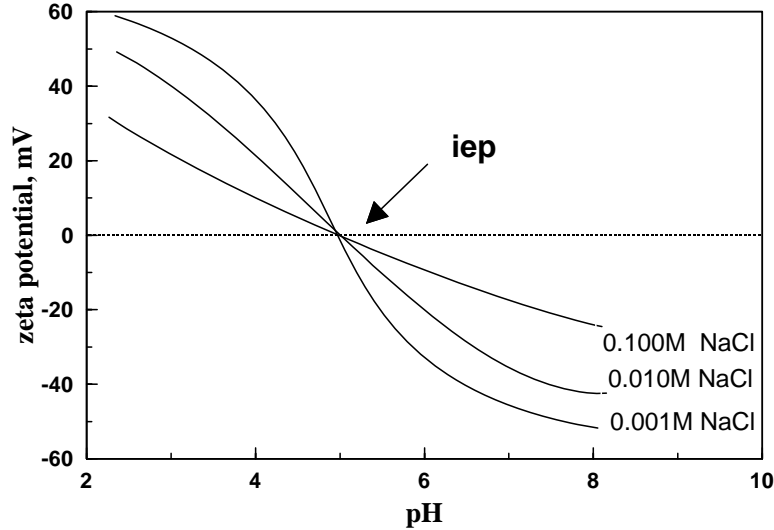
Fig. 12.17. Zeta potential as a function of pH and concentration of electrolyte in the solution. The isoelectric point (iep) is also shown

For a particular concentration of the potential determining ions the zeta potential decreases as ionic strength of the solution, determined by the electrolyte concentration, increases. This results from the compression of the electrical double layer leading to a greater decrease in the potential with the distance from the surface. For metals the electrical charge can also be regulated by applying external potential. At a certain magnitude of the applied potential the metal reaches zero charge and this point is called the potential of zero charge or E_{pzc}. The value of E_{pzc} is connected with the so-called work function (w) that is the work needed to remove electron from metal. The relationship is (Jakuszewski 1962):

$$E_{pzc} = w - 4.78, \qquad (12.13)$$

where E_{pzc} is expressed in relation to so-called hydrogen electrode. Both E_{pzc} and w are expressed in volts. It should be added that the curve describing the relation between metal surface tension (surface energy) and applied external potential E is called the electrocapillary curve, and is given by the Lippmann equation:

$$\partial\gamma/\partial E = -\sigma. \qquad (12.14)$$

where σ stands for surface charge and γ for surface tension.

The electrical charge has a significantly effect on contact angle and flotation. Examinations of flotation data indicate that highest contact angles and best flotation occurs at E_{pzc}, pzc or iep. Figures 12.8 - 12.19 show flotation results of different materials, whose electric state of interface was regulated either by external potential (for conducting substances) and by primary or secondary potential determining ions.

a

b

c
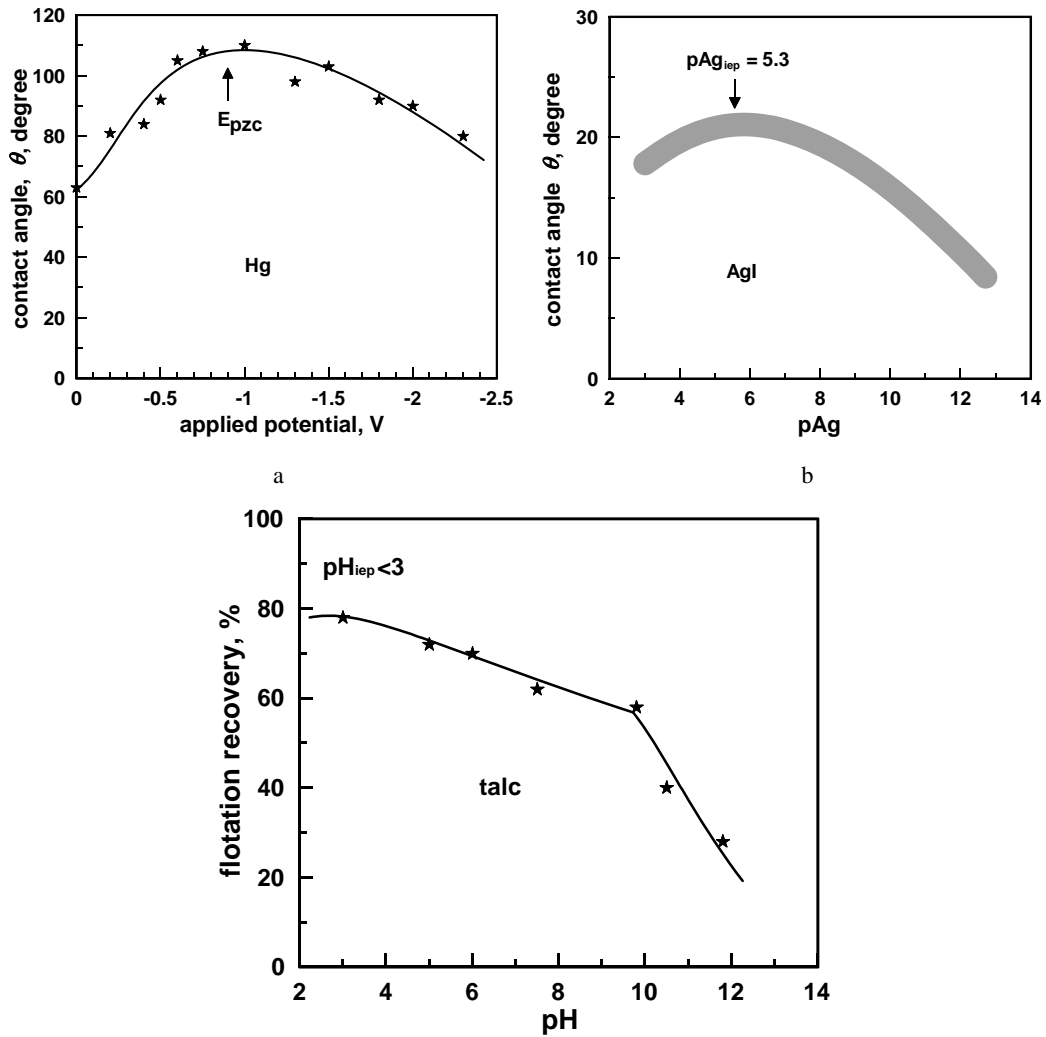
Fig. 12.18. Influence of potential determining factors on contact angle and flotation:
a – mercury, depending on applied potential (activity of electrons)
(after Nakmura et al., 1973), b –iodargyrite (silver iodide) depending on concentration of potential deter-
mining ions (Ag^+) (Billett et al., 1976),
c – talc ($Mg_3[(OH)_2Si_4O_{10}]$) depending on concentration of H^+ ions (Chander et al., 1975)
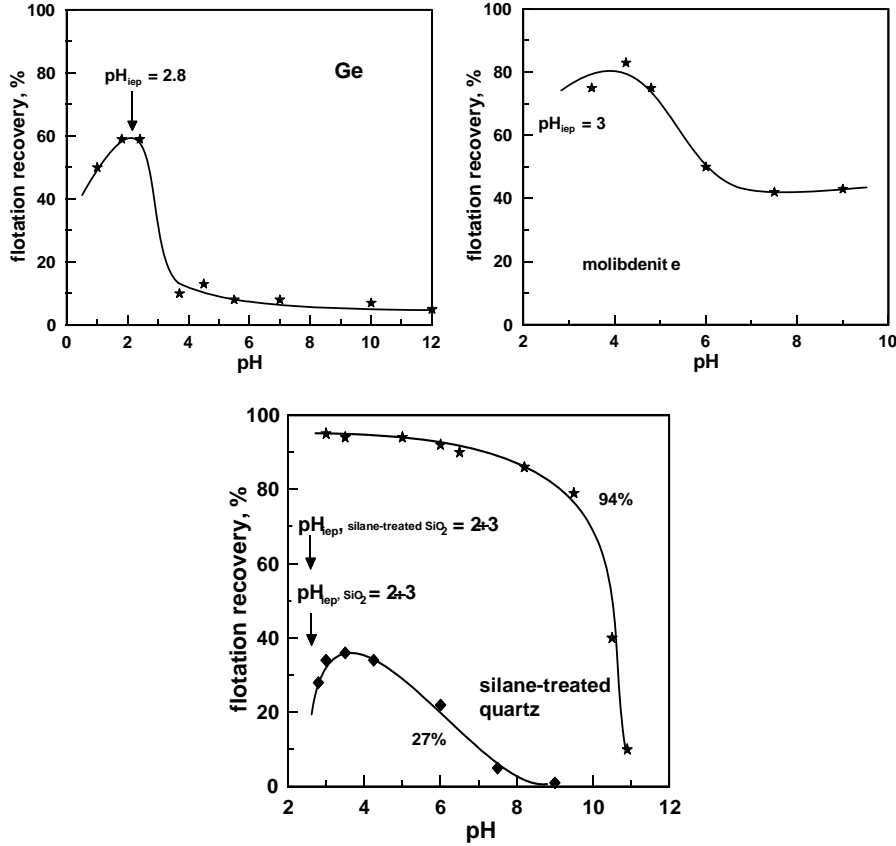
Fig. 12.19. Influence of pH on collectorless flotation of various hydrophobic and rendered hydrophobic materials: a – germanium (Drzymała et al., 1987), b – molybdenite (Chander et al., 1975), c – quartz covered with ether 27 or 94% of silane hydrophobic groups (Laskowski and Iskra, 1970)

A precise description of the effect of electrical charge on wetting angle and flotation is not simple, since any alteration of the solution composition causes changes at all three interfaces influencing the contact angle and flotation. For naturally hydrophobic substances it can be assumed, without a considerable error, that the solid–water interface is the most sensitive to the changes of the electrical charge. Therefore the surface energy γ_{sc} of this interface can be split into a chemical component γ^0_{sc} and the part dealing with the effects involving electrical double layer F^{edl}_{sc} (Ralston and Newcombe, 1992). This can be written as:

$$\gamma_{sc} = \gamma^0_{sc} + F^{edl}_{sc}. \tag{12.15}$$

After inserting this relation into the Young equation we get an expression for a wetting angle, measured through the water phase, depending on potential determining

factor *X*, which causes the increase of the electrical charge and electrical potential at the interface:

$$\cos\theta(\mathrm{pX}) = \frac{\gamma_{sg} - (\gamma_{sc}^0 + F_{sc}^{edl}(pX))}{\gamma_{cg}} = \cos\theta_{pzc} - \frac{F_{sc}^{edl}(\mathrm{pX})}{\gamma c_{cg}} \,, \qquad (12.16)$$

where p*X* denotes negative logarithm of *X* ions concentration (p*X*=-log[*X*]).

Basing on the electrocapillary data and other measurements enabling determination of interfacial energy it can be concluded that since F^{edl}_{sc} can be only negative, therefore, according to equation (12.16) the lowest value of cos θ, i.e. the largest contact angle occurs at pzc, where $F^{edl}_{sc} = 0$. Any decrease of the solid–liquid interfacial energy results in the decrease of the contact angle values, i.e. decreased hydrophobicity.

The value of F^{edl}_{sc} depends on the system subjected to flotation, that is on the kind of material and the method of regulation of the electrical charge. If electrical charge is regulated using external source of electrons, as in the case of mercury, then it is different from substances whose surface potential is determined by the Nernst equation, and still different when the surface is described as a non-nerstian one. Table 12.12 presents F^{edl}_{sc} expressions useful in description of different flotation systems.

Table 12.12. Expression for calculating F_{sc}^{edl}, useful for determination of influence of different potential determining species on contact angle in flotation systems by means of Eq. 12.16 (after Ralston and Newcombe, 1992)

System	Potential determining species	Example	F_{sc}^{edl}
Ideally polarized body	electrons	mercury–water	$F_{sc}^{edl} = -\displaystyle\int_{E_0}^{E-E_0} \sigma_0\, dE$ ***
Nernstian surface*	primary potential determining ions	AgI -Ag$^+$ aqueous solution	$F_{sc}^{edl} = -\displaystyle\int_0^{\psi_0} \sigma_0\, d\psi$ $F_{sc}^{edl} = -\dfrac{8 n_0 kT}{\kappa}\left(\cosh\dfrac{ze\psi_0}{2kT} - 1\right)$ **
Non-nernstian surface	secondary ions	solids–aqueous solution with regulated pH	$F_{sc}^{edl} = -\displaystyle\int_0^{\psi_0} \sigma_0\, d\psi + F_{sw,konf}^{edl}(pX)$ ****

* For nernstian surface $\psi_0 = f(pX)$ fulfills the Nernst equation.

** For edl fulfilling the Gouy–Chapman equation.

*** Modified equation of the Lippmann electrocapillary curve relating surface potential change and applied potential change.

**** $F_{sc}^{edl}(pX)$ is a correction for entropy resulting from the structure of edl.

As it has already been stated, the occurrence of surface charge for naturally hydrophobic and rendered hydrophobic (outside the flotation environment, e.g. silane-treated quartz) worsens flotation (Fig. 12.19c). However, if hydrophobization is not permanent but resulting from the reaction between collector ions on the surface directly in the solution, the effect of concentration of potential determining ions becomes more complicated, since apart from diminishing hydrophobicity and flotation, which results from electrical effects, there also is competition between potential determining and collector ions for the surface.

The above discussion does not take into account the properties of solid–gas (air) and water–gas interfaces. However, both interfaces can contribute to the hydrophobicity of flotation systems. The solid–air interface can, as the pH and ionic strength changes, alter their surface energy due to adsorption of water vapor, which leads to π change. The water–air interface, in turn, has its iep near $pH_{iep}=3.5$ (Tab. 12.11). Thus, the electrical charge of this interface also depends on pH. Similarly, the surface tension of aqueous solutions depends on the electrolyte concentration, i.e. pH and salts regulators. At low electrolyte concentrations surface tension decreases, which is connected with the increase of electrical charge of the interface and it is predicted by the Lippmann equation (12.14), as well as by properly solved Gibbs equation for solutions of different pH (de Bruyn and Agar, 1962), or for salts (Ratajczak, 2001). The effect of electrolytes on the decrease of surface tension finds its proof in the measurements and it can be recorded for all kinds of interfaces. For the water–air interface the presence of small amount of salts results in the so-called Jones-Ray effect (Fig. 12.20a) (Adamson, 1967). At higher electrolyte concentrations the surface tension of aqueous solutions of acids (HCl, HNO_3, $HClO_4$) decreases, while for bases and most salts increases (Fig. 12.20b). There are several theories trying to explain this phenomenon, which are mainly based on the so-called *negative adsorption* (Pugh et al., 1997). Quite probably there is simpler explanation, proposed by Gaudin (1963), that the increase in water surface tension results from additivity of surface tensions of water and electrolyte with certain involvement of the positive and negative adsorption and electrical charge. Indeed, surface tension of pure (undiluted) acids is lower than that of water, while salt surface energy is higher than $\gamma_{cg} = 72.8 mN/m$.

The electrical phenomena at the interfaces can be used for estimation of adsorption. Especially useful can be measurements of zeta potential of particles in the solutions before and after adsorption, as it will be shown in other chapters for the quartz-amine system. It should be also noticed that the zeta potential for both hydrophobic and hydrophilic materials without acidic or basic functional groups are similar and their iep is near $pH = 3.5$ (Fig. 12.21).
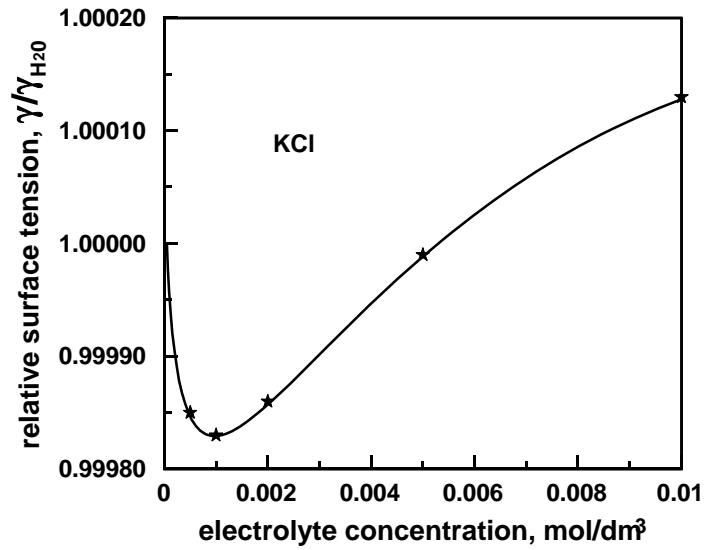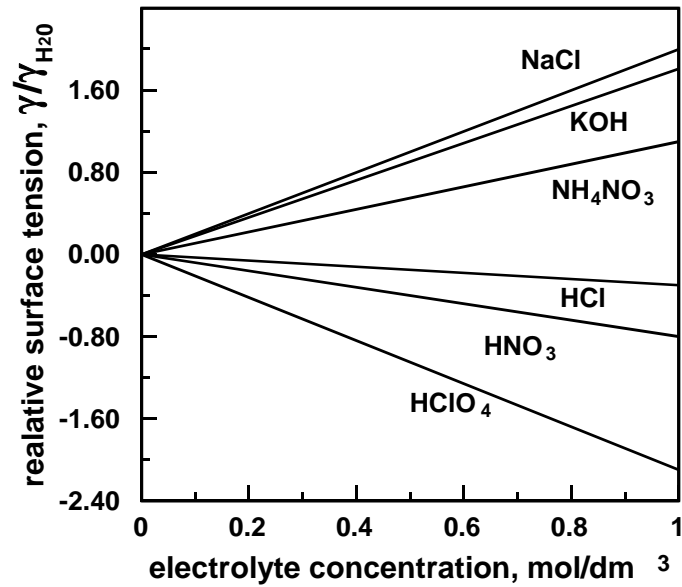
Fig. 12.20. Influence of electrolyte on surface tension of water:
a) the Jones–Ray effect at low concentrations of salts (Adamson, 1967),
b) at greater salt concentrations (Weissenborn and Pugh, 1996)
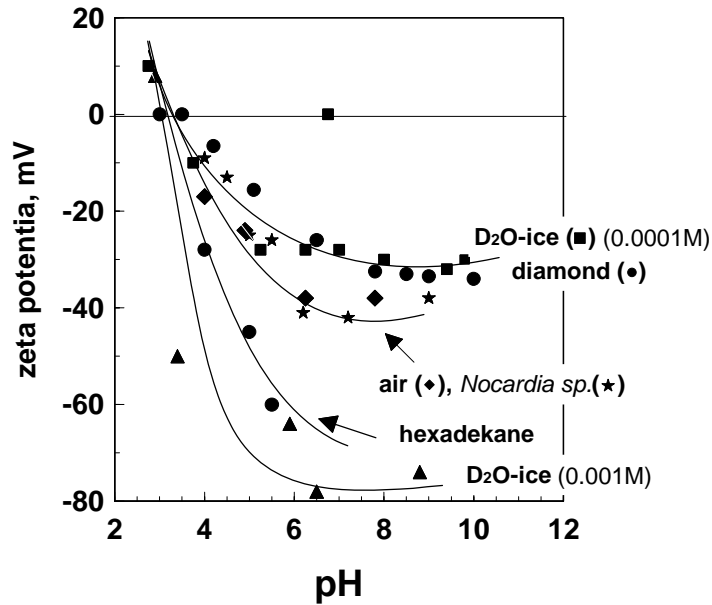
Fig. 12.21. Comparison of zeta potential in aqueous solutions containing 10^{-3} M NaCl
for different materials without functional groups having either acidic or alkaline character
(Drzymała et al., 1999; with permission of Academic Press and the authors)

12.4. Delineation of flotation

Flotation, as any other process of separation, depends on properties of material used as the feed, flotation device and the way flotation is conducted. The main material parameter of the flotation is hydrophobicity. The fact that the hydrophobicity is necessary for flotation (though not always sufficient) can be proved by simple experiments. Gypsum subjected to flotation in water does not float and a drop of water put on a larger piece of gypsum wets completely the surface pointing to the contact angle equals zero. Such a simple experiments can fail in the case of other minerals, e.g. quartz or calcite, which are also hydrophilic and do not float, but a certain contact angle is sometimes detected on these minerals. This can result from adsorption of some contaminants or perhaps the receding contact angle, not the equilibrium one, is important in flotation, which for mentioned above SiO_2 and $CaCO_3$ is zero. In the literature there is disagreement whether or not gold is hydrophobic. Presently, the prevailing opinion is that gold is hydrophilic, yet sorption of air components, including water vapors, can cause its hydrophobicity (Drzymała 1994c). This phenomenon is connected with high surface energy of gold, which easily adsorbs other substances to decrease it. Hydrophilicity of gold can be theoretically predicted on the basis of the Fowkes equa-

tions (12.4) and (12.7), using the Hamaker constant, which is exceptionally high for gold ($\sim 5 \cdot 10^{-19}$J).

The necessity of non-zero contact angle for flotation was also proved by Yarar and Kaoma (1984). They floated naturally hydrophobic substances, including graphite and sulfur, in the presence of increasing amount of ethyl alcohol which lowers the surface tension of the solution. They recorded a cease of flotation as soon as the value of contact angle reached zero. Similar results were obtained by other authors (Yarar and Alvarez 1988, Hornsby and Leja, 1980, Kelebek, 1987).

The condition of non–zero contact angle to facilitate flotation can be also proved by thermodynamic analysis of the process. Flotation can be treated as a process analogical to a chemical reaction. It takes place between particle and bubble both immersed in water:

$$\text{particle} + \text{bubble} = \text{particle-bubble aggregate} \qquad (12.17)$$
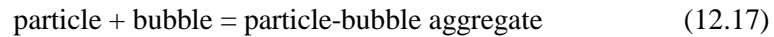
and change of the free enthalpy (thermodynamic potential) (mJ/m^2) of the process can be calculated taking into account the fact that attachment a unit area of particle with a unit area of bubble creates a unit area of the particle–bubble interface:

$$\Delta G_{\text{flotation}} = \Delta G_{\text{products}} - \Delta G_{\text{substrates}} = \gamma_{sg} - (\gamma_{sc} + \gamma_{cg}). \qquad (12.18)$$

Formula 12.18 is know as the Dupre equation (Dupre, 1869). After introducing the Young relation (Eq. 12.1) to Eq. (12.18) (Pockels, 1914), we get the Young-Dupre formula:

$$\Delta G_{\text{flotation}} = \gamma_{cg} \left(\cos\theta - 1\right). \qquad (12.19)$$

It results form equation (12.19) that the contact angle will more than zero when $\Delta G_{flotation}$ is negative. This is in agreement with the second principle of thermodynamics which says that reaction (in this case flotation) may take place when ΔG of the process is negative.

The contact angle in flotation is effected not only by parameters included in the Young equation, i.e. energy of interfaces involved in forming the particle–bubble aggregate but also the size of bubble and particle as well as their densities. Therefore, in some cases contact angle will not be formed, since a particle will be too heavy and will detach from the bubble. Flotation can also fail when the hydrophobic particle is too light (lack of successful collisions). For these reasons each method of flotation features its own upper and lower limits of floating particle size (Ralston, 1992).

The magnitude of the interfacial tension depend on such factors as kind of bonding (covalent, metallic, ionic) between the phases and electrical charge at the interface. On the basis of these and further pieces of information one can build a pyramid of parameters, effecting hydrophobicity (Fig. 12.22a). A complete description of flotation may require more than 100 parameters (Fig. 12.22b).
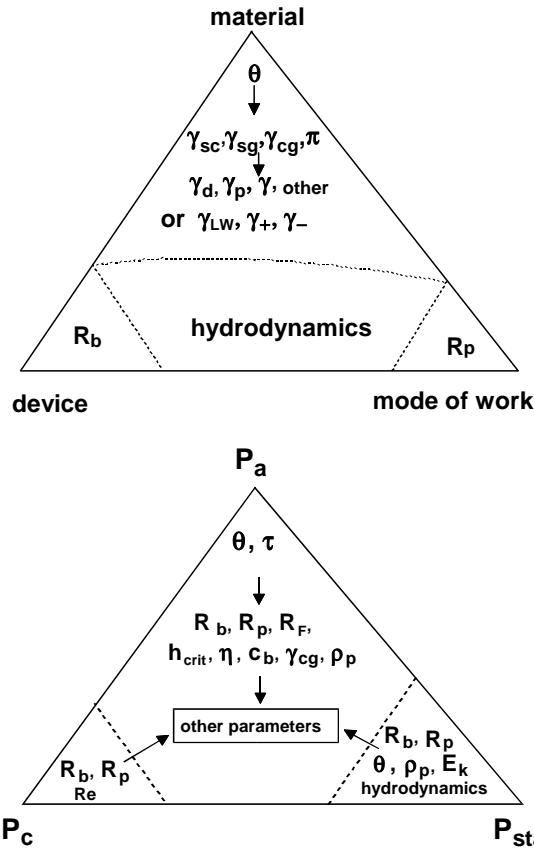
Fig. 12.22. Most important parameters in delineation of flotation:
a – static, b – dynamic delineation (symbols are explained in Table 12.13)

However, flotation is a dynamic, time dependent, process. Very often we want to know how much time is needed for flotation. Complete description of flotation, including the time as a parameter is difficult. There are some general models of flotation which combine many parameters of flotation. On of them is the Schulze model (Schulze, 1984; 1992; 1993; Nguyen et al., 1997) which is most advanced. Other models were proposed by Mao and Yoon (1997), Varbanov Forssberg and Hallina (1993), and Rubinstein and Samygin (1998). The common feature of all models is that they divide flotation into three subprocesses, i.e.:

- collision of bubble with mineral particle (collision)
- forming thin film between bubble and particle, and breaking the film after reaching a critical thickness (h_{kryt}), followed by formation of contact angle
- forming stable particle–bubble aggregate (stability).

The overall probability P of flotation is:

$$P = P_c \, P_a \, P_{stab}, \tag{12.20}$$

where probability of flotation process P is a product of probability of particle collisions with bubble (P_c), particle adhesion to the bubble (P_a), and resistance to detachment of particle from bubble during movement of the bubble-particle aggregate in the flotation cell (P_{stab}).

The second common feature of general models of flotation is relating probability with kinetics of the process. Although equations describing flotation kinetics can assume different forms, it is assumed in most models that kinetic is of the first order:

$$\mathrm{d}N_p \, /\mathrm{d}t = -k \, N_p, \tag{12.21}$$

where:

N_p – concentration of floating particles in a unit volume
k – flotation rate constant
t – flotation time.

The third common feature of the general models of flotation is the relation between the three subprocesses with different flotation parameters. Table 12.13 compares three general models of flotation. More details regarding the models can be found in the original publications.

Table 12.13. Models of flotation

General models of flotation ($dN_p/dt = -k\,N_p$)		
Mao–Yoon (1997)	Schulze (1993)	Varbanov–Forssberg––Hallin (1993)
$k = P_c P_a P_{stab} 0.25\, S_b$	$k = P_c\, P_a\, P_{stab}\, P_{tpc}\, Z N_b$	$k = \delta E U C_b$
$P_c = \left[\dfrac{3}{2} + \dfrac{4\,\mathrm{Re}^{0.72}}{15}\right]\left(\dfrac{R_p}{R_b}\right)^2$	$P_c = \left(\dfrac{R_b}{R_b}\right)^2$	$\delta = f(P_c) = R_p R_b$
$P_a = \exp\left(-\dfrac{E_1}{E_k}\right)$	$P_a = 1 - \exp\left[-\left(\dfrac{\tau_c - \tau_{\min}}{\tau_i}\right)\right]$ $\tau_c = [\pi^2 R_p^3\,(\rho_p + 1.5\rho)/3\eta]^{0,5}(1.39 - 0,46 \ln R_p)$ $\tau_i = 3\eta\, R_F^2\, R_p/8\gamma c_b h^2_{\mathrm{kryt}},$ $h_{\mathrm{kryt}} = 23.3[\gamma(1 - \cos\theta_A)]^{0,16}$	$E = f(P_a)$ $E = 1 - \cos\theta$
$P_{stab} = 1 - P_d$ $P_d = \exp\left[-\dfrac{\gamma\pi R_p^2(1-\cos\theta)^2 + E_1}{E_k'}\right]$	$P_{stab} = 1 - \exp(1 - 1/\mathrm{Bo}'),$ $\omega^* \cong 180° - \theta/2,$ $\mathrm{Bo}' = 4 R_p^2(\Delta\rho g + \rho_p a) + 3R_p(\sin^2\omega^*)\,f(R_b)/C$ $C = |6\gamma\sin\omega^*\sin(\omega^* + \theta)|,$ $f(R_B) = (2\gamma/R_B) - 2R_b\rho g$	P_{stab} taken into account in other parts of expression for k
	$P_{tpc} \cong 1 - \exp(-\tau_v/\tau_{tpc})$ $\tau_v = 0.6(R_p + R_b)^2/\nu$ laminar flow $\tau_v = 13(R_p + R_b)^{2/3}/\varepsilon^{*1/3}$ turbulent flow	$U = g(R_b^2\,\rho + 2 R_p^2\,\Delta\rho)/(9\eta)$ $C_b = 3Q/(4\pi R_b^3\, SV)$

dN/dt – flotation rate,

a – centrifugal acceleration acting on particle-bubble aggregate in a vortex of liquid,

Bo´ – Bond's number,

c_b – rigidity of bubble surface ($c_b = 1$ for rigid uneven surface, $c_b < 1$ for movable smooth surface),

C_b – bubble concentration in pulp (number of bubbles in 1cm^3 of pulp),

E – efficiency of attachment of particles to bubble surface (number of attached particles divided by the number of particles colliding with considered bubble),

E_1 – energy barrier for adhesion of bubble and particle,

E_k – kinetic energy of collision of bubble with particle,

$E_k´$ – kinetic energy of detachment of particle and bubble (calculated from the French–Wilson Eq.),

g – acceleration due to gravity,

h_{kryt} – critical film thickness on surface of particle,

k – rate constant of flotation,

N_b – number of bubbles in flotation cell at a considered time,

N_p – number of particles subjected to flotation at a considered time,

P_a – probability of adhesion of particles to a bubble,

P_d – probability of detachment of particles from a bubble ($P_d = 1 – P_{\text{stab}}$),

P_{stab} – probability of stability of particles-bubble aggregate,

P_{tpc} – probability of formation of particle-bubble-water contact,

Q – flow of air in flotation machine, m^3/s,

R_p – particle radius,

R_b – bubble radius,

R_c – radius of the stream enabling collision of particle with bubble,

R_F – size of thin film between particle and bubble during collision,

Re – Reynolds number,

S – cross section area of flotation machine, m^2,

S_b – area of bubbles leaving flotation cell per time unit and per cross section area ot the cell,

V – rate of ascending bubble, m/s,

V_b –surface velocity of aeration defined as volume rate of aeration normalized per cross section of the flotation column,

U – velocity of particles in relation to velocity of bubble in the pulp,

Z – number of particle collisions per unit time,

γ – surface tension of aqueous solution,

δ – quantity characterizing efficiency of collision between particles and bubbles,

ε^* – dissipation energy in flotation cell,

$\Delta\rho$ – effective density of particle in water,

η – dynamic viscosity,

v – kinematical viscosity,

ρ – pulp density,

ρ_p – particle density,

θ – contact angle,

θ_A – advancing contact angle,

τ_v – life time of liquid vortex in flotation cell which destroys the particle–bubble aggregate,

τ_{tpc} – time needed to form permanent three-phase solid-gas-liquid contact,

τ_c – collision time of bubble and particle,

τ_i – induction time (time of removing liquid film from particle and forming attachment),

τ_{min} – minimal time of contact,

π $= 3.14$,

ω^* $= 180 – \theta/2$.

The value of the periodic flotation rate constant can be determined from the change of particle yield as a function of time, according to the relation:

$$\varepsilon(t) = 1 - \exp(-kt). \tag{12.22}$$

It should be added, that the particle - bubble adhesion takes place not only as a result of collision, but also sliding on the bubble. Therefore, the probability of adhesion will depend on kind of collision and it can have two forms: probability of adhesion through collision (P_{ac}) and probability of adhesion resulting from sliding (P_{asl}). According to Schulze (1992) prevalence of any of these forms of collision depends on many factors, not all of them being known. Generally, it can be stated that collision involving deformation takes place for large and heavy mineral particles which move perpendicularly to the bubble surface. The contact through sliding occurs for small and light particles moving at a low speed. Probability of adhesion, resulting from sliding, can be described with the use of the equation determining particle movement in the area of flowing air bubble:

$$P_{asl} = \sin^2 \varphi_{crit}, \tag{12.23}$$

where φ_{crit} is a critical value of the collision angle which, when exceeded, makes adhesion due to sliding impossible.

The trajectory of moving particles causing either collision or sliding is shown in Fig. 12.23.
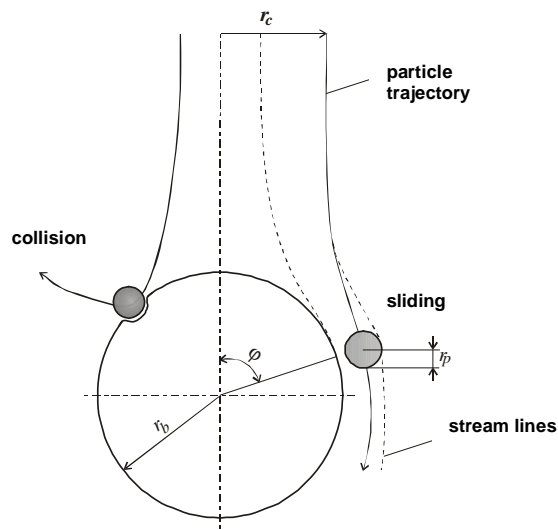
Fig. 12.23. Flotation can take place as a result of either bubble-particle collision or catching particle by bubble

The probability of adhesion resulting from sliding is strictly connected with the character of flow (laminar or turbulent), property of the bubble surface, critical thickness of the film at which its breaking takes place, as well as on particle size, because smaller particles have higher P_{asl} value.

To calculate the conditions for good flotation using general theories of flotation, not only contact angle but also such parameters as size of particles and bubble, induction time, as well as the value of energy barrier between particle and bubble have to be taken into account. It makes delineation of flotation quite complex.

The contact time is an important parameter because is decides about forming a contact angle in dynamic conditions of flotation. For a successful flotation the contact time has to be greater than the induction time. The latter one is measured in the so-called contact time apparatus. The formula presented in Table 12.13, as well as the results of examinations indicate that contact time depends on such parameters as hydrophobicity (Fig. 12.24) and particle size (Fig. 12.25). Figure 12.26 shows, after Laskowski and Iskra (1970), that at the same hydrophobicity, shortening the contact time improves flotation. It can be accomplished for instance by introducing salt to the solution.
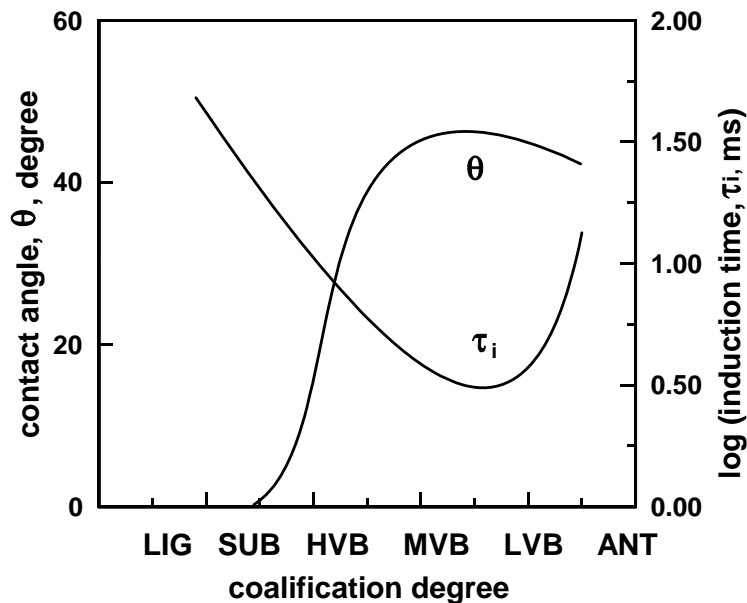
Fig. 12.24. Induction time depends on hydrophobicity
(after Ye and Miller (1988) and Ye et al., 1989).
Various coals from lignite (LIG) to anthracite (ANT).
Symbols LIG, SUB denote type of coal according to American standards

The stability of the particle–bubble aggregates is described by the DLVO theory discussed in details in chapter 13 which deals with oil agglomeration. Difficulties with using the DLVO theory for the description of flotation can be caused by lack of data on zeta potential of bubbles, because such measurements are quite complex. The zeta potential of air bubbles was described by Schulze, 1984; Li and Somaundaran, 1993, Laskowski et al., 1989; Usui and Sasaki, 1978.
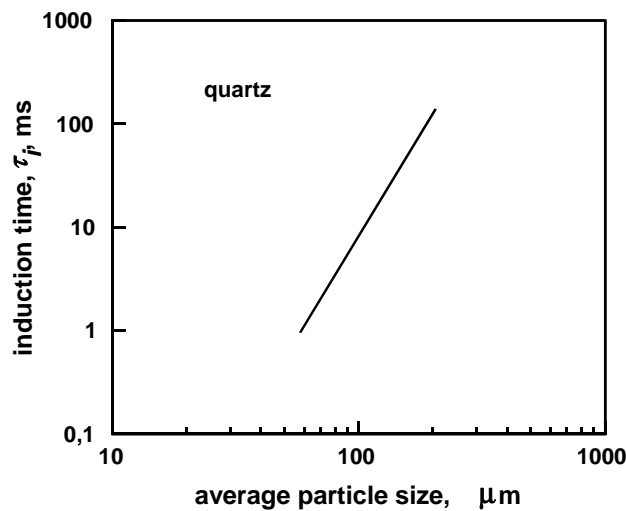
Fig. 12.25. Induction time depends on particle size. Data after Yordan and Yoon, 1986
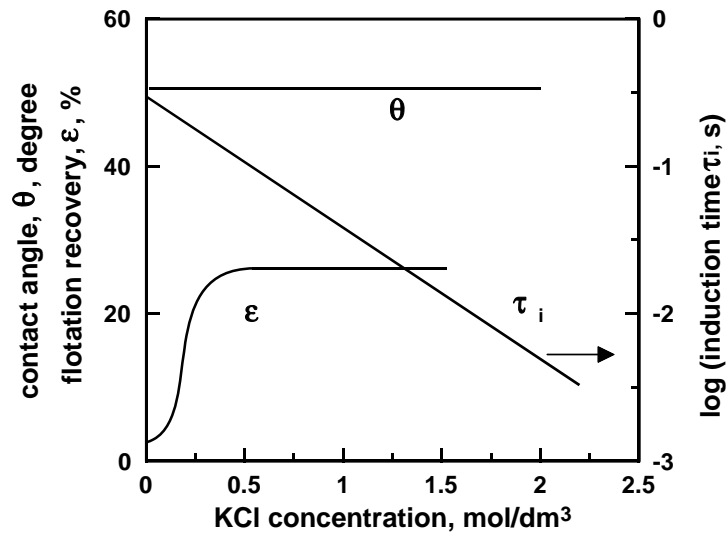
Fig. 12.26. At certain hydrophobicity flotation increases with decreasing induction time
(after Laskowski and Iskra, 1970)

The diagram presenting the dependence of interaction energy E between bubble and mineral particle on distance H between these objects is shown in Fig. 12.27. Energy barriers in the flotation system are indicated.
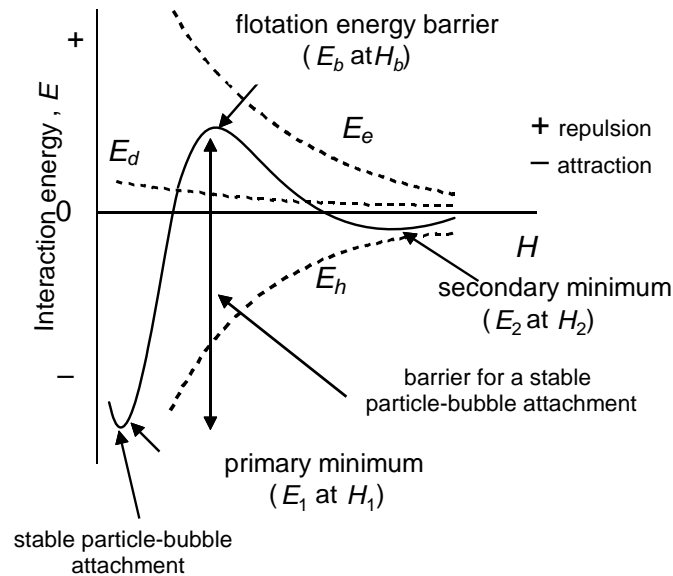
Fig. 12.27. Example of interaction energy E between bubble and particle in water resulting from the DLVO theory: E_e – electrostatic, E_d – dispersion, E_h – hydrophobic interactions. Solid line is the sum of these interactions

To describe the rate of flotation (dN/dt) not only the first but also higher orders kinetic equations can be used. According to Arbiter and Harris (1962), Garcia–Zunga (1935, Soc. Nac. Miner. Santiago, Chile, 47, p. 83) proposed a general equation:

$$\frac{dN}{dt} = -kN^n ,\qquad (12.24)$$

where:
N – number of hydrophobic particles in the cell which are able to float at flotation time t,
n – constant indicating the so-call order of kinetic equation,
k – flotation rate constant.

There are other approaches to kinetics of flotation which are summarized in Table 12.14.

Table 12.14. Models applied for kinetics of flotation
(after Dowling et al., 1985 and Lynch et al. 1981)

Model	Relation
Classic first order	$\varepsilon = \varepsilon_\infty [1 - \exp(-k_1 t)]$
Modified first order	$\varepsilon = \varepsilon_\infty \{1 - 1/(k_2 t)[1 - \exp(-k_2 t)]\}$
For reactor with ideal mixing	$\varepsilon = \varepsilon_\infty [1 - 1/(1 + t/k_3)]$*
Modified for gas–solid adsorption	$\varepsilon = \varepsilon_\infty k_4 t/(1 + k_4 t)$*
Kinetics of second order	$\varepsilon = (\varepsilon_\infty)^2 k_5 t/(1 + \varepsilon_\infty k_5 t)$
Modified second order	$\varepsilon = \varepsilon_\infty \{1 - [\ln(1 + k_6 t)]/(k_6 t)\}$
Two rate constants	$\varepsilon = \varepsilon_\infty [1 - \{\varphi \exp(-k_7 t) + (1 - \varphi) \exp(-k_8 t)\}]$
Distributed rate constants	$\varepsilon = \varepsilon_\infty [1 - \int\limits_0^\infty \exp(-kt)\, f(k, 0)\, dk]$

* Equivalent models because $k_3 = 1/k_4$.

ε – flotation recovery after time t,

ε_∞ – maximum recovery,

φ – fraction of particles having lower flotation rate constant, k_7,

k – flotation rate constant.

12.5. Flotation reagents

12.5.1. Collectors

Flotation requires hydrophobicity of the mineral particle but only a few mineral substances are naturally hydrophobic. Therefore, there is a need to use various reagents, called collectors, to render hydrophilic and slightly hydrophobic particles hydrophobic. The hydrophobizing power of a collectors results from its chemical and physical interactions with the surface and is usually described from physical chemistry point of view. The role of chemistry in the description, analysis and assessment of flotation process is shown in Fig. 12.28.

Flotation process can be used to separate particles from water but it is most often used to separate particles of different materials. In such a case the applied collector has to be selective. Selectivity of a collector relies on favored adsorption of one type of particles of the flotation suspension. Flotation collectors effect not only particle hydrophobicity but also other parameters of flotation, including the time of particle-bubble contact required to form a stable particle-bubble aggregate, as well as the stability of froth.
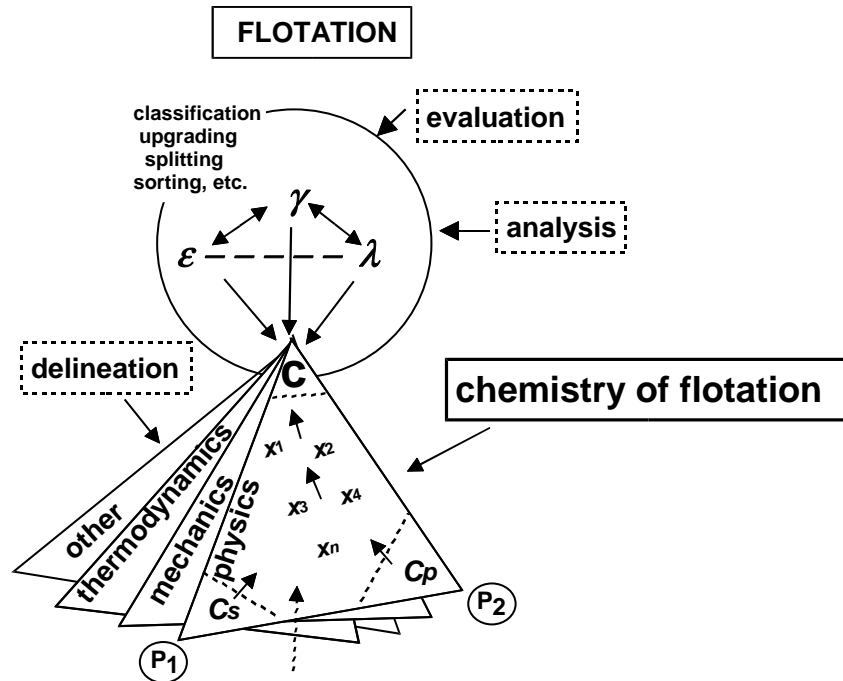
Fig. 12.28. Chemistry plays an important role in flotation

There are many various reagents used as flotation collectors (Gaudin, 1963; Las-kowski, 1969), and there are many possible ways of their classification. One of them is presented in Fig. 12.29. Collectors are usually divided into polar and a non-polar. The non-polar collectors can be further divided into hydrocarbons and their derivates, sulfur organic compounds, and alcohols with their derivates. Generally, the non-polar collectors are insoluble or only slightly soluble in water. The adsorption of alcohol–type collectors takes place mainly due to hydrogen bonding, while in the case of re-maining non-polar collectors the adsorption is due to the van der Waals interactions.

The family of polar collectors can be divided into cationic, anionic, amphoteric and chelating collectors. The cationic collectors have positively charged functional groups, anionic collectors are negatively charged, while amphoteric ionic collectors contain both cationic and anionic functional groups. A characteristic feature of simple ionic collectors is forming single bonds between collector and mineral surface. Far more complex are reaction occurs with the chelating collectors. They form strong chemical rings involving the chelating compound and bulk and surface ions. The adsorption of non-polar, ionic, and chelating collectors is shown in Fig. 12.30.

```
                              collectors
                    ┌──────────────┴──────────────┐
                  ionic                       non-polar
            ┌───────┴────────┐          ┌─────────┴─────────┐
        chelating          simple     sulfur          hydrocarbons
                                      compounds       and derivatives
                                              alcohols

    S-S   →  xanthates
                                     cationic  →  amines
    O-O   →  fatty acids

    N-N   →  diamines            anionic  →  merkaptans

    S-N   →  carbamines
                                                   amino-
    O-S   →  monothiocarbonates   amphoteric  →   alkylacids

    O-N   →  oximes
```
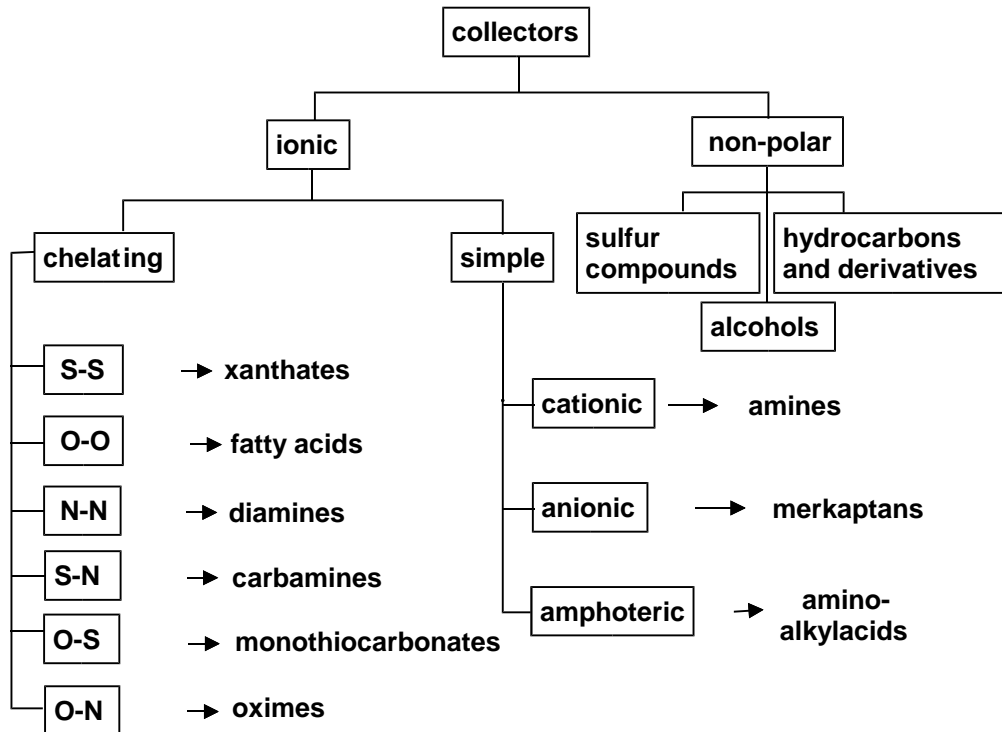
Fig. 12.29. One of several ways of collectors classification

Formation of a surface bond between the ionic collector and a metal ion on the particle surface (–MeOH) can be written as a chemical reaction:

$$R–SH + HO–Me– = R–S–Me– + H_2O \tag{12.25}$$
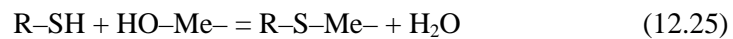
while the formation of a chelating bond, using hydroxamic acid as an example, is given by the reaction:

$$
\begin{array}{c}
R-C=O \\
\;\;\;| \\
HN-\!\!-OH
\end{array}
\;+\; HO-Me \;=\;
\begin{array}{c}
R-C=O_{\searrow} \\
\;\;\;| \quad\;\; Me- \\
HN-\!\!-O^{\nearrow}
\end{array}
\;+\; H_2O \tag{12.26}
$$
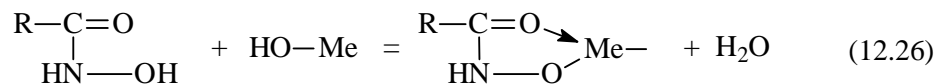
where sign �’ refers to additional coordinate bond with the use of a free electron pair coming from the oxygen atom while Me- denotes metal ion forming the particle surface.

Chelating bonds can be formed by collectors capable of interacting with metal ion on the surface. They form four, five or six-segment ring. One of the bonds is ionic–covalent–metallic in character, while the second one is a coordination bond. The collectors with functional groups containing two atoms out of the group of N, S, P, and O

are capable of forming the chelating bond. Therefore, the chelating collectors can be divided into subgroups such as S-S, O-O, S-O, S-N, and N-P collectors.
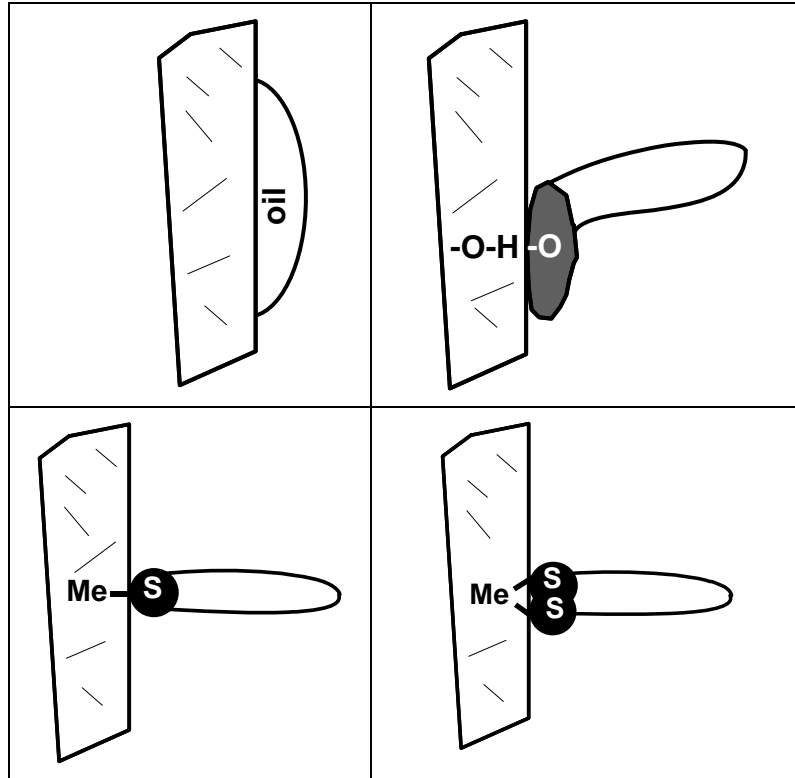
Fig. 12.30. Possible modes of adsorption of collectors at particle-water interface:
a – adsorption of oil on hydrophobic particle with van der Waals forces,
b – adsorption of apolar molecule of collector by means of hydrogen bonding,
c – adsorption of polar collector by means of simple chemical bond
or electrostatic attraction, d – adsorption with formation of chelating bond.
Hydrophobic part of the collector is shown in white while hydrophilic as black
Not to scale.
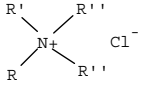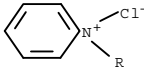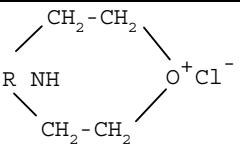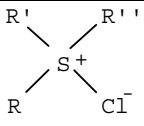
Some researchers believe that certain ionic collectors, although capable of forming chelating bonds, do not form them on mineral surfaces (Sprokin, 1976, Parfitt and Russell, 1977; Cornell and Schindler 1980), especially when four-segment rings are involved.

Tables 12.15–12.20 list, after Nagaraj (1988), selected non-polar, cationic, anionic, amphoteric and chelating collectors. In the tables symbols R, R' and R'' stand for hydrocarbon radicals.

Table 12.15. Nonionic collectors

Collector	Example
Hydrocarbons and derivatives	fuel oil, naphtha, heptane, benzene, halogen derivatives of hydrocarbons
Sulfur compounds	dixanthogen (R–O–C(=S)–S–)$_2$ formic xanthate R–O–C(=S)–S–C(=O)–O–R´, alkyl disulfides R–S–S–R
Alcohol and derivatives	alkylphenyl(polyethoxy) alcohols (Triton, Tergitol, Brij), alkylphenols, higher alcohols

Table 12.16. Ionic collectors

Collector	Example
Cationic	
Primary amines* R–NH$_2$	n-dodecylamine C$_{12}$H$_{25}$–NH$_2$ or C$_{12}$H$_{25}$–NH$_2$·HCl (C$_{12}$H$_{25}$–N$^+$H$_3$Cl$^-$)
Secondary amines* R–(R´)N–H	di-n-amylamine, (C$_5$H$_{11}$)$_2$–NH
Tertiary amines* R–(R´)N–R´´	tri-n-amylamine, (C$_5$H$_{11}$)$_3$–N
Quarternary ammonium salts	
Diamines and triamines	diamine R–NH–(CH$_2$)$_x$–NH$_2$
Pyridinium salts	
Morpholinium salts	
Sulfonium salts	
Anionic	
Mercaptans, R–SH	Due to unpleasant smell mercaptans are not used by industry
amphoteric	
N-dodecyl-2-aminopropionic acid	C$_{12}$H$_{25}$–N$^+$H$_2$–(CH$_2$)$_2$–COO$^-$
other	C$_{12}$H$_{25}$–NH–CH$_2$–COONa, C$_{12}$H$_{25}$–N(CH$_2$–COONa)$_2$, R–(CH$_3$)$_2$N$^+$–CH$_2$–COO$^-$ (alkyl betaines)

* In practice hydrochloric forms of amine are used (for example R–NH$_2$·HCl).

Table 12.17. Selected chelating collectors. Type O–O. Based on Nagaraj, 1988

Collector	Formula	Example
Carbonic acid derivatives (fatty acids)	R–COOH	oleic, linoleic, linolenic, stearic acids
Sulfuric acid derivatives (sulfates)	R–O–SO$_3$H	dodecyl sulfate
Sulfuric acid derivatives (sulfonates)	R–SO$_3$H	dodecyl sulfonates
Phosphoric acid derivatives (phosphates)	(RO)$_2$–P(O)–OH	dialkyl phosphoric acid
Phosphonic acid derivatives (phosphonates, diphosphonates)	(RO)–(R)P(O)–OH R–(PO$_3$H$_2$)$_2$	dialkyl phosphonic acid Flotol-7,9 (1-hydroxyalkylidene-1,1-diphosphonic acid)
Phosphinic acid derivatives (phosphinate)	(R)$_2$–P(O)–OH	dialkyl phosphinic acid
Nitrosophenylhydroxylamine (ammonium salt)	(Ar–N(O$^-$)–N=O)NH$_4$	Cupferron
Salicylaldehyde	OH–Ar–CHO	Salicylaldehyde
Nitrosonaphthols	ON–nA–OH	α-nitroso-β-naphthol, β-nitroso-α-naphthol
Nitrosophenols	R–(OH)Ar(OH)–NO	nitroso alkyl resorcinol
Organic dyes		alizarin and derivatives
Hydroxamic acids	R–CO–NH–OH	Benzohydroxamic acid, potassium octylhydroxamate, IM-50 (C7-C9)

Table 12.18. Selected chelating collectors. Type S–S. Based on Nagaraj, 1988

Collector	Formula	Example
Dithiocarbonates (xanthate)	$\overset{S}{\underset{S}{}}$C - O-	Potassium ethyl xanthate (R–OCSSK)
Trithiocarbonates (tioxanthate)	$\overset{S}{\underset{S}{}}$C - S-	
Dithiophosphates	$\overset{S}{\underset{S}{}}$P(OR)$_2$	Aerofloat ((RO)$_2$P(=S)–SK)
Dithiophosphinates	$\overset{S}{\underset{S}{}}PR_2$	Aerofins
Dithiocarbamates	$\overset{S}{\underset{S}{}}$C - NR$_2$	Sodium diethyldithiocarbamate

Table 12.19. Selected chelating collectors. Type O–N. Based on Nagaraj, 1988

collector	formula	Example
Oximes		α-benzoin oxime
Hydroxyoximes (LIX series)		LIX65N
8-hydroxyquinoline and derivatives		8-hydroxyquinoline (oxine)

Table 12.20. Selected chelating collectors. Type S–N. Based on Nagaraj, 1988

Collector	Formula
Mercaptobenzothiazols	(flotagen)
Mercaptothiodiazoles	
Thiotertrahydroglyoxaline	
Mono- and dithiocarbamates	
Phenylthiourea	

Ionic and some nonionic collectors have very characteristic structure. They consist of a hydrophilic part which is adsorbed on the particle surface and a hydrophobic part which remains in aqueous phase (Fig. 12.30 and 12.31).

$$CH_3CH_2CH_2CH_2\ CH_2CH_2CH_2CH_2 \quad \boxed{COO^-}$$

tail
(hydrophobic)

head
(hydrophilic)
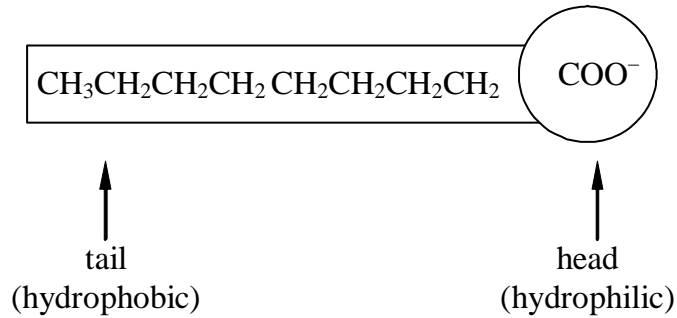
Fig. 12.31. A sketch of structure of ionic collectors using carboxylic acid as an example

Dissolved in water collectors having large hydrophobic part can mutually interact and form, depending on concentration, pre-micelles, micelles, big micelles and other forms (Fig. 12.32). The micelles occur at a certain surfactant concentration called the critical micelle concentration or shortly CMC.

a　　　　**b**　　　　**c**
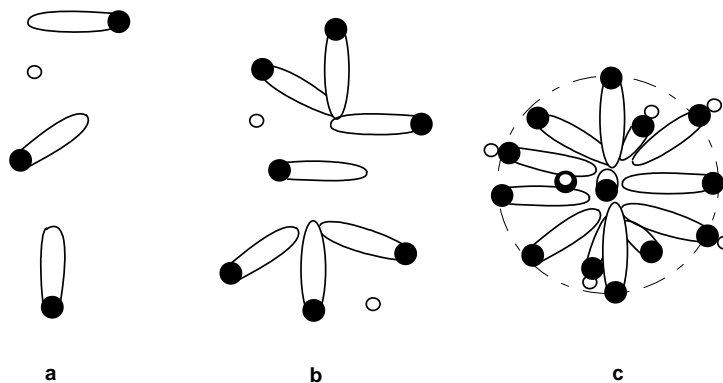
Fig. 12.32. Collector ions can be present in aqueous solution as free ions (a), premicellar species (b) spherical micelles (c). The structures appear with increasing concentration of collector in aqueous solution.
Symbol o denotes ion appositively charged to the collector ion

The CMC values for selected anionic, cationic, and amphoteric collectors are presented in Tables 12.21-12.23.

Table 12.21. Critical micelle concentration (CMC) of selected anionic collectors at room temperature (data after Mishra, 1988)

Anionic surfactant	CMC (kmol/m^3)
Sodium caprylate, C$_8$H$_{17}$COONa	$3.5 \cdot 10^{-1}$
Sodium capriate, C$_{10}$H$_{21}$COONa	$9.4 \cdot 10^{-2}$
Sodium laurate, C$_{12}$H$_{25}$COONa	$2.6 \cdot 10^{-2}$
Sodium myristate, C$_{14}$H$_{29}$COONa	$6.9 \cdot 10^{-3}$
Sodium palmitate, C$_{16}$H$_{33}$COONa	$2.1 \cdot 10^{-3}$
Sodium stearate, C$_{18}$H$_{37}$COONa	$1.8 \cdot 10^{-3}$
Sodium elaidate, trans-C$_{17}$H$_{33}$COONa	$1.4 \cdot 10^{-3}$
Sodium oleate, cis-C$_{17}$H$_{33}$COONa	$2.1 \cdot 10^{-3}$
Sodium dodecyl sulfate, C$_{12}$H$_{25}$SO$_4$Na	$8.2 \cdot 10^{-3}$
Sodium dodecylo sulfonate, C$_{12}$H$_{25}$SO$_3$Na	$9.8 \cdot 10^{-3}$
Sodium dodecylo benzene sulfonate, C$_{12}$H$_{25}$–C$_6$H$_4$–SO$_3$Na	$1.2 \cdot 10^{-3}$

Table 12.22. Critical micelle concentration (CMC) of selected cationic collectors at room temperature (data after Smith, 1988), *m* = number of CH$_2$ groups in w hydrocarbon chain R)

Cationic surfactant	Temperature °C (K)	CMC, kmol/m^3
n-alkylammonium chlorides (R–NH$_3$Cl)	30 (303)	log CMC = 1.31÷0.270*m*
N,N-dimethyl-n-dialkylammonium chlorides, R$_2$(CH$_3$)–N–CH$_3$Cl	30 (303)	log CMC = 2.78÷0.544*m* (*m* = 8, 10, 12)
N,N,N-trimetylalkylammonium bromides, R(CH$_3$)$_2$–N–CH$_3$Br	25(60) (298)(333)	log CMC = 1.98÷0.311*m* (*m* = 8 ÷16)
N-(n-alkyl)-propyl-1,3-diammonium chloride, R(H)$_2$–(CH$_2$)$_3$NH$_3$Cl	25 (298)	log CMC = 1.72÷0.295*m* (*m* = 10÷16)
n-alkylopyridinium bromides	30 (303)	log CMC = 1.70÷0*m* (*m* = 10÷16)

Table 12.23. Critical micelle concentration (CMC) of selected amphoteric collectors at room temperature (data after Smith, 1988)

Amphoteric surfactant	Temperature °C (K)	CMC, kmol/m^3
Diheptanoyl phosphatidylcholine	25 (298)	$1.4 \cdot 10^{-3}$
Dioctanoyl phosphatidylcholine	25 (298)	$2.7 \cdot 10^{-4}$
Didecanoyl phosphatidylcholine	25 (298)	$5.0 \cdot 10^{-6}$
Dipalmitoylophosphatidylocholine	25 (298)	$4.7 \cdot 0^{-10}$
N-dodecyl-2-aminopropionic acid	40 (313)	$1.65 \cdot 10^{-3}$
N, N-dimethyl-N-(3 sulfopropyl dodecylamine	30 (303)	$3.6 \cdot 10^{-3}$
C$_{12}$H$_{25}$(CH$_3$)$_2$–N$^+$–CH$_2$–COO$^-$	30 (303)	$1.7 \cdot 10^{-3}$

Micelles of ionic collectors are not only a collection of ions. Examinations and calculations indicate that on average 45% of ionic micelles ions are bonded with the counter ions (Drzymała, 1990; Dutkiewicz, 1998). Therefore, adsorption layers of ionic collectors contain both surfactant ions and surfactant molecules. Increasing the

concentration of inorganic salts in the solution results in higher number of non-dissociated surfactant molecules in the micelles and adsorbed layers. The micelles easily adsorb at the water-air interface (Fig. 12.33). Micelles are formed by such collectors as oleates, sulfates, sulfonates and other anionic, cationic, amphoteric, and non-ionic surfactants. Certain thiocompounds including xanthates do not form micelles, and therefore, do not adsorb at the water–air interface, and thus, are not called surfactant. The micellization of xanthates requires a higher number of CH_2 groups in the hydrocarbon chain, usually 10 or more groups, while typical xanthates possess from 1 to about 9 groups.
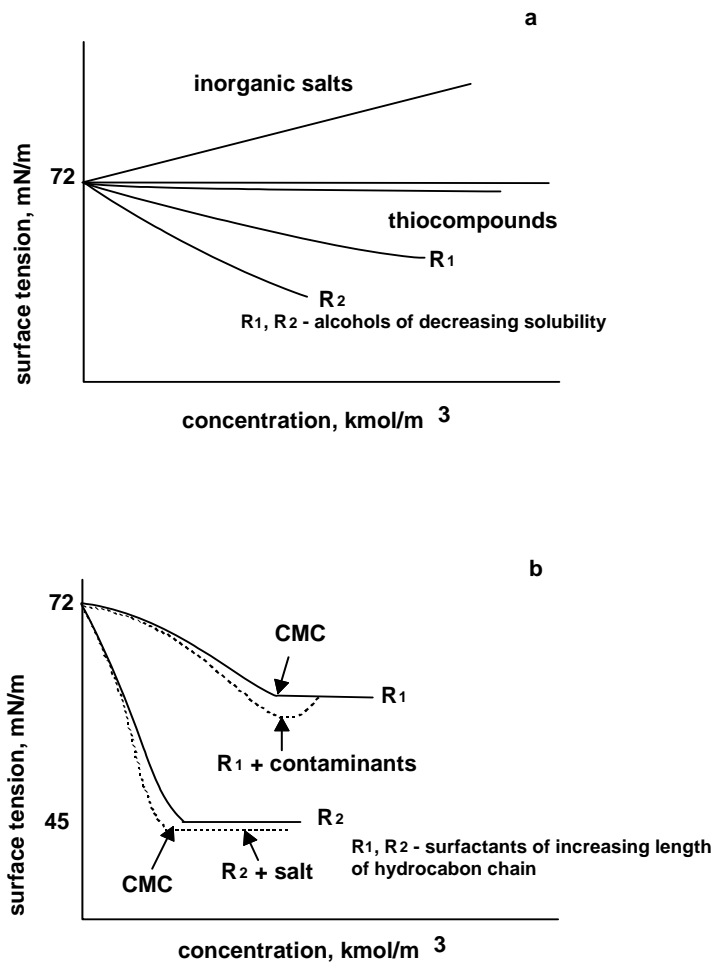
Fig. 12.33. Change of surface tension for aqueous solutions in the presence of collectors: micelle-forming (a) and not forming micelles (b). Surface tension of water in the presence of inorganic salts and alcohols are also presented (after Leja, 1982)

The decrease in the surface tension caused by surface active collectors does not result from a simple mixing of two substances that is water (surface tension 72,8 mN/m) and organic collector (surface tension from 25 to 35 mN/m), but from a considerable adsorption of the hydrophobic surfactant ions or molecules at the water–air interface. Significant adsorption of collector ions at the interface makes the surface tension, in the vicinity of CMC, nearly equal to surface tension of pure (anhydrous) collector. It usually corresponds to a monolayer of the collector at the water-air interface.

The behavior of collectors at the air-water interface is different from that of inorganic salts, since the surface tension of aqueous solutions in the presence of salts, after a slight decrease (Fig. 12.20a), increases as salt concentration increases (Fig. 12.33a).
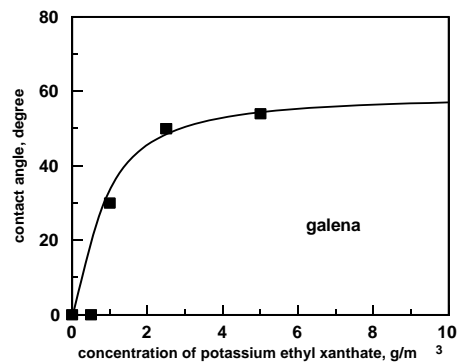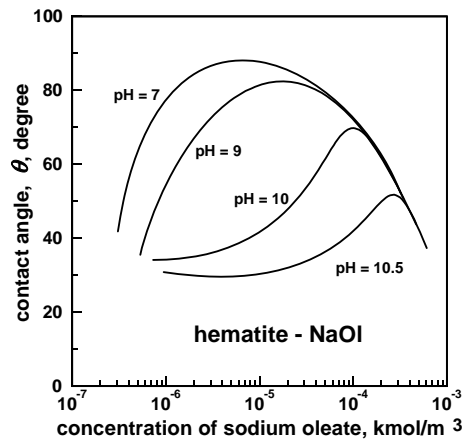
Fig. 12.34. Change of hydrophobicity (contact angle) of mineral particles as a function collector concentration: a – collector not forming micelles (Wark and Cox, 1934, Gaudin, 1963), b – micelles-forming collector (after data of Yap et al., 1981)

The association of collectors influences the hydrophobicity of mineral surface. For non-associating collectors the contact angle increases as the collector concentration increases and reaches plateau a certain constant value (Fig. 12.34a) which is characteristic for a particular hydrocarbon chain (Table 12.24). Table 12.24 shows maximum values of contact angle for different non-associating collectors.

Table 12.24. Maximum contact angle for different collectors
with ethyl and butyl chain.
After Gaudin, 1963

Collector	Chain length*	
	ethyl	butyl
Dithiocarbaminate	60	77
Mercaptane	60	74
Xanthate	60	74
Dithiophosphate	59	76
Trithiocarbonate	61	74
Monothiocarbonate	61	73

* For methyl chain (C_1) $\theta \cong 50°$, propyl (C_3) 68°, C_5 78°, C_6 81°, for greater about 90°, and for C_{16} 98° (Aplan and Chander, 1988).

The long-chained collectors associate and their contact angle, after reaching maximum, begins to decrease (Fig. 12.34) due to formation of a second layer on the existing first layer (Fig. 12.35). In the second layer the collector ion is adsorbed with a hydrophobic part on the hydrophobic part of the collector in the first layer.
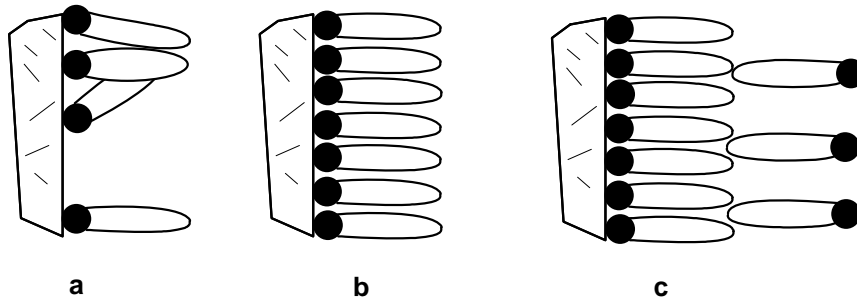
Fig. 12.35. Adsorption of ionic collector on the surface of particle with the formation of hemimicelle (a), monolayer (b) and a second layer leading to hydrophilicity (c)

It should be noticed, however, that no correlation between CMC and the point of diminishing flotation is observed (Fig. 12.36).
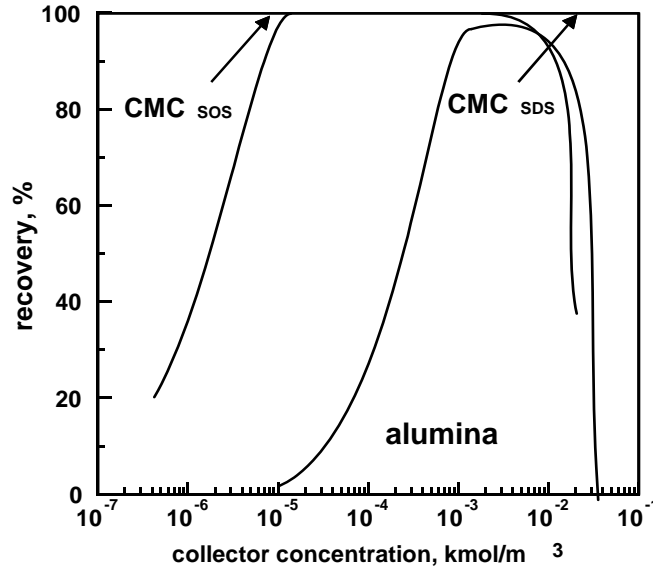
Fig. 12.36. An example of lack of correlation between CMC and flotation (after Freund and Dobias, 1995). SOS – sodium octyl sulfate, SDS – sodium dodecyl sulfate

On the other hand, there is a quite satisfactory correlation between flotation, adsorption, hydrophobicity, and other properties of flotation systems (Fig. 12.37).
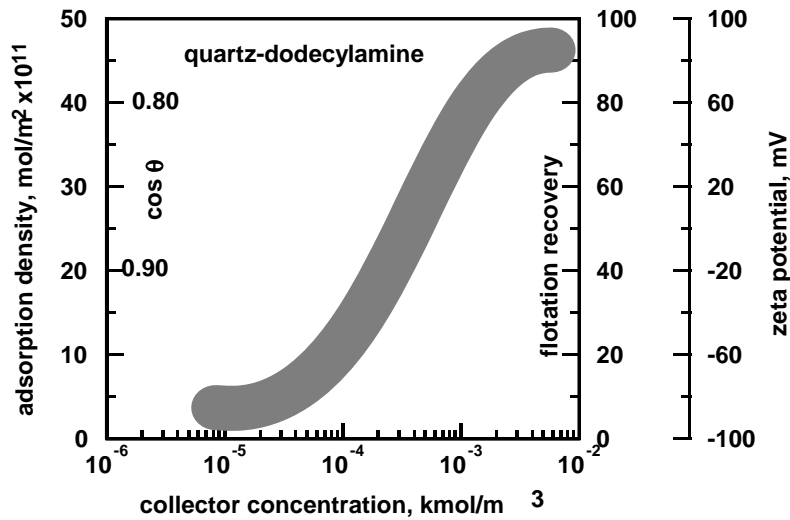
Fig. 12.37. Flotation of particles increases with increasing concentration of collector in the system and is proportional to collector adsorption and hydrophobicity caused by the adsorption. Collector adsorption is manifested by the increase of zeta potential of particles (after Fuerstenau et al., 1964 and Fuerstenau and Urbina, 1988), pH = 6–7

Adsorption of collectors and other compounds occurs, to a different extent, at any interface including those important in flotation, i.e. solid–water, solid–gas and water–gas interface. The property of the interfacial region can be characterized by the Gibbs equation. It is based on thermodynamics and assumption that for two-phase systems there are two pure bulk phases α and β, and a transitory interfacial region σ, situated between the bulk phases. The total internal energy U of each phase of the system will be a sum of different forms of energy:

$$U^\alpha = TS^\alpha - pV^\alpha + \Sigma\mu n^\alpha, \qquad (12.27)$$

$$U^\beta = TS^\beta - pV^\beta + \Sigma\mu n^\beta, \qquad (12.28)$$

$$U^\sigma = TS^\sigma - pV^\sigma + \gamma A + \Sigma\mu n^\sigma, \qquad (12.29)$$

that is thermal TS, surface γA, and chemical $\Sigma\mu n$ energies as well as the volumetric work pV
where:
α, β, σ – phases
T – temperature in kelvins
S – entropy
p – pressure
V – volume
γ – interfacial energy
A – interfacial area
μ –chemical potential
n – number of molecules or ions (or moles) of a given substance.
   Symbol Σ indicates that the chemical energy is a sum of energies of all chemicals species.
   The interfacial region σ contains chemical individuals present in both α and β phases To calculate the excess internal energy U_s of the interfacial area we subtract energies of the α and β phases from the total energy of interfacial region.

$$U_s = TS_s + \gamma A + \Sigma\mu n_s. \qquad (12.30)$$

Total derivative of Eq. (12.30) assumes the form:

$$dU_s = TdS_s + S_s dT + \gamma dA + Ad\gamma + \Sigma\mu dn_s + \Sigma n_s d\mu. \qquad (12.31)$$

   It results from thermodynamics that when a small and reversible change in surface phase σ takes place then:

$$dU_s = TdS_s + \gamma dA + \Sigma\mu dn_s, \qquad (12.32)$$

which means that the remaining segments of Eq. (12.30) have to fulfill the relation:

$$S_s dT + A d\gamma + \Sigma(n_i d\mu_i)_s = 0, \tag{12.33}$$

and for the processes taking place at a constant temperature T and knowing that $\Gamma = (n_1)_s/A$, we obtain the relation:

$$(d\gamma)_T = (-\Sigma\Gamma_i d\mu_i)_T. \tag{12.34}$$

Relation (12.34) is general and complete and describes the state of an interface and it is called the Gibbs equation. Taking into account that the chemical potential μ is determined by the dependence:

$$d\mu_i = RT \, d \ln a_i, \tag{12.35}$$

where α is the activity of a given chemical species, the Gibbs equation can be transformed into:

$$(d\gamma)_T = -RT \, \Sigma\Gamma_i d(\ln a_i)_T = (-RT \, \Sigma\Gamma_i da_i/a_i)_T. \tag{12.36}$$

The Gibbs equation combines three parameters: adsorption (strictly speaking surface excess Γ), activity (or concentration c, since $a = fc$ where f is the activity coefficient) of a chemical species in the solution (a) and the interfacial energy γ. Further transformation of the Gibbs equation is possible taking into account additional data regarding the interfacial region, e.g. dissociative properties of molecules, location of ions or molecules in interfacial region, as well as their mutual interactions. For instance, a change of the interfacial energy resulting from the adsorption of potential determining ions H^+ and OH^- on oxides at constant concentration of other ions originating from dissolved salts (in order to maintain constant ionic strength of the solution) and at a constant temperature, is described by the equation (Bruyn and Agar, 1962):

$$d\gamma = 2.303 \, RT \, (\Gamma_{H^+} - \Gamma_{OH^-}) \, d(pH) = 2.303 RT\sigma_0 \, d(pH). \tag{12.37}$$

where σ_0 is the surface charge.

After relating pH and electric potential, Eq. 12.37 can be transformed into the Lippmann electrocapillary curve. The Lippmann equation can be directly derived from the Gibbs equation (Davis and Rideal, 1963).

The interfacial energy change due to variation of the salt concentration (C_{soli}) in the solution at a constant temperature and pH can be described by the following equation (Ratajczak, 2001):

$$(d\gamma/d\log c_{salt})_{pH} = -2.303 RTF^{-1}(\sigma_+/z_+ - \sigma_-/z_-), \tag{12.38}$$

where:

σ_+, σ_- – ionic components of surface charge (Lyklema, 1972) $\sigma_o = -(\sigma_+ + \sigma_-)$,
z – valence of ions of the salt.

The pH change due to variation of the salt concentration at a constant surface charge and constant temperature is given by the Esin–Markov equation (Lyklema, 1972):

$$(\mathrm{d\,pH}/\mathrm{d\,log}\,a)_{\sigma_0} = \beta, \qquad (12.39)$$

where β is a constant.

The Szyszkowski formula relating a change of the surface tension π (being the difference between the surface tension of pure solvent γ_0 and that of surfactant solution γ) due to increasing mole fraction x (concentration) of the surfactant in the solution fulfills the Gibbs equation (Koopal, 1992) and has the form:

$$\pi = \gamma_0 - \gamma = RT\,\Gamma_m \ln\left(1 + x_i\,K_{i1}^P\right). \qquad (12.40)$$

Equation 12.40 is one of several forms of the equation proposed by Szyszkowski as an empirical relation, which was later found to be a special case of the Gibbs formula in which:

γ_0 – surface tension of solvent

γ – surface tension of solution at a given concentration of surfactant expressed in mole fraction form (x)

Γ_m – constant for a complete monolayer adsorption

x_i – mole fraction

K_{i1}^P – equilibrium constant for the surface reaction:

$$(1)^s + i = 1 + (i)^s, \qquad (12.41)$$

where:

1 – molecule of solvent

i – molecule of adsorbed component

s – surface.

For reaction 12.41 the equilibrium constant, in which concentration is expressed as a mole fraction x, assumes the following form:

$$K_{i1}^P = \left(\frac{x_1 x_i^s}{x_i x_1^s}\right)\left(\frac{f_1 f_i^s}{f_i f_1^s}\right), \qquad (12.42)$$

where f stands for activity coefficient.

Thermodynamically the equilibrium constant is expressed by the relation:

$$K_{i1}^P = \exp\left[\frac{A_i^0(\gamma_1^0 - \gamma_i^0)}{RT}\right], \qquad (12.43)$$

where:

A_i^0 – area occupied by one mole at monolayer adsorption

γ^0 – surface tension of pure substance.

It can be said that the formula for the reaction equilibrium constant for a monolayer adsorption is a bridge between the Szyszkowski and Gibbs equations.

The equations derived from the Gibbs formula as a rule combine two out of three parameters (c, γ, Γ) for finding the third one. Therefore, the Gibbs equations can be divided, as shown in Fig. 12.38, into three families: 1) the relations relating adsorption with concentration $\Gamma = f(c)$, i.e. adsorption isotherm (Γ-c curves), 2) surface tension change with concentration (γ-c curves), and 3) changes of interfacial tension as a function of adsorption (γ-Γ curves), or more often $\pi = \gamma$-$\gamma_0 = f(\Gamma)$).

– for two components
– for more componets

Esin-Markov coefficient
$C_1 = f(C_2)$ $(T, \sigma = const)$

C
concentration

– for organic electrolytes
– for inorganic electrolytes (salts)
– for nonelectrolytes
– Szyszkowski equation
– other

– Langmuir
– Stern-Graham
– Temkin
– Frumkin
– other

γ - c curves

adsorption isotherm

general Gibbs eq.

$d\gamma = -\Sigma\Gamma_i\, d\mu_i$ ($T = const$)

γ, **interfacial energy (or** Π **)**

two-dimensional equation of state

Γ, **surface excess**

– Schofield $\pi[(1/\Gamma) - A_0)] = bkT$
– Volmer (b = 1)

Fig. 12.38. Central role played by the Gibbs equation
in description of relationships between concentration of adsorbing reagent c,
its adsorption Γ and interfacial tension γ
and the place of other equations based on the Gibbs formula

The γ-c curves are applied in mineral processing for monitoring the influence of different reagents (collector, frother, salt, etc.) on thermodynamical properties of interfaces for possible further calculation of hydrophobicity (contact angle) and its changes. The $\pi = \gamma$ - $\gamma_0 = f(\Gamma)$ curves are also useful in mineral processing and they are called the equations of state. The equivalent of either Langmuir's or Szyszkowski's equations for a monomolecular adsorption of substances adsorbing itself without any additional interactions, based on the Gibbs equation for adsorption at a constant temperature, has the following form:

$$\pi = \gamma_0 - \gamma = -RT\,\Gamma_m \ln(1 - x_i^s)\ \text{lub} = -kT\,\Gamma_m \ln(1 - \Gamma_i/\Gamma_m), \qquad (12.44)$$

where Γ_{max} is the density of adsorption when monolayer is formed.

Equation 12.44 describes a rigid adsorption of chemical species which do not change the site of adsorption. For mobile adsorbants, there are other equations and they can be empirical (Shofield and Rideal or Vomer) (Jaycock and Parfitt, 1981), as well as combined empirical and Gibbs equations, which usually contain added information on adsorption conditions and interactions (Davis and Rideal, 1963).

The simplest adsorption isotherm is that of Langmuir. It describes a uniform adsorption leading to a monolayer in which there no interactions between the adsorbing species. The Langmuir adsorption isotherm can also be derived from chemical reactions constants, which at the same time have to fulfill the Gibbs equation. The Langmuir adsorption isotherm has a form:

$$\Gamma_i = \frac{\Gamma_{max} x_i K_{i1}^P}{1 + x_i K_{i1}^P}, \qquad (12.45)$$

where K is the adsorption reaction constant.

There are many adsorption isotherms relating concentration of adsorbed species as a function of their concentration in solution at a constant temperature. They represent complex isotherms which take into account various interactions between adsorbed species as well as simplified isotherms. A simplified Stern–Graham isotherm can be considered as a Langmuir's simplified isotherm. It is valid for low concentration of the substance undergoing adsorption in the solution $(1 > xK^p)$ and it has the form (Hunter, 1987):

$$\Gamma_i = 2rc \exp(-\Delta G_{ads}^0/RT), \qquad (12.46)$$

where:

Γ_i – adsorption, mol/cm^2

ΔG_{ads}^0 – standard free enthalpy of adsorption ($\Delta G_{ads}^0 = -RT \ln K_{ij}$)

r – radius of adsorbed counter ion

c – number of pairs of ions per 1 cm^3 of solution.

When transforming the Langmuir into Stern-Graham equation, Γ_{max} becomes dependent on the size r of ions adsorbed.

There are many other adsorption isotherms, including the Freundlich, (Adamson 1967), Temkin (Davis and Rideal, 1963), Frumkin (Leja, 1982), and other isotherms (Jaycock and Parfitt, 1981). Details on adsorption isotherms can be found in other sources.

Interfacial collector adsorption takes place as a result of the action of different forces. To describe the forces, researchers employ certain chemical rules based on chemical bonds and interactions. In vacuum, ionic, covalent, coordinative, metallic

bonds, as well as van der Waals interactions can take place. In aqueous solutions, additional interactions such as hydrogen bonds, electric interactions between electrically charged surface and entirely or partly hydrated ions in the solution, hydrophobic interactions originating from different structure of water at hydrophobic surface and the structure of ions or molecules undergoing interactions with the surface and showing a tendency to associate can be found. Therefore, a general complete formula for the free enthalpy energy of adsorption of ions, molecules, associated forms, and colloidal objects at interfaces, can be written as follows:

$$\Delta G^0_{ad} = \Delta G^0_{\text{chemical adsorption}} + \Delta G^0_{\text{physical adsorption}} + \Delta G^0_{\text{hydrogen bonding}} \qquad (12.47a)$$

or more precisely:

$$\Delta G^0_{ad} = \{(\Delta G^0_{\text{chem}} + \Delta G^0_{\text{chel}})\} + \{\Delta G^0_{\text{Waals}} + \Delta G^0_{\text{elec}} + \Delta G^0_{\text{CH}_2} + \\ + \Delta G^0_{\text{hydrofob}}\} + \{\Delta G^0_{\text{hydrogen}}\}, \qquad (12.47b)$$

where:

$\Delta G^0_{chem} + \Delta G^0_{chel}$ – free enthalpy describing the effect of simple chemical and coordinative bonds ΔG^0_{chem} leading to chelating structures

$\{\Delta G^0_{Waals} + \Delta G^0_{elec} + \Delta G^0_{CH2} + \Delta G^0_{hydrophob}\}$ - free enthalpy of physical (ΔG^0_{Waals}), electrical (ΔG^0_{elec}), interaction of associating CH_2 groups from hydrocarbon chains (ΔG^0_{CH2}), and hydrophobic interactions ($\Delta G^0_{hydrophob}$)

ΔG^0_{chem} – term resulting from the effect of hydrogen bonds.

It should be added that the van der Waals interactions consist of three other interactions, namely, dispersive (London), induction (Debye inducted dipoles) and orientation (Keesom permanent dipoles) (Laskowski, 1969).

This diversity of forces makes the adsorption and consequently flotation a complex process (Fig. 12.39). In the case of ionic collectors, there are three dominating mechanisms: ionic (electrostatic, physical sorption), chemical, and van der Waals (physical adsorption). The adsorption via chemical bonding usually leads to the best flotation in the vicinity of the *pzc* (Fig. 12.39a). The electrostatic mechanism is typical for substances which are not capable of forming chemical bonds with collectors, e.g. in flotation with anionic collectors which render minerals hydrophobic only up to the isoelectric point (*iep*), while with cationic collectors above the *iep* (Fig. 12.39b). Purely electrostatic mechanism takes place at low collector concentrations. At higher concentrations, apart from electrostatic adsorption, sorption is due to the van der Waals or chemical interactions. Then, the effect of surface electric charge on flotation becomes complicated. The nonionic collectors undergo adsorption on mineral surfaces and then induce flotation due to, first of all, van der Waals forces, especially the London dispersive interaction (Fig. 12.39c). The most efficient adsorption takes place on hydrophobic surfaces leading to an additional increase of hydrophobicity which considerably improves flotation. Other nonionic collectors render minerals floatable due to the hydrogen bonds (Fig. 12.39d).
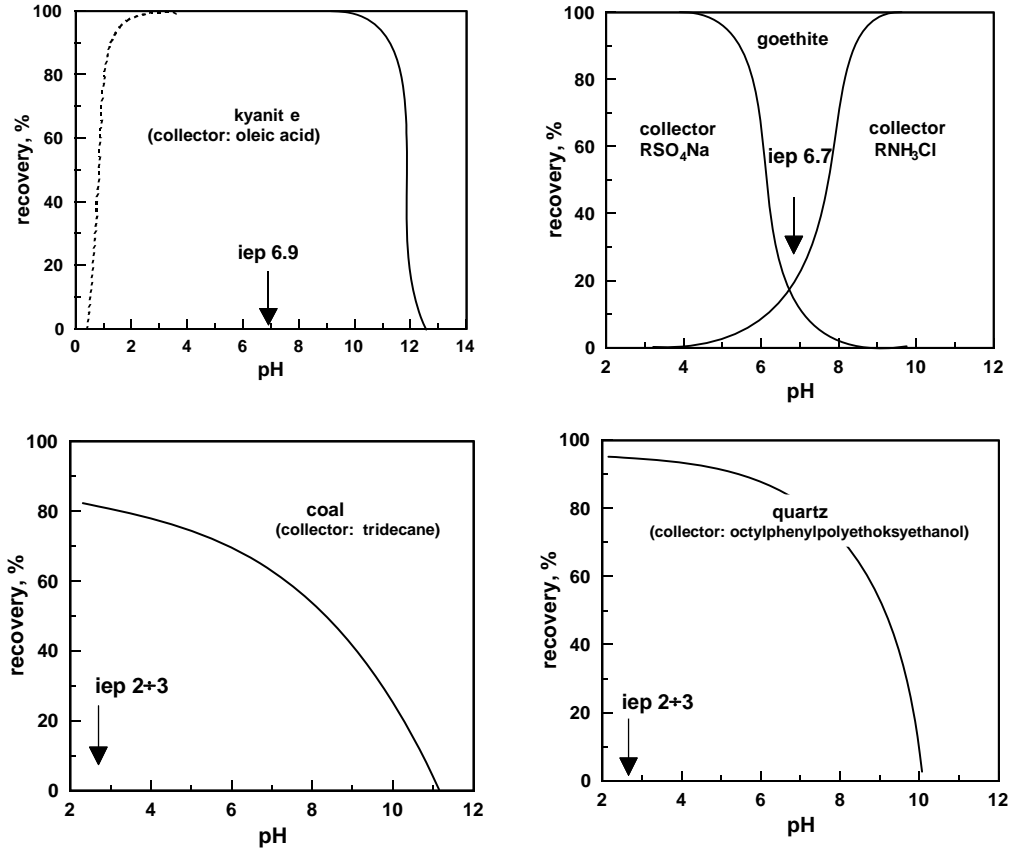
Fig. 12.39. Examples of domination of different mechanisms of adsorption leading to flotation as a function of pH and iep of material: a – chemical adsorption of oleate (10^{-4} M) on an aluminosilicate (kyanite) (maximum flotation is at iep) (Choi i Oh, 1965), b – physical adsorption (electrostatic) of dodecyl sulfate (10^{-3} M) on goethyte (flotation is up to iep, while for dedecyl amine above iep) (after Iwasaki et al., 1960), c – adsorption due to van der Waals interactions of apolar oil with coal (flotation is in vicinity of iep and decreases with increasing surface electrical charge) (Stachurski and Michałek, 1986), d – adsorption of nonionic polymeric collector ($1.6 \cdot 10^{-4}$ M, 10 etoxy units) with hydrogen bonding on quartz (flotation is proportional to the number of undissociated surface –OH groups which maximum number is at iep) (Doren et al., 1975)

Knowing the mechanism of adsorption as well as the extent of adsorption depending on the collector concentration in water, one can calculate the free enthalpy ΔG_{ads} of adsorption on the basis of an appropriate adsorption isotherm and then predict flotation results and selectivity. However, the calculations are far from being easy. Table 12.25 presents ΔG^0_{ads} values for different minerals and collectors based on the Graham-Stern isotherm, which is a simplified form of the Langmuir isotherm (Hunter, 1989).

Table 12.25. Free enthalpy of adsorption ΔG_{ads} calculated from the Graham–Stern isotherm and collector concentration (C_T), at which adsorption is equal to 1 μmol/m^2, $r = 2.5 \cdot 10^{-10}$ m (after Dobias, 1995)

Mineral	Collector	Collector concentration C_T kmol/m^3	ΔG_a kJ/mol
Fluorite	Sodium tetradecyl sulfate	$4 \cdot 10^{-5}$	–26.3
Fluorite	Sodium laurate	$6 \cdot 10^{-5}$	–25.4
Calcite	Sodium dodecyl sulfonate	$2 \cdot 10^{-4}$	–22.4
Fluorite	Sodium dodecyl sulfonate	$3 \cdot 10^{-4}$	–21.4
Scheelite	Sodium dodecyl sulfonate	$3.5 \cdot 10^{-4}$	–21.0
Calcite	Sodium dodecyl sulfate	$7.5 \cdot 10^{-4}$	–19.2
Fluorite	Sodium dodecyl sulfate	$1 \cdot 10^{-3}$	–18.5
Fluorapatite	Sodium dodecyl sulfonate	$2 \cdot 10^{-4}$	–16.8

It results from Table 12.25 that the strongest adsorption involves sodium tetradecyl sulfate on fluorite, while the weakest regards sodium dodecyl sulfonate on fluorapatite.

In flotation, mixtures of two or more collectors are often applied. Then one of them is usually called promoter. Some flotation promoters, when used separately, show a very weak flotation effect. They feature synergism only in the presence of an appropriate collector. Numerous investigations on the flotation promoters involved coal (Sablik, 1998).

12.5.2. Frothers

The main role of frother is to disperse gas, form stable froth and accelerate flotation. These tasks can be achieved because frothers are preferentially adsorbed at the water–gas interface. The sorption is usually accompanied by a decrease in surface tension (Fig. 12.40a). Introduction of a frother into solution results in reduction of air bubbles size (Fig. 12.40b). The bubbles size reduction is connected with a decrease in the surface tension of the solution. It becomes evident when the bubbles are formed in a capillary, since the following relation takes place:

$$d_p = \sqrt[3]{\frac{6a\gamma_{wg}}{g(\rho_c - \rho_g)}} \, , \tag{12.48}$$

where:
γ_{wg} – surface tension of frother aqueous solution
a – capillary diameter
ρ_c – aqueous solution density
ρ_g – gas density
g – gravity.

a   b
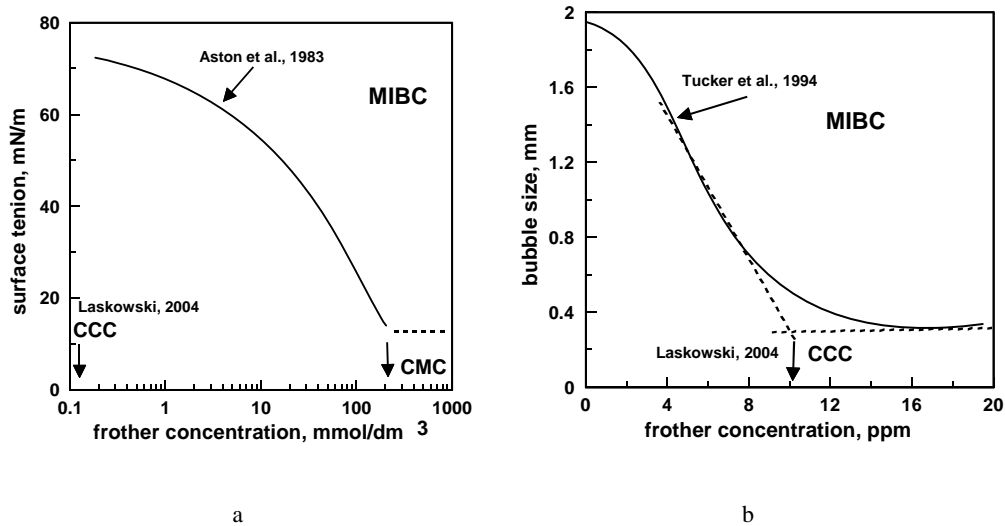
Fig. 12.40. Influence of concentration of frother on properties of the gas–water system for methyl isobutyl carbinol (MIBC) as an example: a – surface tension (Aston et al., 1983), CCC (Laskowski, 2004), and CMC, b – size of bubbles (Tucker et al., 1994) CCC and CMC. For MIBC 1 ppm $\approx 10^{-2}$ mol/dm^3

When many bubbles are created in flotation cells the relation between bubble size and surface tension is less obvious because the size of bubbles reach constant size at very small concentrations when the surface tension drop is not significant in relation to water. Figures 12.40a,b show that methyl isobutyl carbinol (4-methyl-2-pentanol or MIBC) lowers surface tension of aqueous solution down to about 200 mmole/dcm^3 (CMC), while the size of bubbles stabilizes at 0.1 mmol/dm^3 or 10 ppm called by Laskowski (2004) the critical coalescence concentration or CCC.

According to Laskowski (1998) reagents with branched molecule are better frothers because they form less compact films at the gas–water interface.

Air bubbles dispersed in water travel up to the liquid surface and either burst or remain on the surface in a form of froth. And this is another role of frothers in flotation – to form stable froth. The presence of a stable froth is necessary for keeping floated out material on the water surface. This provides enough time to remove floating particles. The froth, however should not be too stable. A stable froth creates problems with its handling. The froth exists when a thin water film is formed around the bubbles and it has the structure preventing a rapid leaking of water from inter-bubble space. This phenomenon prevents bubble disappearance, that is coalescence. The frothers, sorbing themselves on the bubble surface, cause the formation of "rough" layers. This is confirmed by the fact that pure liquids do not form froth, due to the fact that water easily leaks out of thin layers, and therefore the bubble coalescence progresses rapidly.

Froth structure depends on the place in the flotation cell and the extent of mixing (Fig. 12.41). Froth layer undergoes destruction due to bubble breaking as a result of

slow dewatering, while new bubbles are continuously transported from the bottom of the cell. Upper part of the froth is usually of hexagonal shape. In the middle part of the froth the bubbles are round and in the bottom part the froth contains bubbles suspended in water. Hydrophobic particles, present in froth, stick to bubbles. In the spaces between bubble bulk water contains hydrophilic particles mechanically transported to the froth and their amount is usually directly proportional to the amount of water in the froth (Ross, 1991; Waksmundzki et al., 1972). The decrease in content of gangue particles in froth voids can be regulated by froth hydration, i.e. quantity and kind of frother, as well as by appropriate procedures, like spraying the froth with water. The relation between frothing and flotation is not a simple, since both processes are effected by the type of collector used for flotation as well as by interaction between frother and collector. Many problems involving froths, their stability and interactions between frothers and collectors have not been solved. More details about froth in flotation can be found in the "Frothing in flotation II" (Laskowski and Woodburn, 1998).
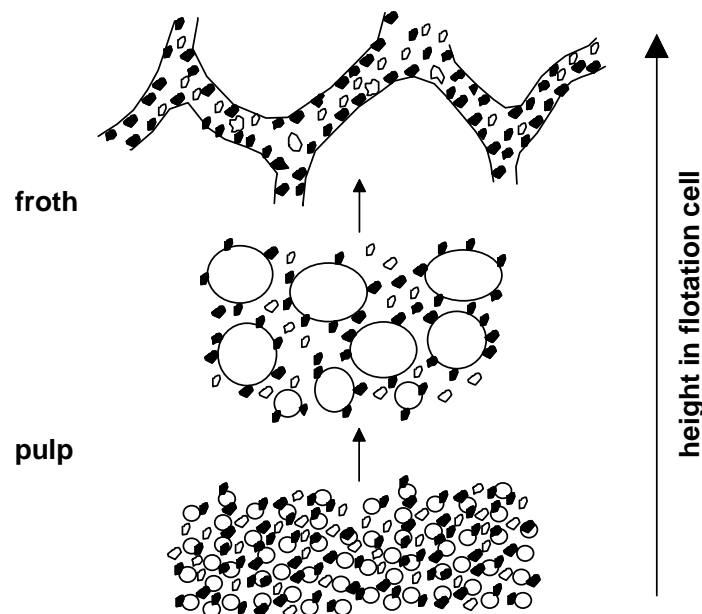
Fig. 12.41. Froth and change of it structure with the position in the flotation cell. Not to scale.

Another role played by the frother is acceleration of the flotation process. This takes place due to diminishing the so called induction time, i.e. the time needed by a bubble to attach itself to a particle and to remove water film between bubble and particle. The effect of diminishing induction time results from the fact that good frothers rapidly change their orientation at interface water-gas at the moment of the collision between bubble and particle on which the collector molecule is adsorbed. To do this

the frother molecule has to behave at interface as a gas film, i.e. it should not associate but to evenly spread at the interface in all stages of flotation, starting from a bubble collision with a particle to the formation a particle–bubble aggregate (Laskowski, 1998).

Table 12.26. Flotation frothers (Laskowski 1998, with some modifications)

Group	Frother
1. aliphatic alcohols	
a) linear	from amyl to decanol
b) branched	iso-amyl 2-ethyl hexanol, methyl isobutyl carbinol (MIBC)
c) with additional group	diacetone
2. Cyclic	
a) linear	cyclohexanol
b) branched	α-terpineol
3. Aromatic	cresols xylenols
4. Alkoxy-hydrocarbons	1,1,3-triethoxybutane
5. Polyglycols and hydrocarbon poly-glycol ethers	$R(X)_nOH$ R=H or C_nH_{2n+1} or any hydrocarbon X=EO (ethylene oxide), PO (propylene oxide) BO (butylene oxide) from 3 to 7

Many chemical compounds can be used as frothers and their classification takes into account either their properties or chemical composition. Classification regarding the properties divides the frothers into acidic, basic, and neutral. Another classification follows the division into normal (standard) frothers and frothers–collectors. The frothers can be divided into aliphatic, cyclic and aromatic alcohols, hydrocarbons with ethoxy groups and polymeric frothers based on polyglycols (Table 12.26) frothers. Aliphatic alcohols contain from four to about 10 carbon atoms and one or more –OH group. The simplest frothers are aliphatic normal alcohols, such as pentanol, hexanol, heptanol. Their solubility in water decreases as molecular weight increases. The solubility of alcohols increases when they contain additional oxygen atom, like in diacetone alcohol. In the industry, branched frothers are commonly used. Methyl isobutyl carbinol (MIBC) belongs to this group. Long-chained amines, sulfonates, sulfates, and fatty acid (Klimpel and Hansen, 1988) are frothers which play also the role of collectors. They are used in flotation of non-sulfide ores. The simple and complex alcohols, especially having high molecular weight and weakly soluble in water belong the nonionic frothers-collectors family. When accompanied by other collectors, they are called promoters.

The properties of froth also depend on salts present in the solution. Investigations by Iskra and Laskowski (unpublished but discussed in details by Laskowski, 1969, pp. 91-93) showed that salts make the foam less voluminous and containing less water. It is caused by so-called salting out of the frother leading to a decreasing surface tension

of frother aqueous solution. Therefore, flotation in the presence of salts generally provides better results (Ratajczak, Drzymala, 2003)

12.5.3. Activators

Activators initiate or improve flotation in the presence of collectors. The question whether or not a reagent is an activator depends not only on reagent properties but also on its interaction with the collector. It happens that activator in the presence of another collector functions as a depressor. It also depends on reagent concentration. Most often cations of hydrolyzing multivalent metals ions are activators. Their list includes Fe^{2+}, Fe^{3+}, Al^{2+}, Pb^{2+}, Mn^{2+}, Mg^{2+}, Ca^{2+}, and other ions. Some anions are also activators, especially fluoride and sulfide ions. There are other activators with a complex structure, known as promoters, which are applied in selected flotation systems, e.g. in coal flotation (Sablik, 1998).

The metal cations become activators due to sorption at the solid-water interface. The adsorption of a particular metal cation takes place within precisely determined pH ranges in the Stern layer of the electric double layer. This results from the difference in the sign of the electric charge of the ion and the surface. The experimental data indicate that the best sorption occurs when the metal ion is in the form of a monohydroxycomplex ($Me(OH)^{n+}$). Figure 12.42 shows flotation of quartz in the presence of different metal cations with the use of sulfonate as a collector (Fuerstenau and Palmer, 1976). Similar relations have been recorded for many other anionic collectors.
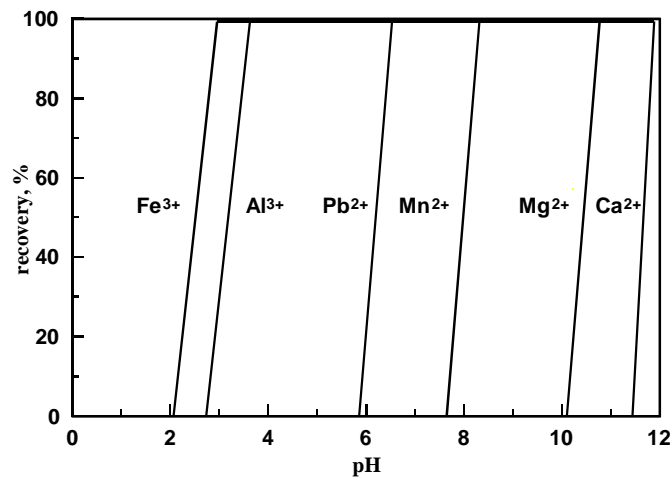
Fig. 12.42. Activating action of hydrolyzing cations of multivalent metals. Flotation of quartz in the presence of 10^{-4} M sulfonate. There in lack of flotation in the absence of activating cations. In presence of 10^{-4} M of cations there is flotation above characteristic pH, at which the dominating species in solution is the monohydroxy complex $MeOH^{n+}$ (Fuerstenau and Palmer, 1976, with permission of SME)

Another mechanism of surface activation with metal cations takes place with sulfide minerals. There is a displacement of the original metal cations from the surface by the added cations as it was described by the reaction in Table 12.27 for sphalerite. The activation reactions are of electrochemical character. On the basis of free enthalpy of reaction ΔG_r^0, a series of metal cations abilities to activate sulfides can be arranged. In the activation series the greater ability of activation the more negative is the value of ΔG_r^0.

Table 12.27 shows the values of ΔG_r^0 for the activation reactions of selected sulfides with different metal ions. The values represent ΔG_r^0 (kJ/mol) for the reactions of sulfides activation with metal ions calculated for the reactions $Me^IS + Me^{II2+} = Me^{II}S + Me^{I,2+}$, taking into account the free energy of formation (ΔG_f^0) of each species i and the relation: $\Delta G_r^0 = \Sigma v_i \ \Delta G_f^0$ in which v means reaction stoichiometric coefficient (see 12.73).

The ΔG_f^0 values are taken from Woods and Garrels (1987), but there are many other sources of such thermodynamic data, e.g. CRS (1986).

Table 12.27. Activation reaction of sphalerite with selected metal cations
and calculated free enthalpy of the reactions

Activation reaction	free enthalpy, ΔG_r^0 (kJ/mol)
$ZnS + Fe^{2+} = FeS + Zn^{2+}$	35.2
$ZnS + Pb^{2+} = PbS + Zn^{2+}$	−17.3
$ZnS + Cu^{2+} = CuS + Zn^{2+}$	−62.9
$ZnS + 2Ag^+ = Ag_2S + Zn^{2+}$	−142.3

Table 12.28. Free enthalpy of the activation reactions for sulfides reacting with metal ions

	Fe^{2+}	Zn^{2+}	Pb^{2+}	Cu^{2+}	Ag^+
FeS		−35.2	−52.5	−98.1	−177,5
ZnS	35.2		−17.3	−62.9	−142,3
PbS	52.5	17.3		−45.6	−125,0
CuS	98.1	62.9	45.6		−79,4
Cu_2S	170.7	136.1	118.2		−6,8
Ag_2S	177.5	142.3	125.0	79.4	

It can be concluded from Table 12.28 that pyrrhotite (FeS) can be activated with all considered cations (ΔG_r^0 is negative), sphalerite with all cation except Fe^{3+}, while galena (PbS) only with Cu^{2+}, and Ag^+ ions. Both cooper sulfides can be activated only with Ag^+, while argentite (Ag_2S) cannot be activated at all (ΔG_j^0 is positive). It can be noticed that activation series for sulfides is, with some exceptions, identical with the so-called galvanic series of metals.

The activation process induces sphalerite flotation in the presence of xanthates after its activation with copper ions (Laskowski, 1969). The activation process can also be harmful as it can lead to a decreased selectivity of sulfides flotation. This phenomenon can be observed during galena separation from copper minerals (Bigosinski, 1998), because galena surface becomes similar to copper minerals.

Fluoride ions can also be applied as activators, especially for silicates, e.g. beryl (Fig. 12.43), while quartz itself is not a subject to activation.
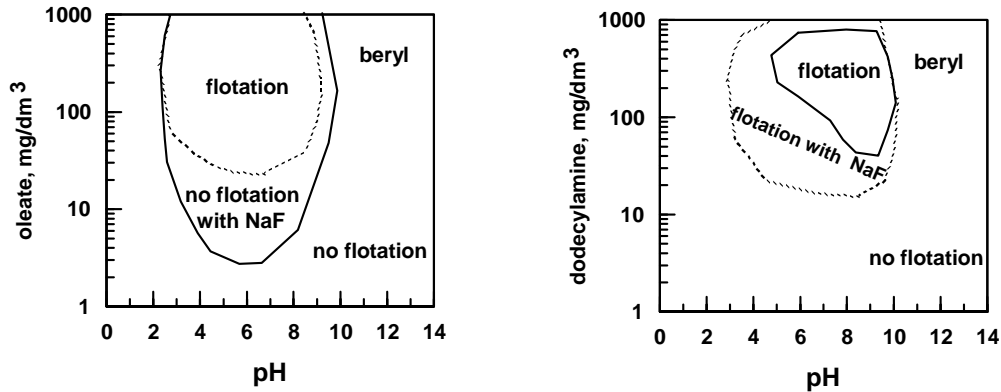
Fig. 12.43. Fluoride ions as activating and depressing media in flotation of silicates:
a – regions of lack of flotation in the presence of oleate as collector,
b – regions of activation in the presence of dodecyl amine as collector (Manser, 1975)

Some authors consider silicate ions as activators. It was proved that at low concentrations the SiO_3^{2-} ion facilitates flotation of some minerals (Kłasen and Mokrousov, 1963) (Fig. 12.44) and coal (Sablik, 1998). The mechanism of this process, however, is not fully known. It is assumed that silicate ions remove foreign ions and particles from the surface, which are present there due to crushing, grinding and other form of contacts with small particles present in the aqueous solution, by peptization (decoagulation).
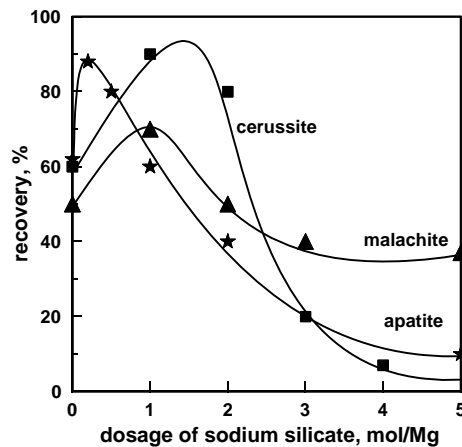
Fig. 12.44. Silicate ions improve flotation results for many minerals,
provided that their concentration is not too high (Klassen and Mokrousov, 1963)

The sulfide ion can also play a role of activator. They are applied as activators in flotation of oxidized minerals. They are added to the system before flotation with xanthates. However, too high sulfide concentration depresses flotation, since the sulfide ions compete with xanthate ions for adsorption sites on the surface. Therefore, it is very often necessary to remove sulfide ions before flotation, that is immediately after the activation process. The mechanism of activation with sulfides relies on forming metal sulfides on the surface of an activated mineral (Fuerstenau and Han, 1988).

According to Sablik (1998), difficult-to-float coals can be activated with hydrocarbon polyglycol ethers, esthers and amines (promoters). The mechanism of their activation is not known.

12.5.4. Depressors

Depressors are used to elevate flotation selectivity. The selectivity is achieved by depressing one or more components of the flotation suspension while the valuable mineral should float without changes. Sometimes the selectivity can be obtained in a reverse process, i.e. through depression of a useful component, while gangue undergoes flotation. Depressor can be organic, inorganic, acid, salt, base, redox, and complexing reagent, etc. The list of often used depressors is presented in Table 12.29.

Table 12.29. Depressors used in flotation

Inorganic depressor	Formula	Organic depressor
Alum	$KAl(SO_4)_2$	starch
Ammonia	NH_3	quebracho
Calgon	polyphosphates	tannin
Sodium cyanide	$NaCN$	lignin derivatives
Sodium dichromate	$Na_2Cr_2O_7$	synthetic polymers
Phosphates	various	acetic acid
Sodium silicate	Na_2SiO_3	dextrin
Fuoric acid	HF	humic acid
Sulfuric acid(IV)	H_2SO_3, SO_2	cellulose derivatives
Sulfuric acid(VI)	H_2SO_4	alginate
Hydrochloric acid	HCl	chitin derivatives
Sodium sulfate(IV)	Na_2SO_3	citric acid
Zinc sulfate(VI)	$ZnSO_4$	hydrazine
Caustic soda	$NaOH$	thioglycolic acid
Oxygen	O_2	chelating compounds
Lime	$Ca(OH)_2$	electrons (redox substances)
Sodium carbonate	Na_2CO_3	
Sodium hydrosulfide	$NaHS$	

Depressors work through different mechanisms. In this monograph they were classified into 3 groups: depressors desorbing collector from the surface, redox depressors

changing the chemical composition of surface, and depressors which decompose collector.

12.5.4.1. Depressors acting through adsorption

Depressors, when adsorbed on mineral surface, block its hydrophobization, that is make the sorption of a collector impossible. When a collector is already present on the surface, the depressor causes its desorption. Activity of depressors depends both on their properties and reactivity of the floating material. Generally, depression results from a competition between depressor and collector ions for the place on the surface of floated particles. The mechanism of action of adsorbing depressors can be described with the use of exchange reactions. Such a description, however, is not simple, since the chemistry of surface reactions is not well known and there is a lack of a complete theory of electric double layer and exact relation between surface charge and surface potential.

The simplest depressor competing with the collector for the places on particle surface is hydrogen ions (H^+). The hydrogen ions simultaneously regulate acidity of the solutions. The list of acids include H_2SO_4 and HCl, while lime, sodium carbonate and caustic soda (NaOH) are the most often used reagents for alkalinity regulation in flotation.

The results of flotation involving pH regulators are usually presented as recovery versus pH curves. Figure 12.45 shows the influence of pH on chalcocite flotation. It can be concluded from the figure that cease of flotation takes place both at low and high pH values.
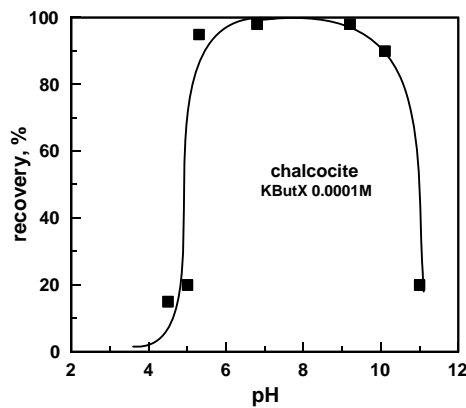
Fig. 12.45. Influence of pH on flotation of chalcocite in the presence of butyl xanthate.
Too high and low pH depresses flotation of minerals

The concentration of hydrogen and hydroxyl ions is presented on one pH scale, since both parameters are related. This results from dissociation of water molecules into ions, according to the reaction:

$$H_2O = H^+ + OH^- \tag{12.49}$$

Reaction equilibrium constants are expressed as a quotient of chemical products activities to chemical substrates activities taking part in the reaction. It should be noticed that species on the right side of the reaction are products while on the left side are substrates. For reaction (12.49) the equilibrium constant is given by:

$$K_{W_a} = \frac{\dfrac{\left(H^+\right)}{c_0}\dfrac{\left(OH^-\right)}{c_0}}{\dfrac{\left(H_2O\right)}{c_0}}, \tag{12.50}$$

where the round parenthesis denote activity. Activities are expressed in kmol/dm^3. The term c_o is constant and always is equal to 1 kmol/m^3, and is introduced to the equation for equilibrium constant to guarantee that the constant is a dimensionless quantity. As c_o always equals 1 kmol/m^3, this quantity is customarily omitted when writing or calculating equilibrium constants. It will be also practiced in this book. Activity, denoted ( ) or a, is, in turn, the product of concentration ([ ] or c) and activity coefficient f, then:

$$a = (\,) = c f = [\,] f. \tag{12.51}$$

For low concentrations the activity coefficient is close to 1. Since in mineral processing low concentrations or reagents are used, it is usually assumed that the activity coefficient is equal to 1. The expression for the equilibrium constant is as follows:

$$K_W = \frac{\left(H^+\right)\left(OH^-\right)}{\left(H_2O\right)} \cong \frac{\left[H^+\right]\left[OH^-\right]}{\left[H_2O\right]}. \tag{12.52}$$

At room temperature (21°C $\cong$ 298K) quantity K_W amounts 1.80·10^{-16} and since at this temperature concentration of water in water [H$_2$O] is 55.56 koml/m^3, the product of OH$^-$ and H$^+$ ions concentration, i.e. ionic water product equals:

$$(H^+)\,(OH^-) = K_W[H_2O] = 1.00\cdot 10^{-14}. \tag{12.53}$$

After finding the logarithm of both sides of this equation:

$$pH = 14 - pOH, \tag{12.54}$$

where pH=$-\log$(H$^+$) and pOH=$-\log$(OH$^-$).

This equation connects concentration of H$^+$ ions with concentration of OH$^-$ ions. Symbol p stands for mathematical function $-\log$ and it can used not only for H$^+$ or OH$^-$ ions, but also any other ion, e.g. pAg = $-\log$(Ag$^+$), pBa = $-\log$(Ba^{2+}) etc.

The mechanism of action of the pH regulating depressors, similarly to the many other depressors, relies on competition with collector ions or molecules. Generally, the competition can be expressed in the form of an exchange reaction:

$$-MC + D = -MD + C \tag{12.55}$$

where:

D   – depressor ion

C   – collector ion

–MC – collector adsorbed or forming surface compound with mineral

–MD – depressor adsorbed or forming surface compound with mineral.

When reaction strictly follows Eq. (12.55), it is possible, on the basis of the equilibrium constants of this reaction,

$$K_M = \frac{[C]\,[-MD]}{[D]\,[-MC]}$$ 12.56),

to obtain the so-called Barski relation

$$\frac{[C]}{[D]} = \frac{[-MD]}{[-MC]} K_M = \text{const},$$ (12.57)

which says that for a particular mineral-collector-depressor system a decrease in flotation takes place at a constant ratio between the concentration of collector and depressor. It means that if collector concentration increases in the solution, to obtain flotation depression we should add more depressor and that the stoichiometric ratio of C to D equals 1. Qualitatively, such a relation holds for many depressor-collector systems. For example, Fig. 12.46 shows lines of flotation – no flotation transition for sulfides floated in the presence of ditiophosphate at different pH values.
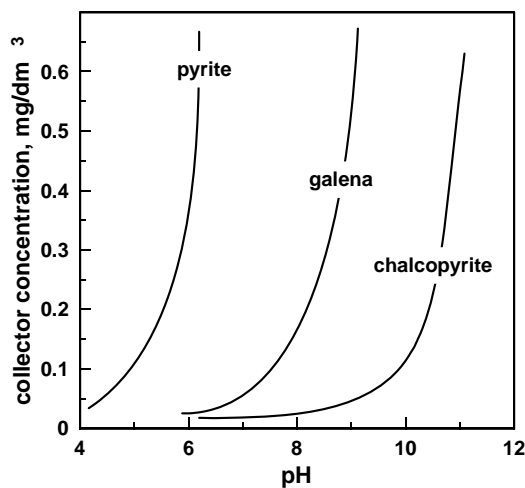
Fig. 12.46. Competition between collector and depressor expressed as edges of transition between flotation and lack of flotation for selected sulfides in the presence of dithiophoshate as collector. The region of flotation occurs on the left side of the curve. The curves were drawn basing on attachment of particles to bubbles measurements (data after Wark and Cox, 1934)

However, it was claimed by Chander (1988) (Table 12.30) that the stoichiometric coefficient for different collector–OH⁻ systems is not equal to 1, but it follows a general relation:

$$\frac{[C]}{[D]^y} = \frac{[\text{collector}]}{[\text{OH}^-]^y} = \text{const} \qquad 12.58$$

Table 12.30. Values of parameter *y* (Eq. 12.58) for selected mineral–collector systems (here pH regulator determines concentration of OH⁻ ions) (after Chander, 1988)

Mineral–collector	*y*	pH range
Galena/KEX	0.65	9–12
Galena/KDEDTP	0.53	6–9
Sphalerite/DEDTC	0.56	6–8
Sphalerite/DBDTC	0.72	7.5–10
Sphalerite/DADTC	0.75	8–11
Chalcopyrite/NaDEDTP	0.71	8.5–11
Chalcopyrite/KEX	-	11–13
Pyrite/NaDEDTP	0.62	4–6
Pyrite/KEX	-	10–12

E – ethyl, D – di, T– tio, A – amyl, B – butyl, X- xanthate, P – phosphate, C – carbonate , K – potassium, Na – sodium. In highly alkaline environment Eq.12.58 is not working

A discrepancy between the Barski formula and Eq. 12.58 was explained by Chander (1988) by the differences between the speeds of collector desorption and depressor adsorption, i.e. lack of equilibrium of the exchange process. A different explanation is possible if we take into account that surface reactions can considerably differ from hypothetical reaction (12.55). Investigation on sulfides proved that on their surfaces there dominate $_{-SMeX}^{-SH}$ groups in the presence of xanthates in neutral medium, while in alkaline medium $_{-SMeX}^{-S^-}$ groups are the prevailing ones (Rönngren et al., 1995). Displacing xanthate groups with OH⁻ groups leads to formation of the –SH–SMeOH and –S⁻–SMeOH groups. Depressing activity of the hydroxyls can be presented as the reaction:

$$\begin{array}{cc} -\text{SH} & -\text{S}^- \\ \end{array}$$
$$-\text{SMeX} + 2\text{OH}^- = -\text{SMeOH} + \text{X}^- + \text{H}_2\text{O} \qquad (12.59)$$
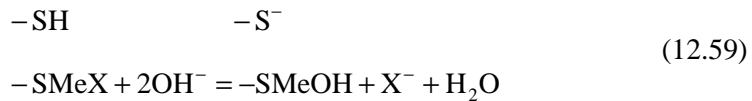
In order to write down equilibrium constant of surface reaction (12.59), one should take into account the fact that concentration of ions taking part in the reaction close to the surface (I_p) is different from the one in the bulk solution (*I*) and is determined by the relations (Drzymala et al. 1979).

$$I_p^- = I^- \exp\left(\frac{F\psi_0}{RT}\right); \qquad I_p^+ = I^+ \exp\left(-\frac{F\psi_0}{RT}\right) \qquad (12.60)$$

where:

I_p – concentration of ion at interface

I – concentration of ion in the bulk solution.

There a negative sign is used for positive ions and a positive sign for negative ions while Ψ_o stands for the surface potential. For negatively charged surface Ψo is negative, while for the surface charged positively is positive. Therefore, the surface equilibrium constant can be presented as:

$$K_{\text{OH}} = \frac{[\text{X}^-]\exp\left(\dfrac{F\psi_0}{RT}\right)[-\text{S}^- - \text{SMeOH}]}{[\text{OH}^-]^2 \exp\left(\dfrac{F\psi_0}{RT}\right)^2 [-\text{SH} - \text{SMeX} - \text{MC}][\text{H}_2\text{O}]} =$$

$$= \frac{[X^-][-\text{S}^- - \text{SMeOH}]}{[\text{OH}^-]^2 \exp\left(\dfrac{F\psi_0}{RT}\right)[-\text{SH} - \text{SMeX} - \text{MC}][\text{H}_2\text{O}]}.$$

(12.61)

Assuming that flotation depression takes place at a constant–S–SMeOH to –SH-SMeX ratio, we obtain the relation:

$$\frac{[\text{X}^-]}{[\text{OH}^-]^2} = K * \exp\frac{F\psi_0}{RT}$$

(12.62a)

Thus, Eq. 12.62a is a slightly different equation from that of Barski. It can be concluded from the above equation that depression depends not only on concentration of collector ions and depressor ions, but also on electric surface potential. The latter one can change as pH changes (from the point of pH_{pzc}) in nernstian mode, i.e. 59mV/pH. This value, however, is usually lower, which can be expressed by introducing an additional factor m. Then Eq. (12.62a) assumes the form:

$$\frac{[\text{X}^-]}{[\text{OH}^-]^2} = K * \exp\frac{Fm\,(\text{pH}_{\text{pzc}} - \text{pH})}{RT}$$

(12.62b)

The equation obtained is quite complicated for it contains three variables. On the basis of measurements for many oxides (Drzymala, 1979), it has been shown that for surface reactions involving ions empirical dependence between surface potential and OH- ions concentration can be used:

$$[\text{OH}^-]^{-(\text{from } 0.5 \text{ to } 0.7)} = K_x \exp\frac{F\psi_0}{RT}$$

(12.63)

where K_x is a constant.

The above relation has been derived by combining the theoretical equation for the surface equilibrium constant with an empirical expression of the following type:

$$pH = pK - n \log [(1/\alpha) - 1)]   \tag{12.64}$$

which represents a modified Temkin isotherm. In Eq. 12.64 α denotes the degree of surface site dissociation, while n and pK are empirical constants.

Introduction of the above relation into general equation (12.63) causes that the effect of OH$^-$ ions on cease of flotation is not so strong as a part OH$^-$ ions is involved in establishing the surface potential. Due to that fact, the general form of the Barski equation becomes:

$$\frac{[X^-]}{[OH^-]^y} \approx k, \qquad \frac{[C]}{[D]^y} \approx k.   \tag{12.65}$$

There is a large group of depressors which especially strongly bind with ions present in the solution as free or surface ions. These depressors are capable of forming chemical compounds of high stability. If a complex is especially stable, it is not possible to desorbed it from the surface by using excessive amount of a collector, since in that case enormously high and impossible-to-achieve collector concentration, higher one than its solubility, should be used. Then, the complex constant can be accepted as a parameter characterizing the depressor's strength. It results from the assumption that the more stable complex the better depressor. To exemplify this statement, Table 12.31 shows concentrations of cyanide needed for sulfides depression in the presence of $1.56 \cdot 10^{-4}$ mole/dm^3 of potassium ethyl xanthate along with equilibrium constants of forming cyanide complexes with iron and copper ions. It can be concluded from the mentioned table that stability constants for iron ions are much higher than those of copper, therefore, cyanide concentration needed for copper sulfides depression is considerably higher than that of iron sulfides. For mixed iron-copper sulfides, for example for bornite, the critical depression concentration assumes intermediate values.

Table 12.31. Comparison of concentration of cyanide necessary for depression of sulfides subjected to flotation with $1.56 \cdot 10^{-4}$ mol/dm^3 of potassium ethyl xanthate and stability constants of formation of cyanide complexes with iron and copper ions. Data after Rogers, 1962 and Chander, 1988

Mineral	Chemical formula	pH range of flotation	Concentration of CN$^-$ (mol/dm^3)	$p\beta = -\log \beta$
1	2	3	4	5
Pyrite	FeS$_2$	7–9	$4.0 \cdot 10^{-6}$	36 (Fe^{2+}(CN)$_6^{4-}$)
Chalcopyrite	CuFeS$_2$	7–11	$1.6 \cdot 10^{-5}$	
Marcasite	FeS	8–10	$1.0 \cdot 10^{-4}$	36 (Fe^{2+}(CN)$_6^{4-}$)
Bornite	Cu$_5$FeS$_4$	8.5–13	$2.5 \cdot 10^{-4}$	
Tetrahedrite	Cu$_3$SbS$_{3,25}$	8.5–13	$8.0 \cdot 10^{-4}$	
Covellite	CuS	9–12	$1.4 \cdot 10^{-3}$	26 (Cu^{2+}(CN)$_4^{2-}$)
Chalcocite	Cu$_2$S	9–13	$7.0 \cdot 10^{-3}$	20 (Cu^{1+}(CN)$_2^-$) 28 (Cu^{1+}(CN)$_4^{3-}$)

A high constant of iron ions complexation is, evidently, responsible for a very stable, irreversible depression of iron sulfides, while copper sulfides depression takes place at much higher CN- concentrations. And it can be reversed, which means that after removing CN- ions from the solution, they will float again. These questions are very important when it comes to selective flotation of sulfide polymetallic ores.

The properties of other complexing depressors can be estimated in the same way. Equilibrium constants can be found in literature or calculated on the basis of thermodynamic data, especially using free enthalpy of forming substances ΔG^0_f (Sillen and Martell, 1964; Garrels and Christ, 1965; Naumov and Others, 1971; CRC, 1986). For this purpose a general reaction of complex forming can be written:

$$\text{Me}^{m+} + n\text{X}^- = \text{MeX}_n^{n-m} . \tag{12.66}$$

Since the central Me^{m+} ion can, depending on reaction conditions, binds different number of complexing ions (ligands), therefore there do exist different constants of the complexing equilibrium. There are constants expressing subsequent stages of a ligand bonding, assigned with symbol K, as well as cumulated constants expressing transition of the central ion to the state of making complexes with certain number of ligands, assigned with symbol β, as presented in Table 12.31. A general equation determining stability constants for the reaction of complexing metal ions with a ligand (depressor) is:

$$\beta_n = \frac{\left[\text{MeX}_n^{n-m}\right]}{\left[\text{Me}^{m+}\right]\left[\text{X}^-\right]^n} = \prod_{i=1}^{n} K_i , \tag{12.67}$$

where Π is a mathematical symbol for multiplying.

For instance, for the reaction of divalent metal ion with four cyanide ions:

$$\text{Me}^{2+} + 4\text{CN}^- = \text{Me(CN)}_4^{2-} . \tag{12.68}$$
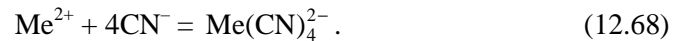
The cumulated constant has the form:

$$\beta_4 = \frac{\left[\text{Me(CN)}_4^{2-}\right]}{\left[\text{Me}^{m+}\right]\left[\text{CN}^-\right]^4} , \tag{12.69}$$

while K_4 will describe the reaction:

$$\text{Me(CN)}_3^- + \text{CN}^- = \text{Me(CN)}_4^{2-} , \tag{12.70}$$
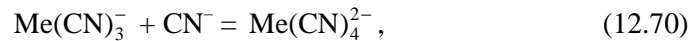
and the expression for the constant is:

$$K_4 = \frac{\left[\text{Me(CN)}_4^{2-}\right]}{\left[\text{Me(CN)}_3^-\right]\left[\text{CN}^-\right]} . \tag{12.71}$$

Equilibrium constants of any arbitrary chemical reaction can be calculated on the basis of the free enthalpy of the reaction, since reaction equilibrium constant *K*, and also *β*, is related according to:

$$\Delta G_r^0 = -RT \ln K, \tag{12.72}$$

and the $\Delta G^0{}_r$ value can be calculated from free enthalpy of formation ΔG_f^0

$$\Delta G_r^0 = \sum \nu_i \, (\Delta G_f^0)_i, \tag{12.73}$$

where Σ means the sum of products of standard free enthalpy of formation of particular species *i* taking part in the reaction and reaction stoichiometric factor *v* being positive for the products and negative for the substrates. As it has already been mentioned, $\Delta G^0{}_f$ values are available in literature.

12.5.4.2. Redox depressors

The course of some minerals flotation can be modified by reagents which are capable of changing the character of the molecules, collector ions, surface species in an electrochemical way. They are redox substances and they can be both oxidizing and reducing reagents. The redox reagents are able to exchange electrons and oxidizing species accepts electrons undergoing reduction, while reducing species give up electrons and undergo oxidations. The reactions involving electrons can cause changes in chemical composition and structure of substance or conditions under which the sorption of flotation reagents occurs through the change of redox potential. The simplest way of effecting flotation with redox potential would be regulation of electrons concentration in the flotation system. Unlike protons (H^+), there are no free electrons in water solution, since they can exist only in a bonded form with the ions or molecules present in the solution. Therefore, the description, performance, as well as control of redox reaction are complicated.

Basic relation describing redox reaction is called the Nernst equation. Its traditional derivation is based on difficult notions of solution pressure or osmotic pressure (Pajdowski, 1993). A better derivation was used by Chander (1988). It is based on reaction equilibrium constant. To derivate the expression for redox reaction involving electrons, first the reaction should be written in a general form:

$$\text{oxidized form of a substance } (u) + \text{electron } (e) =$$
$$= \text{reduced form of a substance } (z), \tag{12.74}$$
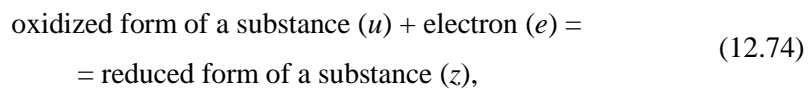
where *e* denotes electron.

A practical example of such a reaction can be iron(III) ions reduction to iron(II) ions:

$$Fe^{3+} + e = Fe^{2+} \tag{12.75}$$

which can be written in a general form as:

$$u + e = z. \tag{12.76}$$

The equilibrium constant for this reaction is given by:

$$K = \frac{[z]}{[u]\,[e]}, \tag{12.77}$$

where the square brackets mean concentration of a particular form which are expressed in $kmol/m^3$.

Now both sides of the equation undergo logarithm operation and then are multiplied by RT:

$$RT \ln K = RT \ln \frac{[z]}{[u]\,[e]}. \tag{12.78}$$

The expression $RT \ln K$ equals the standard potential of chemical reaction $-\Delta G^0$, therefore Eq. (12.78) can be written as:

$$-\Delta G^0 = RT \ln \frac{[z]}{[u]\,[e]}. \tag{12.79}$$

If this equation is divided by nF, i.e. the product of the Faraday constant and the number stating how many electrons are exchanged in the process, i.e. n, then:

$$\frac{-\Delta G^0}{nF} = \frac{RT}{nF} \ln \frac{[z]}{[u]\,[e]}. \tag{12.80}$$

Because $-\Delta G^0/nF$ is known as the standard redox potential E^0, introducing this information results in:

$$E^0 = \frac{RT}{nF} \ln \frac{[z]}{[u]\,[e]} = -\frac{RT}{nF} \ln \frac{[u]}{[z]} - \frac{RT}{nF} \ln e = -\frac{RT}{nF} \ln \frac{[u]}{[z]} + E\ , \tag{12.81}$$

which means that expression E^0, featuring equilibrium constant of the reaction with participation of electrons, was divided into two segments. The first one depends on the concentration of the oxidized and reduced forms of the considered substance while the second one characterizes electrons activity.

Equation (12.81) is the well known Nernst relation. It can be seen after its rearrangement:

$$E = E^0 + \frac{RT}{nF} \ln \frac{[u]}{[z]} = E^0 - \frac{RT}{nF} \ln K*, \tag{12.82}$$

where K^* stands for the equilibrium constant of redox half reaction without taking into account electrons in an explicit form, but taking into account all species taking part in the reaction, including H^+ and OH^- ions. It should be remembered that the concentration of the oxidized species is displayed in the denominator and the reduced form in the numerator.

As it has already been mentioned, depressing action of redox substances relies on transporting electrons which participate in forming new chemical compounds and determine flotation. In the case of some metal sulfides (MS) in the presence of xanthate (X), the following electrochemical oxidation reactions can take place:

$$X^- \rightarrow X_{ads} + e, \tag{12.83}$$

$$2X^- \rightarrow X_2 + 2e, \tag{12.84}$$

$$2X^- + MS \rightarrow MX_2 + S + 2e, \tag{12.85}$$

$$2X^- + MS + H_2O \rightarrow MX_2 + SO_4^{2-} + 8H^+ + 8e, \tag{12.86}$$

$$MS + 6H_2O \rightarrow M(OH)_2 + SO_4^{2-} + 10H^+ + 8e, \tag{12.87}$$
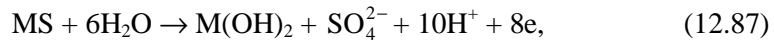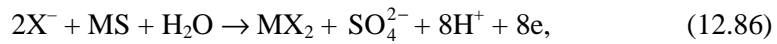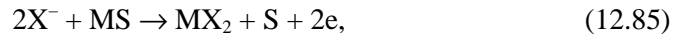
where:
MeX$_2$ – metal xanthate
X$^-$ – xanthate ion in solution
X$_{ads}$ – xanthate adsorbed on the surface
X$_2$ – dixanthogen (on surface as oil or solid).

The species X_2, MeX$_2$ and X$_{ads}$ are generally hydrophobic, M(OH)$_2$ is hydrophilic, while MeS is hydrophilic or slightly hydrophobic (Chmielewski, 1990). Therefore, flotation or its lack depends on the degree of surface occupation by these species. Yet, the condition under which the reactions presented in Eqs. (12.83)-(12.87) can take place is the presence of a reducing itself substance, i.e. the one accepting electrons. The simplest of such substances can be oxygen, which, after accepting electrons, undergoes reduction to O^{2-}.

$$O_2 + 2H_2O + 4e \rightarrow 4OH^- \tag{12.88}$$

There exist many substances capable of redox reactions. Some of them are presented in Table 12.32.

It often happens that hydrogen or hydroxy ions take part in electrochemical reactions (e.g. (12.86)-(12.87)). It is then convenient to present the relation between redox potential of these reactions and pH in E-pH diagrams also called the Pourbaix diagrams (1963) (Letowski, 1975). The diagram for the Cu-H$_2$O system, after Letowski (1975), is shown in Fig. 12.47. E-pH diagrams can be plotted for any system in which

in reaction between the examined substance and the collector, depressor and/or activator takes place with an exchange of electrons (Lekki, 1979).
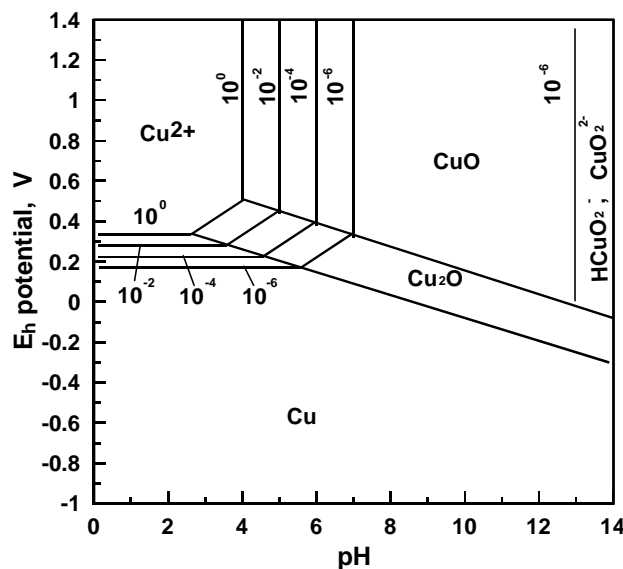
Fig. 12.47. E_h–pH diagram for Cu–H_2O system at 25 °C (298 K). Diagram is based on reactions: Cu_2O + $H_2O = 2CuO + 2H^+ + 2e$ ($E = 0{,}747 - 0{,}0591$ pH); $2Cu + H_2O = Cu_2O + 2H^+ + 2e$ ($E = 0{,}471 - 0{,}0591$ pH); $Cu = Cu^{2+} + 2e$ ($E = 0{,}337 + 0{,}0295 \lg [Cu^{2+}]$); $Cu_2O + 2H^+ = 2Cu^{2+} + H_2O + 2e$ ($E = 0{,}203 + 0{,}0591$ pH $+ 0{,}0591 \lg [Cu^{2+}]$); $Cu^{2+} + H_2O = CuO + 2H^+$ (pH $= 3{,}44 - 0{,}5 \lg [Cu^{2+}]$) (Łętowski, 1975)

On the basis of the Pourbaix diagrams it is possible to predict what E and pH should be used in order to produce proper species on the surface of particles. E value can be either calculated or taken from the tables. It can also be measured with the use of properly prepared electrode, usually made of platinum. The E values are a measure of electrons activity in the system. However, the E values are not absolute, but they are related to a reference system, called standard system, which usually is the potential of the so called hydrogen electrode having E values related to the to normal hydrogen electrode denoted as E_h. In practice, potentials are measured in reference to other electrodes, usually saturated calomel electrode. The standard potential of such electrode must be taken into account. The normal potentials for selected redox reactions related to the hydrogen electrode scale are presented in Table 12.32. To directly determine redox properties of a particular substance the best way is to compare E^0 values for the reactions written in such a way that on the left side there are electrons. If OH^- ions take part in the reaction they should be rewritten in such a way that H^+ ions should occur without OH^- ions. As it can be concluded from Tab. 12.32, the substance of the highest redox potential, i.e. oxidizers, are $S_2O_8^{2-}$ ions, then hypochlorite (ClO^-) and permanganate (MnO_4^-). Strong reducers are also hydrazine, zinc and sulfide ions S^{2-}, since their redox potential is highly negative.

Table 12.32. Standard potentials for selected materials based on standard hydrogen electrode potential (data after Pajdowski, 1993; Barycka and Skudlarski, 1993; Schmidt, 1983 (hydrazine), and other sources

Electrode reaction	Short notation	Normal potential E_h^0 (V)
$S_2O_8^{2-} + 2e = 2\,SO_4^{2-}$	$S_2O_8^{2-}/SO_4^{2-}$	2.050
$ClO^- + 2H^+ + 2e = Cl^- + H_2O$	ClO^-/Cl^-	1.640
$MnO_4^- + 8H^+ + 5e = Mn^{2+} + 12H_2O$	MnO_4^-/Mn^{2+}	1.510
$Cl_2 + 2e = 2Cl^-$	$Cl_2/2Cl^-$	1.360
$O_2 + 4H^+ + 4e = 2H_2O$	O_2/O^{2-}	1228
$Fe^{3+} + e = Fe^{2+}$	Fe^{3+}/Fe^{2+}	0.771
$O_2 + 2e + 2H^+ = H_2O_2$	O_2/H_2O_2	0.680
$(CN)_2 + 2H^+ + 2e = 2HCN$	$(CN)_2/HCN$	0.370
$Fe(CN)_6^{3-} + e = Fe(CN)_6^{4-}$	$Fe(CN)_6^{3-}/Fe(CN)_6^{4-}$	0.363
$Cu^{2+} + e = Cu^+$	Cu^{2+}/Cu^+	0.167
$2H^+ + 2e = H_2$	H^+/H_2	0.000
$SO_4^{2-} + 2H^+ + 2e = SO_3^{2-} + H_2O$	SO_4^{2-}/SO_3^{2-}	–0.103
$N_2 + 4H^+ + 4e = N_2H_4$ (hydrazine)	N_2/N^{2-}	–0.333
$S + 2e = S^{2-}$	S/S^{2-}	–0510
$Zn^{2+} + 2e = Zn$	Zn^{2+}/Zn	–0.763
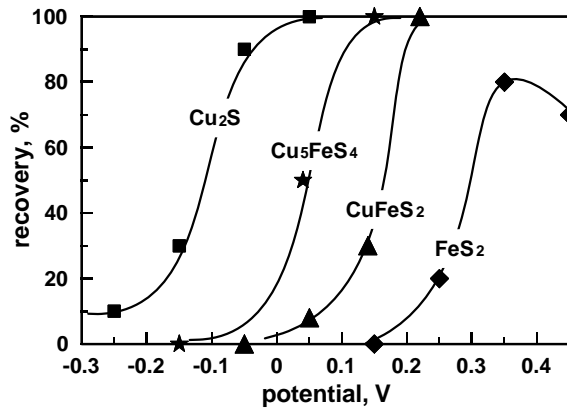
Fig. 12.48. Relationship between flotation recovery of sulfides and potential applied to a platinum wire immersed in aqueous suspension of a sulfide containing ethyl xanthate at $1.44 \cdot 10^{-5}$ kmol/m^3. After Richardson and Walker, 1985

Sulfides flotation and their depression can be regulated not only with the use of redox substances, but also by applying external potential through the wires conducting electrons or electrodes immersed in the suspension. It is necessary to provide a contact between each particle and the electrode delivering or removing electrons and the particles have to be conductive. Although technically difficult, such flotation can be performed. Figure 12.49 shows the effect of applied potential on flotation of selected

metal sulfides. It can be concluded from the mentioned figure that by the means of applied potential one can not only depress, but also activate sulfides for flotation.

12.5.4.3. Depressors decomposing the absorbed collector

Some depressors are capable of destruction of collector molecule or ion absorbed on a mineral surface. Sulfate(IV) ion can serve as an example, which, as it is supposed, decomposes xanthate present on the surface. It works according to the reaction (Yamamoto, 1980):

$$2C_2H_5OC(S)SK + 2K_2SO_3 + 2KHSO_3 + 2O_2 \rightarrow 2C_2H_5OC(S)SOK \rightarrow \\ 2C_2H_5OH + 4K_2S_2O_3 + 2CO_2 \tag{12.89}$$
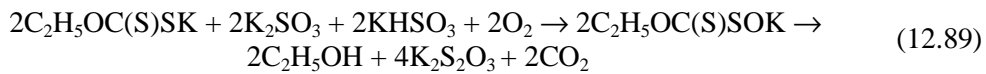
Reaction (12.89) takes place mostly in neutral pH regions.

Removing collectors from particles surface is important when there is a necessity of flotation with one collector and next with another one. In such cases desorption of the first collector using appropriate depressing ions, for instance pH regulators, is carried out. In literature, however, there are not many examples of such depressors.

12.6. Flotation of mineral matter

Many ores and raw materials can be upgraded by flotation. Since ores contain minerals of different properties, a proper collector is needed for flotation of one or a group of minerals. Eigeles (1964) classified materials into six groups according to their flotation response to certain collectors. It is presented in Table 12.33.

Table 12.33. Classification of materials according to their flotation properties (after Eigeles, 1964)

Class	Example	Applied collectors
Non-metals and solids with significant natural hydrophobicity	sulfur, graphite, coal, talc	hydrocarbons, nonionic liquids insoluble in aqueous
Native metals and sulfides	gold, chalcocite chalcopyrite, galena sphalerite	xanthates, aerofloats
Oxidized minerals of non-ferrous metals	cerusite, smithsonite malachite, tenorite, cuprite	xanthates (after sulfidization), anionic and cationic
Oxides, hydroxides and silicates	hematite, ilmenite corundum, cassiterite chromite, feldspars kaolinite	anionic and cationic (with and without activation using metal ions)
Sparingly soluble salts	fluorite, barite, calcite, apatite, dolomite	anionic and cationic
Soluble salts	halite, silvinite, carnalite, kieserite	cationic, seldom anionic

Minerals of the same class feature similar flotation properties. Thus, for their separation the same or similar collectors are used, while minerals of different classes un-

dergo flotation by applying other collecting reagents. These issues are discussed in details in following chapters 12.6.1-12.6.6.

12.6.1. Naturally hydrophobic substances

Graphite, talc, sulfur and some sulfides have a very specific crystalline structure which makes them hydrophobic. They form sheets mutually connected with the van der Waals forces. Crushing and grinding split the particles mostly along the sheets whose surfaces are naturally hydrophobic. Hydrophobic planes easily adsorb different reagents, especially non-ionic, hence their ability to float with non-ionic collectors. Other planes are usually hydrophilic because they contain broken chemical bonds, which easily adsorb hydrophilic hydroxyl groups. This is the reason why particles of many naturally hydrophobic substances upon grinding contain also hydrophilic planes. The latest investigation show that that talc (Michot et al., 1994), graphite Schrader, 1975) and coal (Drzymała, 1999c), known as naturally hydrophobic substances, can be only slightly hydrophobic or completely hydrophilic when, after grinding, the particles are prevented from adsorption of air components such as N_2, CO_2, and pollutants (e.g. hydrocarbons), on their surface. These minerals become hydrophilic when the polluting reagents are removed from their surface, for instance by vacuum degassing. Hydrophilization of naturally hydrophobic substances can also take place as a result of oxygen adsorption. For example, sulfur exposed to air becomes less and less hydrophobic due to oxygen binding.

The presence of hydrophilic planes, oxidation and hydroxylation make flotation of naturally hydrophobic materials inefficient. Therefore, either frothers having collecting properties or collectors and frothers are applied to float naturally hydrophobic materials. Among collectors, usually apolar compounds such as diesel oil and kerosene, are used. Flotation of naturally hydrophobic materials sometimes requires the use of special flotation promoters, especially in the case of oxidized coals. Coal is an organic substance characterized by a complex structure. It is not possible to assign it a determined chemical formula. It is known that coal contains many organic groups: mostly aromatic, then aliphatic, as well as certain amount of oxygen compounds and smaller amount of other elements (S, N). There are very many simplified chemical formulas for coal and one of them is shown in Fig. 12.49.
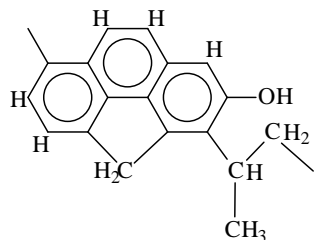
Fig. 12.49. Simplified model of a coal unit. After Krevelen (Czapliński, 1994)

Oxygen present in coal can be found in the form of different functional groups. Their amount changes with the degree of coalification. Coalification results in removal of oxygen and increase in coal aromatization. The last stage of coalification is a complete carbonation of coal, i.e. it contains only elemental carbon (graphite) (Fig. 12.50).
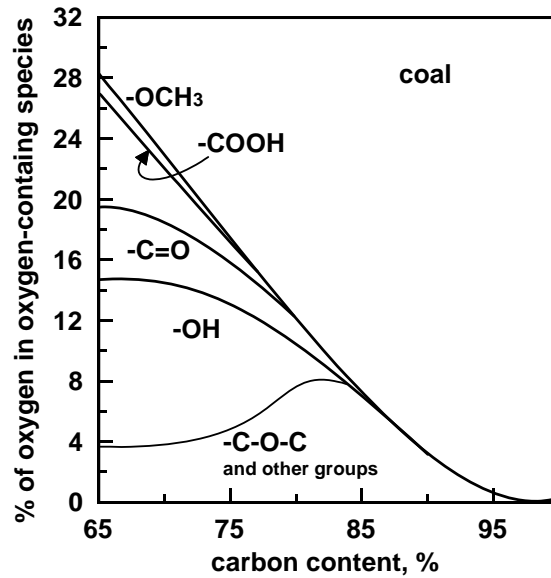
Fig. 12.50. Distribution of oxygen containing groups in coals as a function of their coalification (after Zyla, 1994; with permission of Ucz. Wyd. Nauk.-Dyd. AGH and the author)
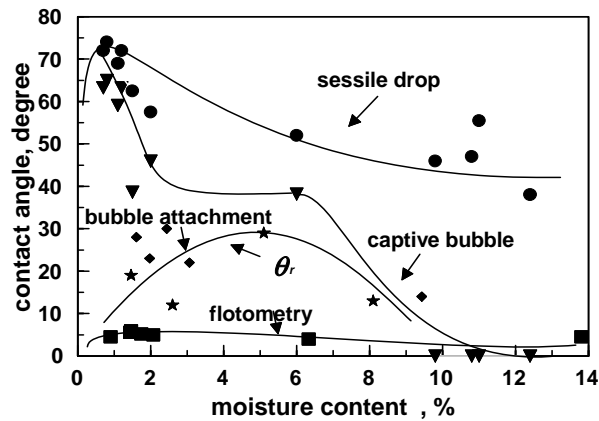
Fig. 12.51. Influence of method of measurement on values of contact angles of coals measured by: sessile drop and captive bubble (Gutierrez–Rodriguez et al., 1984),
bubble attachment (*) – Hanning and Rutter (1989), sessile drop aqueous receding contact angle θ_r) – Good and Keller (1989), flotometric contact angle (Drzymala, 1999c) (permission of © AA Balkema Publishers)

The degree of coalification effects a number of coal properties including its hydro-phobicity (Fig. 12.51). The coal hydrophobicity, measured as contact angle, consid-erably depends on the method of measurement, which was shown in Fig. 12.52. This results from coal heterogeneity and its susceptibility to changes in the course of pre-paratory operations for measurements.
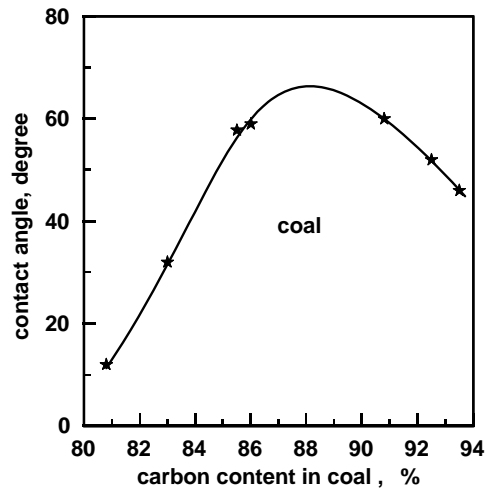
Fig. 12.52. Change of coal hydrophobicity as a function of its coalification
(after Brown, 1962)
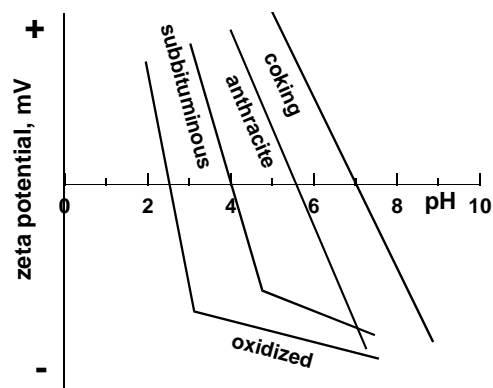
Fig. 12.53. Shape of zeta potential for coal as a function of pH
(after Laskowski and Miller, 1984)

Coal is very easily oxidized by air components. It causes an increase in coal oxy-gen content, especially in the form of carboxyl groups, which, in turn, causes the shift

of the iep to low pH values. This can be demonstrated, for example, by zeta potential measurements (Fig. 12.53).

As the degree of coalification increases, the content of the volatile matter and other components in coal decreases. This could be a base for coal classification. The Polish classification of coal is presented in Table 12.34. Many countries uses their own classification. There also exists the so-called international classification (Czapliński, 1994).

Table 12.34. Polish classification of coal (PN-82/6-97002)

Coal type	Symbol	Volatile matter, %	Roga #*	Application
1	2	3	4	5
Flame	31.1	> 28	< or = 5	Energetic coal for all firebeds
Gas-flame	32.1 32.2	> 28	> 5 to 20 21 to 40	Energetic coal for: all firebeds; gas production
Gas	33	> 28	> 40 to 55	Energetic coal for: grate firing; dust firing; industrial furnaces; gas plant; coke
Gas--coke	34.1 34.2	> 28	> 55	For: coke; gas plant; gas-coke plant
Orthocoke	35.1 35.2	> 26 do 31 > 20 do 26	> 45	For coke
Methacoke	36	> 14 do 20	> 45	For coke
Semicoke	37.1 37.2	> 20 do 28 > 14 do 20	> or = 5	For: special coke mixtures; energy by plants with special firebeds; smokeless fuel
Lean	38	> 14 do 28	<5	As coal 37
Anthracitic	41	> 10 do 14	-	As coal 37
Anthracite	42	≥ 3 do 10	-	For energy by plant with special firebeds
Metaanthracite	43	< 3	-	
Graphite				

*ability of sintering

Typical values of moisture, ash, chemical composition and density of different coal types are presented in Table 12.35.

Table 12.35. Properties of coals (according to Polish classification) on dry and ash-free basis (after Czaplinski, 1994)

Properties–coal type	31	32	33	34	35	37	38	41	42
Moisture, %	9.10	7.45	1.88	2.48	1.15	0.94	0.93	0.98	1.4
Ash, %	4.97	1.24	5.74	5.11	7.89	3.95	5.91	3.69	4.51
Volatile, %	35.29	29.81	26.99	32.36	23.68	16.84	12.67	6.72	5.39
C content, %	66.34	73.58	79.62	79.10	80.19	86.63	85.16	88.59	87.48
H content, %	4.30	4.16	4.66	5.17	4.90	4.51	4.07	3.85	3.87
O+N content, %	13.4	13.19	7.57	7.62	5.31	3.56	2.95	2.17	2.37
Organic S content, %	1.82	0.38	0.53	0.52	0.56	0.77	0.98	0.72	0.73
Real density, g/cm^3	1.48	1.53	1.38	1.35	1.33	1.33	1.41	1.45	1.44
Apparent density, g/cm^3	1.21	1.29	1.34	1.27	1.30	1.20	1.33	1.38	1.38
Porosity, %	18.06	14.19	2.69	4.54	1.69	11.96	5.72	4.82	4.54

The location of hard coals in relation to other carbon-containing substances taking into account carbon, hydrogen, and oxygen content is shown in Fig. 12.54.
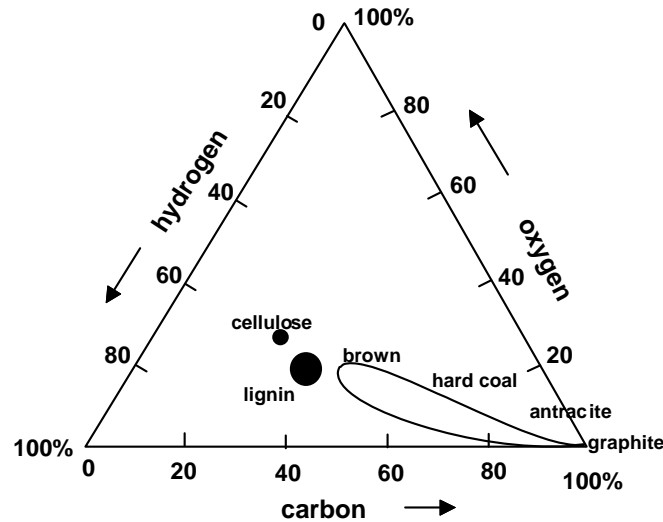
Fig. 12.54. Place of coal among other carbonaceous matters (after Wert and Weller, 1982, with permission of the American Institute of Physics)

Flotation aims at separation of combustible carbonaceous matter from minerals responsible for the formation of ash. Coal contains from a few to tens of percent of ash. Flotation usually involves coal fines, which are difficult to upgrade by other methods. Since coal is naturally hydrophobic, non-polar liquids are used for its flotation. They are mainly products of coal and crude oil distillation. Most often crude oil is used, which is a mixture of hydrocarbons, mostly aliphatic. According to Sablik (1998) post-cumene tar also called the FK reagent can be also used for flotation. It consists of di- and tri-isopropylbenzene, isobuthylbenzene, isopropylindene, diphenylmethane and diphenylpropane. Another collector capable of coal flotation is Pyrolysat (BF), a mixture of high-boiling aliphatic and aromatic hydrocarbons. A good flotation can also be achieved using dibutylmaleate (MDB) or diocthylmaleate (MDO). In coal flotation numerous different substances are used as frothers. They are often waste products coming from local producers, being either pure substances or waste mixtures. Therefore, their chemical composition and commercial names vary considerably and they often change. Generally, pure higher aliphatic alcohols (AC) contaminated with aldehydes, ketones, and esters are used as frothers. They are available on the market in the form of such reagents as Alifal N, Flotanol, Mekol, Reagent HO, ect. Earlier pine oil and products containing phenol were used. Industrially used methyl isobutyl carbinol is a good frother and it is considered as standard in laboratory investigation. Terpenes and polyethylene glycol derivatives can also be used as frothers. In coal flotation various modifying substances are also applied. They are similar, or the same, as

those used in mineral ores flotation. pH regulators (NaOH, H_2SO_4), stability regulators (aqueous-glass, $CaCl_2$), organic colloids (starch, dextrin, tannin) belong to this group. Some coals do not float well and require special reagents called promoters (Sablik, 1998). The well-known cationic collectors (amines, pyridine salts), anionic collectors (sulfonates, sulfates), non-ionic (polyglicolic ethers) can be used as promoters but should be applied in small quantities. Usually they are combined with diesel oil. According to Sablik (1998) activity of coal flotation promoters depends on their adsorption on oxidized coal sites, which provides the sites available for apolar collector. Promoters also cause higher degree of emulsification of diesel oil drops.

Coal flotation takes place due to adsorption of apolar oil at non-polar coal sites. The sorption is physical in character and is caused by the van der Waals forces. Therefore, the best flotation can be observed when there are many non-polar sites, e.g. near iep (Fig. 12.39). It results form the research of Yarar and Leja (1982) that non-oxidized coals float well, while their zeta potential does not considerably effect flotation, although it is possible to see the maximum flotation in the vicinity of neutral pH. Oxidized coals, however, float the worse the lower their zeta potential is. Adsorption of non-polar collector, and thus flotation of coals, is the better the more hydrophobic coal is. As it was shown in Fig. 12.52, the hydrophobicity and coal flotation increases with carbon content up to about 88%, and then it slightly decreases as result of higher number of aromatic groups in coal.

In the presence of simple inorganic salts (NaCl, KCl, etc.), one can notice an increase in coal flotation (Klassen and Mokrousov, 1963; Laskowski, 1966). To observe improved flotation, the salt concentration has to be higher than about 0.1 mol/dm^3. Otherwise flotation is reduced (Li and Somasundaran, 1993). The mechanism of salt flotation, in spite of the attempts by many authors (Klassen and Mokrousov, 1963; Laskowski, 1966; Paulson and Pugh, 1996; Pugh et al., 1997), has not been well explained. Salts does not seem to change the hydrophobicity of the floated material (Laskowki, 1986) but mainly make flotation faster (Yoon, 1982) and shorten the so-called contact time. It can be supposed that the increase in density of aqueous solution also plays a certain role. Salt flotation is not commonly applied because of corrosivity of saline aqueous solutions (Ozbayoglu, 1987).

Sulfur, talc, and graphite also belong to the group of naturally hydrophobic substances. For flotation of sulfur, collectors are used along with frothers. Any apolar compound can serve as a collector. In Poland, at the beginning of sulfur industry development in the sixties of the previous century, kerosene was used as the collector and turpentine as a frother while water-glass was applied as gangue minerals depressor. Since 1970's diesel oil was used and turpentine replaced by mixture of pure alcohols (AC) or byproducts containing AC (Flotanal) (Bara and Kisielewski, 1984). Because of the increased sulfur production from other sources (natural gas, crude oil, exhaust gases desulfurization, coking plants, bituminous shale, underground melting) sulfur ore upgrading has no significance nowadays (Bilans, 1997).
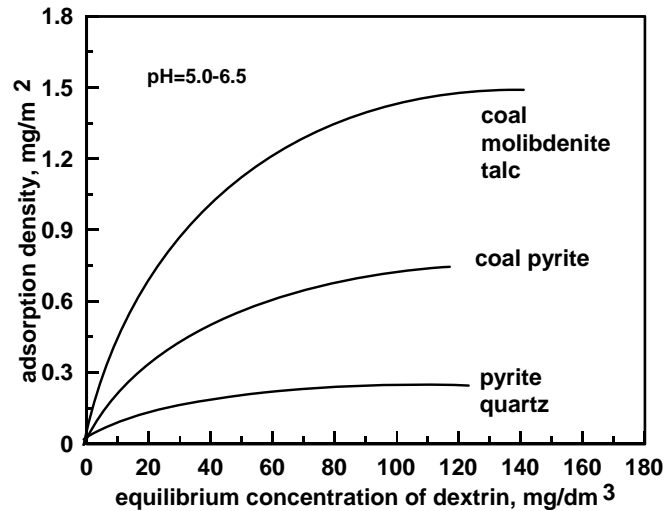
Fig. 12.55. Strong adsorption of dextrin on hydrophobic minerals and coal and weak adsorption on hydrophilic quartz and pyrite (Miller et al., 1984) (Overseas Publishers Association. With permission of Tylor & Francis Ltd.)

Other naturally hydrophobic minerals are talc and graphite. Talc is a silicate (Mg_3 $[(OH)_2Si_4O_{10}]$) and graphite is one of many allotropic varieties of carbon. Presently six allotropic groups of this element are known: graphite (α and β), diamond (diamond and lonsdaleite), carbine (chaoite and cumulene), fullerene (fullerite and nanotubes), carbon (linear and cyclocarbon) (Pierzak and Drzymała, 1998).

Graphite, talc and bituminous matter accompany some ores and raw materials and their easy flotation is an undesirable phenomenon. Additionally, they can alter froth property causing its stabilization. Dextrin is commonly used to depress naturally hydrophobic materials (Laskowski, 1983). Figure 12.55. presents that a considerable adsorption of dextrin on different naturally hydrophobic minerals and negligible adsorption on hydrophilic minerals such as quartz and pyrite occurs. This phenomenon is used for depression of naturally hydrophobic materials.

12.6.2. Native metals and sulfides

Such metals as iron, mercury, copper, gold, and platinum group can be found as native materials (Bolewski and Manecki, 1993). Their flotation is conducted using collector with sulfydryl groups, especially xanthates. To float precious and non-ferrous metals it is necessary to use higher concentrations of sulphydryl collector or collectors containing higher number of CH_2 groups in the hydrocarbon radicals, i.e. five or more. Dithiophosphates as well as xanthate + mercaptobenzothiazole, and dithiophosphate+ mercaptobenzothiazole mixtures (Aplan and Chander, 1988) can be used for flotation.

The hydrophobization mechanism of metal surfaces with sulphydryl collectors is similar to that of sulfides and is of an electrochemical nature. Good flotation of metallic silver, gold, and copper is connected with a high stability constant of metal ions with sulphydryl flotation regents (Fig. 12.56). Metals, not only the native ones, float well with fatty acids and amines (Wark, 1955). Some of them, however, especially Al and Pb, provide small contact angles with amines. Metal sulfides can be floated with different collectors, yet the key role is played by sulphydryl compounds and their alkaline salts (–SNa or –SK). The list of collectors containing sulfur in their structure is presented in Table 12.36 (Aplan and Chander, 1988).
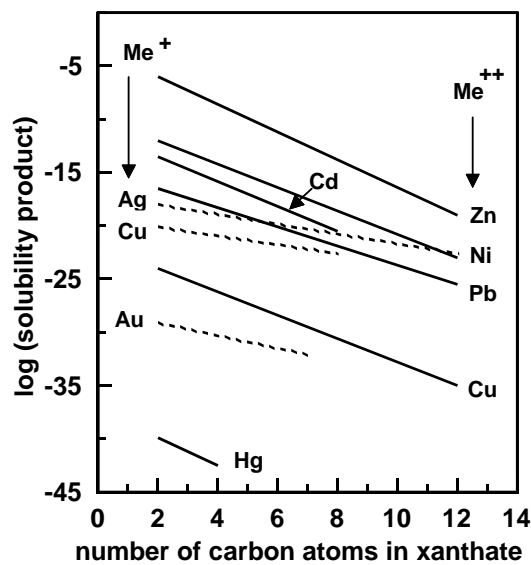
Fig. 12.56. Solubility products of metal xanthatates
(after Aplan and Chander, 1988)

Among sulphydryl collectors the most important are dithiocarbonates (xanthates) and dithiophosphates (aerofloates). Their strong collective activity result from their good reactivity with metal ions, which is expressed by a low solubility product. Figure 12.56 shows the solubility products of mono– and divalent metals with xanthates having different number of carbon atoms in the hydrocarbon radical. Only metal ions which form sulfides of industrial significance were considered.

It results from Fig. 12.56 that xanthates form the most stable compounds with gold, mercury and copper, while the most soluble is the one with Zn^{2+}. Although the constants represent the solubility product for bulk phases not for xanthate-ion compounds on the sulfide surface, there can be observed considerable similarity between metal xanthates solubility and sulfide flotation.

Table 12.36. Collectors containing sulfur applied for flotation of sulfides (after Aplan i Chander, 1988)

Collector type	Formula	Chemical name	Manufacturer and designation	
Mercaptan	R–SH		Pennwalt, Philips	
Dithiocarbonate (xanthate)			AmCy	Dow
	R–O–(C=S)–SK	potassium ethyl	303	Z–3
	R–O–(C=S)–SNa	sodium ethyl	325	Z–4
		potassium isopropyl	322	Z–9
		sodium isopropyl	343	Z–11
		potassium butyl	–	Z–7
		sodium isobutyl	317	Z–14
		potassium sec-butyl	–	Z–8
		sodium sec-butyl	301	Z–12
		potassium amyl	355	–
		sodium amyl	350	Z–6
		potassium sec-amyl	–	Z–5
		potassium hexyl	–	Z–10
Trithiocarbonate	R–S–(C=S)–SNa		Philips (Orform C0800)	
Xanthogen formate	R–O–(C=S)–S–(C=O)–OR´		Dow	Minerec
		R=ethyl, R´=ethyl	Z–1	A
		R=izopropyl, R´=ethyl	–	2048
		R=butyl, R´=ethyl	–	B
Xanthic ester	R–O–(C=S)–S–R'		AmCy	Minerec
		R=amyl, R´=allyl	3302	1750
		R=heksyl, R´=allyl	3461	2023
Monothiophosphate	(R–O–)$_2$(P=S)–ONa		Amcy 194, 3394	
Dithiophosphate	(R–O–)$_2$(P=S)–SNa		AmCy (Aerofloat)	
		sodium diethyl	Na Aerofloat	
		sodium di-isopropyl	Aerofloat 211, 243	
		sodium di-izobutyl	Aerofloat 3477	
		sodium di-isoamyl	Aerofloat 3501	
		sodium di-iso-sec-butyl	Aerofloat 238	
		sodium di-methylamyl	Aerofloat 249	
	(R–O–)$_2$(P=S)–SH	cresylic acid+P$_2$S$_5$	Aerofloat 15	
Dithiophosphinate	(R–)$_2$(P=S)–S–Na		AmCy3418	
Thiocarbamate	R–(NH)–(C=S)–OR´		Dow	Minerec
		N-methyl-O-isopropyl	–	1703
		N-methyl-O-butyl	–	1331
		N-methyl-O-isobutyl	–	1846
		N-ethyl-O-isopropyl	Z–200	1661
		N-ethyl-O-isobutyl	–	1669
Thiourea derivatives	(C$_6$H$_5$NH$_2$)C=S (thiocarbanilide)		AmCy Aero. 130	
Mercaptobenzo-thiazole			AmCy 400 series	

Flotation of sulfides takes place as a result of collectors adsorption. In the case of xanthate flotation of sulfides, hydrophobization mechanism is complex and is not well

understood. This is so because there are many reactions which can create hydrophobization of a sulfide in the presence of xanthates. According to Woods (1988) hydrophobization of sulfides with sulphydryl compounds, especially with xanthates, results from electrochemical reactions in which electrons are transmitted from a collector to a sulfide mineral (anodic process), and then the electrons return to aqueous solution due to catodic reduction of oxygen:

$$O_2 + 2H_2O + 4e = 4OH^- \qquad (12.90)$$

During anodic oxidation, the following products can be formed:
a) chemisorbed xanthate X_{ad} created from X^- ion coming from the aqueous solution and a metal ion sitting in the crystalline structure of sulfide:

$$X^- \rightarrow X_{ad} + e \qquad (12.91)$$
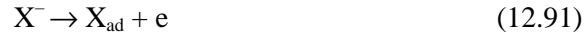
b) dixanthogene X_2, as a result of X^- ion oxidation

$$2X^- \rightarrow X_2 + 2e \qquad (12.92)$$

c) metal xanthate MeX_2, due to the reaction of X- ion with metal sulfide MS

$$2X^- + MS \rightarrow MX_2 + S + 2e, \qquad (12.93)$$
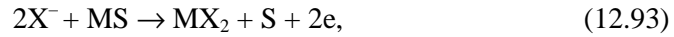
and the product of this reaction is element sulfur S, though other products can also be formed, e.g. thiosulfate, sulfate(IV) or sulfate(VI). The formation of sulfate(VI) can be also written as:

$$2X^- + MS + 4H_2O \rightarrow MX_2 + SO_4^{2-} + 8H^+ + 8e \qquad (12.94)$$
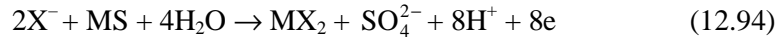
The chemisorbed xanthate X_{ad} can be transformed into either a dithiol:

$$2X_{ad} \rightarrow X_2 \ \text{ or } \ X_{ad} + X^- \rightarrow X_2 + e \qquad (12.95)$$

or metal xanthate:

$$2X_{ad} + M^{2+} + 2e \rightarrow MX_2 \qquad (12.96)$$
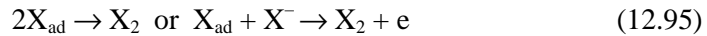
Metal xanthates MX_2 can also be formed on partly oxidized sulfide surface. Surface oxidation can be written as the reaction:

$$MS + 6H_2O \rightarrow M(OH)_2 + SO_4^{2-} + 10H^+ + 8e \qquad (12.97)$$
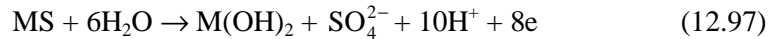
while the formation of metal xanthate as:

$$M(OH)_2 + 2X^- \rightarrow MX_2 + 2OH^- \qquad (12.98)$$

According to Leja (1982), after introduction of xanthate into flotation pulp many other compounds can be formed, for instance xanthogenic acid HX, hydroxyxanthates, perxanthates, disulfide carbonates, etc.

The redox reactions taking place in flotation systems can be shown in a Eh –pH diagram. However, their complexity for metal sulfides in the presence of xanthates and oxygen can be significant due to numerous possible reactions in the system. Therefore, the diagram is usually based on certain assumptions, e.g. the number of considered components and their oxidation degree are limited. Well-constructed diagrams should reflect real conditions in the flotation system and allow to predict quantitatively the presence of different species in the system, especially those which are responsible for flotation. Usually the diagrams provide quantitative information because they are based on the assumption that all predicted reactions would take place without any difficulties within a short period of time, which may not be true.

Figure 12.57 shows a Eh–pH diagram for PbS in the presence of potassium ethyl xanthate (X$^-$) plotted on the basis of redox equations for this system applying the procedure already used for the Cu-H$_2$O system (Fig. 12.57). When drawing the diagram an assumption was made that the highest oxidation form of sulfur is elementary sulfur (S^o). A comparison of real data on flotation for PbS xanthate flotation at varying Eh values and pH=8 (Fig. 12.58) with the areas of predomination of different species present in the flotation system indicates that PbX$_2$ is responsible for a rapid PbS flotation, while the role of dixanthate (X$_2$) is considerably less important. An interpretation of PbS flotation when the sulfide was kept under oxidizing conditions before flotation, is much more difficult since it requires drawing new Eh – pH diagrams at different assumptions.
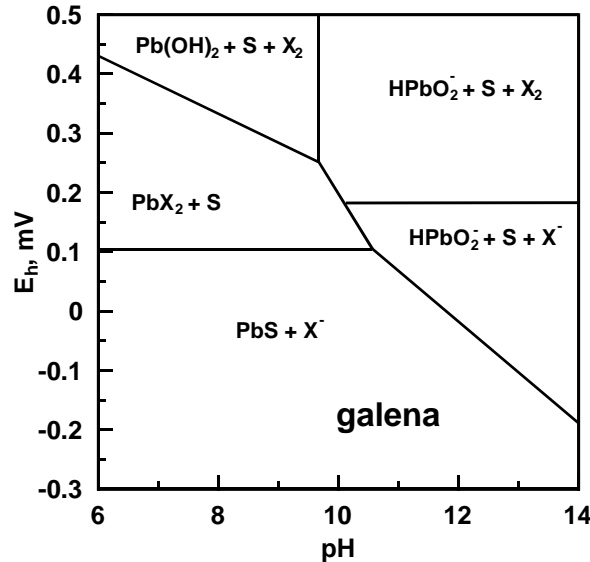
Fig. 12.57. Eh–pH diagram for galena in the presence of ethyl xanthate assuming
that total amount of xanthate species was 10^{-4} M and that elemental sulfur is created during oxidation
(after Woods, 1988)
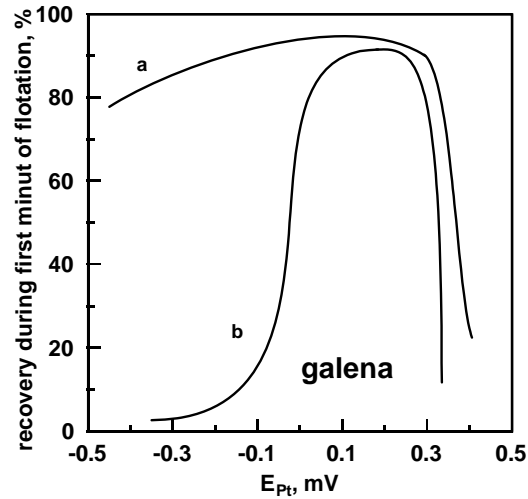
Fig. 12.58. Galena flotation with ethyl xanthate at pH = 8 as a function of applied potential to a platinum electrode in solution: a – galena kept in oxidizing environment before flotation, b – kept in reducing environment (after Richardson, 1995; based on Guy and Trahar, 1985)

Xanthates easily render sulfides hydrophobic. Even a low concentration of xanthate in the solution causes flotation of pyrite (Fig. 12.59). Flotation usually takes place within a wide range of pH. Usually there is a maximum pH value, also called the critical pH (Lekki, 1979) at which flotation disappears. The critical pH depends on the concentration and structure of the collector. Only flotation time, according to Laskowski (1986), who based his claim on the data by Lekki (1980), does not effect the critical pH of flotation.
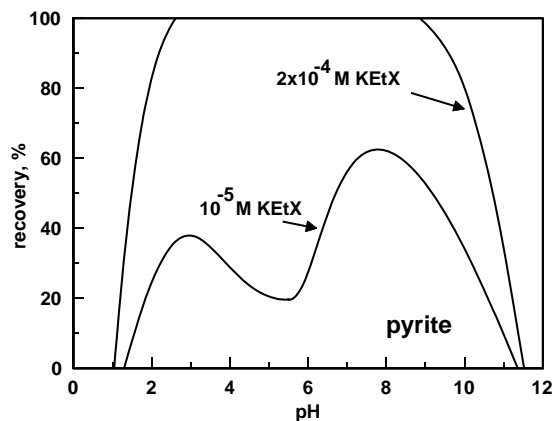
Fig. 12.59. Pyrite flotation in the presence of different concentration of potassium ethyl xanthate (after Fuerstenau et al., 1968)

Sulfide flotation usually takes place at relatively small adsorption of sulphydryl (thiol) collectors. When partly oxidized sulfides are subjected to flotation, xanthate consumption is higher, since some part of it is used for removing the surface oxidized layers by xanthate ions, while the remaining part makes the new surface hydrophobic. The calculated apparent total adsorption of xanthate is equivalent to several or a dozen of statistical monolayers. The flotation improves when longer chain xanthates are used in experiments. Since hydrophobization with xanthates is of electrochemical character, the iep of sulfide does not effects flotation. The isoelectric point on the pH scale, determined from the electrokinetic potential for sulfides is about 5 for ZnS and about 9 for CuS (Lekki, 1979). For oxidized sulfides the iep falls to about 2, i.e. takes the value of elementary sulfur (Ney, 1973).

Sulfides can be also floated with other collectors including oleates (Abramov et al., 1982) and amines. As far as amines are concerned, flotation takes place at low pH values after sulfide ions addition (Aplan et al., 1980).

Application of xanthates requires the use of frothers. Different reagents including simple aliphatic alcohols (AD), branched alcohols (MIBC), complex alcohols (pine oil, α-terpineol), aromatic alcohols (crezoles), polyglycols (Arefroth 65) and Dowforth, as well as trietoxybuthane (TEB) can be used as frothers.

Many papers discuss natural flotation of sulfides. It is known that sulfides having layered (MoS_2, molybdenite; As_2S_3 (auripigment), molecular (As_4S_4, realgar) or chain (Sb_2S_3) structures are naturally hydrophobic (Gaudin et al., 1957; Drzymala, 1994c). Other sulfides which have ionic-covalent-metallic structure, depending on their geological history and the way of their preparation before the measurement, are either hydrophilic or hydrophobic. They are characterized by different contact angles, ranging from very small to that of elementary sulfur. This phenomenon results from formation, due to oxidation, surface layers containing excess of sulfur atom in relation to metal ions, or even elemental sulfur. A further oxidation can lead to hydrophilization of sulfide surface. Metal sulfides from Polish copper deposits are hydrophilic or slightly hydrophobic and their flotometric contact angle is presented in Table 12.37.

Table 12.37. Natural hydrophobicity of sulfides and other minerals mostly from Polish copper deposits in Lubin (LGOM). The hydrophobicity is given in term of contact angle calculated from flotometric data. After Drzymala and Bigosinski (1995), Drzymala (1994) as well as Lekki and Drzymala (1990)

Sulfide	Contact angle	Sulfide	Contact angle
Sulfur	63.2	*covelline	1.9
Pyrite	44.0–0	*djurleite	0
*Bornite	6.5–9.6	*chalcocite	0
*Djurleite – bornite	4.5	*bituminous shale	0
*Galena	4.0	calcite	0
*Chalcopyrite	3.6	quatz	0

* denotes mineral from LGOM.

12.6.3. Oxidized non-ferrous metals minerals

Flotation of this group of minerals can be performed in two different ways. The first approach is designed for sulfides and relies on using thiol collectors after treating the oxidized sulfide surface with sulfide ions. The second path is for silicates, oxides and hydroxides which are floated with either cationic or anion collectors. Lead: cerrusite ($PbCO_3$), vanadinite ($Pb_5[Cl(VO_4)_3]$), anglesite ($PbSO_4$), copper: malachite ($CuCO_3Cu(OH)_2$), azurite ($2CuCO_2Cu(OH)_2$), chrysocola (hydrated cuprum silicate), tenorite (CuO), cuprite (Cu_2O), and zinc: smitsonite ($ZnCO_3$) minerals are suitable for flotation with thiol after sulfidization. Sulfidization of some minerals (cerusite, malachite, azurite) is easily, while with others (anglesite, tenorite, cuprite) experiences difficulty (Leja, 1982).

Sulfidization of mineral relies on treating them with aqueous solutions containing sulfide ions, which react with surface mineral ions, forming metal sulfides and elementary sulfur on the surface. The process, for instance for an oxide, can be written as:

$$-MO + S^{2-} + 2H^+ = -MS + H_2O \qquad (12.99)$$

where –MO is an oxide surface group which becomes metal sulfide –MS under the influence of sulfide ion S^{2-}.

The driving force of this reaction is lesser solubility of metal sulfides in relation to metal oxides. Metal sulfides easily undergo decomposition in the presence of oxygen, forming such oxidized sulfur compounds as thiosulfates, sulfates(IV) or sulfates(VI). Yet, it should be noticed that sulfidization is conducted as a surface reaction. Sulfidization is rather a complicated process.

Sulfide ions regulate redox potential of flotation and they create so low Eh that thiol collector adsorption (e.g. xanthate) does not take place. Therefore, flotation of sulfidized minerals generally does not occur in the presence of sulfide ions (Fig. 12.60, line 3). The best way to create proper Eh is removing sulfide ions from the solution after sulfidization using clean aqueous instead of sulfide solution (Fig. 12.60, line 1) or oxidation of sulfide ions by passing through the solution air (Fig. 12.60, line 2), oxygen, or other oxidizers. However, oxidizing can cause oxidation and the removal of surface sulfide layers which is responsible for flotation.

Some oxidized minerals float with thiols directly without sulfidization, but it requires considerably higher xanthate concentration. According to Fleming (1952) and Leja (1982) vanadinite floats with xanthates at 1 to 2 kg of collector per 1 megagram of the ore, but it requires only 0.1 kg/Mg when sulfide minerals are sulfidized. In the case of chrysocolla, roasting at 773-873 K significantly improves its flotation (Laskowski et al., 1985).
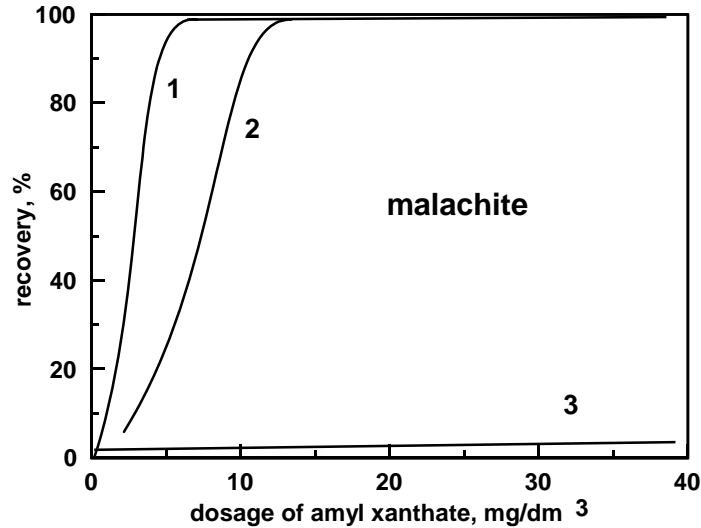
Fig. 12.60. Influence of conditions of flotation on recovery of malachite sulfidized with 960 mg/dm^3 of Na$_2$S·9H$_2$O in the presence of frother (amyl alcohol 60 mg/l): 1 – flotation when after sulfidization the solution is replaced with pure aqueous, 2 – flotation after 25 minutes of air bubbling through the solution containing sulfide ions, 3 – flotation directly after sulfidization in the presence of sulfide ions (after Soto and Laskowski, 1973)

The use of anionic and cationic collectors for flotation of oxidized minerals of non-ferrous metals was discussed in the section on oxide and hydroxide flotation.

12.6.4. Oxides and hydroxides

This is the most numerous and diversified group of minerals. It includes simple oxides (Fe$_2$O$_3$, SnO$_2$), hydroxioxides (AlOOH), as well as complex oxides and hydroxides (spinels, silicates, aluminosilicates). Their flotation can be conducted with different collectors. The selection of a collector depends on mineral properties, including isoelectric point and the ability of a cation which forms the mineral to chemically react with collectors. Detailed discussion of this mineral group would require a separate description of each system and it would be too lengthy. Therefore, only selected flotation systems will be discussed here and application of fatty acids and amines as collectors. Other aspects of flotation of minerals belonging to this group have already been discussed in chapters on flotation reagents (activators, depressants, collectors).

Fatty acids and their aqueous-soluble potassium salts, called soaps, are eagerly used as collectors for oxides, hydroxides, and salts. The most popular is oleic acid which is a cheap by-product the wood industry and is called the tall oil. The tall oil contains oleic acid and such acids as linoleic, linolenic, and abietic. It is known that pH range of flotation of many minerals with fatty aids is similar (Polkin and Najfonov,

1965); Mishra, 1988) (Fig. 12.61). Yet, their mechanisms of adsorption and flotation can be quite different. It results from Fig. 12.61 that some minerals do not float well or do not float at all as quartz (Fig.12.61) or silicates (Table 12.38). This diversity has become the basis of separation of minerals with the use of fatty acids. It can also be concluded from Fig. 12.61 that oleate flotation ceases at extreme pH values. This fact results from a competition of OH^- and H^+ ions. This has already been discussed in chapter 12.5.4.1.
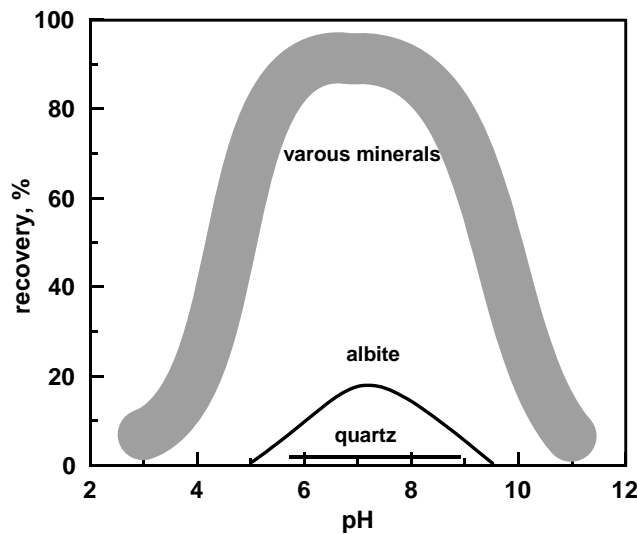
Fig. 12.61. Flotation of many minerals in the presence of 1 kg/Mg NaOl depending on the pH of the solution. Quartz and some silicates do not float under such conditions. Investigated minerals: columbite, zircon, tantalite, ilmenite, rutile, granate, perovskite (based on data of Polkin and Najfonov (1965) supplements with the line of quartz)

Table 12.38. Influence of structure of silicates on their flotation with anionic and cationic collectors (after Manser, 1975)

Collector	Silicate group			
	orthosilicates	pyroxene	amphibole	frame
Anionic	good	week	None	none
Cationic	satisfactory*	satisfactory *	Good	very good

* Flotation depends on pH.

Fatty acids form different species in aqueous solution shown in Fig. 12.62. There are three groups of oleate species: ions (Ol^-, HOl_2^- premicelle), micelles and such phases as liquid oleic acid and acid soap ($NaHOl_2$). All these forms play an important role in flotation process. It should be also noticed that sodium oleate is present in most oleate forms including HOl oil phase, ionic species (acid soap ion) and micelles. Since the structure of minerals and oleate species are diverse, the mechanisms of fatty acids adsorption on mineral surface is highly complex.
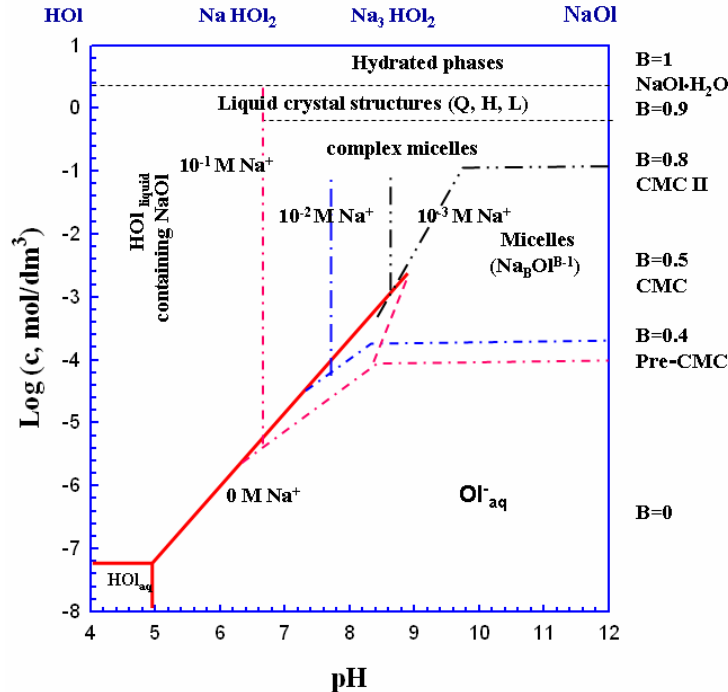
Fig. 12.62. Concentration - pH diagram for sodium oleate aqueous solutions. It shows predominance of various oleate species (Drzymala, 1990): c – activity of oleate species, mol/dm³, B (or β) – degree of binding oleate with sodium ions in associated species (number of sodium ions per one oleate ion in the associate) (data for drawing the diagram are given in Table 12.39. It should be noticed that sodium ions also take part in most oleate species)

There are many hypothesis regarding adsorption of oleate species on mineral surfaces. Two of them seem to be the most realistic. The firs hypothesis, proposed by Lekki (1984) and Laskowski (1981) assumes that flotation is caused by oleate ions which form with mineral-building cations non-soluble soaps. According to such an assumption flotation pH range can be calculated on the basis of oleate soaps solubility product, as flotation takes place when under particular conditions of pH and collector concentrations in the system an oleate soap is formed. The argument of this hypothesis is a good agreement of flotation data with the pH range of soap formation. This is shown in Table 12.40.

According to the second hypothesis, proposed by Fuerstenau and Palmer (1976), adsorption of oleate ions occurs when cations are able to form monohydroxy complexes. It is not important whether the ions originate form mineral crystalline structure or are purposefully introduced into the solution. It has been noticed that flotation of quartz activated by metal ions introduced into the solution is similar to flotation of minerals containing the same metal ion in their crystalline structure. Table 12.41 pre-

sents calculated ranges of metal monohydroxycomplexes formation and observed flotation pH ranges of different minerals. The fact that there is an agreement between flotation and pH ranges of bulk soap formation suggest that both hypothesis can be combined. They become compatible providing that flotation takes place due to forming soaps with hydrolized metal ions present near the mineral surface (Fuerstenau, 1995). These combined hypothesis can be called the activation hypothesis of flotation with fatty acids.

Table 12.39. Reactions and corresponding equilibrium constants of reactions taking place in oleate solution. Activity coefficient of NaOl and HOl in the oily phase and activities of NaHOl$_2$ as well as micellar forms (Na$_\beta$Ol$^{\beta-1}$)$_n$ were assumed to be 1 (Drzymala, 1990)

Nr	Reaction	reaction constant	pK
1	HOl$_{aq}$ $\Leftrightarrow$ H$^+_{aq}$ + Ol$^-_{aq}$	$K_1 = $ (H$^+_{aq}$)·(Ol$^-_{aq}$)/(HOl$_{aq}$)	4.95
2	HOl$_{aq}$ $\Leftrightarrow$ H$^+_{aq}$ + Ol$^-_{aq}$	$K_2 = $ (H$^+_{aq}$)·(Ol$^-_{aq}$)/X$_{HOl\ oil}$	12.3
3	HOl$_{oil}$ $\Leftrightarrow$ HOl$_{aq}$	$K_3 = $ (HOl$_{aq}$)/X$_{HOl\ oil}$	7.35
4	HOl$_{aq}$ + Ol$^-_{aq}$ $\Leftrightarrow$ HOl$_2^-{}_{aq}$	$K_4 = $ (HOl$_2^-{}_{aq}$)/[(Ol$^-_{aq}$)·(HOl$_{aq}$)]	–7.6
5	2Ol$^-_{aq}$ $\Leftrightarrow$ Ol$_2^{2-}{}_{aq}$	$K_5 = $ (Ol$_2^{2-}{}_{aq}$)/(Ol$^-_{aq}$)^2	–4.0
6	HOl$_{oil}$ + Na$^+_{aq}$ $\Leftrightarrow$ NaOl$_{w\ HOl}$ + H$^+_{aq}$	$K_6 = $ (H$^+_{aq}$)·X$_{NaOl\ w\ HOl}$/[(Na$^+_{aq}$)·X$_{HOl\ oil}$]	6.38
7	NaOl$_{In\ HOl}$ $\Leftrightarrow$ Na$^+_{aq}$ + Ol$^-_{aq}$	$K_7 = $ (Na$^+_{aq}$)·(Ol$^-_{aq}$)/X$_{NaOl\ in\ HOl}$	5.92
8	NaHOl$_2$ $\Leftrightarrow$ Na$^+_{aq}$ + H$^+_{aq}$ + 2Ol$^-_{aq}$	$K_8 = $ (Na$^+_{aq}$)·(H$^+_{aq}$)·(Ol$^-_{aq}$)^2	19.01
9	2HOl$_{oil}$ + Na$^+_{aq}$ $\Leftrightarrow$ NaHOl$_2$ + H$^+_{aq}$	$K_9 = $ (H$^+_{aq}$)/[(Na$^+_{aq}$)·(X$_{HOl}$ = 0,8)^2]	5.59
10	0,5 NaHOl$_2$ + (β – 0,5)Na$^+_{aq}$ $\Leftrightarrow$ Na$_\beta$Ol$^{\beta-1}$ + 0,5 H$^+_{aq}$	$K_{10} = $ (H$^+_{aq}$)^{0,5}/(Na$^+_{aq}$)$^{\beta-0,5}$, dla 10^{-3}M Na$^+$ for 10^{-2}M Na$^+$ for 10^{-1}M Na$^+$	4.85 4.58 4.44
11	βNa$^+_{aq}$ + Ol$^-_{aq}$ $\Leftrightarrow$ (Na$_\beta$Ol$^{\beta-1}$)$_n$	$K_\beta = $ 1/[(Na$^+_{aq}$)$^\beta$·(Ol$^-_{aq}$)] or log [Ol$_{total}$] = A – β log (Na$^+_{aq}$) : CMC β = 0,5 premicellar form β = 0,4 cylindrical micelles β = 0,8	 A = –4.4 A = –5.0 A = –1.8
12	–HOl$_s$ $\Leftrightarrow$ –Ol^-_s + H$^+_{aq}$	$K^{int}_{a2} = $ {–Ol^-_s}(H$^+_{aq}$) exp(–$F\psi_0$/RT)/{–HOl$_s$}	4.40
13	–HOl$_s$ + Na$^+_{aq}$ $\Leftrightarrow$ –Ol$^-$Na^+_s + H$^+_{aq}$	$K^{int}_{Na} = $ {–Ol$^-$Na^+_s}(H$^+_{aq}$) exp(–$F\psi_0$/RT)/ /[{–HOl$_s$}(Na$^+_{aq}$) exp(–$F\psi_b$/RT)]	3.3 ±0.3
14	iep		pH=2.0

ψ_0– surface potential,
ψ_b – surface potential at the Na$^+$ ions binding plane
{ } stands for activity of surface species,
parenthesis ( ) denote activity of other species.

Table 12.40. Comparison of calculated pH range of existence of soaps with the range of pH of different minerals according to a hypothesis of Lekki (1984) (data collected by Drzymala, 1986)

Soap	pH range of soap existence[a]	Mineral	pH range of flotation with 10^{-5}M NaOl
FeOl$_3$	2.57–8.01	Magnetite	3.0–8.0[b]
FeOl$_3$	2.57–8.01	Ilmenite	3.7–8.0[c]
FeOl$_3$	2.57–8.01	Hercynite	3.9–8.0[c]
AlOl$_3$	3.98–8.22	Pleonaste	3.6–7.9[c]
MgOl$_2$	7.92–10.37	Pleonaste	8.7–10.4[c]

a) Drzymala (1986), experimental data: b) Luszczkiewicz et al. (1979), c) Lekki (1984).

Table 12.41. Comparison of pH ranges of oleate flotation of minerals as well as activated quartz and pH of existence of metal monohydroxy complexes

Monohydroxy complex	Range of pH at concentration> 10^{-7}M	pH of maximum concentration	Flotation (after [a])		pH of flotation [b]
			mineral	pH of maximum flotation	activated quartz
$FeOH^{++}$	0–3.9	2.7	augite	2.9	2–8*
$AlOH^+$	2.1–5.9	4.3			2–8
$PbOH^+$	3.2–12.4	8.7			
$MnOH^+$	7.6–11.6	9.5	pirolusite	9	
$MgOH^+$	8.4–12.5	10.5	magnesite	10.4	7–13
$CaOH^+$	> 8.5	13.1	Augite	11	7–13
$CuOH^+$	5.1–8.1	6.5			
$FeOH^+$	4.5–12.1	8.7	chromite and other iron minerals	8.7, ~8	

a – Fuerstenau and Palmer (1976), b – Daellenbach and Tiemann (1964).
* The participation of $FeOH^+$ ions in widening the pH range of flotation of activated quartz activated with $FeOH^{++}$ ions cannot be ruled out.

A hypothetical mode of fatty acid adsorption at mineral surface via hydrolized metal cation is shown in Fig. 12.63.

As it results from the oleate forms predominance diagram (Fig. 12.62), the composition, apart from ions, involves non-soluble forms of fatty acids, namely the oil or solid phases. Theoretically, they can attach themselves to mineral surface by hetero-coagulation, contact, and semi-contact (Drzymala, 1986).
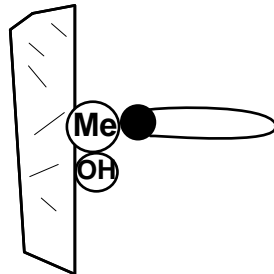
Fig. 12.63. Schematic illustration of adsorption of fatty acid ion on mineral surface through hydrolized metal cation leading to surface hydrophobization

Adhesion by heterocoagulation (Fig. 12.64a) takes place as a result of the van der Waals-London attraction forces between oil or solid phase and solid surface, like in the DLVO theory. The mechanism of this sorption is similar to heterocoagulation. Since electrical double layers between two attracting objects are partly preserved, such attachment can be called a non-contact adsorption, analogically to the nomenclature used by Derjagin (1989) for adhesion of air bubbles to a solid surface. The heteroco-agulation adhesion takes place when interacting objects have opposite electrical charge. If the objects are of the same charge, adhesion is determined by the van der

Waals-London attractive forces. Such adhesion can be described using the DLVO theory. An example of flotation resulting from the heterocoagulation adhesion is oleate flotation of rutile (Purcell and Sun 1963) up to pH about 4,5.

The contact adhesion (Fig. 12.64 b) relies on direct adhesion of oil phase drops to a solid surface. Adhesion force is determined by the force balance determined by the Young equation (12.1), which occur at the three phase boundaries, i.e. aqueous-oil, aqueous-solid, and oil-solid. In turn, the force of interaction of a particular interface depends on dispersion and the non-dispersion forces (polar, chemical, hydrogen bonds and others), which is described by the Fowkes relation (12.4). Flotation at low pH values of such hydrophobic forces as germanium (Drzymała el al., 1987) or mercury (Volke et al., 1984) can serve as an example of contact adhesion.

The semi-contact adhesion consists of adsorption of simple collector ions on the surface and formation of hemicelles or even monolayers which form a bridge for additional adsorption of oily drop or particles of collectors as a result of hydrophobic interaction. Figure 12.64c. presents this kind of sorption. The adhesion is characterized by adsorption isotherms. Flotation resulting from the semi-contact adsorption can take place at low pH values when non-soluble collector phases predominate in the solution and hydrophobization of particle surface is due to adsorption of single soluble collector species. Many minerals can float according to this mechanism.
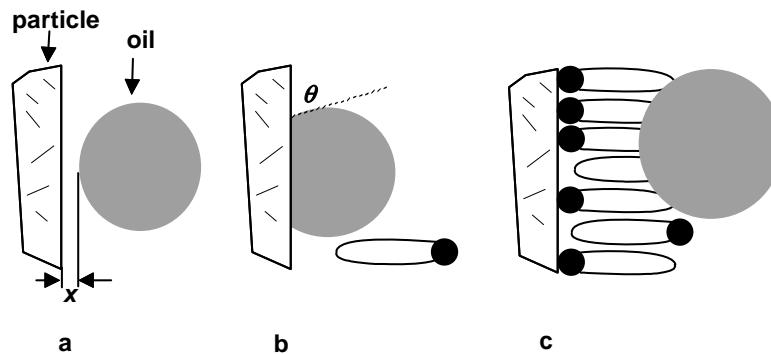
Fig. 12.64. Schematic illustration of modes of adhesion of a colloidal collector (here as an oil drop) to solid surface: a – contactless (heterocoagulation), b – contact, c – semicontact adhesion

Investigations showed that at higher concentrations of fatty acids in the solution the co-adsorption of different species is very common. Coadsorption of oleate ions and oleic acid drops can take place in pH ranges when drops of oleic acid are present in the solution that is in acid or neutral solutions (Leja, 1982). This has already been discussed and shown in Fig. 12.64. Since oleate species are often accompanied by sodium oleate (NaOl), they are frequently present in adsorption layers on minerals. In the case of coadsorption of ionic and micelle species, flotation may be reduced to zero. This phenomenon can be observed at high oleate concentrations and is caused by ad-

sorption of hydrophilic micelles. This can be illustrated by the results of zircon flotation shown in Fig. 12.65.
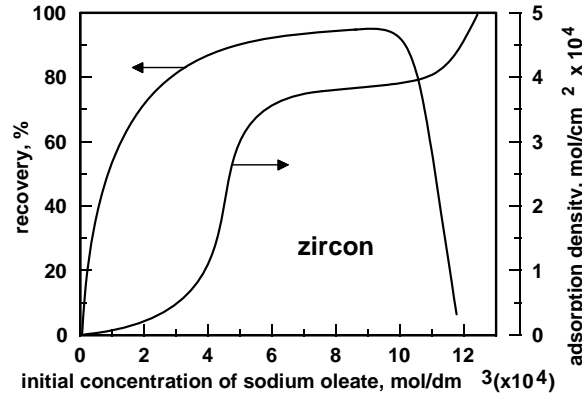
Fig. 12.65. At high oleate species concentrations flotation decreases even though the oleate adsorption increases. It is assumed that it results from adsorption of hydrophilic micelles (based on data of Dixit and Biswas, 1973)
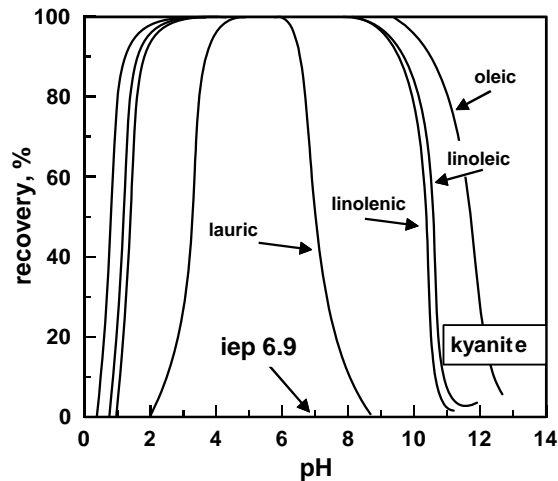
Fig. 12.66. Kyanite flotation with 10^{-4} kmol/m^3 of fatty acids (Choi and Oh, 1965). Applied acids: laurate ($C_{11}H_{23}COOH$), linoleic (C_5H_{11}–CH=CH–CH$_2$–CH=CH–(CH$_2$)$_7$COOH), linolenic CH$_3$–[CH$_2$–CH=CH]$_3$(CH$_2$)$_7$COOH and oleic ($C_{17}H_{33}COOH$)

Oxides and hydroxides flotation depends on the length of hydrocarbon chain of fatty acid applied in flotation, as well as on number of double bonds in the molecule. Fig. 12.66 presents kyanite flotation with different fatty acids. The figure shows that the longer the chain the wider pH range of flotation, which is connected with greater stability constant of created soap. On the other hand, the presence of double bonds at the same number of carbon atoms in hydrocarbon radicals, worsens flotation. It can be

seen in Fig. 12.66 that flotation with linolenic acid, which has three double bonds, takes place in narrower pH range than with linoleic acid, which has two double bonds. Still better is flotation with oleic acid having only one double bond. Oleic, linoleic and linolenic acids have 17 carbon atoms in hydrocarbon radical.

Amines are also used in flotation of oxides and hydroxides. It is assumed that their flotation takes place solely due to physical sorption of amines species on mineral surfaces. Therefore, such parameters as the state of mineral surface, mainly the sign of the electrical charge and hydrophobicity, as well as the chemistry of amine collectors solutions considerably govern flotation. On the basis of the equilibrium constant of amine reaction with water, the CMC and iep of the amine solid phase, presented in Table 12.42, it is possible to draw a diagram expressing predomination of different dodecylamine species in aqueous solutions as a function of pH.

Table 12.42. Equilibrium constants of selected reactions, iep and CMC for dodecylamine in aqueous (after Laskowski, 1988)

Reaction	K
$R–NH_{2\ (aq)}+H_2O \Leftrightarrow R–NH_3^+{}_{(aq)}+OH^-$	$4.3 \cdot 10^{-4}$
$R–NH_{2\ (s)} \Leftrightarrow R–NH_{2\ (aq)}$	$2.0 \cdot 10^{-5}$
micellization	$CMC = 1.3 \cdot 10^{-2}$ M
iep	pH = 11

The dodecylamine domain diagram (Fig. 12.67) proves, that similarly to fatty acids, ions, micelle and amine phases are present in the collector-aqueous system. In contrary to fatty acids, amine ions are positively charged, since in aqueous solution they hydrolyze to $–NH_3^+$. Correctness of the phase diagram for amine drawn on the basis of equilibrium constants was experimentally confirmed by Laskowski (1988) and Laskowski et al. (1988). They found that the iep of non-soluble dodecylamine equals 11 and that in certain pH ranges and concentrations unstable suspension with coagulating colloidal amine particles was formed, while in other areas a stable amine colloidal suspension was present. This is also shown in the diagram.

Typical course of adsorption and flotation of mineral oxides with amines has been already shown in Fig. 12.37 for quartz. Quartz flotation as well as other minerals flotation takes place as a result of electrostatic adsorption of positively charged amine ions with negatively charged sites on particle surfaces. Flotation of minerals with amines generally increases with pH starting from the iep. From a certain pH value flotation decreases as a result of amine precipitation, which takes place along the transition line for the reaction $R\text{-}NH^+{}_{3(aq)} \rightarrow R\text{-}NH_{2(s)}$ presented in the predominance of amine species diagram (Laskowski, 1988). This regularity has been known for a long time (Watson and Manser, 1968; Leja, 1982) but without taking into account the concentration–pH diagram, the decrease in flotation had been attributed to micellization while in fact it is caused by amine precipitation.
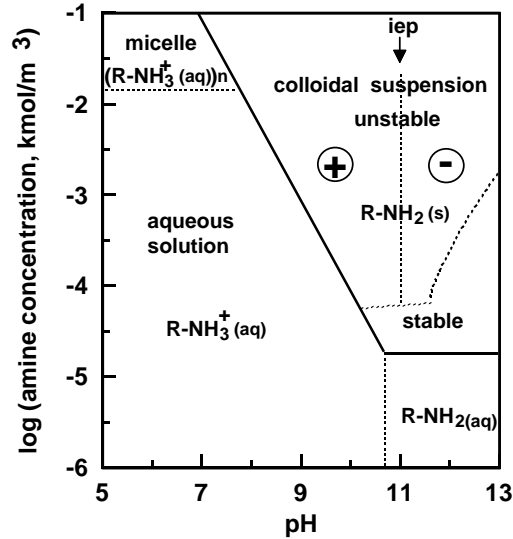
Fig. 12.67. Diagram of predomination of various forms of dodecylamine
as a function of pH of solution (data after Laskowski, 1988)
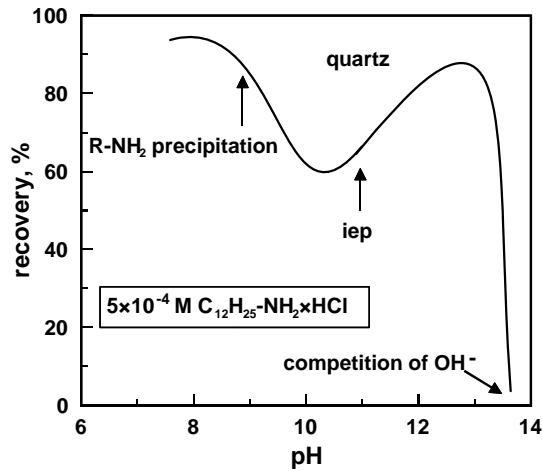
Fig. 12.68. Relationship between quartz flotation with amine and pH. Following a good flotation in alka-
line solutions there is a drop in flotation as a result of precipitation of coagulating amine. At high pH an
increase of flotation is caused by stable of amine suspension (after Laskowski et al., 1988)

As it has already been mentioned amine ions are positively charged up to pH 11
and above this value they become negatively charged. This phenomenon not only af-
fects the properties of amine colloid suspensions but also flotation. This is so because
as pH increases, coagulating amine precipitates and flotation decreases. The decrease
in flotation continues until pH 11, which corresponds to the iep of amine and mini-

mum of its stability. At higher pH values amine suspension becomes stable, flotation slightly increases. However, at pH about 13-14 flotation disappears as a result of competition with OH⁻ ions (Fig. 12.68).

Different amines are applied for flotation. It was established that the longer the hydrocarbon chain of amine the lower amine concentration is needed flotation (Fig. 12.69). Amine with four carbon atoms requires very high amine concentrations, therefore, in practice amines having ten or more carbon atoms in the molecule are used.
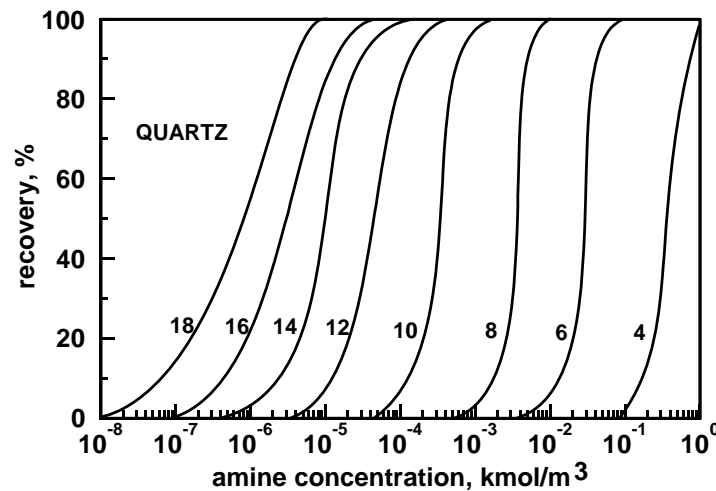
Fig. 12.69. Influence of length of the amine hydrocarbon chain on quartz flotation at pH = 6–7 and increasing concentration of alkylamine acetate (Fuerstenau et al., 1964)

12.6.5. Sparingly soluble salts

Many useful minerals belong to this group. Among them the most important are: fluorite (CaF_2), barite ($BaSO_4$), celestite ($SrSO_4$), calcite ($CaCO_3$), magnesite ($MgCO_3$), dolomite ($CaMg(CO_3)_2$), bastnäsite (($La,Ce)CO_3F$, scheelite ($CaWO_4$), and apatite ($Ca_5F(PO_4)_3$) and its modifications. These minerals can float with different ionic collectors. They float within wide pH and collector concentration ranges (Fig. 12.70).

When sparingly soluble salts type minerals are present in the same ore, there is a need to separate them. Their flotation, at a particular pH, depends on collector concentration. There are differences in flotation resulting from the way the separation is performed as well as the origin of minerals (Fig. 12.71a and b).

Generally, the use of collector alone is not sufficient to selectively separate useful mineral of salt type from the ore. Therefore, the use of depressants for selective flotation of sparingly soluble salt type minerals is necessary. Numerous chemical compounds are applied as depressants, including simple organic substances (water glass),

simple organic (citric) and complex (humic) acids, as well as carbohydrates (starch, dextrin) and tree extracts (tannin, quebracho). Figure 12.72 presents separation of fluorite from calcite by application of mixed $Al_2(SO_4)_3$ + Na_2SiO_3 depressants. Without depressants the separation of fluorite from calcite is not be possible.
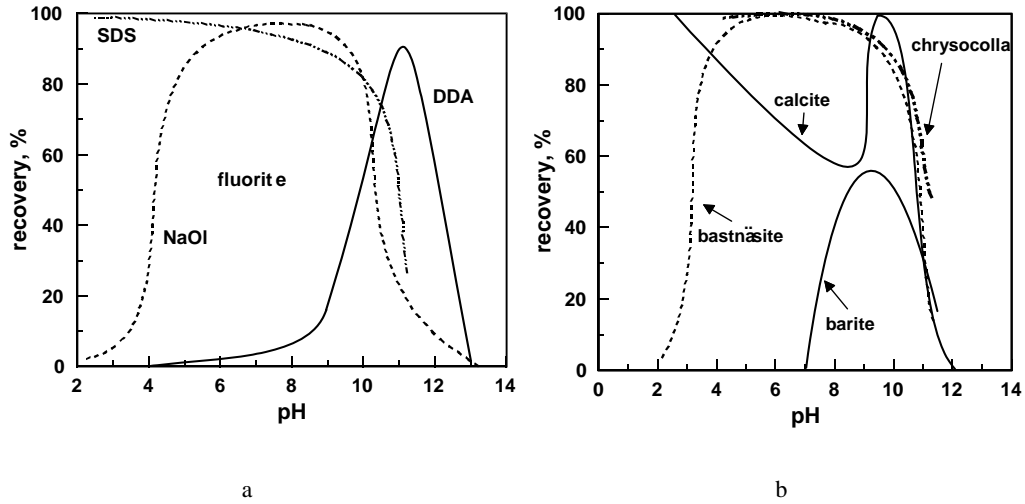
Fig. 12.70. Flotation of sparingly soluble minerals: a) fluorite flotation with sodium oleate ($c_{NaOl} = 2 \cdot 10^{-5}$ M, Pugh, 1986), dedecylamine (DDA) $9 \cdot 10^{-5}$ M (Pugh, 1986), and sodium dodecyl sulfate (SDS) $1 \cdot 10^{-4}$ M (Takamori and Tsunekawa, 1982), b) flotation of different minerals with potassium octyl hydroxamate: chrysocolla $8 \cdot 10^{-4}$ M, bastnäsite $5 \cdot 10^{-4}$ M, calcite $5 \cdot 10^{-4}$ M, barite $1 \cdot 10^{-3}$ M (Fuerstenau and Pradip, 1984). pH range of flotation is usually greater at a higher collector concentration
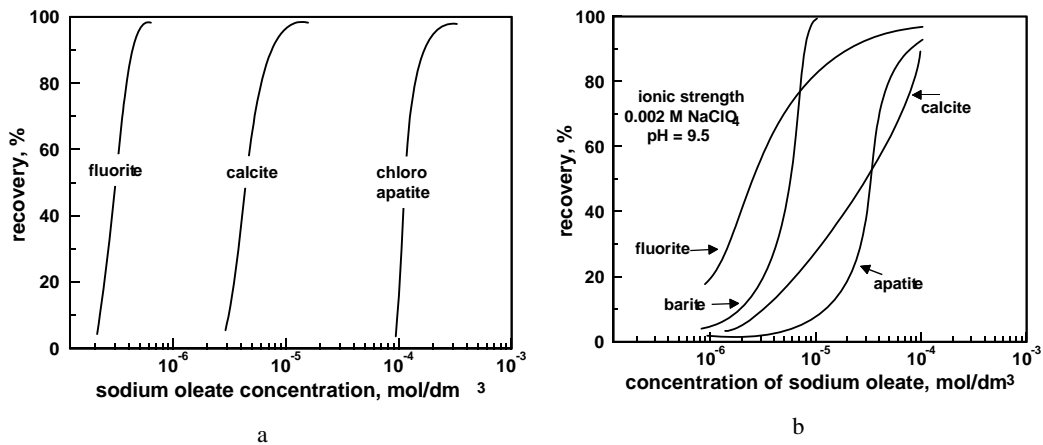
Fig. 12.71. Flotation of sparingly soluble minerals with oleic acid: a – after Finkelstein (1989), natural pH, b – after Parsonage et al., (1982)

Table 12.43 presents collectors and depressors used for separation of barite from fluorite by flotation.

Table 12.43. Influence of different collectors and depressants on barite and fluorite flotation
(table after Pradel, 2000 based on Sobieraj, 1985)

Reagent	Flotation of	
	barite	fluorite
Collectors	Alkyl sulfate	
Pretopon	floats well at pH 8–12	reduced flotation at pH 8
Siarczanol N-2	floats well at pH 4–12	flotation at pH 6–10
Sodium dodecyl sulfate (SLS)	floats well at pH 4–12	cease of flotation at pH > 7
	Alkyl sulfonate	
Oleic sulfosuccinate	floats well at pH 5–12	gradual cease of flotation at pH < 8
Streminal ML	floats well at pH 5–12	floats well at pH 5–12
Sodium kerylbenzosulfonate	floats well at pH 4–12	cease of flotation at pH > 7
	Fatty acids	
Sodium oleate	floats well at pH 6.5–8.5	floats well at pH 4–10
	Other collectors	
Kamisol OC, cationic collector	floats well at pH 3–12	flotation at pH 3–12
Rokanol T-16, nonionic collector	weak collecting power	weak collecting power
Depressant	Tannins	
Quebracho S (+ SLS)	no flotation in alkaline solutions	total cease of flotation in alkaline solutions
Quebracho S (+ Pretopon G)	cease of flotation at pH > 6	cease of flotation at pH > 6
Tannin (+ SLS)	cease of flotation in alkaline solutions	cease of flotation in alkaline solutions
Gallic acid (+ SLS)	cease of flotation in alkaline solutions	cease of flotation in alkaline solutions
Tannin D (+ SLS)	cease of flotation in alkaline solutions	cease of flotation in alkaline solutions
Tannin M (+ SLS)	cease of flotation in alkaline solutions	cease of flotation in alkaline solutions
	Other depressants	
Dextrin (+ sodium oleate)	no flotation in alkaline solutions	flotation at pH 6–9
Glycerol (+ sodium oleate)	full flotation depression at pH 5–11	no flotation in acidic environment; no week flotation in alkaline solutions
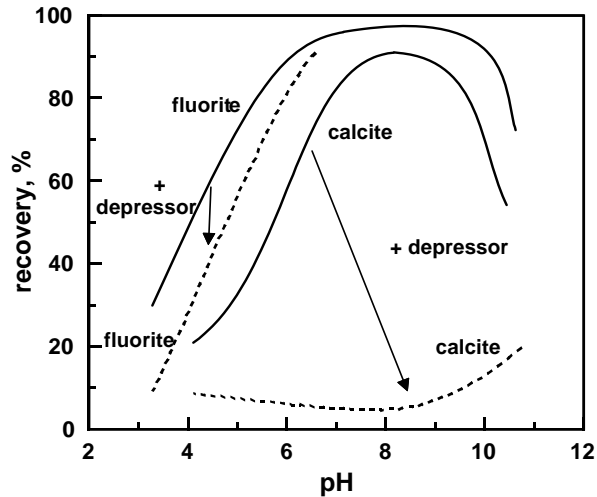
Fig. 12.72. Influence of depressant (70 mg/dm^3 Al$_2$(SO$_4$)$_3$ and 70 mg/dm^3 Na$_2$SiO$_3$) on flotation of fluorite and calcite mixture (dashed line) in the presence of sodium oleate (100 mg/dm^3) (after Abeidu, 1973). Solid line indicates flotation in the absence of depressant

Table 12.44. Solubility products (I$_r$) for selected compounds at 293 K (after Barycka and Skudlarski, 1993)

Compound	I_r	Compound	I_r
1	2	3	4
Fluoride		sulfate	
CaF$_2$	$4.0 \cdot 10^{-11}$	BaSO$_4$	$9.8 \cdot 10^{-11}$
SrF$_2$	$2.5 \cdot 10^{-9}$	SrSO$_4$	$6.2 \cdot 10^{-7}$
MgF$_2$	$6.5 \cdot 10^{-9}$	CaSO$_4$	$9.1 \cdot 10^{-6}$
Chloride		sulfide	
AgCl	$1.8 \cdot 10^{-10}$	HgS	$1.9 \cdot 10^{-53}$
PbCl$_2$	$1.7 \cdot 10^{-5}$	Ag$_2$S	$6.3 \cdot 10^{-50}$
Bromide		Cu$_2$S	$7.2 \cdot 10^{-49}$
AgBr	$4.6 \cdot 10^{-13}$	CuS	$4.0 \cdot 10^{-36}$
PbBr$_2$	$2.8 \cdot 10^{-5}$	PbS	$6.8 \cdot 10^{-29}$
Iodide		ZnS	$1.2 \cdot 10^{-28}$
AgI	$8.3 \cdot 10^{-17}$	NiS	$1.0 \cdot 10^{-24}$
PbI$_2$	$7.1 \cdot 10^{-9}$	CoS	$3.1 \cdot 10^{-23}$
Carbonate		FeS	$5.1 \cdot 10^{-18}$
PbCO$_3$	$7.2 \cdot 10^{-14}$	MnS	$1.1 \cdot 10^{-15}$
ZnCO$_3$	$1.7 \cdot 10^{-11}$	Cyanide	
CaCO$_3$	$7.2 \cdot 10^{-9}$	Hg$_2$(CN)$_2$	$5.0 \cdot 10^{-40}$
MgCO$_3$	$3.5 \cdot 10^{-8}$	CuCN	$3.2 \cdot 10^{-20}$
Hydroxide		chromate	
Fe(OH)$_3$	$4.5 \cdot 10^{-37}$	PbCrO$_4$	$2.8 \cdot 10^{-13}$
Zn(OH)$_2$	$3.3 \cdot 10^{-17}$	BaCrO$_4$	$1.2 \cdot 10^{-10}$
Mg(OH)$_2$	$1.2 \cdot 10^{-11}$	CuCrO$_4$	$3.6 \cdot 10^{-6}$

The mechanism of reaction between polar collectors and sparingly soluble salts minerals is quite complex and the degree of complication is even higher for minerals from the oxide and hydroxide group. It results from the fact that additional parameters become involved, namely concentration of anions and cations in flotation system which are determined by the solubility products of minerals. The solubility products of selected compounds at 293 K, after Barycka and Skudlarski (1993) are gathered in Table 12.44.

The solubility products indicate what the concentration of salt ions in mineral aqueous suspension is. For fluorite the solubility product at 20^0C (293 K) is $9.0 \cdot 10^{-11}$. It means that due to fluorite dissolution the concentration of calcium ions will be c_{Ca++} = $(I_r/4)^{1/3}$ = $2.2 \cdot 10^{-4}$ kmol/m^3, while the concentration of fluoride ions will be twice higher. These values are in agreement with direct measurements of Marinakis and Shergold (1985). Solubility products of other compounds, including salts, can be found in the literature or calculated on the basis of thermodynamic data (free enthalpy of formation) of chemical species taking part in the reaction. The data can be taken from handbooks (CRC, 1986/87) and other sources. When calculating ions concentration one should remember that solubility product I_r is equal to the equilibrium constant of a dissolution reaction K_r, since the activity of the solid phase is 1. Fluorite dissolution can be written as:

$$CaF_2 = Ca^{2+} + 2F^-, \qquad (12.100)$$

and the equilibrium constant of the reaction and the solubility product will be given by:

$$I_r = K_r = \exp(-\Delta G_r^0 / RT) = (Ca^{2+})(F^-)^2/(CaF_2), \qquad (12.101)$$

where
R – gas constant
T – temperature, K.
( ) denotes activity which in technical calculations can be replaced with concentration in kmol/m^3, activity of the solid phase of CaF$_2$ is 1.

In Eq. 12.101 ΔG_r^0 is the standard free enthalpy of reaction calculated from the relation:

$$\Delta G_r^0 = \Sigma \nu_i \, \Delta G_{i,f}^0,$$

where:

$\Delta G_{i,f}^0$ – standard of formation (formation of a given species)

ν_i – stoichiometric coefficient of reaction which is positive for products and negative for substrates.

According to Fuerstenau and Urbina (1988) adsorption of a collector on sparingly soluble minerals can take place physically or chemically, as well as it can be a surface reaction. It is possible to distinguish:

- physical adsorption of a collector due to electrical double layer with preservation of ions hydration (amine on barite),
- chemical adsorption of a collector on non-hydrolized surface ion located in a crystalline structure (fatty acids on barite) or on a hydrolized ion (hydroxamate on bastnesite),
- surface reaction of a collector with surface metal ion leading to its removal from crystalline structure and forming at the interface multilayer collector-metal ions compound having lower solubility than the mineral (oleate on calcite),
- surface reaction of a collector with metal ion situated near the surface (outside crystalline structure) and forming a collector-metal ion compound at the mineral surface (tridecane on hydroxapatite).

The above modes of adsorption after Fuerstenau and Pradip (1984) can schematically be delineate as:

a) physical sorption

$$Me^{++}\!: + H_2O^-collector \rightarrow Me^{++}\!:H_2O^-collector$$
$$Me^{++}\!: + H_2O(OH^-)H_2O \rightarrow Me^{++}\!:H_2O\ OH^-\ H_2O$$

b) chemical sorption

$$Me^{++}\!: + {}^-collector \rightarrow Me^+\!:collector$$
$$Me^{++}\!: + H–collector \rightarrow Me^+\!:collector + H^+$$
$$Me^{++}\!: + OH^- \rightarrow Me^+\!:OH$$
$$Me^+\!:OH + collector^- \rightarrow Me\!:(OH)collector$$

c) adsorption, and then surface reaction

$$Me^{++}\!: + {}^-collector \rightarrow \square\!:(Mecollector)^+$$
$$Me^{++}\!: + H–collector \rightarrow \square\!:(Mecollector)^+ + H^+$$
$$Me^{++}\!: + OH^- \rightarrow \square\!:(MeOH)^+$$
$$Me^{++}\!: + HCO_3^- \rightarrow \square\!:(MeHCO_3)^+$$

d) surface reaction

$$\square\!:(MeOH)^+ + {}^-collector \rightarrow \square\!:(Mecollector)^+ + OH^-$$
$$\square\!:(MeOH)^+ + H\text{-}collector \rightarrow \square\!:(Mecollector)^+ + H_2O$$
$$\square\!:(MeOH)^+ + OH^- \rightarrow \square\!:(MeOH)_2$$
$$\square\!:(MeOH)^+ + 2Hcollector \rightarrow \square\!:Me(collector)_2 + H^+ + H_2O$$
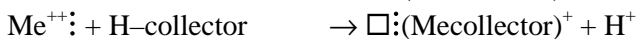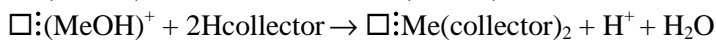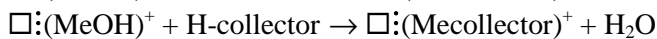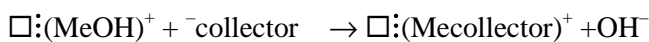
where:

symbol $:$ denotes metal ions surface,

symbol $\square$ denotes site after removing metal ion from the crystalline structure.

The list does not cover all the reaction which can take place between collector ions and mineral ions. A compound of collector and mineral ion can be formed in the bulk

solution and it can undergo sorption on the surface leading to flotation. If the collector–ion compound formed as a result of surface reaction is removed from the surface, flotation is not possible.

It is assumed that chemical reactions between collector and cation dominate in flotation systems involving fatty acids, alkylosulfonates, alkylosulfates, as well as chelating reagents (hydroxamates) while physical adsorption prevails in flotation with amines. Since pH, ionic strength of the solution, concentration of ions released from mineral and the way the mineral is added to a flotation system govern the reactions, the flotation results obtained by different researches can be considerably different both for the same minerals floated by different investigators and for the same minerals of different origin (Fig. 12.71).

A characteristic feature of the discussed flotation systems is possible occurrence of collector multilayers, especially of oleate, on mineral surfaces. According to Rao and Forssberg (1991) the multilayer adsorption of collectors and metal ions (coming from the mineral) compounds is characteristic for the system floated in suspensions having low content of a mineral. The dissolved metal ions form chemical compound with collector ions in the solution and they are adsorbed on the surface of particles which total area is small. Thus, the adsorption is multilayered. If flotation is performed in dense suspensions, the amount of formed ion-collector compound is the same but the surface area of particles is large. It is dictated by the solubility product which is not dependent on the amount of mineral particles in the suspension. The collector-metal ions compounds spread on a very large area, therefore adsorption becomes limited. At appropriate conditions, before multilayer precipitation, there is a monolayer of oleate on calcite, while a double layer exists on such minerals as fluorite, apatite, scheelite and barite (Rao and Forssberg, 1991).

Chemical composition of the mono- or multi- layers depends on the number of metal ions available in the solution. If there are few of them, the adsorption of the collector ions on the surface takes place not only through reaction and bridging with calcium ions, but also with participation of sodium ions, as it has been predicted by Drzymala (1986). According to Rao and Forssberg (1991), depending on the sign of surface potential and its value for calcium minerals, the following reactions, leading to the formation of mono- and double layers of compounds, take place:

➢ on electrically neutral sites:

$$-CaOH + {}^-OOCR = -Ca^+{}^-OOCR + OH^-$$
$$-CaOH + Na^+{}^-OOCR + OH^- = -CaO\ Na\ OOCR^- + H_2O$$
$$-CaOH + Ca^{++}{}^-OOCR + OH^- = -CaO\ Ca\ OOCR^- + H_2O$$

➢ on positively charged sites:

$$-CaOH_2^+ + {}^-OOCR + OH^- = -Ca^+{}^-OOCR + H_2O$$

➢ on negatively charged sites:

$$-CaO^{\delta-}\ Na^+ + {}^-OOCR = -CaO\ Na\ OOCR,\ where\ \delta < 1,$$
$$-CaO^{\delta-}\ Ca^{++} + {}^-OOCR = -CaO\ Ca\ OOCR,\ where\ \delta \leq 1.$$
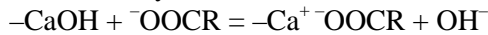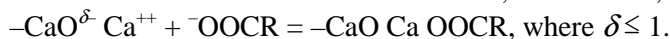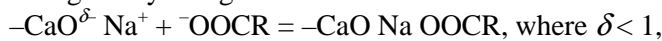
Somasundaran and Ananthapadmanabhan (1986) investigated the role of the relation between mineral ions and collector concentrations. They found out that very often it is possible to record a simple dependence between flotation and onset of formation of collector-metal ions bulk compounds. This is the case for apatite-oleate, dolomite-oleate, magnesite-fatty acids, calcite-fatty acids. If there is in the solution some surplus of cations released from the mineral, the precipitation can occur in the solution, resulting in significant worsening of flotation. The cause of the differences in flotation can also be ions diffusion. If the speed of chemical dissolution is high, the system will tend to form the metal ions-collector compound in the solution. It is better if diffusion advances slowly – then the formation of the compound between a collector and metal ions occurs close to the surface.

To float sparingly soluble salt type minerals one can use hydroxamates of a general formula:

$$R_1\text{—}N\text{—}OH$$
$$R_2\text{—}C\text{=}O$$

. $$(12.102)$$

These compounds can be called N-alkyl hydroxylamine derivatives or carboxylic acids oximes. The characteristic feature of these chelating collector is that they react best at pH about 9 and form multilayers. It suggests that surface layers contain both anions and neutral molecules of hydroxamic acid, as their pK, indicating at which pH concentration of both forms is identical, is about 9 (Fuerstenau and Pradip, 1984).

12.6.6. Soluble salts

Flotation of soluble salts such as halite (NaCl), silvinite (KCl), carnallite (KCl·MgCl$_2$.6H$_2$O), and kieserite (MgSO$_4$·H$_2$O) is conducted with the use of cationic and anionic collectors from their saturated solutions. Flotation of soluble salt type minerals is performed in order to separate one salt form another, as well as to remove from gangue minerals which can be fine particles of alumino-silicates (illite, chlorites) and other minerals, e.g. carbonates (dolomite). The separation of soluble salts is usually based on their surface charge (Table 12.45).

According to Miller et al. (1992) a sign of surface charge of soluble salts is possible to predict using the theory of ions hydration (Table. 12.45). For instance, NaCl is positively charged while KCl is negatively charged and therefore, these minerals can be separated by flotation using amines (in that case KCl floats) or fatty acids (to provoke NaCl flotation) (Miller et al., 1992). Other soluble salt type minerals also follow the electrostatic mechanism and their flotation using amine is shown in Fig. 12.73.

The mechanism of collector - ions interaction in saline solutions is not well known. Very likely there is no a single mechanism of flotation. It has been assumed that KCl flotation takes place as a result of heterocoagulation of positively charged amine col-

lector with negatively charged KCl particles at concentrations higher than amine solubility i.e. when amine in an aqueous solution is present in colloidal form.

Table 12.45. Sign of surface charge for selected soluble salts (after Miller et al., 1992)

Salt	Surface charge sign		Salt	Surface charge sign	
	measured	predicted*		measured	predicted*
LiF	+	+−	KBr	−	+
NaF	+	+	RbBr	−	+
KF	+	+	CsBr	+	+
RbF	+	+	LiI	−	−
CsF	+	+	NaI	−	−
LiCl	−	−	KI	+	
NaCl	+	−	RbI	−	−
KCl	−	+	CsI	+	+−
RbCl	+	+	NaI·2H$_2$O	+	
CsCl	+	+	K$_2$SO$_4$	−**	
LiBr	−	−	Na$_2$SO$_4$·10H$_2$O	−**	
NaBr	−	−	Na$_2$SO$_4$	−**	

 * Predicted from the ions hydration theory for ions in crystalline lattice (Miller et al., 1992).
** Hancer et al., 1997.
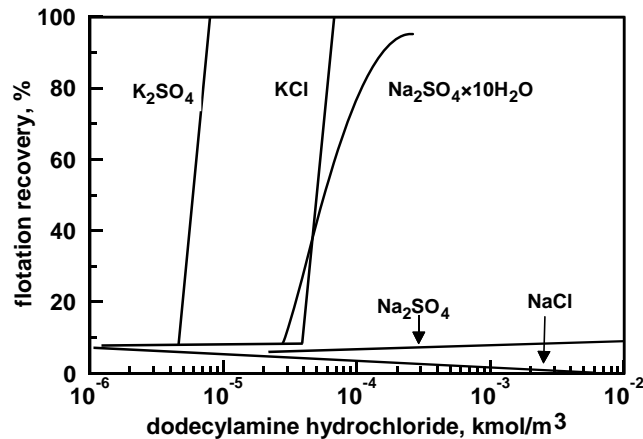
Fig. 12.73. Flotation of different salts in the presence of dodecylamine
(after data of Hancer et al., 1997, data for NaCl after Miller et al., 1992)

This mechanism is valid for K$_2$SO$_4$ flotation, since flotation with amines takes place at concentrations much lower than concentration needed for precipitation. Investigations of Hancer et al. (1997) showed that successful flotation requires thermodynamic stability of a salt. Sodium sulfate can serve as an example since it exists in anhydrous (Na$_2$SO$_4$) and hydrated (Na$_2$SO$_4$ ·10 H$_2$O) forms. Na$_2$SO$_4$ does not float with amine despite its negative charge. Yet, this salt is thermodynamically unstable, since it hydrates and forms Na$_2$SO$_4$·10H$_2$O which floats well because its surface charge is nega-

tive and it is thermodynamically stable at ambient temperature. Thus, the presence of hydrated salt layers does not interfere with amine flotation if the salt is negatively charged. The lack of flotation of halite with amine can be explained by the unmatched size of amine cation and surface sodium ion in NaCl crystalline structure, which is not the case for KCl (Laskowski, 1969).

A technical problem in flotation of soluble minerals is not only the separation of different salts, but also removal of fine gangue particles. The unwanted fine particles significantly increase the consumption of a collector, lower the quality of final products, and harmfully stabilize froth. Reagents like carboxymethylocellulose (CMC), polyacryloamides (PAM), and natural polymers (starches) (Alonso and Laskowski, 1999; Laskowski, 1994) are used as depressors of fine gangue particles. The reagents depressing fine gangue particles which are applied in flotation of soluble salts are also called blinders. Other approaches of separation of gangue fines from salt minerals include selective flocculation of fines with high molecular polyacrylamide followed by flotation of flocculated fines with amine (Perucca and Cormode, 1999). Figure 12.74 presents the effects of selected fined depressants on the results of KCl flotation with amine. In addition to a collector, traditional frothers are used in salt flotation. Mixing frother with a collector to achieve better amine dispersion is recommended.
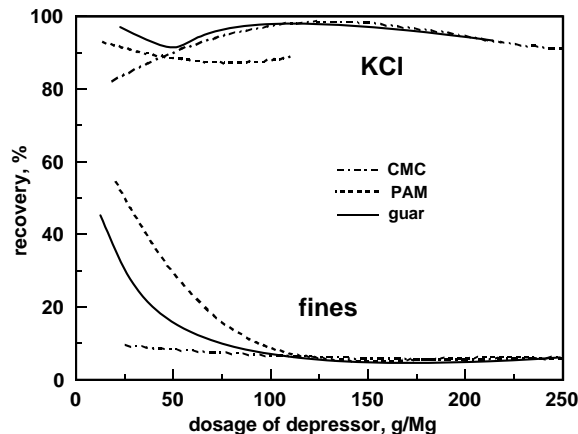
Fig. 12.74. Application of depressants for removing fines of gangue minerals during amine flotation of KCl (after Alonso and Laskowski, 1999). CMC denotes carboxymethylcellulose
PAM - polyacrylamide of low molecular weight, while guar is a natural polysaccharide

12.7. Flotation devices

Flotation can be performed on a small and large scale. The smallest scale involves flotation of a single particle. This can be accomplished in a Hallimond microflotation cell (tube). Tones of material per hour are processed in industrial flotation machines. The microlaboratory scale flotation devices provide a quick and cheap way of deter-

mination of flotation properties of ores and raw materials and their components. Generally, microlaboratory cells are designed to test flotation of one minerals, not mixture of minerals, because in a lean ore a very small sample may have no a single particle of the investigated mineral. It can happen in flotation of gold ore containing several ppm (parts per million) of Au. A disadvantage of small scale flotation devices, except that of Siwek et al., 1981 (Fig. 12.75e), is high mechanical flotation (entrainment) of hydrophilic particles, which masks the true flotation results. The entrainment in the Hallimond tube shown in Fig. 12.75b is governed by the following relation (Drzymala and Lekki, 1989a; 1989b; Drzymala, 1984):

$$a_{max} \, (\rho_p - \rho_w)/\rho_w) = L_H = 0.023 \pm 0.002 \; (cm), \tag{12.103}$$

for density of particles greater than 2.0g/cm^3.

For particles of density lower than 2.09g/cm^3 another expression is used (Drzymala, 1994, 1999):

$$a_{max} \, ((\rho_p - \rho_w)/\rho_w)^{0.75} = L_L = 0.0225 \pm 0.0025 \; (cm), \tag{12.104}$$

where:

ρ_p – particle density,

ρ_w – aqueous density,

a_{max} – maximum particle size which can float mechanically; a_{max} is equal to d_{50}, read from the partition curve representing recovery of mechanical flotation as a function of particle size,

L_L, L_H – constants.

Entrainment decreases as Hallimond cell height decreases. For the cell 1 m in height mechanical flotation of quartz and magnetite decreases from about 100μm to about 20μm (Lukaszewska, 1998). Therefore, relatively large particles (in order of mm in size) should be used for Hallimond tube flotation tests. The appropriate size can be calculated from Eqs (12.103) and (12.104). Another approach to flotation tests in the Hallimond tube, aiming at avoiding mechanical flotation, is conducting flotation measurements within a very short period of time, typically from 15 to 60 seconds. Frequently used microflotation cells are presented in Fig. 12.75.

When working out technological basis of the enrichment of raw materials, laboratory flotation machines are used ranging in capacity from several grams to several kilograms. Their list includes Denver, Mechanobr, Wameco, and IMN laboratory flotation machines. Laboratory flotation columns are less frequently used. Figure 12.76 shows the Mechanobr laboratory flotation machine and its flotation cell, Fig. 12.77 presents the Denver laboratory flotation machine while Fig 12.78 other laboratory flotation devices.
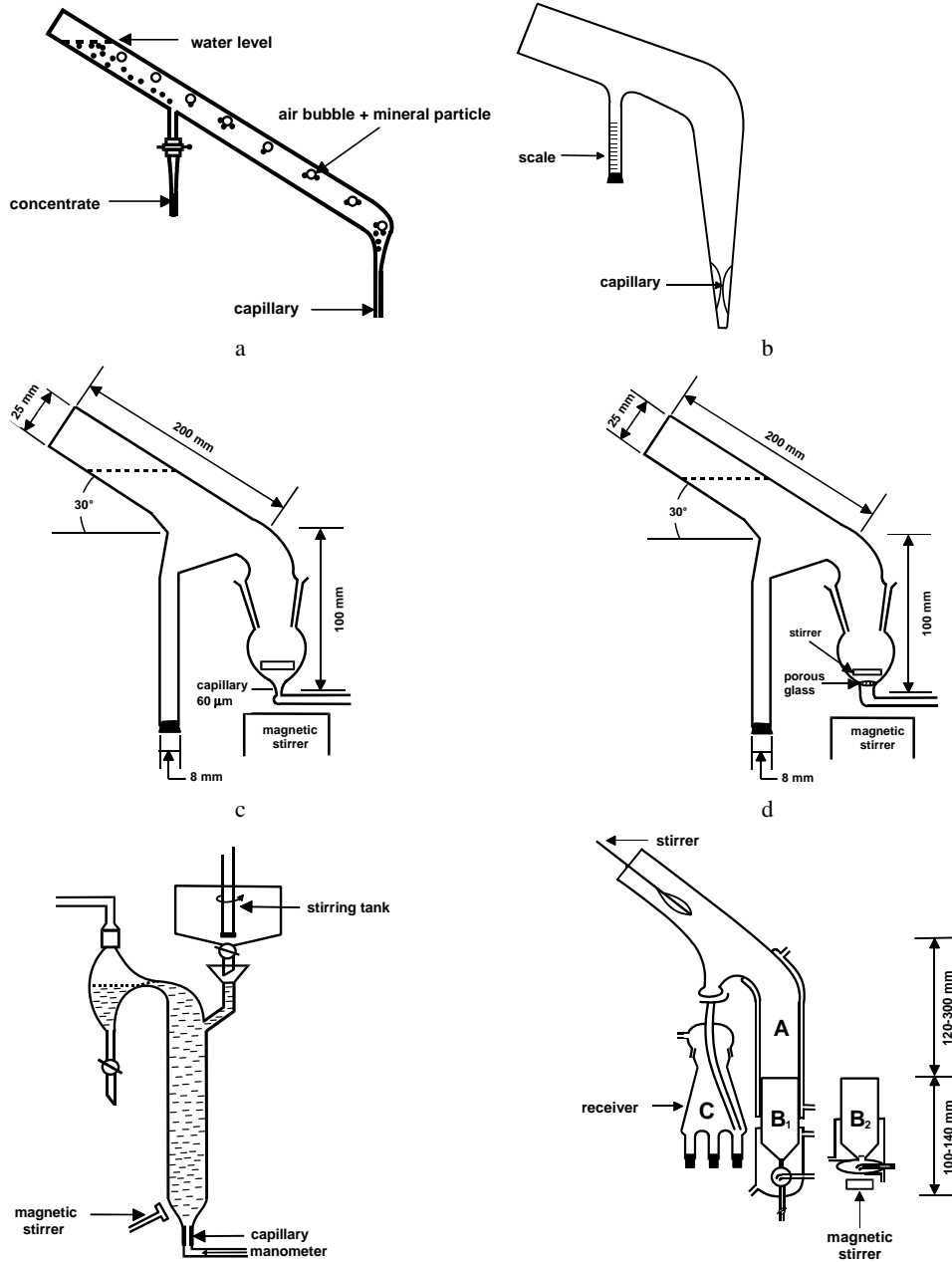
Fig. 12.75. Flotation cells used for flotation on a microlaboratory scale: a – original Hallimond tube (Hallimond, 1944), b – contemporary Hallimond tube designed by Ewers (Sutherland and Work, 1955) equipped with a scale by Lekki (1970), c – modified Hallimond tube (Fuerstenau et al., 1957), d – porous plug version (Nagy et al., 1962), e – cell for fine particles (Siwek et al., 1981), f) universal cell (Dobias, 1983)
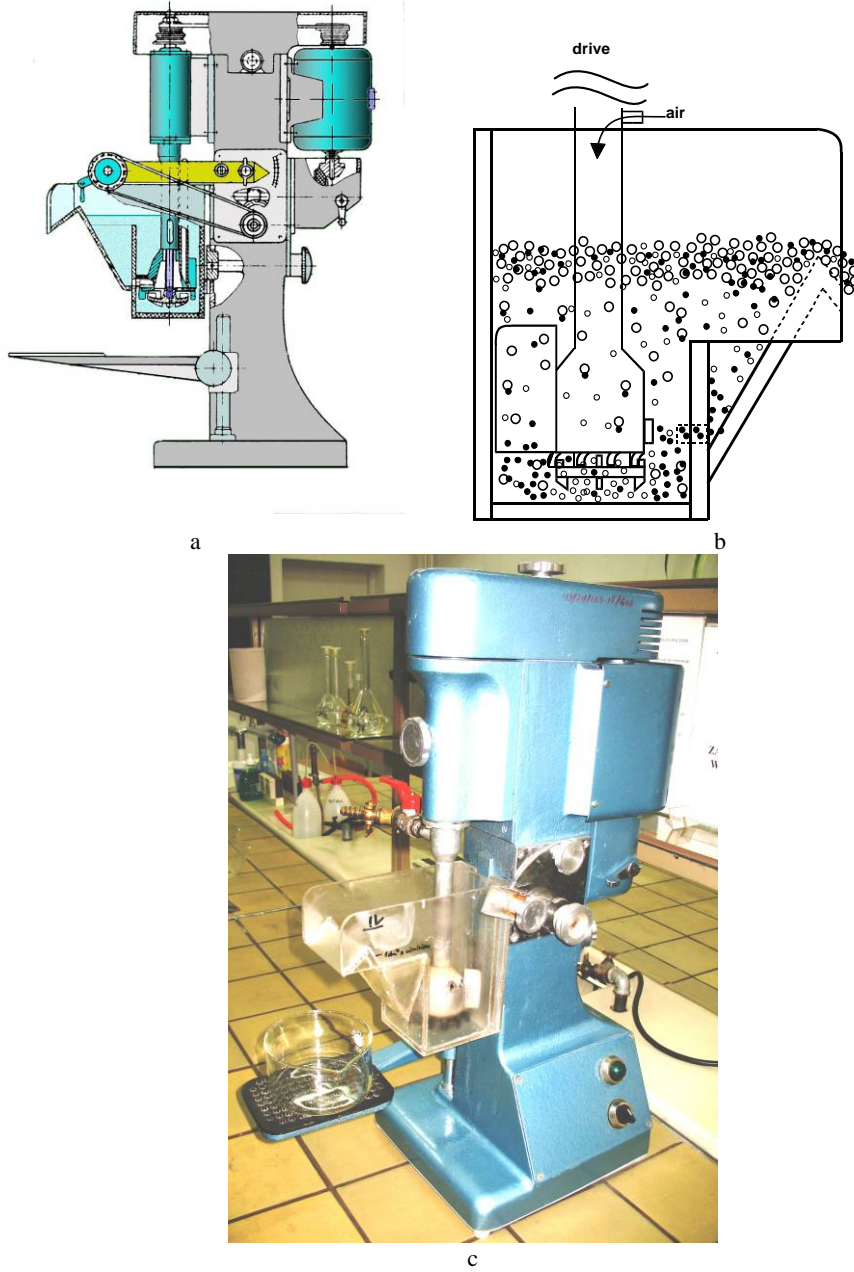
Fig. 12.76. Mechanobr laboratory flotation machine
(with subaeration) (Drzymala, 2001) (a), its flotation cell (b) (after Luszczkiewicz –unpublished, based
on Berger and Efremov, 1962, and its photograph (c)
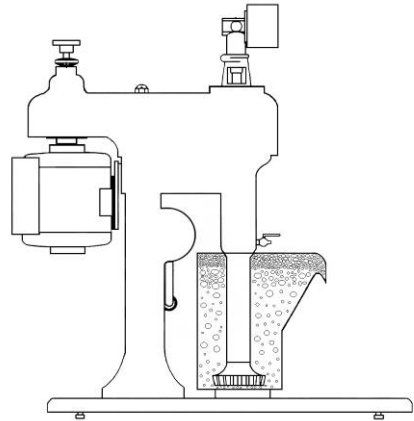
Fig. 12.77. Denver laboratory flotation machine with cell volume 5 dm^3 (Konopacka, 2005 and Bulletin, 1994) (a) and its photograph (b)
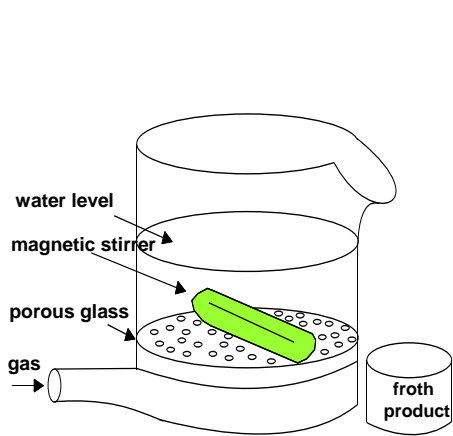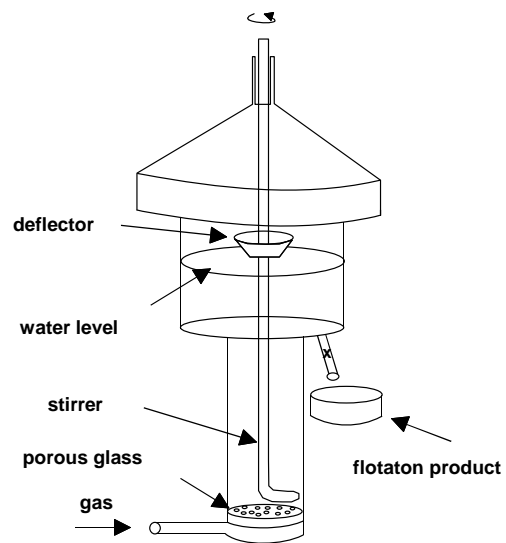
Fig. 12.78. Other laboratory flotation devices. a) Cylindrical cell equipped with magnetic stirrer (Fuerstenau, 1964), b) laboratory flotation device of Partridge and Smith, 1971
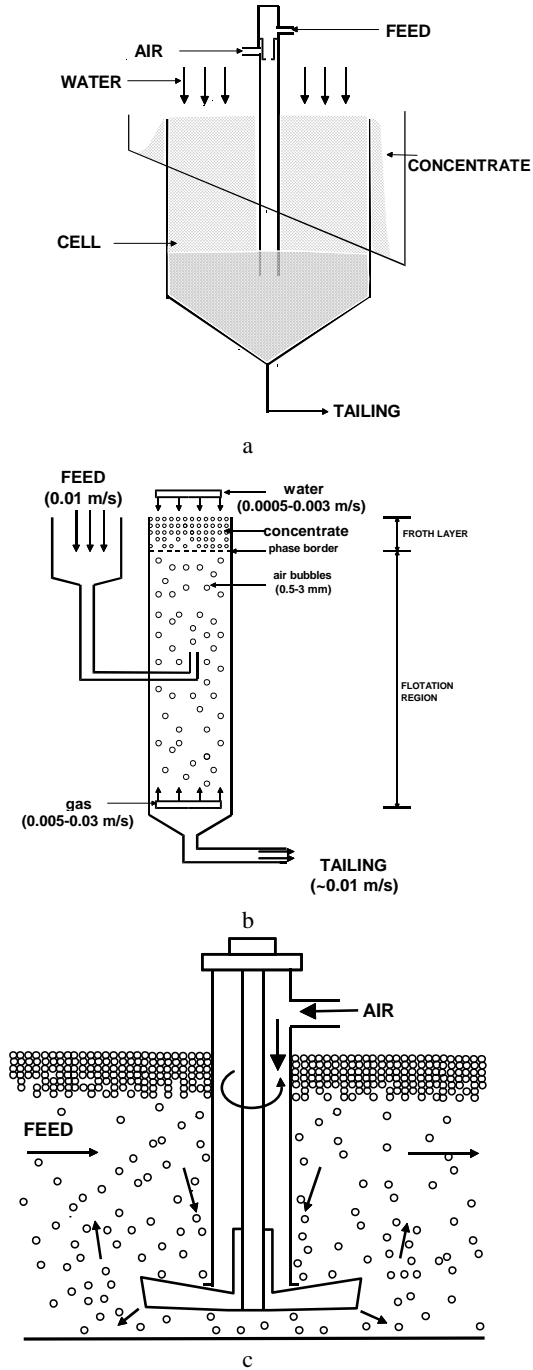
Fig. 12.79. Industrial flotation machines: a – Jameson cell (Evans et al., 1995), b – column cell (Finch et al., 1995), c – tank cell (Denver DR) (Laskowski and Luszczkiewicz, 1989)

Mechanical flotation of hydrophilic particles can be also observed in laboratory and industrial flotation machines. The entrainment is frequently proportional to the amount of water collected along with the concentrate (Ross, 1991). The size of the entrained particles in the Mechanobr laboratory flotation machine is governed by the equation (Hrycyna, 1999):

$$L = d_{50} \, (\rho_p - \rho_w)^{1.65} = 0.1, \qquad (12.105)$$

where:

d – diameter particle at 50% recovery (d_{50}), mm

$\rho = \rho_p - \rho_w$ – density of particle in water, g/cm^3.

Equation (12.105) is valid for the flotation cell 200 cm^3 in volume and using α-terpineol as a frother at concentration of 12.5 mg/cm^3. Equation (12.105) can be used to describe entrainment when only hydrophilic particles are tested. The delineation of entrainment of hydrophilic particles in the presence of floating hydrophobic grains has not been systematically investigated.

Different flotation machines are used by industry. They can be divided into mechanical, pneumatic, mechanical-pneumatic, vacuum, column, and others. Their names include PA, Wemco, Fagergreen, Mechanobr (Sablik, 1998). Mechanical flotation machines are equipped with an impeller which disperses air and stirs particles and bubbles. The pneumatic flotation machines do not have impellers. The air is supplied from an outer source. During depressurizing the air is dispersed and stirs the suspension. Pneumatic Jameson flotation machine is shown in Fig. 12.79a (Evans et al., 1995). The pneumatic-mechanical flotation machines represent a variation of the mechanical ones in which pressurized air is supplied (IZ flotation machine, Szczerba et al., 1999, Denver (Fig. 12.79c), and Agitar). In vacuum flotation machines air bubbles are formed directly on the particle surfaces due to decreased pressure in flotation system.

In Poland flotation machines are used in coal and copper industries (e.g. IMN, IZ, OK, HG, DR types and others).

The capacity of flotation machines can be as high as 100 m^3 and more.

Flotation of some ores and raw materials is conducted in flotation columns. A scheme of flotation column is presented in Fig. 12.79b. Theoretically, they are superior to other flotation machines as the main flotation stage and several cleaning flotation steps take place in the same column in one flotation.

Literature

Abeidu A.M., 1973. Selective depression of calcite from fluorite, Trans. IMM, Section C., 82, C49-C50.

Abramov A.A., Leonov S.B., Sorokin M.M., 1982. Chemistry of flotation systems, Nedra, Moskva, in Russian.

Adamson A.W., 1967. Physical chemistry of surfaces, 3rd edition, Wiley, New York.

Alonso E.A., Laskowski J.S., 1999. Selection of polymers used as slime modifiers in potash ore, in: Polymers in mineral processing, J. Laskowski (ed.), Proc. 3rd UBC-McGill Bi-annual Inter. Symp. on Fundamentals of mineral processing, Met. Soc. CIM Montreal, 405–419.

Aplan F.F., Chander Ch., 1988. Collectors for sulfide mineral flotation, in: Reagents in mineral technology, Surfactant science series, Vol. 27., P. Somasundaran, B.M. Moudgil (eds.), 335–369, Dekker, New York.

Aplan F.F., Simkovich E.Y., Spearin E.Y., Thompson K.C., 1980. In: The physical chemistry of mineral – reagent interactions in sulfide flotation, P.E. Richardosn et al. inni (eds.), US Bureau of Mines, IC 8818, s. 215.

Arbiter N., Cooper H., Fuerstenau M.C., Harris C.C., Kuhn M.C., Miller J.D. and Yap R.F., 1985. Flotation, in: N.L. Weiss (ed.), SME Mineral Process. Handbook Vol. 1, SME, N.Y., 39–109.

Arbiter N., Harris C.C., 1962. Flotation kinetics, in: Froth flotation – 50th anniversary volume, D.W. Fuerstenau (ed.), AIMM/SME, New York, 215–246.

Aston J.R., Drummond C.J. Scales F.J., Healy T.W., 1983. Frother chemistry in fine coal processing, Proc.2nd Australian Coal Prep. Congress, R.I. Whitmore (ed.), Westminster Press, Brisbane, 148–160.

Aveyard R. and Clint J.H., 1995. Liquid droplets and solid particles at surfactant solution interface, J. Chem. Soc., Faraday Trans., 91 (17), 2681–2697.

Aveyard R., Binks B.P., Fletcher P.D.I. and Rutherford C.E., 1994. Measurements of contact angles of spherical monodisperse particles with surfactant solutions, Colloids and Surfaces, 83: 89–98.

Bara D., Kisielewski W., 1984. Analiza zwiększania uzysku przy produkcji siarki metodą flotacyjno-rafineryjną, w: materiały seminarium „Procesy technologiczne surowców mineralnych z uwzględnieniem międzyfazowych zjawisk powierzchniowych”, Baranów Sandomierski, 1–14.

Bartell F.E., Whitney C.E., 1933. Adhesion tension, J. Phys. Chem., 36: 3115–3119.

Barycka I., Skudlarski K., 1993. Podstawy chemii, Wydawnictwo Politechniki Wrocławskiej, Wrocław.

Berger G.S., Efimov I.A., 1962. Methods of separation of mono-mineral fractions, 2nd edition, Gosgeoltechnizdat, Moscow, in Russian.

Bigosiński J., 1998. Wpływ zawartości rozdzielanych składników na wzbogacanie metodą flotacji, Ph.D. thesis, Instytute of Mioning Eng. Wroclaw, Poland

Bilans 1997. Siarka, w: Bilans gospodarki surowcami mineralnymi w Polsce na tle gospodarki światowej – 1995, PAN, Krakow, Poland

Billett D.F, Hough D.B., Ottewill R.H., 1976. Studies on the contact angle of the charged silver iodide-solution-vapour interface, J. Electroanalytical Chem., 74, 107–120.

Bolewski A., Manecki A., 1993. Mineralogia szczególowa, Wyd. PAE, Warszawa.

Brown D.J., 1962. Coal flotation, in: Froths flotation, 50th Anniversary Volume, D.W. Fuers- tenau (ed.), AIME, New York, 518–538.

Bulletin No. L-FLO-1. 1994. Joy Process Equipment Limited (Denver Equipment). England

Chander S., 1988. Inorganic depressants for sulfide minerals, in: Reagents in Mineral Technology, P. Somasundaran i B.M. Moudgil (eds.), Surfactants Science Series, Vol. 27, Chap. 14, 429–469, Dekker, New York.

Chander S., Wie J.M., Fuerstenau D.W., 1975. On the native floatability and surface properties of naturally hydrophobic solids, in: Advances in interfacial phenomena of particulate/solution/gas systems: applications to flotation research, P. Somasundaran and R.B. Grieves (eds.), AICHE Syp. Series, No. 150, Vol. 71, AICHE, New York, 183–191.

Chibowski E., Hołysz L., Zdziennicka F., Gonzalez-Caballero F., 1996. Is the contact angle hysteresis due to film present behind the drop?, in: Surfactants in solutions, A.K. Chattopadhyay and K.L. Mittal (eds.), Dekker, New York, 64, 31–53.

Chmielewski T., 1990. Some aspects of pyrite hydrophobicity – investigation on cleaved electrodes, Journal of Mining and Metallurgy (Glastnik Rudarstwa i Metaurgije), 26(2), 133–144.

Choi H.S., Oh J., 1965. Silicates flotation, J. Inst. Min. Metall, Japan, 81, 614–620.

Clint J.H. and Tylor S.E., 1992. Particle size and interparticle forces of overbased detergents– a Langmuir trough study, Colloids Surfaces, 65(1): 61–67.

Cornell R.M., Schindler P.W., 1980. Infrared study of the adsorption of hydroxy carboxylic acids on α-FeOOH and amorphous iron(III) hydroxide, Colloid and Polymer Sci., 258, 1171–1175.

CRC, 1986/87. Handbook of chemistry and physics, 67th ed. (R.C. Weast (ed.), CRC Press, Boca Raton, Florida, USA.

Crowl V.T. and Wooldridge W.D.S., 1967. A method for the measurement of adhesion tension of liquids in contact with powders, SCI Monograph, 25: 200–212.

Czaplinski A., 1994. Charakterystyka węgli kamiennych i ich właściwości technologiczne, in: Węgiel kamienny, A. Czapliński (red.), Wyd. AGH., Kraków.

Daellenbach C.B., Tiemann T.D., 1964. Chelation of quartz activation ions in oleic acid flotation, Trans. AIME 229, 59–64.

Davies J.T., Rideal E.K, 1963. Interfacial Phenomena, Academic Press, New York.

de Bruyn P.L., Agar G.E., 1962. Surface chemistry of flotation, in: Froth flotation – 50th anniversary volume, D.W. Fuerstenau (ed.), AIMM/SME, New York, 91–138.

Deren J., Haber J., Pampuch R., 1977. Chemia ciała stałego, PWN, Warszawa.

Derjaguin B.V., 1989. Theory of stability of colloids and thin films, Consultants Bureau, New York.

Dixit S.G., Biswas A.K., 1973. Studies on zircon-sodium oleate flotation system: 1-solid-liquid interfacial parameters, Trans. IMM, Sec. C., 82, C200-206.

Dobias B., (ed.), 1993. Coagulation and flocculation, Surfactant Science Ser., 47, Marcel Dekker, N.Y., Chap. 7, 321–353.

Dobias B., 1983. New modified Hallimond tube for study of flotation of minerals from kinetic data, Trans. IMM., Sec.C, 92, C164–166.

Dobias B., 1995. Salt-type minerals, w: Flotation Science and Technology, K.A. Matis (ed.), Dekker, New York, 179–259.

Doren A., Vargas D., Goldfarb J., 1975. Non-ionic surfactants as flotation collectors, Trans. IMM, Sec. C., C34-C37.

Dowling E.C., Klimpel R.R., Aplan F.F., 1985. Model discrimination in the flotation of porphyry copper ore, Minerals and Metallurgical Processing, 2, 87–97.

Drzymala J., 1979. Adsorption isotherm of potential determining ions at oxide/aqueous solution interface, Polish Journal of Chemistry, 53, 1809–1820.

Drzymala J., 1986. O hydrofobizacji powierzchni ciał stałych w wodnych roztworach oleinianowych, Fizykochemiczne Problemy Mineralurgii, 18, 63–84.

Drzymala J., 1989. Chemistry of oleic acid-H2O-NaCl system at 25°, in: Surfactants in Solutions, Vol. 7., K.L. Mittal (ed.), Plenum Press, New York.

Drzymala J., 1990. Własciwosci wodnych roztworów i emulsji oleinianowych, Prace Naukowe Instytutu Chemii Nieorganicznej i Metalurgii Pierwiastków Rzadkich Politechniki Wrocławskiej 61, Monografie 29, Wydawnictwo Politechniki Wrocławskiej, Wroclaw.

Drzymala J., 1994a. Characterization of materials by Hallimond tube flotation. Part 1. Maximum size of entrained particles, Int. J. Miner. Process., 42: 139–152.

Drzymala J., 1994b. Characterization of materials by Hallimond tube flotation, Part 2. Maximum size of floating particles and contact angle, Int. J. Miner. Process., 42, 153–167 oraz errata, Int. J. Miner. Process. 43 (1995), 135.

Drzymala J., 1994c. Hydrophobicity and collectorless flotation of inorganic materials, Advances in Colloid and Interface Sci., 50, 143–185.

Drzymala J., 1995. Określanie możliwości zmniejszenia zawartości ołowiu w koncentratach miedziowych metodami flotacyjnymi przy wykorzystaniu najnowszych osiągnięć z fizykochemii powierzchni, Raport Instytutu Górnictwa Politechniki Wrocławskiej I, 1995.

Drzymala J., 1999a. Characterization of materials by Hallimond tube flotation. Part 3. Maximum size of floating and interacting particles, Int. J. Miner. Process, 55: 203–218.

Drzymala J., 1999b. Entrainment of particles with density between 1.01 and 1.10 g/cm^3 in a monobubble Hallimond flotation tube, Mienerals Eng. 12(3), 329–331.

Drzymala J., 1999c. Flotometric hydrophilicity of coal particles, in: Mining Science and Technology '99, H. Xie i T Golosinski (eds.), Balkema, Rotterdam, 533–537.

Drzymala J., 2001. Hydrofobowość naturalna soli nieorganicznych (in preparation).

Drzymala J., 2001. Ice/aqueous interface, in: Encyclopedia of surface & colloid science, A. Hubbard (ed.), Dekker, New York.

Drzymala J, 2001. Podstawy mineralurgii, Oficyna Wydawnicza PWr.

Drzymala J., Bigosinski J., 1995. Collectorless flotation of sulfides occurring in the fore-Sudetic copper minerals deposit of SW Poland, Mineralogia Polonica, 26, 63–73.

Drzymala J., Chmielewski T., 1992. Flotometry of very hydrophobic materials in the multibubble Hallimond tube, Prace Naukowe Instytutu Górnictwa Politechniki Wroclawskiej, nr 65, Studia i Materialy nr 23, 1992.

Drzymala J., Laskowski J., 1981. Zastosowanie odczynników chelatujących we flotacji, Fizykochemiczne Problemy Mineralurgii, 13, 39–64.

Drzymala J., Lekki J., 1989a. Mechanical, contactless, and collector flotation in the Hallimond tube, J. Colloid Interface Sci., 130: 197–204.

Drzymala J., Lekki J., 1989b. Flotometry – another way of characterizing flotation, J. Colloid Interface Sci., 130, (1), 205–210.

Drzymala J., Lekki J., Kiełkowska M.M., 1987. A study of the germanium-sodium oleate flotation system, Powder Technology, 52, 251–256.

Drzymala J., Lekki J., Laskowski J., 1979. Surface dissociation constants for solid oxide/aqueous solution systems, Colloid and Polymer Sci., 257, 768–772.

Drzymala J., Sadowski Z., Hołysz L., Chibowski E., 1999. Ice/aqueous interface: zeta potential, point of zero charge and hydrophobicity, J. Colloid Interface Sci., 220, 229–234.

Dupre A., Theorie Mecanique de la Chaleur Gauthier-Villars, Paris, 1869, pp. 369ff

Dutkiewicz E.T., 1998. Fizykochemia powierzchni, WNT, Warszawa.

Eigeles M.A., 1964. Principles of non-sulfide minerals flotation, Nedra, Moskva, in Russian.

Ek C., 1992. Flotation kinetics. Innovation in flotation technology, Vol. 208, Kluwer Academic Publishers, London.

Evans G.M., Atkinson B.W., Jameson G.J., 1995. The Jameson cell, in: Flotation Science and Egineering, K.A. Matis (ed.), Dekker, New York, 1995, Chap. 12, 331–362.

Finch J.A., Urbe-Salas A., Xu M., 1995. Column flotation, in: Flotation Science and Engineering, Dekker, K.A. Matis (ed.), New York.

Finkelstein N.P., 1989. Review of interactions in flotation of sparingly soluble calcium minerals with anionic collectors, Transaction IMM, Sec. C, 98, C157–177.

Fleming M.G., 1952. Effects of alkalinity in the flotation of lead minerals, Trans. AIME., 193, 1231–1236.

Fowkes F.M., Riddle F.L., Pastore W.E., Weber A., 1990. Interfacial interactions between self-associated polar liquids and squalane used to test equations for solid-liquid interfacial interactions, Colloids and Surfaces, 43, 367–387.

Fowkes M. F., Attractive forces at interfaces, Ind. and Eng. Chem, 56(12), 40–52.

Freund J., Dobias B., 1995. The role of surface tension, in: Flotation science and technology, K.A. Matis (ed.), Dekker, New York.

Fuerstenau D.W., Healy T.W., Somasundaran P., 1964. The role of the hydrocarbon chain of alkyl collectors in flotation, Trans. AIME, 229, 321–323.

Fuerstenau D.W., Metzeger P.H., Seele G.D., 1957. How to use this modified Hallimond tube for better flotation testing, Eng. Mining Journal, 158 (3), 93–95.

Fuerstenau D.W., Pradip, 1984. Mineral flotation with hydroxamate collectors, in: Reagents in the mineral industry, M.J. Jones and R. Oblatt (eds.), IMM, 161–168.

Fuerstenau D.W., Urbina H., 1988. Flotation fundamentals, in: Reagents in mineral technology, Surfactant Science Series, Vol.. 27, P. Somasundaran and B.M. Moudgil (eds.), Dekker, New York, 1–38.

Fuerstenau D.W., Wiliams M.C., Narayanan K.S., Diao J.L., Urbina R.H., 1988. Assessing the wettability and degree of oxidation of coal by film flotation, Energy and Fuels, Vol. 2(3).

Fuerstenau M.C. 1964. An improved micro-flotation technique. Eng. Min. J., 165(11): 108-109.

Fuerstenau M.C., 1995. Oxide and silicate flotation, in: Flotation science and engineering, K.A. Matis (ed.), Dekker, New York, 89–126.

Fuerstenau M.C., Han K.N., 1988. Activators, in: Frothers, in: Reagents in Mineral Technology, P. Somasundaran (ed.), Surfactants Science series, Vol. 27, Dekker, New York, Chp.13, 411–428.

Fuerstenau M.C., Kuhn M.C., Elgilliani D.A., 1968. The role of dixanthogen in xanthate flotation of pyrite, Trans. AIME, 241, 148–156.

Fuerstenau M.C., Palmer B.R., 1976. Anionic flotation of oxides and silicates, in: Flotation – AM Gaudin memorial volume, Vol. 1, Chap. 7, M.C. Fuerstenau (ed.), AIME, New York, 148.

Garrels R.M, Christ Ch.L., 1965. Solutions, Minerals and Equilibria, Harper and Row, New York.

Gaudin A.M., 1963. Flotacja, Slask, Katowice.

Gaudin A.M., Miaw H.L., Spedden H.R., 1957. Native floatability and crystal structure, in: Electrical phenomena and solid/liquid interface, Proc. 2nd Int. Congr. Surface Activity, London. Butterworths, London, 202–219.

Good R., Keller D.V., 1989. Fundamental research on surface science of coal in support of physical beneficiation of coal, Quarterly Report No. 7, State University of New York at Buffalo, 25.

Gutierrez-Rodriguez J.A., Purcell R.J., & Aplan F.F., 1984. Estimating the hydrophobicity of coal, Colloids and Surfaces 12, 1–25.

Guy P.J., Trahar W.J., 1985. The effects of oxidation and mineral interactions on sulfide flotation, in: Flotation of sulfide minerals, K.S.E. Forssberg (ed.), Elsevier, Amsterdam, 61–79.

Hallimond A.F., 1944. Laboratory apparatus for flotation tests, Mining Magazine, 70, 87–91.

Hancer M., Hu Y., Fuerstenau M.C., Miller J.D., 1997. Amine flotation of soluble sulfate salts, Proc. XX Inter. Mineral Processing Congress, Vol. 3, 715–721, GMDB, Clausthal-Zeller- feld, Germany.

Hanning R.N., Rutter P.R., 1989. A simple method of determining contact angles on particles and their relevance to flotation, Int. J. Miner. Process., 27: 133–146.

He Y.B., Laskowski J.S., 1992. Contact angle measurements on discs compressed from fine coal, Coal Preparation, 10: 19–36.

Heertjes P.M., Kossen N.W.F., 1967. Measuring the contact angles of powder-liquid systems, Powder Technology, 1(1), 33–42.

Hiemenz P.C., 1986. Principles of Colloid and Surface Chemistry, Dekker, New York.

Hornsby D.T., Leja J., 1980. Critical surface tension and the selective separation of inherently hydrophobic solids, Colloids and Surfaces, 1, 425–429.

Hornsby D.T., Leja J., 1983. Critical surface tension of floatability, Colloids and Surfaces, 7(4), 339–348.

Hrycyna E., 1999. Wyniesienie mechaniczne w laboratoryjnej maszynce flotacyjnej typu Mechanobr, M.Sc. thesis, Wydział Górniczy Politechniki Wrocławskiej, Wrocław, Poland.

Huethorst J.A.M. and Leenaars A.F.M., 1990. A new method for determining the contact angle of liquid against solid spherical particles, Colloids and Surfaces, 50: 101–111.

Hunter R.J., 1987. Foundation of colloid science, Vol. 1, Clarendon Press, Oxford.

Iwasaki I., Cooke S.R.B., Colombo A.F., 1960. Report of investigation no. 5593, U.S. Bureau of Mines, USA.

Jakuszewski B., 1962. Współczesne zagadnienia elektrochemii teoretycznej, PWN, Warszawa.

Janczuk B., Chibowski E., Bialotiotrowicz T., 1986. Time dependence wettability of quartz with aqueous, Chem. Papers, 40(3), 349–356.

Janusz W., 1999. Electrical Double layer at the metal oxide-electrolyte interface, in: Interfacial Forces and Fiels: Theory and Applications, J.P. Hsu (ed.), Surfactants Science Series, 85, Dekker, New York, Chap. 4, 135–206.

Jaycock M.J., Parfitt G.D., 1981. Chemistry of interfaces, Ellis Horwood (Wiley), New York.

Johson R.E. Jr., Dettre R.H., 1989. An evaluation of Neumann's „Surface equation of state", Langmuir, 5, 293–295.

Kelebek S., 1987. Wetting behavior, polar characteristics and flotation of inherently hydrophobic minerals, Trans. IMM, Sec. C., 96, C103–C106.

Kitchener J.A., 1992. Minerals and surfaces, in: Colloid chemistry in mineral processing, J.S. Laskowski i J. Ralston (eds.), D.W. Fuerstenau (ed.) Development in Mineral Processing, Vol. 12, 1–35.

Klassen V.I., Mokrousov V.A., 1963. An introduction to the theory of flotation, translation by J. Leja and G.W. Poling, Butterworths, London.

Klimpel R.R., Hansen R.D., 1988. Frothers, in: Reagents in Mineral Technology, Somasundaran and B.M. Moudgil (eds.), Surfactants Science Series, Vol. 27, Dekker, New York, 385–409.

Konopacka 2005, Flotacja solna, Oficyna Wydawnicza PWr.

Koopal L.K., 1992. Adsorption, in: Colloid chemistry in mineral processing, J. Laskowski, J. Ralston (eds.), Elsevier, 37–96.

Kosmulski M., 2001. Chemical properties of material surfaces, Surfactant Science Series, v.102, Dekker, New York

Kwok D.Y., 1999. The usefulness of the Lifshitz–van der Waals/acid–base approach for surface tension components and interfacial tensions, Colloid and Surfaces. A: Physicochemical and Engineering Aspects, 156, 191–200.

Laskowski J., 1966. Flotacja minerałów o naturalnej hydrofobowości w roztworach z podwyższonym stężeniem soli nieorganicznych, Zeszyty Naukowe Politechniki Śląskiej, Górnictwo, Gliwice 1966, no.16.

Laskowski J., 1969. Chemia fizyczna w procesach mechanicznej przeróbki kopalin, Śląsk, Katowice.

Laskowski J., 1981. Redox conditions in flotation: oxides, in: Interfacial phenomena in mineral processing, B. Yarar i D.J. Spottiswood (eds.), Proc. Eng. Found. Conf., Rindge, New Hampshire.

Laskowski J., 1983. Dextrin adsorption by oxidized coal, Colloids and Surfaces, 8, 137–151.

Laskowski J., 1986. The relationship between floatability and hydrophobicity, in: Advances in mineral processing, P. Somasundaran (ed.), SME Littleton, Colorado, USA, 189–208.

Laskowski J., 1994. Flotation of potash ores, in: Reagents for better metallurgy, P.S. Mulukutla (ed.) SME., Littleton, 225–243.

Laskowski J., 1998. Frothers and frothing, in: Frothing in Flotation II, J.S. Laskowski, E.T. Woodburn (eds.), Gordon and Breach, Australia, 1–49.

Laskowski J., 2004, Testing flotation frothers, Physicochemical Problems of Mineral Processing, 38, 13-22

Laskowski J., Fuerstenau D.W., Gonzales G., Urbina R.H., 1985. Studies on the flotation of chrysocolla, Mineral processing and technology review, 1985, Vol. 2, 135–155.

Laskowski J., Iskra J., 1970. Role of capillary effect in bubble particle collision in flotation Trans. IMM, Sec. C., Vol. 79. C6–C10.

Laskowski J., Luszczkiewicz A., 1989, Przeróbka kopalin. Wzbogacanie surowców mineralnych, Wydawnictwo Politechniki Wrocławskiej, Wrocław.

Laskowski J., Miller J.D., 1984. New reagent in coal flotation, in: M.J. Jone and R. Oblatt (eds.), Reagent in the minerals industry, IMM, London, 145–154.

Laskowski J.,1988. Weak electrolyte type collectors, in: Mineral processing and process control, COBRE 87 – International Conference, Vina del Mar, A.L. Mular, G. Gonzalez, C. Barahona (eds.), University of Chile, Vol. 2, 137.

Laskowski J.S., Vuredela R.M., Liu Q., 1988. The colloid chemistry of weak-electrolyte collector flotation, Proc. XVI Inter. Min. Proc. Congr., E. Forsberg (ed.), Elsevier, Amsterdam, 703–715.

Laskowski J.S., Woodburn E.T. (eds.), 1998. Frothing in flotation II, Gordon and Breach, Australia.

Laskowski J.S., Yordan J.L., Yoon R.H., 1989. Electrokinetic potential of microbubbles generated in aqueous solutions of weak electrolyte type surfactants, Langmuir, 5, 373–376.

Lee L.-H., 1996. Correlation between Lewis acid – base surface interaction components and linear solvation energy relationship solvatochromic α and β parameters, Langmuir, 12, 1681–1687.

Leja J., 1982. Surface chemistry of froth flotation, Plenum Press, New York.

Lekki J., 1970, unpublished

Lekki J., 1979. Fizykochemiczne podstawy flotowalności minerałów siarczkowych, Prace Naukowe Instytutu Chemii Nieorganicznej 41, Seria Monografie 16, Wydawnictwo Politechniki Wrocławskiej, 1–112.

Lekki J., 1984. Korelacja oleinianowej flotacji minerałów Fe(II), Al(III) oraz Mg(II) z fazami układu tlenek–oleinian–woda, materiały seminarium, Baranów Sandomierski, 243–259.

Lekki J., Drzymala J., 1990. Flotometric analysis of the collectorless flotation of sulfide materials, Colloids and Surfaces, 44, 179–190.

Letowski F., 1975. Podstawy hydrometalurgii, PWN, Warszawa.

Li C., Somasundaran P., 1993. Role of electrical double layer forces and hydrophobicity in coal flotation in NaCl solutions, Energy and Fuels, 7, 244–248.

Li C., Somasundaran P., Harris C.C., 1993. A levitation technique for determining particle hydrophobicity, Colloids and Surfaces Colloids and Surfaces, A 70: 229–232.

Lukaszewska I., 1998. Flotacja w celce Hallimonda, M.Sc. thesis, Wydział Górniczy Politechniki Wrocławskiej, Wroclaw, Poland

Luszczkiewicz A., Lekki J., Laskowski J., 1979. Floatability of ilmenite, Proc. XIIIth Inter. Min. Proc. Congr., Warszawa, Round Table Seminar, 2, 163–182.

Luszczkiewicz, 2004, unpublished.

Lyklema J., 1972. The Esin and Markov coefficient for double layer with colloid chemical importance, Electroanal. Chem. Interfacial Electrochem., 37, 53–60.

Lyklema J., 1999. The surface tension of pure liquids. Thermodynamic components and corresponding states, Colloid and Surfaces. A: Physicochemical and Engineering Aspects, 156, 413–421.

Lynch A.J., Johnson N.W., Manlapig E.V., Thorne C.G., 1981. Mineral and coal flotation circuits, Chap. 3: Mathematical models of flotation, in: D.W. Fuerstenau (ed.), Development in Mineral Processing, No. 3, Elsevier, Amsterdam.

Manser R.M., 1975. Handbook of silicate flotation, Warren Spring Laboratory, England.

Mao L., Yoon R.H., 1997. Predicting flotation rates using equation derived from first principles, International Journal of Mineral Processing, 51, 171 – 181.

Marinakis K.I., Shergold H.L., 1985. The mechanism of fatty acid adsorption in the presence of fluorite, calcite and barite, Int. J. Mineral Process., 14, 161–176.

Michot L.J., Villieras F., Francois M., Yvon J., Le Dred R., Cases J.M., 1994. The structural microscopic hydrophilicity of talc, Langmuir, 10, 3765–3773.

Miller J.D., Lin C.L., Chang S.S., 1984. Coadsorption phenomena in the flotation of pyrite from coal by reverse flotation, Coal Preparation, 1, 21–32.

Miller J.D., Yalamanchili M.R., Kellar J.J., 1992. Surface charge of alkali halide particles as determined by laser-Doppler electrophoresis, Langmuir, 8, 1464–1469.

Mishra S.K., 1988. Anionic collectors in nonsulfide mineral flotation, in: Reagents in Mineral Technology, Surfactant Science Series 27, P. Somasundaran i B.M. Moudgil (eds.), Dekker, New York, 195–217.

Nagaraj D.R., 1988. The chemistry and application of chelating or complexing agents in mineral separations, in: Reagents in Mineral Technology, Surfactant science series Vol. 27, P. Somasundaran i B.M. Moudgil (eds.), Dekker, New York, 257–334.

Nagy E., Van Cleave A.B., 1962. A study of the characteristics of galena, Can. J. Chem. Eng., 40(2), 776–781.

Nakamura Y., Kamada K., Katoh Y., Watanabe A., 1973. Studies on secondary electrocapillary effects. I – The confirmation of Young-Dupre equation, J. Colloid Interface Sci., 44, 517–524.

Naumov G.B., Ryżenko B.N., Chodakowski J.L., 1971. Handbook, Atomizdat, Moscow, in Russian.

Neumann A.W., 1974. Contact angles and their temperature dependence. Thermodynamic status, measurements, interpretation, and application, Advances in Colloid and Interface Sci., 4(2–3), 105–191.

Neumann A.W., Good R.J., 1979. Techniques of measuring contact angles, in: Surface and Colloid Science, Vol. 11, R.J. Good i R.R. Stomberg (eds.), Plenum Press, New York, 31–91.

Ney P., 1973. Zeta-Poteniale und Flotierbarkeit von Mineralen, Springer-Verlag, Wien–New York.

Nguyen A.V., Schulze H.J., Ralston J., 1997. Elementary steps in particle-bubble attachment, Inter. J. Mineral. Process., 51, 183–195.

Ozbayoglu G., 1987. Coal flotation, in: Mineral processing design, B. Yarar and Z.M. Gogan (eds.), 77–105, Martinus Nijhoff Publisher, Dordrecht.

Pajdowski L., 1993. Chemia ogólna, PWN, Warszawa.

Parfitt R.L., Russell J.D., 1977. Adsorption on hydrous oxides. V – Mechanisms of adsorption of various ions on goethite, J. Soil Sci., 28(2), 297–305.

Parks, G.A., 1965. Isoelectric points of solid oxides, solid hydroxides, and aqueous complex systems, Chemical Reviews, 65(2), 177–198.

Parsonage P., Watson D., Hickey T.J., 1982. Surface texture, slime coating and flotation of some industrial minerals, XIV IMPC, CIM Toronto, V-5.1–V-5.22.

Partridge A. C., Smith G.W. 1971. Small-sample flotation testing a new cell. Trans. Inst. Min. Metall., Sec. C:80: C199–C203.

Paulson O., Pugh R.J., 1996. Flotation of inherently hydrophobic particle in aqueous solutions of inorganic electrolytes, Langmuir 12, 4808-4813.

Perucca C.F., Cormode D.A., 1999. The use of polymers in potash beneficiation at Agrium Potash, in: Polymers in mineral processing, J. Laskowski (ed.), Proc. 3rd UBC-McGill Bi-annual Inter. Symp. on fundamentals of mineral processing, Met. Soc. CIM Montreal, 393–404.

Pierzak J., Drzymala J., 1998. Alotropowe odmiany węgla pierwiastkowego, Prace Naukowe Instytutu Górnictwa Politechniki Wrocławskiej, nr 85, Studia i Materiały nr 27, 63–68, Wrocław.

Pockels A., 1914, Phys. Z., 15, 39.

Polkin S.I., Najfonow T.V., 1965. Concerning the mechanism of collector and regulator interaction in the flotation of silicate and oxide minerals, VII IMPC, Vol. 1., N. Arbiter (ed.) Gordon and Breach, New York, 307–318.

Pourbaix M., 1963. Atlas d'equilibres electrochimiques a 25 °C, Gauthier-Villars, Paris.

Pradel K., 2000. Wykorzystanie efektów kinetycznych do wzbogacania surowców fluorytowo-barytowych, Ph.D. thesis, Instytut Górnictwa Politechniki Wrocławskiej, Wrocław.

Pugh R.J., 1986. The role of the solution chemistry of dedecyloamine and oleic acid collectors in the flotation of fluorite, Colloids and Surfaces, 18, 19–41.

Pugh R.J., Weissenborn P., Paulson O., 1997. Flotation in inorganic electrolytes, Int. J. Miner. Process., 51, 125–138.

Purcell G., Sun S.C., 1963. Significance of double bonds in fatty acids flotation – an electrocinetic study, Trans. AIME, 226, 6–16.

Rönngren L., Sjöberg S., Sun Z.-X., 1995. Complexation at the sulfide aqueous interface, in: Flotation Science and Engineering, K.A. Matis (ed.), Dekker Mew York.

Rönngren L., Sjöberg S., Sun. Z., Forsling W., 1994. Surface reaction in aqueous metal sulfide systems. 5. Surface complexation of sulfide ions, J. Colloid Interface Sci., 162: 227–235.

Ralston J., 1992. The influence of particle size and contact angle in flotation, in: Colloid Chemistry in Mineral Processing, J.S. Laskowski i J. Ralston (eds.), Development in Mineral Processing, D.W. Fuerstenau (ed.), Vol. 12, Chap. 6, 203–224.

Ralston J., Newcombe G., 1992. Static and dynamic contact angles in flotation, in: Colloid Chemistry in Mineral Processing, J.S. Laskowski i J. Ralston (eds.), Development in Mineral Processing, D.W. Fuerstenau (red. serii), Vol. 12, Chap. 6, 173–202.

Rao K.H., Forssberg E., 1991. Mechanism of oleate interactions on salt-type minerals, Part III. Adsorption, zeta potential, and diffuse reflectance FT-IR studies of schelite in the presence of sodium oleate, Colloids and Surfaces, 54(1–2), 161–187.

Ratajczak T., 2001. Mechanizm flotowalności ziarn mineralnych w roztworach soli nieorganicznych, Politechnika Wrocławska, Wrocław, Ph.D. thesis, Wroclaw, Poland.

Richardson P.E., 1995. Surface chemistry of sulfide flotation, in: Mineral surfaces, D.J. Vaughan and R.A.D. Pattrick (eds.), Mineralogical Society Series, No. 5, Chapman and Hall, 261–302.

Richardson P.E., Walker G.W., 1985. The flotation of chalcocite, bornite, chalcopyrite, and pyrite in an electrochemical flotation cell, XVth Inter. Min. Proc. Congr., Vol. 2, 198–210, Soc. Ind. Min. – Bur. Res. Geol. Min., Cannes.

Rogers J., 1962. Principles of sulfide mineral flotation, in: Froth flotation, 50th anniversary volume, D.W. Fuerstenau (ed.), AIMM, New York, Chap. 6, 139–169.

Ross V.E., 1991. Comparison of methods for evaluation of the flotation and entrainment, Trans. IMM, Section C., 100, C121–126.

Rubinstein J.B., Melik-Gaikazyan V.I., 1998. Frothing in flotation II, Chap. 5: Charakterization of flotation froth, Edited by J.S. Laskowski and E.T. Woodburn, Gordon and Breach Science Publishers, Australia.

Rubinstein J.B., Samygin V.D., 1998. Effect of particle and bubble size on flotation kinetics, in: Frothing in flotation II, J.S. Laskowski i E.T. Woodburn (eds.), Gordon and Breach, Australia, Chap. 2, 51–80.

Söhnel O., Garside J., 1992. Precipitation and industrial applications, Butterworth, Oxford.

Sablik J., 1998. Flotacja węgli kamiennych, GIG, Katowice.

Schmidt E.W., 1983. Hydrazine and its derivatives, Wiley, New York.

Schrader M.E., 1975. Ultrahigh vacuum techniques in the measurements of contact angle, IV. Aqueous on graphite (0001), J. Phys Chem., 79, 2508–2515.

Schulze H.J., 1984. Physico-chemical elementary processes in flotation, Developments in Mineral Processing, 4, D.W. Fuerstenau (ed.), Elsevier, Amsterdam, 1984.

Schulze H.J., 1992. Elements of physically – based modelling of the flotation process, Innovation in Flotation Technology, Vol. 208, Kluwer Academic Publishers, London.

Schulze H.J., 1993. Flotation as a heterocoagulation process: possibilities of calculating the probability of flotation, in: Coagulation and flocculation. Theory and applications, Marcel Dekker Inc., New York.

Sillen L.G., Martell A.E., 1964. Stability constants of metal–ion complexes, Chem. Soc., Burlington House, London.

Siwek B., Zembala M., Pomianowski A., 1981. A method for determining fine particle floatabilty, Int. J. Miner. Proces., 8, 85–88.

Smith R.W., 1988. Cationic and amphoteric collectors, in: Reagents in Mineral Technology, Surfactant science series, Vol. 27, P. Somasundaran (ed.), 219–256.

Smolders C.A., 1961. Contact angles, wetting and dewetting of mercury, praca doktorska, University of Ultrecht, Holandia.

Sobieraj S., 1985. Badanie procesu flotacji krajowych rud barytowych, Zeszyty Naukowe Politechniki Śląskiej, 135, 27–45.

Somasundaran P., Ananthapadmanabhan K.P., 1986. In: Advances in mineral processing. P. Somasundaran (ed.), Society of Mining Eng. of AIME, Colorado, 1986, 8.

Sorokin M.M., 1976. Processing of mineral row materials, Izdat. Nauka, Moskva, in Russian.

Soto H., Laskowski J., 1973. Redox conditions in the flotation of malachite with a sulphidizing agent, Trans. IMM., 82, C153–C158.

Spelt J.K., Li D., 1996. The equation of state approach to interfacial tensions, in: Applied surface thermodynamics, A.W. Neumann i J.K. Spelt (eds.), Surfactant Science Series, 63, Dekker, New York, 239–292.

Stachurski J., Michałek M., 1986. Zjawiska elektrokinetyczne w emulsyjnej flotacji różnych typów węgli, referat VIII seminarium naukowo-przemysłowego pt. „Flotacja węgla", Katowice, GIG, 96–104.

Stumm W., Morgan J.J., 1970. Aquatic chemistry, Wiley, New York.

Sutherland K.L., 1948. Kinetics of the flotation process, J. Phys. Chem. 52, 394–425.

Sutherland K.L., Wark I.W., 1955. Principles of flotation, Australasian Institute of Mining and Metallurgy, Melbourne.

Szczerba E., Komorowski J., Skorupska B., 1999. Nowa konstrukcja maszyn flotacyjnych do flotacji gruboziarnistych zawiesin o dużym zagęszczeniu, V międzynarodowa konferencja „Przeróbka Rud Metali Nieżelaznych" ICNOP 99, Instytut Metali Nieżelaznych, KGHM, CBPM Cuprum, 45–58.

Takamori T., Tsunekawa M., 1982. Separation of calcite from fluorite ore by the adsorption – washing – flotation method, XIV IMPC, CIM Toronto, V-1.1–V-1.12.

Tucker J.P., Deglon D.A., Franzidis J.-P., Harris M.C., O'Connor C.T., 1994. An evaluation of direct method of bubble size distribution measurements in a laboratory batch flotation cell, Minerals Eng., 7, 667.

Usui S., Sasaki H., 1978. Zeta potential measurements of bubbles in aqueous surfactant solutions, J. Colloid Interface Sci., 65, 36–45.

van Oss C.J., Giese R.F., Li Z., Murphy K., Norris J., Chaudhury M.K. and Good R.J., 1992. Determination of contact angle and pore sizes of porous media by column and thin layer wicking, J. Adhesion Sci. Technol., 6, 413–445.

van Oss C.J., Giese R.F., Wenzek R., Norris J., Chuvilin J., 1992. Surface tension parameters of ice obtained from contact angle data from positive and negative particles adhesion to advancing freezing fronts, Adhesion Sci. Technol., 6(4), 503–516.

van Oss C.J., Good R.J., 1996. Hydrogen bonding, interfacial tension and the aqueous solubility of organic compounds, J. Dispersion Sci. Tech., 17(4), 433–449.

van Oss C.J., Good R.J., Chaudhury M.K., 1988. Additive and nonadditive surface tension components and the interpretation of contact angles, Langmuir, 4, 884–891.

Varbanov R., Forssberg E., Hallin M., 1993. On the modelling of the flotation process, International Journal of Mineral Processing, 37, 27–43, Elsevier, Amsterdam.

Volke K., Para G., Pawlikowska-Czubak J., Neubert H., 1984. Flotation and adsorption investigation of the system n-dodecanoic acid/mercury at different pH values, Coll. Polymer Sci., 262, 245–251.

Waksmundzki A., Neczaj-Hruziewicz J., Ptanik M., 1972. Mechanism of carryover of gangue slimes during flotation of sulfur ore, Trans. IMM, Section C., 81, C249–251.

Wark I., Cox A.B., 1934. Principles of flotation, Trans. AIMME, 112, part I: 189–302, part III, 267–302.

Washburn, E., 1921. The dynamics of capillary flow, Phys. Rev., 17, 273–283.

Watson D., Manser R.M., 1968. Some factors affecting the limiting conditions in cationic flotation of silicates, Trans. IMM, 77, C57–60.

Weissenborn P.K., Pugh R.J., 1996. Surface tension of aqueous solution of electrolytes: relationship with ion hydration, oxygen solubility, and bubble coalescence, J. Colloid Interface Sci., 184, 550–563.

Wells A.F., 1993. Strukturalna chemia nieorganiczna, WNT, Warszawa.

Wert C.A., Weller M., 1982. Polymeric character of coal, J. Appl. Phys., 53 (10), 6505–6512.

White L.R., 1982. Capillary rise in powders, J. Colloid Interface Sci., 90: 536–538

Woods L.T., Garrels R.M., 1987. Thermodynamic values at low temperatures for natural inorganic materials, Oxford University Press.

Woods R., 1988, Flotation of sulfide minerals, in: Reagents in Mineral Technology, Surfactant science series Vol. 27, P. Somasundaran, B.M. Moudgil (eds.), 39–78.

Yamamoto T., 1980. Complex Sulfide Ores, M.J. Jones (ed.), IMM London, 71.

Yap S.N.Y., Mishra R.K., Raghavan S., Fuerstenau D.W., 1981. The adsorption of oleate from aqueous solution onto hematite, in: Adsorption from aqueous solutions, P.H. Tewari (ed.), Plenum Press, New York, 119–142.

Yarar B., Alvarez J., 1988. Separation of sulfur minerals by the „Gamma flotation" process, XVI Int. Min. Proc. Congr., E. Forssberg (ed.), 547–562, Elsevier, Amsterdam.

Yarar B., Kaoma J., 1984. Estimation of the critical surface tension of wetting of hydrophobic solids by flotation, Colloids and Surfaces, 11, 429–436.

Yarar B., Leja J., 1982. Flotation of weathered coal fines from Western Canada, IX. Int. Coal Prep. Congress, New Delhi, paper C-5.

Ye Y., Khandrika S.M., Miller J.D., 1989. Induction time measurements at a particle bed, Int. J. Miner. Proc. 25, 221–240.

Ye Y., Miller J.D., 1988. Bubble/particle contact time in the analysis of coal flotation, Coal Preparation, 5, 147–166.

Yoon R.H., 1982. Flotation of coal using microbubbles and inorganic salts, Mining Congress J., 68, 76–80.

Yoon R.H., Yordan J.L., 1986. Zeta potential measurements on microbubbles generated using various surfactants, 1986, J. Colloid Interface Sci., 113, 430–438.

Yordan J.L., Yoon R.H., 1986. Induction time measurements for the quartz–amine flotation systems, Annual SME Meeting New Orleans 1986, preprint 86–105, 1–10.

Young T., 1805, Philos.Trans., R. Soc., London, 95, 65

Zisman W.A., 1964. Relation of the equilibrium contact angle to liquid and solid costitution. Contact angle, wettability and adhesion, ACS Advances in Chem. Series, Washington D.C., 43.

Zyla M., 1994. Chemiczny charakter powierzchni węgla kamiennego, w: Węgiel kamienny, A. Czapliński (red.), Wyd. AGH, Krakow.

13. Coagulation

13.1. The nature of coagulation

Coagulation relies on aggregation of fine particles suspended in water into a larger unit called coagulum which, due to gravity force, settles down. Figure 13.1. presents a simplified picture of coagulation.
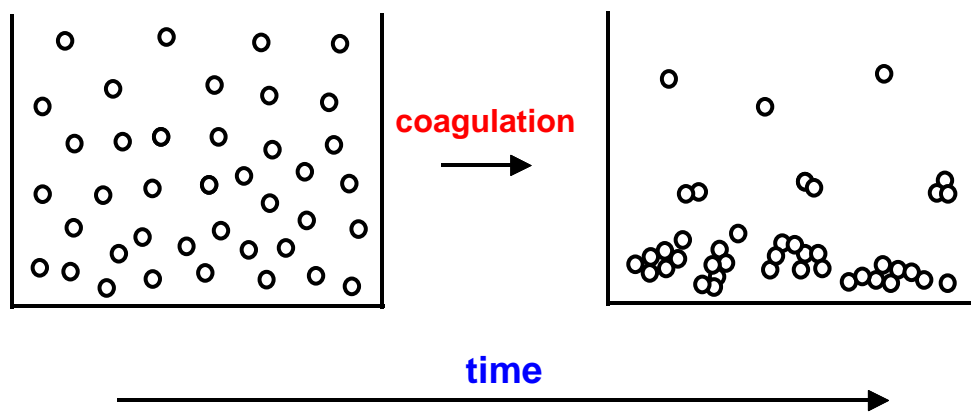
Fig. 13.1. Coagulation

Coagulation of particles is applied in mineral processing, clarification of water, desliming aqueous suspensions for reuse in flotation and upgrading of ores containing very fine particles. When coagulation involves particles of different materials, the process is called heterocoagulation. When coagulation takes place as a result of adhesion to air bubbles and solid particles, it is called flotation, while adhesion of fine to large particles is called slime coating. Coagulation can be carried out selectively and non-selectively. During selective coagulation one kind of particles present in suspension undergoes coagulation, while others do not. Removal of coagulated material, forming a sediment, from uncoagulated particles is accomplished by decantation, drainage, syphonation, etc.

Although coagulation process seems to be simple, its description is complex since coagulation depends on many parameters (Fig. 13.2) which can be divided into those effecting probability of particle collision P_Z, governing particle adhesion P_a, and parameters effecting stability of newly formed coagulates P_{stab} Also time significantly

influences coagulation process. The main parameters governing coagulation, groupped into P_z, P_a, and P_{stab}, are related and form a pyramid-like structure.
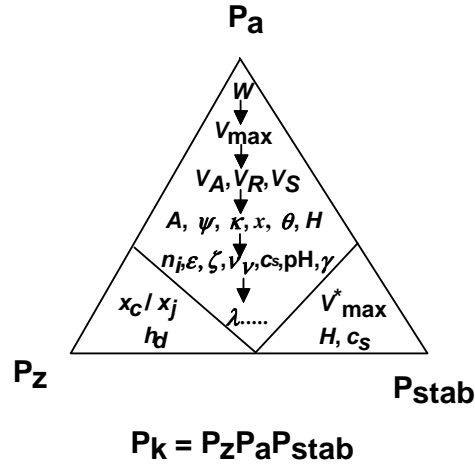
Fig. 13.2. Static delineation of coagulation. Meaning of symbols: P_z – probability of collision of particles, P_a – probability of adhesion of particles, P_{stab} – probability of stability of coagula, W – stability ratio, V_{max} – energy barrier of coagulation, H – distance between particles, V_A – energy of dispersion interactions, V_R – energy of electrostatic interactions, V_s – energy of structural interactions, A – Hamaker constant, ψ – edl potential, $1/\kappa$ – edl thickness, x_c – collision radius, x – particle size, θ – hydrophobicity (contact angle), n – refraction index, ε – dielectric constant, v_v – characteristic frequency, c_s – electrolyte concentration, pH – acidity of the solution, γ – surface energy, T – temperature, g – gravity, n_1 – concentration of particles, V^*_{max} – energy barrier of peptization, ρ – particle density, λ – wavelength of electromagnetic beam, h_d – system hydrodynamics

Figure 13.2 shows that many different parameters contribute to the probability of coagulation P_k, and they can be expressed as a product of probabilities of sub-processes:

$$P_k = P_z P_a P_{stab}. \tag{13.1a}$$

Relationships between particular probabilities and physical parameters of coagulation system are not fully known. Generally, P_z can be expressed as a function of size of coagulating particles (x_i and x_j), as well as of their collision radius x_z and hydrodynamics h_d, P_a as a function of the so-called stability ratio W while P_{stab} as a function energy barrier of decoagulation V_{max}.

$$P_z = f(x_c, x_i, x_j, h_d), \tag{13.1b}$$

$$P_a = f(W) = 1/W, \tag{13.1c}$$

$$P_{stab} = f(V^*_{max}). \tag{13.1d}$$

It means that the main parameter of coagulation process is stability ratio W. As it was shown in Fig. 13.2 the main parameter is dependent on other parameters. The net of related parameters of coagulation may contain as many as 100 parameters (Fig.13.2).

One of the goals of mineral processing is separation of minerals. Particles to be selected have to vary in the value of the main parameter. In the case of coagulation it is stability factor *W*. Stability ratio *W* is a complex parameter, which depends on electrostatic, molecular and structural interaction between particles (see next chapters).

Coagulation is a dynamic process, while P_z, P_a and P_{stab} are static parameters as they are not a function of time. Time, as parameter which determines the results of separation, can be incorporated by appropriate definition of total probability of coagulation P_k, which can be defined as:

$$P_k = \frac{-\dfrac{dn}{dt}}{z_z n_i n_j} , \qquad (13.2)$$

where:
(dn/dt) – coagulation rate,
n_i i n_j – number of particles *i* and *j* in a unit volume,
z_z – number of collisions of particles *i* and *j* in a unit time.
Introducing Eq. (13.2) into Eq. (13.1a) gives

$$-\frac{dn}{dt} = R_{ij} = z_z n_i n_j P_z P_a P_{stab} , \qquad (13.3)$$

that is a general equation of coagulation (Kruyt, 1952; Chander i Hogg, 1987).

13.2. Adhesion of particles

The mechanism of adhesion of particles during coagulation has been explained by the DLVO theory. Acronym DLVO was derived from the names of Russian (Derjagin, and Landau, 1941), and Dutch (Verwey and Overbeek, 1948) researchers who investigated that phenomenon. According to the DLVO theory, coagulation depends on different forces interacting during coagulation. Verwey and Overbeek considered those interactions in terms of energy, while Derjagin and Landau used forces instead. Both approaches are equally useful for the description of coagulation. The energy approach is usually more practical, therefore it will be applied in this work. The use of forces is more suitable for interpretation of coagulation when the measurement and calculations of forces are performed. Special terms disjoining force and disjoining pressure were introduced in 1936 by Derjagin (1989) for forces operating during coagulation. This emphasizes the importance of force approach to coagulation.

The DLVO theory considers aggregation of particles which initially are considerably far away from each other. Coagulation can be schematically expressed by the equation:

$$\qquad\qquad\qquad\qquad\qquad\qquad\qquad\qquad\qquad\qquad\qquad 13.4$$
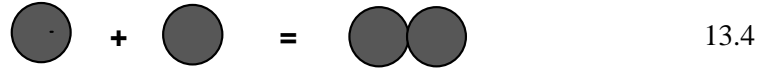
Free enthalpy for two particles which are considerably distant from each other ($H=\infty$), can be expressed as G_∞. After coagulation, when particles stay close to one another at a minimum distance equal the size of atoms in their crystalline lattice, their free enthalpy is G_h. Thus, free enthalpy of coagulation (ΔG_k) equals the difference of free enthalpy after forming coagulum and the energy before coagulation.

$$\Delta G_k = G_h - G_\infty . \qquad\qquad\qquad (13.5)$$

Since the interaction of approaching particles is influenced by various forces, including molecular (m), electrostatic (el), structural (s) and other (Derjagin 1989), free enthalpy of coagulation is given by:

$$\Delta G_k = \Delta G_{k\,d} + \Delta G_{k\,\text{el}} + \Delta G_{k\,s} + \Delta G_{k\,\text{other}}. \qquad\qquad (13.6)$$

According to Eq. (13.6), many factors influence coagulation. As it will be shown in subsequent sections, the most important are Hamaker constant as a measure of molecular forces, potential zeta as a measure of electrostatic interactions, and contact angle, i.e. hydrophobicity of interacting particles as a measure of structural forces.

13.2.1. Molecular interactions

Molecular interactions, also called dispersion interactions, are always present between material objects. Energy of these interactions can be quite considerable and sufficient for maintaining sheets of certain material, for instance graphite, in the form of a compact crystal. Simple calculations of Isrealachvili (1985) indicate that two plain-parallel plates having the Hamaker constant equal to $1 \cdot 10^{-19}$ J (as for instance talc and mica) adhere to one another in the vacuum with a great force leading to pressure of $7 \cdot 10^8$ Pa. Dispersion forces are responsible for interaction of atoms and particles in the gas phase. Due to the existence of dispersion forces gases can be liquefied. Detailed description of gaseous state requires application of real gas equations, which constitute an extension of ideal gas equation, with corrections for dispersion forces and the volume of molecules. The term "dispersion interactions" originates from the observation that these forces are responsible for dispersion, i.e. for dependency of refraction index on the wavelength and dielectric constant on frequency of electric field (Israelachvili 1985).

According to Derjagin (1989) the origin of dispersion force can be described as follows: "Everywhere and always, including in vacuum and at absolute zero there are

spontaneous quantum fluctuations of the electromagnetic filed, even in the absence of external sources. After local fluctuations have arising, they serve as a source of virtual (non-energy-bearing) electromagnetic waves. These waves, when they reach an interface and are partially refracted, form traveling waves in the neighboring phase and in part form standing wave that decay exponentially with increasing distance from the interface. As a result, the wave field, characterized by the tensor of the mean square components of the electromagnetic field, is uniform and isotropic in the bulk phases at sufficient distances from the interface. Close to the interface, however, this tensor is nonuniform and anisotropic. If the interlayer between the two phases is made sufficiently thin, the transition zones with nonuniform distribution of electromagnetic fluctuations begin to overlap. The wave field is changed; in particular, the component of the tensor E_{nn}^2 normal to the interface, is changed. This upsets the equilibrium and, in the general case, gives rise to a disjoining pressure (or molecular attraction), tending to change the thickness of the interlayer (or gap) between the outer phases; the disjoing pressure may be balanced by external forces"

The molecular interaction of a spherical particle (phase) 1 with a particle (phase) 2, through another phase (phase 3), when particles radius r is considerably larger than the distance between particles H, is expressed by:

$$\Delta G_{k,d} = \Delta G_{132}^d = V_A = -\frac{A_{132}R}{12H},$$ (13.7)

where:
H – distance between particles
R – particle radius
A_{132} – the Hamaker constant (in joules).

To calculate the conditions of coagulation, as well as to describe other processes like flotation or foam properties, it is necessary to know the Hamaker constant. Positive values of the Hamaker constant indicate repulsion while negative ones attraction. The Hamaker constant determines the energy of dispersion interaction between particles and other objects like drops, bubbles, thin films, foams, or adsorptive layers. The Hamaker constant is defined as:

$$A = \pi^2 \, C \, \rho^*_1 \, \rho^*_2,$$ (13.8)

where:
ρ^*_1 and ρ^*_2 – number of atoms per volume of objects 1 and 2, respectively
C – proportionality constant between the potential of atom–atom pair and the distance between atoms, also called the London constant.

Since C is of order 10^{-77} J/m^6 while ρ^* is of order $3 \cdot 10^{28}$ m^{-3}, the typical value of the Hamaker constant for condensed (solid and liquid) phases interacting through the vacuum ($A_{131} = A_{101} = A_{11}$) is around 10^{-19} J (Israelachivili, 1985). Vacuum, as a medium for interaction of particles 1 and 2, is usually denoted as 3, or 0, or no symbol is used).

For instance, the Hamaker constant for different substances interacting in vacuum, ranges from $3.8 \cdot 10^{-29}$ J for Teflon to about $5 \cdot 10^{-20}$ J for heavy metals (Drzymala, 1994). The Hamaker constant values for different materials are presented in Table 13.1.

Table 13.1. Hamaker constant A_{11} for selected materials
collected by Drzymala (1994) and other authors

Material	A_{11} ($\times 10^{20}$ J)		A_{11} ($\times 10^{20}$ J)	Material	A_{11} ($\times 10^{20}$ J)
n-pentane (C_5H_{12})	3.8[b]	mica	10.0[b]	MoS_2 (molibdenite)	13.3[e], 9.1[c]
Teflon ($[C_2F_4]_n$)	3.8[b]	MgO (periclase)	10.5[c]	S (sulfur)	23[c]
Acetone (CH_3COCH_3)	4.1[b]	$CaCO_3$ (calcite)	10.1[d]	Fe_2O_3 (hematite)	23.2[a]
Ethanol (C_2H_5OH)	4.2[b]	AsS (realgar)	12.0[c]	C (graphite)	23.8[a]
Water (H_2O)	4.38[a]	FeS_2 (pyrite)	12.0[c]	SnO_2 (cassiterite)	25.6[a]
n-octane (C_8H_{18})	4.5[b]	CaO (lime)	12.5[c]	Si (silicon)	25.6[a]
n-dodecane $C_{12}H_{26}$	5.0[b]	$FeCr_2O_4$ (chromite)	14.0[c]	FeAsS (arsenopyrite)	27[c]
n-tetradecane ($C_{14}H_{30}$)	5.0[b]	ZnS (sphalerite)	14.0[c]	As_2S_3 (auripigment)	28.4[a] 15[c]
Benzene (C_6H_6)	5.0[b]	CdS (greenockite)	15.3[f]	C (diamond)	28.4[a]
n-heksadecane ($C_{16}H_{34}$)	5.1[b]	Al_2O_3 (corundum)	15.5[a]	Cu (copper)	28.4[a]
Cyklohexane (C_6H_{12})	5.2[b]	AgI (iodirite)	15.8[a]	Ge (germanium)	30.0[a]
KCl silvine	6.2[a]	Sb_2S_3 (metastibnite)	16.0[c]	TiO_2 (rutyl)	31.0[a]
C_nH_{2n+2} (paraffin)	6.3–7.3[a]	SiO_2 (quatz)	16.4[a]	PbS (galena)	33[c]
Polystyrene	6.5[b]	$BaSO_4$ (barite)	16.4[a]	Ag (silver)	40.0[a]
CaF_2 (fluorite)	7.2	TiO_2 (anatase)	19.7[a]	Hg (mercury)	43.4[a]
Bornite (Cu_5FeS_4)	7.4[c]	Cu_2S (chalcocite)	21.0[c]	Au (gold)	45.5–50[a]
Poli(vinyl chloride)	7.5[b]	Fe (iron)	21.2[a]	CuS (covelline)	2.8[c] (?)
Pirrothite (FeS)	8.4[c]	Pb (lead)	21.4[a]	[Fe, Ni]$_9$S$_8$) pentlandite	3.3[c] (?)
Talc ($Mg_3[(OH)_2Si_4O_{10}]$)	9.1[c]	Sn (tin)	21.8[a]	$CuFeS_2$ (chalkopyrite)	3.3[c] (?)

a) Visser (1972), b) Israelachvili (1985), c) Lins i współ. (1995), d) Hunter (1987), e) Ebaadi (1981), f) Krupp et al., (1972). Symbol ? denotes uncertain data

Determination of the Hamaker constant is not a simple task. There are two approaches to calculation of the Hamaker constant known as microscopic or macroscopic. Gregory (1969), for example, used the microscopic approach. The Hamaker constant for two identical particles (designated as 1) interacting in a condensed medium 3, i.e. A_{131}, is given by the equation (Sonntag 1982).

$$A_{131} = \frac{27}{64} \frac{h\nu_\nu}{\varepsilon_3^*} \left(\frac{\varepsilon_1^* - 1}{\varepsilon_1^* + 2} - \frac{\varepsilon_3^* - 1}{\varepsilon_3^* + 2} \right)^2 , \qquad (13.9)$$

while for two substances interacting in vacuum (0 or no symbol) (Gregory, 1969) it is described by the relation:

$$A_{12} = A_{102} = \frac{27}{64} \frac{h\nu_{1\nu}\nu_{2\nu}}{(\nu_{1\nu} + \nu_{2\nu})} \left(\frac{\varepsilon_1^* - 1}{\varepsilon_1^* + 2} \right) \left(\frac{\varepsilon_2^* - 1}{\varepsilon_2^* + 2} \right) . \qquad (13.10)$$

For two identical substances interacting in vacuum according to (Gregory, 1969) the equation assumes the form:

$$A_{101} = A_{11} = \frac{27}{64} h \nu_v \left(\frac{\varepsilon_1^* - 1}{\varepsilon_1^* + 2} \right)^2 \qquad (13.11)$$

where:

ε_1^* – terminal (not static as is claimed by Sonntag, 1982) dielectric permeability for phase 1 particle,

ε_2^* – terminal dielectric permeability for substance 2 particle,

ε_3^* – terminal dielectric permeability for condensed medium, that is phase 3,

ν_v – characteristic frequency.

The terminal values of dielectric constant ε_1^*, ε_2^*, or generally ε_n^*, for different substances can be calculated from the index of refraction n_0 within the range of visible light, applying the Maxwell equation $\varepsilon_n = n_0^2$. It should be stressed that ε_n is not static dielectric constant ε_0 referring to zero frequency of electric field. For instance, static dielectric constant for water is 81, while terminal dielectric constant amounts 1.77, since n = 1.323 ($\varepsilon_n^* = n_0^2 = 177$). The n_0 value can be obtained by interpolation of n within a visible range to zero frequency of the electric field or similar dependences (Fig. 13.3.).

Characteristic frequency ν_v of a substance can be also determined from the relationship between refraction index n and frequency within visible light range, according to the equation:

$$\frac{n^2 + 2}{n^2 - 1} = B \nu_v^2 - B \nu^2 = \frac{3\pi m_e M}{e^2 N_a \rho} \frac{\nu_v^2}{s} - \frac{3\pi m_e M}{e^2 N_a \rho} \frac{\nu^2}{s} , \qquad (13.12)$$

where:

m_e – electron mass

e – electron charge

N_a – Avogadro number

s – effective number determining dispersion of electronic oscillators

M – molar mass (g /mol)

ρ – density, g /cm^3.

Plotting the relation:

$$y = \frac{n^2 + 2}{n^2 - 1}$$

as a function of ν^2, within the range of visible light, results in a straight line of inclination B, which enables determination of s. Knowing parameter s and the value of intersection of straight line with axis y, ν_v can be determined. The same value of intersec-

tion enables determination of n_0, and then, from the Maxwell equation ε_0^*. Figure 13.3a shows determination of the values of s, v_v, n_0 and ε_0^* for polystyrene.
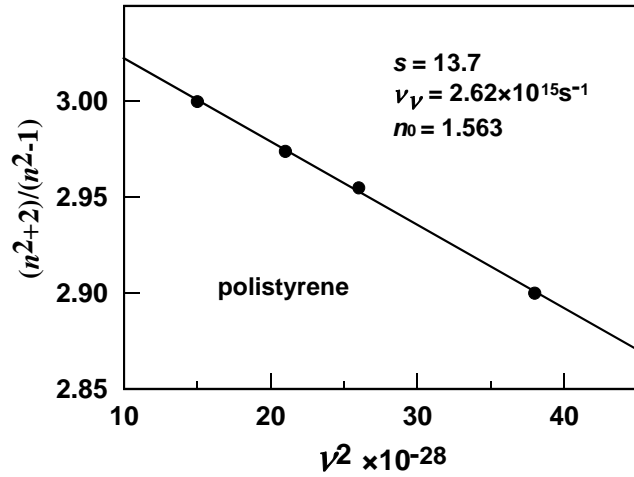
a
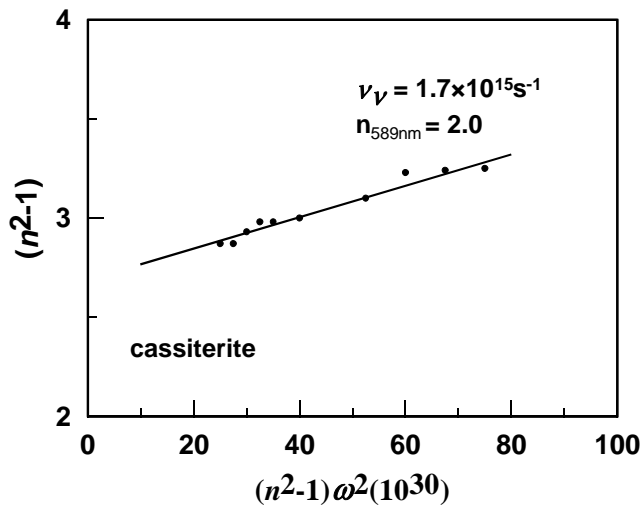
b

Fig. 13.3. Determination of data for calculation of the Hamaker constant basing on refractive index, a) the Gregory (1969) method of calculating s and ε_o, as well as n_o and v_v, needed for calculation of the Hamaker constant, b) the Hough-White (1980) method of v_v determination

The macroscopic approach was proposed by Lifszyc (1954, 1955). For phase 1 interacting with phase 2 through phase 3 as layer of thickness H, the Hamaker constant is included in the following equation (Dzialoszynski et al., 1959)

$$\Pi_m(H) = -\frac{h}{2\pi^2 c_*^3} \times$$

$$\times \int\limits_0^\infty \int\limits_1^\infty p^2 \xi^3 \varepsilon_3^{3/2} \left\{ \begin{array}{l} \left[\frac{(s_1+p)(s_2+p)}{(s_1-p)(s_2-p)} \exp\left(\frac{2p\xi}{c_*} H\sqrt{\varepsilon_3}\right) - 1 \right]^{-1} + \\ \left[\left(s_1 + p\frac{\varepsilon_1}{\varepsilon_2} \right)\left(s_2 + p\frac{\varepsilon_2}{\varepsilon_3} \right) \exp\left(\frac{2p\xi}{c_*} H\sqrt{\varepsilon_3}\right) - 1 \right]^{-1} \end{array} \right\} dpd\xi, \tag{13.13}$$

in which:

$$s_1 = \sqrt{\frac{\varepsilon_1}{\varepsilon_3} - 1 + p^2} \quad s_2 = \sqrt{\frac{\varepsilon_2}{\varepsilon_3} - 1 + p^2}, \tag{13.14}$$

$\Pi_m(H)$ – force of interaction caused by dispersion forces related to unit area (minus sign denotes attraction of plates), also called molecular component of disjoining pressure

h – the Planck constant

$\varepsilon_1, \varepsilon_2, \varepsilon_3$ – functions dependent on imaginary frequency $\omega'' = i\xi$ (i is imaginary number)

ξ – frequency of electromagnetic field

c_* – light speed in vacuum.

This equation is quite complicated, therefore many simplified versions were derived. For example, for plane-parallel particles 1 and 2 in any arbitrary dispersion medium 3, for short distances between particle surfaces, the Hamaker constant is expressed as:

$$A_{102} = \frac{3h}{16\pi^2} \int\limits_0^\infty \left[\frac{\varepsilon_1 - \varepsilon_3}{\varepsilon_1 + \varepsilon_3} \right]\left[\frac{\varepsilon_2 - \varepsilon_3}{\varepsilon_2 + \varepsilon_3} \right] d\xi, \tag{13.15}$$

where: $\varepsilon_1, \varepsilon_2, \varepsilon_3$ area real functions of complex frequency $\omega = \omega' + i\xi$, while ω denotes angular frequency ($\omega = 2\pi\nu$), tj. $\varepsilon(\omega) = \varepsilon'(\omega) + i\varepsilon''(\omega)$.

This equation still remains complicated, therefore many simplified equations for the Hamaker constants were introduced, which in 1980 were collected by Sonntag (1982). The most useful for mineral processing applications can be the equation introduced by Israelachvili (1985) which is based on the Lifszyc equations and presented in the analytical form. For non-metallic substances, when a particle interacts with a particle of a different material 2 through phase 3, the expression for the Hamaker constant assumes the following form:

$$A_{132} = A_{132,\nu=0} + A_{132,\nu>0}, \tag{13.16}$$

$$A_{132,v=0} = \frac{3}{4}kT\left(\frac{\varepsilon_1 - \varepsilon_3}{\varepsilon_1 + \varepsilon_3}\right)\left(\frac{\varepsilon_2 - \varepsilon_3}{\varepsilon_2 + \varepsilon_3}\right), \tag{13.17}$$

$$A_{132,v>0} = \frac{3hv_v}{8\sqrt{2}} \frac{\left(n_1^2 - n_3^2\right)\left(n_2^2 - n_3^2\right)}{\left(n_1^2 + n_3^2\right)^{1/2}\left(n_2^2 + n_3^2\right)^{1/2}\left\{\left(n_1^2 + n_3^2\right)^{1/2} + \left(n_2^2 + n_3^2\right)^{1/2}\right\}}. \tag{13.18}$$

For two identical objects interacting through medium 3 the Israelachvili equation is simplified to:

$$A_{131} = A_{131,v=0} + A_{131,v>0} = \frac{3}{4}kT\left(\frac{\varepsilon_1 - \varepsilon_3}{\varepsilon_1 + \varepsilon_3}\right)^2 + \frac{3hv_v}{16\sqrt{2}}\frac{\left(n_1^2 - n_3^2\right)^2}{\left(n_1^2 + n_3^2\right)^{3/2}}, \tag{13.19}$$

while for two identical object interacting in vacuum, the Hamaker constant takes the form:

$$A = A_{11} = A_{11,v=0} + A_{11,v>0} = \frac{3}{4}kT\left(\frac{\varepsilon - 1}{\varepsilon + 1}\right)^2 + \frac{3hv_v}{16\sqrt{2}}\frac{(n^2 - 1)^2}{(n^2 + 1)^{3/2}}, \tag{13.20}$$

where $\varepsilon_1 = 1$ and $n_3 = 1$.

In the equations from (13.16) to (13.20):

ε – static relative dielectric constant (for water 81),

n – refractive index for light in visible range,

v_v – characteristic frequency equal to the main absorption frequency in the ultraviolet region. $A_{v=0}$ is not higher than 3/4 kT, that is $3 \cdot 10^{-21}$ J at 300 K.

For metals the expression for the Hamaker constant is slightly different because:

$$\varepsilon(v) = 1 - v_p^2/v^2, \tag{13.21}$$

$$\varepsilon(iv) = 1 + v_p^2/v^2, \tag{13.22}$$

thus

$$A = (3/16\sqrt{2})hv_p, \tag{13.23}$$

where v_p is the plasma frequency of free electron gas.

In order to calculate the Hamaker constants using the Israelachvili equation, it is necessary to know the value of characteristic frequency, i.e. frequency of radiation at which the absorption within UV range takes place, as well as index of refraction within the visible range. According to Lins et al. (1995), v_v can be calculated on the basis of the relation between index of refraction and frequency and the Hough-White equation (1980):

$$(n^2 - 1) = (n^2 - 1)\omega^2 \frac{1}{\omega_{UV}^2} + C_{UV} ,$$ (13.24)

where:

n – refractive index of light at appropriate frequency of visible rays

ω – angular frequency of radiation in the visible region for appropriate wavelength λ, at which n was measured (rad s^{-1})

ω_{UV} – angular frequency of absorption in the ultraviolet region.

ω_{UV} is connected with characteristic frequency v_v by the relationship:

$$v_v = \omega_{UV}/2\pi.$$ (13.25)

To determine v_v, the dependence of $(n^2\text{-}1)$ and $(n^2\text{-}1)\omega^2$ should be plotted and approximated with a straight line. The slope of the line, as it results from equation (13.24), has the value $1/\omega_{UV}$, which is recalculated to the value of characteristic frequency v_v using Eq. (13.25). Determination of v_v for cassiterite is presented in Fig. 13.3b. Knowing v_v and the refraction index, the Hamaker constants can be calculated by means of the Israelachvili equation (Eqs (13.19) and (13.20)), substituting n value determined at 589 nm. Parameter $A_{v=0}$ is calculated on the basis of static relative dielectric constants.

Lins et al. (1985) showed that Eq. (13.24) provides estimation of the Hamaker constant for opaque and light absorbing minerals, for which a direct measurement of index of refraction is not possible. Then, the reflection data for a mineral in two different media should be taken into account e.g. in air and oil. Reflection coefficient R_n is related to refraction index n in the following way:

$$R_n = \frac{(n - N)^2 + K_a^2}{(n + N)^2 + K_a^2} ,$$ (13.26)

where:

K_a – absorption coefficient

N – reflection coefficient (for air $N = 1$).

Combination of two equations (13.26) for a mineral in two media, e.g. in air and oil, results in:

$$n = \frac{\frac{(N^2 - 1)}{2}}{\frac{N(1 + R_{n,\text{oil}})}{1 - R_{n,\text{oil}}} - \frac{(1 + R_{n,\text{air}})}{(1 - R_{n,\text{air}})}} .$$ (13.27)

Calculated value n is real only when the value of K_a is not an imaginary number. To check this, K_a should be calculated from the relation:

$$K_a^2 = \frac{R_n(n+1)^2 - (n-1)^2}{(1-R_n)}.$$ (13.28)

More details regarding determination of refraction index of the Hamaker constant for opaque substances can be found in the work by Lins et. al. (1995). The Hamaker constants can be also calculated basing on dispersion component of surface energy using equation (12.7).

To calculate and describe coagulation and heterocoagulation Hamaker constants A_{131} or A_{132}, are used. They reflect interactions between three different phases. These constants can be determined with Eqs (13.16) and (13.23). Their approximated values can be determined using equations (Israelachvili, 1985):

$$A_{12} \approx \sqrt{A_{11}A_{22}},$$ (13.29)

$$A_{131} = A_{313} \approx A_{11} + A_{33} - 2A_{13} = \left(\sqrt{A_{11}} - \sqrt{A_{33}}\right)^2$$ (13.30)

$$A_{132} \approx \left(\sqrt{A_{11}} - \sqrt{A_{33}}\right)\left(\sqrt{A_{22}} - \sqrt{A_{33}}\right),$$ (13.31)

$$A_{132} \approx \pm\sqrt{A_{131}A_{132}}.$$ (13.32)

Table 13.2. Hamaker constants A_{131} for two objects of the same material (1) interacting through another material (3)

Interacting media			Hamaker constant A_{131}
phase 1	phase 3	phase 1	$(\times 10^{20}$ J)
Air	water	air	3.70[a]
Octane	water	octane	0.41[a]
Water	hydrocarbon	water	0.34–0.54[a]
Polistyrene	water	polistyrene	0.95[a]
Quartz (fussed)	water	quartz (fussed)	0.83[a]
Teflon	water	Teflon	0.33[a]
Mica	water	mica	2.0[a]
Ag, Au, Cu	water	Ag, Au, Cu	30–40[a]
Si	water	Si	36[b]
Al_2O_3	water	Al_2O_3	4.12[b]
MgO	water	MgO	1.6[b]
SiO_2 (cryst.)	water	SiO_2 (cryst.)	1.7[b]
$CaCO_3$	water	$CaCO_3$	2.23[b]
CaF_2	water	CaF_2	1.04[b]
Oxides	water	oxides	1.76–4.17[b]
TiO_2	water	TiO_2	1.1[c]

a) Hough and White (1980), b) Ross and Morrison (1988), c)Yotsumoto and Yoon (1993a).

According to Israelachvili (1985), these formulas are not accurate for the systems of high dielectric constants and featuring high values of $A_{v=0}$, like water. In such a case

it is better to use more accurate equations proposed by Gregory (1969), Pashley (1977), Hough and White (1980).

Some Hamaker constants for two objects made of the same material and interacting through a different medium (3) are presented in Table 13.2.

Table 13.3. Hamaker constants A_{132}, for two objects of different materials (1 and 2) interacting through phase 3

Interacting media			Hamaker constant A_{132}
phase 1	phase 3	phase 2	($\times 10^{20}$ J)
Water	octane	air	0.51[a]
Octane	water	air	–0.24[a]
Quartz (fussed)	water	air	–0.87[a]
Quartz (fussed)	octane	air	–0.70[a]
CaF$_2$	liquid He	He vapor	–0.59[a]
Polistyrene	water	gold	2.98[b]
Selenium	water	MgO	2.83[b]

a) Israelachvili (1985), b) Ross and Morrison (1988).

It can be seen in the table that the Hamaker constants can be either positive or negative. Negative value indicates that dispersion forces repel particles, while positive particle attraction. It means that two identical particles always attract each other, while two different objects can either repel or attract one another.

Molecular interactions in coagulation depend not only on the Hamaker constant, but also on the distance between objects and their shapes. Table 13.4 shows different formulas used for calculation of free enthalpy of objects interaction (ΔG_d). These formulas are general and refer to interaction both in vacuum and between objects 1 and 2 through another substance 3, therefore, symbol x as subscript at ΔG^d and the Hamaker constant A was introduced, which can stands for phases 131 or 132. If phase 3 is vacuum, x can indicate interactions between identical objects (11) or two different objects in vacuum (12).

The relations presented in the table sometimes require, especially in the aqueous medium, some corrections, especially at greater separation. The corrections take into account the effect of retardation of molecular interactions. Retardation of interaction becomes considerable when time needed for fluctuation of electric field during propagation from one particle to another is comparable with the fluctuation period. For coagulation process, according to Shenkel and Kitchener (1960), dispersion interaction considering retardation will assume the form:

$$\Delta G_{131}^d = V_A = -\frac{A_{131}R}{12H} f_o \ , \qquad (13.33)$$

where:

$$f_o = \frac{1}{1+1.77P} \; , \tag{13.34}$$

while $P = 2\pi H/\lambda_o$. λ_o is the length of electron wave of oscillation which is usually assumed to be 100 nm. The equation is valid for $P \leq 0.5$. When $P > 0.5$, the following equation should be used:

$$f_o = \frac{2.45}{5P} - \frac{2.17}{15P^2} + \frac{0.59}{35P^3} \; . \tag{13.35}$$

Table 13.4. Equations for free enthalpy of dispersion interactions of objects of different shape (Israelachvili, 1985). x denotes interacting phases, for instance phase 1 with phase 2 through phase 3 (132). When interactions occur through vacuum the symbol is 11 (identical objects) or 12 (different objects)

Interacting objects	Formula	Units
Two atoms	$\Delta G^d = -\dfrac{C}{H^6}$ (C is a constant)	J
Two spheres	$\Delta G_x^d = -\dfrac{A_x(R_1 R_2)}{6H(R_1 + R_2)}$	J
Two flat parallel slabs	$\Delta G_x^d = -\dfrac{A_x}{12\pi H^2}$	J/m^2
Sphere and slab	$\Delta G_x^d = -\dfrac{A_x R}{6H}$	J
Two perpendicular cylinders	$\Delta G_x^d = -\dfrac{A_x \sqrt{R_1 R_2}}{6H}$	J

There are many formulas for the coefficient of retardation f_0 (Czarnecki, 1986).

13.2.2. Electrostatic interactions

Interactions between two electrically charged ions can be described using the Coulomb law (Wróblewski and Zakrzewski, 1984) according to which the interaction energy is inversely proportional to the distance between ions. This dependence is not fulfilled in the case of particles interacting in aqueous suspensions because of diffused electric double layer (edl). When the charged particles approach each other in water, there is at first penetration and then redistribution of charge and potential in the edl. Since the edl penetration is complicated, either the penetration with a constant charge or constant potential for simplicity is usually considered. It is believed that superposition of both electrical double layers most often occurs at constant surface potential and is accompanied by a decrease in the surface charge. When ions passing from the surface into the solution is inhibited, because the rate of approaching particles is higher than the speed of establishing ionic equilibrium, the edl penetration can take place at

constant charge to maintain constant potential, while the surface potential becomes altered. According to Sonntag (1982) both ways lead to practically identical formulas for the energy of particles interactions.

General formula for the electrostatic interaction energy ΔG_{el} of spherical particles of radiuses R_1 and R_2, having different values and edl potential signs Ψ_1 and Ψ_2, when particle radius is of considerable value comparing to the thickness of diffused edl part $1/\kappa$, was derived by Hogg et al. (1966). Its form in the SI system is as follows (Hunter, 1989).

$$\Delta G_{el} = V_R = \frac{\pi \varepsilon \varepsilon_0 R_1 R_2 (\psi_1^2 + \psi_2^2)}{(R_1 + R_2)} \left\{ \frac{2\psi_1 \psi_2}{(\psi_1^2 + \psi_2^2)} \ln\left[\frac{1 + \exp(-\kappa H)}{1 - \exp(-\kappa H)} \right] \right. $$
$$\left. + \ln\left[1 - \exp(-2\kappa H) \right] \right\}, \tag{13.36}$$

where:

ΔG_{el} – change of free enthalpy for the system caused by electrostatic interactions (frequently symbol V_R is used), J

ψ_1 – electrostatic potential of particle, V

ψ_2 – electrostatic potential of another particle, V. When particles are identical $\psi_1 = \psi_2 = \psi_s$

R_1 – radius of spherical particle, m

R_2 – radius of the other spherical particle, m. When particles are identical, $R_1 = R_2 = R$

ε – dielectric constant of medium (usually water), also called relative dielectric permeability (dimensionless quantity, for water $\varepsilon = 81$, at 293,2 K)

ε_0 – dielectric permeability of vacuum, $8.854187817 \cdot 10^{-12}$ $C^2 N^{-1} m^{-2}$ (CRC, 1998)

$1/\kappa$ – Debye radius also called the thickness of edl, m

H – distance between objects, m. For spherical particles it is the distance between most separated spots of particles.

The expression for the thickness of the edl (Debye radius) $1/\kappa$ (m) has the form (Wiese et al., 1976):

$$\kappa = \left(\frac{2z^2 e^2 n_e}{\varepsilon \varepsilon_0 kT} \right)^{1/2} = 3.29 \cdot 10^9 z \sqrt{c_s}, m^{-1}, at\ 298\ K, \tag{13.37}$$

where:

c_s – concentration of electrolyte in the bulk solution, mol/dm^3

z – integer number 1, 2, 3 denoting the valence of the counter ion (without + or – sign), which has major contribution to compensating edl

n_e – electrolyte concentration in the bulk solution as number of pairs of ions per unit volume, m^{-3}

e – elemental electric charge, coulomb (C)

k – Boltzmann constant (1,38·10⁻²³ joule/kelvin, J/K)

T – absolute temperature, kelvin (K).

Positive interaction energy ΔG_{el} indicates repelling, while negative one - attraction. Particle repelling in water, due to electrostatic edl forces, takes place when interacting particles are of identical sings of surface potential. Since ions present in the edl are not mathematical points, in the equations for electrostatic interaction of particles surface potential is replaced by potential in the Stern layer of the edl (Ψ_S). The Stern potential, in turn, is closed to zeta potential. Therefore, zeta potential of particle is used for calculation and description of electrostatic interactions between objects in mineral processing and the ones which take place in nature, including coagulation. It is a correct approximation for low values of surface potentials. It should be stressed, however, that in literature there are many incorrect modifications of the formula for calculating V_R. They result from wrong adaptations of the original equations derived in the electrical units system cgs for the requirements of the SI system. In the SI units a unit of potential is volt (V), of charge is coulomb (C), and the dielectric constant is dimensionless since it is expressed as a relative value in relation to the dielectric permeability in vacuum and is equal to 8.85.10⁻¹² C²N⁻¹m or AsV⁻¹m⁻¹. Since 1 joule (J)=1 volt x coulomb (C) and As (Ampere-second) = J/V and F=C/N, dielectric permeability in vacuum can be also expressed as 8.85·10⁻¹² AsV⁻¹ or Fm⁻¹. A certain indication as to the correctness of the equation including dielectric permeability is the presence of vacuum permeability symbol (most often ε_o) beside the symbol of the dielectric constant for a particle or medium (most often ε).

Changing equations from the cgs electrical system to SI is achieved by replacing ε with 4 $\pi\varepsilon\varepsilon_0$. This problem is discussed in detail in the chapter on the SI units.

Equation 13.36 describes electrostatic interactions for heterocoagulation process, yet it can be applied for the description of coagulation, since during coagulation interaction between identical particles takes place and then $R_1=R_2=R$ and $\Psi_1=\Psi_2=\Psi$.

For identical spherical particles of low potential and high κR values the following approximating equation can be used (Hutner, 1987):

$$\Delta G_{\mathrm{el}} = V_R = 2\pi R\varepsilon\varepsilon_0\psi_S^2 \ln\{1 + \exp(-\kappa H)\}, \qquad (13.38)$$

where Ψ_2 is the Stern potential, usually replaced with the zeta potential (ζ).

For low values of $\kappa R<5$ the edl is very extended. For this case Verwey and Overbeek (1948) introduced a special equation which is highly complicated. Therefore, it is easier to use graphs which can be found in the work of Verwey and Overbeek (1948), as well as in the monograph by Hunter (1987). A simplified expression (with up to 40% error) for $\kappa R<6$ takes the form of:

$$\Delta G_{\mathrm{el}} = V_R = 2\pi R\varepsilon\varepsilon_0\psi_S^2 \exp(-\kappa H). \qquad (13.39)$$

Coagulation processes sometimes take place between spherical and flat particles or between a spherical particle and a flat surface. Then, the expression for electrostatic interactions, according to Sjollem and Busscher (1990) takes the form of:

$$\Delta G_{\text{el}} = V_R = \pi\varepsilon\varepsilon_0 R(\psi_1^2 + \psi_2^2)\left\{\frac{2\psi_1\psi_2}{(\psi_1^2 + \psi_2^2)}\ln\left[\frac{1+\exp(-\kappa H)}{1-\exp(-\kappa H)}\right]\right.$$
$$\left. + \ln\left[1-\exp(-2\kappa H)\right]\right\},$$
(13.40)

which means that interactions, expressed in joules, are twofold stronger than in the case of two spherical particles. When a flat and parallel surface interact with each other, but featuring different surface potentials, the expression for the energy of electrostatic interactions at constant potential V^ψ can be obtained using numerical procedures, while that for low potentials according to the expression (Hutner 1987):

$$\Delta G_{\text{el}} = V_R^\psi = \frac{\varepsilon\varepsilon_0\kappa}{2}\left[(\psi_1^2 + \psi_2^2)(1-\text{ctgh}\,\kappa H) + 2\psi_1\psi_2\,\text{cosec}\,h\,\kappa H\right],$$
(13.41)

where ΔG_{el} for plates is in J/m^2.

For identical surface potentials of both plates ($\Psi_1 = \Psi_2 = \Psi$) Eq. 13.41 is reduced to:

$$V_R^\psi = 2\varepsilon\varepsilon_0\kappa\psi^2(-\kappa H) \text{ J/m}^2.$$
(13.42)

This equation is also true for interactions at constant charge when potentials are low and the two edl slightly superimpose (the plates are far from each other) ($exp(-\kappa H)<<1$) and then interactions can be described by an approximate equation (Sonntag, 1982):

$$\Delta G_{\text{el}} = V_R = \frac{64 n_e kT}{\kappa}\exp(-\kappa H)\left(\exp\frac{ze\psi}{2kT} - 1\right)^2\left(\exp\frac{ze\psi}{2kT} + 1\right)^{-2},$$
(13.43)

where n_c is the number of pairs of ions per 1m^2 and thermodynamic potential of electrostatic interactions ΔG_{el} is expressed in J/m^2.

Table 13.5 presents approximated formulas for energy of electrostatic interactions V_R between the objects of different geometry, placed in medium of dielectric constant constants ε (after Russel et al., 1989).

The equations for electrostatic interactions contain, as a rule, surface potential (Ψ, Ψ_o). Since ions in the edl have certain volume, surface potential is approximated with the Stern potential. This potential, in turn, is approximated with zeta potential, which is easily measurable. The zeta potential can be measured as a function of pH and ionic strength of the solution in which coagulation takes place. The surface, Stern and zeta potentials are mutually related and their values can be calculated. The zeta potential depends on ionic strength of the solution as well as on its pH. At constant ionic

strength zeta potential changes with the pH until it reaches a constant value, which can be constant or slightly dropping towards the pH axis. A change of the zeta potential with pH for many systems can be empirically described using the equation:

$$\zeta = 2\frac{\zeta_{max}}{1+e^{f*(\text{pH}-\text{iep})}} - \zeta_{max}\,.$$

(13.44)

In Eq. (13.44) coefficient $f*$ regulates ζ variations from *iep* to ζ_{max}. A diagram showing typical shape of the zeta potential is presented in Fig. 13.4.

Table 13.5. Approximate formulas for energy of electrostatic interactions $\Delta G_{el} = V_R$ between objects having different geometry in medium of a given dielectric constant ε
(Russel i et al., 1989)

Geometry	limitation	interaction energy V_R
Two parallel slabs	overlap	$64kTn_e\kappa^{-1}\tanh^2(0.25\psi)\exp(-\kappa H)$
Two spheres	constant potential	$2\pi\varepsilon\varepsilon_0\left(\dfrac{kT}{ze}\right)^2 R\psi^2\ln(1+\exp[-\kappa H])$
Two spheres	constant charge	$-2\pi\varepsilon\varepsilon_0\left(\dfrac{kT}{ze}\right)^2 R\sigma_0^2\ln(1-\exp[-\kappa H])$
Two spheres	linear overlap	$4\pi\varepsilon\varepsilon_0\left(\dfrac{kT}{ze}\right)^2\dfrac{R^2}{H+2R}\psi^2\exp(-\kappa H)$
Two spheres	overlap	$32\pi\varepsilon\varepsilon_0\left(\dfrac{kT}{ze}\right)^2 R\tanh^2(0.25\psi)\exp(-\kappa H)$
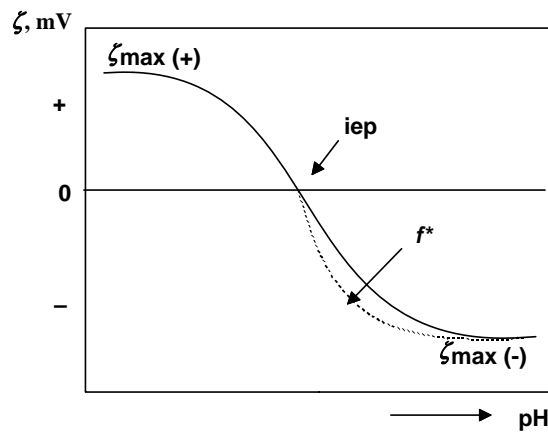
Fig. 13.4. Typical relations between zeta potential and pH
with characteristic terms such as ζ_{max}, iep and curvature coefficient $f*$

Table 13.6. Data for delineation of change of zeta potential as a function of pH in water for various materials

Mineral	pH_{iep}	ζ_{max}	f^*	Ionic strength	Source
γ–Al_2O_3	8.9	39	1.16	0.01 M KNO_3	Wiese and Healy, 1975
γ–Al_2O_3	8.9	76	1.27	0.0001 M KNO_3	Wiese and Healy, 1975
TiO_2	5.8	–42	1.46	0.01 M KNO_3	Wiese and Healy, 1975
TiO_2	5.8	–79	1.29	0.0001 M KNO_3	Wiese and Healy, 1975
Fe_2O_3	6.0	55	1.85	*	Pugh, 1974
Fe_3O_4	6.7	43	1.10	*	Gray et al., 1994
SiO_2 (Fisher)	3.7	–14	0.82	0.1 M NaCl	Cerda and Non-Chhom, 1989
SiO_2 (Fisher)	3.7	–89	0.86	0.001 M NaCl	Cerda and Non-Chhom, 1989
Anthracite	8.0	–44	0.88	*	Ney, 1973
Sulfur	2.2	–32	2.10	*	Ney, 1973
Talc	2.0	–49	0.76	*	Ney, 1973
Bacteria**	3.3	–43	1.00	0.001 M NaCl	Sadowski, 1998
Ice (D_2O)	~3.0	–77	1.45	0.0001 M NaCl	Drzymala et al., 1999
Ice (D_2O)	~3.3	–31	1.00	0.001 M NaCl	Drzymala et al., 1999
Hexadecane	3.1	–70	1.00	0.001 M NaCl	Stachurski and Michalek, 1996
Diamond	~3.0	–77	1.45	0.001 M NaCl	Shergold and Hartley, 1982
Air	3.3	–43	1.00	0.001M NaCl	Li and Somasundaran, 1992

 * In solutions without salt, it can be assumed that the ionic strength is 10^{-4} kmol/m^3, except when the concentration of the reagent which regulates pH is greater. In such a case the ionic strength is determined by the pH value. ** *Nokardia sp.*

Table 13.6 provides the iep, ζ_{max} and f^* constants for different materials in water. A relation between the zeta potential and pH, as well as between the surface potential and pH can be derived on the basis of the equation describing electrical double layer (edl). The dependence between the zeta potential as well as surface potential and pH for the Grahame model of edl is, after Smith (1976), diagrammatically shown in Fig. 13.5.

The slope of the surface potential curve versus pH for non-metals is expressed by:

$$\left[\frac{d\psi_0}{d(\text{pH})}\right]_{\sigma_0 \to 0} = -\frac{2.303 kT}{e} - \frac{kT}{2N_s e^2}\frac{1}{\Theta_c}\frac{d\sigma_0}{d(\text{pH})} \cdot \qquad (13.45)$$

Numerical value of the first right hand term of Eq. (13.45) at 25^{0}C (298 K) is 59 mV per pH unit and is equal to the Galvani potential Φ drop between the bulk of the solid and the solution and is also called the Nernst slope. Since surface potential Ψ_0 is lower than the Galvani potential by the so-called potential chi (χ), $\Psi_0 = \Phi - \chi$, and it changes its value less than 59 mV per pH unit, while this difference is expressed by the second segment of equation (13.45).

solid particle   rigid part   diffusive part   bulk solution

electrical charge σ_0 σ_β σ_d 0

capacity K_1 K_2 C_d

potential ψ_0 ψ_β ψ_d ζ 0

plan name   **S   ISP   OSP**
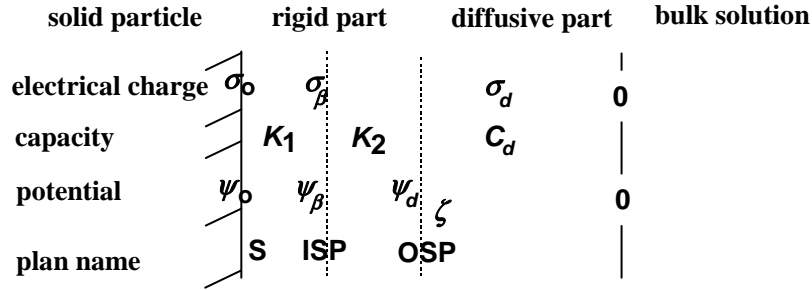
(S - surface. Planes of rigid part of edl : ISP - inner, OSP - outer)

Fig. 13.5. The Grahame model of electrical double layer (edl)

The dependence of the change of zeta potential and pH is very complicated for the Grahame model shown in Fig. 13.5. For a constant ionic strength it is expressed by the relation:

$$\left[\frac{d\zeta}{d(\mathrm{pH})}\right]_{\varsigma\to 0} = \exp(-\kappa\Delta)\left[\frac{d\psi_d}{d\psi_0}\right]_{\varsigma\to 0}\left[\frac{d\psi_0}{d(\mathrm{pH})}\right]_{\varsigma\to 0}, \qquad (13.46)$$

where:

$$\left[\frac{d\psi_d}{d\psi_0}\right]_{\varsigma\to 0} = \left[1+C_d^0\left(\frac{1}{K_1+K_2}\right)\right]^{-1} \qquad (13.47)$$

and relation $\left[\dfrac{d\psi_0}{d(pH)}\right]_{\sigma_0\to 0}$ is described by Eq. (13.45).

Equation (13.46) is simplified. A precise procedure of its derivation and a list of assumptions can be found in the paper by Smith (1976). In Eqs (13.45) and (13.46) the symbols have the following meaning:

ψ_0 – surface potential

ψ_d – potential in the plane of beginning of the diffusive part of edl

σ_0 – surface charge

K_1 – integral capacity of internal part of rigid edl

K_2 – integral capacity of external part of rigid edl

C_d – differential capacity of diffusive part of edl close to iep

k – Boltzman constant

T – absolute temperature

e   – elemental charge

N_s – total number of surface groups available for formation of electrical charge

Θ_c – fraction of surface sites at pzc occupied by either positive or negative charge ($\Theta_c = \Theta_+ = \Theta_-$)

Δ – distance between the slipping plane where the zeta potential is measured and the plane of ψ_d potential ($\zeta = \psi_d \exp(-\kappa\Delta)$)

κ – Debye radius.

The above equations are useful for calculation of various potentials of the edl as well as calculations connected with coagulation.

13.2.3. Structural interaction

Structural interactions are especially important in aqueous systems. They result from the location of water molecules at the water-solid interface and depend mainly on hydrophilicity and hydrophobicity of the surface. Investigations show that hydrophobic structural interactions are considerable at the contact angle, measured through the aqueous phase, greater than 64^0. Hydrophilic structural forces exist for hydrophilic or slightly hydrophobic materials when the angle is less than 15°. For particles of medium hydrophobicity, i.e. for $15^0<\theta_0<64^0$ structural interactions can be neglected.

Forces and energies of structural interactions decrease exponentially with the decreasing distance. Several ways of calculating energy of interactions caused by the structural forces are available in literature. According to Derjagin and Churaev (1989) the free enthalpy ΔG_s of structural interactions for flat particles approaching one another parallel can be expressed by the relation:

$$\Delta G_S = Kl \exp\left(-\frac{H}{l}\right) = E_S^0 \exp\left(-\frac{H}{l}\right),\tag{13.48a}$$

and for spherical particles (Lu et al., 1991):

$$\Delta G_S = K^* lR \ \exp\left(-\frac{H}{l}\right).\tag{13.48b}$$

Table 13.7. Parameters of interactions for identical plane-parallel particles in water
(after Skvarla and Kmet, 1991)

Substance	E_S^0 (mJ/m^2)	l (nm)	Hydrophobicity θ (degree)
Quartz	1.2	0.85	0
Mica	39.8	0.17	0
Montmorillonite	144	2.2	0
CTAB	–22.0	1.0	65
DDOA	–58.0	1.2	94
DMDCHS	–0.4	13.5	100

CTAB –cetylotrimethylammonium ion, DDOA – dioctadecyldimethylamonium ion, DMDCHS – dimethylodichlorosilane

Typical values E_s^0 and l after Skvarla (1991) are presented in Table 13.7. In equations (13.48) and (13.48b) K and K^* are interaction constants, while l is a correlating parameter as well as the parameter determining the layer thickness of oriented water molecules on the surface. Interaction constant K is negative for hydrophobic structural forces, which means that hydrophobic interactions cause particles attraction, while for hydrophilic interactions K is positive, which indicates particles repulsion.

Another approach for calculation of structural interactions between particles and other objects was proposed by van Oss et al. (1990)

$$\Delta G_H^{AB} = \pi R l \Delta G_{H_0}^{AB} \exp\left(\frac{H_0 - H}{l}\right), \tag{13.49}$$

where:

ΔG_H^{AB} – energy of structural interaction as a function of the distance between two spherical objects

$\Delta G_{H_0}^{AB}$ – energy of structural interaction for two plane-parallel surfaces when they attain minimum separation H_0. $\Delta G_{H_0}^{AB}$ is determined by means of contact angle

l – distance of existence of structured water adjacent to surface

R – particle radius.

Van Oss et. al. (1990) assumed that for water $l = 1$nm. Theoretically, for water molecules without hydrogen bonds l amounts about 0.2 nm, but since 10% of water molecules are bound through hydrogen bonds, it can be assumed that l equals 1 nm. The interaction energy, for the particles in contact can be calculated on the basis of the van Oss-Good-Chaudhury (1988) theory according to which:

$$\Delta G_{H_0}^{AB} = -2\gamma_{12}^{AB} . \tag{13.50}$$

Next, γ_{12}^{AB} can be calculated from the relation:

$$\gamma_{12}^{AB} = 2\left(\sqrt{\gamma_1^+ \gamma_1^-} + \sqrt{\gamma_2^+ \gamma_2^-} - \sqrt{\gamma_1^+ \gamma_2^-} - \sqrt{\gamma_2^+ \gamma_1^-} \right), \tag{13.51}$$

in which γ_1^-, γ_1^+, γ_2^- and γ_2^+, or generally γ^- and γ^+, are non-additive parameters of participation of non-dispersion interactions of the total interaction energy

$$\gamma = \gamma^{LW} + \gamma^{AB} = \gamma^{LW} + 2\sqrt{\gamma^+ \gamma^-} . \tag{13.52}$$

The values of these parameters can be determined from contact angles measured in standard liquids. The values of γ^- and γ^+ for standard liquids and some minerals are shown in Table 13.8.

Table 13.8. Values of γ^- and γ^+ for probing liquids and selected minerals. The surface energy of the material is equal to the sum of dispersion (*LW*, sometimes denote as *d*) and nonpolar donor-acceptor (*AB*) components, that is $\gamma = \gamma^{LW} + \gamma^{AB}$ (mJ/m)

Substance	γ	γ^{LW}	γ^{AB}	γ^+	γ^-	Source
Water	72.8	21.8	51	25.5	25.5	van Oss et al., 1990
Decane	23.9	23.9	0	0	0	van Oss et al., 1990
Diiodomethan	50.8	50.8	0	0	0	van Oss et al., 1990
Glycerol	64.0	34.0	30	3.92	57.4	van Oss et al., 1990
Formamide	58.0	39.0	19	2.28	39.6	van Oss et al., 1990
Hectorite	~40	39.9	~0	~0	23.7	van Oss et al., 1990
Sphalerite	60.4	52	8.4	0.2	88.3	Duran et al., 1995
Silica gel	53.3	41.2	12.1	0.7	51.3	Hołysz, 1998
Barite	~55	48.1	~6.7	02±0.1	56.1	Hołysz and Chibowski, 1997

Another approach to the description of hydrophobic structural interactions between spherical particles was proposed by Mao and Yoon (1997). According to them, the energy of hydrophobic interactions can be described by a function similar to the relations for the dispersion interactions, where hydrophobic interaction constant is introduced instead of the Hamaker constant:

$$\Delta G_h = -\frac{R}{12}\frac{K_{131}}{H},$$ (13.53)

where K_{123} is hydrophobic interactions constant.

On the basis of the data by Yoon and Lutterell (1998), the dependence between hydrophobic interaction constant and contact angle can be expressed using the following empirical relation:

$$-\log K_{131} = 3.2 \cos \theta_a + 18.2,$$ (13.54)

where θ_a is the advancing contact angle for water measured through the aqueous phase.

In the case of interactions between different spherical objects such as air bubble and particles, the equation for hydrophobic interactions is of the form:

$$\Delta G_{S,h} = -\frac{R_1 R_2}{6(R_1 + R_2)}\frac{K_{132}}{H_0},$$ (13.55)

where K_{132} is a constant and $K_{132} = \sqrt{K_{131}K_{132}}$.

Other equations for calculating structural interactions can be found in literature. Yotsumoto and Yoon (1993a, 1993b) applied double exponential dependence for the expression of the energy of hydrophobic structural interactions for the spherical particles:

$$\Delta G_{S,w} = V_S = \frac{R}{2}\{C_a D_a \exp(-H/D_a) + C_b D_b \exp(-H/D_b)\},\qquad (13.56)$$

where:

C_a and C_b – constants at the exponential term

D_a and D_b – distance of disappearance of hydrophilic structural interactions.

The equations presented above indicate that the delineation of structural interactions has been neither theoretically nor experimentally established. Most of the observation and equation for the structural forces should be reexamine because they were established before a significant role of microbubbles, commonly present at interfaces, was realized.

13.2.4. Other interactions

Other interactions between objects in a medium can be caused by impurities, especially by the presence of air. Presently there has been a broad discussion in the scientific literature on effects caused by structural forces and air present in the form of microbubbles.

13.2.5. Stability factor *W*

Molecular V_A, electrostatic V_R, structural V_S (hydrophobic $V_{s,h}$ and hydrophilic $V_{s,w}$) and other (due to air) interactions are dependent on the distance between approaching particles and are usually plotted as shown in Fig. 13.6. The lines representing energies can be of different shape because they depend on many parameters. Each kind of interaction can be of either positive or negative sign.
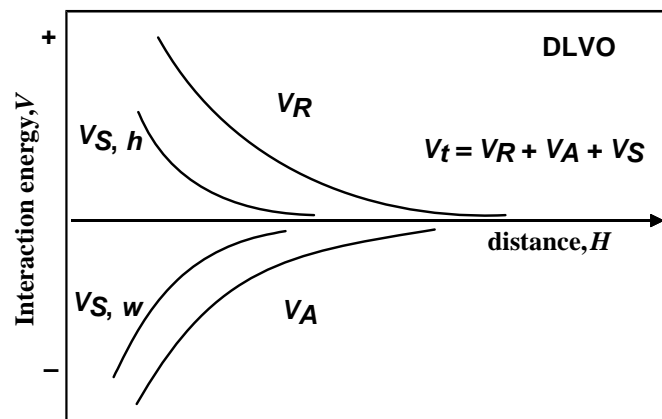
Fig. 13.6. Illustration of the DLVO theory and a set of possible shapes of lines representing energies of interactions between particles during coagulation

When particles interact, their interactions superimpose and since they can be expressed as energies, their values sum up:

$$\Delta G_k = \Delta G_d + \Delta G_{el} + \Delta G_s + \Delta G_{other}, \tag{13.57}$$

which is often written as:

$$V_t = V_A + V_R + V_S + V_{other}. \tag{13.58}$$

Fig. 13.7 shows typical interaction curve V_t illustrating the results of calculations based on the DLVO theory.
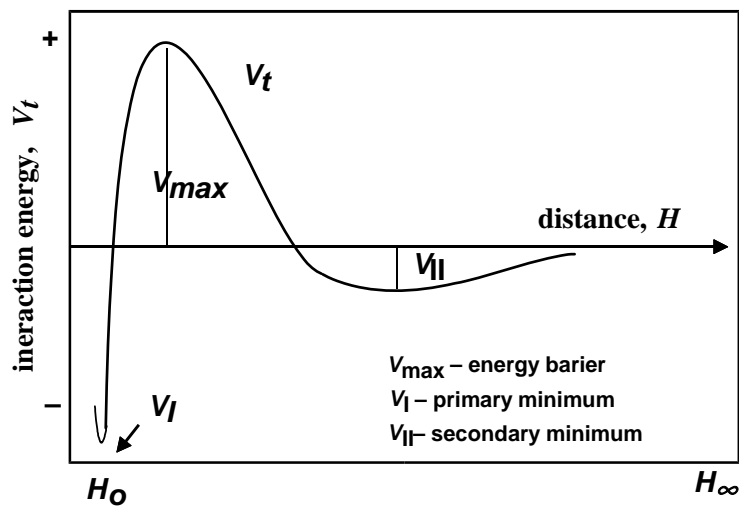
Fig. 13.7. Possible shape of the curve representing total interaction energy of particles V_t during coagulation resulting from the DLVO theory

The DLVO coagulation curves have different shapes. There are some characteristic points for interactions. One is the zero energy of interaction, which occurs when particles are at long distances from one another H_∞. Another is the so-called first minimum which is located at the beginning of the diagram at the distance H_o which equals the distance between atoms in a solid. Any further approach of particles or atoms is not possible as they are exposed to immense repelling forces, equal to those which cause incompressibility of solids.

Equation 13.57 includes the interactions resulting from compressibility through the ΔG_{others} term, which is usually not taken into consideration in the DLVO theory. Therefore, the first minimum in the diagrams of DLVO curves in not present. The course of the DLVO curves between the mentioned terminal points may assume different shapes. When particles have their surfaces electrically charged with opposite signs, they are hydrophobic, and V_A is negative, then all components of the interaction

energy are negative and a barrierless coagulation takes place. In such a case the shape of total interaction curve V_t between points H_∞ and H_0 is simple. It does not contain any maximum or minimum since negative interaction energy indicates attraction of particles. In other cases the curves possess extremes, such as the first and the second minimum. Between the first and second minimum there exist energy barrier, V_{max}. It is a factor which causes that coagulation becomes slow or does not take place at all, as the number of particles possessing sufficient energy to overcome that barrier is the lower the higher barrier is. The value of barrier V_{max} can be expressed in joules. Customarily, the energy barrier is expressed in kT units which represent ratio of the barrier energy in joules to kT unit at the same temperature. At 300 K 1 $kT = 4.14 \cdot 10^{-21}$ J.

The area of energy barrier determines the ability of coagulation, which is characterized by the stability factor W:

$$W = 2R \int_{2R}^{\infty} \frac{1}{r^2} \exp \frac{V_t}{kT} dr , \qquad (13.59)$$

where:

R – particle radius

r – distance between centers of particles determining the radius of the region in which cross section a particle can collide with another particle ($r \cong 2R$).

Parameter W can assume the values from 1 for rapid coagulation, when each collision leads to adhesion, to very high numbers, e.g. 4.10^5, which corresponds to energy barrier V_{max} equal to 15kT. In some cases, for small values of the stability factor W, its value can be slightly lower than 1 and then it should be assumed as 1.

There exist very useful approximated analytical dependence between stability factor W and energy barrier of coagulation (Sonntag, 1982).

$$W \approx \frac{1}{2R\kappa} \exp \left(\frac{V_{max}}{kT} \right) , \qquad (13.60)$$

in which κ means the Debye parameter.

This equation is not fulfilled at $V_{max} = 0$ but basing on definition the value of W is, at this point, equal to 1.

Factor W is the measure of ability of coagulation and it is defined in the following way:

$$W = \frac{\text{number of collisons between particles}}{\text{number of collisions leading to coagulation}} . \qquad (13.61)$$

Factor W determines the probability of particle adhesion as a result of collisions since $P_a = 1/W$. This is a static definition of stability factor W. Its kinetic and kinetic-space definitions based on the collisions ration is:

$$W = \frac{v_f}{v_s} = \frac{j_f}{j_s}, \qquad\qquad (13.62)$$

where:

v – rate of coagulation

j – flux (for instance number of collisions per unit time and surface area)

s and f – symbols representing fast and slow coagulation.

It can be concluded from the definition of the stability factor W that coagulation can be viewed and described on different levels: statically, kinetically and as time–space relations.

The investigation by Prieve and Ruckenstein (1980) proved that W can be also expressed in an empirical form:

$$W = \exp\,[0.92\{(V_{max}/kT) - 1\}] \ \text{(for } (V_{max}/kT) \geq 3). \qquad (13.63)$$

Table 13.9. Half-life $t_{1/2}$ for a hypothetical emulsion containing 1 μm droplets having energy barrier V_{max} located at one radius from the surface of drop (after Friberg, 1991)

Energy barrier V_{max} /kT (in kT units)	$t_{1/2}$	Stability ratio $W = \exp[0.92\{(V_{max}/kT) - 1\}]$ (for $(V_{max}/kT) \geq 3)$*
0	0.8 s	~2
10.0	2.0 h	$3.94 \cdot 10^3$
15.0	1.3 d	$3.92 \cdot 10^5$
17.5	154 d	$3.91 \cdot 10^6$
20.0	5.1 y	$3.90 \cdot 10^7$
50.0	$5.5 \cdot 10^{13}$ y	$3.78 \cdot 10^{19}$

* Empirical equation of Prieve and Ruckenstein (1980). s - second, h - hour, d - day, y - year

Table 13.9 provides typical W and V_{max} values for a hypothetic colloid system consisting of particles 1μ in size. In this table the half-life period of a suspension, calculated from Eq. (13.63) is shown. Detailed calculations of a relation between V_{max} and W can be found in the work of Verwey and Overbeek (1948, p. 169).

13.3. Stability of coagulum

The issue of stability of coagulum is a part of coagulation delineation because it determines the probability of stable coagulum formation (P_{stab}). This issue is considerably less known than the adhesion of particles, described in detail in the previous chapter. Generally, coagulation can be either reversible or irreversible. Irreversible coagulation takes place when the aggregates cannot be destroyed, that is peptized. Irreversible coagulation usually takes places when particles coagulate due to salt addition, and after diluting the suspension, the coagulum does not disintegrate. The degree of coagulation reversibility depends on many factors, mainly at which minimum, the first or

the second one, coagulation has taken place, as well as what forces effect coagulation. According to Derjagin (1989) coagulation is reversible when it takes place at the second minimum. This minimum is usually shallow and the energy needed to release particles from energy well is not high. However, when coagulation takes place at the first minimum, the energy barrier of peptization V^*_{max} is considerable, because the sum of coagulation energy barrier V_{max} and the depth of energy well of the first minimum is V_I is high (Fig. 13.8). According to Derjaguin (1989) the proof of coagulation irreversibility at the first minimum is the fact that initial coagulation phases can be reversed by dilution, while aged coagulation system cannot be peptized, since a considerable part of particles has already been in the state of the first minimum coagulation. If coagulation is irreversible and coagulating particles are small, it can be assumed that P_{stab} equals 1 or approximately 1. If the particles are of a large size and coagulation takes place at the second minimum, this probability can be much lower. The issues connected with V_{max} are discussed in the work by Derjagin (1989).
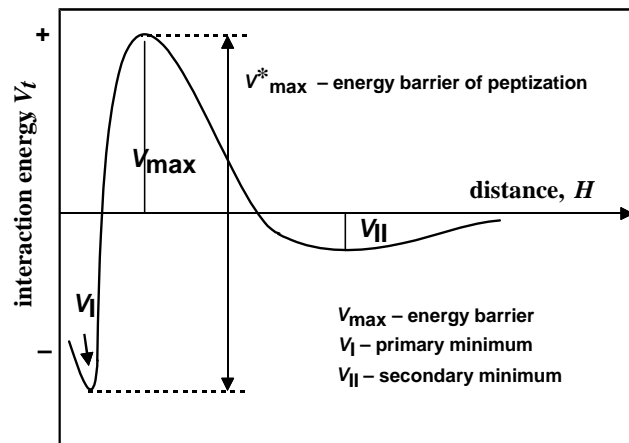
Fig. 13.8. The DLVO curve. The energy barrier of peptization is shown as V^*_{max}

13.4. The probability of particle collision in coagulation process

The probability of particle collision during coagulation depends on particle size and hydrodynamics in the suspension. The probability of coagulation of a large particle x_1 with a smaller one x_2 in a liquid medium is determined by:

$$P_z = \pi\, x_c^2 / \pi\, x_1^2 = (x_c/x_1)^2. \tag{13.64}$$

The equation results from the assumption that not all particles x_2 which meet particle x_1 on their way collide, because such a collision is guaranteed only for the particles

being within a limited collision radius x_c. The right-hand term of expression (13.64) is to the second power, because the probability of collision depends on the ratio between surface column of liquid limiting collision and the particle surface x_1.

The probability of collision, as any other probabilities, can assume the values from zero to one. In the case of rapid coagulation P_c equals 1 because each collision leads to coagulation meaning that other probabilities, including adhesion and stability, also equal 1. In other cases the probability of collision is lower than 1 and depends on the mechanism of collisions. There are only few works thoroughly describing coagulation including probability of collision. Such an equation should have a general form derived from the probability of coagulation (Eq. 13.1a):

$$-\frac{dn}{dt} = z_z n_i n_j P_z P_a P_{stab}, \qquad (13.65)$$

where:
dn/dt – coagulation rate
P_z, P_a i P_{stab} – probability of collision, adhesion, and stability, respectively
z_z – number of collisions of particle i and particle j, which concentrations are n_i and n_j, per time unit.

Chander and Hogg (1987) showed that the formula for coagulation rate is:

$$R_{ij} = -\frac{dn}{dt} = k_m n_i n_j x_i^m \left[P_m\left(\frac{x_j}{x_i}\right) \right] P_a P_{stab}. \qquad (13.66)$$

Therefore, the product of probability of collision and number of collisions is:

$$z_z P_z = k_m x_i^m \ P_m\left(\frac{x_j}{x_i}\right), \qquad (13.67)$$

where x_i and x_j denote the size of primary particle and coagulum, respectively.

The values of particular parameters for collisions caused by Brownian movements and by stirring, are presented, after Chander and Hoggs (1987) in Table 13.10.

Table 13.10. Parameters useful for calculation of number of collisions during coagulation governed by formula (13.66) (after Chander and Hogg, 1987)

Collision mechanism	m	k_m	$Pm(xj/xi)$
Brown motion	0	$\dfrac{2kT}{3\eta}$	$(2 + x_i/x_j + x_j/x_i)$
Mixing	3	$\bar{G}_s/6$	$(1 + x_j/x_i)3$

k – Boltzmann constant, T – absolute temperature, η – liquid viscosity, $\bar{G}_s$ – average shear rate.

13.5. Kinetics and hydrodynamics of coagulation

In mineral processing coagulation is performed in aqueous media containing fine particles forming suspension. The behavior of the suspension depends on the properties of particles and aqueous solution. The particles forming the suspension are subjected to gravity forces and they settle according to the equations presented in the chapter dealing with classification of particles in water. If particles are very small, they are only weekly effected by the gravity force an undergo chaotic brownian motion. Such suspensions are known as colloidal suspension, colloids or sols. The brownian motion result from the diffusion forces. They keep similar concentration of particles in the whole suspension. The size of colloidal particles is usually about one micrometer or less. When particles are of tens of micrometers, they form suspension in which both the gravity and diffusion forces operate. Diffusion of particles resulting from the brownian motion is determined by the Fick law (Laskowski, 1969):

$$j_d = -D \frac{dc}{dh} = -\frac{kT}{6\pi\eta R} \frac{dc}{dh} \,, \tag{13.68}$$

where:
D — diffusion coefficient
k — Boltzmann constant
T — absolute temperature
dc/dh — change of concentration with the position (height) of particle
η — medium viscosity
c — concentration of dispersed particles in mole/m^3 or kg /m^3,
R — particle radius
$\pi = 3.14$.

The sedimentation stream j_g resulting from gravity forces (Laskowski, 1969) is given by:

$$j_g = uc = \frac{mgc}{6\pi\eta R} \,, \tag{13.69}$$

where:
u — settling velocity of particles in a liquid medium which can be calculated using, for instance, the Stokes equation
g — gravity constant
m — real mass of particle in a medium equal to $4/3\pi R^3 (\rho_p - \rho_w)$
ρ_p — particle density
ρ_w — medium density.
Remaining symbols are the same as in Eq. 13.68).

When the particles are subjected to the forces of similar magnitude, then $j_d = j_g$, and it leads to:

$$\frac{dc}{c} = -\frac{mg}{kT}\,dh\,.\tag{13.70}$$

After integrating Eq. (13.70) the Perrin equation is obtained

$$c(h) = c\,\exp\left(-\frac{mgh}{kT}\right).\tag{13.71}$$

It results from the Perrin equation, that the particle concentration $c(h)$ at different heights in non-agitated suspensions depends on particle mass. It can also be concluded from this equation that particle concentration at different heights will be similar if the particle mass is not large.

Forming fine colloidal particles consumes considerable energy needed for creation of new surface. Such systems feature high total energy and the systems with excessive amount of energy are not stable and undergo various alterations, aiming at energy reduction. The main process taking place in suspensions to lower total energy of the system involves particle binding, i.e. coagulation. Another process is recrystallization leading to increasing size of thick particles and dissolving fine particles.

The fine particles are of higher total energy than the large ones. It is described by the Thomson (Lord Kelvin) equation (Adamson, 1963):

$$RT\ln\frac{c_R}{c_o} = \frac{2\gamma V_z}{R}\,,\tag{13.72}$$

where:
c_R – solubility of fine particles having radius R
c_o – solubility of coarse particles
γ – surface energy of material
V_z – molar volume of particle
k – Boltzmann constant
T – temperature, K.

This equation is used for determination of surface energy of the materials. During recrystallization the system diminishes its energy, since fine particles of high surface energy vanish forming larger particles of lower surface energy. This process is usually very slow and, therefore it is not taken into account when discussing stability and coagulation of the suspensions. Another, the most important process of diminishing energy of suspensions, is coagulation. This process takes time. The description of coagulation kinetics is rather complicated since clusters of two particles appear first, and then, after collision with other single particles or clusters finally form coagulum. According to the Smoluchowski theory of coagulation (Sontag, 1982), formula (13.73) can only describe the loss in the number of original particles in the initial period of coagulation.

$$-\frac{dn_1}{dt} = 8\pi D_1 r n_1^2 = k_1 n_1^2 , \tag{13.73}$$

where:

dn_1/dt – rate of disappearance of primary particles
D_1 – diffusion coefficient of primary particle
r – distance between centers of two particles being in contact ($r = 2R$)
k_1 – rate constant
n_1 – concentration of particles in suspension (number of particles in cm^3).

A considerable element of the Smoluchowski theory of coagulation is the so-called half-life period $t_{1/2}$ of suspension also known as coagulation time, within which the number of all particles in 1 cm^3 decreases to its half, which can be expressed by the relation:

$$t_{1/2} = (4\pi \, D_1 r \, n_1)^{-1}. \tag{13.74}$$

Inserting appropriate quantities to Eq. (13.74), the equation for the time of half-coagulation during a rapid coagulation is obtained:

$$t_{1/2} = \frac{3\eta}{4kTn_1} = \frac{2 \cdot 10^{11}}{n_1} \text{(seconds)}. \tag{13.75}$$

These equations have been derived following the assumption that coagulation is caused by diffusion and each collision between particles leads to coagulation. They describe rapid non-barrier coagulation in which any other forces between particles which could prevent coagulation do not exist. More details regarding the kinetics of rapid coagulation according to Smoluchowski can be found in the works and books on colloid chemistry (for instance Sonntag, 1982).

When coagulation is retarded by energy barrier V_{max}, usually caused by the presence of electrical charge on the surface, the disappearance of primary particles is determined by the equation (Sonntag, 1982):

$$-\frac{dn_1}{dt} = \frac{8\pi D_1 n_1^2}{W} , \tag{13.76}$$

where W is stability ratio (Hunter, 1987)

$$W = 2\int_{2}^{\infty} \exp\left(\frac{V_t}{kT}\right)\frac{db}{b^2} , \tag{13.77a}$$

and $b = r/R$ and $r = 2R$.

Another form of this expression is presented by Eq. (13.59). It was proved that it can be made dependent on V_{max} and assume an approximate form, which was presented in Eq. (13.60).

$$W \approx \frac{1}{2R\kappa} \exp\left(\frac{V_{\max}}{kT}\right), \qquad (13.77b)$$

where:

κ – Debye parameter

$V_{\max}$ – energy barrier.

It should be noted that for $V_{\max}=0$, $W=1$, while for $V_{\max}>0$, $W>1$. Coagulation strongly depends on the concentration of salts added to the suspension, for instance for its destabilization. Reerink and Overbeek (Hunter, 1987) showed that there exist both experimental and theoretical relation between stability factor W and salt concentration c_s

$$\log W = -k_a \log c_s + k_b, \qquad (13.78)$$

where k_a and k_b are constant.

It results from Eq. (13.78) that stability of suspensions depends on salt concentration to a certain power k_a, method of coagulation, as well salt type.

Rapid and slow coagulation, in which the driving force is diffusion, is called perikinetic coagulation. Coagulation process can be accelerated through agitation of the system. The process of coagulation supported by agitation is called true coagulation or ortocoagulation. Agitation of the suspension causes the flow of particles and their collisions, which can become a dominating driving force of the process. The flow of particles resulting from agitation is characterized by mean gradient of velocity $\overline{G}$, and its value depends on the intensity of agitation and the medium in which it takes place. Expressions for mean velocity gradient for two systems, with and without agitation, are presented in Table 13.11.

Table 13.11. Expressions for average velocity gradient for different reaction vessels (after Weber, 1972)

Vessel type	Formula
reacting	$\overline{G} = \left(\dfrac{\overline{P}}{V\eta}\right)^{1/2}$
Flowing type with baffles	$\overline{G} = \left(\dfrac{Q\rho_1 g h_f}{V\eta}\right)^{1/2} = \left(\dfrac{g h_f}{v\bar{t}}\right)^{1/2}$
Stationary with paddle stirrer	$\overline{G} = \left(\dfrac{C_D A_\mu \rho_1 v_r^3}{2V\eta}\right)^{1/2}$

$\overline{G}$ – mean velocity gradient, s^{-1}, g – gravity, $\overline{P}$ – power used for stirring the suspension, h_f – head loss in the tank, $\bar{t}$ – mean residence time of liquid in the tank, v – kinematic viscosity of suspension, V – volume of liquid in the reactor, η – viscosity of suspension, Q – flow intensity, ρ_1 – liquid density, C_D – resistance coefficient dependent on impeller shape and flow mode, A_t – cross section of the impeller blade in the plane perpendicular to the direction of movement, v_r – relative rate of blade in relation to liquid (from 0.5 to 0.75 of blade speed).

According to Chander and Hogg (1987), half-life of ortokinetic coagulation can be expressed as:

$$t_{1/2} = \sim 1,5/G_s \, \varphi, \tag{13.79}$$

where:

G_s – mean shear rate, 1/s

φ – volume share of solid particles in the suspension.

Kinetics of coagulation can be also derived from the equations describing particle flow in a unit of time. Relations used for this purpose are presented in Table 13.12.

Table 13.12. Expressions for flux (j) for different system

Flux	Formula	Source
Diffusion due to brownian motion	$j_d = \dfrac{kT}{6\pi\eta \; R} \; \dfrac{dc}{dh}$	1
Gravitational sedimentation	$j_g = \dfrac{mg}{6\pi\eta R} \; c$	1
Fast coagulation	$j_f = 8\pi DRn_1$	2
Slow coagulation	$j_s = \dfrac{8\pi Dn_1}{W}, \quad W = 2R\displaystyle\int_{2R}^{\infty} \exp\,(V_t/kT)\dfrac{dr}{r^2}$	2
Coagulation with stirring	$j_m = j\alpha = \left\{\dfrac{4}{3}(1+q)^3 n_2 G_s R_1^3\right\}\left\{\dfrac{3}{(1+q)^3}\displaystyle\int_0^{\mu^*} x_2^* z^*(x_2^*)dx_2^*\right\}$	3
Rotating disc	$\mathrm{Pe} = \left(\left[\overline{H}+1\right]F_3\overline{n}\right)^{-1}\dfrac{d}{d\overline{H}}\left\{F_1\left[\dfrac{d\overline{n}}{d\overline{H}} + \dfrac{1}{2}\left(\overline{H}+1\right)^2 \mathrm{Pe}F_2\overline{n} + \dfrac{RF_{ex}}{kT}\,\overline{n}\right]\right\}$ $\mathrm{Pe} = 2f_0R^3\omega_d^{3/2}D_\infty^{-1}\nu_k^{-1/2}$ *)	4

*) Peclet number (Pe) is the ratio of convection flow to diffusion flow

Sorce: 1 – Laskowski (1969), 2 – Hunter (1987); 3 – van de Ven (1982); 4 – Dabros and Czarnecki (1980), Dąbroś et al., (1977), Adamczyk and Dabros (1978).

c – concentration of dispersed particles, for instance in g/cm^3, R – particle radius, m – real mass of particle in a medium, η – viscosity of particles, g – gravity, k – Boltzmann constant, T – absolute temperature, f_0 – universal constant for rotation disc, ω_d – angular rate of rotation of disc, ν_k – kinematic viscosity, G_s – mean shear rate, $\pi = 3.14$, dc/dh – change of concentration with change of location h, D – diffusion coefficient, D_∞ – diffusion coefficient for particle infinitely distant from the disc surface, $\overline{n} = n_x/n_\infty$ – dimensionless concentration of particles, n_∞ – concentration of particles infinitely far from the disc surface, n_2 – concentration of particles (number of particles in unit volume), $\overline{H}$ – dimensionless distance equal to H/R (H is the distance between disc surface and the particle), F_{ex} – outer force, its component parallel to axis $\overline{H}$, j – number of particles of radius R_1 ketch per unit time by particle with radius R_1, α – effectivness of ketch by orthokinetic coagulation, $l^* = l/R_1$ (l maximum value of x_2, to which the cross section of ketch operates, $z^* = z/R_1$, where z is a function providing upper limit of cross section of the ketch, $q = l^* - 1$, r – radius of sphere around the particle where the particle can collide with other particles ($r \cong 2R$), F_1, F_2, F_3 – universal functions resulting from particle-surface interaction having a large curvature given in Dabros and Czarnecki (1980), Dabros et al., (1977), Adamczyk and Dabros (1978).

Table 13.12. also shows basic equations needed for the description of heterocoagulation of particles on flat rotating surfaces for the technique called the rotating disc method. This approach is often used for the research describing ability of the system to coagulate, heterocoagulate, as well as slime coating and carrier methods of enrichment.

Equations for kinetics of coagulation considering hydrodynamics are very complicated but only kinetic equations combined with hydrodynamics, allow to obtain full description of coagulation. According to Chander and Hogg (1987) the rate of coagulation at which particular objects (original particles of coagulum) of x_i and x_j, bind with one another to form a large coagulum, are determined by the equation:

$$-\frac{dn_1}{dt} = R_{ij} = k_{ij}\ n_i\, n_j\ E_{ij}\ ,$$
(13.80)

where:

n_i and n_j – concentration numbers for particles (or coagulas) x_i and x_j
k_{ij} – collision frequency coefficient
E_{ij} – product of probabilities of adhesion and stability (resistance) of coagulum to disrupture.

The collision frequency coefficient depends on the type of the driving force of the collision and the size of particle. It can be presented as:

$$k_{ij} = k_m x_i^m P_m\left(\frac{x_j}{x_i}\right),$$
(13.81)

where:

k_m – a constant for a given mechanism
$P_m(x_j/x_i)$ – a function of particle size ratio (power m is an integer number dependent on the mechanism of collision).

Coagulation is usually carried out in two ways: with and without agitation. The latter one involves particle collision resulting from the Brownian motion, while coagulation with agitation is due to shearing forces. The values of factors m and P_m, as well as k_m, in Eq. (13.81) have already been presented in Table 13.10. Both models of coagulation do not have simple solution (Sonntag, 1982), but it can be proved that the mean coagulum size in relation to the initial size x_o undergoes further alteration according to the relation:

$$x = x_0\left(1 + \frac{t}{t_{1/2}}\right)^{1/3}\ ,$$
(13.82)

when collisions result from the Brownian motion, and

$$x = x_o \exp(0.23 \; t/t_{1/2})$$

(13.83)

for systems with agitation. It results from these equations that agitation considerably accelerates coagulation. This can be especially observed for suspensions containing hydrophobic particles which are difficult to coagulate. This process is called the shear-coagulation (Warren, 1992).

13.6. The factors effecting coagulation

Stability of suspensions can be determined in different ways. It can be the measurement of turbidity at appropriate wavelength of light (Fig. 13.9a) (Yotsumoto and Yoon, 1993a), relative stability as turbidity quotient at the initial time and at certain time of coagulation (Fig. 13.9b) (Sadowski and Smith, 1985), the height of the turbidity line as function of time (Fig. 13.9c) (Bodman et al., 1972), the speed of particle falling based on straight-line range of coagulation shown in Fig. 13.9c (Fig. 13.9d) (Bodman et al., 1972), solid concentration at certain height or part of liquid (Fig. 13.9e) (Pugh, 1974), and stability ratio *W* being a quotient of maximum settling rate under certain condition and settling rate when the settling is maximum (Fig. 13.9f) (Wiese and Healy, 1975), as well as other methods.

The stability of suspensions depends on their electrical potential in the Stern layer or a slipping plane, as well as on dispersion or structural interactions. Stability of suspensions is easy to regulate with pH regulators and with soluble salts which strongly effect the zeta potential of particles.

It is shown in Fig. 13.9 a, b, e, and f that suspensions are not stable close to their iep and pzc points. This results from the fact that their zeta potential is at iep equal zero and there is no electrostatic repulsion between particles. On the other hand, the increase in suspension stability at high values of zeta potential results from the appearance of energy barrier which, after Yotsumoto and Yoon (1993a), has been shown in Fig. 13.10.

Stability of two- and multi-mineral suspensions depends on the parameters presented in Fig. 13.9 and, first of all, on the sign of zeta potential. If the sign of zeta potential of both kinds of particles is opposite, a strong attraction of particles leads to a non-barrier heterocoagulation.

If coagulation is carried out by the change of pH or addition of potential-determining ions (Fig. 13.9), a rapid coagulation takes place not only at iep, but also in its vicinity. This results from the fact that electrostatic repelling of particles at low Stern's potentials or zeta potentials are compensated by dispersion forces. Generally, coagulation takes place when the zeta potential of particles is lower than 25 mV and accurate value of the potential depends on the Hamaker constant of particle and the magnitude of structural forces.
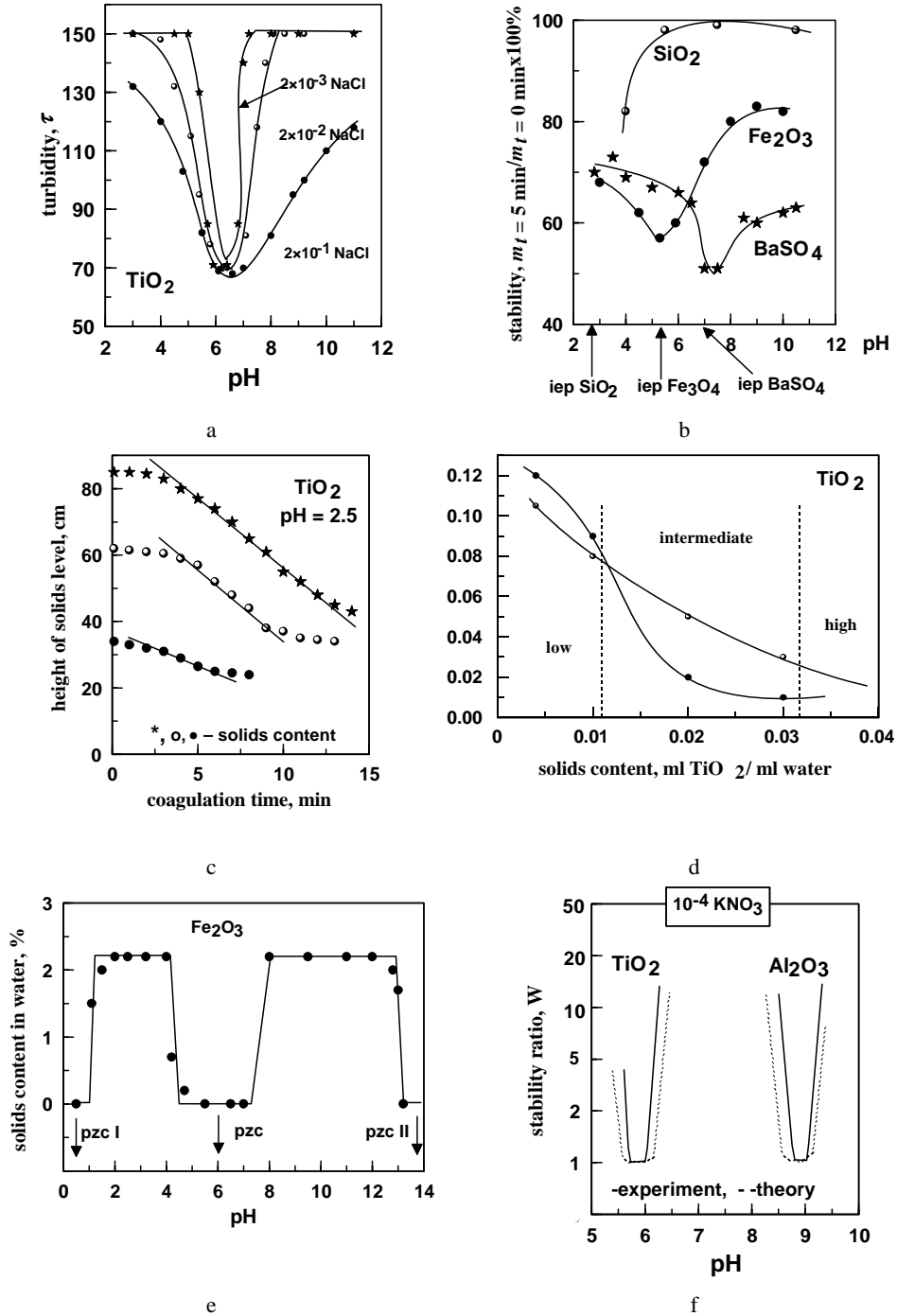
Fig. 13.9. Methods of suspension stability measurements and presentation

Consideration by Derjagin (1989), based on the classical theory DLVO, showed that the conditions under which coagulation, caused by potential-generating ions, takes place are determined by the relation:

$$\frac{\psi_s^2}{A_{131}\kappa_c} = \text{const} ,$$ (13.84)

where:

κ – the Debye parameter for a given salt concentration

ψ_s –the Stern or zeta potential, also dependent on salt concentration.

The relationship agrees with the empirical formula of Eilers–Korff

$$\frac{\zeta_c^2}{\kappa_c} = \text{const} ,$$ (13.85)

in which ζ_c is the zeta potential for a given salt concentration.
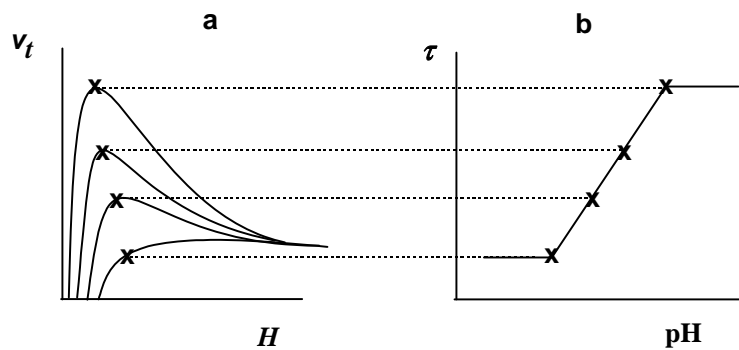
Fig. 13.10. Comparison of the magnitude of energy barrier of interaction of particles V_t (a) with suspension stability (b); τ stands for turbidity of titanium oxide (rutile) suspension, determined experimentally (after Yotsumoto and Yoon, 1993a)

If coagulation is caused by electrolyte (salt) addition, then the ksk (critical concentration of coagulation), which indicates the salt concentration necessary for coagulation, depends on electrical charge of the salt ions. According to Derjagin (1989) and DLVO theory for water at 25^0C at high surface potentials of particles, the ksk amounts (Hunter, 1989):

$$\text{ksk (mol/dm}^3) = \frac{87 \cdot 10^{-40}}{z^6 A_{131}^2} ,$$ (13.86)

where z is a positive number 1, 2, 3… and means counter ion valance which mainly contributes to the compensation of the edl charge. For positively charged surfaces it is an anion, while a cation is for a negatively charged surface. In Eq. (13.86) the

Hamaker constant A_{131} is expressed in joules. This dependence is also in agreement with the empirical equation described by Hardy and Schultz, which says that the ksk is proportional to minus sixth power of counter ion valance and it does not depend on surface potential, i.e.:

$$(ksk)_{z=1} : (ksk)_{z=2} : (ksk)_{z=3} = 1^6 : \left(\frac{1}{2}\right)^6 : \left(\frac{1}{3}\right)^6 = 1 : 0.016 : 0.0014 \tag{13.87}$$

This rule is fulfilled for instance for As_2S_3 and FeOOH colloids (Sonntag, 1982), but it does not function for any other systems. Therefore, a new formula for an accurate description of concentration and valence of electrolyte ions on suspension ksk has still to be worked out. Recently, the Hardy-Schultz relation has been derived following theoretic considerations and it also takes into account the ions of different valence (Hus and Kuo, 1995). According to Glazman and Barboj (Laskowski, 1969) coagulation takes place when the following condition is fulfilled:

$$\psi_s z = \text{const} , \tag{13.88}$$

while according to Hunter (1987) who used the classical DLVO theory, it is:

$$ksk = f\left(\frac{\psi_0^4}{z^2}\right), \tag{13.89}$$

where:
z – valence of counter ion
ψ_0 – surface potential.

Taking the above discussion into account it can be stated that the issue of accurate determination of the conditions of coagulation is complicated and to obtain a complete story it is necessary to incorporate structural forces, as well as to consider the fact that the potential zeta is used for calculation instead of the surface or Stern potentials. Indisputable is the fact that a rapid coagulation always takes place at the iep point and at its vicinity.

Even more difficult is the delineation of heterocoagulation conditions which involves different particles, since both dispersion forces and electrical ones can be positive and negative. When the Hamaker constant for the interaction of different particles in water is positive and the signs of the surface potential are opposite, then a non-barrier heterocoagulation occurs. However, when the Hamaker constant is positive while the potentials are of the same sign, heterocoagulation, under the influence of pH or other potential determining ions, will be governed by the equation (Derjagin, 1989):

$$\frac{\psi_1 \psi_2}{A_{132} \kappa_c} = \text{const} . \tag{13.90}$$

When dispersion forces are positive (repelling) and surface potentials are of the same sign, the system is usually stable. There exist, however, regions of electrolyte concentrations where the above rule does not apply. If the potentials of the same sign are considerably different as to their absolute values and when the ionic force is of a low value, the energy barrier can appear at a long distance between particles, thus the dispersion forces will not effect the interactions and the repelling forces become proportional to the lower potential. When the distances are short, an energy minimum can appear, which indicates attraction (Derjagin, 1984) and the force acting on a unit surface area is determined by the equation:

$$\Pi_{\min} \propto (\psi_1 - \psi_2)^6 / (A_{131})^2. \tag{13.91}$$

13.7. The effect of other substances on the stability of suspensions

The stability of suspensions is effected not only by potential-determining ions and electrolytes in the form of soluble salts, but also other factors, like hydrolyzing cations, solids precipitating from the solution (precipitates), surfactants and polymers (Fig. 13.11).
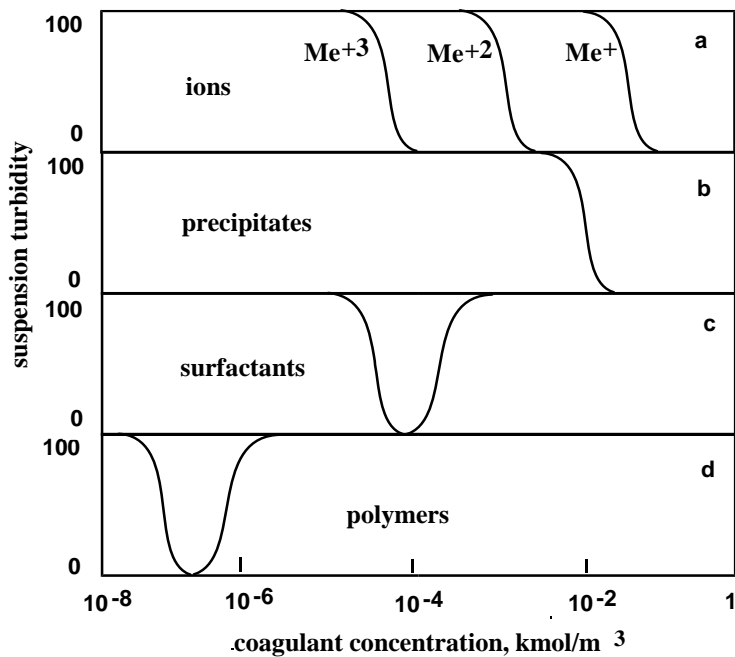
Fig. 13.11. Influence of concentration of various species on coagulation
(after Weber, 1972)

Part a of the figure shows the already discussed rule stating that coagulation of a negatively charged surface due to multivalent cations takes place at considerably lower concentrations than that for monovalent cations. There are two mechanisms of their action. The first one involves lowering the zeta potential as a result of diminishing edl thickness, while another is caused by a specific sorption of ions and their hydrolyzed form.

Many multivalent cations of metals in aqueous solutions undergo reaction with water, i.e. hydrolysis, forming hydrocomplexes. Hydrolysis of multivalent cation becomes considerable when the pH of the solution is regulated by adding, for instance, trivalent iron ions (Fe(III)) forming Fe^{3+} ions and hydrolyzed ions, i.e. hydrocomplexes such as $Fe(OH)^{2+}$, $Fe(OH)_2^+$ and $Fe(OH)_3^0$.

The concentration of particular hydrocomplexes depends on the quantity of added salt of multivalent cation and pH of the solution. The Ca(II) ions behave similarly and their distribution is presented in Fig. 13.12b. The formed hydrocomplexes undergo strong specific adsorption on mineral surfaces. According to Fuerstenau and Han (1988) especially strong sorptive properties are offered by monohydroxycomplexes $Me(OH)_n^+$, (e.g. $Ca(OH)^+$, $Pb(OH)^+$, $Fe(OH)_2^+$ for Fe(III), $Fe(OH)^+$ for Fe(II)). A maximum sorption of a monohydroxycomplex on solids takes place at pH, when there is maximum concentration of these ions in the solution (Fig. 13.12a).

It is believed that the sorption of monohydroxycomplexes of hydrolyzing metal ions on mineral surfaces follows the reaction of exchange:

$$\diagup\hspace{-0.4em}\diagdown\hspace{-1.4em}\Big/ M\text{-}O\text{-}H \;+\; HOM^+ \;\rightarrow\; \diagup\hspace{-0.4em}\diagdown\hspace{-1.4em}\Big/ M\text{-}O\,M^+ + H_2O \qquad (13.92)$$

or through hydrogen bounding

$$\diagup\hspace{-0.4em}\diagdown\hspace{-1.4em}\Big/ M\text{-}O\text{-}H \;+\; HOM^+ \;\rightarrow\; \diagup\hspace{-0.4em}\diagdown\hspace{-1.4em}\Big/ M\text{-}OH \cdots \underset{H}{O}\text{-}M^+ \qquad (13.93)$$
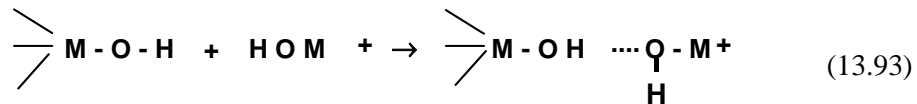
The specific sorption of the hydroxycomplexes of metals causes that the surface potential of negatively charged particles and accompanying potential zeta, become altered towards positive values. The higher concentration of metal monohydroxycomplex, the more considerable alteration of zeta potential, which, as it is shown in Fig. 13.13, is connected with the pH of the solution. At a high sorption, the zeta potential of particles becomes identical with zeta potential of hydrolyzing metal ions and the maximum value of the electrokinetic potential is recorded for pH at which monohydroxycomplex concentration is the highest. At slightly lower pH there exists an additional isoelectric point, called the iep of reversion.

The suspension can be destabilized by adding other substances or precipitation of particles from the solution. Then, heterocoagulation takes place (Fig. 13.11b). Also

surface active substances can be used for coagulation of suspensions (Fig. 13.11c). Their applicability depends on the kind of surfactant. The best are those undergoing significant adsorption on particle surface resulting in the reduction of the zeta potential of particle. Some surfactants additionally cause strong hydrophobization of particles, and the enhancement of coagulation through hydrophobic interactions. However, a too high concentration of a surfactant leads to coagulum disintegration. The phenomenon takes place due to adsorption of a second layer of the surfactant in such a way that its polar part extends into the solution, which provides particle surfaces with high electrical charge, and thus, also with stability.
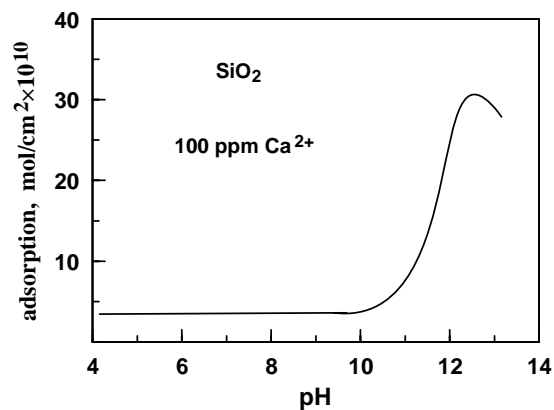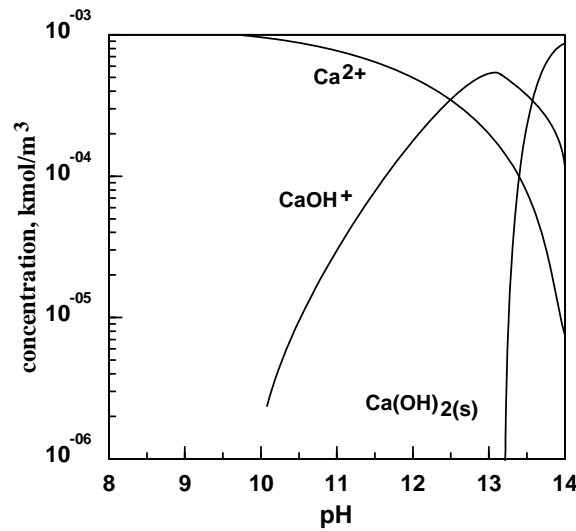
Fig. 13.12. Adsorption of calcium ions on quartz as a function of pH of solution at a total concentration of calcium ions equal to 100 ppm (a), distribution diagram dependent on solution pH (b). Total concentration of $Ca^{2+} = 10^{-3}$ kmol/m^3 (after Fuerstenau and Hana, 1988)

The stability of the suspension can be described and stability factor W and can be calculated in the presence of surfactants using classical coagulation theories. In such a case it is necessary to modify the expressions for the energy of particular interactions, taking into account that the surfactants have been adsorbed on particles. According to Schick (1987) for nonionic surfactants the following relations are valid:

$$V_s = \frac{\pi N_a c_f^2 Z^2 kT}{3\overline{V}\rho_a^2}(0.5 - \chi_F)\,[3(R+\delta) - 0.5Z]\,, \qquad (13.94)$$

$$V_R = 32\pi\varepsilon\varepsilon_0\left(\frac{kT}{ze}\right)^2 (R+\delta)\psi^2 \exp-\kappa H\,, \qquad (13.95)$$

$$V_A = -1/12(A\,...),\qquad (13.96)$$

where:

V_A – a complex function dependent on combination of the Hamaker constant for particle, particles with adsorbed layer and distance between particles

$\overline{V}$ – partial molar volume of water

N_a – the Avogadro number

ρ_a – density of adsorbed layer

δ – thickness of adsorbed layer

c_f – surfactant concentration in adsorbed layer

Z – distance of penetration of adsorbed on particles surfactants

χ_F – the Flory–Huggins parameter of interactions of polymer–solvent

κ – the Debye radius

ε – dielectric constant

ε_0 – dielectric permeability of vacuum

ψ – electrical potential

H – distance

R – particle radius.

Suspensions can be also destabilized using polymers (Fig. 13.11d) of long enough chains, i.e. high molecular mass of one million or more. Such polymers cause coagulation which is called flocculation. It should be noticed, however, that too high concentration of the polymer can lead to restabilization of the suspension as a result of very high electrical charge on particle surface, originating from ionic functional groups of the polymer.

Coagulation and heterocoagulation processes are very important from a practical point of view. But they can be both useful and harmful. Slime coating relying on adhesion of fine gangue particles to useful ore particles due to the forces described by DLVO theory is an example of harmful coagulation. Slime coating causes a decrease

in the selectivity of separation. For instance, hydrophobic surfaces can be rendered hydrophilic as a result of a contact with clay minerals. Such a phenomenon can be also observed in the flotation of coal or metal sulfides. In some cases slime coating is useful and it is used in the so-called carrier methods of enrichment. They depend on controlled adhesion of useful particles to larger particles of other mineral. Sometimes coarse particles are added into the ore, then coarse particles carrying fine particles on their surface are separated.
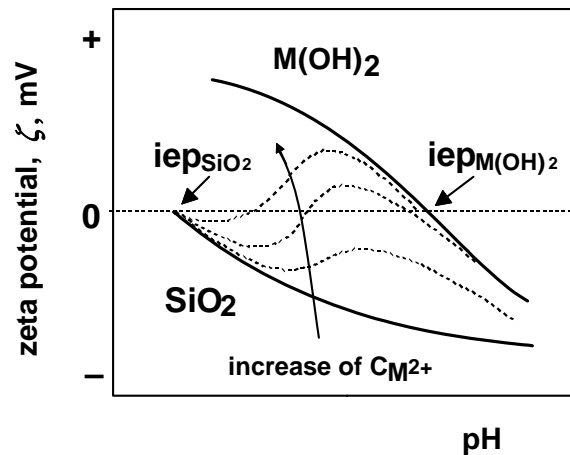
Fig. 13.13. Zeta potential of quartz as a function of pH and concentration of bivalent hydrolyzing cation (James and Healy, 1972)

Coagulation and peptization are also accompanied by other processes or effects known as syneresis, coacervation, ticsothropy, creaming and gelling.

Coacervation is a phenomenon analogical to coagulation but taking place in polymeric colloidal suspensions treated with salts. Such a behaviour can be seen in protein solutions. Syneresis is a phenomenon of increasing compactness of structures of coagulating material. Coagulum is formed due to coagulation and with time coagula become more compact as a result of ordering and increasing number of contact points, which finally leads to higher strength of aggregates. Leaving them alone for a long time can create an unified particle. Transformation of colloid silica into quartz (Sonntag, 1982) following the pattern: silica → silica gel → opal → chalcedone → quartz is an example of syneresis. The term sol has been less and less frequently used to refer to colloid suspension of solids in water. The term gel denotes a colloid system which underwent coagulation forming a strong net–like structure which leads to its characteristic jelly form. The most frequent subject to gelling are organic colloids (starch), less often inorganic ones (silica). Gel–like form of a colloid results from anisotropic properties of particles, which causes formation of three–dimensional structures. With time, the gel undergo consolidation, i.e. synersis. Micelle - the term used previously to describe a particle with its electrical double layer structure around the

colloid particle while presently it is used for description of association of surfactant ions and particles. Coalescence – is a phenomenon of aggregation taking place between small objects in colloidal systems. Is has a broader notion than coagulation, since it involves not only solids but also liquids. Coalescence of oil emulsion leads to separation of phases into oil and, separately, water phases.

13.8. Selective coagulation

When zeta potential of two minerals are of the same sign, the suspension can be either stable or coagulation of one of the components can take place. Such a behavior of particles is a base for selective coagulation. Selective coagulation in the quartz–hematite system after Pugh (1974, 1992) is shown in Fig. (13.14).
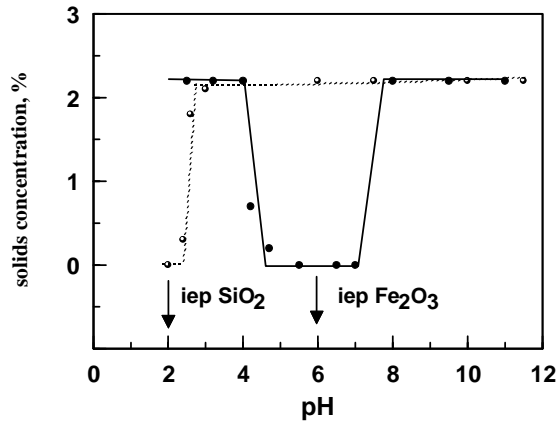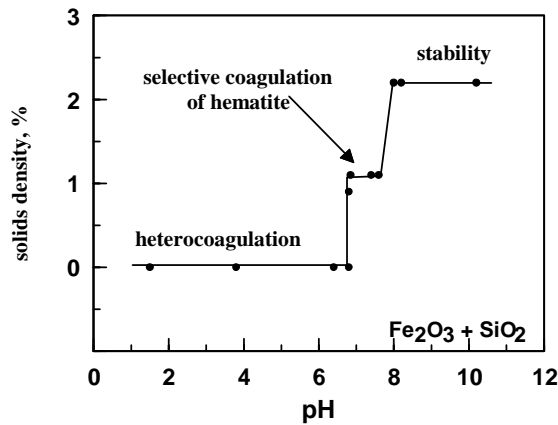
Fig. 13.14. Stability of aqueous suspensions of quartz and separately hematite as a function of pH of solution (a) and the range of selective coagulation of hematite (b). After Pugh 1974 and 1992

Within pH range of 1-7 the suspension of quartz and hematite is unstable and hetero-coagulates due to negatively charged quartz particles and positively charged hematite particles. In a weak alkaline solution, at pH about 7.5, the hematite particles are slight negatively charged and they are stabile. This situation provides the conditions for selective coagulation of hematite. Above pH 8.5 both minerals are highly negatively charged and stable.

Selective coagulation can be also carried out in the quartz–rutile (Pugh 1974, 1992), and coal–ash forming minerals systems (Yoon et al., 1991). In the case of coal, coagulation takes place within a narrow pH range about 10 (Fig. 13.15).
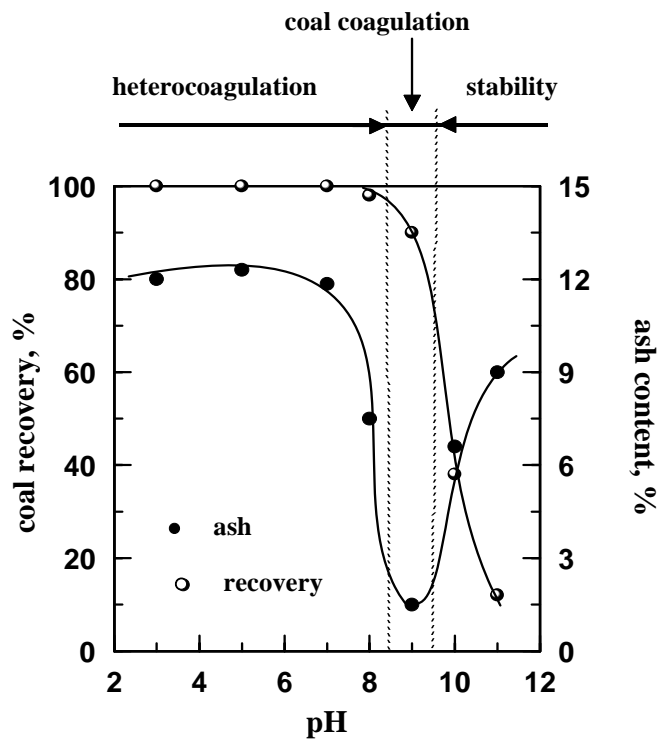
Fig. 13.15. Range of pH stability, coal coagulation, and its heterocoagulation
(after Yoon et al., 1991)

13.9. The structure of coagula

Coagula are formed during coagulation. Characteristic structures of coagula appear when the surface of particle is made of different crystallographic planes of different surface properties. For example they can form the so called "house of cards" structure (Fig. 13.16). Among possible structures, the "face–to–face", "face –to-edge" and

"edge-to-edge" formations can be distinguished. They represent the first order structures which can, like bricks, be arranged as complicated form of a second order. Van Olphen (1963) lists the following structures: edge-to-plane coagulated and aggregated, plane-to-plane face coagulated but not aggregated.

The structure of coagula is complicated and there is a lack of accurate definitions for their description. A list of different formulas used for the description of particle shape can be found, for instance in the work by Sztaba (1964).
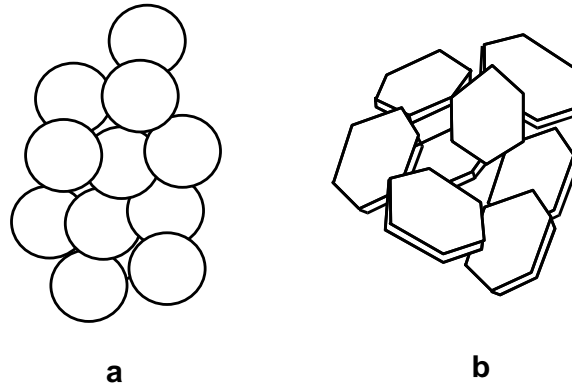
Fig. 13.16. Structure of coagula. Random structure of spherical particles (a)
and house-of-cards structure for flat particles (b) (Hunter, 1993

Czarnecki (1986) applied some of them to determine the particle shape factor ζ_k

$$\xi_k = \frac{1}{\bar{a}\pi\sqrt{2}} \sum_{i=1}^{3} (a_i - \bar{a})^2 \, \text{sign} \sum_{i=1}^{3} (a_i - \bar{a})^3 \quad , \qquad (13.97)$$

where:
a_1, a_2 and a_3 – inertia moment of particle in relation to its main axis of rotation
$\bar{a} = (a_1 + a_2 + a_3)/3$.

The first square element of the equation represents deviation from spherical shape, while the second one, which is to the third power, enables distinguishing between oblong and oblate forms. Factor ζ_k defined in this way bears the following properties: for spherical particles $\zeta_k=0$, for rods $\zeta_k>0$, while for disc coagules $\zeta_k<0$. The term sign in Eq. 13.97 determines the sign of the function, since sign $(y_m)=y_m / |y_m| (=\pm 1)$.

The shape of coagula can be also described with the use of fractals. Fractal geometry, introduced by Mandelbrot (1977, 1982), describes objects which are of the same appearance at different magnifications. Details regarding fractals can be found in many works, including the article by Nowak (1992). A fractal character, repeated at different levels of structure organization, can be assigned to particle aggregates.

The parameter to describe coagula is fractal dimension d which is the measure of coagulum density or the degree of particle binding in coagulum. This fractal dimension of a coagulum is expressed by the relation (Hutner, 1993)

$$d = \log x_1/\log x_2, \tag{13.98}$$

where:

x_1 – quotient of coagulum mass increase

x_2 – quotient of coagulum size (length) increase.

Formula (13.98) can be also written in another form (Feder, 1988; 1988; Koylu et al. 1995, Adachi et al., 1990), e.g.

$$n_k = k_k (R_k/R)^d, \tag{13.99}$$

where:

n_k – number or primary particles in coagulum

R_k – gyration radius of coagulum

R – radius of individual particle in coagulum

k_k – dimensionless coefficient.

According to Hunter (1993), fractal dimension of a coagulum d can be estimated with the use of the measurement of intensity of light diffused by coagulum, since:

$$\ln I = b_\lambda Q_r^{-d} = b \, (4\pi n_p \sin (\theta/2)/\lambda)^{-d}, \tag{13.100}$$

where:

b_λ – constant

Q – vector of light scattering

θ_λ – angle of scattering

λ – wavelength

n_p – number of particles.

Equation (13.100) is valid for Q_r values within the range $R \ll Q_r^{-1} \ll R_k$, where R is a particle radius, while R_k is an aggregate radius. Therefore, this equation becomes useful as soon as noticeable coagulation takes place and a plot of $\ln I$ as a function of Q_r becomes linear with the slope equal to d.

Regular flat (two-dimensional) particle packing in a coagulum would provide fractal dimension 2, while regular three-dimensional fractal dimension 3. Actual value of fractal dimension of spherical coagulum amounts from 1.7 (Koylu, 1995) to 2.2 (Adachi, 1990) i.e. about 2, which indicates their relatively loose packing.

Literature

Adachi Y., Ooi S., 1990. *Geometrical structure of a floc*, J. Colloid Interface Sci., 135(2), 374–384.

Adamczyk Z., Dabros T., 1978. *On the convective diffusion of particles under electrical double – layer forces*, Colloid Interface Sci., 64 (3), 580–583.

Adamson A., 1963. *Chemia fizyczna powierzchni*, Warszawa, PWN.

Bodman S., W., Shah Y.T., Skriba M., 1972. *Settling of flocculated suspension of titanium dioxide and alum mud in water*, Ind. Eng. Chem. Process Des. Develop., 11 (1).

Cerda C., Non-Chhom K., 1989. *The use of sinusoidal streaming flow measurements to determine the electrokinetic properties of porous media*, Colloid and Surfaces, 35, 7–15.

Chander S., Hogg R., 1987. *Sedimentation and consolidation in destabilized suspensions*, in: *Flocculation in Biotechnology and Separation Systems*, Y.A. Attia (ed.), Elsevier, Amsterdam, 279–296.

CRC, 1986/87. *Handbook of chemistry and physics*, CRC Press, Boca Raton.

CRC, 1997/98. *Handbook of chemistry and physics*, CRC Press, Boca Raton.

Czarnecki J., 1986. *The effect of surface inhomogeneities on the interactions in colloid systems and colloid stability*, Advances in Colloid and Interface Science, 24, 283–319.

Dabros T., Adamczyk Z., Czarnecki J., 1977. *Transport of particles to a rotating disk surfcae under an external force field*, Colloid Interface Sci., 62(3), 529–541.

Dabros T., Czarnecki J., 1980. *Wpływ oddziaływań elektrycznych na kinetykę heterokoagulacji*, Fizykochemiczne Problemy Mineralurgii, 12, 47–55.

Derjagin B.V., 1989. *Theory of stability of colloids and thin films*, Consultants Bureau, New York.

Derjagin B.V., Churaev N.V., 1989. *The current state of the theory of long-range surface forces*, Colloids and Surfaces, 41, 223–237.

Derjagin B.V., Landau L., 1941. *Theory of the stability of strongly charged lyophobic sols and of the adhesion of strongly charged particles in solutions of electrolytes*, Acta Physicochim., USSR, 14, 633–662.

Drzymala J., 1994. *Hydrophobicity and collectorless flotation of inorganic materials*, Advances in Colloid and Interface Sci., 50, 143–185.

Drzymala J., 1999. *Characterization of materials by Hallimond tube flotation*, Part 3. *Maximum size of floating and interacting particles*, Int. J. Mineral Processing 55, 203–218.

Drzymala J., Sadowski J., Hołysz L., Chibowski E., 1999. *Ice/water interface: zeta potential point of zero charge, and hydrophobicity*, J. Colloid Interface Sci., 220, 229–234.

Drzymala J., Laskowski J., 1980. *Pomiary elektrokinetyczne w mineralurgii*, Fizykochemiczne Problemy Mineralurgii, 12 (35–45).

Duran J.D.G., Guindo M.C., Delgado A.V., Gonzalez-Caballero F., 1995. *Stability of monodisperse zinc sulfide colloidal dispersions*, Langmuir, 11, 3648–3655.

Działoszyński I.E., Lifszyc E.M., Pitajewski L.P., 1959. *Teoria sił van der Waalsa*, Žurnal Eksp. Teor. Fiz., 37, No. 1, 229–241.

Ebaadi S.H., 1981. *Van der Waals inetractions beween surfactant-coated and bare colloidal particles*, Colloids Surfaces, 2, 155–168.

Feder J., 1988. *Fractals*, Chap. 2, Plenum Press, New York 1988.

Friberg S.E., , 1991. *Emulsion Stability*, in: *Emulsions – a fundamental and practical approach*, J. Sjoblom (ed.), NATO Series (C), Vol. 363, Kluwer Academic Pub., Dordrecht, 1–24.

Fuerstenau M.C., Han K.N., 1988. *Activators*, in: *Reagents in Mineral Technology*, Surfactant Science Series, Vol. 27, P. Somasundaran i B.M. Moudgil (eds.), Dekker, 411–428.

Gray S.R., Langberg D.E., Gray N.B., 1994. *Fine mineral recovery with hydrophobic magnetite*, Int. Journal of Mineral Processing, 41, 183–200.

Gregory J., 1969. *The calculation of Hamaker constants*, Advances in Colloid and Interface Sci., 2, 396–417.

Hogg T., Healy T.W., Fuerstenau D.W., 1966. *Mutual coagulation of colloidal dispersions*, Trans. Faraday Soc., 62, 1638–1651.

Holysz L., 1998. *Surface free energy components of silica gel determined by thin layer wicking method for different layer thicknesses of gel*, J. Mat. Sci., 33, 445–452.

Holysz L., Chibowski E., 1997. *Surface free energy components of barite: effect of sodium dodecyl sulfate*, 9th International Conference on Surface and Colloid Science, Sofia, Bulgaria, B-5, 145–146.

Hough D.B., White L.R., 1980. *The calculation of Hamaker constant from Lifshitz theory with application to wetting phenomena*, Advances in Colloid and Interface Sci. 14, 3–41.

Hsu J.-P., Kuo Y.-C., 1995. *An extension of the Schulze–Hardy rule to asymmetric electrolytes*, J. Colloid Interface Sci., 171, 254–255.

Hunter R.J., 1987. *Foundations of Colloid Science*, Vol. 1, Clarendon Press, Oxford.

Hunter R.J., 1989. *Foundations of Colloid Science*, Vol. 2, Clarendon Press, Oxford.

Hunter R.J., 1993. *Introduction to Modern Colloid Science*, Oxford University Press, Oxford.

Israelachvili J., 1985. *Intermolecular and surface forces*, Academic Press, London.

James R.O., Healy J., 1972. *Adsorption of hydrolyzable metal ions at the oxide-water interface*, Part II, Colloid Interface Sci., 40, 53–64.

Koylu U.O., Xing Y., Rosner D.E., 1995. *Fractal morfology analysis of combustion – generated aggregate using angular light scattering and electron microscope images*, Langmuir, 11, 4848–4854.

Krouyt H.R., 1952. *Colloid Science*, Vol. 1, Elsevier, Amsterdam.

Krupp H., Schnabel W., Walter G., 1972. *The Lifshitz–van der Waals constant*, J. Colloid Interface Sci., 39, 421–423.

Laskowski J., 1969. *Chemia fizyczna w procesach mechanicznej przeróbki kopalin*, Slask, Katowice.

Li C., Somasundaran P., 1992. *Reversal of bubbles charge in multivalent inorganic salt solutions – effect of aluminium*, J. Colloid Interface Sci., 148, 587–591.

Lifszyc E.M., 1954. *The effect of temperature on the molecular forces between condensed bodies*, Doklady Akademii Nauk ZSRR, 97(4), 643–646 (w jęz. rosyjskim).

Lifszyc E.M., 1955. *The theory of molecular attraction forces between solid bodies*, Žurnal Eksperim. Teor. Fiz., 29, No. 1, 94–110.

Lins F.F., Middea A., Adamian R., 1995. *Hamaker constants of hydrophobic materials*, Proc. 1st UBC–McGill Bi-annual International Symposium on Fundamentals of mineral processing, Vacouver, B.C., 61–75.

Lu S. et al., 1991. *Hydrophobic interaction in flocculation and flotation*, Colloid and Surfaces, 57, Part 1: Lu S., Song S., s. 49–60; Part 2: Dai Z., Lu S., s. 61–72; Part 3: Lu S., 73–81.

Mandelbrot B.B., 1977. *Fractals: forms, chance, and dimension*, W.H. Freeman, San Francisco.

Mandelbrot B.B., 1982. *The fractal geometry of nature W.H. Freeman*, San Francisco.

Mao, L., Yoon R.H., 1997. *Predicting flotation rates using a rate equation derived from first principles*, Int. J. Mineral Processing, 51, 171–181

Ney P., 1973. *Zeta Potentiale und Flotierbarkeit von Mineralen*, Springer-Verlag, Wien–New York.

Nowak P., 1992. *Teoria fraktali – nowy sposób opisu obiektów geometrycznie nieregularnych*, Fizykochemiczne Problemy Mineralurgii, 25, 13–24.

Pashley R.M., 1977. *The van der Waals interaction for liquid water – a comparison of the oscillation model approximation and use of the Kramers-Kroning equation with full spectral data*, J. Colloid Interface Sci., 62, 344–347.

Prieve D.C., Ruckenstein E., 1980. *Role of surface chemistry in primary and secondary coagulation and heterocoagulation*, J. Colloid Interface Sci., 73 (2) 539–555.

Pugh R.J., 1974. *Selective coagulation in quartz–hematite and quartz–rutile suspensions*, Colloids and Polymer Sci., 252, 400–406.

Pugh R.J., 1992. *Selective coagulation of colloidal particles*, in: *Colloid Chemistry in Mineral Processing*, J.S. Laskowski i J. Ralston (eds.), Developments in Mineral Processing Vol. 12, Elsevier, Amsterdam, Chap. 8, 243–275.

Ross S., Morrison I.D., 1988. *Colloidal Systems and Interfaces*, Wiley, New York.

Russel W.B., Saville D.A., Schowalter W.R., 1989. *Colloidal Dispersions*, University Press, Cambridge.

Sadowski Z., 1998. Unpublished data.

Sadowski Z., Smith R.W., 1985. *Stability of mineral suspensions in the absence and presence of collectors, dispersants and flocculants*, Minerals and Metallurgical Processing, 217–222.

Schenkel J.H., Kitchener J.A., 1960. *Test of the Derjaguin-Verwey-Overbeek theory with colloidal suspension*, Trans. Faraday Soc., 56, 161–173.

Schick M.J., 1987. *Noniomic surfactants*, Physical Chemistry, Dekker, New York.

Shergold H.L, Hartley C.J., 1982. *The surface chemistry of diamond*, Int. J. Miner. Process., 9, 219–233.

Sjollema J., Bussecher H.J., 1990. *Deposition of polystyrene particles in a parallel plate flow cell.*, Colloids and Surfaces, 47, 323–336.

Skvarla J., Kmet S., 1991. *Influence of wettability on the aggregation of fine minerals*, Int. J. Min. Proces. 32,111–131.

Smith A.L., 1976. *Electrokinetics of the oxide–solution interface*, J. Colloid Interface Sci., 55 (3), 525–530.

Sonntag H., 1982. *Koloidy*, PWN, Warszawa.

Stachurski J., Michałek M., 1996. *The effect of the zeta potential on the stability of a non-polar oil-in-water emulsion*, J. Colloid Interface Sci., 184, 433–436.

Sztaba K., 1964. *Niektóre własności geometryczne zbiorów ziarn mineralnych*, Zeszyty Naukowe AGH nr 85, Seria Rozprawy, z. 25, Kraków.

Van de Ven T.G.M., 1982. *Interactions between colloidal particles in simple shear flow*, Advances in Colloid and Interface Sci., 17, 105–127.

Van Olphen H., 1963. *An introduction to clay colloid chemistry*, Wiley, New York.

Van Oss C.J., Giese R.F., Costanzo P.M., 1990. *DLVO and non-DLVO interactions in hectorite*, Clays and Clay Minerals, 38 (2), 151–159.

Van Oss C.J., Good R.J., Chaudhury M.K., 1988. *Additive and nonadditive surface tension components and the interpretation of contact angles*, Langmuir, 4, 884–891.

Verwey E.J., Overbeek J.Th.G., 1948. *Theory of the stability of lyophobic colloids*, Elsevier, Amsterdam.

Visser J., 1972. *On Hmaker constants; a comparison between Hamker constants and Lifshitz–Van der Waals constants*, Adv. Colloid Interface Sci., 3, 331–363.

Warren L., Pugh R.J., 1992. *Shear-flocculation*, in: *Colloid Chemistry in Mineral Processing*, J.S. Laskowski i J. Ralston (eds.), Developments in Mineral Processing, Vol. 12, Elsevier, Amsterdam, Chap. 8, 243–275.

Weber J.W. Jr., 1972. *Physicochemical Processes for water quality control*, Wiley, New York, s. 69.

Wiese G.R., Healy T.W., 1975. *Coagulation and electrokinetic behavior of TiO$_2$ and Al$_2$O$_3$ colloid dispersions*, Journal of Colloid Interface Sci., 51 (3), 1975.

Wiese G.R., James R.O., Yates D.E., Healy T.W., 1976. *Electrochemistry of the colloid–water interface*, in: *Electrochemistry*, J. O'M. Bockris (ed.), M.T.P. Int. Rev. Sci., Physical Chem., Series 2, Vol. 6, Butterworths, London, 53–102.

Wroblewski A.K., Zakrzewski J.A., 1984. *Wstęp do fizyki*, t. 1, PWN, Warszawa.

Yoon R.H., Honaker R.Q., Luttrell G.H., 1991. *Application of selective hydrophobic coagulation process for upgrading carbonaceous material*, Fizykochemiczne Problemy Mineralurgii, 24, 33–45.

Yoon R.H., Luttrell G.H., 1998. Private information.

Yotsumoto H., Yoon R-H., 1993a. *Application of extended DLVO theory*, I. *Stability of rutile suspensions*, J. Colloid Interface Sci., 157, 426–433.

Yotsumoto H., Yoon R.-H., 1993b. *Application of extended DLVO theory*, II. *Stability of silica suspensions*, J. Colloid Interface Sci.

14. Flocculation

14.1. Introduction

Flocculation is the process in which fine particles, dispersed in water or other liquid, aggregate under the influence of binding compounds called flocculants (Fig. 14.1). A flocculant molecule has to be long and elastic in order to bind particles into aggregates, after adsorption of different parts of a flocculant chain simultaneously on several particles. Newly formed aggregates of fine particles, called flocs, have considerably larger size than initial particles, so due to gravity forces, they settle much faster than single particles, as the fines are the subject to brownian forces. Flocculants are polymers of chain structure, water soluble and their molecular mass in g/mole is about one million. Flocculants are used to accelerate particle settling, improve filtration, enrich ore and raw materials (selective flocculation) and also as modifiers in flotation.
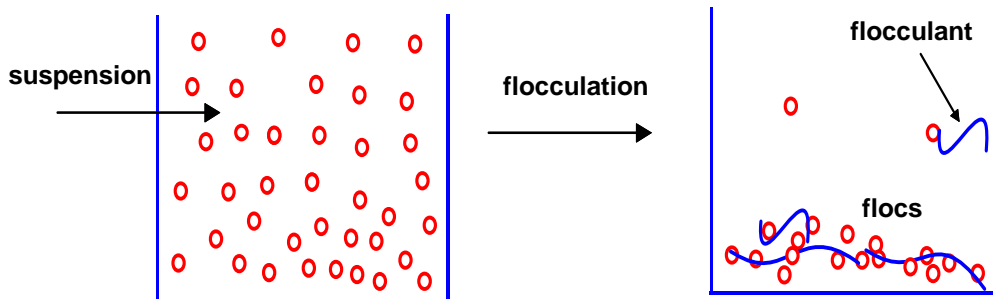
Fig. 14.1. Principle of flocculation

It has not been established so far what should be accepted as the main parameter of flocculation. Taking into account present understanding of the process, it can be assumed that the main parameter is adsorption of the polymer on the particle surface. Since adsorption of a polymer depends on its concentration in suspension, the measure of adsorption can be concentration of a flocculant which provides maximum adsorption $\Gamma_{plateau}$ also called plateau adsorption (Fig. 14.2). Selected $\Gamma_{plateau}$ values for different systems are presented in Table 14.1.
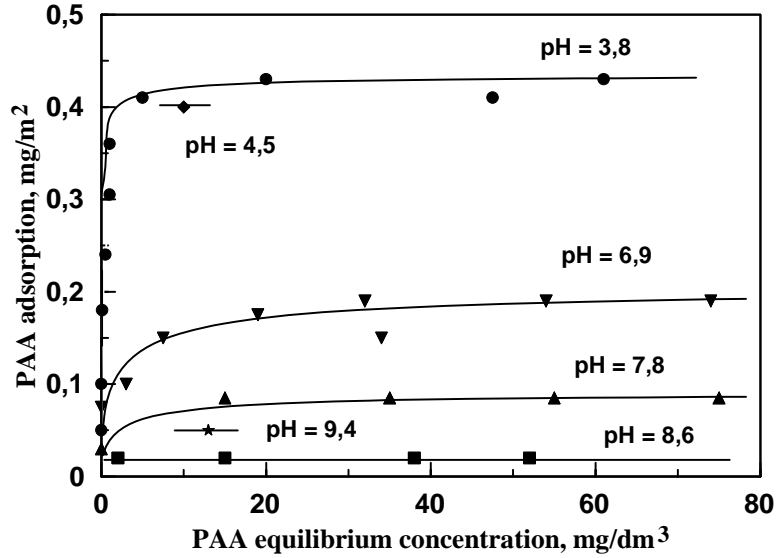
Fig. 14.2. Adsorption isotherm of flocculant on mineral particles at different pH values of the solution. The case of poly(acrylic acid) (PAA)-hematite system (after Drzymala and Fuerstenau, 1987)

When there is no or negligible polymer adsorption, flocculation does not take place, for instance in the case of silica in the presence of poly(acrylic acid) (Tab. 14.1).

Table 14.1. Values of $\Gamma_{plateau}$ for selected particle–flocculant–solution pH systems

System	$\Gamma_{plateau}$, mg/m^2	Source
Fe_2O_3–PAM–pH = 5,2	1.01	Drzymala and Fuerstenau, 1987
Fe_2O_3–PAM–pH = 9,3	0.62	Drzymala and Fuerstenau, 1987
SiO_2–PAM–pH = 4,0	~0.35	Drzymala and Fuerstenau, 1987
SiO_2–PAM–pH = 9,8	~0.15	Drzymala and Fuerstenau, 1987
Fe_2O_3–PAA–pH = 3,8	0.43	Gebhardt and Fuerstenau, 1983
Fe_2O_3–PAA–pH = 7,8	0.08	Gebhardt and Fuerstenau, 1983
TiO_2–PAA–pH = 4,2	0.08	Gebhardt and Fuerstenau, 1983
SiO_2–PAA–pH = 7,0	~0	Gebhardt and Fuerstenau, 1983
Fe_2O_3–PAAM–pH = 3,8	0.61	Drzymala and Fuerstenau, 1987
graphite–PEO–pH = 9,1	0.80	Gochin et al., 1985
anthracite–PEO–pH = 9,1	0.75	Gochin et al., 1985
SiO_2–PAA–pH = 9,8	~0.15	Drzymala and Fuerstenau, 1987

PAA – poly(acrylic acid), PAM – polyacrylamide PAAM – polymer containing half PAA and half PAM groups, PEO – poly(ethylene oxide).

14.2. Flocculants

Flocculants are obtained from polymeric natural products and their modification or as a result of chemical synthesis. Natural flocculants can be produced from starch, cellulose, chitin, proteins, and other natural products (Krishnan and Attia, 1988).
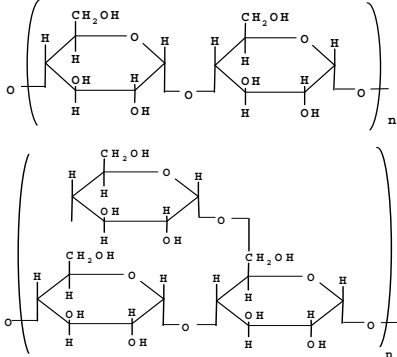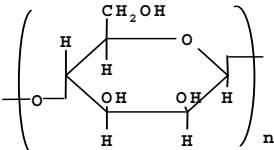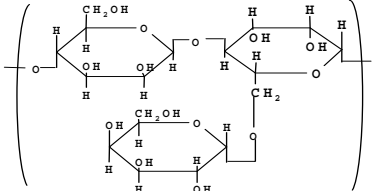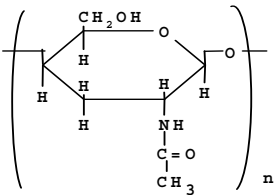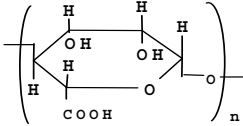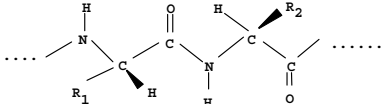
Starch is a white amorphous substance. Heated in water it swells forming a gel. Starch is a carbohydrate and a polysaccharide of chemical formula $(C_6H_{10}O_5)_n$. It can be found in plants in the form of microscopic particles which, when heated in water, stretch out and interact with one another by means of hydrogen bonds through -OH groups. Rice is the richest in starch, containing approximately 80% of this component. Wheat possesses about 75% of starch, while potatoes contain only 20%. Starch consists of two substances: amylose (~20%) and amylopectin (~80%). Amylose is a linear polymer whose chain contains from 200 to 1000 glucose units (D-glucose) combined with α glicoside bonds. Amylopectin is a polysaccharide of molecular mass of about several million, which contains over 1500 glucose groups of branched structure formed by bonds between carbons C-1 and C-6 in glucose units (Table 14.2).

Cellulose is also a polysaccharide and carbohydrate of $C_6H_{10}O_3$ formula. Cellulose, like starch, consists of long chains of D-glucose units, combined not with the α-glicoside bonds as in the case of amylose, but with β-glicoside bonds (Table 14.2). D-glucose, a basic component of both of cellulose and starch, forms one of four monosaccharide structures of $C_6H_{12}O_6$ formula. The remaining ones involve D-mannose, D-galactose and D-fructose. Two forms of D-glucose, α and β, differ not in their structure but in conformation, i.e. positioning in space: –OH and –H groups at the first carbon of the molecule are turned by 180° (Leja, 1982). Such a slight difference results in a significant difference in properties. Cellulose is the main component of fibrous parts of plants and trees. Industry makes use of such cellulose derivatives as: nitrate (explosives), acetate (plastics), xanthate (fabrics), carboxymethyl (mineral processing) and other like hydroxypropyl, hydroxyethyl and methylcellulose.

Galactomanna is a branched polysaccharide composed of D-galactose and D-mannose, which can be found in some plants, while to the industrial products, containing galactomanna, there belong guar, locust, natural gums and taro. The seeds of *cyanopsis tertagonalobus*, a Mediterranean plant, are the main source of guar. The endosperm of its seed, dispersed in water, is used as a flocculant. Seed endosperm can be also applied in the form of hydroxypropyl, hydroxyethyl and carboxymethyl derivatives and as cationic guar.

Chitin is a neutral polymer of $(C_6H_{13}N)_n$ formula which is present in skeletons and armatures of living organisms and mushrooms as one of their components. Chitin consists of N-acetyloglucosomine units. This chemical compound is structurally similar to cellulose. For practical use chitosan is applied, which is a water soluble cationic polysaccharide, obtained by removing some functional groups from chitin with the use of alkalis.

Table 14.2. Natural polymeric flocculants (after Krishnan and Attia, 1988)

Flocculant	Formula
Starch: amylose	
amylopectine	
Cellulose	
Guar	
Chitin	
Alga (compounds)	 (containing also groups: $-OH$, $-SO_3H$ and $-NH_2$)
Protein	

Another source of natural polymer flocculants are algae containing carboxyl groups combined with the first carbon following oxygen in D-glucose unit. There also exist cyclic flocculants of amphoteric character.

There is also a further group of natural polymer substances which consists of gelatine, casein and albumin (Fuerstenau and Urbina, 1988). Proteins are built of about 20 different amino acid and their sequence in a chain varies in different proteins. Since proteins possess chains built of at least 100 segments, practically, there can be countless number of proteins.

In mineral processing, apart from natural ones, synthetic flocculants are used also, which can be of ionic, cationic, and non-ionic character. Typical flocculants belonging to these three groups are shown in Tables 14.3-14.5.

Table 14.3. Anionic flocculants

Type	Name	Formula
Carboxylate	poly(acrylic acid) and its derivatives	$\left(-CH_2-\underset{\underset{\underset{O^-}{\mid}}{\underset{\mid}{C=O}}}{\overset{\overset{R}{\mid}}{C}}-\right)_n$ R = H, CH_3, etc.
Sulfonate	polystyrenosulfonate	$\left(-CH_2-CH-\right)_n$ with phenyl ring bearing $O\leftarrow S\rightarrow O$, O^-
Xanthate	cellulose xanthate starch xanthate	$\left(\underset{\underset{G}{\mid}}{\underset{O}{\mid}}C\overset{S}{\underset{S^-}{<}}\right)_n$ G-O- denotes D-glucose in cellulose or starch
Phosphonate	polyvinylphosphonate	$\left(-CH_2-CH-\right)_n$ with $P=O$, O^-, O^-

Table 14.4. Cationic flocculants
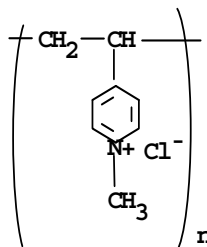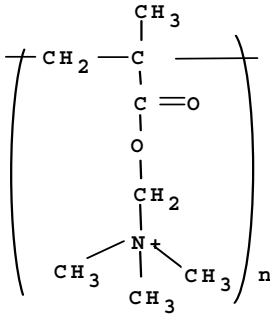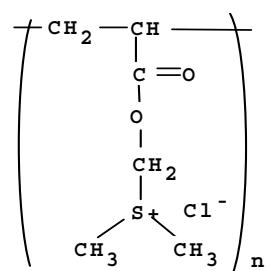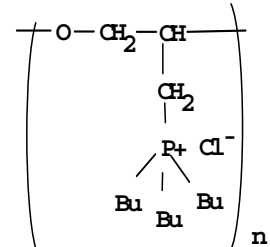
Type	Name	Formula
Ammonic	poly(ethylenimine chloride)	$\left(-CH_2-CH_2-\overset{+}{N}H_2-\right)_n \quad Cl^-$
	poly(N-metyl-4-winyl-piridine chloride)	(structure: CH_2-CH with pyridinium ring, $N^+ Cl^-$, CH_3)$_n$
	poly(2-methacryloxyethyl-trimethylammonium chloride)	(structure: $CH_2-C(CH_3)$, $C=O$, O, CH_2, $N^+(CH_3)_3$)$_n$
Sulfonic	poly(2-akryloxy-ethyldimethylsulfonic chloride)	(structure: CH_2-CH, $C=O$, O, CH_2, $S^+(CH_3)_2$ Cl^-)$_n$
Phosphonic	poly (glycidyl-tributylphosphonic chloride)	(structure: $O-CH_2-CH$, CH_2, $P^+ Cl^-$, Bu, Bu, Bu)$_n$

Table 14.5. Non-ionic flocculants

Type	Name	Formula
Polyalcohols	poly(vinyl alcohol)	$\left(CH_2-\underset{\underset{OH}{\mid}}{CH}\right)_n$
Polyethers	poly(ethylene oxide)	$\left(CH_2-CH-O\right)_n$
Polyamides	polyacrylamide	$\left(CH_2-\underset{\underset{\underset{NH_2}{\mid}}{\overset{\mid}{C}=O}}{CH}\right)_n$
Polycyclic	polyvinylpyrolidinon	$\left(CH_2-\underset{\underset{N}{\mid}}{CH}\right)_n$

Flocculants are also obtained through polymerization of two or more different monomers. Such polymers are called copolymer*s*. They can possess two different monomers situated convertibly in the chain or grouped into blocks (bloc copolymer), as well as attached at different places (attached copolymer).

Another group involves hydrophobic polymers. They are mostly copolymers of styrene and imidazolines, or copolymers of aminomethyled acrylamide with hydrophobic monomers such as methylmetacrylate.

14.3. Flocculation

Flocculation leads to particle aggregates having higher mass than that of a single fine colloidal particle of the initial suspension. They are not influenced by the brownian motion but gravity force, and therefore, they settle down. Figure 14.3 shows particles size distribution for bauxite ore before and after flocculation. Figure 14.3 shows that in the presence of a flocculant the size of particles increases. The d_{50} values for the suspension with and without flocculant are equal 1 and 8 micrometers, respectively, which confirms the claim that flocculation causes considerable increase in the size of fine particles aggregate.
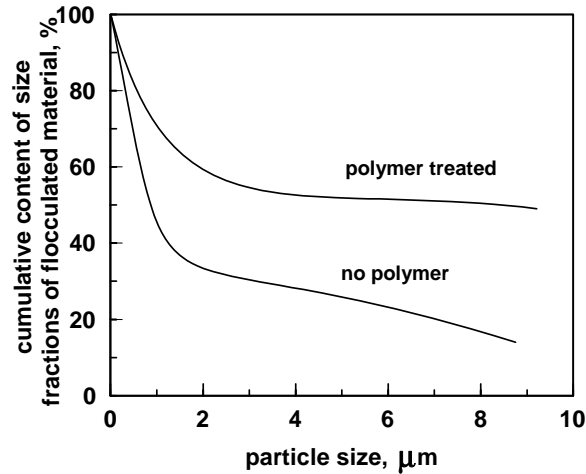
Fig. 14.3. Particles size distribution for an ore before and after flocculation. Flocculant: hydrolized poly-acrylamide. After Atia, 1982; Yu and Atia, 1987

Due to flocculation, the time of suspension clarification decreases and the filtration improves. This results from the structure of the flocculated sediments. The structure of flocs is porous, with numerous channels which are easily penetrated by water. Figure 14.4 shows that the volume of the precipitate in the presence of polymeric flocculant initially increases. Then, the sediment becomes denser and at large doses of flocculant it reaches a constant value.
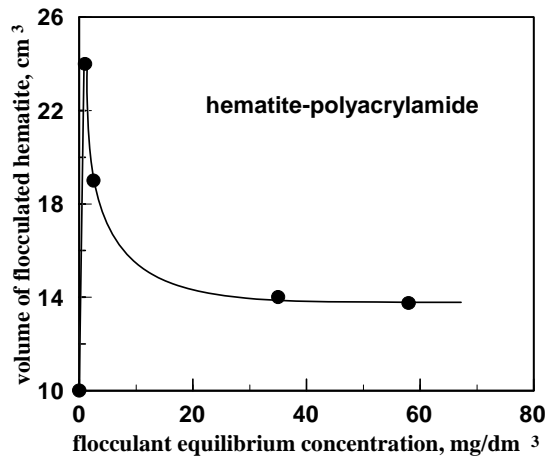
Fig. 14.4. Influence of flocculant concentration on volume of flocculated sediment. After Drzymala and Fuerstenau, 1987

Flocculated sediment volume depends not only on polymer concentration but also on pH of the solution (Fig. 14.5). Kaolin exposed to polyacrylamide, within pH range where the most advantageous flocculation takes place, i.e. pH about 7, nearly doubles its volume. However, it should be stressed that high porosity of a sediment also means higher moisture, which can be undesirable in the case of sediments which are the subject to further processes, especially drying.
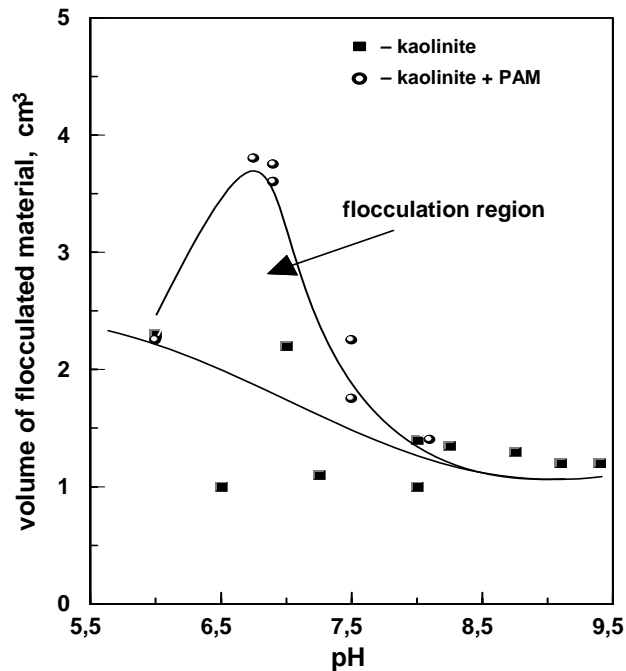
Fig. 14.5. Variation of volume of flocculated sediment as a result of addition polyacrylamide (PAM). After Michael and Morelos, 1955

The action of polymers relies on their ability to adsorb on solid surfaces. A typical adsorption isotherm, that is the course of adsorption at constant temperature has been already shown in Fig.14.2 for the poly(acrylic acid)–hematite system. Adsorption isotherms of a well adsorbing flocculant are very characteristic because adsorption as a the function of equilibrium concentration of a flocculant in the solution increases very rapidly and then reaches *maximal adsorption*, also called the plateau level. It means that at a very small concentration of a flocculant there is a complete adsorption, then the sorption is significant and shortly after that a further sorption does not occur. Maximum adsorption depends on pH of the solution and can assume maximum value $\Gamma_{plateau\ max.}$ According to Hogg (1999) $\Gamma_{plateau\ max}$ can be estimated by means of the equation:

$$\Gamma_{\text{plateau max}} \approx \frac{24M_o}{N_A \xi^2 \beta^2 M^{0.18}} , \qquad\qquad (14.1)$$

where:

M_o – molecular mass of mer

M – molecular mass of polymer

N_A – Avogadro number

ξ – proportionality factor connecting the length of molecule and its hydrodynamic size

β – effective length of bonding in polymeric skeleton.

Typical values of these parameters for polyacrylamide are: $M_o = 71$ g /mol, $M = 10^6$ g /mol, $\xi = 0.67 \div 0.875$, $\beta =$ a few lengths of C–C bond.

The adsorption of polymers, with a certain approximation, is determined by the Langumir isotherm when each segment of a polymer is treated as a unit able to adsorb. This is possible only near the region of concentration close to the plateau adsorption while the most important region of sorption is that of low concentration. A better result provides the Simh-Frischs-Erich isotherm also termed as the SFE isotherm (La Mer and Healy, 1963). There is also a possibility to delineate adsorption basing on probability considerations (Fleer, 1988)

Due to nearly complete sorption of a flocculant, its quantity needed for flocculation is very small, usually several ppm (part per million) units, i.e. several parts by weight of polymer per one million of parts by weight of flocculated material. According to Hogg (1999) adsorption of polymer flocculant on particle surface is not an equilibrium process and, therefore, its delineation requires a completely different approach. He proposed a simplified model in which frequency of polymer molecules collision with a particle determines distribution of adsorbed polymer on the surface, which influences adhesion and flocculation efficiency. The outcome of this model is confirmation of the fact that flocculation results in bimodal distribution of flocs size. The first maximum is recorded for not flocculated and slightly aggregated particles, while the second one refers to considerably flocculated material. Kinetics of polymer adsorption was previously described by Jankovics (Tewari, 1981).

Polymer adsorption onto mineral surface takes place due to typical chemical bonds, i.e. ionic, dispersive (van der Waals), covalent, semipolar, hydrogen of hydrophobic bonds, as well as their combination. When adsorption depends mainly on one kind of bond, the adsorption isotherms, expressed as the function of pH, as well as the relation between sorption at the plateau vs. pH, follow a specific pattern. For instance, adsorption of poly(acrylic acid) (PAA) on mineral particles is of electrostatic character and sorption at plateau depends on the iep. Figure 14.6 shows that adsorption of anionic PAA decreases as pH increases, since the positive electrical charge of the surface also decreases with decreasing pH. It can be also concluded from Fig. 14.6 that quartz and

PAA are negatively charged practically within the whole pH range. On the other hand, adsorption of hydrophobic flocculants easily occurs on hydrophobic surfaces.

Polyacrylamide is an ionic flocculant. Its adsorption takes place mainly as a result of hydrogen bonding with surface hydroxylic groups such as $-OH_2^+$ and $-OH$. Therefore PAM selectivity is insignificant and it adsorbs on all mineral surfaces, though the extent of sorption can be different on various minerals. The adsorption of PAM at the plateau does not depends on the iep of particles and decreases with increasing pH as a results of diminishing number of surface groups $-OH_2^+$ capable of forming hydrogen bonds.

Cationic flocculants can be used for aggregation of negatively charged mineral particles in aqueous solution. It is interesting to add that flocculation is caused by cationic polymers both of a high and a low molecule weight, while other polymers have to be of high molecular mass. According to Attia (1988) such a phenomenon results from the fact that cationic polymers at first neutralize surface charge and then act as a bridging medium.

Adsorption of hydrophobic flocculants takes place as a result of hydrophobic interactions. Therefore they are suitable for flocculation of hydrophobic particles. Flocculants containing xanthate group tend to combine selectively with mineral surfaces, especially with sulfides which contain ions of heavy metals, to form with them covalent or semipolar bonds (Krishnan and Attia, 1988).
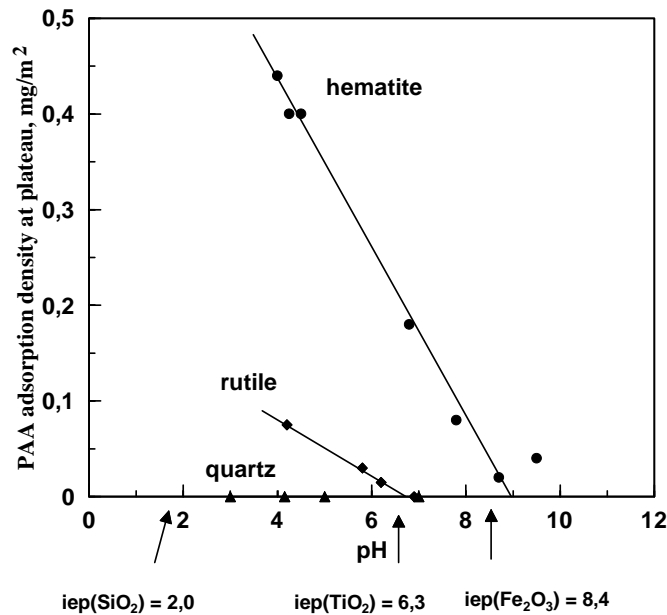
Fig. 14.6. Influence of iep on plateau adsorption of PAA obtained from the adsorption plateau isotherm (after Gebhardt and Fuerstenau, 1983)

On the basis of the discussion presented it can be concluded that flocculants follow a complex mechanism of adsorption and, therefore, it is difficult to select a flocculant without previous experiments. The experiments are also necessary because mineral substances become activated by metal ions which can originate both from minerals subjected to flocculation and from industrial water. Quartz can serve as an example of activations, i.e. making the surface contaminated. Quartz does not flocculate in the presence of poly(acrylic acid), although exposed to hydrolyzing cations it flocculates easily at pH characteristic for each hydrolyzing cation (Fig. 14.7). According to Fuerstenau and Palmer (1976) this activation coincides with the pH range of predomination of monohydroxycomplexes ($[Me^{II}(OH)^+]$) of a given metal. Particle activation can be prevented by the addition of an appropriate chemical to the flocculation system. Therefore, most flocculation processes in the presence of quartz require application of appropriate agents which remove adsorbed ions from its surface before flocculation. In alkaline environment the best "washing" agents are sodium carbonate, while in the acidic environment acids, especially HF. Complexing compounds like sodium versenate (EDA) can be also used.
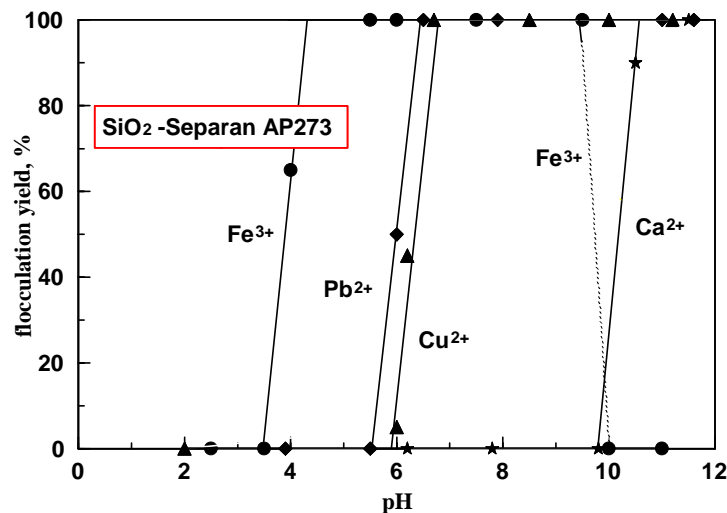
Fig. 14.7. Influence of pH on recovery of flocculated silica by means of anionic flocculant in the presence of 10^{-3} M KNO_3 and $5 \cdot 10^{-4}$ M hydrolyzing metal salts. After Drzymala and Fuerstenau, 1981 with permission of Elsevier Science)

The bonds between polymer and mineral surface are of different stability. In some cases, especially when the suspension is vigorously stirred, bound breaking and their restoration usually takes place mostly on the surface of the same particle. Then flocculation declines and particles undergo dispersion. This process is called restabilization of the suspension or steric stabilization (Fig. 14.8). The latter one also takes place

when molecular mass of polymer is too low and its chains are too short to flocculate particles.
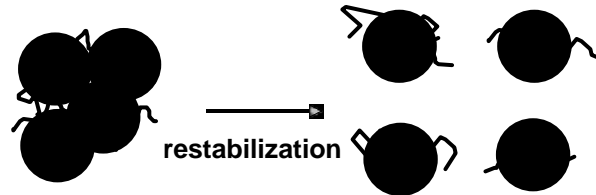
Fig. 14.8. Restabilization of flocculated sediment as a result of braking the polymer-particle attachment followed by reattachment of a polymer but to the same particle

Flocculants can be used for flocculation of fine particles before their thickening in sedimentation tank. Then clarified water is recycled.

The list of flocculants producers and their names can be found in many publications for instance by Lewellyn and Avotins (1988).

14.4. Selective flocculation

As polymer adsorption is different on different minerals, this phenomenon can be utilized in fine particles separation, i.e. selective flocculation, which results in obtaining flocs and suspension of the remaining particles (Fig. 14.9). Selection of flocs from not flocculated material is performed by decantation, syphonation, or overflow from different tank levels. The process of selective flocculation usually consists of four subprocesses:

- preparation of the material to be flocculated (particles dispersion, pH regulation, particle deactivation, etc.)
- selective adsorption of flocculant
- flocs forming and conditioning
- separation of flocs from not flocculated material.

In numerous publications it is stressed that before flocculation suspension has to be subjected to stabilization, i.e. to be completely dispersed. Different dispersing agents are used for this purpose, which has already been described in the chapter on flotation. The claim regarding necessity of stabilization prior to flocculation is not always correct, since there are some systems in which selective flocculation does not have to be preceded by a thorough dispersion of the suspension. Selective flocculation of hematite from quartz containing their mixture can serve as an example. Hematite within pH range from 4 to 9 is not stabile and it undergoes coagulation while quartz heterocoagules with hematite. PAA addition leads to selective flocculation of hematite and, as the mixture in the suspension is stirred, quartz appears in the dispersion.
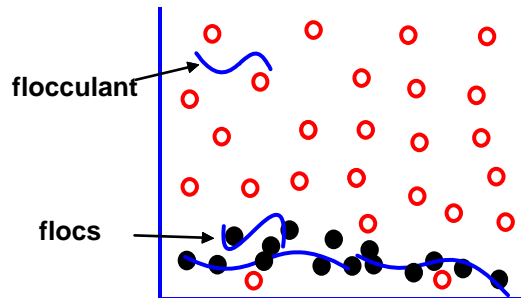
Fig. 14.9. Selective flocculation

The literature provides numerous original and review publications about selective flocculation. This method of separation has been paid closer attention due to vast amounts of fine particles produced by mineral industry which are generally treated as wastes. Selective flocculation, because of its specific character, can be utilized for fine particles enrichment. Attractiveness of this method is based on small amounts of flocculants, usually several ppm, used in flocculation. However, its disadvantage is the necessity of keeping the suspension highly diluted. Yet, the most considerable problem is relatively low selectivity of the process, often resulting from easy activation of mineral surfaces with metal ions. High moisture of floccs is also a problem.

In the literature (e.g. Kisztiszewa-Dimitrowa and Stojew, 1978) there were described numerous applications of selective flocculation for ore and raw materials enrichment on laboratory scale. Only a few, however, were introduced into practice (Attia, 1982). One of them is selective flocculation of quartz-containing taconite (iron ore) used in the Tilden Plant in Michigan, run by the Cleveland Cliffs company from Cleveland, Ohio, USA. This process utilizes flocculation for selective desliming of the ore from quartz. The ore suspension is treated with hydrolized starch which flocculates iron minerals (mainly hematite), while quartz particles are removed from the suspension through decantation while remaining quartz undergoes flotation with the use of amines. The process takes place in an alkaline environment in the presence of Na_2CO_3 and sodium silicate as process regulators.

Another example is silvinite processing in the Saskatchewan Plant by the Cominco company in Canada. The ore contains, apart from silvinite (KCl), 4.5% to 8% of contaminants in the form of dolomite, hematite, quartz, kaolinite, chlorite and anhydrite. These contaminations undergo flocculation with the use of a cation collector Aero 870 (Yu and Attia, 1987). A further example can be kaolin enriched in the USA by Theile Kaolin Company in Georgia, USA. There flocculation is used for removing color contamination in the form of anatase and other titanium and iron minerals from kaolin. Other applications of flocculation including borax, beryl, zircon sand, and phosphates were presented by Richardson and Lawreence (1988).

Literature

Attia Y.A., 1982. Selective flocculation: state of the art review, SME-AIME 111th Annual Meeting, Dallas, Preprint SME 81-360, 1–17.

Drzymala J., Fuerstenau D.W., 1981. Selective flocculation of hematite in the hematite-quartz-ferric ion-polyacrylic acid system. Part 1. Activation and deactivation of quartz, Inter. J. Mineral Processing, 8, 265–277.

Drzymala J., Fuerstenau D.W., 1987. Adsorption of polyacrylamide, partially hydrolized polyacrylamide and polyacrylic acid on ferric oxide and silica, in: Flocculation in bio-technology and separation systems, Y. Attia (ed.), 28–42.

Fleer G.J., 1988. Adsorption of polymers, in: Reagents in mineral technology, Surfactants Science Series, Vol. 27, P, Somasundaran and B.M. Moudgil (eds.), Dekker, N.Y., 105–158.

Fuerstenau D.W., Urbina R.H., 1988. Flotation fundamentals, in: Reagents in mineral techno-logy, Surfactants Science Series, Vol. 27, P. Somasundaran and B.M. Moudgil (eds.), Dekker, N.Y., 1–38.

Fuerstenau M.C., Palmer B. R., 1976. Anionic flotation of oxides and silicates, in: M.C. Fuers- tenau (ed.), Flotation, A.M. Gaudin Memorial Volume, Vol. 1, AIME, New York, Chap. 7, 148–196.

Gebhardt J.E., Fuersternau D.W., 1983. Adsorption of polyacrylic acid at oxide/water interfaces, Colloids and Surfaces, 7, 221–231.

Gochin R.J., Lekili M., Shergold H.L., 1985. The mechanism of flocculation of coal particles by polyethyleneoxide, Coal Preparation, 2, 19–33.

Hogg R., 1999. The role of polymer adsorption kinetics in flocculation, Colloids Surfaces A – Phys. Eng. Aspects, 146, 253–263.

Kisztiszewa-Dimitrowa R., Stojew S.M., 1987. Flokulacja selektywna, Śląsk, Katowice, 1–103.

Krishnan S.V., Attia Y.A., 1988. Polymeric flocculants, in: Reagents in mineral technology, Surfactants Science Series, Vol. 27, P. Somasundaran and B.M. Moudgil (eds.), Dekker, N.Y., 485–518.

La Mer V.K., Healy T.W., 1963. Adsorption-flocculation reactions of macromolecules at the solid-liquid interface, Review of Pure and Applied Chemistry, 13, 112–133.

Leja J., 1982. Surface chemistry of froth flotation, Plenum Press, New York.

Lewellyn M.E., Avotins P.V., 1988. Dewatering/Filtering Aids, in: Reagents in mineral technology, Surfactants Science Series, Vol. 27, P, Somasundaran and B.M. Moudgil (eds.), Dekker, N.Y., 559–578.

Michaels A.S., Morelos O., 1955. Polyelectrolyte adsorption by kaolinite, Industrial and Eng. Chem., 47, 1801–1809.

Richardson P.F., Lawreence J.C., 1988. Industrial Coagulants and Flocculants, in: Reagents in mineral technology, Surfactants Science Series, Vol. 27, P, Somasundaran and B.M. Moudgil (eds.), Dekker, N.Y., 519–558.

Tewari P.H., 1981. Adsorption of polyacrylamide and sulfonated polyacrilamide on Na-kaolinite, in: Adsorption from aqueous solutions, Plenum, London, 143–162.

Yu S., Attia Y.A., 1987. Review of selective flocculation in mineral separations, partially hydrolized polyacrylamide and poliacrylic acid on ferric oxide and silica, in: Flocculation in biotechnology and separation systems, Y. Attia (ed.), 601–635.

15. Oil agglomeration

15.1. Principles

Aggregation of particles and drops of a liquid, both suspended in an immiscible liquid, is referred to as agglomeration. When the liquid used for agglomeration is water immiscible and the process is performed in aqueous environment - it is called oil agglomeration. Oil agglomeration (Fig. 15.1) is most often performed in the following way: oil is added to aqueous suspension of particles and subsequent mixing leads to oil dispersion. At the same time, collision of particles and oil drops causes formation of oil agglomerates. Stopping the mixing initiates a fast settling of aggregates. Agglomerates can be separated form the suspension by either decantation, siphoning, or screening. The most common way is screening through a sieve or screen.
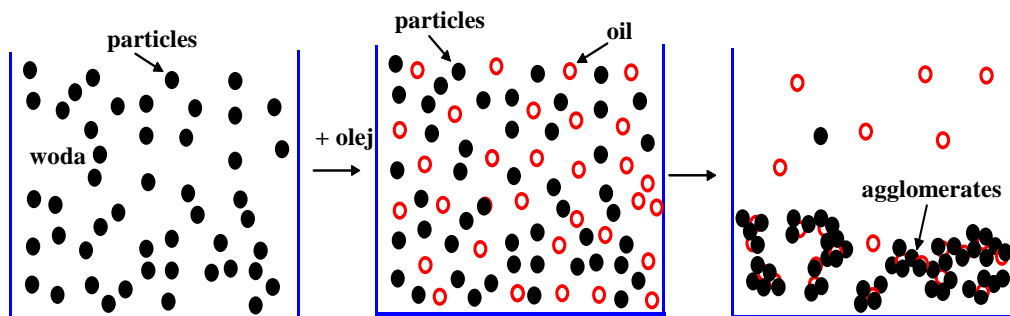
Fig. 15.1. Oil agglomeration

The mechanism of agglomeration is not fully understood. Its complexity results from a great number of variables. Similarly to any other separation process, oil agglomeration can be delineated also from the probability point of view. The probability of oil agglomeration P depends on probabilities of subprocesses such as probability of oil drop–particle collision (P_z), probability of formation of a stable drop-particle aggregate (P_a), and probability of a drop-particle aggregate remaining stable (P_{stab}):

$$P = P_z\, P_a\, P_{stab}. \tag{15.1}$$

Thus, the parameters effecting oil agglomeration are grouped into three families, that is the parameters influencing particle-oil drops collision, parameters responsible for their adhesion, and factors influencing stability of oil agglomerates (Fig. 15.1). It

should be remembered that agglomeration system is interactive because some parameters affect more than one agglomeration subprocess, while the others are combination of different parameters or they are mutually dependent. Therefore, Fig. 15.2, representing parameters effecting oil agglomeration, was shown in the form of a triangle. A similar description of separation processes as an interactive system was earlier proposed by Klimpel (1988), who divided the parameters into machine, operational and chemical dependent factors.

P_a

γ_{ow} and aquaoleophilicity (θ_o)
of solid dependent on pH, Eh, pX,
modifiers,
temperature, etc.

Oil agglomeration

P_z　　　　　　　　　　　　　　　P_{stab}

• mixer design
• stirring
• size of drop and particles
• density of particles and bubbels
• suspension density

• combination of parameters from P_a and P_z groups
• oil viscosity
• surface roughness
• other
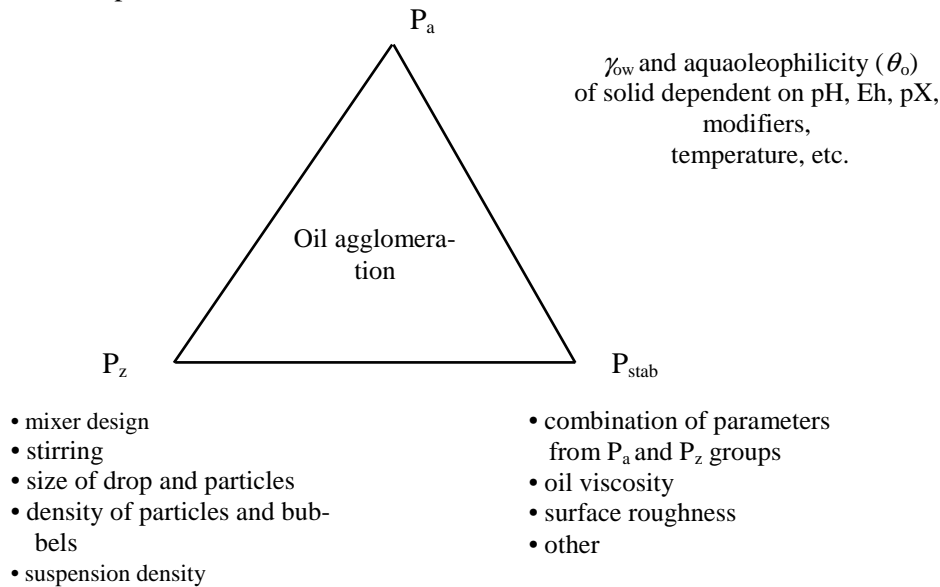
Fig. 15.2. Oil agglomeration as an interactive system

The parameters shown in Fig. 15.2 effect such elements of agglomeration as velocity of agglomeration, physical shape of agglomerates, selectivity of the process, cost, etc. The most important parameters of oil agglomeration are the properties of three involved interfaces, as they result from the nature of particles, water, and oil. Some parameters, especially those from the P_a group, can be easily regulated. The role of interfacial properties is presented in details in the following subchapter.

15.2. Thermodynamics of oil agglomeration

Oil agglomeration is a physicochemical process and can be written as a reaction:

particle (in water) + oil drop (in water) = particle–oil agglomerate (in water)　　　(15.2)

which is illustrated in Fig. 15.3.

water
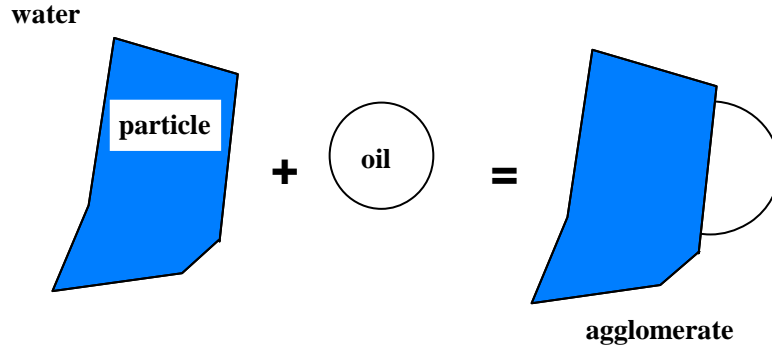
agglomerate

Fig. 15.3. Formation of oil-particle agglomerate as a result of adhesion of oil drop to a particle

As a result of adhesion of a drop and a particles, a new unit area (e.g. 1 cm^2) of the particle–oil interface is formed, at the expense of disappearing of a unit area of particle–water interface and a unit area of the oil–water interface. The process is accompanied by changes of energy. Thus, oil agglomeration can be described as a thermodynamic process resulting from a change in the Gibbs thermodynamic potential also called the free enthalpy (ΔG_{aggl}):

$$\Delta G_{\text{aggl}} = \gamma_{\text{so}} - \gamma_{\text{sw}} - \gamma_{\text{ow}}, \tag{15.3}$$

where:
s – particle
o – oil
w – water
γ_{so} – particle-oil interfacial energy
γ_{sw} – particle-water interfacial energy
γ_{ow} – oil-particle interfacial energy.

Since the γ_{sw} and γ_{so} values are difficult to determine, a solution of Eq. (15.3) requires their combination with the Young equation:

$$\gamma_{\text{sw}} = \gamma_{\text{so}} + \gamma_{\text{ow}} \cos \theta_{\text{o}}, \tag{15.4}$$

which graphical form for a simple particle–oil drop–water system and for oil agglomerate are shown in Fig. 15.4.

Combining Eqs (15.3) and (15.4) one can obtain the relation:

$$\Delta G_{\text{aggl}} = -\gamma_{\text{ow}} (\cos \theta_{\text{o}} + 1), \tag{15.5}$$

where θ_{o} stands for contact angle in the particle-oil-water system measured through the oil phase (Fig. 15.4a).

Equation 15.5 delineates thermodynamics of oil agglomeration for an ideal case shown in Fig. 15.4a. This relation proves that the main parameters of oil agglomera-

tion are θ_o and γ_{ow}. This equation can be applied to approximate delineation of oil agglomeration.
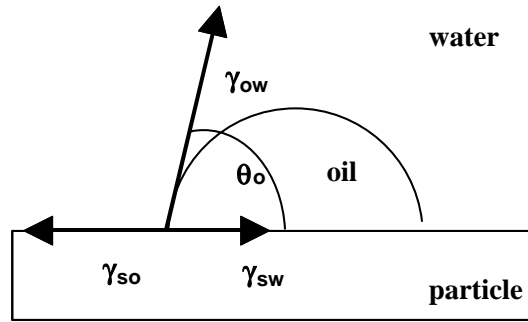
a
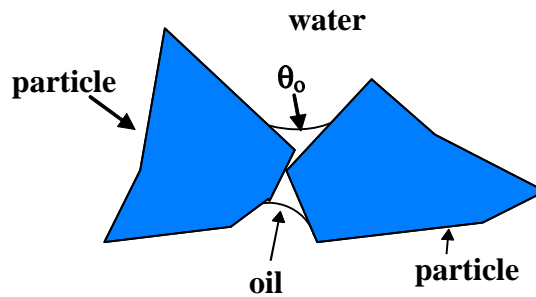
b
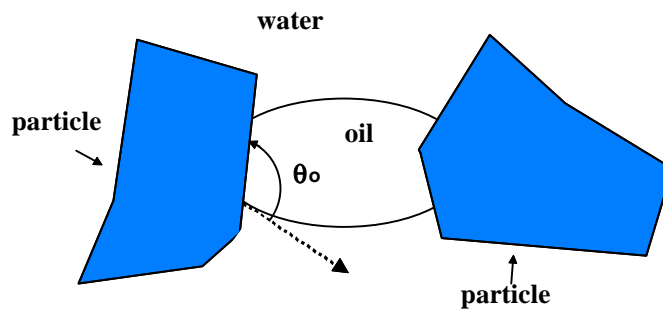
c

Fig. 15.4. Particle-oil drop-water system: a-graphical representation of the Young equation for the particle-oil-water system with a contact angle measured through the oil phase, b- agglomerate when $\theta_o < 90^o$, c-agglomerate when $\theta_o > 90^o$

Table 15.1. Oils used for agglomeration of No. 2 Gas Seam coal and their characteristics along with experimental and calculated results (Drzymala and Wheelock, 2005)

No.	Oil	γ_o mN/m (mJ/m^2)	γ_{ow} mN/m (mJ/m^2)	c_{50} v/w %	ΔG_{ag} mN/m (mJ/m^2)
1	Pentane	17.30	51.06	1.45	–64.13
2	Hexane	18.49	51.10	1.10	–64.97
3	Heptane	20.30	51.10	0.94	–66.07
4	Decane	23.90	51.10	0.65	–67.89
5	Hexadecane	26.35	51.22	0.26	–69.01
6	Paraffin oil	30.1	51.41	0.099	–70.45
7	2-methylpentane	18.41	48.90	0.84	–62.72
8	2,2-dimethylbutane	16.18	49.70	0.68	–61.96
9	2,3-dimetylbutane	17.43	49.80	0.55	–62.96
10	Squalane	29.2	52.30	0.18	–71.07
11	1-octene	21.76	46.51	1.40	–62.37
12	1-tetradecene	26.80	47.77	0.58	–65.73
13	1-octadecene	28.49	47.20	0.36	–65.74
14	Hexanoic acid	27.0	5.8	60	–23.83
15	Heptanoic acid	28.3	7.0	19	–25.48
16	Octanoic acid	28.3	8.5	6.0	–26.98
17	1-butanol	24.6	1.8	500	–18.89
18	1-pentanol	23.78	4.6	135	–20.93
19	1-hexanol	26.21	6.6	35	–24.34
20	1-heptanol	24.50	7.7	12	–24.75
21	1-octanol	27.53	8.1	5	–26.32
22	Benzene	28.85	35.0	12	–53.66
23	Toluene	28.50	36.1	4.7	–54.65
24	Ethyl benzene	29.2	38.4	2.2	–57.17
25	Propyl benzene	28.99	39.6	1.75	–58.30
26	Tetraline	35.44*	27.8*	1.2	–
27	Cyclopentane	22.61	–	2.0	–
28	Cyclohexane	25.50	50.0	0.75	–67.46
29	Cycloheptane	27.84	–	0.60	–
30	Metylcyclohexane	23.85	41.9	0.80	–58.66
31	Propylcycloheksane	26.33	–	0.60	–
32	Metylcyclopentane	22.3	–	0.80	–
33	Ethylcyclopentane	24.9	–	0.80	–
34	Methylene chloride	26.52	28.3	70	–46.15
35	Chloroform	27.14	31.6	25	–49.68
36	Carbon tetrachloride	26.95	45.0	3.5	–63.02
37	Cycloheksene	26.78	44.2	0.75	–62.16
38	Bromoform	41.53	40.9	7.5	–62.06
39	Ethylene chloride	24.15	28.4	37	–45.30
40	Ethylene bromide	38.37	36.5	12	–57.28
41	Ethyl bromide	24.15	31.20	20.4	–48.10
42	Ethyl iodide	29.4	40.0	11.5	–58.83
43	Oleic acid	32.5	15.7	0.55	–35.37
44	*tert*-butylchloride	19.60	23.75	150	–38.31
45	Butylnitrile	28.10	10.40	235	–28.81
46	Tetrachloroethylen	31.70	47.5	2.5	–66.97

* uncertain values.

More detailed thermodynamical consideration of oil agglomeration involving formation of oil bridges of a given size of spherical particles and drops, as well as the shape of oil bridges between particles, leads to more complicated relations. For example calculations by Jaques et al. (1979) showed that ΔG_{aggl} is:

$$\Delta G_{aggl} = \gamma_{ow} [F_1(\psi_1, \theta_o) - \cos \theta_o(1 - \cos \psi_1) - n^2], \qquad (15.6)$$

where:
$F_1(\psi_1, \theta_o)$ – function delineating area of oil bridge
n – oil drop and spherical particle radius ratio
ψ_1 – angle characterizing size of the oil bridge.

The above parameters can be calculated with the use of additional equations and assumptions presented by Jaques et al. (1979). Still other approaches to approximate ΔG_{aggl} were proposed by Keller (1984), as well as by Keller and Burry (1987).

According to Eq. (15.4) the contact angle θ_o is determined by the energy of the three involved interfaces of oil aggregates formed by particles and oil drops immersed in water. To stress the fact that this is the property linking particles with oil in the presence of water, this state, after Yang and Drzymala (1986) will be called *aquaoleophilicity* which can be measured as contact angle θ_o. This term is introduced to differentiate it from hydrophilicity and hydrophobicity, which characterize solid–liquid–gas systems.

Equations (15.5) and (15.6) prove that γ_{ow} and θ_o play a crucial role in oil agglomeration. Drzymala and Wheelock (1990, 2005) verified the applicability of equation (15.5) for oil agglomeration and, at the same time, examined which oils are suitable for coal agglomeration. An American No 2 Gas Seam Peabody coal was subjected to agglomeration applying different organic liquids and measuring suspension turbidity as a function of amount of added oil. During experiments the turbidity of the suspension decreased from a certain constant value until it reached very low values indicating full agglomeration. Parameter $c_{\tau 50}$ was used as an indicator of oil agglomeration, i.e. the concentration of oil needed for lowering the initial suspension turbidity by half, called the concentration of half–agglomeration. The values of $c_{\tau 50}$ obtained and the oils applied are shown in Table 15.1.

Table 15.1 provides ΔG_{aggl} values which can be calculated with the use of Eq. (15.5) as well as measured values of contact angle θ_o and γ_{ow}. Because of the difficulties with measurement and interpretation of θ_o, the calculation of ΔG_{aggl} were performed using the Young equation (Eq. 15.4) and the Fowkes (1964) relation, which tells that the interfacial energy of a selected phase boundary is a sum of surface energy of the components building the interface, reduced by a dispersion effects $2\sqrt{\gamma_1^d \gamma_2^d}$ and other factors X:

$$\gamma_{12} = \gamma_1 + \gamma_2 - 2\sqrt{\gamma_1^d \gamma_2^d} - X, \qquad (15.7)$$

where:

1 and 2 – numbers indicating phases (e.g. 1 means oil, 2 means solid)

γ_1^d and γ_2^d – the so-called dispersion components of surface energy.

In the considered case the Fowkes equation assumes the form:

$$\gamma_{so} = \gamma_s + \gamma_o - 2\sqrt[3]{\gamma_s^d \gamma_o^d} - X. \tag{15.8}$$

Instead of γ_{sw} in the Young formula (Eq. 15.4), one can introduce the Young equation for the solid-oil-water system:

$$\gamma_{sw} = \gamma_s - \gamma_w \cos \theta_w, \tag{15.9}$$

where:

γ_s – surface energy of solid

γ_o – surface energy of oil

γ_w – surface energy of water (surface tension) equal to 72.8 mN/m

γ_{sw} – interfacial energy (solid-water).

θ_w – contact angle of a solid wetted with water measured through the water phase.

Finally one gets an expression for the free enthalpy of oil agglomeration in a form:

$$\Delta G_{aggl} = \gamma_o - \gamma_{ow} - 2\sqrt[3]{\gamma_1^d \gamma_2^d} + \gamma_w \cos \theta_w - X. \tag{15.10}$$

After further assumptions:

a) *X* is closed to zero because hydrophobic particles only weakly interact with the non-dispersive forces

b) $\gamma_w \cos\theta_w$ for the investigated coal is 28.44 mN/m because its $\theta_w = 67°$, and $\gamma_w = 72.8$ mN/m = 72.8 mJ/m²

c) γ_s^d for the investigated coal, as for most bituminous coals is 50 mN/m (Good, 1990)

d) for oils $\gamma_o^d \approx \gamma_o$

one gets approximate expression for the free enthalpy of agglomeration:

$$\Delta G_{aggl} \cong \gamma_o - \gamma_{ow} - 2\sqrt[3]{50\gamma_o} + 28.44, \text{ mN/m lub mJ/m}^2. \tag{15.11}$$

The calculated ΔG_{aggl} values are presented in Table 15.1.

The relations between the amount of oil necessary for half–agglomeration c_{o50} and free enthalpy of agglomeration ΔG_{aggl} for coal No 2 Gas Seam Peabody, subjected to agglomeration with oils (listed in Tab. 15.1) were shown in Fig. 15.5. It results from this figure that there is a good correlation between agglomeration (c_{o50}) and $\Delta G_{aggl} = -\gamma_{ow}(\cos\theta_o + 1)$. The existence of this correlation confirms that main parameters of oil agglomeration are aquaoleophilicity θ_o and γ_{ow}. Figure 15.5. also shows that aliphatic hydrocarbons of high surface tension are the best for oil agglomeration, while aro-

matic hydrocarbons with functional groups (such as butyronitrile, methylene chloride) provide poor results. Alcohols and fatty acids form their own correlation line because they are surface–active substances which decrease water surface tension and contact angle θ_w can reach zero value in their presence. Taking this into account slightly changes of ΔG_{aggl}, since in $\gamma_w \cos\theta_o$ the value of γ_w decreases while $\cos\theta_o$ increases. Thus, the whole expression does not change considerably. This means that alcohols and acids form bonds with the coal surface, probably hydrogen bonds.
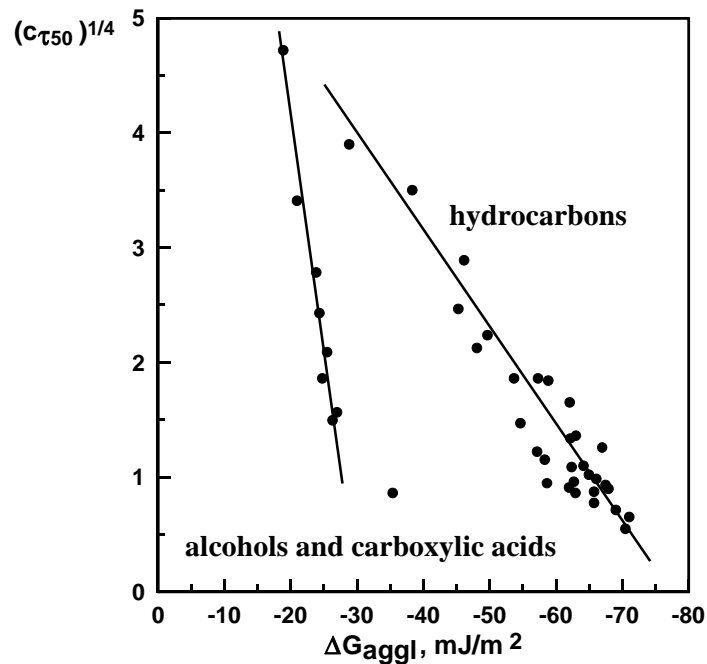
Fig. 15.5. Correlation between amount of oil needed for half-agglomeration ($c_{\tau 50}$) and free enthalpy of agglomeration ΔG_{aggl} calculated with Eq. 15.10

The fact that oil agglomeration is governed by the parameter $\Delta G_{aggl} = -\gamma_{ow}(\cos\theta_o + 1)$ and agglomeration increases with negative value of ΔG_{aggl}, excludes suggestions of other authors that, for instance, only interfacial tension γ_{ow} (Keller and Burry, 1987; Laskowski, 1987), or oil density (Capes, 1979) determine oil agglomeration. The lack of correlation between oil agglomeration and many individual parameters was proved by Labuschagne (1986a). Additional argument that the two parameters play a crucial role in oil agglomeration process, namely aquaoilphility θ_0 and interfacial oil–water (γ_{ow}) tension, is the mechanism of the process, which will be described in one of the subsequent chapters.

15.3. Aquaoleophilicity of agglomerating systems

As it has already been presented, two parameters, aquaoleophilicity θ_o and γ_{ow}, govern oil agglomeration. The interfacial tensions γ_{ow} for most liquids are available in literature or they can be experimentally determined. The measurement of contact angle θ_o is more difficult. This results from the occurrence of considerable hysteresis (Fig. 15.6) caused by heterogeneity of surface energetics, surface roughness, the way of conducting measurement, as well as the applied measurement method. The difference in contact angles measured for advancing and receding oil drop can be up to 80^0. Table 15.2 presents contact angles for advancing and receding oil drops for two coals. Table 15.3 shows "equilibrium" contact angles and the values of oil receding angles for polished coals, measured by Jańczuk and Białopiotrowicz (1988).
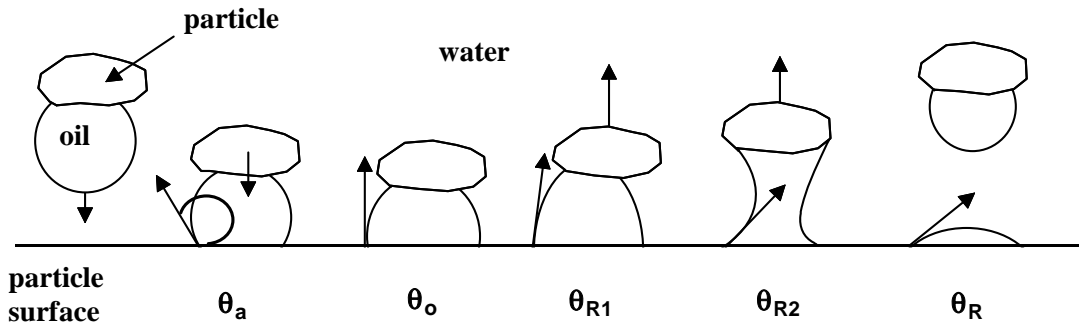
Fig. 15.6. Hysteresis of contact angle of oils in contact with solid surface under water:
θ_A – advancing contact angle of oil, θ_o – hypothetical equilibrium contact angle,
θ_{R1}, θ_{R2} – intermediate angles of retreating oil, θ_R – receding contact angle of oil

Table 15.2. Contact angle for advancing oil drop θ_A, for retreating oil drop θ_R, average contact angle $\theta_{o\ av}$ and their difference $\Delta\theta$ in a coal–heptane drop–water. The contact angle was measured through the oil phase (Drzymala and Wheelock, 1990)

Coal	θ_A	θ_R	$\theta_{o\ av} = (\theta_A + \theta_R)/2$	$\Delta\theta = \theta_A - \theta_R$
Upper Freeport	$123^o \pm 6^o$	$44^o \pm 8^o$	$\sim 84^o \pm 40^o$	79°
Pittsburgh #8	$135^o \pm 2^o$	$55^o \pm 2^o$	$\sim 95^o \pm 40^o$	80°

True contact angle, called the equilibrium contact angle, which should be applied for the Young-type equations (15.4) occurs somewhere between advancing and receding contact angles. Therefore, Leja (1982) claims that contact angle is only an indicator and its measurement should be done in series using the same technique in each series.

Table 15.3. „Equilibrium" contact angle $\theta_{o\ min}$ and receding contact angle $\theta_{o\ max}$
for the coal–water drop–octane measured through the oil phase.
Angle $\theta_{o\ min}$ was measured by a gentle placing a drop on the surface while $\theta_{o\ max}$ by pressing the drop
(measurements and symbols after Janczuk and Bialopiotrowicz, 1988)

Coal*	$\theta_{o\ min}$	$\theta_{o\ max}$
31.1	70.1^o	36.9^o
31.2	68.9^o	36.3^o
32.2	65.6^o	35.1^o
33	67.0^o	33.6^o
34	62.7^o	33.9^o
35	63.0^o	33.1^o

*Polish classification

Aquaoleophilicity, i.e. contact angle of materials wet by oils in water can significantly vary. For Teflon contact angle, measured as the "equilibrium", is about 19° (Jańczuk and Chibowski, 1983). Mean value of the angle, ranging from 40° to 80°, features sulphur, graphite and coals. The highest values of contact angle shows hydrophilic materials such as quartz, calcite, and cellulose. Their contact angle is greater than 90°. Selected values of contact angles for different substances in water in contact with hexadecane, are shown in Table 15.4. It should be noted that, so far, there have nether been discovered substances completely aquaoleophilic on which oil drop would spread forming $\theta_0 = 0$, nor substances completely aquaoleophobic with contact angle equal 180^0. Such values can probably be obtained by appropriate modification with surfactants.

Table 15.4. Contact angle θ_o in the solid-oil (hexadecane)–water system
measured through the oil phase

Solid	θ_o	Source
Teflon	19.5^o	Janczuk and Chibowski, 1983
Sulfur	38°	Janczuk and Chibowski, 1983
Graphite	45°	Drzymala and Wheelock, 1988
Graphite	47°	Janczuk and Chibowski, 1983
Coal (Upper Freeport)	68°*	Good and Keller, 1989
Coal (Illinois #6)	75°	Drzymala and Wheelock, 1988
Plexiglass	75–90°	El-Shimi and Goddard, 1974
Pyrite	105°	Drzymala and Wheelock, 1988
Cellulose	120°	Hamilton, 1972
Quartz	165°	Drzymala and Wheelock, 1988
Nylon	170°	El-Shimi and Goddard, 1974

*Average were value calculated as weighted average of aliphatic, aromatic and ash sites (Table 15.6).

Oil type effects contact angle. Table 15.5 shows that for aliphatic hydrocarbons aquaoleophilicity increases with the length of hydrocarbon chain. For instance, for graphite contact angle with heptane is 69°, while for hexadecane it is equal to 47°.

Table 15.5. Contact angle θ_o in the graphite–oil drop–water system
(data by Janczuk and Chibowski, 1983)

Oil	Graphite	Sulfur
1	2	3
Hexane	69°	56°
Heptane	62°	50,5°
Octane	59.5°	49°
Nonane	58°	46°
Decane	57.5°	43°
Undecane	57.5°	40°
Dodekan	55.5°	37°
Tridecan	54°	36.5°
Tetradekan	52°	39°
Pentadekan	48°	37°
Heksadekan	47°	38°

Precise measurements of coals aquaoleophilicity is difficult because they have aliphatic and aromatic sites, as well as inclusions of gangue minerals, which feature different contact angles equal 32°, 62°, and 103°, respectively (Table 15.6). Average contact angles, calculated on the basis of these numbers, are in agreement with measured contact angles for similar coals (Table 15.4).

Table 15.6. Population of aliphatic ($\theta_o = 32°$), aromatic ($\theta_o = 62°$)
and mineral ($\theta_o = 103°$) sites for different coals. Contact angle measured through the oil phase (decane)
(data after Good and Keller, 1989)

Coal	Type**	$\theta_o = 32°$ % sites	$\theta_o = 62°$ % sites	$\theta_o = 103°$ % sites	θ_o (average*)
Blue Gem	HvBb	22	48	30	67.7°
Upper Freeport	Mvb	25	42	33	68.3°
Taggart	HvBb	18	52	30	68.9°
Illinois #6	HvCb	28	33	39	69.6°

 * weight average
** coal types according to American classification.

In order to find an appropriate oil for agglomeration of a selected substance, it is best to estimate the ΔG_{aggl} values according to Eq. (15.9), as oil agglomeration improves with more negative calculated value of ΔG_{aggl}. It can be assumed that the expression $\gamma_w \cos \theta_w - X$ is constant, but one should know the value of dispersion component of surface energy (γ_o^d) of the examined substance. Such calculations for coals are relatively easy to perform. Table 15.7 shows calculated ΔG_{aggl} values for selected oils with the use of Eq. (15.9) and assuming that for a hypothetic coal $\gamma_w \cos \theta_w - X$ is 100 mN/m and its $\gamma_o^d = 50$ mN/m, as most coals feature γ_o^d equal 50 mN/m (Good et al., 1990). In calculations it was also taken into account that some oils have different γ_o^d and γ_o values and these data were taken from the work by Kloubek (1987).

In Table 15.7 oils were arranged according to their increasing ΔG_{aggl}, values, i.e. to decreasing agglomeration potential. The table gives contact angles values calculated according to the relation:

$$\Delta G_{aggl} = -\gamma_{ow} (\cos \theta_o + 1)$$

Table 15.7. Oils arranged according to ΔG_{aggl} values that is according to decreasing ability of agglomeration by coals. θ_o and ΔG_{aggl} are relative and were calculated taking into account assumptions discussed in the text

Oil	γ_{ow}	γ_o	γ_o^d	$\cos \theta_o$	θ_o	ΔG_{aggl}
Hexadecane	51.1	27.6	27.6	0.382	68	–70.60
n-decane	51.2	23.9	23.9	0.352	69	–69.24
Cyclohexane	50.2	25.5	25.5	0.373	68	–68.91
n-octane	50.8	21.8	21.8	0.335	70	–67.83
n-heptane	50.2	20.4	20.4	0.324	71	–66.47
n-hexane	51.1	18.4	18.4	0.295	73	–66.16
CCl_4	45.0	26.9	26.9	0.428	65	–64.25
n-pentane	49.0	15.8	15.8	0.270	74	–62.21
Ethylbenzene	38.4	29.2	27.8	0.473	62	–56.57
Benzene chloride	37.4	33.6	31.8	0.507	60	–56.36
o-xylene	36.1	30.1	28.0	0.486	61	–53.63
Toluene	36.1	28.5	26.5	0.474	62	–53.20
Benzene	35.1	28.9	26.5	0.476	62	–51.80
Di (2-chloroethyl) ether	28.4	42.8	36.2	0.531	58	–43.49
o-nitrotoluene	27.2	41.5	34.2	0.515	59	–41.20
Nitrobenzene	25.7	43.9	35.2	0.498	60	–38.50
Ethanotiol	26.1	23.2	15.8	0.223	77	–31.91

15.4. Selective oil agglomeration

Oil agglomeration can be applied for selective separation of minerals and substances, especially for coal purification. Selective coal agglomeration consists of aggregation of its combustible parts and removing ash-forming minerals which do not agglomerate. Oil agglomeration takes place due to considerable coal aquaoleophilicity and weak aquaoleophilicity of ash-forming minerals. Intermediate aquaoleophilicity features pyrite, which is another coal component. Therefore, removing pyrite from coal is a difficult task, especially to a satisfactory degree, without application of special organic depressors and/or alkaline pH regulators (Drzymala and Wheelock, 1992; 1994, Capes et al., 1971). Also difficult is removal of organic sulfur from coal as it is bound with the carbonaceous substance. Basing on the data by Killmeyer (1985), Fig. 15.7 compares the curves of coal enrichment by oil agglomeration with other methods. It results from the fact that the best coal separation from gangue components can be achieved by oil agglomeration. Especially good results of separation are recorded

when coal contains clay minerals. Still better ash removing is observed for coals ground to about 10 micrometer (Jacobsen et al., 1990) and even further, to 1 micrometer (Capes, 1984) in size. Such a fine grinding ensures a full release of gangue from the carbonaceous matter and therefore ash removing from majority of coals with the use of oil agglomeration is inversely proportional to particle size in the feed (Capes, 1984).
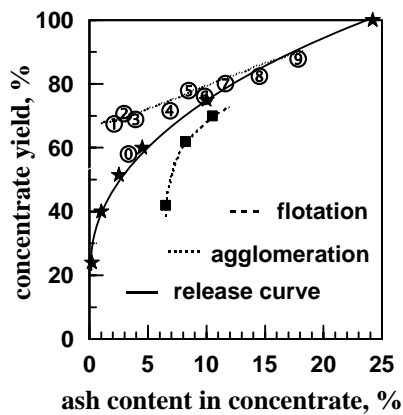
Fig. 15.7. Comparison of coal upgrading by oil agglomeration and a three-step flotation with a release curve based on the gravity-centrifugal in heavy liquids (*float/sink*) methods. Best results were achieved by oil agglomeration. The release curve is for the –0.6 mm size fraction. The numbers denote various modifications of oil agglomeration including: NRCC, Otisca T-process, Dow Solvent, Licado and agglomerating flotation (numerical values were taken from Killmeyer, 1985)

Attempts to apply oil agglomeration for coal cleaning have been undertaken for many years and the history of oil agglomeration until 1980 was described in a review work by Mehotra et al. (1983). Probably the first attempt to apply oil agglomeration in coal enrichment was the described by Cattermol in 1903 (Luis, 1909), while the Trent process was proposed in 1920 (Ralston, 1922). In this classical process about 30% of oil in relation to coal weight was used. Agglomeration was conducted in a container with a mixer and obtained agglomerates were separated on a sieve with 0.15 mm openings.

In 1952 the Convertol process was invented (Müshenborn, 1952) in which less oil was used, that is 3-15% of the coal weight and the obtained fine agglomerates were separated in special centrifuges. Then, Reerink et al. (1956) proposed an improvement in mixing. Another possibility was created by the Shell process (Mondrina and Logman, 1959), which utilizes oil emulsification before its introducing into the reaction mixture. This approach reduced the consumption of oil. In the NRCC (National Research Councul of Canada) process, which has been developed since 1960 (Sirianni et al., 1969), agglomerates are subjected to further processing in order to obtain "*spherical agglomerates*", and sometimes, *pelletizing* in water or in air in special devices. There exist many modifications of oil agglomeration including: LoMAg (Messer, 1968), S.P.S. (Brown et al., 1969), Olifloc (Blankmeister, 1976), T-process, (Keller

and Burry, 1990), Licado (Chi et al., 1989) and agglomeration in pipelines (Brown et al. 1980). Licado is the process in which coal is agglomerated with liquid CO_2 and it accumulates in the upper liquid CO_2 phase, while gangue particles fall to the water phase. In order to maintain carbon dioxide in a liquid form, the process takes place under pressure. In the T-process coal undergoes oil agglomeration with pentane which is recycled at the end of the process, after its evaporation from agglomerates and condensation.

Considerable contribution to the development of oil agglomeration provided the works financed by the National Research Council of Canada which were conducted by Puddington et al. ((Piddington i Sparks, 1975), continued by Capes et al. (e.g. Capes and Jonasson, 1989) and Ignasiak (Pawlak et al., 1990). The effect of the NRCC works was a spherical agglomeration also called the Puddington process, and different modifications of oil agglomeration, e.g. co-agglomeration of coal and limestone aiming at sulfur content decrease in gases after coal burning (Majid et al., 1990), as well as coal agglomeration in pipelines during its transportation at long distances. There are many patents regarding oil agglomeration of coal (Keller and Burry, 1988 with the list of patents until 1982).

Typical scheme of oil agglomeration is shown in Fig. 15.8. Other schemes can be found in a review work by Mehotra et al. (1983).
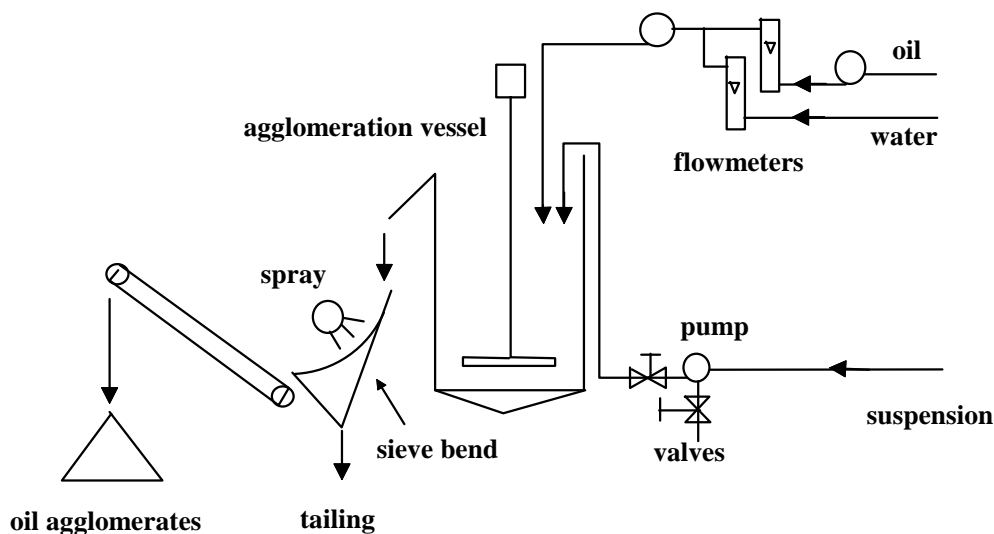
Fig. 15.8. Typical scheme of coal cleaning by means of oil agglomeration (Armstrong, 1978). Other schemes are described by Mehotra et al., 1983

A few systematic investigations on the selectivity of oil agglomeration suggest that the best separation can be obtained when aliphatic hydrocarbons are applied

(Fig. 15.9a and b). Lower quality coal concentrates result from the use of halogen derivatives of aliphatic hydrocarbons (such as CCl_4). The highest amount of ash features the concentrates obtained by oil agglomeration with aromatic hydrocarbons (Keller and Burry, 1987). Figure 15.9a correlates the ash contents in coal agglomerates, adopted from Keller and Burry (1987), and the dose of the oil needed for half-way coal agglomeration (Drzymala and Wheelock, 1989). Figure 15.9b correlates the same ash contents with ΔG_{aggl} of oil agglomeration, taken from Table 15.7. A good correlation between these quantities indicates that oils of high ability to agglomerate the carbonaceous matter are at the same time most selective in removing ash-forming components. This suggests that the difference in ΔG_{aggl} of components determines the selectivity of agglomeration.

a   b
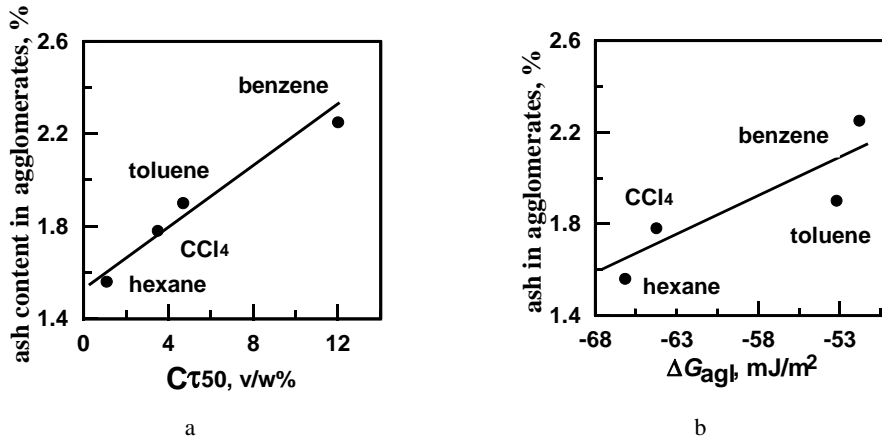
Fig. 15.9. Correlation between ash content in dry agglomerates obtained with different oils and dose of oil needed for half-way agglomeration (a), or free enthalpy of agglomeration (b). Source: ash content – Keller and Burry (1987), $c_{\tau 50}$ values – Drzymala and Wheelock (1989), ΔGaggl – table 15.7

Agglomeration of coal having low aquaoleophilicity can be conducted in the presence of oleic acid (Abdelrahman and Brookes, 1997), which increases affinity of oil towards coal. Hydrophobizing substances are also applied in non-coal materials cleaning which makes the use of oil agglomeration. Some surfactants can be used as hydrophobizing substances, though they should not decrease interfacial tension (γ_{ow}) too much. In such a case oil agglomeration ceases and contact angle can reach the values close to 180° (Kao, 1988/89; Menon and Wasan, 1988). The phenomenon of decreasing γ_{ow} is made use of in oil removing from surface of materials, which takes place during washing.

Oil agglomeration can be applied for upgrading different ores and raw materials, as well as for removing oil contamination from soil (Szymocha et al., 1996). In Table 15.8 there were shown some examples of oil agglomeration used for non-coal substances.

The pH of aqueous solution influences oil agglomeration. Labuschagne (1986b) proved that the same rules are valid for flotation, oil agglomeration, and other surface related processes.

Table 15.8. Application of oil agglomeration for selective and non-selective agglomeration of non-coal materials

Raw material	Hydrophobization substance–oil	Modifier	Remarks	Source
Al_2O_3	dodecylsulphonate–paraffin oils, benzene	pH	pH of agglomeration <7,8, $\theta_o < 90°$	Kavoridis et al., 1981
$(Fe,Mn)WO_4 + SiO_2$	sodium oleate –fuel oil	pH, $FeCl_3$	aggl. of wolframite at pH 7,3	Wei et al., 1986
SnO_2 and $SnO_2 + SiO_2$	*/iso-octane	pH	aggl. of SnO_2, pH < iep = 3,9**	Allen and Veal, 1988
$(Fe,Mn)WO_4$	oleic acid –isooctane	pH	aggl. of wolframite, pH = 6–10	Kelsall and Marinakis, 1984
$(Fe,Mn)WO_4 + SiO_2$	dodecylamine–isooctane	pH	aggl. of wolframite, pH = 2–4	Kelsall and Pitt, 1987
$CaCO_3$	sodium oleate	–	spherical aggl. when $\theta < 90°$	Kawashima et al., 1986
$ZnS + CaCO_3$ (+ graphite)	butyl xanthate–nitrobenzene	$CuSO_4$	aggl. of ZnS pH = 7–8	Farnard et al., 1961
$Fe_3O_4 + SiO_2$	sodium oleate –n-heptane		aggl. of Fe_3O_4	Drzymala, 1994
$Fe_3O_4 + SiO_2$	oleic acid (HOl)–n-heptane		agg. of Fe_3O_4	Drzymala, 1994
Iron ore with apatite	HOl and tall oil–naphtha oils		aggl. of Ca-minerals pH = 10	Sirianni et al., 1968
Iron ore	HOl – naphtha	pH, Na_2SiO_3	pH = 8,5	Uwadiale, 1990
Flotation tailing .$BaSO_4 + CaCO_3 + SiO_2$	fatty acids, other–light oils		aggl. of barytu, pH = 10,2	Meadus and Puddington, 1973
$CaCO_3$, $BaSO_4$, Fe_2O_3, CuO, other	sodium oleate–heptane			Sadowski, 1997
$CaCO_3$, $BaSO_4$	sodium dodecylsulfate (SDS)–heptane		Calcite requires $Ca(SDS)_2$	Sadowski, 1997

* tetra sodium salt of N-octadecyl 1,2 dicarboxyethyl sulfosuccinate.
** too much surfactant may destroy agglomerates.

The best recovery of agglomerated mineral and other materials is usually observed at their pH_{iep}. For coals pH_{iep} is typically within pH range from 2 to 4. Other pH values than pH_{iep} make agglomeration worse, although for many coals the decrease in agglomeration is not significant. The electric properties of materials, characterized by pH_{iep} also effect kinetics of agglomeration. Agglomeration time is the shortest near pH_{iep}. From this pH value up to pH about 8, the time necessary for agglomeration becomes longer (Labuschagne, 1986b), but then it becomes shorter and shorter, espe-

cially at pH 11-12 (Papushin et al., 1984), while the zeta potential within this pH range also decreases. pH also effects the selectivity of coal agglomeration. pH_{iep} values for most coals, oils and gangue minerals are similar and they range from 2 to 4. In this pH range electric charge is low and the particles show a tendency to coagulation and heterocoagulation. Therefore, the selectivity of separation at these pH values is not optimum. The best selectivity is achieved in the alkaline environment, where the gangue features high negative electric charge and is well dispersed (Lai et al., 1989). However, this is not valid for all coals. For some coals one can observe an opposite relation, i.e. a decrease in the ash-forming minerals content as the pH is higher then pH_{iep} (Labuschagne, 1986b). This can result from other properties of the gangue. It should be noted that the above analysis of the selectivity process based on the data by Lai et al. (1989) and Labuschagne (1986b) is not complete, as the authors did not provide full data for drawing the upgrading curves which would answer in details the question about the effect of pH on selective oil agglomeration of coal.

The amount of oil influences oil agglomerates recovery on sieves. Yet, it does not effect separation selectivity, especially for coals, as agglomeration results generally form one smooth upgrading curve. The selection of the upgrading curve for assessment of selectivity of oil agglomeration depends on system specificity and the preferences of a person making the plot. For coal, the Fuerstenau upgrading curves, in the form of coal recovery in the concentrate related to ash recovery in the tailing, is very suitable. Suitable is also the Henry upgrading curves indicating coal concentrate yield versus ash content in the concentrate (Fig. 15.7). Less suitable is the Mayer curve, since it is very flat, unless is plotted as ash recovery in the concentrate vs. concentrate yield.

15.5. The mechanism of oil agglomeration

Physical form of agglomerates, their density, moisture, sphericity, and mechanical resistance are dependent, to a high degree, on aquaoleophilicity of the solid–oil–water system, amount of oil, and the hydrodynamics of the process (intensity and mixing time). There can be distinguished three states of agglomerates (Fig. 15.10).

Pendular state is characterized by the existence of oil bridges formed between particles, joining them into aggregates, called *oil flocs*. Increasing the amount of oil, as well as intensive mixing, can result in increased agglomerate compactness. Therefore, water bridges start to dominate in the aggregates. This condition is called the *funicular state* of agglomerates. In the *capillary state*, there are no bridges since the particles are bound together with oil only. Further oil addition to the system causes formation of a separate oil phase containing the particles which feature considerable aquaoleophilicity ($\theta_0 < 90^0$) and the ones of $\theta_0 >> 90^0$ value remain in the aqueous phase.

Another form can be observed in oil–particle agglomerates when the particles are smaller than oil drops. Then, we deal with so-called *stabilized emulsions*. The form of stabilized emulsion depends on particle aquaoleophilicity (Fig. 15.11). When $\theta_0 > 90^0$ oil drops do not join one another (Fig. 15.11a) while for $\theta_0 < 90^0$ oil drops can be agglomerated (Fig. 15.11b).
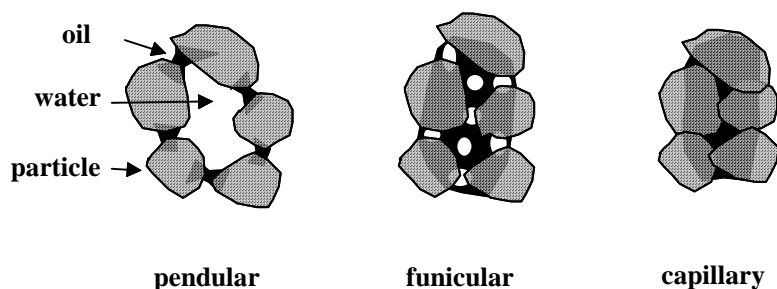
Fig. 15.10. States of oil agglomerates
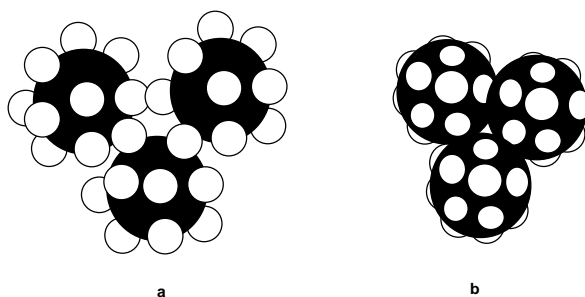
Fig. 15.11. Shape of oil–particles agglomerates when oil drop is larger then particle. Such state is called stabilized emulsion: a – $\theta_o > 90°$, b – $\theta_o < 90°$. Oil drops are black

Particular states of oil agglomeration can be recognized by examining different properties of the system, including agglomerate compactness, resistance, density, moisture, etc. Figure 15.12 shows the change of agglomerate volume in relation to the amount of oil in the system.

In the pendular state the agglomerate volume significantly increases, as added oil amount increases, due to the formation of agglomerate structure.

Funicular state can be recognized due to decreasing agglomerate volume, since the aggregates become more compact and there does decrease the number of water bridges as the amount of added oil increases.

The capillary state is when the agglomerate volume stops decreasing and a further oil addition causes the increase in organic phase volume, and also in aggregate volume.

It results from Fig. 15.12, that the recovery of agglomerates, for instance by sieving, is complete when the aggregates are either in funicular or capillary state.
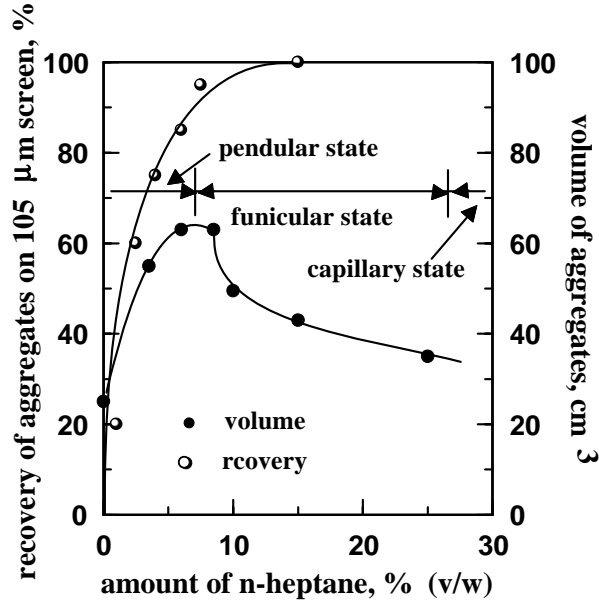
Fig. 15.12. States of agglomerates appearing in a curve showing the volume of agglomerates or their recovery as a function of oil dose (after Drzymala et al., 1986)

The process of oil agglomeration in periodical system, i.e. at constant amount of oil added to predetermined amount of the suspension of solids in water and subjected to mixing with constant intensity, takes place in four stages (Fig. 15.13).
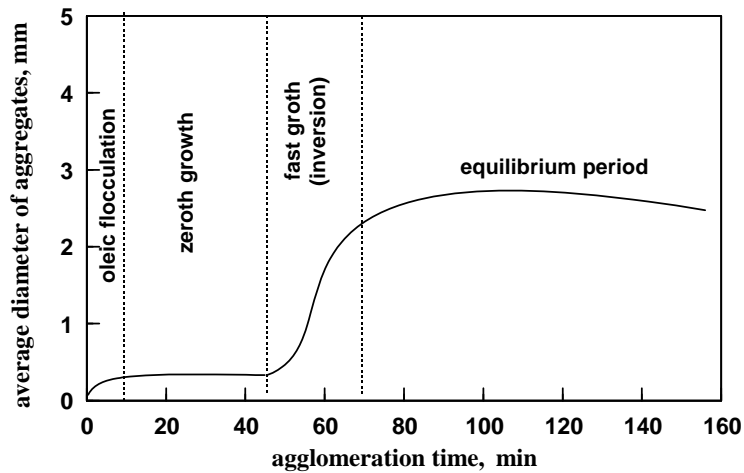
Fig. 15.13. Four stages that can occur during oil agglomeration (after Bemer and Zuiderweg, 1980)

In the first stage, usually short–lasting period, stabilized emulsion and pendular free oil floccules are formed. In the second stage, the system is apparently inert. It is also called the period of zero growth. In this stage a complete transition of emulsion drops, which are stabilized by the particles present on the oil drops surface, into agglomerates of a pendular structure is observed. In the subsequent, third stage, there is a rapid growth of aggregates and their transition into funicular state. This period is also called the period of rapid growth or inversion (Bhattacharyya, 1977). The last stage features final forming of agglomerates (equilibrium period), which, at appropriately intensive mixing, can become spherical due to capillary state of agglomerates or form sphere–like structure.

The length of particular periods and their intensity depend on many factors, mainly on the amount of oil, particle aquaoleophilicity, hydrodynamics (intensity of mixing) and the presence of additives (surfactants, pH regulators, air).

The effect of aquaoleophilicity on the structures forming aggregates, when $\theta_0 < 90^0$ was shown in Fig. 15.14.
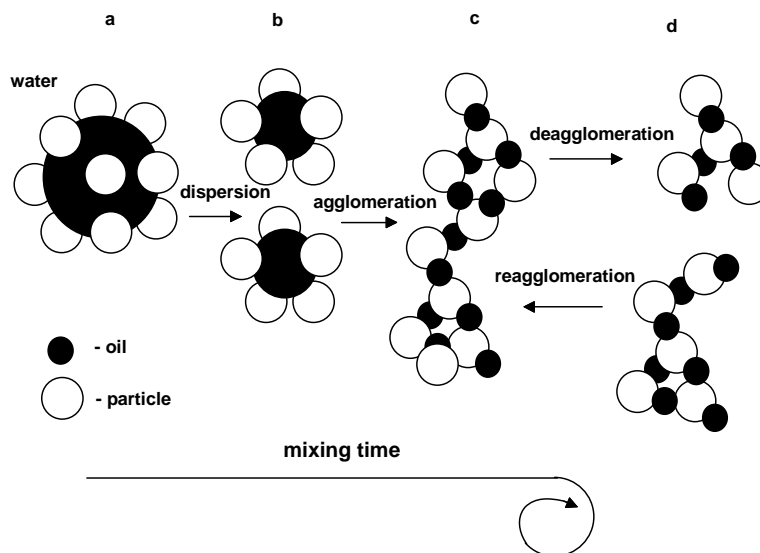
Fig. 15.14. The course of oil agglomeration of weakly aquaoleophilic materials $(\theta_o > 90°)$
as a function of mixing time: a – emulsion stabilized with particles, b – the increase in degree of oil drops dispersion, c – formation of oil flocs (oil drops are smaller than particles),
d – disintegration of agglomerates as a result of mixing and their secondary agglomeration

In the case of weakly aquaoleophilic materials ($\theta_0 > 90°$), due to mixing, the system changes from the state of stabilized emulsion (a and b) to oil flocs in the pendular state

(c and d). In this system, funicular structures (microagglomerates) and spherical agglomerates are not formed. Difficulties in forming funicular bridges or microagglomerates can be explained by analysis of forces occurring in agglomerates, which are subjected to the disrupting forces resulting from stirring of the system (Fig. 15.15). The force of bonding bridge equals the capillary surface energy $\gamma_{ow}\sin\theta$ multiplied by the perimeter which is effected by the force and which is constant in our considerations, as the surface of bridge fixing, until bond disruption, does not change. It results from this analysis, that the bridge resistance force increases as the disrupting increases, i.e. when the distance between particles increases to $x+\Delta x$, as $\theta_0 > \theta_g < 90^0$. The decrease in contact angle results from the fact that the bridge undergoes stretching. Such a behavior of oil bridge is a result of water, which as a surrounding continuous phase, fills the space formed due to particle distancing. When the disrupting force becomes considerable, a rupture of one of the links of the particle–oil drop takes place and oil drops will be present on the surface. During stirring, re-linking can take place between the drops and particle surface, i.e. reagglomeration. Thus, as it was shown in Fig. 15.14, disrupting the bridges causes deagglomeration and in the region of weak disrupting forces the reagglomeration does occur. The system achieves equilibrium state without undergoing inversion, i.e. to the funicular state. The pendular flocs (agglomerates) are weak and cannot be recovered by screening on sieving. Therefore, weakly aquaoleophilic substances cannot be subjected to oil agglomeration. It involves most oxides (quartz, hematite), carbonates (calcite, dolomite) and aluminosilicates.

$\Theta_0 > \Theta_R > 90^0$
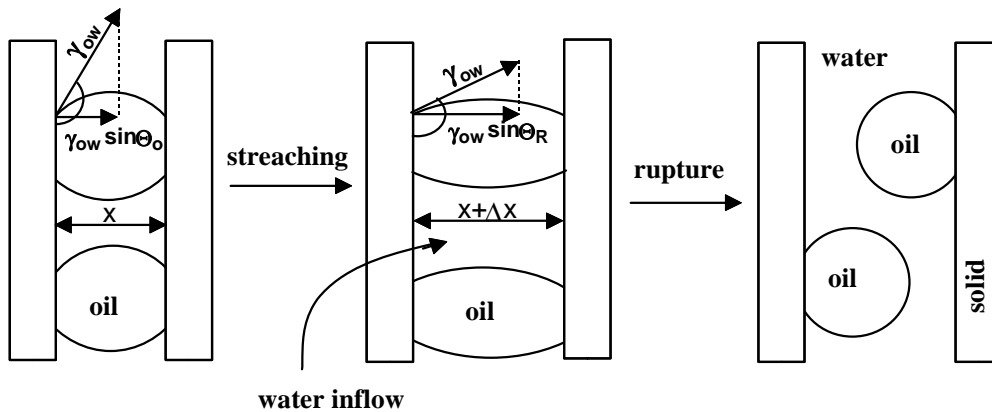
Fig. 15.15. Forces in pendular oil bridge during its rupture. Final state is the formation of drops on the surface of particle

Another course of oil agglomeration occurs for strongly aquaoleophilic materials when $\theta_R < \theta_A < 90^0$. The stages are shown in Fig. 15.16. In the first stage, after introduc-

ing oil, the drops surrounded by particles are formed. They create stabilized emulsion (a). In the course of stirring the size of oil drops decreases (b) until the size of particles and drops becomes similar. Then, we deal with oil agglomerates where particles are linked with one another by pendular oil bridges. The analysis of bridge strength is shown in Fig. 15.17a. On the basis of this figure one can conclude that the bridge rupture leads to a decrease in binding power as in the course of disrupting contact angle decreases from θ_0 to θ_R. This results from the fact that oil bridge, already being very narrow, becomes even more reduced at the half of its length, since the empty space resulting from stretching, is filled not with oil but water present in higher amount between the particles and which constitutes the continuous phase. When bridge is disrupted, instead of having two drops again, four smaller drops are formed on the mineral surface. These drops, due to collisions with other agglomerates, immediately form new bridges. The process of stirring in pendular system for $\theta_R < \theta_0 < 90^o$ leads to oil distribution between particles and to the increase in the number of bridges.
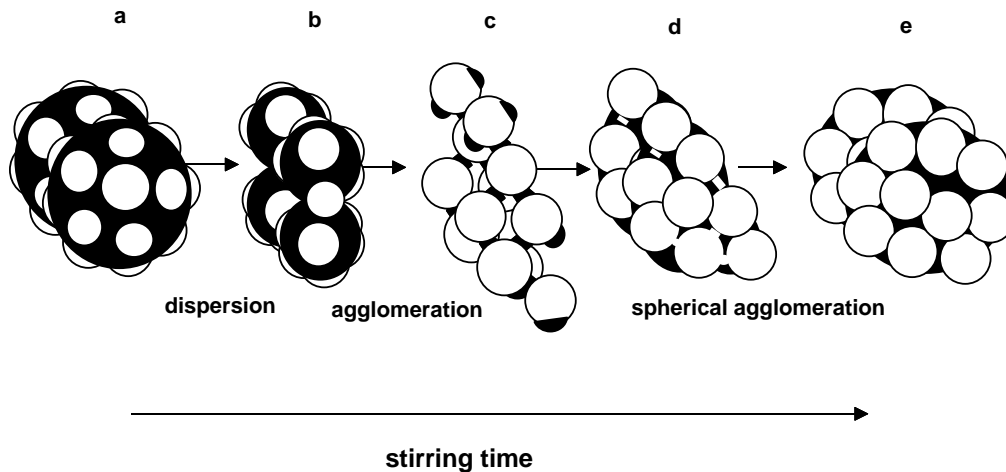
Fig. 15.16. Oil agglomeration of highly aquaoleophilic material ($\theta_o < 90°$)
as a function of mixing time: a – emulsion stabilized with particles, b – increase in oil dispersion degree, c – appearance of oil floccs in pendular state, d – formation of oil floccs (microspheres) in funicular state, e – spherical agglomerates in capillary state

The increase in the number of bridges makes oil the continuous phase (Fig. 15.16d), the bridges become water bridges, and funicular agglomerates are formed. A new kind of bridges alter agglomeration mechanism and requires new analysis of binding forces, which are shown in Fig. 15.17b. Now, the stretching of water bridges encounters considerable resistance as contact angle increases. When the water bridge gets disrupted, water drops appear on the surface and they are removed from the aggregates in subsequent stages of agglomeration. This, in turn, creates the conditions for forming capillary agglomerates which contain exclusively oil (Fig. 15.16e).

a)

$\Theta_R, < \Theta_o < 90^o$,   **pendular state**

b)

$\Theta_R < \Theta_E < 90^o$,   **funicular state**
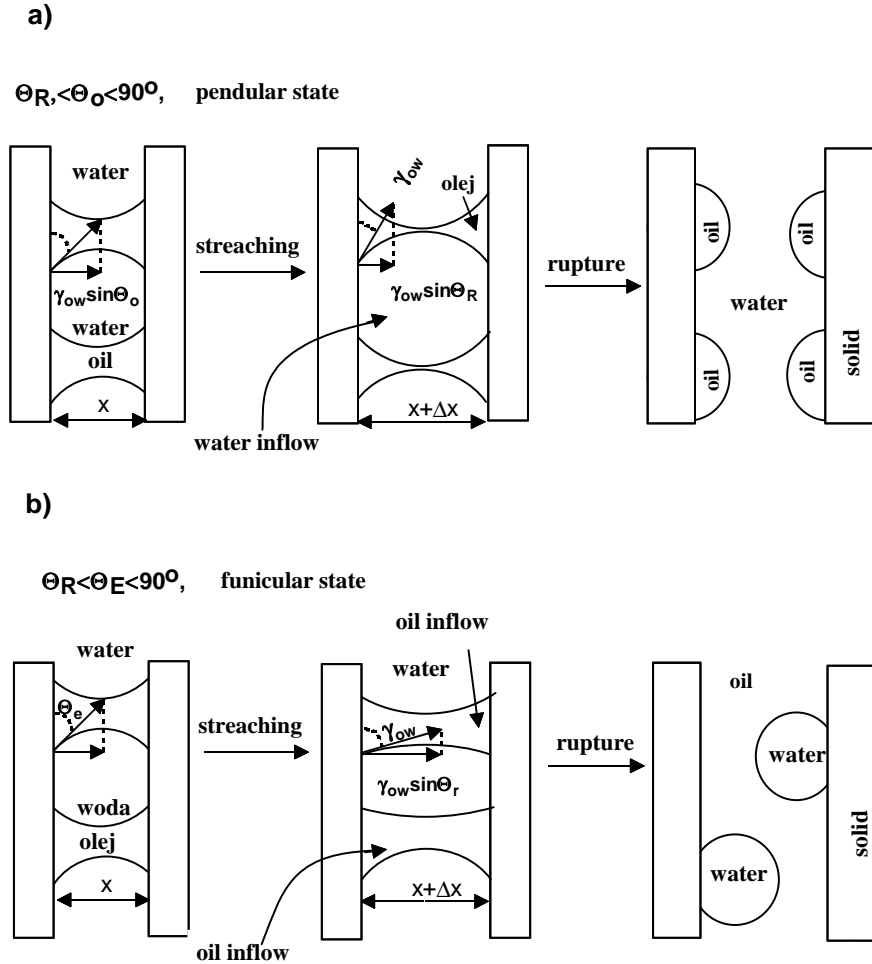
Fig. 15.17. Forces acting in bridges between particles during their rupture when $\theta_R < \theta_o < 90°$, a – pendular bridge (final outcome is the formation of a higher number of bridges), b – funicular water bridge (final outcome is the formation of water drops, which are removed from agglomerates)

The above analysis of bridge resistance represents a much more advanced mechanism of agglomeration than previously proposed by Good and Islam (1991) and proves that the process depends on the $\gamma_{ow}\sin\theta_o$. This is confirmed by already presented results of thermodynamic analysis of the system pointing to the importance of aquaoleophilicity θ_o and γ_{ow}.

The final stage of agglomeration of materials with $\theta_o < 90°$ is the formation of spherical agglomerates which can be easily separated from the suspension by screening or sieving. This mechanism of agglomeration is valid for some coals, especially those which are strongly aquaoleophilic, as well as graphite. Opinions on possible

spherical agglomeration of less aquaoleophilic coals differ considerably; some researchers claim that those coals can undergo agglomeration resulting in microspheres, or even leading to formation of spherical agglomerates, while others do not support this view. The reason of different views is very likely the presence of the air in the agglomerating system. This issue is discussed in details in the next subchapter.

Spherical agglomerates can be formed as a result of agglomeration. Investigation by Kavashimy et al. (1986; Takamori, 1984) proved that diameter D of agglomerates depends on oil–water interfacial tension γ_{ow} and aquaoleophilicity θ_o

$$D^{3-n} = K(1 - \varepsilon/\varepsilon)\gamma_{ow} \cos \theta_o/d\psi, \tag{15.12}$$

where:
n and K – constants
ε – porosity of agglomerates
D – diameter of particles
ψ – saturation of binding liquid.

The dependence of sphere size and oil dose is logarithmic (Fig. 15.18). When too much oil is added to the system, a few or one lump is formed which is called *oil amalgam.*
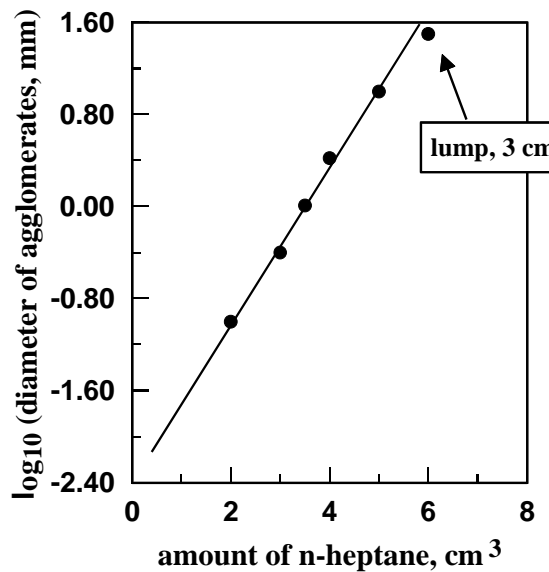
Fig. 15.18. Relationship between the size of agglomerates and oil dose used for their formation (after Drzymala et al., 1986)

A positive technological feature of spherical oil agglomerates is their diminished moisture. Two kinds of moisture can be distinguished in agglomerates: internal and

surface moisture. The internal moisture results from the water content in particles be-
fore their agglomeration. The amount of water M bound with particles is proportional
to the mass of particles forming agglomerate, i.e. to agglomerate volume $\pi D^3/6$ of di-
ameter D. On the other hand, water mass on oil agglomerate surface is proportional to
agglomerate surface, i.e. πD^2, thus:

$$M = K_1(\pi D^2) + K_2\,(\pi D^3/6),\qquad(15.13)$$

where K_1 and K_2 are proportionality coefficients.

Since moisture content W in agglomerates is connected with water content M via
the following the relation:

$$W = \frac{M}{\pi D^3/6},\qquad(15.14)$$

the expression for moisture content in oil agglomerates, depending on their size, is de-
scribed by the equation (Capes et al., 1971):

$$W = \frac{6K_1}{\rho D} + \frac{K_2}{\rho}.\qquad(15.15)$$
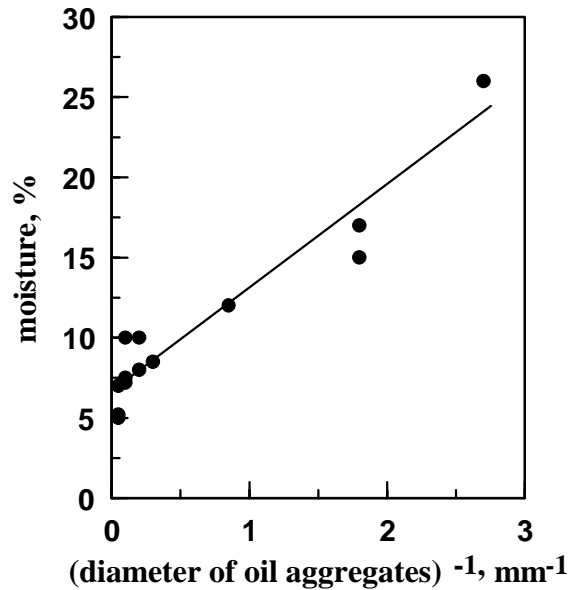
Fig. 15.19. Moisture of oil aggregates increases with decreasing size of aggregates (that is with increasing
reciprocal of aggregates diameter D) (after Capes, 1971)

The relation between agglomerate moisture and a reciprocal of their diameter
should be linear. This is in agreement with the experimental data shown in Fig. 15.19

after Capes (1979). Crossing the moisture line with the axis of moisture content *W* indicates internal moisture of the particles forming agglomerates.

15.6. Air in oil agglomeration of coal

The results of many investigations by Wheelock and his team at Iowa State University (Drzymala et al., 1986; Wheelock et al., 1994; Drzymala and Wheelock, 1996 and 1997; Milana et al., 1997) indicate an important role played by air in coal agglomeration. So far, the mechanism of air effect in oil agglomeration has not been fully understood. It seems now that air acts as a catalyst in oil agglomeration accelerating the process. In some cases the presence of air is indispensable for pushing oil agglomeration beyond the stage of forming stabilized emulsions and pendular oil floccs. The amount of air in intermediate agglomeration forms can be quite high, but it becomes low in the final agglomeration product, i.e. in large agglomerates, microspheres or spherical agglomerates. The role of air in oil agglomeration strongly depends on aquaoleophilicity, namely on contact angle of agglomerated material, especially when it is greater than 90°. Many mineral substances, particularly coals, feature heterogeneous surface and considerable hysteresis of contact angle, which means that their oil advancing contact angle of θ_A markedly differs, even by 80°, from the oil receding contact angle. Moreover, their θ_A can exceed 90° and θ_R be less than 90°. Coals are a good example. (Table 15.2). Therefore, the final outcome of oil agglomeration depends on the way of conducting agglomeration, i.e. whether receding or advancing oil contact angle plays the main role. It seems that air minimizes or eliminates disadvantageous effect of higher than 90° values of oil advancing contact angle in oil agglomeration. The fact that in typical oil agglomeration a decisive role is played by oil advancing contact angle suggest analogy to the flotation process. The latter one is initiated by a collision of an air bubble with a mineral particle. Flotometric examinations (Drzymala, 1999) showed that contact angle of receding water, under the influence of pushing air bubble, is a crucial parameter. Therefore most coals, in spite of their relatively high water advancing contact angle (measured through the aqueous phase, i.e. high hydrophobicity), do not float without collectors, as their receding contact angle is very low.

Oil agglomeration is the process similar to flotation, since an air bubble is replaced by an oil drop. Therefore, one should expect that this process will be determined by the ability of oil drop of spreading on immersed in water particle surface i.e. determined by oil advancing contact angle θ_A. Thus, when θ_A is higher than 90°, complete oil agglomeration does not take place, since as it has been previously described, agglomeration stops at the stage of stabilized emulsion and pendular flocs. The presence of air completely alters the mechanism of the process. First of all, because oil easily spreads on the surface of solids in the air, as well as on water surface in the air or it

forms extremely flat lenses. Investigations by Melik-Gajkazjan (1965), (Laskowski, 1992; Baichenko and Listovnichii, 1989) also proved that oils, binding mineral particles in the presence of air, form a ring (Fig. 15.20a). Due to these rings, fixing of a bubble to a particle, and thus also particle agglomeration, is strong.

Hypothetical course of oil agglomeration in the presence of the air for the materials of low aquaoleophilicity is shown in Fig. 15.20a-d. Although substances with $\theta_A > 90^0$ in the presence of most oils do not form funicular agglomerates (Fig. 15.14), the presence of the air allows oil to spread on particles which leads to forming spherical agglomerates and releasing the air. The ability of air bubbles to agglomerate hydrophobic particles suspended in water is utilized in the so-called "air agglomeration" (Drzymala and Wheelock, 1995). Due to oil ability to spread at the water–air interface, emulsion drops stabilized with particles also can bind gas bubbles. After attachment reorganization takes place, which results in forming characteristic petals (Fig. 15.21), which can be seen under microscope in an appropriate moment of oil agglomeration. This results in formation of spherical aggregates and air, although θ_A for the agglomerating substance is above 90^0.

The influence of the air on oil agglomeration depends on the material used for agglomeration. The most crucial role is played by air when the material's contact angle is $\theta_A > 90^0$ and $\theta_R < 90^0$, which has already been discussed. American Colchester coal behaves in this way. Its spherical agglomeration with isooctane is not possible without the presence of the air (Wheelock et al., 1994; Milana et al., 1997). Pittsburgh No 8 coal also does not agglomerate spherically in the absence of the air (Drzymala and Wheelock, 1996) and its contact angles, as it was shown in Table 15.2, is $\theta_A = 135^o$ and $\theta_R = 55^o$. When the substance of a high aquaoleophilicity is subjected to agglomeration, the result is spherical agglomeration without the presence of the air. American coal No 2 Gas Seem (Wheelock et al., 1994) can serve as a good example.

The air increases the speed of coal agglomeration and makes the formed agglomerates larger. There also increases the recovery of carbonaceous matter and selectivity of coal cleaning (Wheelock et al., 1994).

Additional information on oil agglomeration in the presence of the air can be obtained by torque of impeller measurement during stirring and microscopic observations. The torque during oil agglomeration in the presence of air assumes certain characteristic turning points, which in Fig. 15.22 were marked with letters from A to F. In the first stage of stirring, oil dispersion and formation of stabilized emulsion take place. The ratio of number of emulsion drops to pendular floccs depends on such factors as hydrodynamics, particles and drops size, etc. When coal is highly aquaoleophilic, an inversion takes place and first funicular and next capillary agglomerates are formed, as it was shown, after Bemer and Zuiderweg (1980) in Fig. 15.3. When coal is aquaoleophilic $\theta_R < 90^o$, oil agglomeration will be stopped at the stage of stabilized emulsion or oil floccs. Introduction of the air into the system initiates a number of processes. First, air incorporation into the system takes place (line A-B). Line B-C

characterizes oil flocs and oil petals formation, which is shown in Fig. 15.20 and 15.21. During C-D period, the decreases in torque can be recorded as a result of large funicular flocs formation. Large flocs then change into spherical agglomerates. From point E agglomerates increase their spherical shape and their sizes become similar. Their compactness also increases, which leads to oil pressing out onto the surface. Then, agglomerates become viscous and their adhesion to the other spheres becomes increased. When adhesion reaches an appropriate level, secondary spherical agglomeration occurs, which leads to linking spherical agglomerates into larger units (point F). Adhesion of spherical oil agglomerates, in the form of adhesion coefficient, can be estimated by comparing agglomerate diameter measured with the use of sieve analysis and microscopic analysis (Drzymala and Wheelock, 1988).
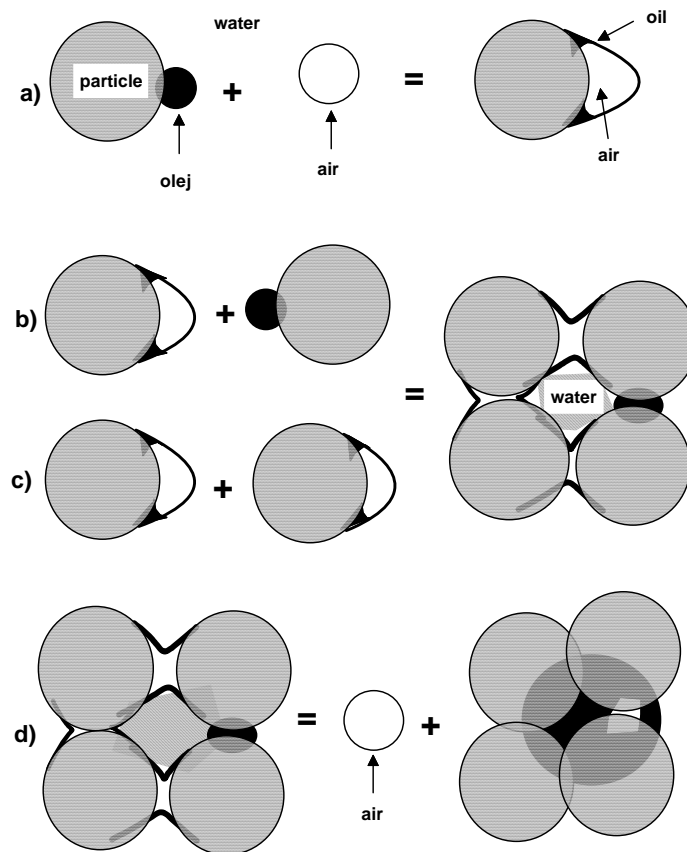
Fig. 15.20. Hypothetical course of oil agglomeration in the presence of the air.
Possible mechanism of formation of oil flocs containing the air (a–c)
and formation of spherical agglomerates (d)
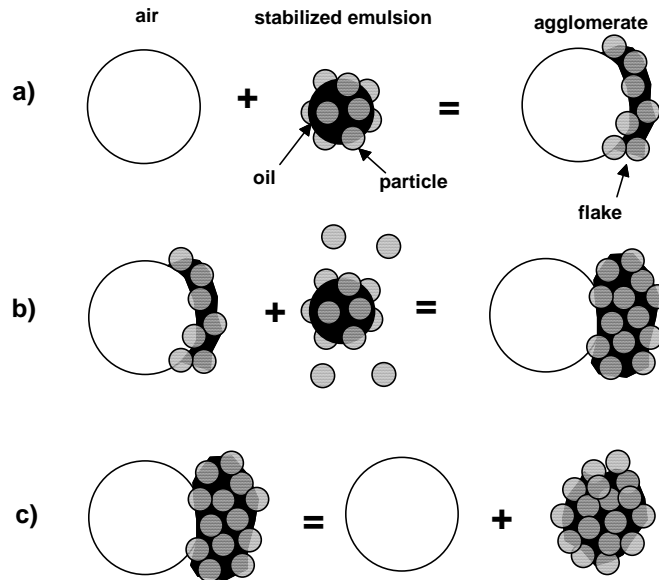
Fig. 15.21. Hypothetical coarse of oil agglomeration in the presence of air.
Possible mechanism of formation of „petals" (a) and spherical agglomerates (b, c)
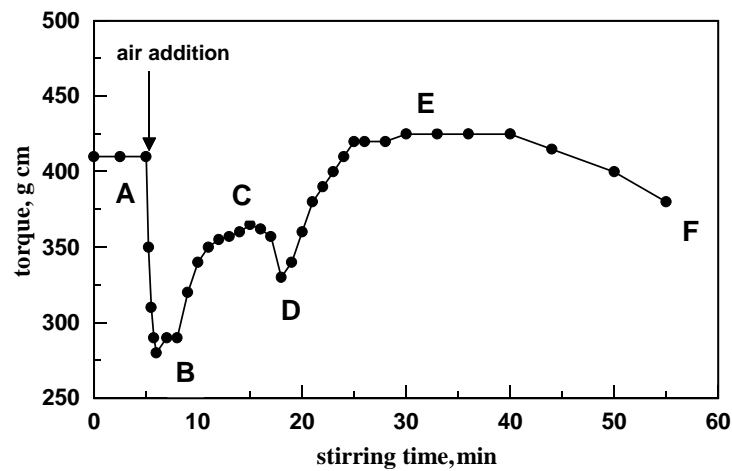
Fig. 15.22. Torque changes during oil agglomeration in the presence of air added as one portion: A –
formation of oil emulsion stabilized by coal particles and formation of microflocs, A–B – air agglomera-
tion (air uptake by the system), B–C – formation of oil flocs and agglomerates in form of petals, C–D –
formation of oil agglomerates (large flocs), D–E – transition between agglomerates (large flocs) and
spherical agglomerates, E–F – increase of sphericity, size similarity and spheres adhesion, F – secondary
agglomeration of spheres (multiplication of spheres size). Results for Pittsburgh No. 8 coal: 30% of coal
in aqueous suspension, 30 % – isooctane (in relation to coal), 9% air content (in relation to coal), tank
diameter – 7.62 cm, impeller diameter – 3.65 cm, impeller velocity 1750 rpm
(after Drzymala and Wheelock, 1996)

Time necessary for reaching point E of spherical agglomeration depends on many factors. Investigation on the influence of different parameters in geometrically similar tanks showed that time t_E (in minutes) needed to obtain spherical agglomeration (point E) for Pittsburgh No 8 coal depends on the energy of stirring P (in watts), system volume V (in dm^3) and the amount of the air C_a (air volume per coal mass unit in per cent) according to the equation (Drzymala and Wheelock, 1996):

$$t_E = 1972 \, (P/V)^{-1,11} \, C_a^{-0.58} \, . \tag{15.16}$$

This equation can be very useful for designing tanks for oil agglomeration on a larger scale.

The air can be introduced into agglomeration systems or it can originate from water in which it is dissolved. The same role as gas bubbles in oil agglomeration can be played by cavities formed due to fast rotation of the impeller (Zhou et al., 1997; Yuschenko et al., 1983).

15.7. Modifications of oil agglomeration

There are many modifications of oil agglomeration, which are briefly described in Table 15.9.

Table 15.9. Modifications of oil agglomeration and their characteristics

Name of method	Characteristics	Source
Vibroacoustic oil agglomeration	ultrasonic stirring (instead of impellers)	Djebdowa and Stojew, 1984
Aggregative flotation	agglomerates are removed by flotation	Wojcik and Taweel, 1984; Pawlak et al., 1990
Agglomeration in mills	agglomeration in special mills (Szego mill)	Trass, 1988
Air assisted oil agglomeration	addition of the air makes agglomeration possible or improves agglomeration	Wheelock et al., 1994; Drzymala and Wheelock, 1997
Oil agglomeration in pipelines	agglomeration durnig transport in pipelines	Brown et al., 1980
Separation of particles to oil phase	aquaoleophilic particles report to the oil phase while aquaoleophilic to the aqueous phase	Shergold, 1981
Peletization	Peletization of particles with oil in the air with a small amount of water or without water	Mehrotra i Sastry, 1986
Oil flotation	Flotation with oil drops instead of the air	Shergold, 1981

Literature

Abdelrahman A.A., Brookes G.F., 1987. An economic assessment of using surfactants in cleaning coal by the oil agglomeartion method, Energy Progress, 7(1), 47–50.

Allen R.P., Veal C.J., 1988. The spherical agglomeration of cassiterite, XVI IMPC, E. Forssberg (ed.), Elsevier, Amsterdam, 1109–1120.

Armstrong L.W., Swanson A.R., Nicol S.K., 1978. Selective agglomeration of fine coal refuse, BHP, Technical Bulletin, 22 (10, 1–6.

Baichenko A.A., Listovnichii A.V., 1989. Rims of an apolar reagent on the surface of a particle being floated, Kolloidnyj Zhurnal of USSR, 51(1), 97–104, 51(1), 123–126.

Bemer G., Zuiderweg F.J., 1980. Growth regimes in the spherical agglomeration process, in: Fine particles processing, Chap. 77, P. Somasundaran (ed.), AIMMPE, New York, 1524–1546.

Bhattacharyya R.N., Moza A.K., Sarkar G.G., 1977. Role of operating variables in oil agglomeration of coal, in: Agglomeration 77, Proc. 2nd Int. Symp. „Agglomeration", K.V.S. Sastry (ed.), AIMMPE, New York, Chap. 54, 910–951.

Blankmeister W., et al., 1976. Optimized dewatering below 10 mm, Seventh International Coal Preparation Congress, Sydney, Australia.

Brown R.B., Brookman H.H., Haupt C.G., 1969. A continuous process for agglomeration and separation, Institute for briquetting and agglomeration, Vol. 11, s. 61.

Brown N.A., Rigby G.R., Callott T.G., 1980. Coking behavior of coals recovered from slurry pipelines using a selective agglomeration technique, Fuel Process. Technol., 3, 101–108.

Capes C.E., Jonasson K., 1989. Application of oil-water contact of coal in beneficiation, in: Interfacial phenomena in coal technology, G.D. Botsaris i Y.M. Glazman (eds.), Dekker, New York, 1989, 115–155.

Capes C.E., 1984. Treatment of coal fines in suspension by agglomeration methods, Proc. Inter. Symp. Powder Technology, 1981, Kyoto, K. Iinoya, J.K. Beddow, G. Jimbo (eds.), Mc Graw Hill, 646–655.

Capes C.E., 1979. Agglomeration, in: Coal Preparation, J.W. Leonard (ed.), Amer. Inst. Mining Metal. And petrol Eng., New York, 10–105/10–116.

Capes C.E., McIlhinney A.E., Sirianni A.F., Puddington I.E., 1971. Agglomeration in coal preparation, Proc. 12th Biennal Conference of the Institute for briquetting and agglomeration, Vol. 12, Vancouver BC, Canada, 53–65.

Chi S.-M., Morsi B.I., Klinzing G.E., Chiang S.-H., 1989. LICADO process for coal cleaning-mechanism, Coal Preparation, 6, 241–263.

Djebdova S., Stojev S., 1984. Vibroacoustical selective agglomeration of coal slimes, Powder Technology, 40, 187–194.

Drzymala J., Wheelock T.D., 1989. Internal report, Chem. Eng. Dep., Iowa State University, Ames, IA.

Drzymala J., Wheelock T.D., 1995. Air agglomeration of hydrophobic particles, Processing of Hydrophobic Minerals and Fine Coal, J. Laskowski i G.W. Poling (eds.), Canadian Institute of Mining , Metallurgy and Petroleum, Montreal Canada, 201–211.

Drzymala J., Wheelock T.D., 1992. Potential pyrite depressants for use in oil agglomeration of fine size coal, Coal Preparation, 10, 189–201.

Drzymala J., Wheelock T.D., 1994. Effect of oxidation and thioglycolic acid on separation of coal and pyrite by selective oil agglomeration, Coal Preparation, 14, 1–11.

Drzymala J., 1999, Flotometric hydrophilicity of coal particles, 1999. Proc. '99 Inter. Symp. Mining Sciece and Technology, Beijing, Balkema, 533–537.

Drzymala J., Markuszewski R., Wheelock T.D., 1986. Influence of air on oil agglomeration of carbonaceous solids in aqueous suspension, Inter. J. Mineral Processing, 18, 277–286.

Drzymala J., Separation of magnetite from synthetic mixture with quartz by oil agglomeration, 1944, Prace Naukowe Instytutu Górnictwa Politechniki Wrocławskiej, nr 76, Studia i Materiały nr 24, 1994, 63–72.

Drzymala J., Wheelock T.D., 1988. Agglomeration with heptane of coal and other materials in aqueous suspensions, Minerals Engineering, 1 (4), 351–358.

Drzymala J., Wheelock T.D., 1997. Air promoted oil agglomeration of moderately hydrophobic coals 2. Effect of air dosage in a model mixing system, Coal Preparation, 18, 37–52.

Drzymala J., Wheelock T.D., 1996. Preliminary characterization of a gas-promoted oil agglomeration process, 1996. Proc. 13th Annual Inetrnational Pittesburgh Coal Conference „Coal – Energy and the Environment", Vol. 2, Shia-Huung Chiang (ed.), The University of Pittsburgh School of Engineering Center for Energy Research, 898–903.

Drzymala J., Wheelock T.D., 2005, Oil agglomeration of solid particles suspended in water by means of organic liquids, Proc. Conf .Oils and Enviroment, AUZO 2005, Gdańsk University of Technology, 98-

El-Shimi A., Goddard E.D., 1974. Wettability of some law energy surfaces, I. Air/liquid/solid interface, Colloid Interface Sci., 48 (2), 249–255.

Farnard J.R., Smith H.M., Puddington I.E., 1961. Spherical agglomeration of solids in liquid suspension, Canadian Journal of Chem. Eng., 94–96.

Fowkes F.M., 1964. Attractive forces at interfaces, Ind. Eng. Chem., 56 (12), 40–52.

Good R.J., Islam M., 1991. Liquid bridges and the oil agglomeration method of coal beneficiation: an elementary theory of stability, Langmuir, 7, 3219–3221.

Good R.J., Keller D.V., 1989. Fundamental research on surface science of coal in support of physical beneficiation of coal, Quarterly report No.7, Dep. Chem. Eng., State University of New York, Buffalo, N.Y.

Good R.J., Srivasta N.R., Islam M., Huang H.T.L., van Oss C.J., 1990. Theory of the acid/base hydrogen bonding interactions, contact angles and the hysteresis of contact: application to coal and graphite surfaces, J. Adhes. Sci. Technol., 4 (8), 607–617.

Hamilton W.C., 1972. Technique for characterization of hydrophilic solid surfaces, J. Colloid Interface Sci., 40 (2), 219–222.

Jacobsen P.S., Killmeyer R.P., Hucko R.E., 1990. Interlaboratory comparison of advanced fine coal beneficiation processes, Processing and utilization of high-sulfur coals III, R. Markuszewski and T.D. Wheelock (eds.), Elsevier, Amsterdam, 109–118.

Jacques M.T., Hovarongkura A.D., Henry J. Jr., 1979. Feasibility of separation process in liquid-liquid solid system: free energy and stability analysis, AIChE Journal, 25 (1), 160–170.

Jańczuk B., Białopiotrowicz T., 1988. Swobodna energia powierzchniowa węgli kamiennych a kąt zwilżania w układzie węgiel–kropla wody–oktan, Przemysł Chemiczny, 67 (2), 76–78.

Jańczuk B., Chibowski E., 1983. Interpretation of contact angle in solid-hydrocarbon-water system, J. Colloid Interface Sci., 95 (1), 268–270.

Kao R.L., Wasan D.T., Nikolov A.D., Edwards D.A., 1988/89. Mechanism of oil removal from a solid surface in the presence of anionic micellar solution, Colloids and Surfaces, 34, 389–398.

Kavouridis C.B., Shergold H.L., Ayers P., 1981. Agglomeration of particles in an aqueous suspension by an immiscible liquid, Trans. IMM Sect.C., C53–C60.

Kawashima Y., Furukawa K., Takenaka H., 1981. Spherical agglomeration, Powder Technology, 30, 211–216.

Kawashima Y., Handa T., Takeuchi H., Takenaka H., 1986. Spherical agglomeration of calcium carbonate dispersed in aqueous medium containing sodium oleate, Powder Technology, 46, 61–66.

Keller D.V., 1984. Methods for processing coal, U.S. Patent No. 4,484,928.

Keller D.V., Burry W.M., 1987. An investigation of a separation process involving Liquid-water-coal systems, Colloids and Surfaces, 22, 37–50.

Keller D.V., Burry W.M., 1988. Time-controlled process for agglomerating coal, U.S. Patent 4,770,766.

Keller D.V., Burry W.M., 1990. The demineralization of coal using selective agglomeration by the T-process, Coal Preparation, 8, 1–17.

Kelsall G.H., Marinakis K.I., 1984. Concentration of fine wolframite particles at the isooctane-water interface, Reagents in the mineral industry, M.J. Jones and R. Oblatt (eds.), Inst. of Mining and Metallurgy, 25–32.

Kelsall G.H., Pitt J.L, 1987. Spherical agglomeration of fine wolframite mineral particles, Chem. Eng. Science, 42 (4), 679–688.

Killmeyer R.P., 1985. Round robin testing of advanced selective agglomeration and flotation processes, Proc. 2nd Annual Pittsburgh Coal Conference, 1985., Pittsburgh Energy Technology Center, 55–62.

Klimpel R.R., 1988. The industrial practice of sulfide mineral collectors, in: Reagents in Mineral Technology, Surfactant Science Series, Vol. 27, P. Somasundaran and B.M. Moudgil (eds.), Dekker, New York, 663–682.

Kloubek J., Interaction at interfaces and induction of surface free energy components, 1987, Collection Czechoslovak Chem. Commun., 52, 271–286.

Labuschagne B.C.J., 1986a. The oil phase selective agglomeration: a structural approach, Proc. 3rd Annual Pittsburgh Coal Conference, Pittsburgh, PA., September 8–12, 47–60.

Labuschagne B.C.J., 1986b. Relationship between oil agglomeration and surface properties of coal: effect of pH and oil composition, Coal Preparation, 3, 1–13.

Lai R.W., Gray M.L., Richardson A.G., Chiang S.H., 1989. Size reduction and selective agglomeration of coal: technical feasibility of cleaning Pittsburgh Seam Coal with isooctane, in: Advances in coal and Mineral Processing Using Flotation, S. Chander and R.R. Klimpel (eds.), SMME Inc. Littleton, Colorado.

Laskowski J.S., 1992, Oil assisted fine particle processing, in: Colloid chemistry in mineral processing, Chap. 12, J. Laskowski and J. Ralston (eds.), Development in Mineral Processing, 12, Elsevier 1992, Amsterdam, 361–394.

Leja J., 1982. Surface chemistry of froth flotation, Plenum Press, New York.

Luis, H., 1909, The dressing of minerals, Edward Arnold, 405

Müschenborn W., 1952. Neue Versuche zur Feinstkohlenschlarmen, Gluckauf, April 12 (15–16), 240–242.

Majid A., Sparks B.D., Capes C.E., Hamer C.A., 1990. Coagglomeration of coal and limestone to reduce sulfur emission during combustion, Fuel, 69 (5), 570–574.

Meadus F.W., Puddington I.E., 1973. The beneficiation of barite by agglomeration, CIM Bulletin, 123–126.

Mehotra V.P., Sastry K.V.S., Morey B.W., 1983. Review of oil agglomeration techniques for processing of fine coals, Interanational Journal of Mineral processing, 11, 175–201.

Mehrotra V.P., Sastry V.S., 1986. Moisture requirements and role of ash and porosity in pelletization of coal fines, Powder Technology, 47, 51–59.

Melik-Gajkazjan V.I., 1965. Physicochemical principles of apolar collector action in flotation of ores and coal, I.N. Płaksin (ed.), Nauka, Moskva 1965, 22–49, in Russian.

Menon V.B., Wasan D.T., 1988. Characterization of oil-water interfaces containing finely divided solids with application to the coalescence of water-in oil emulsions: a review, Colloids and Surfaces, 29 (1), 7–28.

Messer L., 1968. LoMAg technology: low moisture agglomerates and recycled water from coal slurries, American Minechem Corp., Coraopolis, Pa. USA.

Milana G., Vettor A., Wheelock T.D., 1997. Air promoted oil agglomeration of moderately hydrophobic coals, 1. General Characteristics, Coal Preparation, 18, 17–36.

Mondria H., Logman W.H., 1959. Removing root from an aqueous slurry by means of an oil in water emulsion, U.S. Patent No. 2, 903,423.

Papushin Y.L., Elishevich A.T., Sergeev P.V., 1984. Influence of electrostatic interactions on the formation of coal-oil agglomerates, Khim. Tverd. Topl. (Moscow), 3, 96–99.

Pawlak W., Szymocha K., Briker Y., Ignasiak B., 1990. High-sulfur coal upgrading by improved oil ag-glomeration, Processing and utilization of high-sulfur coals III, R. Markuszewski and T.D. Wheelock (eds.), Elsevier, Amsterdam, 279–287.

Puddington I.E. and Sparks B.D., 1975. Spherical agglomeration process, Minerals Sci. Eng., 282–288.

Puddington I.E., Smith H.M., Farnard J.R., 1966. Process for the separation of solids by agglomeration, U.S. Patent No. 3,268,071.

Ralston O.C., 1922. Comparison of froth with the Trent process, Coal Age, 22(23) 911–914.

Reerink G.G., Müschenborn W., Nötzold E., 1956. Production of high grade products especially fuels, from pit, coal or brown coal, U.S. Patent No. 2 769 537.

Sadowski Z., 1997. Spherical agglomeration of fine mineral particles, Proc. XX IMPC (Aachen), Vol. 2., 415–424, GDMB, Claushal–Zellerfeld.

Shergold H.L., 1981. Two-liquid flotation and extraction of fine particles in: Interfacial phenomena in min-eral processing, B. Yarar and J.D. Spottiswood (eds.), Proc. Eng. Found. Conference New Hampshire.

Sirianni A.F., Capes C.E., Puddington I.E., 1969. Recent experience with the spherical agglomeration proc-ess, Canadian Journal of Chemical Engineering, 47, 166–170.

Sirianni A.F., Coleman R.D., Goodhue E.C., Puddington I.E., 1968. Separation studies of iron ore bodies containg apatite by spherical agglomeration methods, CIM Bulletin, 731–735.

Szymocha K., Ignasiak L., Pawlak W., Kramer J., Rojek T., 1996. Results of demonstration tests of the commercial scale clean soil process plant, Proc. Air & Waste Management Association's Annual Meeting & Exhibition. Air & Waste Management Assoc., Pittsburgh, PA USA, 10.

Takamori T., 1984. Recent study on agglomeration-in-liquid in Japan, Proc. Int. Symp. Powder Techn., 1981, Kyoto, Koichi Iinoga, J.K. Beddow, G. Jimbo (eds.) Hemisphere Pub. Corp., Mc Graw-Hill, New York.

Trass O., Bajor O., 1988. Modified oil agglomeration process for coal beneficiation. Part I Mineral matter liberation by fine grinding with Szego Mill, Canadian J. Chem. Eng., 66, 282–285; Part II. Simultane-ous grinding and oil agglomeration, Canadian J. Chem. Eng., 66, 1988, 286–290.

Uwadiale G.G.O.O., 1990. Selective oil agglomeration of Agbaja iron ore, Minerals and metallurgical Proc-essing, 132–135.

Wei D., Wei K., Qiu J., 1986. Hydrophobic agglomeration and spherical agglomeration of wolframite fines, Inter. J. Mineral Processing, 17, 261–27.

Wheelock T.D., Milana G., Vettor A., 1994. The role of air in oil agglomeration of coal at moderate shear rate, Fuel, 73 (7), 1103–1107.

Wójcik W., Tawel A.M.Al., 1984. Beneficiation of coal fines by aggregative flotation, Powder Technology, 40, 179–185.

Yang G.C.C., Drzymala J., 1986. Aquaoleophilicity and aquaoleophobicity of solid surfaces, Colloids and Surfaces, 17, 313–315.

Yuschenko V.S., Yaminsky V.V., Shchukin E.D., 1983. Interaction between articles in a noncontact liquids, J. Colloid Interface Sci., 96 (2), 307–314.

Zhou Z.A., Xu Z., Finch J.A., Hu H., Rao S.R., 1997. Role of hydrodynamic cavitation in fine particles flo-tation, Int. J. Miner. Process., 51, 139–149.

16. SI units

International system of units, in French *System Internationale d'Unit*, usually abbreviated to SI, consists of seven base quantities (Table 16.1).

Table 16.1. SI base units

Base quantity	unit	symbol
Length	meter	m
Mass	kilogram	kg
Time	second	s
Temperature	kelvin	K
Amount of substance	mole	mol
Electric current	ampere	A
Luminous intensity	candela	cd

Remark: temperature in kelvin (K) from that in Celsius (°C) can be calculated using the equation: K = °C + 273.15.

The base SI units provide numerous derived quantities shown in Table 16.2.

Table 16.2. Examples of SI derived units

Quantity	Unit	Symbol	Definition
Force	newton	N	1 kg·m·s^{-2}
Pressure, stress	pascal	Pa	$1 \text{ kg·m}^{-1}\text{·s}^{-2}$
Energy, work, quantity of heat	joule	J	$1 \text{ kg·m}^2\text{·s}^{-2}$
Electric charge	coulomb	C	1 A·s
Electric potential	volt	V	$1 \text{ kg·m}^2\text{·s}^{-3}\text{·A}^{-1}$
Power	watt	W	$1 \text{ kg·m}^2\text{·s}^{-3}$
Frequency	herz	Hz	$2\pi\text{·rad·s}^{-1}$
Electric capacity	farad	F	$1 \text{ kg}^{-1}\text{·m}^{-2}\text{·s}^4\text{·A}^2$
Area	square meter		m^2
Volume	cubic meter		m^3
Speed, velocity	meter per second		m/s
Acceleration	meter per second squared		m/s^2

Derived units can be expressed as combination of other units (Table 16.3).

Table 16.3. Examples of relations between units of SI

Quantity	Relation	Quantity	Relation
farad	F = C/V	amper	A = W/V
volt	V = J/C	pascal	$Pa = N/m^2$
joule	J = N·m	wat	W = J/s

Many relations and laws contain physical constants. Those most useful in minerallurgy are shown in Table 16.4.

Table 16.4. Selected physical constants (CRC, 1997/98)

Constant or number	Symbol	Value
Avogadro number	N_A	$6.02552 \cdot 10^{23}$ molecules per mole
Boltzmann constant	k	$1.38054 \cdot 10^{-23}$ J/K
Elemental electric charge	e	$1.60210 \cdot 10^{-19}$ C
Dielectric permeability of vacuum	ε_0	$8.854 \cdot 10^{-12}$ F/m (*), ($\varepsilon_0 = \mu_0^{-1} c^{-2}$)
Magnetic permeability of vacuum	μ_0	$12.5666370 \cdot 10^{-7}$ N/A^2, $\mu_0 = 4\pi \cdot 10^{-7}$
Speed of light	c	299 792 458 m/s
Planck constant	h	$6.626\ 0755\ 10^{-34}$ J·s
Faraday constant	F	96 485 309 C/mol
Gas constant	R_g	8.3145 J·mol^{-1}·K^{-1}
Numebr pi	π	3.14

* In literature equivalent units can be encountered: $F \cdot m^{-1} = C \cdot V^{-1} \cdot m^{-1} = C^2 \cdot J^{-1} \cdot m^{-1} = C^2 \cdot N^{-1} \cdot m^{-2}$.

Sometimes the values of physical quantities are either small or large. Then, they can be expressed as multiples and submultiples of the base units. The applied multiplications are shown in Table 16.5.

Table 16.5. SI prefixes used to form SI units

Name	Factor	Symbol	Name	Factor	Symbol
yotta	10^{24}	Y	deci	10^{-1}	d
zetta	10^{21}	Z	centi	10^{-2}	c
exa	10^{18}	E	mili	10^{-3}	m
peta	10^{15}	P	micro	10^{-6}	μ
tera	10^{12}	T	nano	10^{-9}	n
giga	10^{9}	G	pico	10^{-12}	p
mega	10^{6}	M	femto	10^{-15}	f
kilo	10^{3}	K	atto	10^{-18}	a
hecto	10^{2}	H	lepto	10^{-21}	z
deka	10^{1}	Da	yocto	10^{-24}	y

Remark: SI base units of mass is kg while initial unit for multiplication is gram

The SI units were created in sixties of the previous century. In scientific literature there can still be found formulas expressed in other systems such as cgse (centimeter–gram–second– electrostatic) or cgsm (centimeter–gram–second- magnetic or electromagnetic). The use of the non-SI units is not wrong, but not disclosing this fact is a serious fault since others using the formulas can make mistakes in calculations, introducing into equations in the electrostatic system the values in the SI units. This leads not only to erratic calculations but also to false interpretations of the data. The problem mentioned above is not, unfortunately, rare. Table 16.6 presents different versions of the same formula for energy of electrostatic interactions of two spheres. The expression has a crucial meaning for the description and interpretation of many phenom-

ena, including coagulation. Table 16.6 shows that the formulas in the cgse system are frequently not accurately adjusted to the SI units, which causes the occurrence of many untrue versions of the same expressions.

Table 16.6. Correct and incorrect versions of the same equation in SI and cgse

Equation for V_r	Source	Remarks
$\dfrac{\varepsilon R_1 R_2 (\psi_1^2 + \psi_2^2)}{4(R_1 + R_2)} \left\{ \dfrac{2\psi_1\psi_2}{(\psi_1^2 + \psi_2^2)} \ln\left[\dfrac{1+\exp(-\kappa H)}{1-\exp(-\kappa H)}\right] + \ln\left[1-\exp(-2\kappa H)\right] \right\}$	Hogg, Healy, Fuerstenau, 1966	correct cgs system
$\dfrac{\varepsilon R_1 R_2 (\psi_1^2 + \psi_2^2)}{4(R_1 + R_2)} \left\{ \dfrac{2\psi_1\psi_2}{(\psi_1^2 + \psi_2^2)} \ln\left[\dfrac{1+\exp(-\kappa H)}{1-\exp(-\kappa H)}\right] + \ln\left[1-\exp(-2\kappa H)\right] \right\}$	Mao, Yoon, 1997 Laskowski, 1988	cgse, though the text sugests SI lack of $4\pi\varepsilon_0$ before ε
$\dfrac{\varepsilon\varepsilon_0 R_1 R_2 (\psi_1^2 * \psi_2^2)}{4(R_1 + R_2)} \left\{ \dfrac{2\psi_1\psi_2}{(\psi_1^2 * \psi_2^2)} \ln\left[\dfrac{1+\exp(-\kappa H)}{1-\exp(-\kappa H)}\right] + \ln\left[1-\exp(-2\kappa H)\right] \right\}$ *denotes + (Sadowski used multiplying sign)	Sonntag, 1982 Sadowski, 1994	SI, lack of π before ε and 4 should be removed
$\dfrac{\varepsilon\varepsilon_0 R_1 R_2 (\psi_1^2 + \psi_2^2)}{(R_1 * R_2)} \left\{ \dfrac{2\psi_1\psi_2}{(\psi_1^2 + \psi_2^2)} \ln\left[\dfrac{1+\exp(-\kappa H)}{1-\exp(-\kappa H)}\right] + \ln\left[1-\exp(-2\kappa H)\right] \right\}$ *denotes symbol =, correctly +	Czarnecki, 1986	SI, lack of π before ε
$\dfrac{\pi\varepsilon\varepsilon_0 R_1 R_2 (\psi_1^2 + \psi_2^2)}{(R_1 + R_2)} \left\{ \dfrac{2\psi_1\psi_2}{(\psi_1^2 + \psi_2^2)} \ln\left[\dfrac{1+\exp(-\kappa H)}{1-\exp(-\kappa H)}\right] + \ln\left[1-\exp(-2\kappa H)\right] \right\}$	Dabros and Czarnecki, 1980; Hunter,1989	SI, correct

A practical rule of correction of any formula in cgse to the SI unit is simple (Hutner, 1987), since dealing with cgse equations when the dielectric constant is present (dimensionless since expressed in relation to vacuum), it should be replaced by $4\pi\varepsilon\varepsilon_0$, i.e. $4\pi\varepsilon\varepsilon_0$ (SI) $= \varepsilon$ (cgse).

Although it does not mean at all that one cannot use the equations in cgse any longer. Yet it should be remembered that a unit of electrical potential in cgse is not volt (V) but electrostatic unit of potential (units of ES pot.), while a unit of charge is not coulomb (C) but electrostatic unit of charge (esu). One should also know that 1 *V*

$$= \frac{1}{300} esu = \frac{1}{300} \frac{\sqrt{g \cdot cm}}{s}$$ and that 1 C $= 3 \cdot 10^9$ esu. Then, after inserting into an equa-

tions in the cgse the units of esu while to SI equations the units of SI (volt, coulomb, farad) we obtain the same relations and results. If in reports, publications as well as presentation cgse units are used, this fact should be explicitly disclosed. Table 16.7 gives other useful formulas for both systems. This should be helpful when recognizing which system the expressions refer to.

Table 16.7. Selected equations expressed both in SI and cgse units

Expression	SI units	cgse system	Relation
Debye parameter	$\kappa = \left(\dfrac{2n_o F^2 z^2}{\varepsilon\varepsilon_0 RT} \right)^{1/2}$	$\kappa = \left(\dfrac{8\pi n_o F^2 z^2}{\varepsilon RT} \right)^{1/2}$	$4\pi\varepsilon\varepsilon_0$ (SI) $= \varepsilon$ (cgs)
Electrical double layer charge (Gouy–Chapman)	$\sigma_d = -(8n_o\varepsilon\varepsilon_0 kT)^{1/2} \sinh\left(\dfrac{2\mathrm{e}\,\psi_d}{kT} \right)$	$\sigma_d = -\left(\dfrac{\varepsilon kTn_o}{2\pi} \right)^{1/2} \sinh\left(\dfrac{2\mathrm{e}\,\psi_d}{kT} \right)$	$4\pi\varepsilon\varepsilon_0$ (SI) $= \varepsilon$ (cgs)
Electrostatic interactions	$V_R = 2\pi\varepsilon\varepsilon_0 R\psi_0^2 \ln(1+\exp(-\kappa D))$	$V_R = \dfrac{\varepsilon R\psi_0^2}{2} \ln(1+\exp(-\kappa D))$	$4\pi\varepsilon\varepsilon_0$ (SI) $= \varepsilon$ (cgs)
Coulomb's law	$F = \dfrac{1}{4\pi\varepsilon\varepsilon_0} \dfrac{Q_1 Q_2}{D^2}$	$F = \dfrac{1}{\varepsilon} \dfrac{Q_1 Q_2}{D^2}$	$4\pi\varepsilon\varepsilon_0$ (SI) $= \varepsilon$ (cgs)

n_o – number of ion pairs per cm^3

z – ion valence

Q – electrical charge {coulomb (SI) or esu (cgse)},

ψ_0 – surface potential {volt (SI) or esu (cgse)},

ψ_d – diffusive edl potential

F – Faraday constant

D – distance {m (in both systems)}

R – particle size {m (in both systems)}

π – 3.14

T – temperature {kelvin (in both systems)}

ε – dielectric constant {dimensionless (in both systems)}

ε_0 – dielectric permeability of vacuum (8.854·10^{-12} F/m) present only in SI

e – elemental electric charge

$R_g T/F = kT/$e {dimensionless quotients (in both systems)}.

The value of the gas constant R_g, Faraday constant F, Boltzmann constant k in SI were given in Table 16.4.

More details regarding application of both unit systems and recalculations can be found in many publication, for instance by Hunter (1987) or Atkins (1978).

Literature

Atkins P., 1978. Physical chemistry, Oxford University Press, Oxford, 316, 338.

CRC, 1997/8. Handbook of chemistry and physics, ed. 78, D.R., Linde (ed.), CRC Press Boca Raton.

Czarnecki J., 1986. The effect of surface inhomogeneities on the interactions in colloidal systems, Advances in Colloid and Interface Sci., 24, 283–319.

Dabros T., Czarnecki J., 1980. Wpływ oddziaływań elektrycznych na kinetykę heterokoagulacji, Fizyko-chemiczne Problemy Mineralurgii, 12, 47–55.

Hogg R., Healy T.W., Fuerstenau D.W., 1966. Mutual coagulation of colloidal dispersions, Trans. Faraday Soc., 62, 1638–1651.

Hunter R.J., 1987. Foundation of Colloid Science, Vol. 1, Clarendon Press, Oxford, Appendix A, 639–640.

Laskowski J.S., 1988. Dispersing agents in mineral processing, in: Froth flotation, Development in Mineral Processing, 9, S.H. Castro Flores i J. Alvarez Moisan (eds.), Elsevier, Amsderdam.

Mao L., Yoon R-H., 1997. Predicting flotation rates using a rate equation derived from first principles, Inter. J. Mineral Process, 51, 171–181.

Sadowski Z., 1994. Hydrofobowa agregacja zawiesin minerałów węglanowych i siarczanowych, Wydawnictwa UMCS, Lublin.

Sonntag H., Koloidy, PWN, Warszawa 1982.

17. Index

The book deals with mineral processing and is designed for all interested in principles of science and practice of this discipline. The book offers a new and fresh look at understanding of different separation methods applied for enrichment of ores and raw materials. Common structure and features of all separation methods are extensively discussed. The first chapter of the book offers basic information helpful in understanding the Nature (Big Bang theory, elemental particles, molecules, formation of minerals and ores). The second part deals with the structure and properties of separation methods and presents different approaches (upgrading, classification, sorting, distribution, etc.) used for analysis of separation results. In the third part different methods of separation are presented including comminution, screening, hydraulic classification, flotation, coagulation, flocculation, oil agglomeration as well as gravity, magnetic, electric, dielectric, and thin liquid film separations. In the last part the SI units were presented.

The book is based on monograph Podstawy mineralurgii (Foundations of minerallurgy, in Polish) printed in 2001.

Jan Drzymala is a professor of mineral processing and chemistry at the Wroclaw University of Technology (Poland). He has got experience in research and teaching of minerals processing in Poland, USA, and France. He has published more that 100 scientific papers, including two monographs.